1994
XV Brazilian National Meeting on Particles and Fields

SBF
SOCIEDADE BRASILEIRA DE FÍSICA

Proceedings of the

XV Brazilian National Meeting

on Particles and Fields

(XV Encontro Nacional de Física de Partículas e Campos)

October 4–8, 1994

Angra dos Reis, Brazil

Editors

M. S. Alves (UFRJ)
M. E. Araújo (UnB)
C. A. Bonato (UFPb)
C. D. Chinelatto (Unicamp)
S. A. Dias (CBPF)

A. Foerster (UFRGS)
G. C. Marques (IFUSP)
S. F. Novaes (IFT/UNESP)
M. T. Thomaz (UFF)

XV Brazilian National Meeting on Particles and Fields

The Brazilian National Meeting on Particles and Fields (Encontro Nacional de Física de Partículas e Campos) is a scientific meeting held every year that assembles the Brazilian Physics community working in Field Theory, Cosmology and Gravitation, Particle Physics Phenomenology, and Experimental High Energy Physics. The most important aim of this meeting is to enable the interchange of information among the entire community through the presentation of short communications of the submitted papers and the panel session. An overview of the research in the area is achieved through invited review talks of wide interest.

The XV Brazilian National Meeting on Particles and Fields was held at Angra dos Reis, Rio de Janeiro, from 4–8 October, 1994. It was organized under the auspices of Sociedade Brasileira de Física (SBF) with the support of Coordenação de Aperfeiçoamento de Pessoal de Nível Superior (CAPES), Centro Latino–Americano de Física (CLAF), Conselho Nacional de Desenvolvimento Científico e Tecnológico (CNPq), Fundação de Amparo à Pesquisa do Estado de São Paulo (FAPESP), do Rio de Janeiro (FAPERJ), do Rio Grande do Sul (FAPERGS), and Financiadora de Estudos e Projetos (FINEP).

The meeting had 270 participants and consisted of seven plenary and eight parallel talks given by invited speakers, nine of them from abroad. We also had 105 short communications and 93 panels, where Brazilian researchers in the area had an opportunity to present the final results of their research projects and to discuss their works in progress.

During this meeting, Prof. José Leite Lopes and Prof. Carlos Aragão de Carvalho Filho delivered talks to honor Prof. C. M. G. Lattes and Prof. J. J. Giambiagi, respectively. On the night of October 6, a round table was organized to discuss the financial support in Science and Technology with the participation of members of the Ministério da Ciência e Tecnologia, Financiadora de Estudos e Projetos (Finep), Fundação de Amparo à Pesquisa do Estado de São Paulo (FAPESP), and Centro Latino Americano de Física (CLAF).

We would like to thank the SBF staff for all their efforts, in particular Neusa M. L. Martin for organizing these Proceedings.

May 1995   The Organizing Committee

ÍNDICE

I. PALESTRAS DE REVISÃO E SEMINÁRIOS

II. CONTRIBUIÇÕES CIENTÍFICAS

A. Cosmologia e Gravitação

B. Física Experimental de Altas Energias

D. Teoria de Campos

High Energy Neutrino Astronomy
and its Telescopes

F. Halzen

Department of Physics, University of Wisconsin, Madison, WI 53706

Doing astronomy with photons of energies in excess of a GeV has turned out to be extremely challenging. Efforts are underway to develop instruments that may push astronomy to wavelengths smaller than 10^{-14} cm by mapping the sky using high energy neutrinos instead. Neutrino astronomy, born with the identification of thermonuclear fusion in the sun and the particle processes controlling the fate of a nearby supernova, will reach outside the galaxy and make measurements relevant to cosmology. The field is immersed in technology in the domains of particle physics to which many of its research goals are intellectually connected. To mind come the search for neutrino mass, cold dark matter (supersymmetric particles?) and the monopoles of the Standard Model. While a variety of collaborations are pioneering complementary methods by building telescopes with effective area in excess of 0.01 km^2, we show here that the natural scale of a high energy neutrino telescope is 1 km^2. With several thousand optical modules and a price tag unlikely to exceed 100 million dollars, the scope of a kilometer-scale instrument is similar to that of experiments presently being commissioned such as the SNO neutrino observatory in Canada and the Superkamiokande experiment in Japan.

Overview

In the past year we have witnessed the first activity in the commissioning of a novel type of telescope which detects elusive high energy neutrinos to probe mysteries in a variety of fields including astronomy and astrophysics, cosmic ray and particle physics. Most of all, however, one hopes to be surprised as historically, new ways of looking at the sky have led to unexpected discoveries. Large volumes of deep ocean and lake water as well as the Antarctic ice cap are being instrumented to trap cosmic neutrinos. With the present flurry of activity, scientists are hopefully taking the first steps in the future construction of kilometer-scale neutrino detectors consisting of a million billion liters (a teraliter) of instrumented natural water or ice. These instruments should be able to study the Universe beyond our galaxy and watch cosmic cataclysms without having to wait for a once-in-a-century miracle like a nearby supernova.

The penetrating power of the neutrino has been successfully exploited by particle physicists, who realized some time ago that by illuminating matter with an intense neutrino beam one can glean information on structure deep inside protons. In a very poor choice of words for a physicist, one could say that neutrinos are a diagnostic tool to "X-ray" protons or nuclei. The technique contributed in important ways to the discovery of quarks and is conceptually simple, though technologically very challenging. A very intense beam of accelerated protons is shot into a "beam-dump" which typically consists of a kilometer-long mound of earth or a 100-meter-long block of stainless steel. Particle physics does the rest. Protons interact with nuclei in the dump and produce a large multiplicity of pions in each collision. Neutral pions decay into two photons, while charged pions decay into a muon and a neutrino. The material in the dump will eventually absorb the photons and muons so that only neutrinos exit at the opposite end, forming an intense and controlled beam ready to perform neutrino microscopy of matter.

Can we use neutrinos to X-ray the Universe? Are there cosmic beam-dumps producing neutrinos in space? Recall that all that is needed is a proton beam, energetic enough to produce pions, and target material to act as the

dump. The answer is definitively positive: cosmic ray experiments have revealed the existence of cosmic protons with energies up to 10^{20} eV. When these particles interact with the Earth's atmosphere, the collision energy exceeds by more than a hundred times those achievable with CERN's LHC. The cosmic ray beam will produce neutrinos in any target material. The target may be as ordinary as the Earth's atmosphere and as exotic as the cosmic photons which fill outer space.

Incredibly, we have no clue where these cosmic rays come from and how they can be accelerated to such energies. The highest energy cosmic rays are, almost certainly, of extra-galactic origin. Beyond our galaxy, powerful quasars and active galaxies stand out as the most likely sites from which particles can be hurled at Earth with joules of energy. The idea is rather compelling as bright quasars are also the dominant source of high energy photons. Quasars are the brightest sources in the Universe; some are so far away that they are messengers from the earliest of times. Their powerful engines must be extremely small as their luminosities are often observed to change by an order of magnitude over time periods as short as a day. Only black holes, a billion times more massive than our sun, will do. It is anticipated that beams accelerated near the black hole produce neutrinos on the ambient matter in the active galaxy, e.g. on the photons with an average density of $10^{14}/cm^3$. Neutrino astronomers believe that the high energy neutrino sky will glow uniformly with bright active galaxies far outshining our Milky Way. But the results may be even more spectacular. As is the case in man-made beam dumps, photons from celestial accelerators may be absorbed in the dump. It is important to realize that high energy photons, unlike weakly interacting neutrinos, do not carry information on cosmic sites shielded from our view by more than a few hundred grams of intervening matter. The neutrino sky may divulge sources with no counterpart in any wavelength of light. Neutrino telescopes may reveal the sources of the enigmatic high energy cosmic rays, thus resolving one of the most lingering puzzles in astronomy.

Some mixture of elementary particle physics and astrophysics allows us to compute that quasars will emit roughly one neutrino for every proton. As we know the frequency with which cosmic rays reach Earth, we can estimate the neutrino luminosity associated with quasars. Kilometer-size instruments are required to *guarantee* their detection and to do real astronomy. The most spectacular discoveries may however be within reach of the smaller detectors now under construction. In order to achieve large effective telescope area, it is unfortunately necessary to abandon the low-energy thresholds of existing supernova or solar neutrino detectors. There is no free lunch. One simply optimizes the instrument to efficiently catch those neutrinos that are easy to catch, i.e. those with very high energies, typically 1-100 GeV and above, which have a relatively large probability of being absorbed by protons in the detector and producing telltale electrons or muons. The accelerator physicist's method for building a neutrino detector will typically use lead absorber to filter out all particles but the neutrinos, wire chambers to detect electrons and muons produced in neutrino charge exchange interactions, and electronics with a combined price tag of roughly 10^4 US dollars per m^2. Such a 1 km^2 detector would cost 10 billion dollars. Realistically, we are compelled to develop methods which are more cost-effective by a factor of one hundred in order to be able to commission neutrino telescopes with effective area of order 1 km^2. Obviously, the proven technique developed by existing underground detectors such as Kamiokande and IMB cannot be extrapolated to kilometer scale. All present telescopes do however exploit the well-proven Cherenkov technique used by these detectors.

We recall that the interaction of neutrinos with matter is so weak that they will have to penetrate the full thickness of the Earth in order to have some chance of being captured. Detectors of astrophysical neutrinos must therefore be orders of magnitude larger than familiar astronomical instruments. Large volumes of water or ice are needed to trap a few neutrinos. When these collide with nuclei of matter, they will spawn muons which will act as observable tracers of the presence and direction of neutrinos: see Fig. 1. High energy muons are marvelous particles. They can, unlike electrons, travel through kilometers of water and ice, thus allowing one to extend the reach of the
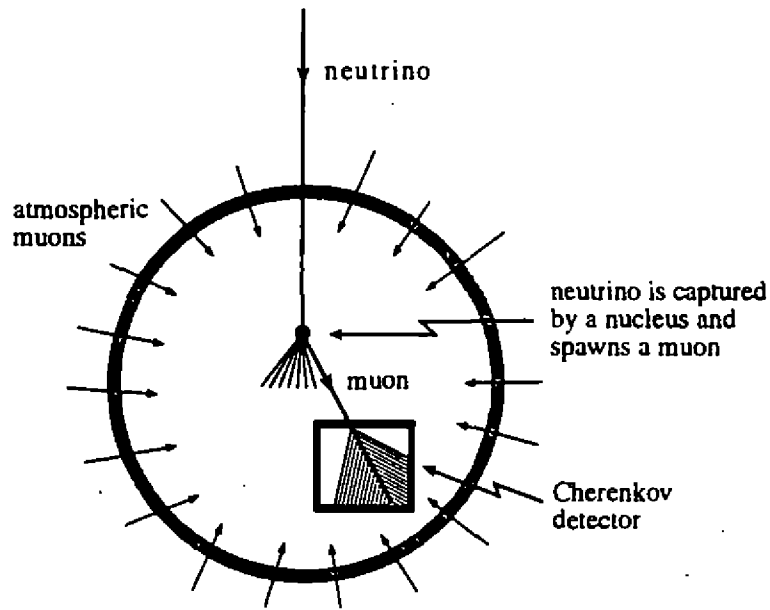
Fig. 1

detector well beyond the actual instrumented volume. Also, high energy muons are nicely aligned with the direction of their parent neutrino. The muons point back to the neutrino sources to better than 1 degree, a deviation which decreases with increasing neutrino energy.

In a Cherenkov detector the direction of the neutrino is inferred from the muon track. It is measured by mapping the cone of Cherenkov light radiated by the muon as it travels through the detector. A high energy muon, travelling faster than the speed of light in water or ice, will radiate photons in the form of a "Cherenkov cone" of light. The arrival times of the Cherenkov photons, recorded by a grid of optical detectors, are used to map the shape of the cone and thus reconstruct the direction of the radiating muon. The photons can be detected with commercial photomultiplier tubes which represent a robust and cheap technology. All this sounds relatively straightforward until one faces the fact that the detector is constantly bombarded with muons produced by cosmic rays in the Earth's atmosphere. These are the decay products of cosmic ray pions and totally unrelated to neutrinos. Near the Earth's surface these muons are over ten billion times more numerous than those signaling the arrival of cosmic neutrinos. In a detector shielded by a kilometer-thick layer of water or ice, the number is reduced and hopefully manageable. Manageable means that the direction of every down-going muon is flawlessly measured so that it can be unambiguously categorized as signal or background. The trick is to use the Earth as a filter: muons travelling *upwards* through the detector must be spawned by neutrinos because the Earth (about 12500 km of it) will shield out atmospheric cosmic ray muons. Neutrino telescopes point into the ground, with the South Pole telescope studying the northern skies.

In this paper we will first review the theorized sources of high energy cosmic neutrinos. We start with those sources whose detection can be guaranteed with sufficiently large telescopes. Although we subsequently list the many science goals of the high energy neutrino telescopes, we will concentrate on two particularly exciting challenges: the observation of neutrino emission by active galaxies and the search for WIMPS, the particles making up the cold dark matter. We finally describe the techniques for detecting neutrinos as well as the four major experiments which are proceeding with construction, each of which has different strengths and faces different challenges. For the construction of a kilometer-scale detector one can imagine any of the above detectors as the basic building block for the ultimate telescope. A world-wide effort is underway to agree on a technology to realize the dream of building the

ultimate instrument. The present efforts described in this article will hopefully be more than engineering projects. The most exciting and unexpected discoveries may be those made by the small, prototype detectors. Although nothing can be guaranteed, history is on our side. The photon sky has been probed with a variety of instruments sensitive to wavelengths of light as large as 10^4 cm for radio-waves to 10^{-14} cm for the GeV-photons detected with space-based instruments. Astronomical instruments have now collected data spanning 60 octaves in photon frequency, an amazing *expansion of the power* of our eyes which scan the sky over less than a single octave just above 10^{-7} cm. The lensmakers in Flanders developed the telescope to make an early inventory of the goods on ships crossing the English Channel. Little did they know that Galileo would use the same instrument to discover the moons of Jupiter. The first X-ray telescope was built to study the sun and moon; its successors discovered all kind of wonderful objects like neutron stars and accreting binaries. The gamma ray instruments developed by the US to search for thermonuclear explosions in the Soviet Union discovered the still enigmatic gamma ray bursts. Each wavelength of light has a story like this to tell. Maybe the most dramatic is the accidental discovery of the cosmic photon background with apparatus studying *sky-interference with telephone communications.* Hopefully, in a not-too-distant future, short wavelength neutrinos will contribute their own bizarre tale.

1. Guaranteed Cosmic Neutrino Beams

In heaven, as on Earth, high energy neutrinos are produced in beam dumps which consist of a high energy proton (or heavy nucleus) accelerator and a target in which gamma rays and neutrinos are generated in roughly equal numbers in the decays of pions produced in nuclear cascades in the beam dump. For every π^0 producing two gamma rays, there is a charged π^+ and π^- decaying into $\mu^+ \nu_\mu$. If the kinematics is such that muons decay in the dump, more neutrinos will be produced. For back-of-the-envelope calculations it is useful to know that roughly one neutrino is produced for each interacting proton in a typical astrophysical beam dump. It should be stressed immediately that in efficient cosmic beam dumps with an abundant amount of target material, high energy photons may be absorbed before escaping the source. Therefore, the most spectacular neutrino sources may have no counterpart in high energy gamma rays.

By their very existence, high energy cosmic rays do guarantee the existence of definite sources of high energy cosmic neutrinos[1]. They represent a hadron beam of known luminosity, with particles accelerated to energies in excess of 10^{20} eV. Cosmic rays produce pions in interactions with i) the interstellar gas in our galaxy, ii) the cosmic photon background in our Universe, iii) the sun, and finally iv) the Earth's atmosphere, which represents a well-understood beam dump. These interactions are the source of fluxes of diffuse photons and neutrinos. The atmospheric neutrino beam can be used to study neutrino oscillations over oscillation lengths varying between 10 and 10^4 km[1].

A rough estimate of the *diffuse fluxes* of gamma rays and neutrinos from the galactic disk can be obtained by colliding the observed cosmic ray flux with interstellar gas with a nominal density of 1 proton per cm^3. The target material is concentrated in the disk of the galaxy and so will be the secondary photon flux. The gamma ray flux has been identified by space-borne gamma ray detectors. It is clear that a roughly equal diffuse neutrino flux is produced by the decay of charged pion secondaries in the same collisions that produced the photons. Conservatively, assuming a detector threshold of 1 TeV, one predicts three neutrino-induced muons per year in a 10^6 m^2 detector from a solid angle of 0.07 sr around the direction of Orion. There are several concentrations of gas with similar or smaller density in the galaxy. The corresponding *number of neutrino* events from within 10 degrees of the galactic disc is 50 events per year for a 10^6 m^2 detector at the South Pole which views 1.1 steradian of the outer Galaxy with an average density of 0.013 grams/cm^2.

A guaranteed source of extremely energetic diffuse neutrinos is the interaction of ultra high energy, extra-galactic,

cosmic rays on the microwave background. The major source of energy loss is photoproduction of the Δ resonance by the cosmic proton beam on a target of background $2.7°$ photons with a density of $\sim$400 photons/cm^3 and an average energy of 7×10^{-4} eV. For cosmic ray energies exceeding

$$E_p \approx \frac{m_\Delta^2 - m_p^2}{2(1 - \cos\theta)_\varepsilon} \approx \frac{5 \times 10^{20}}{(1 - \cos\theta)} \text{ eV} .$$ (1)

where θ is the angle between the proton and photon directions, the photopion cross-section grows very rapidly to reach a maximum of 540 μb at the Δ^+ resonance ($s = 1.52$ GeV^2). The Δ^+ decays to $p\pi^0$ with probability of 2/3, and to $n\pi^+$ with probability 1/3. The charged pions are the source of very high energy muon-neutrino fluxes. In addition, neutrons decay producing a flux of lower energy ν_e.

The magnitude and intensity of the cosmological neutrino fluxes is determined by the maximum injection energy of the ultra high energy cosmic rays and by the distribution of their sources. If the sources are relatively near at distances of order tens of Mpc, and the maximum injection energy is not much greater than the highest observed cosmic ray energy (few $\times 10^{20}$ eV), the generated neutrino fluxes are small. If, however, the highest energy cosmic rays are generated by many sources at large redshift, then a large fraction of their injection energy would be presently contained in γ-ray and neutrino fluxes. The reason is that the energy density of the microwave radiation as well as the photoproduction cross-section scale as $(1 + z)^4$. The effect would be even stronger if the source luminosity were increasing with z, i.e. if cosmic ray sources were more active at large redshifts — 'bright phase' models. Early speculations on bright phase models led to the suggestion of kilometer-scale neutrino detectors over a decade ago[2].

The other guaranteed extraterrestrial source of high energy neutrinos is the Sun. The production process is exactly the same as for atmospheric neutrinos on Earth: cosmic ray interactions in the solar atmosphere. Neutrino production is enhanced because the atmosphere of the Sun is much more tenuous. The scaleheight of the chromosphere is $\sim$115 km, compared with 6.3 km for our upper atmosphere. The decisive factor for the observability of this neutrino source is the small solid angle (6.8×10^{-5} sr) of the Sun. A detailed calculation shows that the rate of neutrino-induced upward-going muons is higher than the atmospheric emission from the same solid angle by a factor of $\sim$5. The rate of muons of energy above 10 GeV in a 10^5 m^2 detector is 50 per year. Taking into account the diffusion of the cosmic rays in the solar wind, which decreases the value of the flux for energies below one TeV, cuts this event rate by a factor of 3. Folded with a realistic angular resolution of 1 degree, observation of such an event rate requires, as for the previous examples, a 1 km^2 detector.

2. Active Galactic Nuclei: Almost Guaranteed?

Although observations of PeV (10^{15} eV) and EeV (10^{18} eV) gamma-rays are controversial, cosmic rays of such energies do exist and their origin is at present a complete mystery. The cosmic-ray spectrum can be understood, up to perhaps 1000 TeV, in terms of shockwave acceleration in galactic supernova remnants. Although the spectrum suddenly steepens at 1000 TeV, a break usually referred to as the "knee" cosmic rays with much higher energies are observed and cannot be accounted for by this mechanism. This failure can be understood by simple dimensional analysis. The EMF in the supernova shock is of the form

$$E = ZeBRc .$$ (2)

where B and R are the magnetic field in the galaxy and the radius of the shock. For a proton Eq. (2) yields a maximum energy

$$E_{max} = [10^5 \text{ TeV}] \left[\frac{B}{3 \times 10^{-6} \text{G}}\right] \left[\frac{R}{50 \text{ pc}}\right]$$ (3)

and therefore E is less than 10^5 TeV for the typical values of B, R shown. The actual upper limit is much smaller than the value obtained by dimensional analysis because of inefficiencies in the acceleration process.

Cosmic rays with energy in excess of 10^{20} eV have been observed. Assuming that they are a galactic phenomenon, the measured spectrum implies that 10^{34} particles are accelerated to 1000 TeV energy every second. We do not know where or how. We do not know whether the particles are protons or iron or something else. If the cosmic accelerators indeed exploit the 3μGauss field of our galaxy, they must be much larger than supernova remnants in order to reach 10^{21} eV energies. Equation (2) requires that their size be of order 30 kpc. Such an accelerator exceeds the dimensions of our galaxy. Although imaginative arguments exist to avoid this impasse, an attractive alternative is to look for large size accelerators outside the galaxy. Nearby active galactic nuclei (quasars, blazars...) distant by order 100 Mpc are the obvious candidates. With magnetic fields of tens of μGauss over distances of kpc near the central black hole or in the jets, acceleration to 10^{21} eV is possible; see Eq. (2).

One can visualize the accelerator in a very economical way in the Blanford-Zralek mechanism. Imagine that the horizon of the central black hole acts as a rotating conductor immersed in an external magnetic field. By simple dimensional analysis this creates a voltage drop

$$\frac{\Delta V}{10^{20}\text{volts}} = \frac{a}{M_{BH}}\,\frac{B}{10^4 G}\,\frac{M_{BH}}{10^9 M_\odot} \ . \tag{4}$$

corresponding to a luminosity

$$\frac{\mathcal{L}}{10^{45}\text{erg s}^{-1}} = \left(\frac{a}{M_{BH}}\right)^2 \left(\frac{B}{10^4 G}\right)^2 \left(\frac{M_{BH}}{10^9 M_\odot}\right)^2 . \tag{5}$$

Here a is the angular momentum per unit mass taken to be the black hole mass M_{BH}.

All this was pretty much a theorist's pipe dream until recently the Whipple collaboration reported the observation of TeV (10^{12} eV) photons from the giant elliptical galaxy Markarian 421[3]. With a signal in excess of 6 standard deviations, this was the first convincing observation of TeV gamma rays from outside our Galaxy. That a distant source such as Markarian 421 can be observed at all implies that its luminosity exceeds that of galactic cosmic accelerators such as the Crab, the only source observed by the same instrument with comparable statistical significance, by close to 10 orders of magnitude. More distant by a factor 10^5, the instrument's solid angle for Markarian 421 is reduced by 10^{-10} compared to the Crab. Nevertheless the photon count at TeV energy is roughly the same for the two sources. The Whipple observation implies a Markarian 421 photon luminosity in excess of 10^{43} ergs per second. It is interesting that these sources have their highest luminosity above TeV energy, beyond the wavelengths of conventional astronomy. During May 1994 Markarian 421 was observed to increase its flux by a factor 10 in one day, strongly suggesting the catastrophic operation of a high energy hadronic accelerator.

Why Markarian 421? Whipple obviously zoomed in on the Compton Observatory catalogue of active galaxies (AGNs) known to emit GeV photons. Markarian, at a distance of barely over 100 Mpc, is the closest blazar on the list. As yet TeV gamma rays have not been detected from any other AGNs. Although Markarian 421 is the closest of these AGNs, it is one of the weakest; the reason that it is detected whereas other, more distant, but more powerful, AGNs are not, must be that the TeV gamma rays suffer absorption in intergalactic space through the interaction with background infra-red photons. TeV gamma rays are indeed efficiently absorbed by infra-red starlight and this most likely provides the explanation why astronomers have a hard time observing much more powerful quasars such as 3C279 at a redshift of 0.54. Production of e^+e^- pairs by TeV gamma rays interacting with IR background photons is the origin of the absorption. The absorption is, however, minimal for Mrk 421 with $z = 0.03$, a distance close enough to see through the IR fog. This implies that all of the AGNs may have significant very high energy components but that only Markarian 421 is close enough to be detectable with currently available gamma-ray telescopes. The opportunities for neutrino astronomy are wonderfully obvious.

This observation was not totally unanticipated. Many theorists[1] have identified blazars such as Markarian 421 as powerful cosmic accelerators producing beams of very high energy photons and neutrinos. Acceleration of particles

is by shocks in the jets (or, possibly, also by shocks in the accretion flow onto the supermassive black hole which powers the galaxy) which are a characteristic feature of these radio-loud active galaxies. Many arguments have been given for the acceleration of protons as well as electrons[1]. Inevitably beams of gamma rays and neutrinos from the decay of pions appear along the jets. The pions are photoproduced by accelerated protons on the target of optical and UV photons in the galaxy, which reaches densities of 10^{14} per cm^3. The latter are the product of synchrotron radiation by electrons accelerated along with the protons.

Powerful AGNs at distances of order 100 Mpc and with proton luminosities of 10^{45} erg/s or higher are obvious candidates for the cosmic accelerators of the highest energy cosmic rays. Their luminosity often peaks at the highest energies and their proton flux, propagated to Earth, can quantitatively reproduce the cosmic ray spectrum above spectrum 10^{18} eV[4]. Some have argued that all cosmic rays above the "knee" in the spectrum at 10^{15} eV may be of AGN origin. The neutrino flux from such accelerators can be calculated by energy conservation:

$$\mathcal{L}_p N \epsilon_{eff} = 4\pi d^2 \int dE[E \, dN_\nu/dE] \, , \tag{6}$$

where N_ν is the neutrino flux at Earth, d the average distance to the sources, N the number of sources and ϵ_{eff} the efficiency for protons to produce pions and therefore neutrinos in the AGN beamdump. Assuming the production of 1 neutrino per interacting proton, we obtain

$$E\frac{dN_\nu}{dE} = \frac{N\epsilon_{eff}}{4\pi}\frac{7.5 \times 10^{-10}}{E\,(\text{TeV})} \, cm^{-2}\,s^{-1}\,sr^{-1} \tag{7}$$

for $\mathcal{L}_p = 10^{45}$ erg/s and $d = 100$ Mpc. We here assumed an E^{-2} energy spectrum extending to 10^{20} eV energy. With ϵ_{eff} of order 10^{-1} to 10^{-3} and the number of relatively nearby sources N in the range 10 to 1000, it is a reasonable estimate that $N\epsilon_{eff} = 1$. The total energy in excess of 1 EeV (10^{18}-10^{20} eV) is 5×10^{-9} erg/cm²/s. This number nicely matches the energy density of the extra-galactic cosmic rays in the same interval of energy, as it should, assuming again that 1 neutrino is produced for every proton in the AGN dump. The flux of Eq. (7) is at the low end of the range of fluxes predicted by Biermann et al. and by Protheroe et al. and Stecker et al. in models where acceleration is in shocks in the jet[4] and accretion disc[5,6], respectively.

The above discussion suggests a very simple estimate of the AGN neutrino flux that finesses all guesses regarding the properties of individual sources:

$$4\pi \int_{10^{17}eV} dE[E \, dN_\nu/dE] \simeq \mathcal{L}_{CR}$$
$$\simeq 7.2 \times 10^{-9}\,erg\,cm^{-2}\,s^{-1} \, . \tag{8}$$

which simply states that AGNs generate 1 neutrino for each proton. $\mathcal{L}_{CR}$ is obtained by integrating the highest energy $E^{-2.71}$ component of the cosmic ray flux above 10^{17} eV. Assuming an E^{-2} neutrino spectrum we recover the result of Eq. (7). Is is now clear that our flux is a lower limit as protons should be absorbed in ambient matter in the source or in the interstellar medium.

3. Intermezzo: The Case for a Kilometer-Scale Detector

Observing AGNs has become a pivotal goal in the development of high energy neutrino telescopes. The architecture of detectors is often optimised for the detection of AGN neutrinos. Neutrinos are observed via the muons they produce in the detector volume. At high energy it is possible to enhance the effective volume of detectors by looking for neutrino-induced muons generated in charged-current interactions of ν_μ in the water or ice outside the instrumented detector volume. The effective detector volume is then the product of the detector area and the muon

range in rock R_μ. TeV muons have a typical range of one kilometer, which leads to a significant increase in effective detector volume. The average muon energy loss rate is

$$\left\langle \frac{dE}{dX} \right\rangle = -\alpha(E) - \beta(E) \times E , \tag{9}$$

where X is the thickness of material in g/cm^2. The first term represents ionization losses, which are approximately independent of energy, with $\alpha \sim 2$ MeV g^{-1}cm^2. The second term includes the catastrophic processes of bremsstrahlung, pair production and nuclear interactions, for which fluctuations play an essential role. Here $\beta \sim 4 \times 10^{-6}$ g^{-1}cm^2. The critical energy above which the radiative processes dominate is

$$E_{cr} = \alpha/\beta \approx 500 \, \text{GeV}. \tag{10}$$

To treat muon propagation properly when $E_\mu > E_{cr}$ requires a Monte Carlo calculation of the probability P_{surv} that a muon of energy E_μ survives with energy $> E_\mu^{min}$ after propagating a distance X.

The probability that a neutrino of energy E_ν on a trajectory through a detector produces a muon above threshold at the detector is

$$P_\nu(E_\nu, E_\mu^{min}) = N_A \int_0^{E_\nu} dE_\mu \frac{d\sigma_\nu}{dE_\mu}(E_\mu, E_\nu)$$
$$\times R_{eff}(E_\mu, E_\mu^{min}) . \tag{11}$$

where

$$R_{eff} = \int_0^\infty dX \, P_{surv}(E_\mu, E_\mu^{min}, X) . \tag{12}$$

and σ_ν is the cross section for a neutrino of energy E_ν to produce a muon of energy E_μ. The flux of ν_μ-induced muons at the detector is given by the convolution of the neutrino spectrum ϕ_ν with the muon production probability (11) as

$$\dot\phi_\mu(E_\mu^{min}, \theta) = \int_{E_\mu^{min}} \left\{ dE_\nu \, P_\nu(E_\nu, E_\mu^{min}) \right.$$
$$\left. \times \exp[-\sigma_t(E_\nu) X(\theta) N_A] \phi_\nu(E_\nu, \theta) \right\} . \tag{13}$$

The exponential factor here accounts for absorption of neutrinos along the chord of the Earth, $X(\theta)$, before they interact to produce muons. Absorption becomes important for $\sigma(E_\nu) \gtrsim 10^{-33}$ cm^2 or $E_\nu \gtrsim 10^7$ GeV.

The event rate in a detector is obtained by multiplying Eq. (13) by its effective area. From Eqs. (7),(13) we obtain order 300 upcoming muon events per year in a 10^6 m^2 detector. It is not a comfortably large rate, as the flux is indeed distributed over a number of sources. There is, however, no competing background. Hopefully one will be able to scrutinize a few nearby sources with good statistics. We should recall at this point that our back-of-the-envelope estimate yields a flux at the lower end of the range of fluxes predicted by detailed modeling. Optimistic predictions exceed our estimate by over an order of magnitude and are, possibly, within reach of the first-generation telescopes now being commissioned.

4. The Neutrino Sky: Summary

The neutrino sky at GeV-energy and above is summarized in Fig. 2. Shown is the flux from the galactic plane as well as a range of estimates (from generous to conservative) for the diffuse fluxes of neutrinos from active galaxies and from the interaction of extra-galactic cosmic rays with cosmic photons. At PeV energies and above all, sources dominate the background of atmospheric neutrinos. In order to deduce the effective area of an instrument required to study the fluxes in the figure, the detection efficiency must be included using Eq. (13). At the highest energies this efficiency approaches unity and 1 event per km^2 per year corresponds to the naive estimate of 10^{-16} neutrinos
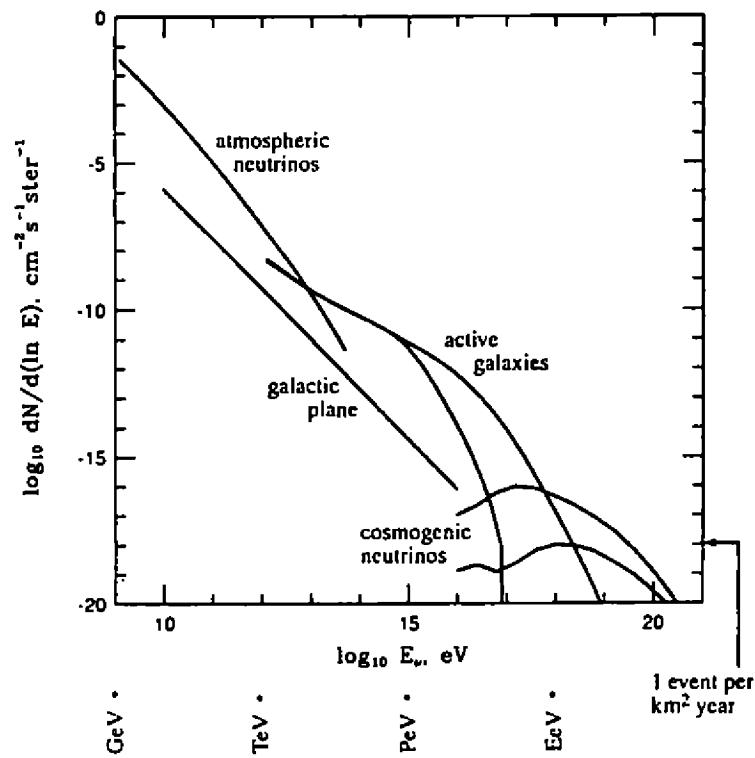
Fig. 2

per cm^2 second. At TeV–PeV energy the 1 event level per year corresponds to a flux of 10^{-14}–10^{-15} per cm^2 second. As before, we conclude that the diffuse flux from AGN yields order 10^3 events in a kilometer-size detector per year in the TeV-energy range.

It should be emphasized that high energy neutrino detectors are multi-purpose instruments. Their science reach touches astronomy, astrophysics and particle physics. Further motivations for the construction of a km^3 deep underground detector include[1]:

1. The search for the t'Hooft-Polyakov monopoles predicted by the Standard Model.

2. The study of neutrino oscillations by monitoring the atmospheric neutrino beam. One can exploit the unique capability of relatively shallow neutrino telescopes. i.e. detectors positioned at a depth of roughly 1 km. to detect neutrinos and muons of similar energy. In a ν_μ oscillation experiment one can therefore tag the π progenitor of the neutrino by detecting the muon produced in the same decay. This eliminates the model dependence of the measurement inevitably associated with the calculation of the primary cosmic ray flux. Surface neutrino telescopes probe the parameter space $\Delta m^2 \gtrsim 10^{-3}$ eV^2 and $\sin^2 2\theta \gtrsim 10^{-3}$ using this technique. Recently, underground experiments have given tantalizing hints for neutrino oscillations in this mass range.

3. The search for neutrinos from the annihilation of dark matter particles in our galaxy.

4. The capability to observe the thermal neutrino emission from supernovae[7] (even though the nominal threshold of the detectors exceeds the neutrino energy by several orders of magnitude!). The detector will be able to monitor our galaxy over decades in a most economical fashion.

5. Further study of the science pioneered by space-based gamma ray detectors such as the study of gamma ray bursts and the high energy emission from quasars.

It is intriguing that each of these goals individually point to the necessity of commissioning a kilometer-size detector. In order to illustrate this, I will discuss the search for the particles which constitute the cold dark matter.

5. Indirect Search for Cold Dark Matter

It is believed that most of our Universe is made of cold dark matter particles. Big bang cosmology implies that these particles have interactions on the order of the weak scale, i.e. they are WIMPs[8]. We know everything about these particles (except whether they really exist!). We know that their mass is of order of the weak boson mass and we know that they interact weakly. We also know their density and average velocity in our galaxy, as they must constitute the dominant component of the density of our galactic halo as measured by rotation curves. WIMPs will annihilate into neutrinos with rates whose estimate is straightforward. Massive WIMPs will annihilate into high energy neutrinos. Their detection by high energy neutrino telescopes is greatly facilitated by the fact that the sun conveniently represents a dense and nearby source of cold dark matter particles.

Galactic WIMPs, scattering off protons in the sun, lose energy. They may fall below escape velocity and be gravitationally trapped. Trapped dark matter particles eventually come to equilibrium temperature, and therefore to rest at the center of the sun. While the WIMP density builds up, their annihilation rate into lighter particles increases until equilibrium is achieved where the annihilation rate equals half of the capture rate. The sun has thus become a reservoir of WIMPs which annihilate into any open fermion, gauge boson or Higgs channels. The leptonic decays of heavy quarks and weak bosons produced in the annihilation channels $b\bar{b}$ and W^+W^- turn the sun into a source of high energy neutrinos. Their energies are in the GeV to TeV range, rather than in the familiar KeV to MeV range from thermonuclear burning. These neutrinos can be detected in deep underground experiments.

We illustrate the power of neutrino telescopes as dark matter detectors using as an example the search for a 500 GeV WIMP with a mass outside the reach of present accelerator and future LHC experiments. A quantitative estimate of the rate of high energy muons of WIMP origin triggering a detector can be made in 5 easy steps.

Step 1: The halo WIMP flux ϕ_χ.

It is given by their number density and average velocity. The cold dark matter density implied by the observed galactic rotation curves is $\rho_\chi = 0.4$ GeV/cm^3. The galactic halo is believed to be an isothermal sphere of WIMPs with average velocity $v_\chi = 300$ km/sec. The number density is then

$$n_\chi = 8 \times 10^{-4} \left[\frac{500 \text{ GeV}}{m_\chi} \right] \text{ cm}^{-3} \tag{14}$$

and therefore

$$\phi_\chi = n_\chi v_\chi = 2 \times 10^4 \left[\frac{500 \text{ GeV}}{m_\chi} \right] \text{ cm}^{-2}\text{s}^{-1}. \tag{15}$$

Step 2: Cross section σ_{sun} for the capture of WIMPs by the sun.

The probability that a WIMP is captured is proportional to the number of target hydrogen nuclei in the sun (i.e. the solar mass divided by the nucleon mass) and the WIMP-nucleon scattering cross section. From dimensional analysis $\sigma(\chi N) \sim \left(G_F m_N^2\right)^2/m_Z^2$ which we can envisage as the exchange of a neutral weak boson between the WIMP and a quark in the nucleon. The main point is that the WIMP is known to be weakly interacting. Details are not relevant for our rate estimate. We obtain for the solar capture cross section

$$\Sigma_{\text{sun}} = n\sigma = \frac{M_{\text{sun}}}{m_N}\sigma(\chi N)$$
$$= \left[1.2 \times 10^{57}\right]\left[10^{-41} \text{ cm}^2\right]. \tag{16}$$

Step 3: Capture rate N_{cap} of WIMPs by the sun.

N_{cap} is determined by the WIMP flux (15) and the sun's capture cross section (16) obtained in the first 2 steps:

$$N_{\text{cap}} = \phi_\chi \Sigma_{\text{sun}} = 3 \times 10^{20} \text{ s}^{-1}. \tag{17}$$

Step 4: Number of solar neutrinos of dark matter origin.

The sun comes to a steady state where capture and annihilation of WIMPs are in equilibrium. For a 500 GeV WIMP the dominant annihilation rate is into weak bosons

$$\chi\bar\chi \to WW \to \mu\nu_\mu . \tag{18}$$

Each W produces muon-neutrinos with a branching ratio which is roughly 10%. As we get 2 W's for each capture, the number of neutrinos generated in the sun is

$$N_\nu = \frac{1}{5} N_{cap} \tag{19}$$

and the corresponding neutrino flux at Earth is given by

$$\dot\phi_\nu = \frac{N_\nu}{4\pi d^2} = 2 \times 10^{-8} \mathrm{cm}^{-2}\mathrm{s}^{-1} , \tag{20}$$

where the distance d is 1 astronomical unit.

Step 5: Event rate in a high energy neutrino telescope.

For (18) the W-energy is approximately m_χ and the neutrino energy half that by two-body kinematics. The energy of the detected muon is given by

$$E_\mu \simeq \frac{1}{2} E_\nu \simeq \frac{1}{4} m_\chi . \tag{21}$$

In the second step we used the fact that, in this energy range, roughly half of the neutrino energy is transferred to the muon. Simple estimates of the neutrino interaction cross section and the muon range can be obtained as follows

$$\sigma_{\nu-\mu} = 10^{-38} \mathrm{cm}^2 \frac{E_\nu}{\mathrm{GeV}} = 2.5 \times 10^{-36} \mathrm{cm}^2 \tag{22}$$

and

$$R_\mu = 5 \mathrm{\ m} \frac{E_\mu}{\mathrm{GeV}} = 625 \mathrm{\ m} . \tag{23}$$

which is the distance covered by a muon given that it loses 2 MeV for each gram of matter traversed. We have now collected all the information required to compute the number of events in a detector of area $10^6 \mathrm{\,m}^2$. For the neutrino flux given by (20) we obtain

$$\#\,\mathrm{events/year} = 10^6 \times \phi_\nu \times \rho_{H_2O} \times \sigma_{\nu-\mu} \times R_\mu$$
$$\simeq 1000 \tag{24}$$

for a 1 km^2 water Cherenkov detector, where R_μ is the muon range and $\phi_\nu \times \rho_{H_2O} \times \sigma_{\nu-\mu}$ is the analog of Eq. (13). Notice that this corresponds to 10 events per year for a $10^4 \mathrm{\,m}^2$ telescope, an area typical for the instruments presently under construction.

The above exercise is just meant to illustrate that high energy neutrino telescopes compete with present and future accelerator experiments in the search for dark matter and supersymmetry; see below. The above exercise can be repeated as a function of WIMP mass. The result is shown in Fig. 3. (The two branches as well as the structure in the curves are related to details of supersymmetry. These are, for all practical purposes, irrelevant). Especially for heavier WIMPs the technique is very powerful because underground high energy neutrino detectors have been optimized to be sensitive in the energy region where the neutrino interaction cross section and the range of the muon are large. Also, for high energy neutrinos the muon and neutrino are aligned along a direction pointing back to the sun with good angular resolution. A kilometer-size detector probes WIMP masses up to the TeV-range, beyond which they are excluded by cosmological considerations. The technique fails for low masses only for those
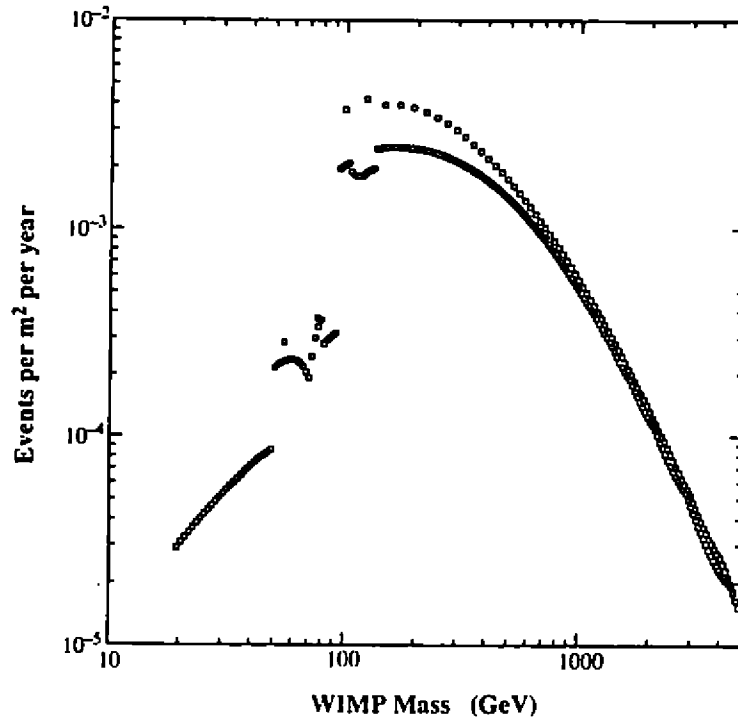
Fig. 3

mass values already excluded by unsuccessful accelerator searches. Competitive direct searches for dark matter will have to deliver detectors reaching better than 0.05 events/kg/day sensitivity.

Particle physics provides us with rather compelling candidates for WIMPs. The Standard Model is not a model: its radiative corrections are not under control. A most elegant and economical way to revamp it into a consistent and calculable framework is to make the model supersymmetric. If supersymmetry is indeed Nature's extension of the Standard Model, it must produce new phenomena at or below the TeV scale. A very attractive feature of supersymmetry is that it provides cosmology with a natural dark-matter candidate in the form of a stable lightest supersymmetric particle[8]. This is, excluding the axion, the only candidate because supersymmetry completes the Standard Model all the way to the GUT scale where its forces apparently unify. Because supersymmetry logically completes the Standard Model with no other new physics threshold up to the GUT-scale, it must supply the dark matter. So, if supersymmetry, then dark matter and accelerator detectors are on a level playing field. The interpretation of the above arguments in the framework of supersymmetry is explicitly stated in Ref. [9].

6. DUMAND et al.: Complementary Technologies

We have presented arguments for doing neutrino astronomy on the scale of 1 kilometer. In order to achieve large effective area, it is unfortunately necessary to abandon the low MeV thresholds of detectors such as IMB and Kamiokande. One focuses on high energies where: i) neutrino cross sections are large and the muon range is increased; see Equation (13), ii) the angle between the muon and parent neutrino is less than 1 degree, and iii) the atmospheric neutrino background is small. The accelerator physicist's method for building a neutrino detector uses absorber chambers with a few x, y wires and associated electronics with a price of roughly 10^4 US dollars per m^2. Such a 1 km^2 detector would cost 10 billion dollars. Realistically, we are compelled to develop methods which are more cost-effective by a factor 100 in order to be able to commission neutrino telescopes with area of order 1 km^2. Obviously, the proven technique developed by IMB, Kamiokande and others cannot be extrapolated to kilometer scale. All present high energy telescope designs do however exploit the well-proven Cherenkov technique.

implemented with the use of conventional photomultiplier tubes.

In a Cherenkov detector the direction of the neutrino is inferred from the muon track, which is measured by mapping the associated Cherenkov cone travelling through the detector. The arrival times and amplitudes of the Cherenkov photons, recorded by a grid of optical detectors, are used to reconstruct the direction of the radiating muon. The challenge is well-defined: record the muon direction with sufficient precision (i.e., sufficient to unambiguously separate the much more numerous down-going cosmic ray muons from the up-coming muons of neutrino origin) with a minimum number of optical modules (OM). Critical parameters are detector depth, which determines the level of the cosmic ray muon background, and the noise rates in the optical modules, which will sprinkle a muon trigger with false signals. Sources of noise include radioactive decays such as potassium decay in water, bioluminescence and, inevitably, the dark current of the photomultiplier tube. The experimental advantages and challenges are different for each experiment and, in this sense, they nicely complement one another as engineering projects for a large detector. Each has its own "gimmick" to achieve neutrino detection with a minimum number of OMs:

1. AMANDA uses sterile ice, free of radioactivity;

2. Baikal triggers on pairs of OMs;

3. DUMAND and NESTOR shield their arrays by over 4 km of ocean water.

Detectors under construction will have a nominal effective area of 10^4 m^2. The OMs are deployed like beads on strings separated by 20–60 meters. There are typically 20 OMs per string separated by 10 meters or more. Baikal is presently operating 36 optical modules, 18 pointing up and 18 down, and the South Pole AMANDA experiment started operating 4 strings with a total of 80 optical modules in January 94. The first generation telescopes will consist of roughly 200 OMs. Briefly,

1. AMANDA is operating in deep clear ice with an absorption length in excess of 60 m, similar to that of the clearest water used in the Kamiokande and IMB experiments. The ice provides a convenient mechanical support for the detector. The immediate advantage is that all electronics can be positioned at the surface. Only the optical modules are deployed into the deep ice. Polar ice is a sterile medium with a concentration of radioactive elements reduced by more than 10^{-4} compared to sea or lake water. The low background results in an improved sensitivity which allows for the detection of high energy muons with very simple trigger schemes which are implemented by off-the-shelf electronics. Being positioned under only 1–2 km of ice, it is operating in a cosmic ray muon background which is two orders of magnitude larger than deep-ocean detectors such as DUMAND. The challenge is to reject the down-going muon background relative to the up-coming neutrino-induced muons by a factor 10^6. The group claims to have met this challenge with an up/down rejection which is similar to that of the deep detectors.

   Although residual bubbles are found at depths as large as 1 km, their density decreases rapidly with depth. Ice at the South Pole should be bubble-free below 1100–1300 m, as it is in other polar regions. The effect of bubbles on timing of photons has been measured by the laser calibration system deployed along with the OMs. After taking the scattering of the light on bubbles into account, reconstruction of muons has been demonstrated by a successful measurement of the characteristic fluxes of cosmic ray muons.

   The polar environment turned out to be surprisingly friendly but only allows for restricted access and one-shot deployment of photomultiplier strings. The technology has, however, been satisfactorily demonstrated with the deployment of the first 4 strings. It is clear that the hot water drilling technique can be used to

deploy OM's larger than the 8 inch photomultiplier tubes now used to any depth in the 3 km deep ice cover. AMANDA will deploy 6 more strings in 1995 at a depth of 1500 meters.

2. BAIKAL shares the shallow depth of AMANDA and large background counting rate of tens of kHz from bioluminescence and radioactive decays with DUMAND. It suppresses its background by pairing OMs in the trigger. Half its optical modules are pointing up in order to achieve a uniform acceptance over upper and lower hemispheres. The depth of the lake is 1.4 km, so the experiment cannot expand downwards and will have to grow horizontally.

   The Baikal group has been operating an array of 18(36) Quasar photomultiplier (a Russian-made 15 inch tube) units deployed in April 1993(94). They have reached a record up/down rejection ratio of 10^{-4} and, according to Monte Carlo, will reach the 10^{-6} goal to detect neutrinos as soon as the full complement of 200 OMs is deployed. They expect to deploy 97 additional OMs in 1995.

3. DUMAND will be positioned under 4.5 km of ocean water, below most biological activity and well shielded from cosmic ray muon backgrounds. A handicap of using ocean water is the background light resulting from radioactive decays, mostly K^{40}, plus some bioluminescence, yielding a noise rate of 60 kHz in a single OM. Deep ocean water is very clear with an absorption length of order 40 m in the blue. The deep ocean is a difficult location for access and service. Detection equipment must be built to high reliability standards and the data must be transmitted to the shore station for processing. It has required years to develop the necessary technology and learn to work in an environment foreign to high energy physics experimentation, but hopefully this will be accomplished satisfactorily.

   The DUMAND group has successfully analysed data on cosmic ray muons from the deployment of a test string. They have already installed the 25 km power and signal cables from detector to shore as well as the junction box for deploying the strings. The group will proceed with the deployment of 3 strings of 24 OMs in 1995.

4. NESTOR is similar to DUMAND, being placed in the deep ocean (the Mediterranean), except for two critical differences. Half of its optical modules point up, half down like Baikal. The angular response of the detector is being tuned to be much more isotropic than either AMANDA or DUMAND, which will give it advantages in, for instance, the study of neutrino oscillations. Secondly, NESTOR will have a higher density of photocathode (in some substantial volume) than the other detectors, and will be able to make local coincidences on lower energy events, even perhaps down to the supernova energy range (tens of MeV). OMs are deployed on titanium "umbrellas" which open up when lowered in the water.

5. Other detectors have been proposed for near surface lakes or ponds (e.g. GRANDE, LENA, NET, PAN and the Blue Lake Project), but at this time none are in construction[10]. These detectors all would have the great advantage of accessibility and ability for dual use as extensive air shower detectors, but suffer from the 10^{10}–10^{11} down-to-up ratio of muons, and face great civil engineering costs (for water systems and light-tight containers). Even if any of these are built it would seem that the costs may be too large to contemplate a full kilometer-scale detector.

7. Sketch of a Kilometer-Size Detector

In summary, there are four major experiments proceeding with construction, each of which has different strengths and faces different challenges. For the construction of a 1 km scale detector one can imagine any of the above

detectors being the basic building block for the ultimate 1 km³ telescope. The redesigned AMANDA detector (with spacings optimized to the absorption length of 60 m), for example, consists of 5 strings on a circle of 60 meter radius around a string at the center (referred to as a 1 + 5 configuration). Each string contains 13 OMs separated by 15 m. Its effective volume for TeV-neutrinos is just below 10^7 m³. Imagine AMANDA "supermodules" which are obtained by extending the basic string length (and module count per string) by a factor close to 4. Supermodules would then consist of 1 + 5 strings with 51 OMs separated by 20 meters on each string, for a total length of 1 km. A 1 km scale detector then may consist of a 1 + 7 + 7 configuration of supermodules, with the 7 supermodules distributed on a circle of radius 250 m and 7 more on a circle of 500 m. The full detector then contains 4590 phototubes, which is less than the 9000 used in the SNO detector. Such a detector (see Fig. 4) can be operated in a dual mode:

1. It obviously consists of roughly 4 × 15 the presently designed AMANDA array, leading to an "effective" volume of ~ 6 × 10⁶ m³. Importantly, the characteristics of the detector, including threshold in the GeV-energy range, are the same as those of the AMANDA array module.

2. The 1 + 7 + 7 supermodule configuration, looked at as a whole, instruments a 1 km³ cylinder with diameter and height of 1000 m with optical modules. High energy muons will be superbly reconstructed as they can produce triggers in 2 or more of the supermodules spaced by large distance. Reaching more than one supermodule (range of 250 m) requires muon energies in excess of 50 GeV. We note that this is the energy for which a neutrino telescope has optimal sensitivity to a typical E^{-2} source (background falls with threshold energy, and until about 1 TeV little signal is lost).
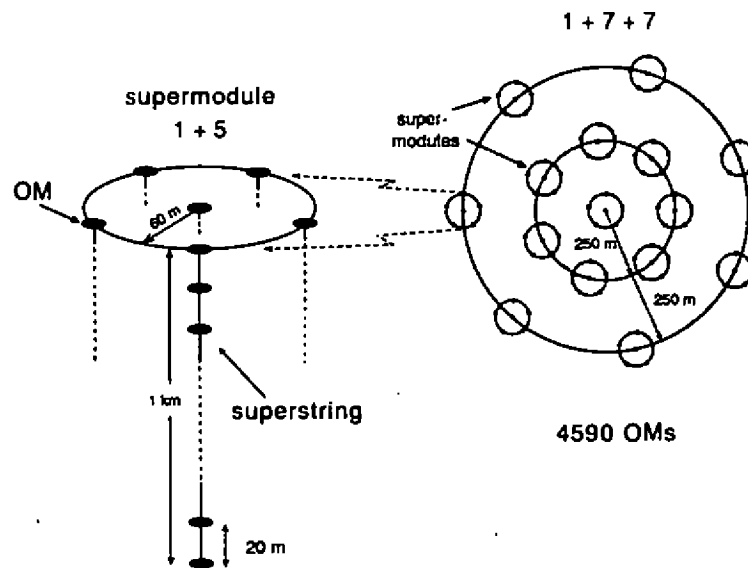
Fig. 4

Alternate methods to reach the 1 km scale have been discussed by Learned and Roberts[11].

What are the construction costs for such a detector? AMANDA's strings (with 20 OMs) cost $150,000 including deployment. By naive scaling the final cost of the postulated 1 + 7 + 7 array of supermodules is of order $50 million, still below that of Superkamiokande (with 11,200 × 20 inch photomultiplier tubes in a 40 m diameter by 40 m high stainless steel tank in a deep mine). It is clear that the naive estimate makes several approximations over- and underestimating the actual cost.

Acknowledgements

References

1. T. K. Gaisser, F. Halzen and T. Stanev, *Physics Reports*, in press.

2. V.S. Berezinsky *et al.*, *Proc. of the Astrophysics of Cosmic Rays*; Elsevier, New York (1991).

3. M. Punch *et al.*, *Nature* **358**, 477–478 (1992).

4. K. Mannheim and P.L. Biermann, *Astron. Astrophys.* **22**, 211 (1989); K. Mannheim and P.L. Biermann, *Astron. Astrophys.* **253**, L21 (1992); K. Mannheim, *Astron. Astrophys.* **269**, 67 (1993).

5. A.P. Szabo and R.J. Protheroe, in *Proc. High Energy Neutrino Astrophysics Workshop* (Univ. of Hawaii, March 1992, eds. V.J. Stenger, J.G. Learned, S. Pakvasa and X. Tata, World Scientific, Singapore).

6. F.W. Stecker, C. Done, M.H. Salamon and P. Sommers, *Phys. Rev. Lett.* **66**, 2697 (1991) and **69**, 2738(E) (1992).

7. F. Halzen, J. E. Jacobsen and E. Zas, *Phys. Rev.* **D49**, 1758 (1994).

8. J. R. Primack, B. Sadoulet, and D. Seckel, *Ann. Rev. Nucl. Part. Sci.* **B38**, 751 (1988).

9. F. Halzen, M. Kamionkowski, and T. Stelzer, *Phys. Rev.* **D45**, 4439 (1992).

10. J.G. Learned, *Proc. of the 13th European Cosmic Ray Symposium*, Geneva 1992, CERN (1992).

11. J. G. Learned and A. Roberts, *Proceedings of the 23rd International Cosmic Ray Conference*, Calgary, Canada (1993); F. Halzen and J.G. Learned, *Proc. of the Fifth International Symposium on Neutrino Telescopes*, Venice (1993), ed. by M. Baldo-Ceolin.

On the Role of Vector Supersymmetry in Topological Field Theory

Olivier Piguet*

Département de Physique Théorique. Université de Genève
24, quai Ernest Ansermet, CH - 1211 Genève 4 (Switzerland)

Vector supersymmetry is typical of topological field theory. Its role in the construction of gauge invariant quantities is explained, as well as its role in the cancellation of the ultraviolet divergences. The example of the Chern-Simons theory in three dimensions is treated in details.

1. Introduction

A main characteristics of topological gauge theories (see [1] for a general review) is their lack of local observables. In particular there is no energy-momentum tensor because of their metric independence and, moreover, the gauge field configurations satisfying the equations of motion are pure gauges. Observables are integrated gauge invariant objects like Wilson loops, or currents localized on the boundary, if any, of the base manifold. Other important physical, gauge invariant quantities are the possible anomalies and the counterterms which correspond to the possible renormalization of the coupling constants. We shall deal here with the latter category of gauge invariant objects. which are represented by space-time integrals.

The aim of this talk is to show how a supersymmetry generated by a space-time vector valued supercharge happens to hold, and to show that this supersymmetry generator may be used in a a natural way for the explicit construction of the gauge invariant objects considered. Its role in the complete cancellation of the ultraviolet divergences in topological theories will also be explained.

In order to keep the argument as simple and self-contained as possible, I shall concentrate on the 3-dimensional Chern-Simons theory. Sect. 2 will be devoted to the description of the model, of its gauge fixing and to its BRS invariance. Sect. 3 will present some simple facts about the BRS cohomology which will be needed later on. Vector supersymmetry will be introduced in Sect. 4 and the solution of the problem in Sect.5. Some conclusions are proposed at the end.

The notations are those of [2]. Generally the statements are given without proof. The proofs may be found in [2], unless they are well-established or an explicit reference is given.

2. The $D = 3$ Chern-Simons model

2.1 The Chern-Simons action

The Chern-Simons term[3, 4] in three space-time dimensions is given by the gauge invariant action

$$S_{CS} := -\frac{k}{4\pi} \int d^3x \; \varepsilon^{\mu\nu\rho} \mathrm{Tr} \left(A_\mu \partial_\nu A_\rho - \frac{2i}{3} A_\mu A_\nu A_\rho \right) . \tag{2.1}$$

The number k plays the role of the inverse of the coupling constant[1] and A_μ is a Lie algebra valued gauge field. as well as all the fields we shall introduce later on. Denoting such a generic field by φ, we define

$$\varphi(x) := \varphi^a(x)\tau_a , \tag{2.2}$$

where the matrices τ are the generators of the group and obey

$$[\tau_a, \tau_b] = if_{abc}\tau_c , \qquad \mathrm{Tr}(\tau_a\tau_b) = \delta_{ab} . \tag{2.3}$$

---

[1] The parameter k is actually quantized[4], but this is irrelevant in perturbation theory, which is a (formal) expansion at zero coupling, hence at infinite k.

The gauge transformations read

$$\delta A_\mu(x) = \partial_\mu \omega(x) + i[\omega(x), A_\mu(x)] =: D_\mu \omega(x) , \qquad (2.4)$$

with $\omega := \omega^a \tau_a$. The gauge group is chosen to be simple and compact. These transformations change the integrand of the action (2.2) into a total derivative, leaving thus the action invariant if there are no boundary contributions and if the topology is trivial [4].

Expression (2.2), although referred here to the flat Euclidean space-time. has an intrinsic geometrical meaning and can be defined on an arbitrary three dimensional manifold $\mathcal{E}$ in a natural way. Indeed one remarks that the Chern-Simons action (2.2) being the integral of a 3-form, does not depend on the metric $g_{\mu\nu}$ which one may introduce on $\mathcal{E}$. Explicitly, defining the gauge connection 1-form

$$A := A_\mu dx^\mu , \qquad (2.5)$$

one can write the Chern-Simons action as

$$S_{\text{CS}} = -\frac{k}{4\pi} \int_\mathcal{E} \text{Tr} \left(A \, dA - \frac{2i}{3} A^3 \right) , \qquad (2.6)$$

the wedge symbol $\wedge$ for the multiplication of forms being omitted.

The main consequence of the metric independence is the vanishing of the energy-momentum tensor associated to the Chern-Simons action:

$$T_{\text{CS}}^{\mu\nu} = \frac{\delta S_{\text{CS}}}{\delta g_{\mu\nu}} = 0 . \qquad (2.7)$$

Another important feature of the theory is the peculiar form of the gauge field equations:

$$F_{\mu\nu} := \partial_\mu A_\nu - \partial_\nu A_\mu - i[A_\mu, A_\nu] = 0 , \qquad (2.8)$$

which means that there is also no field strength. Thus there is no local gauge invariant quantity at all, in other words there are no local observables. But this remark does not imply that the present theory is physically empty. Two types of observables may be defined. The first one is provided by the Wilson loops, that is by the gauge invariant quantities associated to the closed loops C:

$$\text{Tr} \, \text{P} \, \exp i \oint_C A_\mu dx^\mu , \qquad (2.9)$$

where the symbol P means the "path ordered product". The second type of observables are present in case the 3-manifold possesses a 2-dimensional boundary : there exists then a set of conserved chiral current which are localized on the boundary and which generate an infinite dimensional algebra of conserved charges [5, 6, 7].

2.2. Gauge Fixing

We shall fix the gauge à la Landau, adding to the Chern-Simons action (2.2) the term

$$S_{\text{gf}} := \text{Tr} \int d^3x \, (B\partial^\mu A_\mu - \bar{c}\partial^\mu(\partial_\mu c + i[c, A_\mu])) , \qquad (2.10)$$

where the Lie algebra valued fields B, c and $\bar{c}$ are a Lagrange multiplier, the ghost and the antighost, respectively.

The gauge-fixed action

$$\tilde{S} := S_{\text{CS}} + S_{\text{gf}} , \qquad (2.11)$$

is invariant under the nilpotent BRS transformations

$$sA_\mu = D_\mu c := \partial_\mu c + i[c, A_\mu] , \qquad sc = ic^2 .$$

$$s\bar{c} = B , \qquad sB = 0 . \qquad (2.12)$$

The gauge fixing part of the action of course depends on the metric, chosen here as the flat Euclidean one[2] $\delta_{\mu\nu}$.

---

[2]See [8] for the generalization to a curved manifold.

Remark. The gauge fixing part of the action is *s*-exact, i.e. it is a BRS variation:

$$S_{gf} = s\mathrm{Tr} \int d^3x \; \bar{c}\partial^\mu A_\mu \; . \tag{2.13}$$

2.3 The Slavnov-Taylor Identity

The BRS variations of most of the fields being nonlinear, one has to couple them to external fields in order to control their possible renormalizations. We thus add to the action the piece

$$S_{\text{ext}} := \int d^3x \; \mathrm{Tr} \left(\rho^\mu D_\mu c + i\sigma c^2 \right) \; , \tag{2.14}$$

so that the total classical action

$$S(A, c, \bar{c}, B, \rho, \sigma) := \bar{S} + S_{\text{ext}} \tag{2.15}$$

obeys the Slavnov-Taylor identity

$$\mathcal{S}(S) := \int d^3x \; \mathrm{Tr} \left(\frac{\delta S}{\delta \rho^\mu} \frac{\delta S}{\delta A_\mu} + \frac{\delta S}{\delta \sigma} \frac{\delta S}{\delta c} + B \frac{\delta S}{\delta \bar{c}} \right) = 0 \tag{2.16}$$

which plays the role of the Ward identity associated to the BRS invariance.

Remark. Here, at the classical level, the Slavnov-Taylor identity simply expresses the BRS invariance of the action. At the quantum level, the classical action is replaced by the vertex functional[3]

$$\Gamma(A, c, \bar{c}, B, \rho\sigma) = S(A, c, \bar{c}, B, \rho\sigma) + O(\hbar) \; . \tag{2.17}$$

i.e. by the generating functional of the 1-particule irreducible (1PI) Green functions:

$$\left. \frac{\delta^n \Gamma}{\delta\varphi(x_1) \cdots \delta\varphi(x_N)} \right|_{\varphi=0} = \langle 0|T(\varphi(x_1) \cdots \varphi(x_N))|0\rangle_{1PI} \; ,$$

where φ stands for any field. Then the Slavnov-Taylor identity (2.17) has to hold with S replaced by Γ.

The Slavnov-Taylor identity thus expresses the BRS invariance in a functional form or, equivalently, in the form of identities between Green functions.

The gauge fixing condition may also be expressed in a functional form:

$$\frac{\delta S}{\delta B} = \partial A \; , \tag{2.18}$$

Applying the functional operator $\delta/\delta B$ to the Slavnov-Taylor operator defined by (2.17) yields the identity (true for any functional $\mathcal{F}$)

$$\frac{\delta}{\delta B} \mathcal{S}(\mathcal{F}) = \mathcal{S}_{\mathcal{F}} \frac{\delta \mathcal{F}}{\delta B} + \frac{\delta \mathcal{F}}{\delta \bar{c}} \; , \tag{2.19}$$

where we have defined the "linearized" Slavnov-Taylor operator

$$\mathcal{S}_{\mathcal{F}} := \mathrm{Tr} \int d^3x \; \left(\mathrm{Tr} \frac{\delta \mathcal{F}}{\delta \rho^\mu} \frac{\delta}{\delta A_\mu} + \frac{\delta \mathcal{F}}{\delta A_\mu} \frac{\delta}{\delta \rho^\mu} + \frac{\delta \mathcal{F}}{\delta \sigma} \frac{\delta}{\delta c} + \frac{\delta \mathcal{F}}{\delta c} \frac{\delta}{\delta \sigma} + B \frac{\delta}{\delta \bar{c}} \right) \; . \tag{2.20}$$

Applying the identity (2.20) for $\mathcal{F} = S$ and making use of the Slavnov-Taylor identity(2.17) and of the gauge condition (2.19) yields the "ghost equation"

$$\mathcal{G}\Gamma = 0 \; , \quad \text{with} \quad \mathcal{G} := \frac{\delta}{\delta \bar{c}} + \partial^\mu \frac{\delta}{\delta \rho^\mu} \; . \tag{2.21}$$

---

[3] In perturbation theory considered as a formal power expansion in $\hbar$, i.e. in the number of loops of the Feynman graphs, the zeroth order – the classical theory – coincides with the tree graph approximation.

The latter implies that the antighost $\bar{c}$ and the external field ρ appear only in the combination

$$\hat{\rho}^\mu = \rho^\mu + \partial^\mu \bar{c} \ . \tag{2.22}$$

2.4. Stability

The linearized Slavnov-Taylor operator (2.21) may be interpreted as the "derivative at the point $\mathcal{F}$" of the nonlinear map S, defined by (2.17). from the space of the field functionals into the complex numbers. For $\mathcal{F}$ equal to the action S, it can be shown to be nilpotent as a consequence the Slavnov-Taylor identity:.

$$\mathcal{S}_S{}^2 = 0 \ , \tag{2.23}$$

and its action on the fields reads

$$\mathcal{S}_S \varphi = s\varphi \ , \quad \varphi = A, c, \bar{c}, B \ ,$$

$$\mathcal{S}_S \rho^\mu = \frac{\delta S}{\delta A_\mu} \ , \tag{2.24}$$

$$\mathcal{S}_S \sigma = \frac{\delta S}{\delta c} \ .$$

One sees that it coincides with the BRS operator s when applied to the dynamical fields, and yields equations of motion if applied to the external fields.

The operator $\mathcal{S}_S$ allows one to characterize the stability of the theory defined by the Slavnov-Taylor identity and by the gauge condition. This means the following. Given an action S obeying the equations (2.17) and (2.19), let us ask for the most general solution S' in the neighbourhood of S. Writing

$$S' = S + \epsilon \Delta \ , \tag{2.25}$$

with ϵ "small", we find that the perturbation Δ has to obey the two conditions

$$\mathcal{S}_S \Delta = 0 \tag{2.26}$$

and

$$\frac{\delta \Delta}{\delta B} = 0 \ . \tag{2.27}$$

Due to the ghost equation (2.22), it must of course obey the further condition

$$\mathcal{G} \Delta = 0 \ , \tag{2.28}$$

which however is not independent due to the commutation rule

$$\left[\frac{\delta}{\delta B}, \mathcal{S}_S \right] = \mathcal{G} \ . \tag{2.29}$$

A model given by an action S is "stable" if the most general perturbation Δ can be obtained by a redefinition of the parameters and of the field variables.

It is very important to distinguish the "physical" perturbations from the "unphysical" ones. The latter perturbations are those which correspond to a mere redefinition of the fields: they indeed don't affect the physical outcome of a theory, e.g. the scattering amplitudes in a usual gauge theory. It turns out that the unphysical $\mathcal{S}_S$-invariant perturbations are those that take the form of a $\mathcal{S}_S$-variation:

$$\Delta_{\text{unphys}} = \mathcal{S}_S \hat{\Delta} \ . \tag{2.30}$$

Perturbations corresponding to the redefinition of gauge parameters are unphysical, too, and have the same form.

On the other hand, the physical perturbations correspond to the redefinition of physical parameters like the coupling constants and the masses. They are characterized by the property:

$$\mathcal{S}_S \Delta_{\text{phys}} = 0 \ , \quad \text{but} \quad \Delta_{\text{phys}} \neq \mathcal{S}_S \hat{\Delta} \text{ for any } \hat{\Delta} \ . \tag{2.31}$$

Solving (2.27) with a nilpotent operator S_S is thus a problem of cohomology. The next section will deal with this.

3. Cohomology and Descent Equations

3.1 Cohomology and Observables

In ordinary gauge theories the observables are defined, at the classical level, as gauge invariant local polynomial of the *physical fields* (gauge and matter fields). "Local" from now on will mean that these polynomials are made of products of the fields and of their derivatives at a common space-time point x. They may integrated (e.g. Wilson loops) or not (e.g. currents). In the quantum theory, defined e.g. by the renormalized perturbation theory, local field polynomials P become local "operators", or, in the framework of the Green functions, local "insertions" which may be represented by the generating functional

$$P \cdot \Gamma = P + O(\hbar) \tag{3.1}$$

of the 1-particule irreducible Green functions

$$\langle 0|T(P\ \varphi(x_1)\varphi(x_2)\cdots)|0\rangle_{1PI} .$$

The right-hand-side of (3.2) expresses the fact that the tree graph approximation corresponds to the classical approximation. But now P may depend on unphysical fields such as the ghost fields and the external fields.

The quantum version of an observable is then defined as an insertion given by a quantum extension of a local polynomial O of the *physical and unphysical fields*, which is BRS-invariant but not a BRS variation (the linearized Slavnov-Taylor operator (2.21) for $\mathcal{F} = \Sigma$ must be used):

$$S_S O = 0 , \quad \text{but} \quad O \neq S_S \hat{O} \text{ for any } \hat{O} . \tag{3.2}$$

In other terms, quantum observables are defined as cohomology classes of the "coboundary operator" S_S in the space of the local functionals.

We have seen that topological gauge theories such as the Chern-Simons theory do not possess x-dependent local observables. But they possess quantities which are gauge invariant in the sense defined above, i.e. defined by the cohomology of S. We have already encountered the example of the nontrivial BRS-invariant perturbations of the action in Subsect. . Another important example is that of the gauge anomalies[4].

3.2. The Descent Equations

The structure we shall discuss here applies to the gauge invariant quantities which are expressed as space-time integrals. But, in order to keep simplicity, we shall consider in more details only the case of the perturbation Δ introduced in Subsect. . With

$$\Delta = \int d^3x\ Q^0(x) , \tag{3.3}$$

It follows from the BRS invariance condition (2.27) that the BRS variation of the integrand must be a total derivative[5]:

$$S_S Q^0 = \partial_\mu Q^{1\mu} . \tag{3.4}$$

The conditions (2.28) and (2.29) imply that Δ – as well as all the quantities which we shall derive from it – do not depend on the Lagrange multiplier B and depend on the antighost $\bar{c}$ and the external field ρ^μ only through the combination (2.23). The relevant variables are therefore the fields A_μ, c, $\hat{\rho}^\mu$ and σ.

Applying S_S to (3.5) and using the nilpotency of S_S now imply that the variation of $Q^{1\mu}$ is the total derivative of an antisymmetric tensor:

$$S_S Q^{1\mu} = \partial_\nu Q^{2[\mu\nu]} . \tag{3.5}$$

Repeating the argument twice leads to

$$S_S Q^{2[\mu\nu]} = \partial_\rho Q^{3[\mu\nu\rho]} , \quad S_S Q^{3[\mu\nu\rho]} = 0 . \tag{3.6}$$

---

[4] Their absence in the Chern-Simons theory was actually shown in ref. [9].
[5] The exponents give the ghost number. By convention the ghost number of c is equal to 1.

The process stops here because the rank of an antisymmetric tensor is bounded by the space-time dimension.

In the notation of differential forms, these "descent equations" read

$$S_S \omega_3^0 = d\omega_2^1 ,$$

$$S_S \omega_2^1 = d\omega_1^2 ,$$

$$S_S \omega_1^2 = d\omega_0^3 ,$$ (3.7)

$$S_S \omega_0^3 = 0 .$$

with

$$\Delta = \int \omega_3^0 .$$ (3.8)

Here. d is the exterior derivative (with $d^2 = 0$), and the forms ω_{3-g}^g of ghost number g and degree $3 - g$ are defined by:

$$\omega_3^0 = \frac{1}{3!} \varepsilon_{\mu\nu\rho} Q^0 dx^\mu dx^\nu dx^\rho ,$$

$$\omega_2^1 = \frac{1}{2} \varepsilon_{\mu\nu\rho} Q^{1\rho} dx^\mu dx^\nu ,$$

                                                                                            (3.9)

$$\omega_1^2 = \frac{1}{2} \varepsilon_{\mu\nu\rho} Q^{2\nu\rho} dx^\mu ,$$

$$\omega_0^3 = \frac{1}{3!} \varepsilon_{\mu\nu\rho} Q^{3\mu\nu\rho} .$$

Remark. The formalism of the differential forms is the natural one in the present context of a topological theory. Indeed. (3.9) as well as the descent equations (3.8) never involve the metric, but only the differentiable structure of the manifold. To the contrary the metric enters explicitly. although in a spurious way, in the notation in terms of the tensors Q, the latter being the Hodge duals of the forms ω.

3.3. Solution: Existence and Uniqueness

In order to solve the descent equations. let us begin by the last and simplest of them. It is clear that, since ω_0^3 is a 0-form of ghost number 3, its most general invariant expression is given by

$$\omega_0^3 = x \frac{i}{3} \text{Tr} \, c^3 .$$ (3.10)

with x an arbitrary coefficient. In order to find the solution for the other forms, and in particular for ω_3^0 yielding the quantity Δ (3.9) of interest, one has to climb up the descent equations. Each step represents a cohomology problem. but for nonintegrated objects. This cohomology can be shown to consists only of invariant 0-forms made with the ghost field c alone, without derivative[6]. This result was just used above in order to solve the last descent equation. However. since the next steps involve forms of higher degree, the cohomology is then trivial. As it can be shown, this implies that, once the 0-form ω_0^3, i.e. the coefficient x, is given, the general solution for the 3-form ω_3^0 is *unique* up to the BRS variation of a an arbitrary 3-form and the exterior derivative of an arbitrary 2-form:

$$\omega_3^0 = \bar{\omega}_3^0 + S_S \bar{\omega}_3^{-1} + d\bar{\omega}_2^0 ,$$ (3.11)

where $\bar{\omega}_3^0$ is a particular solution. We will show in the next section how a supersymmetry generated by a vector operator indeed gives a particular solution. and what this implies.

4. The Vector Supersymmetry

Since the action depends on the metric only through the gauge fixing part (2.11), which is a BRS variation. the energy-momentum tensor will be a BRS variation as well:

$$T^{\mu\nu} = \frac{\delta S_{gf}}{\delta g_{\mu\nu}} = S_S Q^{\mu\nu} .$$ (4.1)

---

[6]This is very peculiar to the topological theories. In ordinary Yang-Mills theories the cohomology depends on the invariantsdraft constructed with the ghost c and on those made with the Yang-Mills strength F as well [10. 11. 12].

Although the conservation of $T^{\mu\nu}$ does not strictly imply that of $Q^{\mu\nu}$, it turns out [13] that $Q^{\mu\nu}$ is indeed conserved[7]. It follows that there exists a conserved vector charge Q_μ of ghost number -1. This charge generates infinitesimal "vector supersymmetry" transformations, displayed here for all the fields in regard with their BRS transformations (see (2.25)):

$$
\begin{aligned}
\mathcal{S}_S c &= ic^2 & Q_\mu c &= -A_\mu \\[4pt]
\mathcal{S}_S A_\nu &= D_\nu c & Q_\mu A_\nu &= \frac{2\pi}{k}\varepsilon_{\mu\nu\rho}\hat\rho^\rho \\[4pt]
\mathcal{S}_S \hat\rho^\nu &= -\frac{k}{4\pi}\varepsilon^{\nu\rho\sigma} F_{\rho\sigma} + i\{c,\hbar^\nu\} & Q_\mu \hat\rho^\nu &= -\delta_\mu^\nu\sigma \\[4pt]
\mathcal{S}_S \sigma &= D_\nu \hat\rho^\nu + i[c,\sigma] & Q_\mu\sigma &= 0 \\[4pt]
\mathcal{S}_S \bar c &= B & Q_\mu \bar c &= 0 \\[4pt]
\mathcal{S}_S B &= 0 & Q_\mu B &= -\partial_\mu\bar c \; .
\end{aligned}
\tag{4.2}
$$

The variation of the action under these supersymmetry transformations reads

$$
\mathcal{W}_{(\xi)}^S S := \int \sum_{\text{all fields } \varphi} \delta_\xi^S \varphi \frac{S}{\delta\varphi} = \Delta_\mu^{\text{class}} := \int \mathrm{Tr}\left(\frac{2\pi}{k}\varepsilon_{\mu\nu\rho}\rho^\nu\partial^\rho B + \rho^\tau\partial_\mu A_\tau - \sigma\partial_\mu c\right) \; .
\tag{4.3}
$$

where we have denoted the infinitesimal supersymmetry transformation of parameter ξ^μ by

$$
\delta_\xi^S := \xi^\mu Q_\mu \; .
\tag{4.4}
$$

We see that the action is actually invariant for vanishing external fields ρ and σ. For the quantum theory, where the action S is replaced by the functional Γ, (4.4) is interpretated as a (broken)Ward identity for vector supersymmetry. The breaking $\Delta_\mu^{\text{class}}$ vanishes when the external fields are set to zero. Moreover, being *linear* in the quantized fields. it does not need to be renormalized – whence the superscript "class". It is therefore harmless[8].

The geometrical aspect of the supersymmetry transformation laws is much more apparent if one write them – for all the fields except $\bar c$ and B – in the language of differential forms. Introducing the forms

$$
\tilde\rho = \frac{1}{2}\varepsilon_{\mu\nu\rho}\hat\rho^\mu dx^\nu dx^\rho \; , \qquad \tilde\sigma = \frac{1}{3!}\sigma dx^\mu dx^\nu dx^\rho,
\tag{4.5}
$$

(the form A being already defined by (2.6)). and denoting by i_ξ the interior derivative, or contraction, with respect to the the vector ξ^μ, one can write, in an obviously metric independent way,

$$
\begin{aligned}
\mathcal{S}_S c &= ic^2 & \delta_\xi^S c &= -i_\xi A \\[4pt]
\mathcal{S}_S A &= dc + i\{c, A\} & \delta_\xi^S A &= -\frac{2\pi}{k}i_\xi\tilde\rho \\[4pt]
\mathcal{S}_S \tilde\rho &= \frac{k}{4\pi}(dA + iA^2) + i\{c,\tilde\rho\} & \delta_\xi^S \tilde\rho &= -i_\xi\tilde\sigma \\[4pt]
\mathcal{S}_S \tilde\sigma &= d\tilde\rho + i\{A,\tilde\rho\} + i\{c,\tilde\sigma\} & \delta_\xi^S \tilde\sigma &= 0 \; .
\end{aligned}
\tag{4.6}
$$

Now, with the help of the properties

$$
d^2 = 0 \; , \qquad \{d. i_\xi\} = \mathcal{L}_\xi \; . \qquad \{i_\xi, i_{\xi'}\} = 0 \; .
\tag{4.7}
$$

where $\mathcal{L}_\xi$ denotes the Lie derivative along the vector ξ, it is easy to check that the algebra

$$
\mathcal{S}_S = 0 \; . \qquad \left\{\mathcal{S}_S, \mathcal{W}_{(\xi)}^S\right\} = \mathcal{W}_{(\xi)}^\Gamma \; . \qquad \left\{\mathcal{W}_{(\xi)}^S, \mathcal{W}_{(\xi')}^S\right\} = 0 \; .
\tag{4.8}
$$

holds, where

$$
\mathcal{W}_{(\xi)}^\Gamma := \int \sum_{\text{all fields } \varphi} \mathcal{L}_\xi\varphi\frac{\delta}{\delta\varphi}
\tag{4.9}
$$

---

[7] This actually happens in every topological model studied up to now.

[8] This would not be the case for an arbitrary gauge fixing. One can check that, at least among the family of the linear covariant gauges, vector supersymmetry selects the Landau gauge. In particular a Feynman-type gauge would violate supersymmetry. Some noncovariant gauges, like the axial gauge, are also possible [14, 15, 16].

is the generator of the space-time translations[9]. This shows that the BRS, supersymmetry and translation generators $\mathcal{S}_S$, $\mathcal{W}_{(\xi)}^S$ and $\mathcal{W}_{(\xi)}^T$ obey a superalgebra of the Wess-Zumino type.

Let us end this section by noting that the supersymmetry Ward identity (4.4) imposed to the theory yields the constraint

$$\mathcal{W}_{(\xi)}^S \Delta = 0 \qquad (4.10)$$

on the perturbation (2.26), which has to be obeyed together with the previous constraints (2.27), (2.28) and (2.29).

5. Solving the Descent Equations

We have mentioned in Subsect. that the descent equations (3.8) admit a unique solution - modulo a total derivative and a BRS variation - once the bottom 0-form is given. We shall show in the present section, on the example of the equations (3.8), how vector supersymmetry allows to find that solution.

This is done with the help of the operator[10]

$$\nabla := dx^\mu \mathcal{W}_\mu , \qquad (5.2)$$

where we have introduced the components $\mathcal{W}_\mu^S$ of the supersymmetry generator (4.4) - and also $\mathcal{W}_\mu^T$ for the translations - defined by

$$\mathcal{W}_{(\xi)}^S =: \xi^\mu \mathcal{W}_\mu^S , \qquad \mathcal{W}_{(\xi)}^T =: \xi^\mu \mathcal{W}_\mu^T . \qquad (5.3)$$

It is clear from the algebra (4.9) which now reads

$$\mathcal{S}_S{}^2 = 0 , \qquad \{\mathcal{S}_S, \mathcal{W}_\mu^S\} = \mathcal{W}_\mu^T , \qquad \{\mathcal{W}_\mu^S, \mathcal{W}_\nu^S\} = 0 , \qquad (5.4)$$

that

$$\prod_{k=1}^{n} \mathcal{W}_{\mu_k}^S = 0 \quad \text{if } n \geq 3 . \qquad (5.5)$$

Hence

$$\nabla^n = 0 \quad \text{if } n \geq 3 . \qquad (5.6)$$

The algebra (4.9) also implies the commutation relation[11]

$$[\nabla, \mathcal{S}_S] = d . \qquad (5.7)$$

The particular solution of the descent equations we are looking for reads

$$\omega_p^{3-p} = \frac{1}{p!} \nabla^p \omega_0^3 , \qquad p = 0, \cdots, 3 . \qquad (5.8)$$

This is readily checked using the commutation relation (5.8). The corresponding perturbation Δ (3.9) of the action then reads

$$\Delta = \frac{1}{3!} \int \nabla^3 \omega_0^3 = ix \int \text{Tr} \left(\frac{k}{6\pi} A^3 + \bar{\sigma} c^2 + \bar{\rho}\{A, c\} \right) . \qquad (5.9)$$

This is only one of the BRS invariant solutions corresponding to the same zero 0-form ω_0^3, as we already know. Another possible solution is e.g. the one which leads to the Chern-Simons action (2.2):

$$\Delta = x \Sigma_{CS} . \qquad (5.10)$$

(One can actually check that (5.10) and (5.11) differ by a BRS variation.) The solution (5.11) would correspond to a renormalization of the parameter k. However the Chern-Simons action Σ_{CS} is not supersymmetric and one has thus to discard this solution.

---

[9] In the flat space and with the constant vector fields considered here, this Lie derivative takes the simple form of an infinitesimal translation $\xi^\mu \partial_\mu$. In a general curved manifold $\mathcal{L}_\xi$ generates the diffeomorphisms along the vector field ξ, and supersymmetry transformations become superdiffeomorphisms [8].

[10] A more intrinsic definition of ∇, suitable for the generalizations, is provided by its action on the individual fields (in the differential form notation):

$$\nabla c = -A , \quad \nabla A = -\frac{2\pi}{k} \bar{\rho} , \quad \nabla \bar{\rho} = -\bar{\sigma} , \quad \nabla \bar{\sigma} = 0 . \qquad (5.1)$$

[11] This is Sorella's "decomposition of the exterior derivative" [17]. .

On the other hand, the solution (5.10) being obtained by the triple application of the supersymmetry operator is supersymmetric due to the identity (5.6) taken for $n = 4$. Moreover, it is the only supersymmetric one, as we shall check below. But before, let us mention that, like (5.11), it also corresponds to a renormalization of k, however combined with a renormalization of the field amplitudes.

Let us write the general solution, which differs from (5.10) by an arbitrary BRS variation (restricted by having the same quantum numbers and dimension as the action):

$$\Delta_{\text{general}} = \Delta + S_S \int \text{Tr} \left(y \bar{\sigma} c + z \bar{\rho} A \right)$$

$$= \Delta + \int \text{Tr} \left(y(i\bar{\sigma}c^2 + \bar{\rho}dc + i\bar{\rho}\{A,c\}) + z \left(\frac{k}{4\pi}(dAA + iA^3) - \bar{\rho}dc \right) \right) .$$

But the variational part in the right-hand side is not supersymmetric for any ratio of the parameters y and z; this shows that indeed (5.10) is the unique perturbation of the action which is both BRS invariant and supersymmetric.

6. Ultraviolet Finiteness

6.1. Classical Perturbation

Gauge theories quantized in the Landau gauge are characterized by a remarkable property, which may be stated in words as the nonrenormalization of the insertions depending on the ghost field c not differentiated. This property is expressed by the "antighost equation" [18] which, in the present case reads

$$\bar{\mathcal{G}}S := \int d^3x \left(-i\frac{\delta}{\delta c} + \left[\bar{c}, \frac{\delta}{\delta B} \right] \right) S = \Delta_{\text{class}}^{\mathcal{G}} := \int d^3x \left([\rho^\mu, A_\mu] - [\sigma, c] \right) , \tag{6.1}$$

where the breaking $\Delta_{\text{class}}^{\mathcal{G}}$, like the one of the supersymmetry Ward identity, is linear in the quantum fields, hence not subject to renormalization. For the perturbation Δ defined in Subsect. , this leads to the further constraint

$$\int d^3x \frac{\delta}{\delta c} \Delta = 0 . \tag{6.2}$$

Now. it is visible that (5.10) violates this latter constraint. and thus must be discarded. As a final result, taking into account all the constraints dictated by the initial theory on the perturbation Δ leads to the solution

$$\Delta = 0 . \tag{6.3}$$

6.2. Counterterms Induced by the Radiative Corrections

Up to now, we have spoken only of the classical theory, and more specifically of its stability. The outcome is that the classical theory is not only stable: its parameters themselves are completely fixed.

Going to the quantum theory, in the perturbative framework, requires the investigation of two points.

1) Absence of anomalies

One has to check the validity to all orders of the Slavnov-Taylor identity (2.17), of the supersymmetry Ward identities (4.4), and as well of the constraints given by the gauge condition. the ghost equation and the antighost equation. In other words one has to check that all these identities do not suffer from anomalies. It has actually been verified [9, 13. 2] that algebraic consistency forbids the appearance of such anomalies.

2) Absence of counterterms

One has to check the stability of the theory upon the radiative corrections: these corrections must be interpretable at each order as a renormalization of the parameters of the theory. For this one has to study all possible counterterms to the action. The counterterms are of course constrained by the symmetries and identities imposed to the Green functions. It is a very general feature of renormalization theory [2] that these constraints on the counterterms are identical to the constraints on the perturbation of the classical action we have already spoken about. We can therefore retain our previous result (6.4). This simply means the absence of any free counterterm – hence of

any free parameter once those of the classical theory have been fixed. The usual interpretation in the framework of a renormalization via a cut-off procedure is the ultraviolet finiteness of the theory. One can however offer a more physical interpretation [13], namely that the quantum theory keeps intact the *scale invariance* of the original classical theory.

7. Conclusion

The role of vector supersymmetry, as we have seen, is twofold.

Its first role is to realize explicitly Sorella's decomposition of the external derivative (5.8), thus providing the operator ∇ for the construction of solutions to the descent equations.

The second aspect of this supersymmetry is its role in the cancellation mechanism of the ultraviolet divergences. In fact, as we have seen in the Chern-Simons example, supersymmetry alone is not sufficient. The special coupling of the ghost c as expressed by the "antighost equation" (6.2) is also needed. One actually observes a "conspiration" between both conditions: supersymmetry selects the unique element (5.10) among the whole family of BRS invariant counterterms, and it is just this element which is killed by the the condition (6.3) following from the antighost equation.

Many of the results shown here for the three-dimensional Chern-Simons theory have been generalized to a whole class of topological theories. including the BF models [19, 20, 21, 22], the bosonic string [23, 24], four-dimensional topological Yang-Mills theory [25, 26], etc.

References

[1] D. Birmingham, M. Blau, M. Rakowski and G. Thompson, *Phys. Rep.* 209 (1991) 129;

[2] O. Piguet and S.P. Sorella, *Algebraic Renormalization*, submitted to "Lecture Notes in Physics" (Springer);

[3] A.S. Schwarz, Baku International Topological Conference. Abstracts, vol. 2, p. 345, (1987);

[4] E. Witten, *Commun. Math. Phys.* 121 (1989) 351;

[5] G. Moore and N. Seiberg, *Phys. Lett.* B220 (1989) 422;

[6] A. Blasi and R. Collina, *Int. J. Mod. Phys.* 7 (1992) 3083;
    Phys. Lett. B243 (1990) 99;

[7] S. Emery and O. Piguet, *Helv. Phys. Acta* 64 (1991) 1256;

[8] C. Lucchesi and O. Piguet, *Nucl. Phys.* B381 (1992) 281;

[9] A. Blasi and R. Collina, *Nucl. Phys.* B345 (1990) 472;

[10] J. Dixon, "Cohomology and renormalization of gauge theories", I, II, III, *unpublished preprints, 1976-1977;*
    J. Dixon, *Commun. Math. Phys.* 139 (1991) 495;

[11] M. Dubois-Violette, M. Henneaux, M. Talon and C.-M. Viallet,
    Phys. Lett. B289 (1992) 361;

[12] F. Brandt, N. Dragon and M. Kreuzer,
    Phys. Lett. B231 (1989) 263; *Nucl. Phys.* B332 (1990) 224, 250;
    F. Brandt, PhD Thesis (in German), *University of Hanover (1991), unpublished;*

[13] F. Delduc, C. Lucchesi, O. Piguet and S.P. Sorella, *Nucl. Phys.* B346 (1990) 313;

[14] A. Brandhuber, M. Langer, O. Piguet, M. Schweda and S.P. Sorella,
    Phys. Lett. B300 (1993) 92;

[15] A. Brandhuber, M. Langer, S. Emery, O. Piguet, M. Schweda and S.P. Sorella,
    Helv. Phys. Acta 66 (1993) 551;

[16] S. Emery and O. Piguet, *Helv. Phys. Acta* 67 (1994) 22;

[17] S.P. Sorella, *Commun. Math. Phys.* 157 (1993) 231;

[18] A.Blasi, O. Piguet, S.P. Sorella, *Nucl. Phys.* B356 (1991) 154:

[19] M. Abud, J.-P. Ader and L. Cappiello, *Nuovo Cimento* 105A (1992) 1507:

[20] J.C. Wallet, *Phys. Lett.* B235 (1990) 71:

[21] N. Maggiore and S. P. Sorella, *Nucl. Phys.* B377 (1992) 236:
N. Maggiore and S. P. Sorella, *Int. J. Mod. Phys.* A8 (1993) 929:

[22] C. Lucchesi, O. Piguet and S. P. Sorella, *Nucl. Phys.* B395 (1993) 325:

[23] L. Baulieu, C. Becchi and R. Stora, *Phys. Lett.* B180 (1986) 55:
L. Baulieu and M. Bellon, *Phys. Lett.* B196 (1987) 142:

[24] C. Becchi, *Nucl. Phys.* B304 (1988) 513:

[25] M. Werneck de Oliveira, *Phys. Lett.* B307 (1993) 347;

[26] A. Brandhuber, O. Moritsch, M. Werneck de Oliveira, O. Piguet and M. Schweda, *Nucl. Phys.* B431 (1994) 173:

Theory of Brain Function, Quantum Mechanics and Superstrings

D. V. Nanopoulos*

Center for Theoretical Physics, Department of Physics

Texas A&M University, College Station, TX 77843-4242, USA:

and

Astroparticle Physics Group, Houston Advanced Research Center (HARC),

The Mitchell Campus, The Woodlands, TX 77381, USA:

and

CERN Theory Division, 1211 Geneva 23, Switzerland

Recent developments/efforts to understand aspects of the brain function at the *sub-neural* level are discussed. MicroTubules (MTs), protein polymers constructing the cytoskeleton, participate in a wide variety of dynamical processes in the cell. Of special interest to us is the MTs participation in bioinformation processes such as *learning* and *memory*, by possessing a well-known binary error-correcting code $[K_1(13,2^6,5)]$ with 64 words. In fact, MTs and DNA/RNA are *unique* cell structures that possess a code system. It seems that the MTs' code system is strongly related to a kind of *"Mental Code"* in the following sense. The MTs' periodic paracrystalline structure make them able to support a *superposition* of coherent quantum states, as it has been recently conjectured by Hameroff and Penrose, representing an *external* or *mental order*, for sufficient time needed for *efficient* quantum computing. Then the quantum superposition collapses spontaneously/dynamically through a new, string-derived mechanism for collapse proposed recently by Ellis, Mavromatos, and myself. At the moment of collapse, organized *quantum exocytosis* occurs, *i.e.*, the simultaneous emission of neurotransmitter molecules by the synaptic vesicles, embedded in the "firing zone" of the presynaptic vesicular grids. Since in the superposition of the quantum states only those participate that are *related* to the "initial signal", when collapse occurs, it only enhances the probability for "firing" of the *relevant* neurotransmitter molecules. That is how a *"mental order"* may be translated into a *"physiological action"*. Our equation for quantum collapse, tailored to the MT system, predicts that it takes 10,000 neurons $\mathcal{O}(1 \text{ sec})$ to dynamically collapse, in other words to process and imprint information. Different observations/experiments and various schools of thought are in agreement with the above numbers concerning *"conscious events"*. If indeed MTs, with their fine structure, vulnerable to our quantum collapse mechanism may be considered as the *microsites of consciousness*, then several, unexplained (at least to my knowledge) by traditional neuroscience, properties of consciousness/awareness, get easily explained, including *"backward masking"*, *"referal backwards in time"*, etc. Furthermore, it is amusing to notice that the famous puzzle of why the left (right) part of the brain coordinates the right (left) part of the body, *i.e.*, the signals travel maximal distance, is easily explained in our picture. In order to have timely quantum collapse we need to excite as much relevant material as possible, thus signals have to travel the maximal possible distance. The *non-locality* in the cerebral cortex of neurons related to particular missions, and the related *unitary sense of self* as well as *non-deterministic free will* are consequences of the basic principles of quantum mechanics, in sharp contrast to the "sticks and balls" classical approach of conventional neural networks. The proposed approach clearly belongs to the *reductionist* school since quantum physics is an integrated part of our physical world. It is highly amazing that string black-hole dynamics that have led us to contemplate some modifications of standard quantum mechanics, such that the quantum collapse becomes a detailed dynamical mechanism instead of being an "external" ad-hoc process, may find some application to some quantum aspects of brain function. It looks like a big-universality principle is at work here, because both in the black hole and the brain we are struggling with the way information is processed, imprinted, and retrieved.

"...the Astonishing Hypothesis - that each of us is the behavior of a vast, interacting set of neurons."

Francis Crick in
The Astonishing Hypothesis

"...what will they think? - What I tell them to think."

Orson Welles in
Citizen Kane

Prooimion

Theory of brain function, quantum mechanics, and superstrings are three fascinating topics, which at first look bear little, if any at all, relation to each other. Trying to put them together in a cohesive way, as described in this task, becomes a most demanding challenge and unique experience. The main thrust of the present work is to put forward a, maybe, foolhardy attempt at developing a new, general, but hopefully scientifically sound framework of Brain Dynamics, based upon some recent developments, both in (sub)neural science and in (non)critical string theory. I do understand that Microtubules [1, 2] are not considered by all neuroscientists. to put it politely, as the microsites of consciousnes, as has been recently conjectured by Hameroff and Penrose [3, 4]. Also, I do know that, the *one interpretation* of non-critical string theory, put forward by Ellis, Mavromatos, and myself [5, 6], which has led to *not* just an incremental change. but a total rethinking of the Quantum Mechanics *doctrine(s)* from the ground up, is not universally, to put it mildly, accepted. Leaving that aside, and time will tell, the emerging big picture *"when microtubules meet density matrix mechanics"*, as the reader hopefully will be able to judge for her(him)self, is rather astonishing. It looks like the modified quantum dynamics [5, 6] of microtubules [1, 2] may indeed lead [3, 4] to a rather concise, experimentally verifiable (presently and in the immediate future) theory of brain function [7]. Since this is a rather vast, multidisciplinary, and multidimensional subject, I kept in mind that *potential* readers may include (high-energy) physicists, biologists, biochemists, neuroscientists, medical doctors, including psychiatrists, psychologists, and psychotherapists, etc. Thus, I have tried my best to obey the *"technical minimality"* principle, and at the same time, to make it as self-contained and informative, as possible, by not assuming that psychoanalysts know about *"quantum coherence"*. or formal string theorists know about the Freudian *"unconscious proper"*, even if, in the latter case, they believe that *they know everything, and so why bother?!*

A concrete, technically elaborated proposal materializing some of the general ideas that I have tried to put forward here, has been worked out by Mavromatos and myself [7], work that I strongly encourage the interested reader to consult. I am fully aware of the rather speculative nature of the ideas presented here *and* of the sometimes circumstantial looking experimental evidence used to support them. Nevertheless, the way that different structures/mechanisms, from completely disconnected fields of knowledge, *fit and bind* together to produce such a *coherent*, dynamical scheme of the Brain function, makes it very hard to ignore the whole thing, by just believing that it is all coincidental, and nothing more than a grand illusion! It goes without saying that the responsibility for all views expressed here is completely mine.

1   Introduction

The brain is our most valuable asset. The workings of the brain enable us to *think*, a fundamental function that, among other things, make us aware of our own existence or self-aware: *cogito, ergo sum.* Our perceptions of the universe, concerning its physical structure, form and function according to the universal physical laws, emerge from processed-in-the-brain representations of, hopefully, objective physical reality. Understanding the way that the brain functions is the primordial prerequisite for a complete physical understanding of the dynamic universe that

---

*E-mail: dimitri@phys.tamu.edu or nanopoud@cernvm.cern.ch

we are part of. Undoubtedly, the brain is a very complicated system and thus to understand its function we need a coordinated effort involving several, if not all, branches of natural sciences: biology, neuroscience, biochemistry, physics, information theory/computer science, medicine, pharmacology, etc. We may eventually need some well-organized excursions to the realms of the science of mental life or psychology, for some extra help. Alas. the compartmentalization of science in our epoch, the highly technical jargon used in every field today, and the endemic narrow mindness, expressed best by the dictum *scientific conformity means intellectual stultification*, make the study of brain function a titanic struggle. Nevertheless, we ought to try to figure out, as explicitly as possible, as detailed as possible, and as predictive as possible, what are the most fundamental brain constituents and how they interact, so that they eventually produce this miracle that is called brain function, or put it differently, what makes the brain *tick!* This kind of *reductionist* approach has turned out to be very successful in the past, both in biology and in physics. The discovery of the double-helical structure of DNA, its identification with the gene, and the subsequent breaking of the genetic code, three bases for one aminoacid, in biology, as well as the discovery of electroweak unification and its subsequent spontaneous breaking that led to the Standard Model of the strong and electroweak interactions, in particle physics, are glowing examples of applied reductionism. In the case of the brain function, things are a bit more complicated and delicate extra care is needed, because the *mind* pops into the picture and thus the workings of the associated *Mental World* have to be addressed one way or another!

There are two extremes in handling the mental world problem:

* *Strong Artificial Intelligence* (SAI). purporting that the brain is just a computer and the only thing we have to figure out is the algorithm.

* *Cartesian or dualistic view*, assuming that brain and mind are *two distinct entities*, in interaction with each other.

$$
\begin{array}{ccc}
\text{Brain} & \overline{} & \text{Mind} \\
\cap & \overrightarrow{} & \cap \\
\text{(Attainable physical world)} & & \text{(Mental world)} \\
||| & & ||| \\
W_1 & & W_2
\end{array}
\qquad (1)
$$

where the mental world contains perceptions, ideas, memories, feelings, acts of volition, etc. I believe that both the above extremes are needlessly exaggerated. Instead I would like to propose here a new *unified approach* in which there is an "effective" mental world *emerging* from the physical world, but with distinct qualities

$$
\begin{array}{ccccccc}
W & \supset & W_1 & \otimes & W_2 & \longrightarrow & W_1 \\
||| & & & & \updownarrow & \uparrow & \\
\text{physical world} & & & & \text{causes} & \text{``collapse''} &
\end{array}
\qquad (2)
$$

Hard-core *materialists* are very welcome to be W_2-*world* "*blind*" and just concentrate on the transition $W \longrightarrow W_1$. in a kind of "just the facts ma'am" attitude! The present approach combines two new ideas/mechanisms developed recently, one in biology/neuroscience and one in superstring theory:

i. It has been suggested by Hameroff (for some time now) [1] that *MicroTubules* (MT), cytosceletal protein polymer paracrystalline structures within the neurons [1, 2], may be the fundamental units or microsites where most of the brain function originates. Furthermore, Hameroff and Penrose argued very recently [3, 4] that quantum effects may play a central role in the MT functioning and they were *desperately* looking for an explicit "*collapse of the wavefunction*" mechanism, that would validate their claims.

ii. It has been suggested by Ellis, Mavromatos and myself that, in *one interpretation* of non-critical string theory, one gets naturally modifications of Quantum Mechanics, leading among other things to a new explicit *"collapse of the wavefunction"* mechanism and *a microscopic arrow of time* [5, 6].

The present proposal is to combine (i) and (ii).

It is remarkable that the string-derived collapse of the wavefunction mechanism fits "hand-in-glove" to the MT hypothesis. Thus, by complementing (i) with (ii), a rather detailed and spelled out scenario of brain function *emerges*. Namely, because the stringy collapse of the wavefunction is due to the truncation of the unattainable global degrees of freedom, the scheme depicted as Eq. (2) naturally emerges. W_2 should be identified with the physical "global state space" *isomorphic* to the "effective" mental world in the following sense: the *collapse of the wavefunction* is what causes the system to "decide" its course of action, thus being completely identifiable with the Jamesian[1] view of *consciousness*, as a *selecting agency*. The W_2 global states are the agents of collapse!

In this approach, the "collapse of the wavefunction" will result in well-coordinated, organized *exocytosis*, *i.e.*, the *simultaneous* emission of neurotransmitter molecules by the synaptic vesicles, embedded in the "firing zone" of the presynaptic vesicular grids [9]. From then on, standard neurophysiology applies. *e.g.*, setting the motor in action, etc. Clearly, the strong correlation between the "effective" mental world and the "collapse of the wavefunction" (through the "global state space") makes it clear how a mental intention (*e.g.*, I wish to bend my index finger) is *physically* and *causally* related to the motor action (*e.g.*, bending my index finger). Eventually, we may even be able to develop a *"mental code"*, *i.e.*, a dictionary that would translate feelings, intentions, etc directly into specific neurochemical states charting out detailed neurotransmitter molecule topologies. Actually, even if this statement sounds extremely far-fetched speculation and off-the-wall, the *universality* of the "effective" mental world for all humans, with of course all its diversity, cries out for an objective mapping between mental and specific neurochemical processes. A good analogy here is the *"genetic code"*, a well-tabulated dictionary between "base" sequencing in DNA and aminoacid, thus protein, production on the ribosomes [10]. Proteins, of course, are our basic building blocks that are responsible for the way we look, move, etc.

In section 2, I will discuss *Brain Mechanics*, *i.e.*, some very general arguments of what the brain is supposed to do and how it does it, while in section 3, I will present some elements of *Quantum Mechanics*, useful in our subsequent discussions. Section 4 provides a view of some *Brain morphology and modeling*, based upon classical notions and some criticism and problems they are facing. Section 5 provides some elements of *string*-derived *density matrix mechanics*, an extension of orthodox Quantum Mechanics, while sections 6 and 7 discuss the *biochemical* and *physical profile* of *Microtubules* (MT) respectively, and their potentially important role in brain function. Section 8 shows how *microtubule* dynamics, in a stringy-derived *density matrix mechanics* framework, may yield a *unified model* of Brain and Mind, a *quantum theory of brain function*, while the final Section 9 covers the emerging *quantum psychophysics*.

2 Brain Mechanics

The brain is a rather complicated physical system in constant interaction with the external world or environment. Very generically and in *grosso modo* the brain functions as follows:

---

[1] William James (1842-1910), the father of American (physiological) psychology, observed that consciousness is not a thing or a substance, but rather a *process* [8].

(i) Imagine that the brain is in some state $|A\rangle$, when some *external stimulus* is applied, for some given period of time, then

(ii) after the removal of the external stimulus, the brain is in some state $|B\rangle$, which in principle should have in some way *coded* (or recorded) the "message" that was carried by the external stimulus, in such a way that

(iii) "later" it is possible to *retrieve* (or recall) the message directly from the state $|B\rangle$, keeping in mind that

(iv) it is possible that the brain has not necessarily gone directly from $|A\rangle$ to $|B\rangle$, but many intermediate steps may have occurred: $|A\rangle \rightarrow |A_1\rangle \rightarrow |A_2\rangle \rightarrow \cdots \rightarrow |B\rangle$, i.e., the *information* (or message) has been *processed* in the brain before it was recorded.

There are some fundamental properties that characterize successful brain function, namely: *long-term stability* and *non-locality*, as strongly suggested by the plethora of experimental data. While the need for long-term stability is rather obvious, non-locality, i.e., coherent neuronic activity at spatially remote cortical locations, makes the classical treatment of the brain function rather questionable. At the same time, non-locality is strongly suggestive of *quantum treatment* [11, 12, 13]. Since we are concerned here clearly with macroscopic states, and at the same time we need to invoke quantum treatment, we have to look at the so-called *Macroscopic Quantum States* (MQS), which are abundant in the quantum world. Superconductivity, superfluidity, magnetization, etc are typical examples of MQS with very specific characteristics:

(i) For special "structures" and "conditions",

(ii) a critical degree of coherence may be achieved that leads to an

(iii) *ordered state*, that is highly stable.

Consider for example *Magnetization*: the special "structures" are the *Weiss regions*, small regions in a ferromagnet within which all electron spins are polarized in a specific direction. Though, because there are many small regions and polarizations, on the average there is no magnetization visible in the ferromagnet. If we now apply a sufficiently strong magnetic field $\vec{B}$ or we decrease sufficiently the temperature (below the P. Curie point), i.e., the special "conditions", the ferromagnet exhibits magnetization because now all electron spins in the whole *macroscopic* crystal, are polarized in the same direction, strongly correlated with each other, thus leading to a highly stable *macroscopic coherent* (or quantum) *state*, the *ordered state*.

In a more physical language, the transition from an unordered state (e.g., many Weiss-regions) to an ordered state (e.g., magnetization) is called a phase transition. The value(s) of the crucial parameter(s) (e.g., the magnetic field $\vec{B}$ or temperature T) at the transition point characterize the phase transition and define the *critical point* (e.g., Curie temperature). It should be apparent that an ordered state contains some *information* (e.g., all electron spins polarized in the same direction) than the unordered state (electron spins randomly polarized). On the other hand, the unordered state is more *symmetric* (randomly distributed electron spins are rotationally invariant, i.e., there is no *preferred direction*), while the ordered state exhibits less symmetry (polarized electron spins have chosen spontaneously a specific direction, thus breaking the rotational symmetry). Thus, ordered states are the net result of *spontaneous symmetry breaking* that triggers the phase transition. There are certain characteristics of phase transitions very useful for our subsequent discussions

(i) *Universality*: many, qualitatively and quantitatively different, systems can be described by the same phase transition.

(ii) *Attractor*: by varying suitably the system parameters, they can be brought close to their *critical values*, so as to cause a phase transition. It is not necessary to be infinitesimally close to the critical point. The critical point acts as an *attractor* for anything in its environment. In other words, we don't really need a *fine-tuning* of our system parameters to reach an ordered state.

(iii) *Evolution equations*: All the basic properties of phase transitions (including (i) and (ii) above) can be encoded in a set of evolution equations called renormalization group equations (RGEs). They describe deviations (and approach) from (to) criticality, as well as other characteristics of phase transitions [14].

Macroscopic coherent (or quantum) states, or ordered states have some highly exclusive characteristics:

(i) *Long-range/term stability*: highly stable, long-range correlations between the fundamental elements are maintained by wave-like, self-propagating excitation loops (*e.g.*: phonons, spin-waves, magnons, etc.) that *Regulate* the behavior of the "other" fundamental elements and *Feedback* to the original fundamental element that caused the "disturbance". I will call this the $R+F$ property of MQS.

(ii) *Non-locality*: clearly MQS, as its very nature indicates may go beyond microscopic locality.

(iii) *Emergence*: MQS have *new properties* that are *not* present at the fundamental elements level. The new properties characterize states at a *hierarchical level above* the level where the fundamental interactions among the fundamental constituents apply. For example, superconductivity is a new property/phenomenon, *i.e.*, emerging from a *collective treatment* of electrons under special circumstances, while of course each electron follows at the fundamental level the laws of quantum electrodynamics.

Let us use now the physical language of MQS and phase transitions to describe *by analogy*, for the time being, the basic functions of the Brain:

(I) *Uncoded Brain*: random signals, unattended perception are some of the characteristics of this case. It corresponds to the random polarizations in the many, small Weiss regions of the ferromagnet.

(II) *Learning*: An *external stimulus* is applied, say for a few seconds, that "straightens out" or "puts an order" to the random neuronic signals so that they are able to represent some *coherent piece* of information. It corresponds, in the case of the ferromagnet, to applying for some time an external magnetic field $\vec{B}$ or lowering the temperature below the Curie point. They cause the *breaking* of the multi-domain small structures with their random polarizations,and thus they lead to the ordered state, where all electron spins, throughout the whole ferromagnet. are strongly correlated to all point in the *same direction*. We are talking about a phase transition or, in the spirit of the previous discussion, a spontaneous breaking of some symmetry. Clearly. it depends on the nature of the external stimulus with which specific fundamental elements will interact and set them "straight". so that a corresponding MQS, or ordered state, is created. Realistically, in order to be able to *encode* all qualitatively different signals and create a coherent *unitary sense of self*, a tremendous number of qualitatively different ordered states is needed, *i.e.*, practically an infinite number of qualitatively different spontaneously broken symmetries. Furthermore, these symmetries should be accompanied by a set of *selection rules*, thus providing a physical *filter* against undesirable, irrelevant "stray" signals. A very tall order indeed,

if one recalls the fact that, until now, the only "known" (observable) spontaneously broken symmetry, at the fundamental level, is the one describing the electroweak interactions. Just *one*, which is kind of short with respect to the desirable *infinity* of spontaneously broken symmetries! We will see later how string theory takes care of this problem.

(III) *Coded Brain* or *Memory*: the resulting, highly stable, coherent "*firing*" of a bunch of involved neurons, not necessarily localized, corresponding, in the case of the ferromagnet, to the stability and macroscopic nature (including non-locality) of the *emerging* magnetization (*ordered*) state. Such a kind of naturally organized, coherent neuron firing, not necessarily localized, may provide the solution to the so-called "binding problem". More later.

(IV) *Recall Process*: In this picture, a *replication weak* signal, *sufficiently* resembling the *learning* signal, may excite momentarily the ordered state, but, thanks to its R+F property, it will relax back to its previous form. It is this, ordered-state—excitation—ordered-state process that make us aware of recalling something, i.e., we "feel" it! It corresponds in the case of the ferromagnet, to apply a *weak* magnetic field $\vec{B}'$, not necessarily exactly parallel to the original $\vec{B}$, which will force the electron spins to oscillate, *momentarily*, before they relax back to their equilibrium, i.e., we recover the ordered state, thanks of course to the R+F property of MQS. It should be stressed that it is not necessary for the replication signal to be exactly identical to the learning signal in order to recall full information, thanks to the *attractor* property of the phase transitions, discussed above. In phase-transition language, the recall memory process corresponds to the act of an *irrelevant operator*. It should not escape our attention that the endemic, in the framework of phase transitions, R+F and *attractor* properties fascilitate tremendously the retrieving of information, without the need of *complete* identity of the replication and learning signal. Otherwise, it would take extraneous *fine-tuning*, which here translates to very long time periods, in order to retrieve information. Imagine what would happen if we need to see all the details of a fast approaching, hungry lion, including say the length and shape of its claws, before we run up a tree! Not very practical indeed.

The above presented generic picture for the brain function may sound plausible and promising. But, is there any "*experimental*" evidence for its support? The answer is *yes*. The main observational tool is the ElectroEncephaloGram (EEG). It is usually assumed that the EEG waveforms emerge from the summation of local neuron firings, but things are a bit more complicated. One would expect that *asynchronous* firing of randomly distributed neurons would produce a zero net effect on the scalp electrodes. By studying electric potentials evoked during sensory stimulation and during learning trials, E. R. John has been able to show that these evoked potentials arise from the firing of large and disperse neural groups and that they are radically different from those obtained by the spontaneous random cortical activity [15]. *Temporal rearrangement* within the neural groups characterizes the externally evoked potentials. Furthermore, Sayers et. al.[16], presented independent evidence strengthening the temporal rearrangement case, by studying EEG *phase coherence*. Frequency components of the EEG spectrum obtained during spontaneous cortical activity show a random configuration of phase relations, which shifts to a distinct pattern of *phase coherence* immediately following sensory stimulation. Amazingly enough, imposing the *phase characteristics* of the evoked potential on the spontaneous waveform, we can reproduce the characteristic shape of the observed evoked waveform [16]. These findings support E. R. John's [15] case for temporal rearrangement, while at the same time it falsifies the kind of classical expectation that the EEG arises from the summation of

neural firings, which would imply that just the *amplitude characteristics* is the only difference between spontaneous and evoked waveforms. Clearly, it seems that the external stimulus does not just add energy to the brain, but it organizes it in a *coherent way*, in a similar fashion that an external field $\vec{B}$ acts on a ferromagnet! It seems that the analogy between brain function and critical phenomena dynamics may be quite useful and fruitful.

In the *unified approach* suggested here (see Eq. (2)) the "effective" mental world (W_2) is *actively* interacting with the emerging MQS, and thus through the R+F property of the MQS *and* the subsequent triggering by W_2 of the collapse of the MQS, it provides the solution to the age-old problem of how intentional/emotional acts are strongly correlated to body acts, as explained in the Introduction. It should be stressed that *emergence* here has a multi-valued meaning: it encompasses the natural (Darwinian [17]) evolution and selection, the development of brain in specific subjects and eventually the "conscious" moment under consideration.

3   Quantum Mechanics

The physical principles that govern the microworld, as provided by Quantum Mechanics (QM), are *profoundly* different from the ones that the macrocosmos obeys. The "microworld" here denotes anything at and below the molecular level: molecules, atoms, electrons, nuclei, protons, neutrons, quarks. As Linus Pauling taught us, chemistry is nothing else but applied quantum mechanics at the atomic and molecular level. Interestingly enough, Molecular Biology holds a very intriguing position between the macro and micro worlds in the following sense: *ab initio*, Molecular Biology is concerned with the structure and function of the cell [10], which is mainly composed of *macromolecular structures* (DNA, RNA, proteins, ...) and as such, *most of the time* and for many purposes, are sufficiently and accurately described by classical physics. Nevertheless, we should not be carried away and discard QM from the picture by interpreting *most of the times* as implying *at all times!* After all, as Watson and Crick [18] taught us, the double helical structure of DNA, which is the source of DNA's fundamental genetic properties is due to the quantum mechanical H-bonds between purines (A,G) and pyrimidines (T,C): always a double H-bond for A=T and a triple H-bond for G $\equiv$ C. It is in the *stability* and *universality* of these H-bonds, as verified experimentally by Chargaff [19], that the secret of the genetic code lies! Since my central thesis here, as emphasized earlier, is that quantum mechanics plays *also* a very fundamental role in the emergence of the mental world from the physical world, *i.e.*, in the brain-mind relation, I will discuss very briefly some elements of QM, that I will need later.

The central dogma of Quantum Mechanics is the *particle-wave duality*: it depends on the particular circumstances if a *quantum state* is going to express itself as a particle or as a wave [20]. Consider for example a particle travelling in spacetime. Its quantum state is described by a *wavefunction* $\Psi(\vec{x},t)$ obeying a Schrödinger-type equation of the form

$$i\hbar\frac{\partial\Psi}{\partial t} = H\Psi \tag{3}$$

where $\hbar$ ($\equiv 1$ in natural units) is the Planck constant, and H is a system-dependent operator, called the *Hamiltonian* of the system. It provides the *unitary, time-evolution* of the system, and with eigenvalues identifiable with the different energy levels of the system. A fundamental, and *immensely crucial* for us here, property of the quantum equation (3) is its *linearity*. Imagine that $\Psi_1,\Psi_2,\ldots,\Psi_n$ are different solutions of (3), then clearly the *linear superposition*

$$\Psi = \sum_{i=1}^{n} c_i(t)\Psi_i . \tag{4}$$

with c_i arbitrary complex numbers, is also a solution of (3). This is the mathematical statement of *Quantum Superposition*. Let us discuss next its physical meaning. Suppose that we would like to describe quantum mechanically the following "history" of a particle, say an electron: it starts at some initial point around $(\vec{x}_0, t_0)$, it *goes through* a wall that contains n slits, say $1, 2, \ldots, n$, *without us knowing which specific one*, and it ends up at some final point around $(\vec{x}_f, t_f)$. Let $\Psi_1, \Psi_2, \ldots, \Psi_n$ denote the wavefunctions of the electron, referring to the case that the electron went through the slit $1, 2, \ldots, n$, respectively. Since we don't know the specific slit that the electron went through, we are *obliged* to take as the wavefunction of the electron, a linear superposition of $\Psi_1, \Psi_2, \ldots, \Psi_n$, i.e., (4). The physical meaning then of the c_i's becomes clear: $|c_i|^2$ is the *probability* that the electron went through the slit i, and thus c_i is referred to as the *the probability amplitude*. Notice that conservation of probability entails that at any time t

$$\sum_{i=1}^{n} |c_i(t)|^2 = 1 \tag{5}$$

The *probability density* to find the electron at some specific point $(\vec{x}_a, t_a)$, after it has passed through the slits and before it ends up at $(\vec{x}_f, t_f)$ is given by

$$|\Psi(\vec{x}_a, t_a)|^2 = |\sum_{i=1}^{n} c_i \Psi_i|^2 . \tag{6}$$

Clearly, this is a standard *wave-like behavior* and (4) may be interpreted as describing a quantum state evolving in a *coherent way*, or obeying the fundamental quantum mechanical principle of *quantum coherence*, the physical meaning of *linear superposition*. Imagine now, that we would like to find out through which specific slit the electron went through. Then, we have to make a "*measurement*" or "*observation*", i.e., to concentrate on those aspects of the quantum system that can be *simultaneously magnified* to the classical level, and from which the system must then choose. In other words, we have to *disturb* the system (electron in our example) with the *magnifying device*, which results in *de-coherence*, thus (6) is replaced by

$$|\Psi(\vec{x}_a, t_a)|^2 \quad \overset{\text{``measurement''}}{\underset{\text{``collapse''}}{\longmapsto}} \quad \sum_{i=1}^{n} |c_i|^2 |\Psi_i|^2 \tag{7}$$

In other words, we get classical probabilities, highly reminiscent of a standard *particle-like behavior*. The "measurement"/"observation" process has caused decoherence of the wavefunction and thus led to its *collapse* to a *specific state*. Here are then, in a nutshell, our basic quantum mechanical rules, that constitute *quantum reality*:

(i) A quantum system can, in principle, be in many states *simultaneously* $(\Psi_1, \Psi_2, \ldots, \Psi_n)$ and its quantum state $\Psi = \sum_{i=1}^{n} c_i \Psi_i$, a *pure state*, evolves *coherently* and according to the quantum equation (3), *as long as* we don't *disturb* it. This is *quantum linear superposition* or *quantum parallelism*, leading to wave-like behavior.

(ii) A "measurement"/"observation" forces the quantum state Ψ to *decide* what it wants to be, with probability $|c_i|^2$ that the Ψ quantum state will turn out to be the i-th state (described by Ψ_i), *after* the "measurement"/"observation". This is the "*collapse of the wavefunction*", leading to classical particle-like behavior.

Incidentally, the famous Heisenberg *uncertainty principle* [21] is nothing else but a quantitative expression of our intuitive statement above that a "measurement"/"observation" disturbs the system in an *uncontrollable way*, entailing always uncertainties in the outcome, *e.g.*,

$$\Delta x \cdot \Delta p \geq \hbar . \tag{8}$$

Clearly. (8) indicates the fact that it is impossible to "measure" *simultaneously*, at a desirable level, both the position and the momentum of a particle. Notice that this is a *fundamental principle*, and has nothing to do with the potentially difficult and practical problems that face experimentalists. Whatever she does, she cannot beat the uncertainty principle.

The endemic. in the Quantum World, wave-particle duality is responsible for the necessity of the two-step approach to quantum dynamics discussed above. This kind of approach is very different from the deterministic approach of classical dynamics and, in a way, it creates a *schism* in our understanding of the Universe. There is the classical world and there is the quantum world, each following its own laws which. frankly, do not seem to have much common ground. It may even, sometimes, lead to some embarrassments [12]. like *e.g.*, the *Schrödinger's cat* paradox. a peculiar situation where a quantum event may oblige us to treat a cat as 50% alive and 50% dead! Furthermore. in the passage from the quantum to the classical world it is not clear at all who is there to decide that we crossed the quantum-classical border!

This *dualistic* view of the world (classical versus quantum) is reminiscent of the ancient needs for heavenly-terrestial dynamics, abolished by Galileo and Newton for universal dynamics. or for space and time dynamics. abolished by Einstein for spacetime dynamics, or for electromagnetic and weak interactions, abolished recently for electroweak interactions. It looks to me that this classical versus quantum dualistic view of the world *cries out*, once more, for a *unified approach* which for many practical purposes would *effectively* look like two separate worlds (classical and quantum). Any resemblance with the unified approach I discussed in the Introduction for the brain versus mind problem is *not* accidental! A *unified approach* for classical *and* quantum dynamics will be attempted in section 5, but let me prepare the ground here by generalizing a bit the notion of quantum state and the likes. What we are really after is some kind of formalism that enables us to express. at least in principle, the two-step process of quantum dynamics in a more uniform language. Let us represent a given quantum state α by a state vector $|\alpha\rangle$, while $\langle\alpha|$ denotes the complex conjugate state vector α^*, and let us assume that this state vector has "length" one: $\langle\alpha|\alpha\rangle = 1$. Consider now a complete set of orthonormal state vectors $|i\rangle$: $\langle j|i\rangle = \delta_{ij}$, implying that any *pure state* can be written as $|\Psi^a\rangle = \sum_i c_i^a |i\rangle$, with c_i complex numbers obeying the conservation of probability condition $\sum_i |c_i|^2 = 1$ (see (4),(5)). Then the *scalar product* $\langle\Psi^b|\Psi^a\rangle = \sum_i c_i^{*b} c_i^a$ expresses the *probability amplitude* that starting with the state vector $|\Psi^a\rangle$ we end up in the state $|\Psi^b\rangle$. Actually, we can consider all the tensor products $|\Psi^k\rangle\langle\Psi^l|$ with the understanding that $\langle\Psi^l|\Psi^k\rangle = \text{Tr}(|\Psi^k\rangle\langle\Psi^l|) = \sum_i c_i^{l*} c_i^k$. It is very convenient to introduce the notion of the *density matrix* $\rho \equiv |\Psi\rangle\langle\Psi|$ with matrix elements $\rho_{ij} = c_i c_j^* |i\rangle\langle j|$ and such that $\text{Tr}\rho = \text{Tr}(|\Psi\rangle\langle\Psi|) = \langle\Psi|\Psi\rangle = \sum_i c_i c_i^* = 1$. *i.e.*, the conservation of probability condition. Notice that, in the case of a *pure state*, the description of a quantum system by the state vector $|\Psi\rangle$ or by the density matrix ρ is *equivalent*. For example. the measurable quantities $\langle\Psi|A|\Psi\rangle$ correspond to $\text{Tr}(\rho A)$. with A denoting the quantum operator representing the "measurable quantity". etc. The quantum equation (3) becomes in the density matrix approach

$$\dot{\rho} \equiv \frac{\partial\rho}{\partial t} = \frac{i}{\hbar}[\rho, H].$$ (9)

which is nothing else but the *quantum analogue* of the classical statistical mechanics *Liouville equation*, describing the time evolution of the phase-space density function. The great advantage of the density matrix approach is its ability to describe not only *pure states*, but also *mixed states*. Imagine that for *practical reasons* it is impossible to know the exact *pure state* of our quantum system. *i.e.*. we only know that we have a combination of different *pure states* $|\alpha\rangle = \sum_i c_i^\alpha |i\rangle$, $\alpha = 1, 2, \ldots$, each with *classical probability* p_i. Clearly, in this case we cannot use the

quantum equations (3) or (9) because it is only applied for *single* pure states, but we can still use the density matrix approach. Write the density matrix of the system as a *mixed state*

$$\rho = \sum_a p_a |a\rangle \langle a| \ . \tag{10}$$

then the probability that a "measurement"/"observation" will find our system in some pure state $|\Psi\rangle = \sum_i d_i |i\rangle$ is given by

$$P_\Psi = \mathrm{Tr}(\rho |\Psi\rangle \langle \Psi|) = \sum_a p_a |\langle \Psi|a\rangle|^2 \ , \tag{11}$$

which is a sum of products of classical and quantum probabilities! Notice that in the case of a single *pure state*, say $|b\rangle$, all $p_{a\neq b} = 0$ and $p_b = 1$ in (10), and a "measurement"/"observation" causes the "collapse of the wavefunction" $|b\rangle$, that implies turning a *pure state* $\rho = |b\rangle \langle b|$ into a *mixed state* $\rho = \sum_i |c_i^b|^2 |i\rangle \langle i|$, which is nothing else but (7)! Of course, in the case of a "measurement"/"observation" we *open* the system under consideration, and clearly (9) needs modification, *i.e.*, addition of extra terms that represent the "disturbances". On the other hand, since the "collapse of the wavefunction" implies loss of quantum coherence, there is no way to use a wave equation like (3), or possible modifications, to represent the "disturbances". The notion of description of a quantum state by state vectors or wavefunctions really gives in to the density matrix approach, thus the correct approach for a *unification* of classical and quantum dynamics. Usually, when we deal with realistic quantum systems, composed of different independent or loosely interacting parts, it helps to express the quantum state of the system as the product of different independent components. Imagine, for example, a particle called π^0 decaying into two photons γ_1 and γ_2. Since π^0 has no spin, the most general description of the system of two photons is given by

$$|\Psi\rangle = c_1 |\gamma_1\rangle_+ |\gamma_2\rangle_- + c_2 |\gamma_1\rangle_- |\gamma_2\rangle_+ \ , \tag{12}$$

where the subscripts indicate the polarizations of the two photons, always opposite, such that the whole system has angular momentum zero, corresponding to the spinless π^0. Imagine that a "measurement"/"observation" is done on the system by measuring say the polarization of γ_2 and found to correspond to the $-$ one. After the "measurement"/"observation" we know that $c_1 = 1$ and $c_2 = 0$, thus without "measuring" the polarization of γ_1, we know it is the $+$ one. Einstein found it very disturbing, that some "measurement" on one part of the system has an "instantaneous" effect on some other *distant* part. Sometimes this is referred to as the *Einstein-Podolsky-Rosen* (EPR) puzzle [22, 12], and it is a very clear proof of the *non-local* nature of the quantum world! Experiments done in the mid-80's have confirmed [23], beyond any shadow of doubt, the *non-local nature* of quantum mechanics, and the failure of classical spacetime notions to describe quantum reality.

The Macroscopic Quantum States (MQS), mentioned in section 2, correspond here to something like

$$|\Psi\rangle = \sum_i c_i |1\rangle_i |2\rangle_i \cdots |N\rangle_i \ . \tag{13}$$

where $|k\rangle_i$ refers to the quantum state of the k-th fundamental constituent in the i-th macroscopic quantum state. Of course, for a MQS N is $\mathcal{O}(N_{\mathrm{Avogadro}} \approx 6 \times 10^{23})$, a rather larger number and in several occasions the index i can also run into large numbers. For example, in the case of a ferromagnet, the *ordered state* would be described by (13), and if $|k\rangle_i$ indicates the spin polarization of the k-th electron, then *only* one $c_i \neq 0$. While in the case of *quasicrystals*, describable also by (13), not only is N large $(\mathcal{O}(N_{\mathrm{Avogadro}}))$, but *also* the linear combinations may involve a huge number of *alternatives*, *i.e.*, the i-index can be also large. *Quasicrystals* are rather intriguing

physical structures that may need quantum mechanics in an essential way for their understanding. According to Penrose [12], the quasicrystal assembly cannot be reasonably achieved by the local adding of atoms one at a time, in accordance with the *classical* picture of crystal growth, but instead there must be a non-local essentially quantum mechanical ingredient to their assembly. Instead of having atoms coming individually and attaching themselves at a continually moving growth line (standard classical crystal growth), one must consider using something like (13), an evolving quantum linear superposition of many different alternative arrangements of attaching atoms. There is not one *single* thing that happens, many alternative atomic arrangements must coexist! Some of these linearly superposed alternatives will grow to very large conglomerates, and at certain point the "collapse of the wavefunction" will occur and thus more specific arrangements will be singled out, and so on, until a good-sized quasicrystal is formed. But why is Nature employing such an intriguing mechanism? Penrose claims [12] that maybe "energetics" is the answer. Usually, crystalline configurations are configurations of *lowest energy*, and the correct arrangement of atoms can be discovered simply by adding one atom at a time, and solving its own minimizing problem, etc. In quasicrystal growth, finding the lowest energy state is a very complicated and difficult problem, because it involves a large number of atoms *at once*, and thus, we have a *global, non-local* problem to solve. Clearly, a quantum mechanical description, a la (13), seems appropriate where many different combined arrangements of atoms are being "tried" simultaneously, and eventually collapsing, through physical environment tangling, to the "energetically" and "enviromentally" appropriate arrangements, the *observable* quasicrystal.

It should be stressed that the QM rules have been in place and in successful use for about 70 years now, and have led to a most deep understanding of the microworld. Nevertheless, the fundamental mechanism triggering the "collapse of the wavefunction" has escaped us, until I believe recently, when string theory enabled us to put a definite proposal on the table, to be discussed in section 5. Intriguingly enough, Molecular Biology and Neurobiology in particular, lies just in the classical-quantum interface and thus very interesting phenomena may occur. So, let us turn our attention now to the detailed structure of the brain.

4 Brain Morphology and Modeling

The human brain is the most complicated object, as far as we know, in the Universe. At a first look, it is amazing that this seemingly amorphous mass is capable of executing all these miraculous operations that control our actions and make us aware of the world around. A closer look though points to a rather recursively hierarchical structure and a very elaborate organization [24, 12]. An average brain weighs about 1.3 kg, and it is made of: $\sim 77\%$ water, $\sim 10\%$ protein, $\sim 10\%$ fat, $\sim 1\%$ carbohydrates, $\sim 0.01\%$ DNA/RNA, and the rest other stuff. The largest part of the human brain, the *cerebrum*, is found on the top and is divided down the middle into left and right cerebral hemispheres, and front and back into *frontal, parietal, temporal*, and *occipital lobes*. Further down, and at the back lies a rather smaller, spherical portion of the brain, the *cerebellum*, and deep inside lie a number of complicated structures like the thalamus, hypothalamus, hippocampus, etc. It seems that what make humans more advanced than other animals is not only the largeness of the cerebrum, but also its proportion of brain as a whole, the largest in the animal kingdom!

Both the cerebrum and the cerebellum have comparatively thin outer surface layers of grey matter and larger inner regions of white matter. The grey regions constitute what is known as the *cerebral cortex* and the *cerebellar cortex*. It is in the grey matter where various kinds of computational tasks seem to be performed, while the white matter consists of long nerve fibers (axons) carrying signals from one part of the brain to another. It is the *cerebral*

cortex that is central to the higher brain functions, speech, thought, complex movement patterns, etc. On the other hand, the *cerebellum* seems to be more of an "automaton". It has to do more with precise coordination and control of the body, and with skills that have become "second nature". Cerebellum actions seem almost to take place by themselves, without thinking about them. They are very similar to the unconscious reflex actions, *e.g.*, reaction to pinching, which may not be mediated by the brain, but by the upper part of the spinal column. Thus, it seems highly likely that the phenomena of consciousness, that we are mainly concerned here, have much more to do with the cerebrum than with the cerebellum or the spinal cord. So, from now on, we will concentrate on the cerebral cortex.

Various parts of the cerebral cortex are associated with very specific functions. We distinguish several regions. The *visual cortex*, a region in the occipital lobe at the back of the brain, is responsible for the reception and interpretation of vision. The *auditory cortex*, in the temporal lobe, deals mainly with analysis of sound, while the *olfactory cortex*, in the frontal lobe, deals with smell. The *somatosensory cortex*, just *behind* the division between frontal and parietal lobes, has to do with the sensations of touch. There is a very specific mapping between the various parts of the surface of the body and the regions of the somatosensory cortex. In addition, just in *front* of the division between the frontal and parietal lobes, in the frontal lobe, there is the *motor cortex*. The *motor cortex* activates the movement of different parts of the body and, again here, there is a very specific mapping between the various muscles of the body and the regions of the motor cortex. All the above mentioned regions of the cerebral cortex are referred to as *primary*, since they are the one most directlt concerned with the input and output of the brain. Near to these primary regions are the *secondary* sensory regions of the cerebral cortex, where information is processed, while in the *secondary motor* regions, conceived plans of motion get translated into specific directions for actual muscle movement by the primary motor cortex. But the most abstract and sophisticated activity of the brain is carried out in the remaining regions of the cerebral cortex, the *association cortex*. It is right here that information from various different sensory regions is analyzed in a rather complex way, memories are laid down, pictures of the outside world are constructed, general plans are conceived, etc. This is the anatomic, morphological structure of the brain, on which my observations of section 2 were based on! There is a rather well-known and extremely curious phenomenon that I call *X-ism*. It is the *right* (*left*) cerebral hemisphere which is concerned *exclusively* with the *left* (*right*) hand side of the body, so that virtually all nerves must *cross over* from one side to the other as they enter or leave the cerebrum! Furthermore, as I mentioned above, the vision cortex is right at the back, while the eyes are at the front, the feet-related region of the somatosensory cortex is at the top, whereas the feet are at the bottom, and the left (right) auditory cortex is related to the right (left) ear! It seems that the cerebral neurosignals prefer to follow the longest possible path, and since this X-ism is not observed in the cerebellum, whose action appears to be completely unconscious, it is not inconceivable that the emergence of consciousness is facilitated by the cerebral X-ism. In our unified scheme, such a strange correlation between consciousness and X-ism seems to be born out of the dynamics.

Let us now continue our fascinating trip inside the brain, and let us concentrate on its basic building blocks, the nerve cells or neurons. Among the about 200 types of different basic types of human cells, the neuron is one of the most specialized, exotic and remarkably versatile cell. The neuron is highly unusual in three respects: its *variation in shape*, its *electrochemical function*, and its *connectivity*, *i.e.*, its ability to link up with other neurons in networks. Let us start with a few elements of neuron microanatomy [24, 12]. There is a central starlike bulb, called the *soma*, which contains the nucleus of the cell. A long nerve fibre, known as the *axon*, stretches out from one end

of the soma. Its length, in humans, can reach up to *few cm*, surprisingly long for a single cell! The raison d'etre of the axon is to transmitt the neuron's output signal, *i.e.*, it acts like a wire. The axon has the ability of multiple bifurcation, branching out into many smaller nerve fibers, and the very end of which there is always a *synoptic knob*. At the other end of the soma and often springing off in all directions from it, are the tree-like *dendrites*, along which input data are carried into the soma. The whole nerve cell, as basic unit, has a cell membrane surrounding soma, axon. synoptic knobs, dendrites. Signals pass from one neuron to another at junctions known as *synapses*. where a synaptic knob of one neuron is attached to another neuron's soma or dendrites. There is very narrow gap. of a few nm, between the synaptic knob and the soma/dendrite to where the *synaptic cleft* is attached. The signal from one neuron to another has to propagate across this gap. The workings of the nerve signals are another wonder of Nature!

A nerve fiber is a cylindrical tube containing a mixed solution of NaCl and KCl, mainly the second, so there are Na^+, K^+. and Cl^- ions within the tube. Outside the tube the same type of ions are present but with more Na^+ than K^+. In the *resting* state there is an excess of Cl^- over Na^+ and K^+ inside the tube. giving it a negative charge. while it has positive charge outside. A nerve signal is nothing else but a region of *charge reversal* travelling along the fiber. At its head, *sodium gates* open to allow the sodium to flow inwards and at its tail *potassium gates* open to allow potassium to flow outwards. Then. metabolic pumps act to restore order and establish the *resting state*, preparing the nerve fiber for another signal. Amazingly enough, there is no major material (ion) transport that produces the signal, just in and out local movements of ions, across the cell membranes. *i.e.*, a *small* and *local* depolarization of the cell! Eventually, the nerve signal reaches the attached synaptic knob, at the very end of the nerve fiber, and triggers it to emit chemical substances, known as *neurotransmitters*. It is these substances that travel across the synaptic cleft to another neuron's soma or dendrite. It should be stressed that the signal here is not electrical, but a chemical one. What really is happening is that when the nerve signal reaches the synaptic knob, the local depolarization cause little bags immersed in the *vesicular grid*, the *vesicles* containing molecules of the neurotransmitter chemical (*e.g.*, acetylcholine) to release their contents from the neuron into the synaptic cleft. the phenomenon of *exocytosis*. These molecules then diffuse across the cleft to interact with *receptor proteins* on receiving neurons. On receiving a neurotransmitter molecule, the receptor protein opens a gate that causes a local depolarization of the receiver neuron. The nerve signal has been transmitted!

It depends on the nature of the synaptic knob and of the specific synaptic junction, if the next neuron would be encouraged to *fire*. *i.e.*. to start a new signal along its own axon, or it would be discouraged to do so. In the former case we are talking about *excitory synapses*, while in the latter case about *inhibitory synapses*. At any given moment, one has to add up the effect of all excitory synapses and subtract the effect of all the inhibitory ones. If the net effect corresponds to a positive electrical potential difference between the inside and the outside of the neuron under consideration, *and* if it is bigger than a critical value, then the neuron *fires*. otherwise it stays mute.

For our concerns here, the fundamental dynamical process of neural communication can be summarized in the following three steps:

1. The neural axon is an *all* or *none* state. In the *all* state a signal, called a *spike* or *action potential* (AP). propagates indicating that the summation performed in the soma produced an amplitude of the order of tens of mV. In the *none* state there is no signal travelling in the axon, only the resting potential (~ -70mV). It is essential to notice that the presence of a travelling signal in the axon, *blocks* the possibility of transmission of a second signal.

2. The nerve signal, upon arriving at the ending of the axon, triggers the emission of neurotransmitters in the synaptic cleft, which in turn cause the receptors to open up and allow the penetration of ionic current into the *post synaptic* neuron. The *efficacy* of the synapse is a parameter specified by the amount of penetrating current per presynaptic spike.

3. The post synaptic potential (PSP) diffuses toward the soma, where all inputs in a short period, from all the presynaptic neurons connected to the postsynaptic are summed up. The amplitue of individual PSP's is about 1 mV, thus quite a number of inputs is required to reach the "firing" threshold, of tens of mV. Otherwise the postsynaptic neuron remains in the *resting* or *none* state.

The cycle-time of a neuron, *i.e.*, the time from the emission of a spike in the presynaptic neuron to the emission of a spike in the postsynaptic neuron is of the order of *1-2 msecs*. There is also some recovery time for the neuron. after it *"fired"*, of about *1-2 msecs*, independently of how large the amplitude of the depolarizing potential would be. This period is called the *absolute refractory period* of the neuron. Clearly, it sets an upper bound on the spike frequency of 500-1000/sec. In the types of neurons that we will be interested in, the spike frequency is considerably lower than the above upper bound, typically in the range of 100/sec, or even smaller in some areas, at about 50/sec. It should be noticed that this rather exotic neural communication mechanism works very efficiently and it is employed *universally*, both by vertebrates and invertebrates. The vertebrates have gone even further in perfection, by protecting their nerve fibers by an *insulating coating* of *myelin*, a white fatty substance, which incidentally gives the *white matter* of the brain, discussed above, its color. Because of this insulation, the nerve signals may travel undisturbed at about 120 meters/second, a rather high speed!

A very important and significant anatomical fact for our discussion, is that each neuron receives some 10^4 synaptic inputs from the axons of other neurons, usually one input per presynaptic neuron, and that each branching neural axon forms about the same number ($\sim 10^4$) of synaptic contacts on other, postsynaptic neurons. A closer look at our cortex then would expose a mosaic-type structure of assemblies of a few thousand densely connected neurons. These assemblies are taken to be the basic cortical processing *modules*, and their size is about $1(\text{nm})^2$. The neural connectivity gets much sparcer as we move to larger scales and with much less feedback, allowing thus for autonomous local collective, parallel processing and more serial and integrative processing of local collective outcomes. Taking into account that there are about 10^{11} nerve cells in the brain (about 7×10^{10} in the cerebrum and 3×10^{10} in the cerebellum), we are talking about 10^{15} synapses! Counting one synapse per second, you will find yourself counting past 30 million years after you started! Undoubtedly, the brain is very special, and it should not be unreasonable to expect it to give rise to mental properties [25].

While the dynamical process of neural communication suggests that the brain action looks a lot like a computer action, there are some fundamental differences having to do with a basic brain property called *brain plasticity*. The interconnections between neurons are not fixed, as is the case in a computer-like model, but are changing all the time. Here I am referring to the synaptic junctions where the communication between different neurons actually takes place. The synaptic junctions occur at places where there are *dendritic spines* of suitable form such that contact with the synaptic knobs can be made. Under certain conditions these dendritic spines can shrink away and break contact, or they can grow and make new contact, thus determining the *efficacy* of the synaptic junction. Actually, it seems that it is through these dendritic spine changes, in synaptic connections, that long-term memories are laid down, by providing the means of storing the necessary information. A supporting indication of such a conjecture is the fact that such dendritic spine changes occur within *seconds*. which is also how long it takes

for permanent memories to be laid down [12].

Furthermore, a very useful set of phenomenological rules has been put forward by Hebb [26], the *Hebb rules*, concerning the underlying mechanism of brain plasticity. According to Hebb, a synapse between neuron 1 and neuron 2 would be strengthened whenever the firing of neuron 1 is followed by the firing of neuron 2, and weakened whenever it is not. A rather suggestive mechanism that sets the ground for the emergence of some form of *learning!* It seems that *brain plasticity* is not just an incidental complication, it is a *fundamental property* of the activity of the brain. Brain plasticity and its time duration (few *seconds*) play a critical role, as we will see later, in the present unified approach to the brain and the mind.

Many mathematical models have been proposed to try to simulate "learning", based upon the close resemblance of the dynamics of neural communication to computers and implementing, one way or another, the essence of the Hebb rules. These models are known as *Neural Networks* (NN) [27].

Let us try to construct a neural network model for a set of N interconnected neurons. The activity of the neurons is usually parametrized by N functions $\sigma_i(t)$, $i = 1, 2, \ldots, N$. and the synaptic strength, representing the synaptic efficacy, by $N \times N$ functions $j_{i,k}(t)$. The total stimulus of the network on a given neuron (i) is assumed to be given simply by the sum of the stimuli coming from each neuron

$$S_i(t) = \sum_{k=1}^{N} j_{i,k}(t)\sigma_k(t) \tag{14}$$

where we have identified the individual stimuli with the product of the synaptic strength ($j_{i,k}$) with the activity (σ_k) of the neuron producing the individual stimulus. The dynamic equations for the neuron are supposed to be, in the simplest case

$$\frac{d\sigma_i}{dt} = F(\sigma_i, S_i) \tag{15}$$

with F a non-linear function of its arguments. The dynamic equations controlling the time evolution of the synaptic strengths $j_{i,k}(t)$ are much more involved and only partially understood, and usually it is *assumed* that the j-dynamics is such that it produces the synaptic couplings that we need or postulate! The simplest version of a neural network model is the Hopfield model [28]. In this model the neuron activities are conveniently and conventionally taken to be "*switch*"-like, namely ± 1, and the time t is also an integer-valued quantity. Of course, this *all*(+1) or *none*(−1) neural activity σ_i is based on the neurophysiology discussed above. If you are disturbed by the ± 1 choice instead of the usual "binary" one ($b_i = 1$ or 0), replace σ_i by $2b_i - 1$. The choice ± 1 is more natural from a physicist's point of view corresponding to a two-state system, like the fundamental elements of the ferromagnet, discussed in section 2, *i.e.*, the electrons with their spins up (+) or (−).

The increase of time t by one unit corresponds to one step for the dynamics of the neuron activities obtainable by applying (for all i) the rule

$$\sigma_i(t + \frac{i+1}{N}) = \text{sign}(S_i(t + i/N)) \tag{16}$$

which provides a rather explicit form for (15). If, as suggested by the Hebb rules, the j matrix is *symmetric* ($j_{i,k} = j_{k,i}$), the Hopfield dynamics [28] corresponds to a sequential algorithm for looking for the minimum of the Hamiltonian

$$H = -\sum_i S_i(t)\sigma_i(t) = -\sum_{i,k=1}^{N} j_{i,k}\sigma_i(t)\sigma_k(t) \tag{17}$$

Amazingly enough the Hopfield model, at this stage, is very similar to the dynamics of a statistical mechanics *Ising-type* [14], or more generally a *spin-glass*, model [29]! This *mapping* of the Hopfield model to a spin-glass

model is highly advantageous because we have now a justification for using the statistical mechanics language of phase transitions, like critical points or attractors, etc, to describe neural dynamics and thus brain dynamics, as was envisaged in section 2. It is remarkable that this simplified Hopfield model has many *attractors*, corresponding to many different *equilibrium* or *ordered* states, endemic in spin-glass models, and an unavoidable prerequisite for successful storage, in the brain, of many different patterns of activities. In the neural network framework, it is believed that an internal representation (*i.e.*, a pattern of neural activities) is associated with each object or category that we are capable of recognizing and remembering. According to neurophysiology, discussed above, it is also believed that an object is memorized by suitably changing the synaptic strengths. *Associative memory* then is produced in this scheme as follows (see corresponding (I)-(IV) steps in section 2): An external stimulus, suitably involved, produces synaptic strengths such that a specific learned pattern $\sigma_i(0) = P_i$ is "printed" in such a way that the neuron activities $\sigma_i(t) \sim P_i$ (II *learning*), meaning that the σ_i will remain for all times close to P_i, corresponding to a stable attractor point (III *coded brain*). Furthermore, if a *replication signal* is applied, pushing the neurons to σ_i values *partially* different from P_i, the neurons should evolve toward the P_i. In other words, the memory is able to retrieve the information on the whole object, from the knowledge of a part of it, or even in the presence of wrong information (IV *recall process*). Of course, if the external stimulus is very different from any preexisting $\sigma_i = P_i$ pattern, it may either create a new pattern, *i.e.*, create a new attractor point, or it may reach a chaotic, random behavior (I *uncoded brain*).

Despite the remarkable progress that has been made during the last few years in understanding brain function using the neural network paradigm, it is fair to say that neural networks are rather artificial and a very long way from providing a realistic model of brain function. It seems likely that the mechanisms controlling the changes in synaptic connections are much more complicated and involved than the ones considered in NN, as utilizing cytoskeletal restructuring of the sub-synaptic regions. *Brain plasticity* seems to play an essential, central role in the workings of the brain! Furthermore, the "*binding problem*", alluded to in section 2, *i.e.*, how to *bind* together all the neurons firing to different features of the same object or category, *especially* when more than one object is perceived during a *single* conscious perceptual moment, seems to remain unanswered.

We have come a long way since the times of the "*grandmother neuron*", where a *single* brain location was invoked for self observation and control, indentified with the pineal glands by Descartes [30]! Eventually, this localized concept was promoted to *homunculus*, a little fellow inside the brain which observes, controls and represents us! The days of this "*Cartesian comedia d'arte*" within the brain are gone forever!

It has been long suggested that different groups of neurons, responding to a common object/category, fire *synchronously*, implying *temporal correlations* [31]. If true, such correlated firing of neurons may help us in resolving the binding problem [32]. Actually, brain waves recorded from the scalp, *i.e.*, the EEGs, suggest the existence of some sort of *rhythms*, *e.g.*, the "*α-rhythms*" of a frequency of 10 Hz. More recently, oscillations were clearly observed in the visual cortex. Rapid oscillations, above EEG frequencies in the range of 35 to 75 Hz, called the "*γ*-*oscillations*" or the "*40 Hz oscillations*", have been detected in the cat's visual cortex [33, 34]. Furthermore, it has been shown that these oscillatory responses can become *synchronized* in a stimulus-dependent manner! Amazingly enough, studies of auditory-evoked responses in humans have shown inhibition of the 40 Hz coherence with *loss of consciousness* due to the induction of general anesthesia [35]! These remarkable and striking results have prompted Crick and Koch to suggest that this *synchronized* firing on, or near, the beat of a "*γ-oscillation*" (in the 35–75 Hz range) might be the *neural correlate* of *visual awareness* [36, 32]. Such a behavior would be, of course, a very

special case of a much more general framework where coherent firing of *widely-distributed* (*i.e.*, *non-local*) groups of neurons, in the "beats" of x-oscillation (of specific frequency ranges), *bind* them together in a mental representation, expressing the *oneness* of *consciousness* or *unitary sense of self*. While this is a remarkable and bold suggestion [36, 32], it is should be stressed that in a physicist's language it corresponds to a phenomenological explanation, not providing the underlying physical mechanism, based on neuron dynamics, that triggers the synchronized neuron firing. On the other hand, the Crick-Koch proposal [36, 32] is very suggestive and in compliance with the general framework I developed in the earlier sections, where macroscopic *coherent* quantum states play an essential role in awareness, and especially with respect to the *"binding problem"*. We have, by now, enough motivation from our somehow detailed study of brain morphology and modeling, to go back to quantum mechanics and develop a bit further, using string theory, so that to be applicable to brain dynamics.

5 Stringy Quantum Mechanics: Density Matrix Mechanics

Quantum Field Theory (QFT) is the fundamental dynamical framework for a successful description of the microworld, from molecules to quarks and leptons and their interactions. The *Standard Model* of elementary particle physics, encompassing the strong and electroweak interactions of quarks and leptons, the most fundamental point-like constituents of matter presently known, is fully and wholy based on QFT [37]. Nevertheless, when gravitational interactions are included at the quantum level, the whole construction collapses! Uncontrollable infinities appear all over the place, thus rendering the theory inconsistent. This a well-known and grave problem, being with us for a long, long time now. The resistance of gravitational interactions to conventionally unify with the other (strong and electroweak) interactions strongly suggests that we are in for changes both at the QFT front and at the gravitational front, so that these two frameworks could become eventually compatible with each other. As usual in science, puzzles, paradoxes and impasses, that may lead to major crises, bring with them the seeds of dramatic and radical changes, if the crisis is looked upon as an opportunity. In our case at hand, since the Standard Model, based upon standard QFT, works extremely well, we had not been forced to scrutinize further the basic principles of the orthodox, Copenhagen-like QFT. Indeed, the mysterious "collapse" of the wavefunction, as discussed in section 3, remained always lacking a dynamical mechanism responsible for its triggering. Had gravity been incorporated in this conventional unification scheme, and since it is the *last known* interaction, any motivation for changing the ground rules of QFT, so that a dynamical mechanism triggering the "collapse" of the wavefunction would be provided, would be looked upon rather suspiciously and unwarranted. Usually, to extremely good approximation, one can neglect gravitational interaction effects, so that the standard QFT applies. Once more, *usually* should not be interpreted as *always*. Indeed, for most applications of QFT in particle physics, one assumes that we live in a *fixed, static, smooth* spacetime manifold, *e.g.*, a Lorentz spacetime manifold characterized by a Minkowski metric ($g_{\mu\nu}$ denotes the metric tensor):

$$ds^2 \equiv g_{\mu\nu}dx^\mu dx^\nu = c^2 dt^2 - d\vec{x}^2 \tag{18}$$

satisfying Einstein's special relativity principle. In such a case, standard QFT rules apply and we get the miraculously successful Standard Model of particle physics. Unfortunately, this is not the whole story. We don't live exactly in a *fixed, static, smooth* spacetime manifold. Rather, the universe is *expanding*, thus it is not *static*, and furthermore unavoidable *quantum fluctuations* of the metric tensor $g_{\mu\nu}(x)$ defy the *fixed* and *smooth* description of the spacetime manifold, at *least* at very short distances. Very short distances here do not refer to the nucleus, or even the proton radius, of 10^{-13}cm, but to distances comparable to the Planck length, $\ell_{Pl} \sim 10^{-33}$cm, which in

turn is related to the smallness of G_N, Newton's gravitational constant! In particle physics we find it convenient to work in a system of units where $c = \hbar = k_B = 1$, where c is the speed of light, $\hbar$ is the Planck constant, and k_B is the Boltzman constant. Using such a system of units one can write

$$G_N \equiv \frac{1}{M_{Pl}^2} \equiv \ell_{Pl}^2 \tag{19}$$

with $M_{Pl} \sim 10^{19}\,\text{GeV}$ and $\ell_{Pl} \sim 10^{-33}\text{cm}$.

It should be clear that as we reach very short distances of $\mathcal{O}(\ell_{Pl})$, fluctuations of the metric $\delta g_{\mu\nu}(x)/g_{\mu\nu}(x) \sim (\ell_{Pl}/\ell)^2 \sim \mathcal{O}(1)$, and thus the spacetime manifold is not well defined anymore, and it may even be that the very notion of a spacetime description evaporates at such Planckian distances! So, it becomes apparent that if we would like to include quantum gravity as an item in our unification program checklist, we should prepare ourselves for major revamping of our conventional ideas about quantum dynamics and the structure of spacetime.

A particularly interesting, well-motivated, and well-studied example of a *singular* spacetime background is that of a *black hole* (BH) [38]. These objects are the source of a singularly strong gravitational field, so that if any other poor objects (including light) cross their "horizon", they are *trapped* and would never come out of it again. Once in, there is no way out! Consider, for example, a quantum system consisting of two particles a and b in lose interaction with each other, so that we can describe its quantum *pure* state by $|\Psi\rangle = |a\rangle |b\rangle$. Imagine now, that at some stage of its evolution the quantum system gets close to a black hole, and that for some unfortunate reason particle b decides to enter the BH horizon. From then on, we have no means of knowing or determining the exact quantum state of the b particle, thus we have to describe our system not anymore as a *pure* state $|\Psi\rangle$, but as a *mixed* state $\rho = \sum_i |b_i|^2 |a\rangle \langle b_i|$, according to our discussion in section 3 (see (10,11)). But such an evolution of a *pure state* into a *mixed state* is not *possible* within the conventional framework of quantum mechanics as represented by (3) or (9). In conventional QM *purity* is eternal. So, something drastic should occur in order to be able to accomodate such circumstances related to singularly strong gravitational fields. Actually, there is much more than meets the eye. If we consider that our pure state of the two particles $|\Psi\rangle = |a\rangle |b\rangle$ is a quantum fluctuation of the vacuum, then we are in more trouble. The vacuum always creates particle-antiparticle pairs that almost momentarily, and in the absence of strong gravitational fields, annihilate back to the vacuum, a rather standard well-understood quantum process. In the presence of a black hole, there is a very strong gravitational force that may lure away one of the two particles and "trap" it inside the BH horizon, leaving the other particle hanging around and looking for its partner. Eventually it wanders away from the BH and it may even be detected by an experimentalist at a safe distance from the BH. Because she does not know or care about details of the vacuum, she takes it that the BH is decaying by emitting all these particles that she detects. In other words, while *classical* BH is supposed to be stable, in the presence of quantum matter, BH do decay, or more correctly *radiate*, and this is the famous *Hawking radiation* [38, 39]. The unfortunate thing is that the Hawking radiation is *thermal*, and this means that we have lost vast amounts of *information* dragged into the BH. A BH of mass M_{BH} is characterized by a *temperature* T_{BH}, an *entropy* S_{BH} and a *horizon radius* R_{BH} [38, 39, 40]

$$T_{BH} \sim \frac{1}{M_{BH}}; \quad S_{BH} \sim M_{BH}^2; \quad R_{BH} \sim M_{BH} \tag{20}$$

satisfying, of course, the first thermodynamic law, $dM_{BH} = T_{BH}dS_{BH}$. The origin of the huge entropy ($\sim M_{BH}^2$) should be clarified. Statistical physics teaches us that the *entropy* of a system is a measure of the information *unavailable to us* about the detailed structure of the system. The entropy is given by the number of different

possible configurations of the fundamental constituents of the system, resulting always in the same values for the macroscopic quantities characterizing the system, e.g., temperature, pressure, magnetization, etc. Clearly, the fewer the macroscopic quantities characterizing the system, the larger the entropy and thus the larger the lack of information about the system. In our BH paradigm, the macroscopic quantities that characterize the BH, according to (20), is *only* it mass M_{BH}. In more complicated BHs, they may posses some extra "*observables*" like electric charge or angular momentum, but still, it is a rather small set of "observables"! This fact is expressed as the "*No-Hair Theorem*" [38], i.e., there are not many different long range interactions around, like gravity or electromagnetism, and thus we cannot "measure" safely and from a distance other "observables", beyond the mass (M), angular momentum ($\vec{L}$), and electric charge (Q). In such a case, it becomes apparent that we may have a huge number of different configurations that are all characterized by the same $M, Q, \vec{L}$, and this the huge entropy (20). Hawking realized immediately that his BH dynamics and quantum mechanics were not looking eye to eye, and he proposed in 1982 that we should generalize quantum mechanics to include the *pure state* to *mixed state* transition, which is equivalent to *abandoning* the quantum superposition principle (as expressed in (3) or (9)), for some more advanced quantum dynamics [41]. In such a case we should virtually abandon the description of quantum states by wavefunctions or state vectors $|\Psi\rangle$ and use the more accomodating density matrix (ρ) description, as discussed in section 3, *but* with a *modified* form for (9). Indeed, in 1983 Ellis, Hagelin, Srednicki, and myself proposed (EHNS in the following) [42] the following modified form of the conventional Eq. (9)

$$\frac{\partial\rho}{\partial t} = i[\rho, H] + \delta\!\!\!/H\rho \tag{21}$$

which accomodates the *pure state—mixed state* transition through the extra term $(\delta\!\!\!/H)\rho$. The existence of such an extra term is characteristic of "*open*" quantum systems, and it has been used in the past for *practical reasons*. What EHNS suggested was more radical. We suggested that the existence of the extra term $(\delta\!\!\!/H)\rho$ is *not due* to *practical reasons* but to some fundamental, dynamical reasons having to do with quantum gravity. Universal quantum fluctuations of the gravitational field ($g_{\mu\nu}$) at Planckian distances ($\ell_{Pl} \sim 10^{-33}$cm) create a very *dissipative* and *fluctuating* quantum vacuum, termed *spacetime foam*, which includes virtual Planckian-size black holes. Thus, quantum systems *never* evolve undisturbed, even in the *quantum vacuum*, but they are continously interacting with the spacetime foam, that plays the role of the *environment*, and which "opens" spontaneously and dynamically *any* quantum system. Clearly, the extra term $(\delta\!\!\!/H)\rho$ leads to a *spontaneous dynamical decoherence* that enables the system to make a transition from a pure to a mixed state accomodating Hawking's proposal [41]. Naive approximate calculations indicate that $\langle\delta\!\!\!/H\rangle \sim E^2/M_{Pl}$, where E is the energy of the system, suggesting straight away that our "low-energy" world ($E/M_{Pl} \leq 10^{-16}$) of quarks, leptons, photons, etc is, for most cases, extremely accurately described by the conventional Eq. (9). Of course, in such cases is not offensive to talk about wavefunctions, quantum parallelism, and the likes. On the other hand, as observed in 1989 by Ellis, Mohanty, and myself [43], if we try to put together more and more particles, we eventually come to a point where the decoherence term $(\delta\!\!\!/H)\rho$ is substantial and decoherence is almost instantaneous, leading in other words to an instantaneous *collapse* of the wavefunction for large bodies, thus making the transition from quantum to classical *dynamical* and not by decree! In a way, the Hawking proposal [41], while leading to a major conflict between the standard QM and gravity, motivated us [42, 43] to rethink about the "collapse" of the wavefunction, and it seemed to contain the seeds of a dynamical mechanism for the "collapse" of the wavefunction. Of course, the reason that many people gave a "cold shoulder" to the Hawking proposal was the fact that his treatment of quantum gravity was semiclassical, and thus it could be that all the Hawking excitement was nothing else but an artifact of the bad/crude/unjustifiable

approximations. Thus. before we proceed further we need to treat better Quantum Gravity (QG). String Theory (ST) does just that. It provided the *first*, and presently *only* known framework for a consistently quantized theory of gravity [44].

As its name indicates, in string theory one replaces *point like* particles by *one-dimensional, extended, closed, string* like objects, of characteristic length $\mathcal{O}(\ell_{Pl}) \sim 10^{-33}$cm. In ST one gets an *automatic, natural* unification of *all* interactions *including* quantum gravity, which has been the *holy grail* for particle physics/physicists for the last 70 years! It is thus only natural to address the hot issues of black hole dynamics in the ST framework [44]. Indeed. in 1991, together with Ellis and Mavromatos (EMN in the following) we started a rather elaborate program of BH studies. and eventually, we succeeded in developing a new dynamical theory of string black holes [45]. One *first* observes that in ST there is an *infinity* of particles of different masses, including the *Standard Model* ones, corresponding to the different excitation modes of the string. Most of these particles are unobservable at low energies since they are very massive $M \gtrsim \mathcal{O}(M_{Pl} \sim 10^{19} \text{ GeV})$ and thus they cannot be produced in present or future accelerators, which may reach by the year 2005 about 10^4 GeV. Among the *infinity* of different types of particles available, there is an *infinity* of massive "gauge-boson"-like particles, generalizations of the W-boson mediating the weak interactions, thus indicating the *existence* of an *infinity* of *spontaneously broken gauge symmetries,* each one characterized by a specific *charge,* generically called Q_i. It should be stressed that, even if these stringy type. spontaneously broken gauge symmetries do not lead to long-range forces, thus *classically* their Q_i charges are unobservable at long distances, they do become observable at long distances at the *quantum level.* Utilizing the quantum Bohm-Aharonov effect [46]. where one "measures" phase shifts proportional to Q_i. we are able to "measure" the Q_i charges from adesirable distance! This kind of Q_i charge. if available on a black hole, is called sometimes and for obvious reasons, *quantum hair* [47]. From the infinity of stringy symmetries, a relevant for us here. specific, *closed subset* has been identified, known by the name of $W_{1+\infty}$ *symmetry*, with many interesting properties [48]. Namely, these $W_{1+\infty}$ symmetries cause the mixing [49], in the presence of singular spacetime backgrounds like a BH. between the massless string modes, containing the *attainable localizable low energy world* (quarks. leptons. photons, etc), let me call if the W_1-*world, and* the massive ($\geq \mathcal{O}(M_{Pl})$) string modes of a very characteristic type, the so-called *global states.* They are called *global states* because they have the peculiar and unusual characteristic to have *fixed* energy E and momentum $\vec{p}$, and thus. by employing the uncertainty type relations, a la (8), they are extended over *all* space and time! Clearly, while the *global states* are as *physical* and as *real* as any other states. still they are *unattainable* for *direct observation* to a *local observer.* They make themselves noticeable through their *indirect* effects. while interacting with, or agitating, the W_1 *world.* Let me call the global state space, the W_2-*world.*

The *second* step in the EMN approach [45] was to concentrate on spherically symmetric 4-D stringy black holes, that can be *effectively* reduced to 2-D (1 space + 1 time) string black holes of the form discussed by Witten [50]. This effective dimensional reduction turned out to be very helpful because it enabled us to concentrate on the real issues of BH dynamics and bypass the technical complications endemic in higher dimensions. We showed that [45], as we suspected all the time, stringy BH are *endorsed* with W-hair, *i.e..* they carry an *infinity* of charges W_i, correponding to the $W_{1+\infty}$ symmetries. characteristic of string theories. Then we showed that [45] this W-hair was sufficient to establish *quantum coherence* and avoid *loss of information.* Indeed, we showed explicitly that [45] in stringy black holes there is no Hawking radiation, *i.e.,* $T_{BH} = 0$, and no entropy, *i.e.,* $S_{BH} = 0$! In a way. as it should be expected from a respectable quantum theory of gravity, BH dynamics is not in conflict with quantum mechanics. There are several intuitive arguments that shed light on the above, rather drastic results. To start

with, the *infinity* of W-charges make it possible for the BH to *encode* any possible piece of information "thrown" at it by making a transition to an altered suitable configuration, consistent with very powerful selection rules. It should be clear that if it is needed an *infinite* number of *observable* charges to determine a configuration of the BH, then the "measure" of the unavailable to us information about this specific configuration should be virtually zero, i.e., $S_{BH} = 0$! The *completeness* of the W-charges, and for that matter of our argument, for establishing that $S_{BH} = 0$, has been shown in two complementary ways. Firstly, we have shown that [45] if we *sum over* the W-charges, like being unobservables, we reproduce the whole of Hawking dynamics! Secondly, we have shown that the $W_{1+\infty}$ symmetry *acts* as a phase-space volume (area in 2-D) preserving symmetry, thus entailing the *absence* of the extra $W_{1+\infty}$ symmetry violating $(\delta\!\!\!/\!\!\!\!/)\rho$ term in (21), thus reestablishing (9), i.e., safe-guarding quantum coherence. Actually, we have further shown that [45] stringy BHs correspond to "extreme BHs", i.e., BH with a harmless horizon, implying that the infinity of W-charges neutralize the extremely strong gravitional attraction. In such a case, there is no danger of seducing a member of a quantum system, hovering around the BH horizon, into the BH, thus eliminating the raison d'etre for Hawking radiation! Before though icing the champagne, one may need to address a rather fundamental problem. The low-energy, attainable physical world W_1, is made of electrons, quarks, photons, and the likes, all very well-known particles with well-known properties, i.e., mass, electric charge. etc. Nobody, though, has ever added to the identity card of these particles, lines representing their W-charges. In other words, the W_1-world seems to be W-charge blind. How is it possible then for an electron falling into a stringy BH, to excite the BH through $W_{1+\infty}$-type interactions, to an altered configuration where it has been taken into account all the information carried by the electron? Well, here is one of the miraculous mechanisms, endemic in string theories. As discussed above. it has beeen shown [49] the in the presence of singular spacetime backgrounds, like the black hole one, a mixing, of purely stringy nature, is induced between states belonging to different "mass" levels, e.g., between a *Local* (L) state ($|a\rangle_L$) of the W_1 world, with the *Global* states (G) ($|a_i\rangle_G$) of the W_2 world

$$|a\rangle = |a\rangle_L + \sum_g |a_g\rangle_G$$
$$\text{or} \qquad (22)$$
$$|a\rangle_W = |a\rangle_{W_1} \oplus |a\rangle_{W_2}$$

Notice that any resemblance between the symbols in (22) and (2) is *not* accidental and will be clarified later. Thus, we see that when a low energy particle approaches/enters a stringy BH, its global state or W_2 components while *dormant* in flat spacetime backgrounds, get *activated* and this causes a quantum mechanical coherent BH transition, always satisfying a powerful set of selection rules. In this new EMN scenario [45] of BH dynamics, if we start with a *pure state* $|\Psi\rangle = |a\rangle_W |b\rangle_W$, we end up with a *pure state* $|\Psi'\rangle = |a'\rangle_W |b'\rangle_W$, even if our quantum system encountered a BH in its evolution, because we can *monitor* the $|b\rangle$ part through the Bohm-Aharonov-like W_i charges! So everything looks dandy.

Alas, things get a bit more complicated, before they get simpler. We face here a new purely stringy phenomenon, that has to do with the global states, that lead to some dramatic consequences. Because of their *delocalized* nature in spacetime, the global or W_2-states can neither (a) appear as *well-defined asymptotic states*, nor (b) can they be integrated out in a *local path-integral formalism*, thus defying their detection in local scattering experiments!!! Once more, we have to abandon the language of the scattering matrix S, for the superscattering matrix $\$ \neq SS^\dagger$. or equivalently abandon the description of the quantum states by the wavefunction or state vector $|\Psi\rangle$, for the density matrix ρ [51]. Only this time it is for real. While string theory provides us with consistent and complete quantum dynamics, including gravitational interactions, it does it in such a way that *effectively* "*opens*" our low energy attainable W_1 world. This is not anymore a possible artifact of our treatment of quantum gravity, this is

the *effective quantum mechanics* [51, 5, 6] that emerges from a consistent quantum theory of gravity. An intuitive way to see how it works is to insert $|a\rangle_W$ as given in (22) into (9), where $\rho_W \equiv |a\rangle_W \langle a|_W$, collect all the $|a\rangle_{W_2}$ dependent parts, treat them as *noise*, and regard (9) as describing *effectively* some quantum *Brownian* motion. i.e., regard it as a *stochastic differential equation*, or *Langevin equation* for $\rho_{W_1} = \sum_i p_i |a_i\rangle_{W_1} \langle a_i|_{W_1}$ (see (10)), where the p_i's depend on $|a\rangle_{W_2}$ and thus on the W_2 *world* in a *stochastic way* [52]. In the EMN approach [51, 52, 5, 6] the emerging equation, that reproduces the EHNS equation (21) with an explicit form for the $(\delta \not{H})\rho$ term, reads (dropping the W_1 subscripts)

$$\frac{\partial \rho}{\partial t} = i[\rho, H] + iG_{ij}[\alpha_i, \rho]\beta^j \tag{23}$$

where G_{ij} denotes some *positive definite* "*metric*" in the string field space, while β^j is a characteristic function related to the field α_j and representing *collectively* the agitation of the W_2 *world* on the α_j dynamics and thus, through (22), one expects $\beta^j \approx \mathcal{O}((E/M_{Pl})^n)$, with E a typical energy scale in the W_1-world system, and $n = 2, 3, \ldots$

Before I get into the physical interpretation and major consequences of (23), let us collect its most fundamental, *system-independent* properties, following *directly* from its specific structure/form [51, 5, 6]

I) *Conservation of probability P* (see (5) and discussion above (9))

$$\frac{\partial P}{\partial t} = \frac{\partial}{\partial t}(\mathrm{Tr}\rho) = 0 \tag{24}$$

II) *Conservation of energy, on the average*

$$\frac{\partial}{\partial t} \langle\langle E \rangle\rangle \equiv \frac{\partial}{\partial t}[\mathrm{Tr}(\rho E)] = 0 \tag{25}$$

III) *Monotonic increase in entropy*/microscopic arrow of time

$$\frac{\partial S}{\partial t} = \frac{\partial}{\partial t}[-\mathrm{Tr}(\rho \ln \rho)] = (\beta^i G_{ij}\beta^j)S \geq 0 \tag{26}$$

due to the positive definiteness of the metric G_{ij} mentioned above, and thus *automatically* and *naturally* implying a *microscopic arrow of time*.

Rather remarkable and useful properties indeed.

Let us try to discuss the physical interpretation of (23) and its consequences. In conventional QM, as represented by (9), one has a *deterministic*, *unitary* evolution of the quantum system, and it is *only when* one feels compelled to "measure"/"observe" the system, that the probabilistic element of QM *emerges*. One, of course, tacitly assumes the existence of a fixed, smooth spacetime background that does not "disturb" the system, acting simply as the *arena* in which things are happening, and thus leaving the system "*closed*". The characteristics of such "closed" systems include, of course, conservation of energy and no *definite arrow of time* or *no flow of time*, which is reflected in the forms of (9), (18), which are invariant under $t \to -t$! When we decide to "open" the system we basically perform a "measurement", i.e., we force the system to "decide" what it wants to be, by choosing a very specific state, out of many coexisting possible ones, i.e., we are talking about the "collapse" of the wavefunction. That's in a nutshell the Copenhagen interpretation of QM, leaving too much to be desired, and too much on the "eye" of the "observer"! We need to do better. In the *density matrix mechanics*, as represented by (23), and as emerged, in one *interpretation* from string theory, one has a *stochastic, indeterministic* evolution of the quantum system, *ab initio*, due to the *unavoidable* existence of *spacetime foam*. The *uncontrollable, universal* quantum fluctuations of the spacetime metric at very short distances ($\mathcal{O}(\ell_{Pl})$), containing creation and annihilation of virtual Planckian-size

BH, *agitate* through the global or W_2-*world* states, our low-energy quantum system, rendering it *dynamically* and *spontaneously* "*open*". This is an *objective, universal* mechanism, independent of any "observer", that is always "up and working", thus *eroding* the quantum coherence and eventually leading to a *dynamical, spontaneous collapse*. It should be clear that the *natural* "*opening*" of our quantum system is due to our *inability* to take into account all the detailed effects of the global states, because of their delocalized nature, and thus we do *truncate* them, arriving at the *Procrustean Principle*, a *new universal principle* [6] that goes beyond the standard uncertainty principle (8). Furthermore, since this new dynamical mechanism of the "collapse" of the wavefunction, as emerged in the EMN approach [51, 5, 6], is an *objective spontaneous, time-ordered*, and thus an *orchestrated* one, I propose here to call it *synchordic collapse*.[2] Schematically, one can represent this new mechanism of the "collapse" of the wavefunction, by using (22), as follows

$$
\begin{array}{ccccccc}
 & & & & & synchordic & \\
W & \supset & W_1 & \otimes & W_2 \longrightarrow & \text{cause} & \underline{\qquad} & W_1 \\
||| & & ||| & & ||| & & collapse & \\
\text{Physical World} & & \text{Attainable} & & \text{Global} & & & \\
\text{(including all local} & & \text{Physical World} & & \text{States} & & & \\
\text{and global states)} & & \text{(including all local,} & & \text{World} & & & \\
 & & \text{low-energy states)} & & & & &
\end{array}
\qquad (27)
$$

which makes it apparent that the *global* or W_2-*world* states are the *agents* of the *synchrodic collapse*, as being the raison d'etre of *stochasticity* in quantum dynamics. Also, notice the similarity between (2) and (27), rather remarkable and very suggestive! The most *amazing* and *astonishing* thing is that, despite the well-known fact that usually open, dissipative systems defy quantization and energy conservation, our naturally "open" system, as represented by (23) and as explicitly indicated in (24), (25), and (26), is *different* [53, 54]. It is susceptible to quantization, it *conserves energy* in the mean, and *monotonically increases* its entropy, leading to loss of information, quantitatively expressed as *quantum decoherence*, and thus supplementing us with a very *natural, universal, objective microscopic arrow of time*! In the EMN approach [51, 5, 6], *time is a statistical measure of the interactions (quantum gravitational friction) between the local, low-energy world* W_1 *and the global or* W_2-*world states, in the presence of singular spacetime backgrounds (spacetime foam)*. The strong emerging correlation between loss of information, quantum decoherence leading to wavefunction collapse and the dynamical appearance of *flowing* time, I believe is unprecedented in physics.

Clearly, the role of the *magic* extra term proportional to β^j in (23), is *multifunctional*, as exemplified by making use of the *dissipation-fluctuation theorem* of statistical mechanics [14]. It can be viewed as a *dissipative term* that destroys quantum coherence, by damping the off-diagonal elements and *also* it can be seen as a *noise term able* to drive the system away from its equilibrium position and, after some time, bring it back to the same position or bring it to some other equilibrium position. In other words, we may interpret (23) as a renormalization group equation (RGE), as discussed in section 2, describing the evolution of the system between different *phases*, each corresponding to one of the *infinite* spontaneously broken $W_{1+\infty}$ symmetries. Clearly, at an *equilibrium position*, or at a *critical point*, all β^j do vanish, thus recovering naturally (9) from (23), or equivalently recovering standard QFT as applied to particle physics for the past 70 years. In principle, in fixed, smooth spacetime backgrounds, hopefully corresponding to *critical points* in our new stringy language, there is a *decoupling* of the global states from the local, low-energy states in (22), *i.e.*, all c_g's do vanish, and thus implying vanishing β^j in (23). Before though, we are carried away from the highly promising stringy big quantum picture that emerges here, it should

---

[2] chord=string in greek: synchordia something like symphonia.

pay to have a closer look at some numerical details, if not for any other reason, just as a *reality check*! Indeed, one can work out, using (23), the time that it takes for quantum decoherence, or equivalently the quantum coherence lifetime τ_c, as defined by the off-diagonal elements damping factor [43]: $\exp[-Nt(m^6/M^3)(\Delta X)^2]$, for a system of N constituents of mass m, assuming that its center of mass gets finally pinned down within ΔX, and is given by

$$\tau_c = \frac{M^3}{Nm^6(\Delta X)^2} \tag{28}$$

where M stands for $M_{SU} \approx (1/10)M_{Pl} \approx 10^{18}\,\text{GeV}$, the characteristic string scale [55]. What about the value of m? The most natural value for it would be $m \approx m_{\text{nucleon}} \approx 1\,\text{GeV}$ for the following reason. Our attainable low-energy world, as far as we know is made up of electrons, protons, and neutrons: that is what constitute us, *i.e.*, our cells, our proteins, our DNA, etc, and also that is what everything else we use, *i.e.*, the "apparatus", is made of. Of course, protons and neutrons are mainly made of up (u) and down (d) constituent quarks, but for my arguments they are of comparable mass and thus would give the same results. Now, since the bulk of matter is due to nucleons, and not to electrons ($m_{\text{nucl}} \approx 1836 m_e$), the shortest coherence lifetimes that we are interested in would be provided by $m \approx m_{\text{nucl}}$. Furthermore, independent of the complicated structure that you may consider, *e.g.*, a complicated protein polymer structure, a la Microtubules (MTs), the virtual Planckian BHs have such high energy that they "see" and interact/agitate with the most fundamental constituents of the complicated structure, *i.e.*, up and down quarks and electrons, thus as explained above, justifying the identification $m \approx m_{\text{nucl}} \approx 1\,\text{GeV}$ in (28). Thus, using $M \sim 10^{18}\,\text{GeV}$, $m \sim 1\,\text{GeV}$, and $(\Delta x) \sim 1\text{nm} \equiv 10^{-7}\text{cm}$. (28) yields

$$\tau_c = \frac{10^{16}}{N}\,\text{sec} \tag{29}$$

a rather suggestive formula. In the case of a single ($N = 1$) hydrogen atom. (29) becomes $\tau_H \sim 10^{16}\text{sec}$, the present age of the universe! In other words, standard QM applies extremely accurately in microsystems, as of course, we want, because of the spectacular successes of QM in the microworld. On the other hand, if we take a piece of ice, containing say $N \sim N_{\text{Avogadro}} \approx 10^{24}$ nucleons, then we get $\tau_c^{\text{ice}} \approx 10^{-8}$ sec, a rather short-lived quantum coherence implying that for macroscopic objects ($N \sim N_{\text{Avogadro}}$) QM rules fail and classical physics emerges *naturally*, *dynamically*, *spontaneously*, and *objectively*! The *Schrödinger's cat* paradox is automatically resolved: within $\mathcal{O}(10^{-8}\text{sec})$ the cat would be dead or alive, not the fifty/fifty stuff anymore. Furthermore, the "measurement"/"observation" problem gets a similar satisfactory resolution. Indeed, performing a "measurement"/"observation" on a quantum system implies bringing it in "*interaction*" with some suitable *macroscopic apparatus* ($N_{\text{macr}} \sim \mathcal{O}(N_{\text{Avog}})$), thus triggering an almost *instantaneous* "collapse" of the wavefunction of the quantum system, as suggested by (29) with $N \approx N_{\text{macr}} + N_{\text{quant.syst}} \sim \mathcal{O}(N_{\text{Avog}})$. The *magic step*, as indicated in (7), and which constitutes basically the one-half of quantum mechanics *it does need not to be postulated*, but it comes out from the stochastic dynamics, as provided by the agitating global or W_2-*world* states. It should not escape our notice that there is no quantum-classical border, but a continuous and smooth transition. Furthermore, as (28) indicates, the Avogadro number, a measure of the macroscopicity of the system, is basically dynamically determined to be the inverse of the dimensionless product of the gravitational strength ($\sqrt{G_N}$) times the characteristic strong interaction scale ($\Lambda_{\text{QCD}} \sim \mathcal{O}(0.1\,\text{GeV})$) times the electromagnetic fine structure constant ($\alpha = 1/137$)

$$N_{\text{Avogadro}} \sim \frac{1}{\sqrt{G_N}\,\Lambda_{\text{QCD}}\,\alpha} \tag{30}$$

I do hope that I have convinced the reader that the performed *reality check* has been rather successful and illuminating.

It is highly remarkable that stringy modified QM or *density matrix mechanics* is offering us, see ((23),(27)), a new *unified approach* to quantum dynamics, by turning a *deterministic* wave-type equation into a *stochastic differential* equation able to successfully describe *both* evolution and "measurement" of quantum systems. At the same time, a *unified picture* of the quantum and classical world is emerging, as promised in section 3, without the need of raising artificial borders between the quantum and the classical, the transition between them is dynamical and smooth. The fundamental property of string theory that allows all these "miraculous events" to occur is its defining property, *i.e.*, the need of 2-dimensions (1 space + 1 time) to describe a 1-dimensional (1-D) *extended* object and its accompanying *infinity* of excitation modes/particles, due exactly to its extended nature. While a pointlike particle "runs" on a *world-line*, a string sweeps a *world-sheet*. Eventually, all 4-D spacetime physics would be mappings of corresponding physics in the 2-D stringy world-sheet. The existence of the $W_{1+\infty}$ symmetry was first established in 2-D "world sheet" physics and then mapped into 4-D spacetime physics. The *infinity* of spontaneously broken stringy gauge symmetries, and the very existence of the *global states*, *somehow* can trace back their origin to the *2-dimensionality* of the world-sheet! In other words, the stringy nature of the modified quantum mechanics prevails, as should be apparent at each and every turn!

The alert reader may have already noticed the stunning similarity between the string dynamics in singular spacetime backgrounds, like black holes and spacetime foam, and the brain mechanics presented in section 2. Presence or lack of quantum coherence and its cause, the existence of an *infinite* number of possible equilibrium or critical points corresponding to an *infinite* number of spontaneously broken "gauge" (stringy) symmetries with *appropriate selection rules*, the possibility of "running" away from one equilibrium point, and eventually coming back to it, or end up at another equilibrium point, in a *timely* manner, etc. etc. If we could only find a structure in the brain that it renders the EMN string dynamics [45, 51, 52, 5, 6] applicable, we would then be able to provide a rather explicit answer to most of the problems raised in sections 2 and 4. Namely, the *binding problem*; how the brain represents a *physical, objectively real, flowing time? free will*, etc. etc.

Well, these brain structures *do exist* and they are called

6   MicroTubules (MT) I: The biochemical profile

Living organisms are collective assemblies of cells which contain collective assemblies of organized material, including membranes, organelles, nuclei, and the *cytoplasm*, the bulk interior medium of living cells. Dynamic rearrangements of the cytoplasm within *eucaryotic cells*, the cells of all animals and almost all plants on Earth, account for their changing shape, movement, etc. This extremely important cytoplasmic structural and dynamical organization is due to the presence of networks of inteconnected protein polymers, which are referred to as the *cytosceleton* due to their boneline structure [1, 2]. The cytosceleton consists of *Microtubules* (MT's), action microfilaments, intermediate filaments and an *organizing complex*, the *centrosome* with its chief component the *centriole*, built from two bundles of microtubules in a separated T shape. Parallel-arrayed MTs are interconnected by cross-bridging proteins (*MT-Associated Proteins*: MAPs) to other MTs, organelle filaments and membranes to form *dynamic networks* [1, 2]. MAPs may be contractile, structural, or enzymatic. A very important role is played by contractile MAPs, like dynein and kinesin, through their participation in cell movements as well as in intra-neural, or axoplasmic transport which moves material and thus is of fundamental importance for the *maintenance* and *regulation* of *synapses*. The structural bridges formed by MAPs stabilize MTs and prevent their disassembly. The MT-MAP "complexes" or *cytosceletal networks* determine the cell architecture and dynamic functions, such a *mitosis*, or *cell division, growth,*

differentiation, movement, and for us here the very crucial, *synapse formation and function,* all essential to the living state! It is usually said that *microtubules* and *ubiquitous* through the entire biology! [1, 2]

Microtubules [1, 2, 3] are hollow cylindrical tubes, of about 25 nm in diameter on the outside and 14 nm on the inside, whose walls are polymerized arrays of *protein subunits.* Their lengths may range from tens of nanometers during early assembly, to possible centimeters (!) in nerve axons within large animals. The protein subunits assemble in longitudinal strings called *protofilaments,* thirteen (13) parallel protofilaments laterally align to form the hollow *"tubules".* The protein subunits are "barbell" or "peanut" shaped *dimers* which in turn consists of two globular proteins, *monomers,* known as *alpha (α)* and *beta (β) tubulin.* The α and β tubulin monomers are similar molecules with identical orientation within protofilaments and tubule walls. In the polymerized state of the MT, one monomer consists of 40% α-helix, 31% β-sheet and 29% random coil. The α-tubulin consists of four α-helixes, four β-sheets, and two random coils, while the β-tubulin has six α-helixes, one β-sheet, and seven random coils. Each *monomer* consists of about 500 aminoacids, is about 4nmx4nmx4nm, and weighs 5.5×10^4 daltons or equivalently its atomic number is 5.5×10^4, and has a *local polarity.* Each *dimer,* as well as each MT, appears to have an electric polarity or dipole, with the negative end oriented towards the α-monomer and the positive end towards the β-monomer. The dipole character of the dimer originates from the 18 Calcium ions (Ca^{++}) bound within each β-monomer. An equal number of negative charges required for the electrostatic balance are localized near the neighboring α-monomer. Thus, MTs can be viewed as an example of *electret* substances, *i.e.,* oriented assemblies of dipoles, possessing *piezoelectric* properties, pretty important in their functions including their assembly and disassembly behavior. The dimers are held together by relatively weak Van der Waals hydrophobic forces due to dipole coupling. Each dimer has 6 neighbors which form slightly skewed *hexagonal lattices* along the entirety of the tube, with a "leftward" tilt, and several *helical patterns* may be "seen" in the relations among dimers. Imagine a MT slit along its length, and then opened out flat into a strip. One then finds that the tubulins are ordered in sloping lines which rejoin at the opposite edge 5 or 8 places displaced (5+8=13), depending on the line slope, it is to the right or to the left. The crystal-like symmetry packing of the tubulin in MTs is very suggestive for a possible use of MTs as *"information processors".* It should be rather obvious that such a delicate, fine MT organization is there for some good reason.

Further evidence for the very special role that MTs are made to play is provided by the very interesting assembly and disassembly behavior. Dimers self-assemble in MTs, apparently in an *entropy-driven* process which can *quickly* change by MT disassembly and reassembly into *another orientation.* It seems that Guanosine TriPhosphate (GTP) hydrolysis to Guanosine DiPhosphate (GDP) provide the energy that binds the polymerizing tubulin dimers, while biochemical energy can also be pumped into MTs by phosphorylation/dephosphorylation of MAPs. In fact, each tubulin dimer, as a whole, can exist in two different geometrical configurations or *conformations,* induced, *e.g.,* by the GTP-GDP hydrolysis. In one of these they bend 29° to the direction of the microtubule. It seems that these two conformations *correspond* to two different states of the dimer's electric polarization, where these come about because an electron, centrally placed at the α-tubulin/β-tubulin junction, may shift from one position to another, the textbook, gold-platted case of a *quantum-mechanical two-state system* [20]! Several "on-off" functions linked to Ca^{++} binding could do the job. The Ca^{++} concentration changes could alter the conformational states of certain tubulin subunits, which may be pre-programmed to undergo conformational changes in the presence of Ca^{++}, through GTP, glycosylation, etc. Furthermore, a calcium-calmodulin complex could facilitate charge and/or energy transfer, similar to the way acceptor impurities act in semiconductors! The Ca^{++} may delocalize an electron from its orbital spin mate, both electrons belonging to an aromatic aminoacid ring within a hydrophobic pocket, resulting

in an unstable *electron "hole"*. and thus enhancing the probability for either a charge transfer from an adjacent subunit, and/or transfer of energy to an adjacent subunit. Tubulins in MTs may also be modified by binding various ligands, MAPs, etc. Then, given the fact that the genes for α and β tubulins are rather complex, providing a varying primary tubulin structure, *e.g.*, at least 17 different β-tubulins can exist in mammalian brain MTs, one easily sees that the number of different possible combinations of tubulin states and thus the *information capacity* within MTs may be very large indeed! It should be stressed that proteins undergo conformational motions over a wide range of time and energy scales. However, significant conformational changes related to protein function generally occur within the $(10^{-9} - 10^{-12})$ sec time scale. The conformational changes are related to cooperative movements of protein sub-regions and charge redistributions, thus *strongly linked* to *protein function* (signal transmission, ion channel opening, enzyme action, etc) and may be triggered by factors including phosphorylation, GTP hydrolysis, ion fluxes, electric fields, ligand binding, and neighboring protein conformational changes. In the case of MTs, the *programmable* and *adaptable* nature of the tubulin conformational states can be easily used to *represent* and *propagate* information. Further evidence for some of the extraordinary tasks that may be undertaken by the MTs, due to their specific fine structure, is their fundamental role in *mitosis*, or *cell division*. The *centriole*, as we discussed above, consists basically of two cylinders of nine triplets of MTs each, forming a kind of separated T. At some point, each of the two cylinders in the *centriole* grows another, each apparently dragging a bundle of MTs with it, by becoming a focal point around which MTs assemble. These MT fibers connect the centriole to the separate DNA strands in the nucleus, at the *centromeres*, and the DNA strands separate, thus initiating cell division. Another, indeed extraordinary mechanism from the many contained in Nature's magic bag of tricks! The interelation and parallelism between MTs and DNA goes much further. The *centriole*, a rather critical part of the *centrosome* or *MT's organizing center*, seems to be a kind of *control center* for the cytosceleton. Thus, it seems that we have two *strategic centers* in a single cell: the *nucleus*, where all the fundamental genetic material of the cell resides, controlling the cell's heredity and governing the production of proteins, of which the cell itself is composed! On the other hand, the *centrosome*, with the MT-composed *centriole* as its chief component seems to control the cell's movements and its organization. As DNA is the common genetic database containing hereditary information, *microtubules* are *real time executives* of dynamic activities within living cells. One may wonder at this point, that while DNA's very suggestive double-helical structure enables it to possess a code, the *genetic code* [10], nothing of similar caliber occurs within microtubules. This is a false alarm! So, let us take things from the beginning. One nucleotide of DNA is composed of three elements: a *base*, ribose, and *phosphate group*. Four types of bases are present: Adenine (A), Thymine (T), Guanine (G), and Cytosine (C), belonging to two basic categories, a purine base (A,G) and a pyrimidine base (T,C). Nucleotides are inteconnected by hydrogen bonds organizing them in a specific double-helix structure (A=T. G≡C). From the aspect of organization of structure, one such double-helix may be considered as an *aperiodic crystal*. "Aperiodic" signifies the irregular interchange of bases *inside* the helix, while the phospates and riboses are located on the outside making up a *periodic crystal* structure. The irregular repetition of bases within the helix represents properties of the living beings which make sense, from an information point of view, only as *code system*. In the genetic code, one triplet of bases, the *codon*, codes one aminoacid. The basic genetic code is coded by 20 aminoacids and there exists a "stop" as three more codons. Thus, there exist 61 codons which code 20 aminoacids, from the $4^3 = 64$ possible combinations of four bases of triplets. Then, the messenger RNA (mRNA) is synthesized from the one strand of the DNA double helix, while the other strand of the double helix remains in the nucleus making possible the synthesis of another chain of DNA. The complete genetic

information is preserved and remains inside the nucleus. From mRNA through carrier RNA (tRNA) to ribosomal RNA (rRNA) there is a continual transmission of the genetic information message, making in effect proteins. the other side of the genetic code. One crucial point to emphasize here is the following [56]: it is well known that the protein's catalytic or other functions strongly depends on its *exact 3-dimensional* structure, thus making it a Tantalian job to try to exactly reproduce genetically a protein! Nature, though. is more subtle. All a gene has to do is to get the *sequence* of the aminoacids correct in that protein. Once the correct polypeptide chain has been synthesized, with all its side chains in the right order, then following the laws of quantum mechanics, called Chemistry in this particular case. the protein would fold itself up correctly into a unique 3-D structure. A difficult 3-dimensional (reproduction) problem has been recast as a much easier attractible 1-dimensional one! A very good lesson to be appreciated and remembered and maybe to be used in other similar circumstances.

Until recently, it was widely believed that MTs were just base elements of the cytosceleton and that they played a role in the mitotic spindle and active transport. More careful study of the MT's structure, notably by Koruga [57]. showed that MTs possess also a. *code system*! One should not be surprised by such a finding. Recall that the two different *conformational states* of a tubulin dimer can switch from one to the other. due to alternative possibilities for their *electric polarization*. Clearly, the state of each dimer would be influenced by the polarization states of each of its six neighbors, due to the Van der Waals forces between them. thus giving rise to certain specific rules governing the conformation of each dimer in terms of the conformations of its neighbors. This would allow all kind of messages to be propagated and processed along the length of each microtubule. These propagating signals appear to be relevant to the way that microtubules transport various molecules alongside them, and to the various interconnections between neighboring microtubules through MAPs. The repetitive geometric lattice array of MT units may serve as a *matrix* of directional transfer and transduction of biochemical, conformational, or electromagnetic energy. It seems highly plausible that the continuous grids of intramural MT could function as programable switching matrices capable of information processing. Within neurons. transfer of MT conformational charge or energy state could be driven by travelling nerve action potentials and/or associated transmittance Ca^{++} flux. Such a view is supported by the fact that velocities of action potentials and accompanying Ca^{++} flux $\mathcal{O}(10-100)$m/sec would result in time intervals for 4nm tubulin subunit transfers of about 10^{-10} sec. consistent with the observed nanosecond range of protein conformational oscillations [58]! Taking into account the intraneural MT density, the neural fraction of the brain, and average neural firing rates, *parallel computing* in MT coupled to action potentials could reach 10^{26} transfers/sec (*bits*) in the human brain!

Koruga observed [57] that the hexagonal packing [59] of the α and β tubulin subunits in MT with *13 protofilaments* corresponds to *information coding*. He noticed that hexagonal packing and face-centered cubic packing of spheres have equal density and thus he used both to explain MT organization. It is known that the Oh(6/4) symmetry group describes face-centered-cubic sphere packing and *derives* information coding laws [60]. In the case of hexagonal packing, the centers of the spheres should lie on the surface of a cylinder (with radius equal to the Oh(6/4) unit sphere) and the sphere values in the axial direction (lattice) of the cylinder by order of sphere packing is the *same* as in the dimension in which face-centered-cubic packing is done. There should be two kinds of spheres (white and black) on the cylinder surface, but linked such that they have the dimension value in which the face-centered-cubic packing is done, leading to an "helical symmetry". Amazingly enough, the MTs satisfy all these desiderata! Thus, the MTs possess one of the best known [60] *binary error-correcting* codes. the 6-binary dimer $K_1[13,2^6,5]$, where the distance between spheres in order of packing is 5 and with $2^6 = 64$ *words*!!! It should

be noticed that information theory suggests that the optimal number of spheres (white and black corresponding to, say, α and β monomers) for information processing is 11, 12, or 13! A rather amazing result, supported further by the fact that 13 (=5+8) seems to be almost universal amongst mammalian MTs. Thus 13 is our lucky number! In addition, symmetry theory suggests that on the surface of a circular cylinder in axial direction of the MT, there must be a code of length of 24 monomer subunits (or 12 dimers), the code $K_2[24, 3^4, 13]$ corresponding to a 4-dimer ternary sequence [57]. It is under the influence of the above discussed Ca^{++}-calmodulin "complex" that 6-binary dimers of K_1 code give 4-dimer ternary sequence of K_2 code, corresponding to biophysical transfer of information from one point to other in MT, by transforming the hexagonal surface organization into a new cubic state. Undoubtedly, microtubule symmetry and structure are optimal for information processing. Thus microtubules along with DNA/RNA are unique cell structures that possess a code system, signifying their singularly important position. Like in the case of DNA/RNA, the specific structure of MTs led to the conclusion that they possess code systems which can be utilized in the neuron dynamic information activities, and other dynamical biological activities as well. It is very hard to believe that the detailed, fine, paracrystalline MT structure, which, among the many other useful functions, enables MTs to possess the K-codes, is just accidental and parochial. It is not very hard to speculate that, since the MTs are strongly involved in erocytosis, which is the most fundamental process that may somehow transform intentions/feelings/etc into neural action, the K-codes may be used as a dictionary translating psychological "orders" into physiological actions! In other words, the DNA/RNA provide the genetic code, while the MTs provide the mental code or K-code. As such, MTs become primary suspects for further investigations concerning their possible role as the microsites of consciousness. One should not worry that, at this stage of our investigation, the mechanism of "real time" regulation and control by MT or other cytoskeletal filaments seems to be missing, because it will be provided soon, once we study their physics in the light of density matrix mechanics, presented in the previous section. Before we get to this fascinating subject, let us provide some further phenomenological/experimental evidence that indeed neural MTs have to do a lot with learning, memory, cognition, and thus, eventually, with consciousness ...

Our story starts thousands of millions of years ago, when the then popular cytosceleton-less procaryotic cells became entangled with spirochetes possesing whiplike tail composed of cytosceletal proteins. This, fortunate for us, symbiosis produced the eucaryotic cells, possessing cytoskeletons [61, 3]. All this is well, but it has led to the following puzzle. Single eucaryotic cell organisms, the protozoa, like the amoeba and the paramecium, without possessing a single neuron or synapse, still appear able of cognitive and adaptive activities. Amoebae have been seen to hunt for food and paramecia to avoid obstacles! How is this possible? The only logical explanation left is that the key structure is the cystosceleton, including MTs, that act as the nervous system of single cells, as has been observed almost half a century ago, by the famous neuroscientist C. S. Sherrington [62]. Indeed, the paramecium seems to use its cytosceleton for coordinated action, in the form of metachronal waves. Furthermore, metachronal waves of ciliary beating in paramecea are reversibly inhibited by the general anesthisogon, chloroform [63]. In addition, it has been shown that signal transduction in sensory cilia is due to propagating conformational changes along ciliary microtubule subunits [64]!

Further evidence, in modern times, that links the cytosceleton with cognitive function is provided by the following findings:

1. Experiments with trained goldfish show that the drug colchicine produces retrograde amnesia, by affecting memory fixation, through interference with the MTs responsible for the structural modification of certain

synapses [65].

2. Production of tubulin and MT activities correlate with peak learning, memory and experience in baby chick brains [66].

3. Experiments with baby rats show that when they first open their eyes, neurons in their visual cortex begin producing vast quantities of tubulin [67].

4. Selective dysfunction of animal brain MTs by the drug colchicine causes defects in learning and memory which mimic the symptons of Alzheimer's disease (AD). It has been reported that in rats, continuous MT disruption induced by chronic colchicine administration results in a dose-dependent learning deficit, and retention is also impaired. It has also been stressed that these colchicine-induced cognitive defects resemble those of AD, *i.e.*, amnesia of recent learning and loss of formerly established memories [68].

5. It has been hypothesized [69], and very recently supported by detailed experimental studies [70], that impairment of MTs, leading to tangled and dysfunctional neural cytosceleton, may be one explanation for the pathogenesis of Alzheimer's disease (AD) [71].

6. In specific hippocampal regions of the brain of schizophrenic patients, neuronal distorted architecture found due to a lack of 2 MAPs (MAP-2 and MAP-5) [72].

Arguably, we have plenty of evidence that, the cytosceleton, and in particular the microtubules, have been rather instrumental through the whole *natural evolution*, from the amoeba and paramecium to humans, and they even helped or were deeply involved in *natural selection*. All these facts, I believe, make it difficult to justify the rather popular attitude of taking the neuron as the fundamental, structureless unit and try to explain the brain function from there on. An analogous attitude would be to try to understand Chemistry by *only* accepting the existence of *structureless* a-toms, in their original Democritean form. We can make a bit of progress but we cannot go that far! The Pauli exclusion principle, of pure quantum mechanical origin, seems to play a rather fundamental role in understanding the periodic table, ... We should come to terms with the *complexity* of the neuron, and we should not treat it just as a *switch*. It will be wiser to concentrate on the *nervous system* of the *neuron*, namely the *microtubule network* [1, 3]. By avoiding taking this rather natural step, we are vulnerable to the accusations of being micro-behaviorists or micro-functionalists, by treating the whole neuron as a black box. Personally, I don't feel comfortable with such an accusation!

So, let us concentrate now on the detailed structure of the neural MTs. Each individual neuron, as being an eucaryotic cell, has its cytosceleton. Due to the unfortunate for us, fact that neurons do not multiply after the brain is fully formed, there seems to be no role for a *centriole* in the neural cell. Indeed, centrioles seem to be absent in the neuron's centrosome, which as usual, is found close to the neuron's nucleus. Neural MTs can be very long indeed, in comparison with their diameter, of order of $O(10nm)$ and can reach lengths of mms or more! There are about 450 MTs/μ^2 or about 7×10^5 tubulins/μ^3, along the neural axon. Furthermore, as we mentioned above, the potential *computing* brain power increases substantially if the tubulin diners (of characteristic two-state conformational frequency of $10^{10}Hz$) are taken to be the basic computational units. Indeed, in the case of the "neuron unit", we get something like 10^{14} basic operations per sec ($= 10^{11}$ neurons x 10^3 signals/(neuron sec)), while in the case of the "tubulin dimer unit" we get something like 10^{28} basic operations per sec ($= 10^{11}$ neurons x

10^7 tubulin/neuron x 10^{10} signals/(tubulin sec))! A rather remarkable gain on brain power by replacing "neuron-type" switches with "*microtubular information processors*", even if we reduce it for efficiency, non-participation, etc. down to, say, 10^{25} "bits". The neural MTs can grow or shrink, depending on the circumstances, they transport neurotransmitter molecules, they are running along the lengths of the axons and dendrites and they do form communicating networks by means of the connecting MAPs. Neural MTs seem to be responsible for *maintaining* the synaptic strengths, while they are able to effect *strength-alterations* when needed. It also seems that neural MTs play a fundamental role in organizing the growth of new nerve endings, piloting them towards their connections with other neuron, thus contributing or being mainly responsible for the formation of neural networks *in vivo*. Neural MTs extend from the *centrosome*, near the nucleus, all the way up to the presynaptic endings of the axon, as well as in the other direction, into the dendrites and dendritic spines, the postsynaptic end of the synaptic cleft. These dendritic spines are subject to growth and degeneration, a rather important process for *brain plasticity*, in which the overall interconnections in the brain are suffering continuous and subtle changes, and as we discussed in section 4, out of reach for the conventional neural networks (NN) approach to brain function. As a further indication for the involvement of neural MTs in *exocytosis*, or the release of neurotransmitter chemicals from the presynaptic vesicular grid, Penrose has emphasized [3] the existence and role of certain substances, called *clathrins*, found in the presynaptic endings of axons, and *associated* with MTs. Clathrins are built from protein trimers, known as *triskelions*, which form three-pronged structures. The clathrin triskelions fit together in an incredulous way, to form very beautiful configurations, basically identical in general organization to the carbon molecules known as "fullereness" or "bucky balls" [73], but much bigger, since the single carbon atoms are replaced by an entire clathrin triskelion involving several aminoacids. Thus, clathrins have a very fascinating geometrical structure, of a truncated icosahedron, that should be related to their important role in the release of neurotransmitter chemicals.

If what is happening in the synaptic clefts, involving always microtubule networks in a rather fundamental way both at the presynaptic and postsynaptic stage, reminds you of the quasicrystals discussed at the end of section 3, you are right. Brain plasticity shares some similarities with quasicrystal growth [12]. Also, I do hope that I have presented significant evidence indicating the direct involvement of MTs in the control of brain plasticity, and thus coming to a point, where the physics of MTs needs to be discussed.

7 MicroTubules (MT) II: The physical profile

The remarkable biological/physiological properties of MTs discussed in the previous section is a typical example of the amazing *high degree of order* present in biological systems. Usually, bioscientists pay more attention to the functional organization rather than to the spatial/physical structure, but we should always remember that, if we would like to understand function we should study structure [56]. The DNA story is a good example at hand, emphasizing the strong structure-function correlation [18]. The basic physical framework for understanding biological order was put forward by Fröhlich [74]. As we discussed in the previous section, proteins are vibrant, dynamic structures in physiological conditions. A variety of recent techniques have shown that proteins and their component parts undergo conformational transformations, most significantly in the "nanosecond" $10^{-9} - 10^{-10}$ sec range, as predicted by Fröhlich. It should be stressed that these motions are *global changes* in protein conformation *rather than* rapid *thermal fluctuations* of side chains or local regions. About 25 years ago, Fröhlich suggested [74] that such *global* protein changes are *completely triggered* by charge redistributions such as dipole oscillations or electron movements within specific *hydrophobic* regions of proteins. Hydrophobic regions within proteins are comprised of

non-polar side chains of aminoacids which exclude water. Incidentally, and for later use, general anesthesia gas molecules apparently act there to prevent protein conformational responsiveness [75]. Fröhlich's basic conjecture was that quantum-level events such as the movement of an electron within these hydrophobic regions act as a *trigger/switch* for the conformational state of the *entire* protein. The movement of an electron among resonant bond orbitals of aminoacid and side chains such as aromatic rings of tyrosine, is a good example of Fröhlich's electrons. Fröhlich considered an ensemble of high-frequency oscillators that can be subjected to an external electric field and allowed to strongly interact among themselves. He conjectured that, if biochemical energy such as ATP or GTP hydrolysis were supplied to the dipolar system, a new state would be formed that is characterized by a *long-range coherence*, as manifested by a macroscopic occupation of a single mode. He provided some physical evidence, that coherent excitation frequencies in the range $10^9 - 10^{10}$ Hz were possible in such biological systems. He further predicted metastable states (longer-lived conformational state patterns stabilized by local factors) and travelling regions of dipole-coupled conformations. Such global protein conformations appear suitable for computations: finite states which can be influenced by dynamic neighbor interactions. There is some experimental evidence for Fröhlich's excitations in biological systems that include observations of GHz-range phonons in proteins [76], sharp-resonant non-thermal effects of GHz irradiation on living cells [77], GHz-induced activation of microtubule pinocytons in rat brains [78], Raman detection of Fröhlich frequency energy [79] and the demonstration of propagating signals in microtubules [80]. Fröhlich's basic physical ideas [74] seem to make a lot of sense, but is there any structure(s) that may realize them, or is it another theoretical pipedream? Lo and behold, microtubules just fit the bill. The entire MT may be viewed within the context of the Fröhlich framework, as a regular array of coupled dipole oscillators interacting through resonant long-range forces. Furthermore, as we discussed in the previous section in detail, in the case of MTs we have an explicit mechanism involving the calcium-calmodulin "complex" for the electron movement in the hydrophobic pocket. In addition, coherent vibrations within regions of an MT may take the form of *kink-like excitations* separating adjacent regions with opposite polarization vectors, with the dipole orientations in the direction of the MT axis. The extra energy needed for the creation of kink-like excitations may be provided by GTP hydrolysis, as discussed in the previous section. It is known that the energy produced during GTP hydrolysis is delivered to assembled MTs, although the precise manner in which this energy is utilized is still not understood. Amazingly enough, the free energy released in GTP hydrolysis is about 10Kcal/mole (0.42eV/molecule), or about the energy content of a kink-like excitation! Recently rather detailed and interesting studies of the physics of microtubules, at the *classical level*, have been undertaken by several groups [81, 82, 83], as it is discussed next.

Microtubules are viewed as polymers of subunit proteins, the tubulins, and as such they may be considered as lattices of oriented dipoles. There are three types of arrangements of dipoles in lattices: (i) random, (ii) parallel-aligned or *ferroelectric*, and (iii) regions of locally frozen orientations or *spin-glass* [29]. As discussed in section 2, depending on the values of the parameters characterizing the system (temperature and external electric field look the most relevant here) the system may exhibit different phases. In the ferroelectric phase, there is a long range order (global dipole alignment), encouraging the propagation of kink-like excitations and thus able of MT signaling and assembly/disassembly. On the other hand, the spin-glass phase with its locally frozen dipole orientations seems to be useable for efficient information processing and computations. So, it seems that the MTs organize cell activities by operating in two different phases, accessible by slightly changing the temperature and the external electric field. A rather remarkable operational biological system [1, 57, 81, 82, 83].

The basic characteristics of the physical MT model, put forward in Ref. [81, 82], is that the MT's strong uniaxial

dielectric anisotropy align the dipole oscillators so that they can be effectively described by *only one degree of freedom*! In fact, experiments have shown [84] that a tubulin undergoes a conformational change induced by GTP-GDP hydrolysis in which one monomer shifts its orientation by 29° from the dimer's vertical axis, as we discussed in the previous section. Thus, the relevant degree of freedom, identifiable with an "order parameter", is the projection on the MT cylinder's axis of the monomer's displacement from its equilibrium position. The mobile electron on each dimer, as discussed in the previous section, can be localized either more toward the α-monomer or more toward the β-monomer. The latter possibility is associated with changes in dimer conformation. and thus we should identify the "order" parameter with the amount of β-state distortion when the latter is projected on the MT longitudinal axis. Using the language of Quantum Mechanics (see section 3) I will denote the two *conformational states* of the dimer as $|\alpha\rangle$ and $|\beta\rangle$ referring respectively to the cases of the mobile electron being on the α- or β-court and with $|\alpha\rangle \rightarrow |\beta\rangle$ the *quantum transition* triggered by the movement of the electron from the one court to the other. The archetypal of a two-state quantum system indeed! The remarkable inherent symmetry of a MT enables one to view it effectively as nearly perfect *one-dimensional crystal* and thus including time, as a *highly symmetric 2-dimensional physical system*. Furthermore, one should take into account the fact that the whole MT cylinder represents a *"giant dipole"*. When the cross section of a MT is viewed using electron microscopy, the MT's outer surfaces are surrounded by a "clear zone" of several nm which apparently represents the *oriented* molecules of cytoplasmic water called sometimes *"vicinal"* water. and enzymes. It seems that the MT produces an electric field. Therefore, it is assumed that. together with the polarized water surrounding it, a MT generates a nearly uniform intrinsic electric field parallel to its axis. The existence of a solvent in the environment of the MT, assumed for simplicity to be just water, has some further consequences. The water provides a dielectric constant ($\epsilon \sim 80$) that reduces the long-range electrostatic energy between the dimer dipoles, and at the same time, it provides a viscous medium that damps out vibrations of dimer dipoles.

All the above detailed physical structure is taken into account in a *classical* mean field theory approach to the dynamics of the MT [81, 82]. One mimics the overall effect of the surrounding dimer-dipoles on a *chosen site n*. by qualitatively describing it by a double-well quartic potential, a standard method, applied in the past rather successfully in similar systems. *e.g.*, in dipolar excitations of ferroelectrics [85]. The potential then. for the β-displacement $u_n(t)$ along the longitudinal symmetry (x) axis of the MT cylinder, in the continuous limit $u_n(t) \rightarrow u(x,t)$, where $u(x,t)$ represents a *1+1 dimensional classical field*, takes the form

$$V(u) = -\tfrac{1}{2}Au^2(x,t) + \tfrac{1}{4}Bu^4(x,t)$$ (31)

with $B > 0$ and $A = -(+\text{const})(T - T_c)$. where T_c denotes the critical temperature of the system. The equation of motion then reads

$$M\frac{\partial^2 u}{\partial t^2} - kR_0^2\frac{\partial^2 u}{\partial x^2} - Au + Bu^3 + \gamma\frac{\partial u}{\partial t} - qE = 0$$ (32)

where M denotes the mass of the dimer. k is a stiffness parameter. R_0 is the equilibrium spacing between adjacent dimers, γ is the viscous water damping coefficient, and E is the electric field due to the "giant" MT dipole discussed above, with q the effective mobile charge of a single dimer. Detailed studies [81. 82] of the dynamical equation (32), in the appropriate parameter range. have revealed very interesting results/properties. Indeed, for temperatures below the critical temperature $T_c \approx 300°$K. the coefficient A in (31) is positive, thus putting the system into the ferroelectric phase, characterized by long-range order, *i.e.*, all dipoles aligned along the MT longitudinal direction. In this phase, Eq. (32) admits travelling waves in the form of displaced *classical* kink-like solitons with *no energy*

loss [86]. The kink-like soliton propagates along the protofilament with a fixed velocity v, which for $T < T_c$, *i.e.*, in the ferroelectric phase is well approximated by [81, 82]

$$\vec{v} \approx 2 \times 10^{-5}(\text{m/sec})\vec{E}/(1\text{V/m}) \tag{33}$$

implying, for a characteristic average value of $E \approx 10^5\text{V/m}$, $v \approx 2\text{m/sec}$ and thus a propagating time, from one end to the other of an $O(1\mu)$ MT, $\tau \approx 5 \times 10^{-7}$ sec. As (33) suggests, the kink-like soliton travels preferentially in the direction of the intrinsic electric field, thus transferring the energy that created it, *i.e.*, chemical GTP-GDP hydrolysis type energy, towards a specific end where it can be used to detach dimers from the MT, in accordance with experimental observations [87], concerning the assembly/disassembly of MTs [88]. The role of MAPs, the lateral cross-bridging proteins, as MTs *stabilizers* becomes clearer now. From the physical point of view, these bridges represent *lattice impurities* in the MT structure, and it is well-known that impurities play a very important role in soliton propagation. Kinks may be totally reflected by an attractive impurity, for a specific range of the kink propagating velocities, thus MAPs may significantly reduce the MT disassembly. Furthermore, the addition of an *external* electric field introduces a new control mechanism in the MT dynamics. As (33) suggests, depending on the relative direction and sign of the two fields (external versus internal) the kink-like solitons may travel faster or stop altogether! Here we have a mechanism that turns MTs to artificial information strings [81, 82, 83]. Each kink-like soliton can be viewed as a bit of information whose propagation can be controlled by an external electric field! Nevertheless, while the ferroelectric phase can be useful for signaling and the assembly/disassembly of MTs, it is to "straight" for *information processing* and *computation*! For such operations one has to move to the spin-glass phase [29]. Detailed studies show [82] that as we increase the temperature above the critical one T_c, while keeping the electric field at appropriate small values, the coefficient A in (31) becomes negative, signaling the formation of a *metastable* phase, the spin-glass phase, before eventually reaching the naively expected *random* phase, where all dipoles are distributed randomly. To understand the existence and properties of the spin-glass phase better, it helps to notice that an MT, as a regular array of coupled local dipole states, can be mapped to an anisotropic two-dimensional *Ising model* [14] on a *triangular lattice*, so that the effective Hamiltonian is

$$H = -\sum j_{ik}\sigma_i\sigma_k \tag{34}$$

with the effective spin variable $\sigma_i = \pm 1$ denoting the dipole's projection on the MTs longitudinal axis, and the exchange constants j_{ij}, representing the interaction energy between two neighboring lattice sites, are given by

$$j_{ij} = \frac{1}{4\pi\epsilon}\left(\frac{3\cos^2\theta - 1}{r_{ij}^3}\right)p^2 \tag{35}$$

In (35), p is the dipole moment $p = qd$, where $d \approx 4$nm; r_{ij} is the distance between sites i and j, and θ is the angle between the dipole axis and the directions between the two dipoles. Explicit calculations using MT X-ray diffraction data, have succeeded to determine all relevant parameters (j_{ij}, θ, and r_{ij}) relevant to the MT system and be found in Ref. [82]. As is well-known [29], such a system is able to exhibit *frustration* in its ground state, *i.e.*, there will always be a conflict between satisfying all the *energy requirements* for the "+" bonds (two-parallel dipoles) and "−" bonds (parallel-antiparallel dipoles). That leads to the *spin-glass phase* where spin orientations are locally "frozen" in random directions due to the fact that the ground state has a multitude of equivalent orientations. For each triangle, reversing the spin on one side with respect to the remaining two leads to an equivalent configuration. In a MT with about 10^4 dipoles or dimers the degeneracy of the ground state is of the order of $6^{10.000}$, a very large number

indeed! Small potential barriers separating the various equivalent arrangements of spins play a fundamental role. Relaxation times are very long for the various accessible states giving them *long-term stability*! All these properties of the spin-glass phase makes it optimal for computational applications. The spin-glass phases allow easy formation of *local* ordered states, each of which carries some information content and is relatively stable over time. thus the perfect candidate for information processing and computation. It is highly remarkable that tubulin subunits in closely arrayed neural MTs (450 MT/μ^2) have a density of about 10^{17}tubulins/cm^3. very close to the theoretical limit for charge separation [89]. Thus, cytosceletal arrays have *maximal* density for information storage via charge. and the *capacity* for *dynamically coupling* that information to mechanical and chemical events via *conformational states* of proteins. Furthermore, the switch between the different phases (*ferroelectric, spin-glass* and *random*) is achieved through various physical means. *e.g.*, temperature or electric field changes. both within easily attainable physiological conditions! For example, as the intrinsic electric field is raised above. about 10^4V/m, easily attainable in MTs, the MT state switches from the spin-glass to the ferroelectric phase. While the similarities between the equations (34) and (17) as well as between the brain function phases of section 2 and the MT phases discussed here. are striking and rather suggestive, some further steps are needed before shouting *eureka*.

The treatment of MT dynamics [81, 82] presented above is based on *classical* (mean) *field theory*. For some physical issues this is an acceptable approximation. given the fact that MTs may sometimes have macroscopic dimensions. On the other hand, our main purpose would then evaporate. since the central issue of quantum coherence and its loss would remain mute and its relevance or not to brain function would remain unaswered. Usually, after the classical treatment of a system, one goes directly to *quantize* the dynamics of the system in a standard way. Alas. things here are not so easy. We have seen that there are very important, *dissipative. viscous* forces. due. for example, to the existence of water molecules that play a very important role in the support and propagation of classical kink-like solitons, but on the other hand, as is well-known, render the possible quantization of the dynamical system, rather impossible! Amazingly enough. very recently [7] together with N. Mavromatos we have been able to map the $1+1$ dimensional MT physical model discussed above to a $1+1$ dimensional *non-critical* string theory [90, 91]. the precursor of the $1+1$ black-hole model [50] discussed in section 5. Should we be surprised by such a mapping? Probably, not that much. To start with, there are not that many different theories in $1+1$ dimensions, and even seemingly completely different theories may belong to the same *universality class*, discussed in section 2. implying very similar physical, "*critical*" properties. In fact, the possibility of casting the $1+1$ dimensional MT dynamics in the. rather simple, double-well quartic potential form (31). stems from the well-known equivalence [14]between such a quartic potential and the one-dimensional *Ising model, i.e.*, interacting one-dimensional "spin" chains, similar to the MTs protofilaments! Furthermore, one can "derive" [92] a $1+1$-dimensional non-linear σ model (resembling the $1+1$ dimensional, *non-critical* string theory [90, 91]) as the infrared limit of the Heisenberg (anti)ferromagnet model (resembling the $1+1$-dimensional MT electret). The consequences of such a mapping of the $1+1$ MT dynamics on to a suitable $1+1$ *non-critical* string theory are rather far-reaching. All the interesting and novel results discussed in section 5. when appropriately translated. hold also true for the MT system. including the construction of a *completely integrable* $1+1$ dimensional model for the MTs. admitting *consistent* (mean-field) *quantization*. Furthermore. the *completely integrable* nature of the MT system. implying the existence of an "infinity" of quantum numbers labelling the states of the system (like the Black-Hole $W_{1+\infty}$ *hair* discussed in section 5). make it possible to store and eventually retrieve information in a *coherent way*. The practically infinite dimensional degeneracy of the spin-glass ground state. discussed above with its remarkable information processing/computation

abilities, is, of course, due to the available "infinity" of quantum numbers, characterizing the system. In any case, the *consistent quantization* of the MT-dynamics/system, make the possible appearance of large-scale coherent states, the MQS of section 2, not only plausible, but also feasible. But, as we discussed in detail in section 5, there is no "closed" system in Nature. Because of the *Procrustean Principle* [6], a concise, synoptic expression of the spacetime foam effects, all physical systems are rendered necessarily "open", and thus eventually "collapse". The MT system is no exception to the rule. On the contrary, the above discussed mapping of the 1+1-dimensional MT dynamics to a 1+1-dimensional *effective non-critical* string theory, as observed by N. Mavromatos and myself [7], simplify things considerably in this context too! After all, the central issue of section 5 was basically how to take into account s

More specifically, in the case of the MT system the *conformational, quantum* transitions of the dimers ($|\alpha\rangle - |\beta\rangle$)) create abrupt distortions of spacetime, thus enhancing the possibility of creation and annihilation of virtual, Planck-size black holes. The Planckian black holes interact with the MT system, through the global string states[3] (the W_2 *world* of (27)), which *agitate* the MT system in a *stochastic way*, as described by (23), but with a monotonic increase in entropy (26) supplying the MT system with a *microscopic arrow of time*, badly needed specifically in biological systems, while allowing for loss-free energy propagation (25). Furthermore, the W_2 global states lead to *synchordic collapse* (27) with a time period τ_c (29). While all these facts start painting a rather fascinating picture, one may justifiably wonder that the brain, being a hot, wet, noisy environment, is the complete *antithesis* of what is really needed for quantum effects to develop! In other words, even if we could be able to produce a macroscopic quantum state (MQS), would not be that *environmental effects* take over and "destroy" everything before any "useful" quantum effects take place? There are different ways/levels of answering this question in our framework here. The MT-dynamics, including viscous water and all, can be *mapped* to a *non-critical* string theory and as such MTs may be viewed as "open" systems obeying consistent quantum dynamics as contained in (23). One then is entitled, if so desired, to ignore completely the mapping, and just use (23) as a successful phenomenological equation describing the MT system, but with all parameters entering (23) determined appropriately by the *physical environment*. One then hopes to reproduce most of the interesting results mentioned above, without reference to the rather specific and detailed quantum gravitational framework used above. In principle, I don't see anythig wrong with such an *agnostic approach*, beyond losing some predictive power. Nevertheless, it should be stressed that the amazing shielding of the whole neuronal axon through the insulating coating of *myelin*, as discussed in section 4, and the whole astonishing fine paracrystalline structure of the MT network provide just the right environment for the fluorishing of quantum effects. One may even wonder if Nature, or more precisely *natural selection* supported throughout evolution, all these fine structures in a random, parasitic way or, as I believe, because they were needed to perform useful work. *Survival of the finest!*

It is encouraging that further studies of the MT dynamics strongly indicate that the MT's filamentous structure may be due to spontaneous symmetry breaking effects, a la superconductivity, and provided further evidence for the MTs' usefulness to support and sustain quantum coherence. Indeed, considering the layer of ordered water outside and inside MTs, Del Giudice, et. al.[93] proposed that the formation of MT's cylindrical structure from tubulin subunits may be understood by the concept of self-focusing of electromagnetic energy by ordered water. Like the Meissner (symmetry breaking) effect for superconducting media, electromagnetic energy would be confined inside filamentous regions around which the tubulin subunits gather. Del Giudice, et. al.[93] showed that this self-focusing should result in filamentous beams of radius 15nm, precisely the inner diameter of microtubules! Furthermore, Jibu,

---

[3] It should be remarked that the effective non-critical string picture advocated in Ref. [7], applies more generally to the case where the W_2-*world* does not correspond *necessarily* to Planckian states but describes complicated, yet unknown, biological effects in the brain.

et. al.[94], have proposed that the quantum dynamical system of water molecules and the quantized electromagnetic field confined inside the hollow MT core can manifest a specific collective dynamical effect called *superradiance* [95] by which the MT can transform *any incoherent, thermal* and *disordered* molecular, atomic or electromagnetic energy into *coherent photons* inside the MT. Furthermore, they have also shown [94] that such *coherent photons* created by superradiance penetrate perfectly along the internal hollow core of the MT as if the optical medium inside it were made "transparent" by the propagating photons themselves. This is the quantum phenomenon of *self-induced transparency* [96]. *Superradiance* and *self-induced transparency* in cytoskeletal MTs can lead to "*optical*" *neural holography* [1]. Neurons (and maybe other cells) may contain microscopic coherent optical supercomputers with enormous capacity. Thus Jibu, *et. al.*[94], suggest that MTs can behave as *optical waveguides* which result in coherent photons. They estimate that this quantum coherence is capable of superposition of states among MT spatially distributed over *hundreds of microns*! These in turn are in superposition with other MTs hundreds of microns away in other directions and so on...

It seems to me that we have accumulated enough evidence to safely assume that the MT structure and dynamics are not only, strongly supportive of the onset of long-range quantum coherence, but they are also very protective of quantum coherence, shielding it from standard physical environmental effects, modulo, of course, the menace of the spacetime foam. So, finally we have in place all the physical and biological facts needed to put forward our thesis about a *unified theory* of the Brain-Mind dynamics promised in the Introduction.

8 Microtubules and Density Matrix Mechanics (I): Quantum Theory of Brain Function

Let us assume that an "external stimulus" is applied to the brain. This, of course, means that some well-defined physical signal, presumably representing some form of information, interacts with the brain. The physical content of the signal (energy content, ...) starts to "straigthen up" the *relevant* regions of the brain, as analyses of EEGs, discussed in section 2, have shown [16]. In our picture, the detailed microstructure, both physical and biological, of the MT network entails that this "external stimulus" would initially *trigger/cause coherent* vibrations of the *relevant* part of the MT network. Eventually, it is most probable that the "*prepared*", by the external stimulus, quantum state of the system Ψ would be a quantum *superposition* of many states or many *alternatives*, all taking place at once. This is extremely likely to occur in the *spin-glass* phase with its huge degeneracy, thus basically allowing the *relevant part* of the MT network to perform many-many quantum (parallel) computations *at once*, while processing the data contained in the "external stimulus". After some time r_c, as given by (28) or (29), and because of the *global* or W_2-*world states* the *relevant* MT wavefunction would "*collapse*" to one specific state. The W_2-*world states* have forced the system to "decide" what it wants to be, by triggering it *to choose one* among many alternative states. Notice that since the MT network is rather *extensive*, from the "*sensory*" *cortex* to the *association cortex* to the *motor cortex* (see section 4), the whole process of *input→processing→output* is well-coordinated/correlated through the *magic* properties of the *chosen* quantum state. The dynamically *emerging*, due to *synchordic collapse* (see (22)) *chosen* state has all the desirable properties (see section 2), like long-term stability and non-locality, as being one of the many possible states of the spin-glass phase, to be of primary importance in *brain function* and "*decision making*"! Indeed as we have stressed numerous times by now, one of the most important functional roles of the MTs, is their strong involvement in *brain plasticity* and *exocytosis* (see sections 4.6). MTs control the shrinkage or growth of dendritic spines (*brain plasticity*) and by triggering the "*unlocking*" of the presynaptic vesicular grid.

thus allowing *one* vesicle to "fire" or emit its content of neurotransmitters towards the synaptic cleft, they control exocytosis. Certainly MTs are the *masters* of the *neurophysiological game*. The whole *neurophysiological response* to the "external signal" *depends* on the specific form of the *chosen* state of the *relevant part* of the MT network, which in turn, at least *partially* depends on the W_2-*world states* in a *stochastic way* (see sections 5,7). That is how, finally they may lead to *learning* or *memory recall* or, through the motor cortex, to *action*, or *nothing*, as discussed in sections 2,4,6. It should be stressed that the biological/physical properties of the MTs, as discussed in sections 6 and 7, are rather suggestive of their important role in the brain function. The very existence of the K-codes [57], related to the MT *conformational states*, which in turn are *strongly correlated* to *protein function* (see section 6) make it apparent that *everything*, from bioinformation transmission to memories lay down, to decision making, to movement, is *MT-driven*, and thus, as mentioned above, at least *partially, global states* or W_2-world states dependent! Actually, I cannot refrain from recalling here the analogy between *brain plasticity* and *quasicrystal growth* discussed in sections 3,4,6. In the case of quasicrystals, the ground state, *i.e.*, the state with *minimal energy*, is determined by employing many-many alternatives *at once, i.e.*, parallel "computations" of energy considerations *at once*, depending, of course, on the physical environment, *e.g.*, solvent, etc, until the quasicrystal grows enough, so that *synchordic collapse* occurs, with *one* final macroscopic state possible, the one that the experimentalists look at [12]! In the case of *brain plasticity*, including dendritic spine growth and shrikage, a very similar situation occurs, though now we are dealing with a much more involved situation where many *minimization conditions* have to be satisfied simulataneously, corresponding to the very complex nature of the brain, and thus in a way, make *imperative* the posssibility of *quantum computation*, as provided by the *MT network* in a *stringy modified quantum mechanics* or *density matrix mechanics framework*!

While the above emerging quantum theory of brain function has several suggestive and *qualitatively* sound features, it would be nice to be able to make some *quantitative statements* as well, in other words work out some predictions or even postdictions! Indeed, this is possible. To start with, in order for this new dynamical theory to "hold water" at all, we first have to check whether the very phenomenon of *exocytosis* is of quantum nature, as we claim, or whether it can be explained on the basis of statistical or thermal fluctuations. Well, the answer is on our favor. Ecccles [9] and Beck and Eccles [97] have shown that *exocytosis* is a *quantum phenomenon* of the presynaptic vesicular grid. They noticed that the synaptic vesicles forming an hexagonal array, are packaged between the presynaptic dense projections in a triangular array, composing the presynaptic vesicular grid, having *paracrystalline properties* [98]. Any similarity with the MT hexagonal paracrystalline structure is not accidental, since the *boutons* are the end points of MTs! There are about *10.000 vesicles* per synaptic unit or *bouton*, of which only (30-80) belong to the *"firing zone"* of the paracrystalline presynaptic vesicular grid [98] and of which, *only one* (1) "fires" about (5.000-10,000) neurotransmitter molecules, in a *probabilistic* ($\sim$ 0.3 − 0.4) way. Thus, the probability of quantum (vesicular) emission is a *holistic* property of the presynaptic vesicular grid of the bouton! Actually, they further noticed [9, 97] that this probability *is not a fixed number*, but can be increased or decreased by physiological or pharmacological treatment [99]! This is exactly what the doctor ordered. Indeed, one can *schematically* identify the *prepared state* Ψ, discussed with the one represented by (13), where the $|k\rangle_i$ refers now to the specific $|\alpha\rangle$ *or* $|\beta\rangle$ conformational state of the k-th tubulin dimer in the i-th relevant macroscopic (MT-network) quantum state, and N is the number of tubulins involved. Then, the system suffers *synchordic collapse*

$$|\Psi\rangle = \sum_i c_i\,|1\rangle_1\,|2\rangle_i \cdots |N\rangle_i \longrightarrow \rho w_1 = \sum_{i=1} p_i\,|1\rangle_i \cdots |N\rangle_i\,{}_i\langle N| \cdots {}_i\langle 1| \tag{36}$$

where ρ_{W_1} has been discussed in Section 5 (just above (23)), with the p_i denoting *probabilities* depending in an *stochastic way* on the W_2-*world states*. Since, the MT network extends all the way to the relevant vesicular grids, it becomes apparent that we expect a *synchordic, simultaneous* (EPR-like [22, 12]), *probabilistic* "firing" of all the *boutons* involved, triggering thus the appropriate standard neurophysiological action! Thus, not only do we expect *quantum exocytosis* to occur, but we also do expect to be able to *influence*, through the *stochasticity* brought by the *global* or W_2-*world states*, the probabilistic outcome, allowing thus for (see below) *free-will!* And indeed it is happening [9, 97, 98, 99]. So far so good. Another immediate prediction or natural expectation, that one has in this new dynamical theory, concerns the *time difference* between say an "*external order*" and "*action*". According to our new picture advanced here, there is some time-lapse between the input and the output, characterized *mainly* by τ_c, the quantum coherence lifetime, as given by (28),(29), *i.e.*, the time that takes for information processing and quantum computation. The way that (29) has been derived should make it clear that it was meant to apply in the MT network system! The only thing we are missing is the value of N. It seems to be a consensus, very rare in Brain Science, that the basic *module* of 10^4 neurons, discussed in section 4, should be able to "decide" something useful! In this case

$$N \approx 10^4 \frac{\text{neurons}}{\text{module}} \cdot 10^8 \frac{\text{tubulins}}{\text{neuron}} \cdot 10^5(Z_{\text{tubulin}})(10\% \text{ efficiency}) \approx 10^{16} \tag{37}$$

implying, when inserted in (29)

$$\tau_c^{\text{"Brain"}} \approx \mathcal{O}(1 \text{ sec}) . \tag{38}$$

a rather long time compared to the neuron cycle-time of about (1-2) msecs and to *neurosignal* velocity of about 100 m/sec, as discussed in section 4. Let me stress at this point that the rather long time of $\mathcal{O}(1 \text{ sec})$ should not be compared with *cerebellum* guided reflections, as discussed in section 4, of much smaller reaction time, since they have become of second nature and there is no "*thinking*" or "*decision making*" involved. For the skeptical reader, who may feel queasy with our philosophy to use the nucleon mass ($m_{\text{nucleon}} \approx 1$ GeV) as the fundamental mass unit (m) in (28) and thus yielding (29), we offer the following hopefully soothing remarks. It has been noticed in [7] that it is reasonable, in the case of an assembly of tubulin dimers as in microtubules, to assume that the pertinent moving mass is the effective mass M^* of the kink background. This effective mass M^* has been estimated to be [81] $M^* \approx 3m_{\text{nucleon}}$! By inserting now M^* as the fundamental mass unit in (28), where N denotes, in this interpretation, the number of tubulin dimers $N_T \approx 10^{12}$, as provided by (37), we get *again* $\tau_c^{\text{"Brain"}} \approx \mathcal{O}(1 \text{ sec})$! For yet another way, the third way of reproducing (38) see [7]. So, we feel kind of confident that (38) provides indeed a rather indicative, *canonical* value of the time lapse needed, in our scheme, for an "*event*" to be perceived *consciously*, under normal circumstances. Clearly, (28),(29) and (37) spell out *explicitly* the dependence on different parameters involved in getting 38) and thus enabling us to derive estimates for $\tau_c^{\text{"Brain"}}$ in circumstances different that the normal/canonical one discussed above. Individual *conscious events* may occur at different time scales depending on the number (N), effective mass (M^*), etc, of the tubulin dimers involved in the *prepared* coherent state Ψ (36). For example, the "γ-*oscillations*" (or "40 Hz *oscillations*") [33, 34] discussed at the end of section 4, *may be* due to the successive, synchordic collapses of an *extended* MT-network. Indeed, it is plausible that the *relevant* MT-network involves either a bigger number of, or longer, neurons than the *canonical* values used in (28),(29), (37) to yield (38), thus enabling us to get in this case $\tau_c^{\text{"Brain"}} \approx \mathcal{O}(1/50 \text{ sec})$, without much sweat and pain. It is too early yet, to get down to such specifics, and would be foolhardy to claim that everything has been explained! Simply, it does not seem inconceivable to be able to accomodate such "γ-*oscillations*" in our scheme, thus providing a microscopic, physical

explanation to the phenomenological Crick-Koch proposal [36, 32] that synchronized firing in the "γ-range" might be the neural correlate of visual awareness. Generalizing this notion to other "x-oscillations" we may naturally lead to the solutionof the *binding problem* or *unitary sense of self*! It is highly remarkable and astonishing the *synergy*, in our scheme, between *Planck scale physics, atomic and subatomic physics* providing the relevant parameters in (28), thus leading to (29), *and Neurobiology* (37), to eventually yield the estimate (38), seemingly in the right ballpark! Indeed, as discussed in sections 4 and 6, *learning* or *memory laydown*, closely related to *brain plasticity*, involving shrinkage or growth of dendritic spines are supposed to occur [100] within $O(seconds)$, in amazing agreement with our prediction (38)!

Further evidence that our prediction (38), and more generally, that our new quantum theory of brain is making sense relies upon rather complicated experiments, including clinical studies, that have been discussed in detail by Penrose [12, 3], so I will be rather concise. These are experiments that have been performed on *human subjects*, and have to do with the time that *consciousness* takes to act and to be enacted, *i.e.*, they are concerned with the *active* and *passive* role of *consciousness* respectively. In the first one, performed by Kornhuber, *et. al.*[101] on a number of human subjects volunteered to have electrical signals recorded at a point on their heads, *i.e.*, EEGs, and they were asked to flex their index finger of their right hands suddenly at various times, at *free-will*. Averaged over many trials, Kornhuber's experiments showed that the decision to flex the finger appears to be made a *full second* or even *1.5 seconds before* the finger is actually flexed. Furthermore, if *free-will* is replaced by reponse to the flash of a light signal, then the reaction time for finger flexing is, at least, five times shorter than the *free-will* one! In the second experiment, by Libet, *et. al.*[102], subjects who had to have brain surgery consented to having electrodes placed at points in the brain, in the somatosensory cortex. The upshot of Libet's experiment [102] was that when a stimulus was applied to the skin of the patients, *skin-touch*, it took about $O(second)$ before they were *consciously aware* of that stimulus, despite the fact that the brain itself would have received the signal of the stimulus in about 0.01 sec, and a pre-programmed "reflex" response to such a stimulus could be achieved by the brain in about 0.1 sec! Furthermore, cortical stimuli of less than $O(sec)$ are not perceived at all, and a cortical stimulus over $O(sec)$ is perceived from $O(sec)$ onwards! It is even possible that a cortical stimulus can even *"backward mask"* an earlier skin stimulus, indicating that *awareness* of the skin stimulus had actually not yet taken place by the time of cortical stimulus. The *conscious perception* can be prevented ("masked") by a later event, provided that the event occurs within $O(sec)$. In addition, when a cortical stimulation lasting for more than $O(sec)$ is followed by a skin stimulation, within the original $O(sec)$, *both signals* were perceived, but in *reversed order*! The subject would think that first was the skin-touch, followed by the cortical stimulation, *i.e.*, a *referal backwards in time* for the skin stimulus of about $O(sec)$. Though for the cortical stimulation, assumed to occur this time after the skin-touch, there is no *referal backwards in time*, implying that this is *not* simply an overall error in the internally perceived time. These are rather dramatic results with far-reaching consequences for the understanding of *consciousness* [103, 12, 3]. In our new dynamical theory they admit a rather simple and straightforward explanation. Indeed, the Kornhuber type experiments [101], concerning *active* consciousness, imply that indeed there is a time-lapse between input—output of about $O(sec)$ as suggested by (38), and not in the naively expected $O(msec)$ range from simplistic "neurosignal" analysis. One may imagine, as discussed in detail above, that the external stimulus, flex the finger at *free-will* in this particular case, sets the *relevant preconscious state* "*in gear*", and eventually, through the involvement of *global or W_2-world states*, the "collapse" of the wavefunction occurs, leaving only one specific state, the *conscious state*, that carry the order to *physiologically* flex the index finger! The strong correlation between *free-will* and the

global or W_2-world states should be apparent. Clearly, if *free-will* is replaced by *reflective response* to an external stimulus, then we expect much smaller reaction time, since basically there is no conscious thinking involved and thus the situation is very similar to cerebellum reflective actions. Concerning the Libet type experiments [102], involving *passive consciousness*, again we can provide simple explanations. Since it takes about $O(\text{sec})$ for *conscious perception* in our new dynamical theory, if the cortical stimulus is removed in time less than $O(\text{sec})$, we feel nothing, since presumably it did not succeed to "prepare" the *preconscious states*, thus it acts simply like random noise. On the other hand, if it lasts about $O(\text{sec})$, then it is able to "straighten" the *relevant* states up, and thus it is able to create *conscious perception*, that we "feel" it! On the other hand, the skin-touch, as more "real" and *effective*, would always felt after $O(\text{sec})$, *except* when, during the $O(\text{sec})$, a *relevant* cortical stimulus is applied that *eliminates* the skin-touch's efforts to "prepare" a *preconscious state and* let it "run" or "*compute*", to be more specific. In a way, since the cortical stimulus is applied before the "collapse" of the skin-touch related wavefunction, quantum superposition, even if it is approximate, suggests that indeed something like $|\Psi_{\text{skin-touch}} + \Psi_{\text{cort.stim.}}|^2 \approx 0$ is possible, thus providing a possible quantum explanation to the "*backwards masking*" effect! Concerning the *referal backwards in time* puzzle, one should recall that a *microscopic arrow of time*, presumably responsible for the *consciously perceived time ordering*, past, present, future, is *only* present in the EMN approach [5, 6, 51], and as such is strongly correlated with the spontaneous collapse. The skin-touch case as more "effective", involving more "mass"/"energy" movement in its process (*longest way*) may have a "collapse" characteristic time τ_c, as given in (29), smaller than the cortical stimulus case (*shortest way*), thus because $(\tau_c)_{s-t} < (\tau_c)_{c-s}$, *independently* of the time of their application, we always feel that the skin-touch occurred always first! A rather interesting application of the EMN approach [5, 6, 51]. Incidentally, if this new approach to brain dynamics is right, one may understand the famous X-*ism* phenomenon, referred to in section 4. The neurons seem to follow the principle of the *longest possible path*, because in such a case they *activate* the most "mass"/"energy" movement possible, thus *shortening* the "decision" time τ_c given by (28) or (29), thus contributing better to hierarchical and non-local actions of the brain. This kind of microphysical explanation is, of course, supportive of an evolutionary natural selection, where in this case survival of the fittest reads survival of the longest neuron ... It should not be very surprising that the modern man is around only 50,000 years and that the dawn of civilizations was about 10,000 years ago! It is a lot of fine-complicated structure to put together, starting from the very simple amoeba or paramecium and eventually evolving to humans with their extremely long microtubule networks.

Another very suggestive key feature, supporting further the eminent direct connection between coherent MT conformational oscillations and the emergence of *consciousness*, is the fact that *absence* of conformational oscillations, as caused by general anethesia molecules, leads to *loss* of consciousness [75, 3]. We have already discussed in section 6 the case of *reversible inhibition* of of paramecium's methachronal waves by chloroform [63]. *Metachronal waves* are paramecium's best shot for a conscious event! What about higher organisms? It is rather well-known that brains of patients under general anethesia are commonly quite active: EEG, evoked potentials and other brain functions persist despite lack of consciousness. In a way, general anethesia, at the right level, implies *absence* of consciousness. It has been suggested [75, 3] that, as *anesthetic gas* diffuse into individual nerve cells, their electric dipole properties (unrelated, in principle, to their ordinary chemical properties) can interrupt the actions of MTs. They interfere through weak Van der Waals forces, with the normal switching actions of the tubulins. "blocking" the crucial tubulin electrons, as discussed in section 6. It should be stressed that although there seems to be no generally accepted *detailed* picture of the action of anesthetics, it is widely believed that it is the Van der Waals

interactions of these substances with the conformational dynamics of the brain proteins that do the job. Here, the relevant brain proteins are identified with the tubulin dimers consisting the MT network. Such a detailed scenario for the workings of general anesthesia seem to explain easily some of its key features. For example, it is a rather remarkable fact that general anethesia can be induced by a large number of completely different substances of no chemical affinity whatsoever, e.g., from ether to chloroform to xenon! In our case it is just the electric dipole properties of these substances that need to be similar and not necessarily their chemical properties. Furthermore, if the general anesthesogon concentrations are not too high, complete reversibility or recovery of consciousness is achieved, indicating that the temporary Van der Waals "blocage" of the crucial tubulin electron has ended and conformational oscillations reoccur. On the other hand, general anesthetics, which are known to bind to micro-tubules, at high enough concentrations cause their depolymerization [104], implying in our picture partial or total *irreversible* loss of consciousness. It is also known that anesthetics may disrupt hydrophobic links among MAPs which interconnect MTs into functional coherent networks [105]. These, rather simple, in our framework, expla-nations of certain *puzzling* features of general anesthesia provide further positive evidence and credibility to our central thesis here, that MTs are the microsites of consciousness. We have argued before that quantum coherence in MT networks leads eventually, through synchordic collapse, to conscious events, while we see here that *systematic, organized, prevention* of quantum coherence, a la general anesthesia, leads to *loss* of consciousness!

It is remarkable how well the MT's biological/physical structure fits within the density matrix mechanics frame-work. We were able not only to derive several qualitatively interesting results, but as I showed above, we were able to get some highly desirable *numbers* too! Nevertheless, we should not be carried away and we should also not lose perspective of what we want to achieve, i.e., how the *whole* brain works and what is *consciousness*, etc. There is a cognitive hierarchy, and what we have showed is that the MT information processing may provide the basement level, implying that everything else is build upon it. The neuron synapse is the next layer up leading to yet another layer, the *neural synaptic network* or *module*, that it is able to operate cooperatively by utilizing dense interconnectedness, parallelism, associative memory and learning due to synaptic plasticity, as we explained above. At intermediate cognitive levels the motor and sensor *maps* represent the body and the outside world, while the next to highest cognitive level appears to be comprised of anatomically and functionally recognizable brain systems and centers (i.e., respiratory center, ...). The highest cognitive level is *global brain function*, which *correlates* with awareness, thought or *consciousness*. Clearly, this hierarchical structure is *susceptile* to *quantum treatment*, because of the very special dynamics that characterize the MT network. In a way, one may consider the conformational ($|\alpha\rangle$ or $|\beta\rangle$) states of the tubulin dimers assembled in microtubules, as the basic units of the quantum system. While the more evolved hierarchical structures comprised of neurons, modules, modules of modules, and, eventually the whole brain, may be viewed as the "measuring apparatus" providing the bulk of the "mass"/"energy" needed in *synchordic collapse*. Recall that, in the case if quantum mechanics discussed in section 3 (around (7)), it is only after the "collapse" of the wavefunction has occured that we are able to discuss with certainty, "observable" properties of the system. Likewise, in our case here, it is only after the *synchordic collapse* has occured that we can "*feel*" *consciously an event*. As we discussed above, it depends on the individual conscious event, i.e., on the specifics of the *relevant* MT-network involved, of how long is going to take before we "*feel*" it. Thus, we get in our scheme a dynamically organized *time-ordered* appearance of conscious events, corresponding to the synchordic collapse of the *relevant* MT-network involved, representing the very nature of the event under consideration. At each instant, and in a *cohesive way*, the "*sum*" of the conscious events consists of what we call *consciousness*! If

$c_i(t)$ refers to the i-th conscious event at time t, then consciousness C at time t may *symbolically* be represented by $C(t) = \sum_i c_i(t)$. This is how *consciousness emerges hierarchically* in our dynamical scheme. It looks like, at each moment, we "*read*" the outputs $(c_i(t))$ of the different "*microscopic measuring apparati*", we "*decide*" $(C(t))$ and we *proceed* accordingly, and so on, ad infinitum, meaning here our lifetime span! A very simplistic analogy would be the way we use the panel of our cars, with all its numerous indicators, showing us, at each moment, how we are doing with gas, oil, temperature, water, etc. and thus, "forcing" us to "decide" if we have to stop or not for gas, etc. As I mentioned above, while discussing the phenomenon of "*backwards masking*" and "*referal backwards in time*", *conscious time*, i.e., past, present, future make sense only when it refers to *conscious events*. In our scheme, conscious events are due to synchordic collapse which, as discussed in section 5, introduces a microscopic arrow of time, providing thus, naturally, time-ordering! It is amazing that the mechanism that we have proposed [52] to explain the origin and arrow of cosmic time, applies all the way down to the MT-networks, explaining the origin and arrow of consciousness. Putting it differently, in our scheme, the notions of cosmic and conscious time are naturally identified as one may naively expect, and as it was, since long, suspected.

So, we expect to see a kind of *fractal phenomenon* occuring in which we have quantum coherence (and synchordic collapse) extended over a MT, over hundreds of MTs comprising the neuron, over thousands of neurons comprising the module, over tens of modules (incidentally explaining the "40 Hz oscillations" discussed above and in section 4), etc. Actually, there is enough space in our dynamical, hierarchical scheme to accomodate *neural networks* [28, 27], attempts to use *synchronized neural firing* [33] in explaining the *binding problem* [36, 32], *and* eventually Neural Darwinism [25]. Eventually the whole brain is involved, one way or another, but coherently and in a correlated way, subjected to *synchordic collapse*, thus explaining the "*binding problem*" or the "*unitary sense of self*" problem. Furthermore, the *stochastic nature* of the synchordic collapse, due to the existence of the *global or W_2-world states*, provides a very plausible explanation of *free-will*.

In order to see how our new dynamical theory of brain function, spelled out in a rather detailed manner above, would work in practice, it would be interesting and perhaps amusing to present a very simple example. Let us consider (36), in the admittedly very unrealistic, case of only two superimposed quantum states: $\Psi = c_1(t)\Psi_1 + c_2(t)\Psi_2$, where Ψ_i stands for $|1\rangle_i |2\rangle_i \cdots |N\rangle_i$, and with $c_1(0) = c_2(0) = \frac{1}{\sqrt{2}}$. Then, if we denote by γ the synchordic collapse frequency ($\gamma \equiv 1/\tau_c$ (28)), and assume that the finally *chosen* state will be, say Ψ_1, then one may deduce that [42, 43] $|c_1|^2 = (1 + e^{-2\gamma t})^{-1}$. In Fig. 1., $|c_1|^2$ is plotted against time (t), for different values of γ, corresponding, in our scheme, to rather indicative *psychological* or *personality* states, providing thus our *psychological* or *personality profile*! Depending on the value of γ, the curves are *schematically* denoted as "*visible*", "*violet*", "*ultraviolet*", and "*infrared*". A common feature of all these curves is the increase with time of $|c_1|^2$, until it reaches some rather big (close to 1) value (say ≈ 0.9), at which point one safely may assume that synchordic collapse is occuring. At this moment, we pass from the *superimposed* $(c_1\Psi_1 + c_2\Psi_2)$ quantum state, identified here with the *preconscious state*, to the *chosen* (Ψ_1) state, identified here with the *conscious state* or *event*, i.e., we "*feel*" it! Fig. 1.(a) indicates a *normal psychological state*, in which things happen in a straightforward way as represented by the canonical, standard ("*visible*") value of $\gamma = 1$ Hz, corresponding to $\tau_c^{\text{"Brain"}} \approx \mathcal{O}(1\,\text{sec})$ (38). Fig. 1.(b) indicates *excitement* ("*violet*"), in other word things are happening quicker by involving, maybe, more tubulins (increase N in (37) and thus (28,29) increasing γ, say $\gamma = 2$ Hz or $\tau_c^{\text{"Brain"}} \approx \mathcal{O}(0.5\,\text{sec})$. Clearly, in this case there is less time for quantum computations, and maybe, not enough time for very wise "decisions", thus we may start acting a bit incoherent in the social sense! This case gets much worse in the presence of "stimulants", where

maybe many more than the usual tubulins get involved and thus the synchordic collapse frequency gets much bigger ("*ultraviolet*") disrupting, eventually, complete "collapse", as schematically indicated in Fig. 1.(c). In this "*high*" *state* [106], while we are "closer" to a coherent quantum superposition, we clearly act in a completely incoherent, and thus unacceptable, social way. On the other end of the *synchordic collapse* frequency sector, in the "*infrared*" limit, lies the *dream state* as indicated in Fig. 1.(d). Indeed, during our sleep, basically by definition, the brain is working in a very slow, subnormal mode entailing thus rather small values of γ (see Fig. 1.(d)). In such a case, a quantum superposition, initiated presumably in a *parasitic* way, may last much longer than a *normal state* case, and thus, eventually, may get lost in the *environmental* background, one way or another, before suffering our specific *synchordic collapse*, the agent of *conscious events*. That is why in most cases, we don't *remember* our dreams! Furthermore, as we all know, when we dream of someone, the person in the dream is usually a *mixture* of two or three rather similar people, read quantum superposition of *relevant* quantum states in our scheme, and eventually disappear without leaving any strong imprint in our memory, read absence of complete synchordic collapse in our scheme! Of course, it may happen, as in the case of not being quite asleep, that γ gets close to its "normal" value (*e.g.*, $\gamma \approx 0.9$ in Fig. 1.(d)), in which case complete synchordic collapse is achievable and we do, then, vividly remember our dream or nightmare! It is amazing and worth mentioning,that a similar, but phenomenologically postulated picture explaining the *Dream states*, or *Rapid-Eye-Movement* (REM) *sleep state*, has been put forward in Ref. [107],[32](p.161-2). There, words like "disturbed", "superimposed", "condensation" are used to describe *Dream states* in a generic way, without any reference to Quantum Physics. Here we see that such an explanation [107, 32] seems to emerge naturally from the quantum aspects of our dynamical scheme.

It should be strongly emphasized that in order to be able to provide positive evidence or refute our scheme, further experiments are badly needed and their results eagerly awaited. MT dynamics have to be studied in *vivo* and in *vitro*. We need to have a clear experimental picture about their assembly and disassembly properties, including their growth; we also need to have experimental information on which specific mechanism, if any, of the ones that have been suggested, is responsible for sustaining quantum coherence of the conformational states. We need further clinical studies of the "*funny*" time related phenomena. We also need to understand experimentally *and* theoretically, the role played by the K-code(s) in bioinformation processing, and their connection to the genetic code. Is it accidental that both codes have 64 words? Is it accidental that MT-networks look suspiciously similar to "quantum computers"? Can we use them in *vitro* for quantum computing? Is it accidental that microtubules, as participants in centrioles, are partially responsible for *mitosis* or cell division, thus "*interacting*" directly with the DNA, maybe thus being able to bring in *environmental information*, since MT-networks extend all the way to the cell membrane? Is it accidental that both *DNA* and MTs, the unique cellular structures known to posses a code system, are *effectively* 1+1 dimensional? Is it accidental that as we move from micro-organisms to macro-organisms, the amount/length of *normal* and *selfish or junk* DNA and the length of MTs do increase? Probably not, but we have to, and we are going to find out.

9   Microtubules and Density Matrix Mechanics (II): Quantum Psychophysics

Any scientifically sound theory of brain function, by its very nature, has not only to provide a credible picture of what is happening at the very microscopic (basic) level but it should also accomodate naturally all phenomena observed at the very macroscopic (top) level, *i.e.*, *personality* level as described by *psychology*. Psychology is usually

defined as the science of mental life, where the latter includes feelings. desires. intentions, cognitions, reasonings. decisions. and the like. It is advisable and useful. for our purposes here. to distinguish between *Jamesian psychology* [8]. or psychology of the *conscious*, and *Freudian*[4] *psychology* [108. 109] or psychology of the *unconscious*. I use here the term *Freudian psychology* instead of the. maybe. more proper one *psychoanalysis* for the following reasons. As defined by Freud [108], *psychoanalysis* falls under the head of psychology. not of medical psychology. nor of the psychology of the morbid processes. but simply psychology. Psychoanalysis is certainly not the whole psychology. but its substructure and perhaps its entire foundation (unconscious→conscious)! But. *psychoanalysis* is also a method of psychotherapy. *i.e.*, it consists of techniques for treating emotionally disturbed people. Since this last property of psychoanalysis is. commonly. the prevailing one. and since the therapy shouldn't swallow up the science. I prefer to stick to the term Freudian psychology. as the theoretical system. background of psychology. and view psychoanalysis strictly as a method of psychotherapy. We describe next the essentials of Jamesian psychology [8] and how they fit in (or are explained) within our scheme. which also seems able to accomodate the basics of Freudian psychology [108. 109]. *i.e.*, we will move from the *conscious* to the *preconscious* to the *unconscious*! The relevance of the connection of Jamesian views of consciousness to Copenhagen Quantum Mechanics has been *repeatedly* and *forcefully* emphasized by II. Stapp [13].

The brain-mind interaction is of central importance in Jamesian thought [8]. James opposed. vigorously, sterile. (pseudo)scientific. prevailing at his time, views purporting that feelings. no matter how intense that may be present can have *no causal efficacy* whatever. He counterattacked by making a positive argument for the efficacy of con- sciousness by considering its distribution. For James. consciousness is at all times primarily a *selecting agency*. being present when choices must be made between different possible courses of action [8]. Clearly, such distribution makes sense *only* if consciousness plays a role. one way or another. in making these selections. James went even further. developing his principal claim about the unity of each conscious thought [8]. It is the whole thoughts. he argued. that are the proper fundamental elements of psychology. not some collection of elementary components out of which thoughts are assumed to be formed by aggregation. In other words. even if each thought has components. these component thoughts are experienced together in a particular way that makes the experienced whole an essentially new *emerging* entity! He even had the courage to speculate that if all these properties were not to be born out of his contemporary physics (what we now call Classical Physics). physics has to be modified! All this activity was taking place in the 1890's!! [8] What a *wise* man. indeed. Coming back to the 1990's. it is stricking to notice that James views of consciousness are *mapped*. almost *one-to-one* to our dynamical theory of brain function. Our *central thesis* suggest. that every *conscious event* is the *psychological counterpart* of a *related*. specific *synchordic collapse event* in the brain. that triggers a specific neutral activity. described here by MT-dynamics. strongly correlated and *quantum computably*. responding to stimuli. An *isomorphism*, or a *one-to-one mapping* seems to emerge between *conscious events*. in a generic sense. and *specific neural patterns*, described by *specific* MT-networks, generated by. and thus strongly dependent on. synchordic collapse. By, just. recalling that it is synchordic collapse that causes the quantum MT-system to *"decide"* its course of action in a fundamentally *integrative character*. EPR-like [22, 3] way. and using the isomorphism available in our scheme. one should be able to reproduce. almost *verbatim*. the Jamesian views of consciousness. If. James' proposal about consciousness is not the mental or psychological version. or counterpart. of our physical/physiological views about consciousness. frankly. I don't know what would ever be. However. in order to complete our *isomorphism* between mental events and neural patterns described by MT-network states. we

---

[4]Sigmund Freud (1856-1939), founder of psychoanalysis and arguably the single most important figure in pointing out the role of *unconscious processes* in our behavior and feelings.

clearly have to discuss the preliminary phase that "prepares" the specific set of superimposed MT quantum states, of which only one is going to be selected or chosen. But then, we naturally have been led to the domains of the other great master of modern psychology.

Freud [108] felt that consciousness was only a thin slice of the total mind, that like an iceberg, the larger part of it existed below the surface of awareness. He said that scientific work in psychology will consist in translating unconscious processes into conscious ones, and thus filling the gaps in conscious perceptions! He argued that the personality is a complex and intricate energy system [109]. The form of energy that operates the personality and enables it to perform work is called psychic energy. He assumed that psychic energy comes from the energy of the body, but he was agnostic on how this transformation takes place. He insisted, though, that there is nothing mystical, vitalistic or supernatural about the concept of psychic energy [109]. It performs work as does any other form of energy, but in this case is psychological work, thinking, perceiving, and remembering. There is a continuously transformation taking place of bodily energy to psychic energy and viceversa.

A mental event is conscious or not, according to Freud [108, 109], depending upon the magnitude of energy invested in it and the intensity of the resisting force! A person feels pain or pleasure when the magnitude of the pain or pleasure exceed a certain catheris value which is called the threshold value. Likewise, (s)he perceives an object in the world when the perceptual process is energized beyond a threshold value. Sometimes even when the catheris exceed the treshold, the feeling or perceptions may not become conscious because of the inhibiting effects of an anti-catheris which prevents it from becoming conscious! Freud [108, 109] differentiated between two qualities of unconsciousness, the preconscious and unconscious proper. A preconscious state is one which can become conscious quite easily because of weak resistance, and in sharp contrast, to an unconscious proper state where the opposing force is rather strong! Actually, there is a continuous spectrum of unconsciousness. At the one end, ending at the unconscious proper state, there is memory that can never become conscious, because it has no association with language, while at the other end, including the preconscious state, there is memory which is "on the tip of the tongue".

Freud assumed that, since a relatively large concentration of energy in a mental process is required in order for it to become conscious, we can be conscious of only one thing at a time [109]. However, the rapid shifting of energy from one idea, memory, perception or feeling to another provides for a wide range of conscious awareness within a short time-lapse! The perceptual system is like a radar mechanism which rapidly scans and takes many quick pictures of the world. When the perceptual system discovers a needed object, or apprehends potential danger in the external world, it comes to rest and focuses its attention upon the object or danger. Ideas and memories, i.e., mental representations of past experiences, are summoned form the preconscious to help the person adjust to the situation confronting him. When the danger is past or the need is satisfied, the mind turns its attention to other matters [108, 109].

Concerning the nature of the "unconscious proper", Freud suggested [109] that "threatening" events could be repressed in memory so that they were not ordinarily available for conscious recall. Freud's analysis of repression, the selective inability to recall, is a form of Darwinism (survival of the fittest) as applied to the mental world to become the Freudian suppression of the "threatening". "Threatening" events belong to the set of the "unconscious proper events". Freud developed further [108, 109] a theory about the fate of the repressed events, connecting them, partially, to dreams! Dreams are filled with disguised or symbolic representations of repressed desires. When the disguise becomes too transparent, the dreamer usually wakes up. Anxiety dreams and nightmares, for example, are

caused by the emergence of repressed desires which makes the person anxious. He noticed that somatically. sleep is an act which reproduces intra-uterine existence,[5] fulfilling the condition of repose, warmth and absence of stimulus. The feature characterizing the mind of a sleeping person is an almost complete withdrawal from the surrounding world and the cessation of all interest in it. Freud pictured [109] the situation which leads to dream formation as follows: the *preconscious* dream-wish is formed. which expresses the *unconscious* impulse in the material of the *preconscious* day-residues. This dream-wish must be sharply distinguished from the day-residues. it need not have existed in waking life and it may already display the *irrational character. e.g.*, a person in the dream is the *mixture* of two or three rather similar people. etc. noticeable in all that is unconscious when we come to translate it into terms of consciousness! The logical validity, freshness. and stunning resemblance to our presently holding views about brain function. characterizing *Freudian psychology* [108, 109]. are properties very hard to miss. Since his time, ample evidence has accumulated from the study of neurosis, hypnotism. and parapraxes to show that his basic views about the action of the unconscious and its role in behavior, were essentially correct.

After our, hopefully, enjoyable and useful excursion to Freud-land, we have all that is needed to complete the above-discussed *isomorphism* between mental events and neural patterns, described by MT-quantum states. Freud's *psychic energy* as opposed to *bodily energy* and the transformation into each other. corresponds to the exchange of energy/interactions between the W_1-*world* or *attainable physical world localizable states* and the W_2-world or *global states*. as explicitly indicated in (27). Notice. as (25) explicitly shows. that there is *conservation of energy* in our scheme! Furthermore. the "preparation" of the *relevant superimposed* MT-quantum states depends on the *nature* and *intensity* of the stimulus, as discussed in sections 2.4,7.8. *i.e.*, if it can "easily" "straigthen up" the *relevant* states. corresponding to a *preconscious state*. or if. it can "hardly" have any effect on the states, corresponding to "unconscious proper" *states*. In the case of *preconscious states*. identifiable with the *relevant superimposed quantum states*. synchordic collapse follows easily, turning it into a *conscious state!* In the case of "unconscious proper" *states*. identifiable with either isolated, not easily reproduced. or random states, nothing happens! Clearly, there is a continous spectrum of quantum states from the "*preconscious*" to the "*unconscious proper*". In the case that an "unconscious proper" *stata* gets "prepared". then synchordic collapse leads to Freud's "threatening events". For example, while we sleep being "off guard", "unconscious proper" states may be partially and *parasitically* prepared. even in disguised form, and may lead to nightmares! On the other hand, synchordic collapse, of variable effectiveness. of presumably partially *parasitically prepared preconscious dream-states*, as discussed in the previous section (see Fig. 1.(d)) reproduces Freud's basic views about dream formation discussed above. If our dynamical theory of brain function. with its now completed *isomorphism* between mental events and MT-quantum dynamics states has not reproduced, almost *verbatim* the basic elements of Freudian psychology, I don't know what would ever do. Needless to say, Freud's terms are psychological. while ours are structural. It is in this sense that we consider the *mental world* somehow *isomorphic* to the W_2-*world of physical global states* that help to "*prepare*" and eventually dismantle. by "*synchordic collapse*". the *relevant superimposed* MT-quantum states of the W_1-attainable physical world constituted by tubulin-dimer conformational states, as depicted clearly in (2) and (27). It should be mentioned here (see relevant discussions in sections 6,8) the rather fundamental role played by the K-code(s) [57] possessed by the microtubules, in advancing and completing our *isomrphism* between the mental world and the W_2-world, by acting as a dictionary translating *psychological orders* into *physiological actions*. It is in this sense that I propose to call the K-code(s). the *Mental Code*, playing in a way the role of the *genetic code*. but in the mental world.

---

[5]There is. presently, evidence to suggest that in the *womb*, especially in the third trimester. *Dream or REM sleep* occurs more than 8 hours a day [107].

It should be stressed once more here (see the appropriate discussion in section 5, between (22) and (23), that there is nothing mystical or supernatural about the W_2 *world global states*, or the way they interact with the W_1-*world attainable physical states*, except that, due to their *delocalized nature*, sometimes, a bit different than normal, novel properties may emerge! Through the above mentioned *isomorphism*, these novel properties are transmitted to the mental world, which thus is an (*emerging*) part of the physical world, but with (*inherited*) distinct qualities. Notice further, that in particle physics at very high energies, we only talk about electroweak interactions, and only at low energies we may talk about "*effective*" electromagnetic and weak interactions. Similarly here and in a *unified theory* sense, we should talk only about the *physical world* (W) when *all states, localized* and *delocalized* are accounted for (2,27), and only talk about the *attainable physical world* (W_1) and the *mental world* and their interactions, *i.e.*, an *effectively emerging dual world* (1), *only* when the delocalized states get truncated, which happens realistically most of the time! Incidentally, if all these kind of (post) modern views sound pretty drastic, let me remind you that *Empedocles* (490-430 B.C.), the famous, ancient greek, presocratic philosopher, in his "cosmic phantasy", ascribed to the whole universe the same animistic principle as is manifested in each individual organism! If he was not describing, in his way, the W_2-world global, delocalized states. I don't know whatever would do better. He certainly was the first complete *effective* dualist! Hopefully, this emerging compromising resolution of the age-old problem concerning the brain-mind relation, will bring peace, once and for all, to the different quarters of *dualists* and *non-dualists*, and avoid further *duels*! Nevertheless, as I already mentioned in the Introduction (just after (2)), hard-core *materialists* may, if they so wish, concentrate their attention on the physical relation/transition between the W-*physical world* and the W_1-*attainable physical world*. It is *immaterial* to me!

The interface between psychology and physics (*psychophysics*) has always been rather interesting, thought-provoking, challenging, sometimes controversial, but certainly not dull. Before Darwin, man was set apart from the rest of the animal kingdom by virtue of having a soul. The evolutionary doctrine made man a part of nature, an animal among other animals. Man became an object of scientific study, no different save in complexity, from other forms of life. Literally at the same time (1860), Fechner founded the science of psychology, by showing that the mind could be studied scientifically and that it could be measured quantitatively. At about the same time, the physical formulation of the *principle of conservation of energy*, notably by Helmholtz, stating that energy is a quantity that can be transformed, but it cannot be destroyed, had rather far reaching consequences for biology and psychology. It made possible an even more radical view of man. This is the view that man is an *energy system* which obeys the same physical laws that regulate, say, the fall of an apple or electromagnetic phenomena. Thanks to Freud's genius, the physical dynamics extended to apply to man's *personality*, and not only to her/his body. This really amazing visionary step, as taken by Freud, led to *dynamical psychology* [108], *i.e.*, one that studies transformation and exchanges of energy within the *personality*, as well as between the *personality* and the body. It is an amusing coincidence to notice that Freud's chef d'oevre "*The Interpretation of Dreams*" [108], and Planck's revolutionary paper on energy quantization, *both* appeared in 1900 (!), and *both* after considerable hesitation and self-doubt!!! The dynamical scheme presented here, is nothing more than a supermodest attempt to continue the psychophysical tradition described above, by combining the most recent advances in quantum dynamics, as described in non-critical superstring theory [5, 6, 7], with the amazing progress in microtubules and their dynamics [1]-[4]. A *unified scheme* of brain-mind dynamics emerges, consistent with all known laws of physics, notably including the law of conservation of energy, and at the same time, providing satisfactory answers to age-old problems such as what is *consciousness*, the *binding problem* or *unitary sense of self, free-will* and the like, involving parts or the entire

activity of the brain. Indeed, *conscious thoughts* seem to correspond to metastable states of the brain associated with particular integrated patterns of neural excitations, that are *selected* by *synchordic collapse*, from among a plethora of such neural patterns described by MT-network states (quantum) mechanically generated according to (3.4). Since *synchordic collapse* is due to the truncation of *global delocalized* states, our *consciousness* is nothing else but a *localized* aspect of a global. integrative process. There is a new image of man emerging, in which human consciousness is placed in the inner workings of a non-local global process that link the whole universe together. defying classical physics and observations of usual everyday life. It seems, that we are *intimately* and *integrally* connected into the same global process that is actively creating the form of the universe, as we suggested in [52]. thus providing a whole new meaning to the. presently fashionable. expression *global village*. There seems to be a *central organizing principle* at work, essentially what I called *the Protean Principle* at the end of my review "As time goes by ..." [6]. This new view of man's place in the universe is an essential "*paradigm shift*". We are not *just* small. irrelevant, struggling for survival creatures in a meaningless universe, but through our dynamically created consciousness, *we participate actively* in the intrinsically global process that forms the world around us. *We are brains with strings attached!* I do believe that this, scientifically geared. "paradigm shift" in our *Weltanschauung*. or "world view", is bound to have a tremendous impact, but mostly presently unimaginable. in all forms of human behavior form the individual to the social level. Some visionary people have already started talking about the dawn of the *brain man*, at the dawn of *third wave* [110] of civilization. characterized by strongly declining muscle work and fastly increasing brain work, that succeeds the "*second wave*" related to the industrial revolution of 300 years ago. and which in turn succeeded the "*first wave*" related to the agricultural revolution of 10.000 years ago. This is just the *dawn* of the *Homo Quantum* ...

Acknowledgements

References

[1] S. R. Hameroff. *Ultimate Computing: Biomolecular Consciousness and Nanotechnology* (North-Holland, Amsterdam, 1987). *and* Journal of Consciousness Studies, 1 (1994) 91.

[2] P. Dustin, *Microtubules* (Springer-Verlag. New York, 1984), second edition; V. Meininger and S. Binet. International Review of Citology, 114 (1989) 21.

[3] R. Penrose. *Shadows of the Mind* (Oxford University Press, Oxford. 1994).

[4] S. R. Hameroff and R. Penrose. paper to appear.

[5] For reviews see: J. Ellis, N. Mavromatos, and D. V. Nanopoulos, in Proceedings of the International Symposium on Black Holes. Membranes, Wormholes, and Superstrings. edited by S. Kalara and D. V. Nanopoulos (World Scientific. Singapore 1993). p 51; in *Recent Advances in the Superworld*. Proceedings of the HARC Workshop, edited by J. L. Lopez and D. V. Nanopoulos (World Scientific, Singapore 1994). p. 3 (hep-th/9311148); to appear in Proceedings of the International School of Subnuclear Physics 31th Course. Erice, July 1993 (hep-th/9403133); in Proceedings of the First International Conference on "Phenomenology of Unification from Present to Future", Rome, March 1994 (hep-th/9405196).

[6] For a non-technical (*as possible*) account see: D. V. Nanopoulos, "*As time goes by ...*", Rivista del Nuovo Cimento. 17 No. 10 (1994).

[7] N. Mavromatos and D. V. Nanopoulos, "*Non-critical String Theory Formulation of Microtubule Dynamics and the Quantum Origin of Consciousness*, CERN-TH/95-127.

[8] W. James. *The Principles of Phychology*. 1890. Reprinted (Dover, New York. 1950), and "Does Consciousness exist?" in the *Writings of William James*, edited by J. J. McDermott (University of Chicago Press, Chicago. 1977) p. 169-83.

[9] J. C. Eccles, Proc. R. Soc. Lond. B227(1986) 411; A. Fogelson and R. Zucker, Biophys. J. 48 (1985) 1003.

[10] J. D. Watson, *Molecular Biology of the Gene* (W. A. Benjamin, Menlo Park, CA. 1976).

[11] L. M. Ricciardi and H. Umezawa. Kybernetic 4 (1967) 44; C. I. J. M. Stuart, Y. Takahashi, and H. Umezawa, Journal of Theoretical Biology 71 (1978) 605 *and* Foundations of Physics 9 (1979) 301.

[12] R. Penrose. *The Emperor's New Mind* (Oxford University Press, Oxford. 1989).

[13] H. P. Stapp, *Mind, Matter and Quantum Mechanics* (Springer-Verlag, New York. 1993).

[14] N. Goldenfeld, *Lectures on Phase Transitions and the Renormalization Group* (Addison-Wesley, New York. 1992).

[15] E. R. John. Science 177 (1972) 850; E. R. John, F. Bartlett, M. Shimikochi, and D. Kleinman, Journal of Neurophysiology 36 (1973) 893; F. Bartlett and E. R. John, Science 181 (1973) 764; E. R. John, in *The PsychoBiology of Consciousness*, ed. by R. J. and J. M. Davidson (Plenum Publishing Corporation, New York, 1980) p. 129.

[16] B. McA. Sayers, H. A. Beagley, and W. R. Henshall, Nature 247 (1974) 481; B. McA. Sayers and H. A. Beagley, Nature 260 (1976) 461.

[17] C. Darwin. *On the origin of species by means of natural selection or the preservation of favoured faces in the struggle for life* (Murray, London, 1859).

[18] J. D. Watson and F. Crick, Nature 171 (1953) 737, *ibid* 964.

[19] E. Chargaff. *Experientia* 6 (1950) 201; Fed. Proc. 10 (1951) 654; J. Cell. Comp. Physiol. 38 (1951) 41.

[20] For a readable and enjoyable account of the basics of quantum mechanics see: R. P. Feynman, R. Leighton, and M. Sands, *The Feynman Lectures on Physics*, Volume III (Addison-Wesley, 1963).

[21] W. Heisenberg, Zeitschr. Phys. 43 (1927) 172.

[22] A. Einstein. B. Podolsky, and N. Rosen. Phys. Rev. 47 (1935) 777.

[23] For a review see: A. Aspect and P. Grangier. "Experiments on EPR-type correlations with pairs of visible photons", in *Quantum Concepts in Space and Time*, edited by R. Penrose and C. J. Isham (Oxford University Press, 1986).

[24] E. R. Kandel and J. H. Schwartz. *Principles of Neural Sciences* (Appleton and Lange, Norwalk, Conn, 1991). 3rd edition; V. Braitenberg and A. Shulz. *Anatomy of the Cortex* (Springer-Verlag, Berlin, 1991).

[25] G. M. Edelman. *Bright air, brilliant fire* (BasicBooks, New York, 1992).

[26] D. O. Hebb. *The organization of behavior* (Wiley, New York, 1949), and *Essay on Mind* (Lawrence Erlbaum Associates, Hillsdale, N.J. 1980).

[27] For an introductory book see: T. Khanna. *Foundations of Neural Networks* (Addisson-Wesley, 1990).

[28] J. J. Hopfield. Proc. Nat. Acad. Scien. USA 70 (1982) 2554, *ibid* 81 (1984) 3088; Phys. Today, 47 (February 1994), p. 40, and reference therein.

[29] M. Mézard, G. Parisi. and M. Virasoro, *Spinglass theory and beyond* (World Scientific, Singapore, 1987); D. J. Amit. *Modeling brain function* (Cambridge University Press, Cambridge, 1989); D. L. Stein, *Spin glasses in biology* (World Scientific, Singapore, 1992).

[30] R. Descartes. *Meditations on first philosophy*, ed. S. Tweyman (Routledge, London, 1993), from the original *Medidationes de prime philosophia* (Paris, 1641).

[31] P. M. Milner, Phychol. Rev. 81 (1974) 521; C. Von der Marlsburg and W. Schneider. Biol. Cybern. 54 (1986) 29.

[32] F. Crick. *The Astonishing Hypothesis* (Charles Scribner's Sons, New York, 1994).

[33] C. M. Cray and W. Singer, Proc. Nat. Acad. Sci. USA 86 (1989) 1698; R. Eckhorn, *et. al.*, Biol. Cybern. 60 (1988) 121; C. M. Cray, *et. al.*, Nature 338 (1989) 334; A. K. Engel, *et. al.*, Proc. Nat. Aca. Sci. USA 88 (1991) 6048 and Science 252 (1991) 1177.

[34] For a review see: W. Singer, Ann. Rev. Physiol. 55 (1993) 349.

[35] C. Madler and E. Poppel, Naturwissenschaften, 74 (1987) 42; G. Plourde and T. W. Picton, Anesth. Analg. 71 (1990) 460.

[36] F. Crick and C. Koch, Semin. Neuroscien. 2 (1990) 263; C. Koch, Current opinion in neurobiology, 3 (1993) 203; F. Crick and C. Koch, Scient. Amer., September 1992, p. 111.

[37] See for example, M. Kaku, *Quantum Field Theory* (Oxford University Press, Oxford, 1993).

[38] For a readable account see: S. W. Hawking, *A Brief History of Time* (Bantam Books, New York, 1989).

[39] S. Hawking, Comm. Math. Phys. 43 (1975), 199.

[40] J. Bekenstein, Phys. Rev. D12 (1975), 3077.

[41] S. Hawking, Comm. Math. Phys. 87 (1982), 395.

[42] J. Ellis, J.S. Hagelin, D.V. Nanopoulos and M. Srednicki, Nucl. Phys. B241 (1984), 381.

[43] J. Ellis, S. Mohanty, and D. V. Nanopoulos. Phys. Lett. B 221 (1989) 113, *ibid* B 235 (1990) 305.

[44] See for instance, M.B. Green, J.H. Schwarz and E. Witten, *String Theory*, Vol. I and II (Cambridge Univ. Press 1986).

[45] J. Ellis, N.E. Mavromatos and D.V. Nanopoulos, Phys. Lett. B267 (1991), 465; *ibid* B272 (1991), 261; *ibid* B276 (1992), 56; Phys. Lett. B278 (1992), 246; Phys. Lett. B284 (1992), 27, 43; Phys. Lett. B288 (1992), 23; Phys. Lett. B289 (1992), 25; Phys. Lett. B296 (1992), 40.

[46] Y. Aharonov and D. Bohm, Phys. Rev. 115 (1959) 485.

[47] L. M. Krauss and F. Wilczek, Phys. Rev. Lett. 62 (1989) 1221.

[48] For a review see, C. Pope, L. Romans, and X. Shen, in *Strings 90*, edited by R. Arnowitt, et. al. (World Scientific. Singapore 1991), p. 287.

[49] S. Chaudhuri and J. Lykken, Nucl. Phys B396 (1993), 270.

[50] E. Witten, Phys. Rev. D44 (1991). 314.

[51] J. Ellis. N.E. Mavromatos and D.V. Nanopoulos, Phys. Lett. B293 (1992), 37.

[52] J. Ellis, N.E. Mavromatos, and D. V. Nanopoulos, CERN-TH.7480/94 (hep-th/9503162).

[53] B. Misra, I. Prigogine and M. Courbage, *Physica* A98 (1979), 1; I. Prigogine, *Entropy, Time, and Kinetic Description*, in *Order and Fluctuations in Equilibrium and Non-Equilibrium Statistical Mechanics*, ed G. Nicolis et al. (Wiley, New York 1981); B. Misra and I. Prigogine, *Time, Probability and Dynamics*, in *Long-Time Prediction in Dynamics*, ed G. W. Horton, L. E. Reichl and A.G. Szebehely (Wiley, New York 1983); B. Misra, *Proc. Nat. Acad. Sci. U.S.A.* 75 (1978), 1627.

[54] R. M. Santilli, Hadronic J. Vol. I, pages 223, 574 and 1279 (1978); *Foundations of Theoretical Mechanics*, Vol. I (1978) and II (1983), Springer-Verlag, Heidelberg/New York; *Lie-admissible Approach to the Hadronic Structure*, Vol. I (1978) and II (1982), Hadronic Press, Palm Harbor, Fl,; see also J. Fronteau, A. Tellez-Arenas and R.M. Santilli, Hadronic J. 3 (1979), 130; J. Fronteau, Hadronic J. 4 (1981), 742.

[55] V. Kaplunovsky, Nucl. Phys. B 307 (1988) 145; erratum B382 (1992) 436; I. Antoniadis, J. Ellis, R. Lacaze, and D. V. Nanopoulos, Phys. Lett. B 268 (1991) 188; S. Kalara, J. L. Lopez, and D. V. Nanopoulos, Phys. Lett. B 269 (1991) 84.

[56] F. Crick, *What a mad pursuit* (BasicBooks, New York, 1988).

[57] D. L. Koruga, Annals of the N.Y. Academy of Sciences, 466 (1986) 953; Biosystems, 23 (1990) 297; Nanobiology, 1 (1992) 5.

[58] J. R.Lakowicz and G. Weber, Biochemistry 12 (1973) 4171.

[59] R. D. Erickson, Science 181 (1973) 705.

[60] J. Leech, Canad. J. Math 10 (1964) 657; J. Leech and N. J. A. Sloane, Can. J. Math. 28 (1971) 718; F. J. MacWilliams and N. J. Sloane. *The theory of error correcting codes: 674* (North Holland, Amsterdam, 1977); N. J. Sloane, Sci-ent. Amer. 250 (1984) 116.

[61] L. Sagan, J. Theor. Biol. 14 (1967) 225.

[62] C. S. Sherrington. *Man on his nature* (Cambridge University Press, Cambridge 1951) second edition.

[63] B. Parducz. Acta Biol. Acad. Scien. Hung. 13 (1962) 299.

[64] J. Atema, J. Theor. Biol. 38 (1973/4) 181.

[65] J. Cronly-Dillon, D. Carden, and C. Birks, J. Exper. Biol. 61 (1974) 44.

[66] R. Mileusnic, S. P. Rose, and P. Tillson, Neuro. Chem. 34 (1980) 1007.

[67] D. Moshkov, et. al., Acta Histochemica Supp-Band. XLI (1992) 241.

[68] G. Bensimon and R. Chernot, Pharmacol. Biochem. Behavior. 38 (1991) 141.

[69] S. S. Matsuyama and L. F. Jawik, Proc. Nat. Acad. Scie. USA 86 (1989) 8152.

[70] V. M. Y. Lee, B. J. Balin, L. Otvos, and J. Q. Trojanowski, Science 251 (1991) 675.

[71] For further references and a report on recent developments see W. Roush, Science 267 (1995) 793.

[72] S. E. Arnold, V. M. Y. Lee, R. E. Gur and J. Q. Trojanowski, Proc. Nat. Acad. Sci. USA 88 (1991) 10850.

[73] R. F. Curl and R. E. Smalley, Scient. Amer. 265 (1991), No. 4, 32.

[74] H. Fröhlich. Inter. Jour. Quant. Chem. 2 (1968) 641; Nature 228 (1970) 1093; Proc. Nat. Acad. Sci. USA 72 (1975) 4211; in *Modern biochemistry.* ed. by F. Guttmann and H. Keyzer (Plenum Press, New York, 1986) p. 241: see also: *Neural Network World,* 4 (1994) No. 3 issue that contains a series of articles devoted to Fröhlich's hypothesis.

[75] N. P. Franks and W. R. Lieb. Nature 300 (1982) 487; S. R. Hameroff and R. C. Watt, Anest. Analg. 62 (1983) 936.

[76] L. Genberg, et. al., Science 251 (1991) 1051.

[77] W. Grundler and F. Keilmann. Phys. Rev. Lett. 51 (1983) 1214.

[78] C. Neubauer. ct. al., Bioelectromagnetics. 11 (1990) 261.

[79] L. Genzel, et. al., Biopolymers, 22 (1983) 1715.

[80] P. Vassilev. et. al., Bioch. Biophys. Res. Comm. 126(1) (1985) 559.

[81] M. V. Sataric. J. A. Tuszyński and R. B. Zakula, Phys. Rev. E48 (1993) 589.

[82] J. A. Tuszyński, et. al., paper to appear in J. Theor. Biol. (1995).

[83] S. R. Hameroff and R. C. Watt. J. Theor. Biol. 98 (1982) 549; S. Rasmussen, et. al., Physica D42 (1990) 428.

[84] R. Melcki. et. al., Biochem. 28 (1989) 9143; S. N. Timasheff, et. al., J. Cell Biol. 107 (1988) 243.

[85] M. A. Collins. et. al., Phys. Rev. B19 (1979) 3630.

[86] P. Lal. Phys. Lett. A111 (1985) 389.

[87] T. Horio and H. Hotani. Nature 321 (1986) 605.

[88] T. Mitchison and M. Kirschner. Nature 312 (1984) 232, *ibid* 237. *and* Cell 45 (1986) 329; H. Hotani. et. al., Nanobiology 1 (1992) 61; Y. Engelborghs. Nanobiology 1 (1992) 97.

[89] F. Gutmann, in *Modern Biochemistry,* ed. by F. Gutmann and H. Keyzer (Plenum Press, New York, 1986).

[90] I. Antoniadis, C. Bachas, J. Ellis and D.V. Nanopoulos. Phys. Lett. B211 (1988). 393; Nucl. Phys. B328 (1989). 117; Phys. Lett. B257 (1991). 278.

[91] D.V. Nanopoulos, in *Proc. Int. School of Astroparticle Physics.* HARC-Houston (World Scientific. Singapore. 1991). p. 183.

[92] N. Dorey and N. E. Mavromatos, Nucl. Phys. B 386 (1992) 614; N. Mavromatos. Nucl. Phys. B (Proc. Suppl.) 336 (1993) 145.

[93] E. Del Giudice. et. al., Nucl. Phys. B 275[FS 17] (1983) 185.

[94] M. Jibu. et. al., Biosystems 32 (1994) 195.

[95] R. H. Dicke. Phys. Rev. 93 (1954) 99.

[96] S. L. McCall and E. L. Hahn. Phys. Rev. Lett. 18 (1967) 908.

[97] F. Beck and J. C. Eccles. Proc. Nat. Acad. Sci. USA 89 (1992) 11357.

[98] K. A. Kert.K. Peper, and C. Sandri, in *Cholinergic Mechanisms.* ed. P. G. Waser (Raven Press. New York. 1975) p. 43; A. Triller and H. Korn. J. Neurophysiol. 48 (1982) 708.

[99] J. J. Jack. S. J. Redman, and K. Wong. J. Physiol.. Lond. 321 (1981) 111; G. D. S. Hirst, et. al., J. Physiol.. Lond. 321 (1981) 97; H. Korn and D. S. Faber, in *New insights into synaptic function.* ed. by G. M. Edelman, W. E. Gall, and W. M. Cowan (Wiley. New York, 1987) p. 57.

[100] E. R. Kandel. *The cellular basis of behavior* (Freeman. San Francisco, 1976).

[101] L. Deeke, B. Grötzinger, and H. H. Kornhuber, Biol. Cybernetics. 23 (1976) 99; for more recent experiments and their implications see: B. Libet, in *The principle of design and operation of the brain* ed. by J. C. Eccles and O. D. Creutzfeldt. Experimental Brain Research series 21 (Springer-Verlag, Berlin. 1990) p. 185; B. Libet. *Reveu de Métaphysique et de Morale* 2 (1992) 255.

[102] B. Libet, et. al.. Brain 102 (1979) 193.

[103] E. Harth. *Windows on the Mind* (Harvester Press. Hassocks. Sussex, 1982).

[104] A. C. Allison and J. E. Nunn. *The Lancet* 2 (1968) 1326.

[105] S. A. Lewis, et. al.. Nature 342 (1989) 498.

[106] *The Beatles.* "With a little help from my friends". in *Sgt. Pepper's Lonely Hearts Club Band* LP (EMI. London. 1967).

[107] F. Crick and G. Mitchison. Nature 304 (1983) 11 and J. Mind Behav. 7 (1986) 229.

[108] S. Freud. *The Standard Edition of the Complete Psychological Writings.* Vol. 1-24 (Hogarth Press. London. 1953-1974).

[109] For a concise, readable. and stimulating account of the basics of Freudian psychology see. C. S. Hall. *A Primer of Freudian Psychology* (Mentor. New York, 1979); for much of the best that Freud wrote on psychological theory in a concise volume see. S. Freud, *General Psychological Theory* (Collier Books. New York. 1963).

[110] A. and H. Toffler, *War and Antiwar* (Warner Books Inc.. New York. 1995).
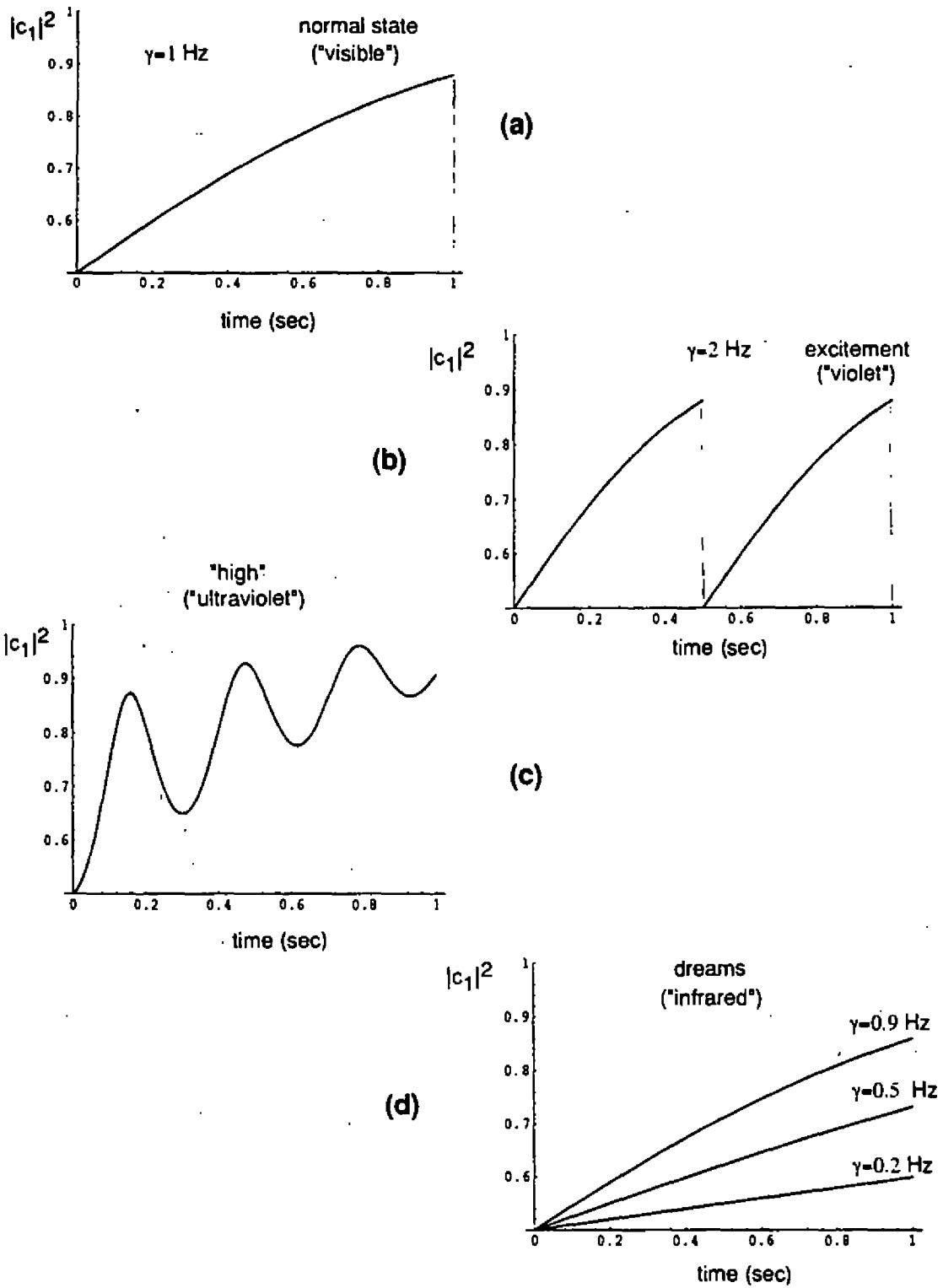
Figure 1.: *Psychological* or *Personality* profile as a function of time, parametrized by different values of the MT-network synchordic collapse frequency γ ($\equiv 1/\tau_c^{\text{Brain}}$), as indicated in (a) through (d).

Event Generators in Particle Physics

Torbjörn Sjöstrand*

Theory Division, CERN, CH-1211 Geneva 23, Switzerland

This presentation gives an introduction to the topic of event generators in particle physics. The emphasis is on the physics aspects that have to be considered in the construction of a generator, and what lessons we have learned from comparisons with data. A brief survey of existing generators is also included. As illustration, a few topics of current interest are covered in a bit more detail: QCD uncertainties in W mass determinations and $\gamma p/\gamma\gamma$ physics.

1 Introduction

The ultimate goal of particle physics is to find and understand *the* underlying theory of the Universe. Experimental progress in this direction requires exploration at ever higher energies. This way one hopes to gain access to new particles and reactions not allowed at lower energies, to observe hints of symmetries that are spontaneously broken at some high energy scale, and to profit from a smaller $\alpha_s(Q^2)$. The latter point also implies a reduced dependence of non-perturbative physics, such as confinement and hadronic wave functions, that are not all too well understood. Experimental data are consistent with the hypothesis that, above some grand unification scale, the three couplings of the standard model come together (at least if supersymmetry is included in the game) [1]. So it is no wonder that theorists' folklore says that physics is simpler at higher energies.

From an experimental point of view, this is all wrong. If the energy of a process is increased, the amount of cascading is also increased. With cascading I here mean, in a very broad sense, all the mechanisms that increase the number of quanta that are needed to describe the event as times goes by: decays of exotic new particles or the familiar W and Z resonances, initial- and final-state QCD parton showers, fragmentation mechanisms that turn partons into hadrons, and decays of ordinary unstable particles. The lower cut-off of the cascading is given essentially by the pion mass, independently of the full energy of the process. So higher energies means a larger energy range over which cascading can occur, i.e. higher multiplicities, and thus larger experimental challenges.

The evolution of experimental particle physics is therefore towards larger complexity. In the fifties and sixties, the emulsion and bubble chamber data of the time showed every single vertex of the processes studied, usually with two or three outgoing particles. Around 1980, the turn-on of higher-energy e^+e^- and $\bar{p}p$ colliders gave events with tens of charged particles, sometimes even above 100. When we today plan ahead for the LHC, the expected average charged multiplicity per event is above 100. At nominal luminosity, with around 20 events overlayed in each single beam crossing, any physics will have to be dug out among 4000 charged or neutral particles!

There are ways to get back to some kind of simplicity. One is to consider (semi-) inclusive quantities, such as jets, where a set of particles is characterized just by a summed energy and a direction vector. These jets approximate the partons of a simpler perturbative description, but with a non-negligible smearing that has to be understood for precision physics. Another is to search only for especially clean (parts of) final states. As an example, a 200 GeV Higgs particle can decay into two Z^0's, each of which can subsequently decay to a lepton pair. So the observation

---

of events with four well isolated leptons, with invariant mass distributions peaked in the appropriate places, would provide clear evidence for new physics. However, there is a price to be paid, in that the clean states normally have small branching ratios. When we search for a process that is rare in the first place, this may not always be acceptable. Combine this with an unrealistic definition of 'isolation' of leptons among 4000 other particles, and a promising signal may be gone. Remove the isolation criterion, and leptons from the decays of top quarks and bottom mesons will completely overwhelm the new physics. It then becomes imperative to understand the finer details of detector acceptance and resolution, to devise an analysis strategy that cuts away these backgrounds without too much of a loss to the signal.

As we see, it is seldom possible to avoid all the complications of high-multiplicity events. Furthermore, even if we firmly believe in QCD today, it is somewhat embarrassing that we know so little about how confinement really works. After all, this is a unique chance that the standard model provides us with to study strong-coupling physics! One line of approach is to devise models that allow various aspects of confinement to be tested by a judicious analysis of data. The foremost place where the two aspects above (experimental demands and theoretical curiosity) come together is event generators.

2 Event Generator Survey

In real life, an accelerator provides events. These events are registered in a detector as electronics signals. A data acquisition system stores a digitized and compressed version of the information, often only for the 'promising' part of the full event rate. In an event reconstruction program, the digitized electronics signals are turned back into a list of particle momenta and charges. The reconstructed events can then be used for physics analysis.

In the 'virtual reality' world, event generators take the rôle of the accelerator in providing the events. The response of the detector is then modelled in a detector simulation program. The most frequently used such program is GEANT [2]. This program provides an output in a format identical to that of the experimental data acquisition system, except that the original physics event input is also kept for later reference. Therefore the same reconstruction programs can be used, and the same physics analysis strategies. Comparisons between real data and simulated data form an important ingredient for the final results that can be published.

While event generators are not always as fast as desirable, the real bottleneck is detector simulation, where (for some applications) it is necessary to trace hadronic and electromagnetic shower evolution in excruciating detail. For many studies it is therefore common to jump directly from the event generator to the physics analysis. Detector effects are then completely neglected, or simulated by simple geometrical cuts and rule-of-thumb smearing of momentum vectors.

The phenomenologist is not normally concerned with the detector-specific aspects, and therefore may use the event generator as it is to explore various potentially interesting aspects. He/she might, for instance, introduce 'crackpot' alternative models just to check whether one should expect any testable consequences.

The description above may help illustrate why generators are useful. Let us try to give a somewhat more formalized list, subdivided by interest group. For the event generator author

- it allows theoretical studies of very *complex* multiparticle physics, by a subdivision of the complete problem into more manageable subtasks;
- it gives a larger flexibility in the spectrum of physical quantities that can be studied (no need to worry whether an observable is infrared finite or not in perturbative QCD);
- it provides a vehicle for the dissemination of interesting theoretical ideas to the experimental community;
- it allows a larger feedback from the experimental community, and hence a faster path for improved under-

standing of the underlying physics; and

- it is a source of fun and satisfaction (for some of us) to attack the non-trivial challenges.

For the experimental physicists (and many phenomenological ones as well), an event generator can be used

- to predict event rates and topologies, and hence to estimate the feasibility of an intended physics study in the first place;

- to simulate possible backgrounds, and hence to devise analysis strategies that optimize signal-to-background ratios;

- to study detector requirements, and hence to optimize the detector design and trigger strategy; and

- to study detector imperfections, and hence to evaluate acceptance corrections.

To the lists above, a final point should be added: nature is random! We are all familiar with the quantum mechanical uncertainty principle, with the principle of superposition, with the collapse of the wave function at measurements, and so on. What this means is that each event is unique. Had we had a perfect understanding of QCD, and infinite computing power, it would still have been a formidable task to enumerate all possible hadronic final states allowed, e.g. at LEP, as a function of the complete setup of all quantum numbers of the event (flavours, momenta, decay vertices, spins, ...), to calculate the complete matrix element for each such state, and to sum it all up to arrive at something as straightforward as a charged multiplicity distribution. It is therefore natural to subdivide the complete process into a sequence of smaller steps: the Z^0 decaying to a specific $q\bar{q}$ flavour; these developing a shower by consecutive branchings $q \rightarrow qg$ and $g \rightarrow gg$; fragmentation of a complex partonic system as the iterative production of one particle at a time; a sequential chain of secondary hadronic decays; and so on. In each step, nature is assumed to make a random choice between the allowed possible outcomes, and the relative probabilities may be calculated or modelled. This sequence of random choices may be simulated in an event generator by the use of random numbers. After each new step the set of possible states that could be reached is larger and more varied, until the final output has the full complexity observable in nature. Therefore, just as each experimental event is unique, so is each generator event. It is the average over many events that should be compared, and the fluctuations around this average.

There is one catch: the basic description of quantum mechanics is in terms of amplitudes rather than probabilities. One therefore has to watch out that a probabilistic description does not lose some of the fundamental aspects associated with interference terms. There is no generic recipe to handle this problem, but often nature is kind to us, so that reasonable ways out can be found.

There exist a wide range of generators, and by now the zoology may be quite confusing. However, in view of their increasing importance, a number of workshops have been devoted in part to collect information and critically compare all main generators by topic. Surveys are available for LEP 1 [3], for HERA [4], and for hadron colliders [5], and another will appear within the framework of the current LEP 2 workshop.

Generators can be designed for different purposes, and therefore also be quite different in size. The two with the widest scope are HERWIG [6] and PYTHIA/JETSET [7], which can be used for e^+e^-, ep and pp collision alike, which contain a wide range of allowed subprocesses, and which are attempts to cover all the aspects of the way from a hard process to a complex multihadronic final state. Almost in the same class is ISAJET [8], which is primarily intended for pp physics. The development and support of programs like these can easily be full-time efforts, where many model aspects related to non-perturbative QCD have to be developed from scratch.

There is then a broad spectrum of other generators, with more specific scopes. Some are devoted to the study of QCD parton shower evolution, or to the non-perturbative fragmentation modelling, or to more precise descriptions of particle decays, or to the simulation of multiparton matrix elements, or to multiple QED radiation, or to higher-

order (including loop graphs) corrections to electroweak processes, or to a multitude of other tasks. Most of them do not contain models for fragmentation. So long as non-hadronic final states are considered, or observables not so sensitive to fragmentation, these programs are often superior to the general-purpose ones above. Therefore, the choice is sometimes between describing a few things very precisely or 'everything' at a reduced level of precision. In practice, often both are needed.

In the following, the discussion will tend to be centred more around the former kind of approach, firstly because this is where my own interests lie. and secondly because it gives me the chance to address a wide range of topics.

3 $e^+ e^-$ Physics

Jet physics started in earnest when the experiments at PETRA observed clean two- and three-jet events. Experience has shown that a sensible approach is to divide the process into four consecutive steps:

1. A hard process e^+e^- — γZ — $q\bar{q}$. This process is perturbatively calculable in the standard model. Often initial-state QED radiation is also included in the description. The 'final state' of this step is given by the q flavour and angular distribution, plus possibly the distribution of additional photons.

2. A stage where perturbative QCD is applicable. Full second-order matrix-element calculations have been performed for the jet rate, which means that the production of two-, three- and four-jet events can be described consistently to that order. The game gets increasingly more complicated for each new order, however, at the same time as higher-order effects are clearly visible in the data. The alternative is therefore to adopt the parton-shower approach, wherein the evolution towards higher parton multiplicities is described as a sequence of branchings at decreasing virtualities. of the kinds q — qg, g — gg and g — $q\bar{q}$. This is an approximation to the correct answer. which should be good in the collinear limit but less good for widely separated jets. A standard method is to match the first branching of the shower to the first-order matrix element, so that a reasonable description is thereby obtained over the full kinematical range.

3. The fragmentation stage. When the shower is evolved towards smaller virtualities, the running α_s becomes larger, and ultimately a limit is hit where perturbation theory breaks down. In models this scale typically comes out to be around 1 GeV. Below this scale, the coloured partons are somehow transformed into colourless hadrons. Currently only phenomenologically motivated models are available, today normally string or cluster fragmentation.

4. Secondary decays occur since many of the hadrons produced above are unstable. Normally also this step involves non-perturbative physics, but experimentally determined branching ratios [9] can here often be used as input.

3.1   Parton Showers

The parton-shower picture is derived within the framework of the leading-logarithm approximation, LLA. In this picture, only the leading terms in the perturbative expansion are kept in a systematic manner. Some subleading corrections are included, as we shall see, but most are neglected. The overall theoretical picture is rather encouraging: there is reason to believe that neglected effects are small, and the predictive power of this approach is increasing year by year.

Phenomenologically, the main reason for the LLA success is our ability to formulate it in terms of a probabilistic picture, suitable for event generation. The probability $\mathcal{P}$ that a branching a — bc will take place during a small

change $dt = dQ_{evol}^2/Q_{evol}^2$ of the evolution parameter $t = \ln(Q_{evol}^2/\Lambda^2)$ is given by the evolution equations [10]

$$\frac{dP_{a \to bc}}{dt} = \int dz \frac{\alpha_s(Q^2)}{2\pi} P_{a \to bc}(z) . \tag{1}$$

For gluons it is necessary to sum over all allowed final-state flavour combinations b and c to obtain the total branching probability. The $P_{a \to bc}(z)$ are the Altarelli-Parisi splitting kernels

$$P_{q \to qg}(z) = C_F \frac{1 + z^2}{1 - z} .$$

$$P_{g \to gg}(z) = N_C \frac{(1 - z(1 - z))^2}{z(1 - z)} ,$$

$$P_{g \to q\bar{q}}(z) = T_R(z^2 + (1 - z)^2) , \tag{2}$$

with $C_F = 4/3$, $N_C = 3$, and $T_R = n_f/2$, i.e. T_R receives a contribution of $1/2$ for each allowed $q\bar{q}$ flavour. The z variable specifies the sharing of four-momentum between the daughters, with daughter b taking fraction z and c taking $1 - z$.

Starting at the maximum allowed virtuality t_{max} for parton a, the t parameter may be successively degraded. This does not mean that an individual parton runs through a range of t values: each parton in the end is associated with a fixed t value, and the evolution procedure is just a way of picking that value. It is only the ensemble of partons in many events that evolve continuously with t, cf. the concept of structure functions. The probability that no branching occurs during a small range of t values, δt, is given by $(1 - \delta t \, dP/dt)$. When summed over many small intervals, the no-emission probability exponentiates

$$\mathcal{P}_{no-emission}(t_{max}, t) = \exp \left(-\int_t^{t_{max}} dt' \frac{dP_{a \to bc}}{dt'} \right) . \tag{3}$$

This is (almost) what is normally called the Sudakov form factor. Thus the actual probability for a branching of a given t is the naive probability, eq. (1), multiplied by the probability that a branching has not already taken place, eq. (3). Compare with the exponential decay law of radioactive decays, with a t-dependent decay probability.

Once the branching of parton a has been selected, the products b and c may be allowed to branch in their turn, and so on, giving a tree-like structure of branchings at successively smaller t values. The branching of a given parton is stopped whenever the evolution parameter is below t_{min}.

Very valuable input for model builders is provided by the theoretical studies of corrections beyond leading log, such as coherence effects [11, 12, 13]. The latter come in two kinds:

- The intrajet coherence phenomenon is responsible for a decrease of the amount of soft gluon emission inside jets. It has been shown that an ordering in terms of a decreasing emission angle takes into account the bulk of soft gluon interference effects. Algorithms which contain angular ordering are loosely said to produce coherent showers, while those without generate conventional ones.

- The interjet coherence phenomenon, responsible for the flow of particles in between jets, with constructive or destructive interference depending on colour configuration ('colour drag phenomena'), cf. [12]. This form of coherence is not just a direct consequence of the ordering of (polar) emission angles mentioned above, but also requires that azimuthal angles of branchings be properly distributed.

The angular ordering may be understood as follows, for the example of a branching $q_0 \to qg$. In the branching, the original q_0 colour is inherited by the gluon, while the q and g share a new colour-anticolour pair. A soft gluon g' (emitted at large angles) corresponds to a large (transverse) wavelength, so the soft gluon is unable to resolve the separate colour charges of the q and the g, and only feels the net charge. This is nothing but the original charge carried by the q_0. Such a soft gluon (in the region $\theta_{q_0 g'} > \theta_{qg}$) could therefore be thought of as being emitted

by the q_0 rather than by the q–g system. If one only considers the emission that should be associated with the q or the g, to a good approximation, there is a complete destructive interference in the regions of non-decreasing opening angles, while partons radiate independently of each other inside the regions of decreasing opening angles ($\theta_{qg'} < \theta_{qg}$ and $\theta_{gg'} < \theta_{qg}$), once azimuthal angles are averaged over. The details of the colour interference pattern are reflected in non-uniform azimuthal emission probabilities.

Parton-shower programs generally give a good account of LEP data [14]: thrust distributions, jet masses, the number of jets as a function of the resolution parameter, and so on. In some variables, deviations are visible, such as the four-jet relative angular distributions used to test the triple-gluon vertex [15]. This is not so surprising, since the parton shower does not contain any explicit information about the four-jet matrix elements. So, while the overall rate of four-jet emission is well described, some of the azimuthal angular distributions are not correctly simulated.

Many of the above distributions do not test coherence specifically. Better signals are a slower increase in multiplicity as a function of energy, or in a characteristic depletion of particle production at low momenta [13]. The data clearly speak in favour of coherence. Recently, two new tests have been performed. One is to consider the rate of particle pairs as a function of the relative angle, and specifically the difference in rate between the pairs almost back-to-back and those almost collinear [16]. Another is to classify events as either three- or two-jet ones at some given resolution scale, and then compare the average number of additional sub-jets that are found when the resolution parameter is reduced [17]. Again incoherent models fail to describe the data, while the coherent ones do very well. The only catch is that all the tests above probe not only the perturbative but also the non-perturbative aspects of the models, so some caution is necessary in not overinterpreting the results.

Recently, the b-quark rate in hadronic Z^0 decays has been a topic of some controversy. The experimentally observed $b\bar{b}$ rate is about two standard deviations above the theoretically predicted one in the standard model [18]. This may not seem enough of a deviation to worry anybody but, given the excellent agreement with the standard model in almost every other respect, it is natural to closely scrutinize every hint of even the slightest crack in the shiny wall. One possibility put forward is that there is a larger rate of secondary $b\bar{b}$ production, i.e. branchings $g \to b\bar{b}$, than assumed in current shower programs. Since the absolutely overwhelming contribution comes from primary $Z^0 \to b\bar{b}$ production, the small excess observed translates into a requirement to enhance the $g \to b\bar{b}$ rate by at least a factor of 4. The issue has been studied in some detail [19], by comparing parton-shower programs with resummed matrix-element calculations. The conclusion is that parton showers seem accurate in this respect to about the 20% level. This does not include general uncertainties such as what is the proper b quark mass (not necessarily the same for the high-virtuality $Z^0 \to b\bar{b}$ vertices as for the close-to-threshold $g \to b\bar{b}$ ones), but it is still difficult to imagine a total error of a factor of 2, let alone one of 4. The discrepancy, if there is one, is therefore likely to be found elsewhere. One example might be in uncertainties in the shape of the b fragmentation function, specifically how often a B hadron is so slow that no secondary vertex is registered in the detector.

3.2 Fragmentation

The fragmentation process has yet to be understood from first principles, starting from the QCD Lagrangian. This has left the way clear for the development of a number of different phenomenological models. Being models, none of them can lay claims to being 'correct'. The best one can aim for is a good representation of existing data, plus a predictive power for properties not yet studied or results at higher energies.

All existing models are of a probabilistic and iterative nature. This means that the fragmentation process as a whole is described in terms of one (or a few) simple underlying branchings, of the type jet → hadron + remainder-jet, string → hadron + remainder-string, cluster → hadron + hadron, or cluster → cluster + cluster. At

each branching, probabilistic rules are given for the production of new flavours, and for the sharing of energy and momentum between the products.

Three main schools are usually distinguished, string fragmentation (SF), cluster fragmentation (CF) and independent fragmentation (IF) [20]. These need not be mutually exclusive: it is possible to have models which contain both cluster and string aspects, or models which interpolate between independent and string fragmentation. Local parton–hadron duality (LPHD) is a fourth approach, wherein the perturbatively calculable rate of partons is assumed directly translatable into corresponding rates of hadrons; it is not a complete scheme in the sense of the others, but it is useful for some observables.

While the evolution of fragmentation models was rapid in the early eighties, no really new algorithms have been introduced in the last ten years, and only a modest amount of refinement of the existing approaches has been performed.

For lack of time, and because of personal bias, in the following I concentrate on the string fragmentation approach [21].

While non-perturbative QCD is not solved, lattice QCD studies lend support to a linear confinement picture (in the absence of dynamical quarks), i.e. the energy stored in the colour dipole field between a charge and anticharge increases linearly with the separation between the charges, if the short-distance Coulomb term is neglected. This is quite different from the behaviour in QED, and is related to the presence of a three-gluon vertex in QCD. The details are not yet well understood, however.

The assumption of linear confinement provides the starting point for the string model, most easily illustrated for the production of a back-to-back $q\bar{q}$ jet pair. As the partons move apart, the physical picture is that of a colour flux tube (or maybe colour vortex line) being stretched between the q and the $\bar{q}$. The transverse dimensions of the tube are of typical hadronic sizes, roughly 1 fm. If the tube is assumed to be uniform along its length, this automatically leads to a confinement picture with a linearly rising potential. In order to obtain a Lorentz covariant and causal description of the energy flow due to this linear confinement, the most straightforward way is to use the dynamics of the massless relativistic string with no transverse degrees of freedom. The mathematical, one-dimensional string can be thought of as parametrizing the position of the axis of a cylindrically symmetric flux tube. From hadron spectroscopy, the string constant, i.e. the amount of energy per unit length, is deduced to be $\kappa \approx 1$ GeV/fm.

As the q and $\bar{q}$ move apart, the potential energy stored in the string increases, and the string may break by the production of a new $q'\bar{q}'$ pair, so that the system splits into two colour singlet systems $q\bar{q}'$ and $q'\bar{q}$. If the invariant mass of either of these string pieces is large enough, further breaks may occur. In the Lund string model, the string break-up process is assumed to proceed until only on-mass-shell hadrons remain, each hadron corresponding to a small piece of string.

In order to generate the quark–antiquark pairs $q'\bar{q}'$, which lead to string break-ups, the Lund model invokes the idea of quantum mechanical tunnelling. This leads to a flavour-independent Gaussian spectrum for the transverse momentum of $q'\bar{q}'$ pairs. Tunnelling also implies a suppression of heavy quark production, u : d : s : c $\approx$ 1 : 1 : 0.3 : 10^{-11}. Charm and heavier quarks hence are not expected to be produced in the soft fragmentation.

A tunnelling mechanism can also be used to explain the production of baryons. This is still a poorly understood area. In the simplest possible approach, a diquark in a colour antitriplet state is just treated like an ordinary antiquark, such that a string can break either by quark–antiquark or antidiquark–diquark pair production. The production probabilities are then given by the effective diquark masses assumed, plus simple flavour Clebsch-Gordan coefficients of the baryon wave functions. In this approach, the baryon and antibaryon are produced next to each other, and share (at least) two quark flavours. A more complex scenario is the 'popcorn' one, where diquarks as such do not exist, but rather quark–antiquark pairs are produced one after the other. Part of the time, this scenario

gives back an effective diquark picture, but in addition configurations are possible where one or more mesons are produced in between the baryon and antibaryon, and where therefore these two are no longer required to be as strongly correlated in flavour content.

In general, the different string breaks are causally disconnected. This means that it is possible to describe the breaks in any convenient order, e.g. from the quark end inwards. Results, at least not too close to the string endpoints, should be the same if the process is described from the q end or from the $\bar{q}$ one. This 'left–right' symmetry constrains the allowed shape of fragmentation functions $f(z)$, where z is the fraction of $E + p_L$ that the next particle will take out of whatever remains. Here p_L is the longitudinal momentum along the direction of the respective endpoint, opposite for the q and the $\bar{q}$. Two free parameters remain, which have to be determined from data.

If several partons are moving apart from a common origin, the details of the string drawing become more complicated. For a $q\bar{q}g$ event, a string is stretched from the q end via the g to the $\bar{q}$ end, i.e. the gluon is a kink on the string, carrying energy and momentum. As a consequence, the gluon has two string pieces attached, and the ratio of gluon/quark string forces is 2, a number that can be compared with the ratio of colour charge Casimir operators, $N_C/C_F = 2/(1 - 1/N_C^2) = 9/4$. In this, as in other respects, the string model can be viewed as a variant of QCD, where the number of colours N_C is not 3 but infinite. Fragmentation along this kinked string proceeds along the same lines, as sketched for a single straight string piece. Therefore no new fragmentation parameters have to be introduced.

The more prominent features of LEP data are well described by the string model, when combined with the parton-shower approach mentioned before. One recent example is detailed comparisons of quark and gluon jet fragmentation, which have been made possible by the high statistics and good flavour tagging capabilities of LEP experiments [22]. It is now clearly established that gluon jets have a softer particle momentum spectrum and a broader angular distribution than quark jets of the same energy, and that the results are in excellent agreement with the model predictions. However, as a consequence of the increased statistics, also discrepancies start to show up. This is most notable in the flavour composition, i.e. in the rate of various mesons and baryons: even with a rather large number of free parameters available, the current string fragmentation approach is somewhat off in many places and fails miserably in some [23]. So the conclusion seems to be that the general space–time structure of fragmentation is under control, but that the detailed mechanism of flavour production and hadron formation is still not so well understood.

3.3 W$^+$W$^-$ Events

Based on the above sections, the situation might seem rather satisfactory: if both perturbative and non-perturbative QCD aspects appear reasonably well under control, then, from now on, effectively we can forget about QCD whenever we go about the business of testing the standard model in the weak sector. However, this is not quite true, and as an example we can consider determinations of the W mass. The m_W will be *the* critical observable of LEP 2, which should allow new precision tests.

The problem is that QCD interference effects between the W$^+$ and W$^-$ decays undermine the traditional meaning of a W mass in the process $e^+e^- \to W^+W^- \to q_1\bar{q}_2 q_3\bar{q}_4$. Specifically, it is not even in principle possible to subdivide the hadronic final state into two groups of particles, one of which is produced by the $q_1\bar{q}_2$ system of the W$^+$ decay and the other by the $q_3\bar{q}_4$ system of the W$^-$ decay: some particles originate from the joint action of the two systems.

In order to understand which QCD interference effects can occur in hadronic W$^+$W$^-$ decays, it is useful to examine the space–time picture of the process. Consider a typical c.m. energy of 170 GeV, a W mass $m_W = 80$

GeV, and a width Γ_W = 2.08 GeV. The averaged (over the W-mass distribution) proper lifetime for a W is $\langle\tau\rangle \approx (2/3)\hbar/\Gamma_W \approx 0.06$ fm. This gives a mean separation of the two decay vertices of 0.04 fm in space and 0.07 fm in time. A gluon with an energy $\omega \gg \Gamma_W$ therefore has a wavelength much smaller than the separation between the W^+ and W^- decay vertices, and is emitted almost incoherently either by the $q_1\bar{q}_2$ system or by the $q_3\bar{q}_4$ one. Only fairly soft gluons, $\omega \lesssim \Gamma_W$, feel the joint action of all four quark colour charges. On the other hand, the typical distance scale of hadronization is about 1 fm, i.e. much larger than the decay vertex separation. Therefore the hadronization phase may contain significant interference effects.

A complete description of QCD interference effects is not possible since non-perturbative QCD is not well understood. The concept of colour reconnection/rearrangement [24] is therefore useful to quantify effects (at least in a first approximation). In a reconnection two original colour singlets (such as $q_1\bar{q}_2$ and $q_3\bar{q}_4$) are transmuted into two new ones (such as $q_1\bar{q}_4$ and $q_3\bar{q}_2$). Subsequently each singlet system is assumed to hadronize independently according to the standard algorithms, as outlined above. Depending on whether a reconnection has occurred or not, the hadronic final state is then going to be somewhat different.

In the following, we will first discuss perturbative effects and subsequently non-perturbative ones. Further details may be found in [25].

Until today, perturbative QCD has mainly been applied to systems of primary partons produced almost simultaneously. The radiation accompanying such a system can be represented as a superposition of gauge-invariant terms, in which each external quark line is uniquely connected to an external antiquark line of the same colour. The system is thus decomposed into a set of colourless $q\bar{q}$ antennae/dipoles. Neglecting interferences, the $e^+e^- \to W^+W^- \to q_1\bar{q}_2\,q_3\bar{q}_4$ final state can be subdivided into two separate dipoles, $\widehat{q_1\bar{q}_2}$ and $\widehat{q_3\bar{q}_4}$. Each dipole may radiate gluons from a maximum scale m_W downwards. Within the perturbative approach, colour transmutations can result only from the interferences between gluons (virtual as well as real) radiated in the W^+ and W^- decays. A colour reconnection then corresponds to radiation, e.g. from the dipoles $\widehat{q_1\bar{q}_4}$ and $\widehat{q_3\bar{q}_2}$. The emission of a single primary gluon cannot give interference effects, by colour conservation, so interference terms only enter in second order in α_s.

The general structure of the results is well illustrated by the interference between the graph where a gluon with momentum k_1 (k_2) is emitted off the $\widehat{q_1\bar{q}_2}$ ($\widehat{q_3\bar{q}_4}$) dipole and the same graph with k_1 and k_2 interchanged:

$$\frac{1}{\sigma_0}d\sigma^{\text{int}} \simeq \frac{d^3k_1}{\omega_1}\frac{d^3k_2}{\omega_2}\left(\frac{C_F\,\alpha_s}{4\pi^2}\right)^2\frac{1}{N_C^2-1}\,\chi_{12}\,H(k_1)\,H(k_2)\ . \tag{4}$$

Note that the interference is suppressed by $1/(N_C^2-1) = 1/8$ as compared to the total rate of double primary gluon emissions. This is a result of the ratio of the corresponding colour traces.

The so-called profile function χ_{12} controls decay–decay interferences. It quantifies the overlap of the W propagators in the interfering Feynman diagrams. Near the W^+W^- pair threshold, χ_{12} simplifies to

$$\chi_{12} \approx \frac{\Gamma_W^2}{\Gamma_W^2 + (\omega_1 - \omega_2)^2}\ . \tag{5}$$

Other interferences (real or virtual) are described by somewhat different expressions, but have the same general properties. The profile functions cut down the phase space available for gluon emissions with $\omega \gtrsim \Gamma_W$ by the alternative quark pairs. The possibility for the reconnected systems to develop QCD cascades is thus reduced, i.e. the dipoles are almost sterile.

The radiation pattern $H(k)$ is given by

$$H(k) = \widehat{q_1\bar{q}_4} + \widehat{q_3\bar{q}_2} - \widehat{q_1q_3} - \widehat{\bar{q}_2\bar{q}_4}\ , \tag{6}$$

where the radiation antennae are

$$\hat{ij} = \frac{(p_i \cdot p_j)}{(p_i \cdot k)(p_j \cdot k)} \,. \tag{7}$$

In addition to the two dipoles $\widehat{q_1\bar{q}_4}$ and $\widehat{q_3\bar{q}_2}$, which may be interpreted in terms of reconnected colour singlets, one finds two other terms, $\widehat{q_1q_3}$ and $\widehat{\bar{q}_2\bar{q}_4}$, which come in with a negative sign. The signs represent the attractive and repulsive forces between quarks and antiquarks. The effects of the reconnected almost sterile cascades should appear on top of a dominant background generated by the ordinary-looking no-reconnection dipoles $\widehat{q_1\bar{q}_2}$ and $\widehat{q_3\bar{q}_4}$. The negative-sign interference terms are therefore perfectly physical, and distort the overall radiation pattern in the same direction as the positive-sign ones.

We now turn to the possibility of reconnection occurring as a part of the non-perturbative hadronization phase. This requires model building, beyond what is already available in the standard string fragmentation approach. Specifically, the string model does not constrain the nature of the string fully. At one extreme, the string may be viewed as an elongated bag, i.e. as a flux tube without any pronounced internal structure. At the other extreme, the string contains a very thin core, a vortex line, which carries all the topological information, while the energy is distributed over a larger surrounding region. The latter alternative is the chromoelectric analogue to the magnetic flux lines in a type II superconductor, whereas the former one is more akin to the structure of a type I superconductor. We use them as starting points for two contrasting approaches, with nomenclature inspired by the superconductor analogy.

In scenario I, the reconnection probability is proportional to the space–time volume over which the W^+ and W^- strings overlap, with saturation at unit probability. A consideration of distances in the W^+W^- system shows that each W can effectively be viewed as instantaneously decaying into a string spanned between the partons, from a quark end via a number of intermediate gluons to the antiquark end. The strings expand, both transversely and longitudinally, at a speed limited by that of light. They eventually fragment into hadrons and disappear. An overlap of the W^+ and W^- strings may be calculated by making an ansatz for each individual string field, uniform in the longitudinal direction and falling off as a Gaussian of approximately 0.5 fm width in the transverse direction, and an average proper time of decay of $\tau_{frag} \approx 1.5$ fm. This gives a model with one free parameter, the constant of proportionality between the space–time integral of the overlap and the probability of a reconnection.

In scenario II it is assumed that reconnections can only take place when the core regions of two string pieces cross each other. This means that the transverse extent of strings can be neglected, which leads to considerable simplifications compared with the previous scenario. Such an approach does not introduce any new parameters. The reconnection probability comes out to be about 35% at 170 GeV; the free parameter of model I has been adjusted to give the same answer at this energy. This probability does not vary by more than a factor of 2 over the full LEP 2 energy range.

Comparing scenarios I and II above with the no-reconnection scenario, it turns out that reconnection effects are very small. The change in the average charged multiplicity is at the level of a per cent or less, and similar statements hold for rapidity distributions, thrust distributions, and so on. This is below the experimental precision we may expect, and so may well go unobserved. One would like to introduce more clever measures, which are especially sensitive to the interesting features, but so far we have had little success.

Ultimately, the hope would be to distinguish between scenarios I and II, and thereby to gain some insight into the nature of the confinement mechanism. In principle, there are such differences. For instance, the reconnection probability is much more sensitive to the event topology in scenario II, since the requirement of having two string cores cross is more selective than that of having two broad flux tubes overlap.

We now come to the W mass. Experimentally, m_W depends in a non-trivial fashion on all particle momenta of an

event. Errors in the W mass determination come from a number of sources [26], which we do not intend to address here. Therefore we only study the extent to which the average reconstructed W mass is shifted when reconnection effects are added, but everything else is kept the same. Even so, results do depend on the reconstruction algorithm used. We have tried a few different ones, which however are all based on the same philosophy: a jet finder is used to define at least four jets, events with two very nearby jets or with more than four jets are rejected, the remaining jets are paired to define the two W's, and the average W mass of the event is calculated. Events where this number agrees to better than 10 GeV with the input average mass are used to calculate the systematic mass shift.

In scenario I this shift is consistent with being zero, within the 10 MeV uncertainty in our results from limited Monte Carlo statistics (160,000 events per scenario). Scenario II gives a negative mass shift, of about -30 MeV; this also holds for several variations of the basic scheme. A simpler model, where reconnections are always assumed to occur at the centre of the event, gives a positive mass shift instead: about $+30$ MeV if results are rescaled to a reconnection probability of 35%. We are therefore forced to conclude that not even the sign of the effect can be taken for granted, but that a real uncertainty of ±30 MeV does exist from our ignorance of non-perturbative reconnection effects. Studies show that pure perturbative effects could add at most about 5 MeV to this, while the potential interplay between perturbative and non-perturbative effects (one W decaying inside the hadronic field of the other W) has been assumed no larger than that.

Since the three sources are not independent, the numbers are added linearly to get an estimated total uncertainty of 40 MeV. In view of the aimed-for precision, this is non-negligible, and should be a cause for worry. It is not impossible that one could tailor-make experimental algorithms that are less sensitive to these effects, however.

Potential reconnection effects may not be the only uncertainty. Currently we are studying the uncertainties that could come from Bose-Einstein effects [27]. The underlying reason is the same as for the W reconnections: the two W's decay so close to each other compared with typical hadronization distances and Bose-Einstein radii. For a pair of nearby π^0's, say, the production amplitude then should be symmetrized with respect to which π^0 comes from which W. Even neglecting reconnection phenomena, the concept of a W mass on the hadron level is then undermined. The Bose-Einstein phenomenon is very poorly known, so we cannot definitely claim that there have to be observable effects. However, attempts at modelling indicate that the uncertainty in the W mass can well turn out to be comparable with or even larger than the one quoted for reconnection phenomena.

4 Hadronic Physics

The need for event generators is excellently illustrated by the recent CDF top paper [28]. In order to reach a conclusion, generators are used at every step of the way: to study the signal, potential backgrounds, detector response and imperfections, and so on. This shows how critical the generator aspects are, for better or for worse.

While hadron colliders are well suited to reach energies higher than e^+e^- ones (cf. the Tevatron and LEP), there are disadvantages. Hadrons have a complicated internal structure of quarks and gluons. This means that hadronic collisions are more complex than leptonic ones. Leptoproduction ep events are intermediate to the e^+e^- and the pp/$\bar{p}p$ ones, with a simple probe on a complicated target. Therefore the experience from HERA will be invaluable in reaching a better understanding of the hadronic structure in its broadest sense, i.e. also including aspects such as initial-state QCD radiation, interference between initial- and final-state radiation, and beam-jet fragmentation. However, from an event-generator point of view, ep and e^+e^- processes may be viewed as special cases of the hadron-hadron description. I therefore now jump directly to the latter kind of processes.

A summary of the physics in hadronic event generators is the following:

• An event is normally classified by the 'hardest' (i.e. the one with largest momentum transfer) interaction that

occurs. This can be a process such as $qg \to qg$, $q\bar{q}' \to W^+$, $q\bar{q} \to t\bar{t}$. or anything else. The corresponding matrix element is perturbatively calculable. Not all events need contain a hard. calculable subgraph. exceptions are found among elastic. diffractive and low-$p_\perp$ events.

- In order to calculate a cross section, the squared matrix element has to be multiplied by two parton-distribution functions. which describe the partonic content of the two incoming hadrons. The analogy with e^+e^- and ep physics is made more transparent if one introduces parton distributions also for leptons. The evolution is here not given by QCD processes but by QED branchings such as $e \to e\gamma$. The probability that the electron retains a fraction x of the full momentum if it is probed at a scale Q^2 is fully perturbatively calculable. unlike the QCD case.

- The initial-state radiation that gave rise to the two incoming partons has to be reconstructed. i.e. the inclusive parton-distribution description has to be turned into an exclusive set of radiated partons.

- Also partons in the final state can radiate further. in the same spirit as described for e^+e^- events.

- Not all partons of an incoming hadron take part in the hard interaction. A remnant is left behind. 'attached' to the hard interaction by its colour charge. Nothing forbids several partons being kicked out, by independent (semi-)hard interactions. All this gives a 'beam jet' structure that still is not so well understood.

- Again outgoing coloured partons turn into colourless hadrons by fragmentation. Normally the fragmentation process is assumed universal. i.e. the same models can be used as in e^+e^-. This need not be correct. — universality is known to break down if one tries to extrapolate from pp collisions to heavy-ion ones — but it is a reasonable starting point.

- Unstable particles decay, just as in e^+e^-.

Below we give some further details on the topics not already covered for e^+e^-.

4.1 Hard Processes and Parton Distributions

The wide range of physics processes that are of interest in hadronic physics leads to a need for generators to contain a bit of everything. For instance. PYTHIA contains the following major groups:

- Hard QCD processes. e.g. $qg \to qg$.
- Soft QCD processes. such as diffractive and elastic scattering. and minimum-bias events.
- Heavy-flavour production. e.g. $gg \to t\bar{t}$.
- Prompt-photon production. e.g. $qg \to q\gamma$.
- Photon-induced processes. e.g. $\gamma g \to q\bar{q}$.
- Deep inelastic scattering. e.g. $q\ell \to q\ell$.
- W/Z production, such as $e^+e^- \to \gamma^*/Z^0$ or $q\bar{q} \to W^+W^-$.
- Standard model Higgs production. where the Higgs is reasonably light and narrow, and can therefore still be considered as a resonance.
- Gauge boson scattering processes. such as $W_LW_L \to W_LW_L$ (L = longitudinal), when the standard model Higgs is so heavy and broad that resonant and non-resonant contributions have to be considered together.
- Non-standard Higgs particle production. within the framework of a two-Higgs-doublet scenario with three neutral (h^0, H^0 and A^0) and two charged ($H^\pm$) Higgs states.
- Production of new gauge bosons, such as a Z', W' and R (a horizontal boson, coupling between generations).
- Production of fourth-generation fermions.
- Leptoquark (L_Q) production.

- Technicolour, e.g. gg — η_{techni}.

- Compositeness, e.g. d* and u* production.

- Other deviations from standard model processes, e.g. due to contact interactions or a strongly interacting gauge boson sector.

The list is by no means a survey of all interesting physics. Most notable is the absence of supersymmetric particle production and decay, but many other examples could be found: axigluons, baryon number violating processes, and so on. Also, within the scenarios studied, not all contributing graphs have always been included, but only the more important and/or more interesting ones. In many cases, various approximations are involved in the matrix elements coded. Other generators contain also other processes, and sometimes in other approximations, so there is a lot of complementarity.

The cross-section for a process $ij \to k$ is given by

$$\sigma_{ij \to k} = \int dx_1 \int dx_2 \, f_i^1(x_1, Q^2) \, f_j^2(x_2, Q^2) \, \sigma_{ij \to k}(s) \ . \tag{8}$$

Here σ is the cross-section for the hard partonic process, as codified in the matrix elements for each specific process. For processes with many particles in the final state it would be replaced by an integral over the allowed final-state phase space.

The $f_i^a(x, Q^2)$ are the parton distribution functions, which describe the probability to find a parton i inside beam particle a, with parton i carrying a fraction x of the total a momentum, when the a is probed at some squared momentum scale Q^2 that characterizes the hard process. Since we do not understand QCD in the low-Q^2 region, a derivation from first principles of the parton distributions of hadrons does not yet exist. It is therefore necessary to rely on parametrizations, where experimental data are used in conjunction with the evolution equations for the Q^2 dependence, to pin down the parton distributions. The most complete selection of distributions is found in PDFLIB [29].

The input from HERA has provided further stimulus for studies in this field. What is the small-x behaviour? Do parton distributions saturate? What is the rôle of the pomeron and rapidity-gap events? A number of questions remain to be answered.

4.2   Initial- and Final-State Radiation

For parton showers, a separation of radiation into a hard scattering and initial- and final-state showers is arbitrary, but very convenient. There are also situations where it is appropriate: for instance, the process $e^+e^- \to Z^0 \to q\bar{q}$ only contains final-state QCD radiation, while $q\bar{q} \to Z^0 \to e^+e^-$ only contains initial-state QCD radiation. Similarly, the distinction of emission as coming either from the q or from the $\bar{q}$ is arbitrary. In general, the assignment of radiation to a given mother parton is a good approximation for an emission close to the direction of motion of that parton, but not for the wide-angle emission in between two jets, where interference terms are expected to be important. For such configurations the matrix-element approach is better, if possible.

In both initial- and final-state showers, the structure is given in terms of branchings $a \to bc$, specifically $e \to e\gamma$, $q \to qg$, $q \to q\gamma$, $g \to gg$, and $g \to q\bar{q}$. These processes are characterized by the splitting kernels and evolution equations given earlier.

Each parton is associated with some virtuality scale Q^2, which gives an approximate sense of time ordering to the cascade. In the initial-state shower, Q^2 values are space-like ($m^2 < 0$) and gradually increasing as the hard scattering is approached, while Q^2 is time-like ($m^2 > 0$) and decreasing in the final-state showers. Emission angles increase on the way in to the hard interaction and decrease again thereafter. Only the energy per parton is decreased at both stages, as more and more partons are created and share the original energy.

A closer look reveals further differences. In a final-state branching, the two daughters are on an equal footing, both being time-like (or on the mass shell). In the initial-state branching, the mother parton and one daughter parton are space-like, whereas the other daughter is time-like (or on the mass shell). It is the space-like daughter that goes on towards the hard interaction, while the other daughter may initiate a time-like cascade on a side branch, just as in final-state radiation. The initial-state cascade may be viewed as a virtual fluctuation, wherein an initial parton almost on the mass shell is resolved into a set of partons with the same net invariant mass. Such fluctuations are born and die continuously in the proton wave function. It is the hard interaction that provides the momentum transfer to turn the space-like virtualities of the two incoming partons into time-like virtualities of the outgoing partons. It thereby also allows all the side branches to be promoted from a status of virtual fluctuations into one of final-state partons. Space-like fluctuations in principle are allowed on the side branches, but then remain purely virtual and are not observable in the final state.

A sequential evolution of the shower in time is not very convenient for generator applications, since the momenta of the incoming partons are then not known beforehand, which makes a matching to a desired hard scattering very costly in terms of efficiency. A common solution is backwards evolution [30], wherein the evolution equations are rewritten to act in the opposite direction for inital-state showers, i.e. from a given daughter-parton, the mother that produced it (together with a sister) is reconstructed. The procedure can then be started at the hard scattering, with known kinematics, and traced back to the two shower initiators.

Shower evolution is cut off at some lower scale Q_0, typically around 1 GeV for QCD branchings. The same cut-off scale is also used to regularize the soft-gluon-emission divergences in the splitting kernels. From above, a maximum scale Q_{max} is introduced, where the showers are matched to the hard interaction itself. The relation between Q_{max} and the kinematics of the hard scattering is uncertain, and the choice made can strongly affect the amount of well-separated jets.

We already mentioned a few open questions in the description of parton distributions; clearly, also these are reflected in corresponding uncertainties in the structure of initial-state parton showers. On top of this, the coherence conditions that we encountered for final-state radiation have a much more complicated and poorly understood analogue for the initial state [31]. Although existing parton shower programs do rather well by comparison with experiments, it should therefore not be a surprise that the level of confidence is not as high as in e^+e^- annihilation. However, progress is being made. For instance, CDF recently presented an interesting study that shows the importance of angular ordering in the initial-state radiation or, more specifically, how the angles in the shower are matched to the hard scattering angle [32].

4.3   Beam Remnants and Multiple Interactions

In a hadron–hadron collision, the initial-state-radiation algorithm reconstructs one shower initiator in each beam, by backwards evolution from the hard scattering. This initiator only takes some fraction of the total beam energy, leaving behind a beam remnant that takes the rest. For a proton beam, a u quark initiator would leave behind a ud diquark beam remnant, with an antitriplet colour charge. The remnant is therefore colour-connected to the hard interaction, and forms part of the same fragmenting system. Often the remnant is more complicated, e.g. a g initiator would leave behind a uud proton-remnant system in a colour octet state, which can conveniently be subdivided into a colour triplet quark and a colour antitriplet diquark, each of which are colour-connected to the hard interaction. The energy sharing between these two remnant objects, and their relative transverse momentum, introduces additional degrees of freedom.

So far we have assumed that each event only contains one hard interaction, i.e. that each incoming particle has only one parton that takes part in hard processes, and that all other constituents sail through unaffected. This

is appropriate in e^+e^- or ep events, but not necessarily so in hadron–hadron collisions. Here each of the beam particles contains a multitude of partons, and so the probability for several interactions in one and the same event need not be negligible. The dominant mechanism is expected to be that disjoint pairs of partons, with one parton from each beam, undergo 2 — 2 scatterings.

The dominant 2 — 2 QCD cross sections are divergent for $p_\perp$ — 0. and drop rapidly for larger $p_\perp$. Probably the lowest-order perturbative cross-sections will be regularized at small $p_\perp$ by colour coherence effects: an exchanged gluon of small $p_\perp$ has a large transverse wave function and can therefore not resolve the individual colour charges of the two incoming hadrons; it will only couple to an average colour charge that vanishes in the limit $p_\perp$ — 0. Customarily, some effective $p_{\perp min}$ scale is therefore introduced, below which the perturbative cross-section is either assumed completely vanishing or at least strongly damped. Phenomenologically, in some approaches. $p_{\perp min}$ comes out to be a number of the order of 1.5-2.0 GeV [33].

In a typical 'minimum-bias' event one therefore expects to find one or a few scattering(s) at scales around or a bit above $p_{\perp min}$, while a high-$p_\perp$ event also may have additional scatterings at the $p_{\perp min}$ scale. The probability to have several high-$p_\perp$ scatterings in the same event is small, since the cross-section drops so rapidly with $p_\perp$.

The understanding of a multiple interaction is still very primitive, and even the experimental evidence that it exists at all is rather weak [34]. The approach taken to this problem therefore varies significantly from one generator to the next. This may not always be appreciated by the normal user, since any approach by necessity contains a number of free parameters, and these parameters have been tuned by comparisons with essentially the same experimental data. Only when a broad range of properties are studied, preferably at several different energies, can one hope to better understand this complex part of physics.

HERA may provide very interesting possibilities to test these issues: a deep inelastic scattering should only give one interaction, but in the Q^2 — 0 limit the hadronic nature of the photon takes over (see below) and one comes back to a hadron–hadron physics scenario with the possibility of multiple interactions.

4.4 γp and $\gamma\gamma$ Events

There are many reasons for being interested in γp and $\gamma\gamma$ physics. The process $ep \to e\gamma p \to eX$ is a main one at HERA and $e^+e^- \to e^+e^-\gamma\gamma \to e^+e^-X$ will be a main one at LEP 2 and future linear e^+e^- colliders. Therefore, these events are always going to give a non-negligible background to whatever other physics one is interested in. However, more importantly, collisions between real photons provides the richest spectrum of (leading-order) processes that is available for any choice of incoming elementary particles. For instance, since the photon has a hadronic component, all of hadronic physics is contained as a subset of the possibilities. A correct description of the components of the total γp and $\gamma\gamma$ cross sections is therefore the ultimate challenge of 'minimum-bias' physics. (Leaving heavy-ion physics aside.) This also explains why γp and $\gamma\gamma$ events here appear under the heading of hadronic physics. In the following I will describe the approach developed in [35].

To first approximation, the photon is a point-like particle. However, quantum mechanically, it may fluctuate into a (charged) fermion–antifermion pair. The fluctuations γ — $q\bar{q}$ are of special interest to us, since such fluctuations can interact strongly and therefore turn out to be responsible for the major part of the γp and $\gamma\gamma$ total cross sections, as we shall see. On the other hand, the fluctuations into a lepton pair are uninteresting, since such states do not undergo strong interactions to leading order, and therefore contribute negligibly to total hadronic cross sections. The leptonic fluctuations are perturbatively calculable, with an infrared cut-off provided by the lepton mass itself. Not so for quark pairs, where low-virtuality fluctuations enter a domain of non-perturbative QCD physics. It is therefore customary to split the spectrum of fluctuations into a low-virtuality and a high-virtuality part. The former part can be approximated by a sum over low-mass vector-meson states, usually (but not necessarily) restricted to

the lowest-lying vector multiplet. Phenomenologically, this Vector Meson Dominance (VMD) ansatz turns out to be very successful in describing a host of data. The high-virtuality part, on the other hand, should be in a perturbatively calculable domain.

In total, the photon wave function can then be written as

$$|\gamma\rangle = c_{\text{bare}}|\gamma_{\text{bare}}\rangle + \sum_{V=\rho^0,\omega,\phi,J/\psi,\Upsilon} c_V|V\rangle + \sum_{q=u,d,s,c,b} c_q|q\bar{q}\rangle + \sum_{\ell=e,\mu,\tau} c_\ell|\ell^+\ell^-\rangle . \tag{9}$$

In general, the coefficients c_i depend on the scale μ used to probe the photon. Introducing a cut-off parameter p_0 to separate the low- and high-virtuality parts of the $q\bar{q}$ fluctuations, one obtains $c_q^2 \approx (\alpha_{\text{em}}/2\pi)2e_q^2\ln(\mu^2/p_0^2)$. The VMD part corresponds to the range of $q\bar{q}$ fluctuations below p_0 and is thus μ-independent (assuming $\mu > p_0$). The major contribution comes from the ρ^0, $c_\rho \approx 0.04$. Finally, c_{bare} is given by unitarity: $c_{\text{bare}}^2 \equiv Z_3 = 1 - \sum c_V^2 - \sum c_q^2 - \sum c_\ell^2$. In practice, c_{bare} is always close to unity. Usually the probing scale μ is taken to be the transverse momentum of a $2 \to 2$ parton-level process. Our fitted value $p_0 \approx 0.5$ GeV then sets the minimum transverse momentum of a perturbative branching $\gamma \to q\bar{q}$.

The subdivision of the above photon wave function corresponds to the existence of three main event classes in γp physics:

1. The VMD processes, where the photon turns into a vector meson before the interaction, and therefore all processes allowed in hadronic physics may occur. This includes elastic and diffractive scattering as well as low-$p_\perp$ and high-$p_\perp$ non-diffractive events.

2. The direct processes, where a bare photon interacts with a parton from the proton.

3. The anomalous processes, where the photon perturbatively branches into a $q\bar{q}$ pair, and one of these (or a daughter parton thereof) interacts with a parton from the proton.

All three processes are of $O(\alpha_{\text{em}})$. However, in the direct contribution the photon structure function is of $O(1)$ and the hard-scattering matrix elements of $O(\alpha_{\text{em}})$, while the opposite holds for the VMD and the anomalous processes. The VMD component contributes about 80% of the total γp cross section, but less in the jet cross section: at intermediate $p_\perp$ values the anomalous processes are contributing most and at large $p_\perp$ values the direct processes dominate.

The difference between the three classes is easily seen in terms of the beam jet structure. The incoming proton always gives a beam jet containing the partons of the proton that did not interact. On the photon side, the direct processes do not give a beam jet at all, since all the energy of the photon is involved in the hard interaction. The VMD ones give a beam remnant just like the proton, with a 'primordial $k_\perp$' smearing of typically up to half a GeV. The anomalous processes give a beam remnant produced by the $\gamma \to q\bar{q}$ branching, with a transverse momentum going from p_0 upwards. Thus the transition from VMD to anomalous should be rather smooth.

A generalization of the above picture to $\gamma\gamma$ events is obtained by noting that each of the two incoming photons is described by a wave function of the type given in eq. (9). In total, there are therefore three times three event classes. By symmetry, the 'off-diagonal' combinations appear pairwise, so the number of distinct classes is 'only' six: VMD×VMD, VMD×direct, VMD×anomalous, direct×direct, direct×anomalous and anomalous×anomalous. The pattern of their relative importance is the same as for the γp process: VMD×VMD dominates the total cross section and direct×direct the jet cross section at large $p_\perp$.

When pp (or $\bar{p}p$), γp and $\gamma\gamma$ events are compared at a common energy, the above ansatz leads to characteristic differences. There are most jets in $\gamma\gamma$ events and least in pp ones, not surprisingly, and this is also reflected in the total transverse energy flow, in the multiplicity distribution, and so on. Indications along these lines now start to appear at HERA, e.g. in the inclusive $p_\perp$ spectrum of charged particles [36]. The excess of jets in $\gamma\gamma$ events is observed at TRISTAN [37] and LEP 2 should have much more to say.

5   Summary and Outlook

This talk has only scratched the surface of the aspects that have to be programmed in a modern, versatile generator. If one looks back, the evolution has been explosive. The first version of the Lund Monte Carlo, in 1978, was about 200 lines long (and coded on punched cards!). Today, PYTHIA/JETSET together is over 30,000 lines of code, supplemented by a 300 pages long physics description and manual [7]. The growth in physics potential of the programs has been fairly linear over these years (a roughly constant number of persons contributing a rather constant number of new aspects per year), whereas the increase in the code itself has been closer to an exponential. This in part reflects changes in programming style, in part the trend to address more subtle and difficult-to-program problems as the simpler are 'solved'.

Of course, Lund is only one family of generators. Historically one should presumably start with models based on pure phase space or longitudinal phase space, but the first event generator in a more modern sense (that I am aware of) is the Artru–Mennessier model of 1974 [38]. The Field–Feynman ansatz of 1978 [39] had an enormous impact (partly due to the magic of the name Feynman). Starting with PETRA, the use of event generators has taken off, so that today there is hardly any experimental analysis presented or planned without the help of generators.

Initially there was a lot of scepticism, and it is not so easy to say when that disappeared. In retrospect it is tempting to call the UA1 experiences of 1984 the watershed. The 'discoveries' of supersymmetry and of top [40] can be traced back at least in part to a poor understanding of the signal, of the backgrounds, and of the detector response, and the only way one has found to do better in cases like these is to have more elaborate event generation and detector simulation programs.

Today, the problem is rather the opposite: some people have too deep a faith in generators. For instance, in the LEP 1 workshop our main recommendation was that 'Due to the large uncertainties present in any realistic QCD Monte Carlo, physics studies must be based on the use of at least two complete and independent programs.' [3], but this rule is not always followed. It is therefore important to remember the size and complexity of current-day generators. Hopefully this talk has given you some insight into the different aspects and assumptions that enter, and the many question marks that still remain. Even if the 'pioneering days' may be past, there is every need for continuing studies, e.g. in the area of multiparticle production, to address the new problems that come along. This way, hopefully, event generators will remain in the heartland of phenomenological and experimental particle physics.

Acknowledgements

References

[1] U. Amaldi, W. de Boer and H. Fürstenau, Phys. Lett. B260 (1991) 447

[2] R. Brun et al., GEANT 3, CERN Report DD/EE/84-1 (1987, revised)

[3] Z Physics at LEP 1 — Vol. 3: Event Generators and Software, eds. G. Altarelli, R. Kleiss and C. Verzegnassi, CERN 89-08 (1989)

[4] Physics at HERA — Vol. 3: Monte Carlo Generators, eds. W. Buchmüller and G. Ingelman (DESY, 1992)

[5] T. Sjöstrand, Z. Phys. C42 (1989) 301;
F. Anselmo et al., in 'Large Hadron Collider Workshop', eds. G. Jarlskog and D. Rein, CERN 90-10 (1990), Vol. II, p. 130;
I.G. Knowles and S.D. Protopopescu, in 'Workshop on Physics at Current Accelerators and Supercolliders', eds. J.L. Hewett, A.R. White and D. Zeppenfeld, ANL-HEP-CP-93-92 (1993)

[6] G. Marchesini, B.R. Webber, G. Abbiendi, I.G. Knowles, M.H. Seymour and L. Stanco, Comput. Phys. Commun. 67 (1992) 465

[7] T. Sjöstrand and M. Bengtsson, Comput. Phys. Commun. 43 (1987) 367;
H.-U. Bengtsson and T. Sjöstrand, Comput. Phys. Commun. 46 (1987) 43;
T. Sjöstrand, Comput. Phys. Commun. 82 (1994) 74, CERN-TH.7112/93

[8] F.E. Paige and S.D. Protopopescu, in 'Physics of the Superconducting Super Collider 1986', eds. R. Donaldson and J. Marx (1987), p. 320

[9] Particle Data Group, L. Montanet et al., Phys. Rev. D50 (1994) 1173

[10] G. Altarelli and G. Parisi, Nucl. Phys. B126 (1977) 298;
Yu.L. Dokshitzer, Sov. Phys. JETP 46 (1977) 641

[11] A.H. Mueller, Phys. Lett. B104 (1981) 161;
B.I. Ermolaev and V.S. Fadin, JETP Lett. 33 (1981) 269

[12] Yu.L. Dokshitzer, V.A. Khoze and S.I. Troyan, Sov. J. Nucl. Phys. (Yad. Fiz.) 47 (1988) 1384

[13] Yu.L. Dokshitzer, V.A. Khoze, A.H. Mueller and S.I. Troyan, Basics of Perturbative QCD (Editions Frontières, Gif-sur-Yvette, 1991)

[14] T. Hebbeker, Phys. Rep. 217 (1992) 69;
S. Bethke and J.E. Pilcher, Annu. Rev. Nucl. Part. Sci. 42 (1992) 251

[15] L3 Collaboration, B. Adeva et al., Phys. Lett. B248 (1990) 227;
OPAL Collaboration, M.Z. Akrawy et al., Z. Phys. C40 (1991) 49;
VENUS Collaboration, K. Abe et al., Phys. Rev. Lett. 66 (1991) 280;
DELPHI Collaboration, P. Abreu et al., Phys. Lett. B255 (1991) 466;
ALEPH Collaboration, D. Decamp et al., Phys. Lett. B284 (1992) 151

[16] A.A. Syed, Particle Correlations in Hadronic Decays of the Z^0 Boson (Ph.D. Thesis, Nijmegen, 1994)

[17] S. Catani, B.R. Webber, Yu.L. Dokshitzer and F. Fiorani, Nucl. Phys. B383 (1992) 419;
OPAL Collaboration, R. Akers et al., Z. Phys. C63 (1994) 363;
ALEPH Collaboration, D. Busculic et al., preprint CERN-PPE/94-208

[18] D. Schaile, CERN-PPE/94-162, to appear in the proceedings of the XXVII International Conference on High Energy Physics, Glasgow, July 1994

[19] M.H. Seymour, Lund preprint LU TP 94-7 (1994), to appear in Nucl. Phys. B

[20] T. Sjöstrand, Int. J. Mod. Phys. A3 (1988) 751

[21] B. Andersson, G. Gustafson, G. Ingelman and T. Sjöstrand, Phys. Rep. 97 (1983) 31

[22] OPAL Collaboration, P.D. Acton et al., Z. Phys. C58 (1993) 387, and in preparation

[23] R.J. Hemingway, OPAL-CR173, to appear in the proceedings of the XXVII International Conference on High Energy Physics, Glasgow, July 1994

[24] G. Gustafson, U. Pettersson and P. Zerwas, Phys. Lett. B209 (1988) 90

[25] T. Sjöstrand and V.A. Khoze, Phys. Rev. Lett. 72 (1994) 28, Z. Phys. C62 (1994) 281

[26] LEP 2 workshop presentation by L. Camilleri at the LEPC open meeting, CERN, November 1992

[27] L. Lönnblad and T. Sjöstrand, in preparation

[28] CDF Collaboration, F. Abe et al., Phys. Rev. D50 (1994) 2966

[29] H. Plothow-Besch, Comput. Phys. Commun. 75 (1993) 396

[30] T. Sjöstrand, Phys. Lett. 157B (1985) 321;
M. Bengtsson, T. Sjöstrand and M. van Zijl, Z. Phys. C32 (1986) 67

[31] M. Ciafaloni, Nucl. Phys. B296 (1987) 249;
S. Catani, F. Fiorani and G. Marchesini, Nucl. Phys. B336 (1990) 18;
G. Marchesini and B.R. Webber, Nucl. Phys. B349 (1991) 617

[32] CDF Collaboration, F. Abe et al., Phys. Rev. D50 (1994) 5562

[33] T. Sjöstrand and M. van Zijl. Phys. Rev. **D36** (1987) 2019

[34] AFS Collaboration. T. Åkesson et al.. Z. Phys. **C34** (1987) 163;
UA2 Collaboration. J. Alitti et al., Phys. Lett. **B268** (1991) 145;
CDF Collaboration, L.J. Keeble et al., in 'The Fermilab Meeting DPF 92', eds. C.H. Albright, P.H. Kasper, R. Raja
and J. Yoh (World Scientific. Singapore. 1993). Vol. 2, p. 1002

[35] G.A. Schuler and T. Sjöstrand. Phys. Lett. **B300** (1993) 169. Nucl. Phys. **B407** (1993) 539. CERN-TH.7193/94 (1994)

[36] H1 Collaboration. I. Abt et al.. Phys. Lett. **B328** (1994) 176

[37] TOPAZ Collaboration. H. Hayashii et al.. Phys. Lett. **B314** (1993) 149;
AMY Collaboration. B.J. Kim et al., Phys. Lett. **B325** (1994) 248

[38] X. Artru and G. Mennessier. Nucl. Phys. **B70** (1974) 93

[39] R.D. Field and R.P. Feynman, Nucl. Phys. **B136** (1978) 1

[40] UA1 Collaboration. G. Arnison et al.. Phys. Lett. **139B** (1984) 115 and **147B** (1984) 493

Triviality of $(\lambda_0\phi^4)_{s+1}$ in the Lee Approximation

F.A.B. Coutinho, J.F. Perez and W.F. Wreszinski

Instituto de Física, Universidade de São Paulo

The issue of (non) triviality of $(\lambda_0\phi^4)_{s+1}$ where s denotes the space dimension, and λ_0 the "bare" coupling constant, remains as one of the most important conceptual questions in quantum field theory [1]. In this note we summarize some of the ideas in two recent papers ([2], [3]).

Unfortunately, there are no rigorous results on triviality for $s = 3$ [1]. It is also important to compare this case, which is conventionally renormalizable with $s = 2$, which is superrenormalizable. Folklore predicts triviality in the former-case, and nontriviality in the latter [1].

Our basic result concerns the so called Lee approximation.

The Lee approximation has a long history, reviewed in ([4], chapter 11)]. We are basically interested in the model X_{s+1} ([4], pg. 69), defined by

$$H_\epsilon = H_0 + V_\epsilon$$

on symmetric Fock space where H_0 is the free Hamiltonian for a scalar Boson field, and V_ϵ is the cut-off (in our notation)

$$V_\epsilon = \lambda \int_{B_\epsilon} \prod_{i=1}^{4} \int \frac{d\vec{p_i}}{\sqrt{\mu_i}} \delta(\vec{p_1} + \vec{p_2} - \vec{p_3} - \vec{p_4}) a^*(\vec{p_1}) a^*(\vec{p_2}) a(\vec{p_3}) a(\vec{p_4}) \tag{1}$$

with $\mu_i \equiv \mu(\vec{p_i}) = \sqrt{\vec{p_i}^2 + m^2}$.

H_ϵ is singular for $\epsilon \to 0$. In this model, s is the space dimension. In which sense is this model an "approximation" to $(\lambda_0\phi^4)_{s+1}$? For this purpose, it is convenient to return to the interaction term in the nonrelativistic approximation, which may be written, up to multiplicative constants, in momentum space as [2],

$$\int_{B_\epsilon} \prod_{i=1}^{4} \int \frac{d\vec{p_i}}{\sqrt{\mu_i}} \delta(\vec{p_1} + \vec{p_2} - \vec{p_3} - \vec{p_4}) a^+(\vec{p_1}) a^+(\vec{p_2}) a(\vec{p_3}) a(\vec{p_4}) \tag{2}$$

with $\mu_i \simeq m_0 c^2$. If relativistic kinematics is preserved, i.e., $\mu_i = \mu(\vec{p_i}) = \sqrt{\vec{p_i}^2 + m^2}$ we are led to [2].

The significance of the Lee approximation may be understood from the model's limitations. As in the non relativistic limit (nrl), where creation and annihilation processes are kinematically suppressed, such procsses are neglected in the Lee approximation: here, too, the number operator commutes with the Hamiltonian, with Fock space decomposing into dynamically independent sectors. Further, due to the absence of vacuum polarization, the free and physical vacuum are identical, and hence no space cutoff is necessary to make the Hamiltonian a well-defined operator (Haag's theorem does no apply). However, the difficulties due to high momenta are present, and renormalization of mass and coupling constant are necessary. It will be seen that these features suffice to furnish results on triviality which are consistent with folklore. The main reason is that relativistic kinematics introduces a sort of ultraviolet cutoff in comparison with the nrl, compare [1] and [2] (where in the latter $\mu_i \simeq m_0 c^2$). Indeed, there is no Thomas effect when the kinematics is relativistic [2], and may restrict the analysis of the model to the $N=2$ particle sector.

One of our basic results [2, 3] is Theorem. In the Lee approximation the theory is either trivial or unbounded from below in some N-sector for N sufficiently large (hence physically unacceptable) if $s = 3$, and is nontrivial with semibounded Hamiltonian if $s = 2$. The above result is the first one supporting the folklore for $s = 3$.

References

1. R. Fernandez, J. Frohlich and A. Sokal-Random Walks, Critical Phenomena and Triviality in Quantum Field Theory, Springer-Verlag, 1992

2. F.A.B. Coutinho, J.F. Perez and W.F. Wreszinski On the Triviality of $(\lambda_0\phi^4)_d + 1$ in the Nonrelativistic and Lee Approximations - submitted to Ann. Phys. (N.Y.)

3. F.A.B. Coutino, J.F. Perez and W.F. Wreszinski - A Variational Proof of the Thomas Effect - submitted to J. Math. Phys.

4. K. Hepp, Théorie de la Renormalisation, Springer, 1969

5. T. Frederico. Phys. Lettl B282, 409 (1992)

On Universal Vassiliev Invariants[*]

Daniel Altschuler

Institut für Theoretische Physik, ETH-Hönggerberg, CH-8093 Zürich, Switzerland

and

Laurent Freidel

Laboratoire de Physique Théorique ENSLAPP,
Ecole Normale Supérieure de Lyon, 46, allée d'Italie, 69364 Lyon Cedex 07, France

Vassiliev's knot invariants [1] contain all the invariants, such as the Jones, HOMFLY and Kauffman polynomials, which can be obtained from a quantum group deformation $U_h(\mathcal{G})$ of the Hopf algebra structure of enveloping algebras $U(\mathcal{G})$, where $\mathcal{G}$ is a semisimple Lie algebra.

For a compact semisimple Lie group G with Lie algebra $\mathcal{G}$, Wilson loops in the quantized Chern-Simons model give knot invariants associated to $U_h(\mathcal{G})$ at special values $h = 2\pi i\, k^{-1}$, k a positive integer. The coefficients of the expansion in powers of h of these observables are examples of Vassiliev invariants. This is a particular case of a general theorem [2], which states that for all h the coefficients of the power series expansion of the invariants associated with semisimple Lie algebras are Vassiliev invariants.

By treating the Chern-Simons model with the conventional methods of perturbation theory, the coefficients of the powers of h of the observables can be computed [3]. Feynman diagrams and Feynman rules are the main tools of the computation. Given a knot, or more generally a link L, and the degree n (order in perturbation theory) or power of h in which one is interested, the corresponding invariant $V_n(L)$ results from the application of a Feynman rule $W_{\mathcal{G}}$ to a finite linear combination $Z_n^{CS}(L)$ of diagrams. The vector space D_n of diagrams of degree n is of finite dimension, and $Z_n^{CS}(L) \in D_n$ depends on L and on the form of the Chern-Simons action. The Feynman rule $W_{\mathcal{G}}$ depends on $\mathcal{G}$ and the representations occuring in the definition of the observables. It is an element of the dual space D_n^*, and $V_n(L) = \langle W, Z_n^{CS}(L) \rangle$.

Here we have used Bar-Natan's way [4] of describing Feynman rules and diagrams. He found that the diagrams and rules of Chern-Simons theory obey a small number of fundamental properties, and this led him to define general diagrams and rules, the latter which he called weight systems, by these same properties. Kontsevich [5] discovered an integral formula for an invariant $Z_n(L) \in D_n$, which plays for generic h the same role as $Z_n^{CS}(L)$ does for the special values in the Chern-Simons case. The main ingredient hiding behind it is the flat connection associated with the Knizhnik-Zamolodchikov equations. The formal power series $Z(L) = \sum_{n \geq 0} Z_n(L)\, h^n$ is called the universal Vassiliev invariant, since by varying W in $\langle W, Z(L) \rangle$ one gets all the invariants constructed from a deformation of the identity solution of the Yang-Baxter equation.

The knot invariants constructed using the representations of $U_h(\mathcal{G})$ have been generalized to all quasi-triangular Hopf algebras by Reshetikhin and Turaev [6]. Their construction is purely combinatorial, the proof of invariance consists in verifying that the Reidemeister moves do not change the relevant expressions. Recently, similar combinatorial definitions of universal Vassiliev invariants have appeared [7]. In our paper [9] we show that the combinatorial and the analytic definition of Kontsevich are equivalent. It turns out that the main contribution to $Z(L)$ is a type of series called ordered exponential in the physics literature. Ordered exponentials satisfy many interesting identities

---
[*]Talk given by the first author

which makes them very powerful. A crucial step in the proof of equivalence is to identify an expression for the Drinfeld associator [8] among the Kontsevich integrals. We do it quite naturally using only Drinfeld's definition of the associator as a monodromy operator between solutions of the Knizhnik-Zamolodchikov differential equations.

References

[1] V. A. Vassiliev. *Cohomology of knot spaces*, in "Theory of singularities and its applications" (ed. V. I. Arnold). Advances in soviet mathematics, AMS, 1990.

[2] J. Birman and X. S. Lin, Invent. Math. **111** (1993) 225.

[3] E. Guadagnini, M. Martellini and M. Mintchev, Phys. Lett. **B227** (1989) 111.
D. Bar-Natan, *Perturbative Chern-Simons Theory*. Princeton University preprint, 1990.
S. Axelrod and I. Singer. *Chern-Simons perturbation theory*. in the proceedings of the XXth International conference on differential geometric methods in theoretical physics. June 3-7, 1991. New York City (World Scientific. Singapore. 1992).

[4] D. Bar-Natan, *On the Vassiliev knot invariants*, Harvard University preprint, 1992.

[5] M. Kontsevich, *Vassiliev's knot invariants*, to appear in Advances in Soviet Mathematics.

[6] N. Reshetikhin and V. G. Turaev, Commun. Math. Phys. **127** (1990) 1.

[7] S. Piunikhine, *Combinatorial expression for universal Vassiliev link invariant*, Harvard University preprint, 1993.
P. Cartier, C. R. Acad. Sci. Paris Série I **316** (1993) 1205.

[8] V. G. Drinfeld. Leningrad Math. J. **1** (1991) 1419.
V. G. Drinfeld. Leningrad Math. J. **2** (1991) 830.

[9] D. Altschuler and L. Freidel, *On Universal Vassiliev Invariants*, to appear in Commun. Math. Phys.

Topologia de Schwarzschild

E. M. Monte e M. D. Maia

Edmundo@alpha.mat.unb.br   Maia@alpha.mat.unb.br

Através da caracterização de um espaço-tempo com simetria esférica, como subvariedade local de um espaço pseudo-Euclideano de dimensão seis e com diferentes assinaturas, investigamos a existência de uma diferença na topologia (não-Euclideana), $R^2 \times S^2$ da subvariedade. Esta diferença topológica está associada a diferença de assinatura do espaço ambiente. Examinamos especificamente os exemplos conhecidos, do espaço-tempo de Schwarzschild e de sua extensão máxima, o espaço de Kruskal. Verificamos que em algumas situações, como por exemplo o caso apresentado por Kasner, o espaço-tempo está simplesmente imerso. Por outro lado, com base em argumentos de causalidade e da preservação da estrutura dos cones de luz no espaço-tempo, sugerimos a necessidade de se caracterizar um mergulho propriamente dito em lugar de uma simples imersão, de modo a tornar a subvariedade compatível com as propriedades físicas do espaço-tempo.

Introdução

Vamos considerar o seguinte problema: "Determinar a geometria e a topologia do espaço físico externo a um corpo aproximadamente esférico de massa m. "

Gostaríamos de modelar nosso espaço físico através de um espaço-tempo quadridimensional [1]. A geometria para o nosso problema é descrita pela solução de Schwarzschild.

Observamos que devemos retirar as regiões, $r = 0$ e $r = 2m$ da variedade espaço-tempo nas coordenadas (t, r, θ, ϕ). Para garantirmos a existência de uma métrica associada ao nosso espaço, exigimos que este seja conexo e assim definimos,

a) Espaço-tempo exterior de Schwarzschild: (V_4, g)

Onde $V_4 = P_I^2 \times S^2$, $P_I^2 = \{(t,r) \in R/ \ r > 2m\}$ e S^2 a esfera de raio r. A métrica g é dada pela solução de Schwarzschild.

b) Buraco Negro de Schwarzschild: (B_4, g)

Onde $B_4 = P_{II}^2 \times S^2$, $P_{II}^2 = \{(t,r) \in R/ \ 0 < r < 2m\}$ e S^2 a esfera de raio r. Novamente a métrica g é dada pela solução de Schwarzschild.

É fato bastante conhecido que (B_4, g) e (V_4, g) podem ser estendidas para $r = 2m$. A extensão de $(E, g) = ([P_I^2 \cup P_{II}^2] \times S^2, g)$ foi dada por Kruskal [2], porém Fronsdal [3], um ano antes, obteve de forma indireta e usando o formalismo de imersão a indicação de tal extensão, $(E', g') = (Q^2 \times S^2, g')$, onde Q^2 é chamado de plano de Kruskal [1].

2. Topologia de Schwarzschild

Modelamos primeiramente nosso espaço físico por $(E, g) = ([P_I^2 \cup P_{II}^2] \times S^2, g)$. Temos que E é desconexo, já que é formado por duas componentes conexas desconectadas. Quando obtemos a extensão $(E', g') = (Q^2 \times S^2, g')$, através da imersão de Fronsdal, encontramos que E' é conexa. Conseguimos um espaço-tempo conexo para o nosso modelo matemático do campo gravitacional fora do corpo esférico.

Veja que $Q^2 \subset R^2$ e $[P_I^2 \cup P_{II}^2] \subset R^2$. É fácil ver que a topologia de Q^2 é dada por uma base de abertos de

R^2 [5], enquanto que a topologia de $[P_f^2 \cup P_{II}^2]$ é dada por uma base de abertos de R^2 menos a superfície $r = 2m$. Logo obtemos topologias diferentes para (E, g) e (E', g'), esta última sendo do tipo $R^2 \times S^2$.

Tomamos uma curva $\alpha(t)$ sobre (E, g), esta última mergulhada local e isometricamente em (E_6, η) e em (E_6, η'). Escrevemos em coordenadas,

$Y(\alpha(t)) = (Y_1(\alpha(t)), ..., Y_6(\alpha(t)))$ e $Y'(\alpha(t)) = (Y'_1(\alpha(t)), ..., Y'_6(\alpha(t)))$,

Onde observamos que no primeiro caso Y_1 e Y_2 sendo funções periódicas de t podem levar pontos distintos da variedade imersa em um mesmo ponto, possibilitando aparecer problemas de causalidade em (E, g). esta última antes de ser imersa poderia ter sido considerada sem estes problemas. Vemos que para a imersão de Fronsdal não temos estes problemas e lembramos que (E', g') foi obtida desta imersão.

Uma diferença topológica aparece entre (E', g') e (E, g), vinda do fato de termos mudado as coordenadas de imersão e da mudança de assinatura de E_6 [6].

Analisando o comportamento qualitativo de cones de luz, vemos que em (E, g) não podemos definir cones de luz em $r = 2m$, enquanto em (E', g') sim.

Como foi visto a imersão de Kasner é uma imersão mas não é um mergulho, já que esta última possui auto-intersecções, para intervalos apropriados do parâmetro t. No caso de Fronsdal, um cálculo simples mostra que de fato $Y' = Y'(x^i)$ é uma imersão além de ser um homeomorfismo, ou seja é um mergulho.

Note que a partir das definições de imersão e mergulho podemos caracterizar a topologia do espaço-tempo imerso em questão. Isto sugere uma metodologia para determinarmos propriedades glogais de um espaço-tempo .

Concluimos que (E', g') é o espaço-tempo que descreve o campo gravitacional exterior a um corpo de massa m e simetria esférica. A topologia deste campo é do tipo $R^2 \times S^2$, não Euclideana.

Referências

1. S.Hawking, G.Ellis - The Large Scale Structure of Space-Time, Cambridge (1973)

2. M.Kruskal - Phys.Rev., 119, 1743 (1960)

3. C.Fronsdal - Phys.Rev., 116, 778 (1959)

4. E.Kasner - Am.J.Math. 43, 130 (1965)

5. J. Dugundji - Topology, Boston (1966)

6. E.Monte e M.Maia - Preprint, XIV ENFPC (1993)

Classification of Second Order Symmetric Tensors in Kaluza-Klein-Type Theories

J. Santos,* M. J. Rebouças,† and A.F.F. Teixeira‡

* *Universidade Federal do Rio G. do Norte. Departamento de Física*

Caixa Postal 1641, 59072-970 Natal - RN. Brazil

† † *Centro Brasileiro de Pesquisas Físicas*

Departamento de Relatividade e Partículas

Rua Dr. Xavier Sigaud 150, 22290-180 Rio de Janeiro - RJ. Brazil

Using the theory of Jordan matrices we discuss the algebraic classification of second order symmetric tensors (Ricci tensor) on five-dimensional (5-D) Lorentzian manifolds M, extending previous results on this issue. We show that a symmetric two-tensor R can be classified in four Segre types and their twenty-two degeneracies. Using real half-null pentad bases for the tangent space $T_p(M)$ to M at p we derive a set of canonical forms for R_{ab}, generalizing the canonical forms for a symmetric two-tensor on 3-D and 4-D space-times manifolds.

1. Introduction

The algebraic classification of the Ricci part S_{ab} of the Riemman tensor in 4-D space-times (Segre classification) has been discussed by several authors [1] and is of interest in understanding some purely geometrical features of space-times [2-4], in classifying and interpreting matter field distributions [5-10], in determining limits of non-vacuum space-times [11], and as part of the procedure for checking the local equivalence of space-times [12].

Kaluza-Klein-type theories in five and more dimensions is of interest in at least two contexts. In gauge theories they have been used as a way to unify the fundamental interactions in physics. From a technical viewpoint, on the other hand, they have been employed as a tool for obtaining exact solutions in four dimensions [13].

In this work we briefly discuss the algebraic classification of second order symmetric tensors defined on 5-D Lorentzian manifolds M, extending previous results on this subject [14,15]. For a detailed account of our results see ref. [16].

2. Classification and Canonical Forms

In this work M is a real 5-D manifold endowed with a Lorentzian metric g of signature $(-++++)$. $T_p(M)$ denotes the tangent vector space to M at a point $p \in M$, and any tensorial lower case latin indices range from 0 to 4.

Let R_{ab} be the covariant components of a second order symmetric tensor R at $p \in M$. Given R_{ab} we may use the metric tensor to have the mixed form $R^a{}_b$ of R at $T_p(M)$. In this form the symmetric two-tensor R may be looked upon as a real linear operator $R : T_p(M) \longrightarrow T_p(M)$. If one thinks of R as a matrix $R^a{}_b$, one can formulate the eigenvalue problem

$$R^a{}_b V^b = \lambda \delta^a{}_b V^b. \tag{2.1}$$

*internet: janilo@dfte.ufrn.br
†internet: reboucas@cat.cbpf.br
‡internet: teixeira@cat.cbpf.br

where λ is scalar and V^b are the components of a generic eigenvector $V \in T_p(M)$. The fact that we have δ^a_b rather than g_{ab} on the right hand side of equation (2.1) makes apparent that we have cast the non-standard eigenvalue problem involving the hyperbolic (real) metric $R_{ab} V^b = \lambda g_{ab} V^b$ into the standard form (2.1) well known in linear algebra textbooks. However, R^a_b is no longer symmetric in general and the eigenvalue problem (2.1) gives rise to the Jordan block diagonal matrices.

When all eigenvalues of R are real similarity transformations exist under which R^a_b takes at p either one of the following Jordan canonical forms [16]:

$$
\begin{pmatrix}
\lambda_1 & 1 & 0 & 0 & 0 \\
0 & \lambda_1 & 1 & 0 & 0 \\
0 & 0 & \lambda_1 & 0 & 0 \\
0 & 0 & 0 & \lambda_2 & 0 \\
0 & 0 & 0 & 0 & \lambda_3
\end{pmatrix},
\quad
\begin{pmatrix}
\lambda_1 & 1 & 0 & 0 & 0 \\
0 & \lambda_1 & 0 & 0 & 0 \\
0 & 0 & \lambda_2 & 0 & 0 \\
0 & 0 & 0 & \lambda_3 & 0 \\
0 & 0 & 0 & 0 & \lambda_4
\end{pmatrix},
\quad
\begin{pmatrix}
\lambda_1 & 0 & 0 & 0 & 0 \\
0 & \lambda_2 & 0 & 0 & 0 \\
0 & 0 & \lambda_3 & 0 & 0 \\
0 & 0 & 0 & \lambda_4 & 0 \\
0 & 0 & 0 & 0 & \lambda_5
\end{pmatrix}.
$$

$\quad\quad$ (a) Segre type [311] $\quad\quad\quad\quad\quad$ (b) Segre type [2111] $\quad\quad\quad\quad$ (c) Segre type [1,1111]

or one of the possible block-degenerated Jordan matrices. Here $\lambda_1, \cdots, \lambda_5 \in \mathbb{E}$. The Segre type is a list of digits inside square brackets, where each digit refers to the multiplicity of the corresponding eigenvalue, which clearly is equal to the dimension of the corresponding Jordan block. The comma in type [1,1111] is used to separate eigenvalues associated to timelike and spacelike eigenvectors. We remark that the Lorentzian character of the metric g on M, together with the symmetry of R_{ab}, rule out the Segre types [5], [41], [32] and [221] and degeneracy thereof (see ref. [16] for details).

When R^a_b complex eigenvalues one can show [16] that it is necessarily diagonalizable over the complex field and possesses three real eigenvalues, i.e., only the Segre type [$z\bar{z}$111] and its specializations are permitted.

As far as the canonical forms are concerned, although the most general decomposition for the Ricci tensor in 5-D is given by

$$
\begin{aligned}
R_{ab} = \ & 2\rho_1\, l_{(a}m_{b)} + \rho_2\, l_a l_b + \rho_3\, x_a x_b + \rho_4\, y_a y_b + \rho_5\, z_a z_b + \rho_6\, m_a m_b \\
& + 2\rho_7\, l_{(a}x_{b)} + 2\rho_8\, l_{(a}y_{b)} + 2\rho_9\, l_{(a}z_{b)} + 2\rho_{10}\, m_{(a}x_{b)} + 2\rho_{11}\, m_{(a}y_{b)} \\
& + 2\rho_{12}\, m_{(a}z_{b)} + 2\rho_{13}\, x_{(a}y_{b)} + 2\rho_{14}\, x_{(a}z_{b)} + 2\rho_{15}\, y_{(a}z_{b)},
\end{aligned}
\tag{2.2}
$$

with $\rho_1, \ldots, \rho_{15} \in \mathbb{R}$, it is possible to show [16] that semi-null pentad bases with non-zero inner product

$$
l^a m_a = x^a x_a = y^a y_a = z^a z_a = 1
\tag{2.3}
$$

can be introduced at a point $p \in M$, such that the possible Segre types and the corresponding canonical forms for a second order symmetric tensor R at $p \in M$ are given by

Segre type	Canonical form	
[1,1111]	$R_{ab} = 2\rho_1\, l_{(a}m_{b)} + \rho_2\, (l_a l_b + m_a m_b) + \rho_3\, x_a x_b + \rho_4\, y_a y_b + \rho_5\, z_a z_b,$	(2.4)
[2111]	$R_{ab} = 2\rho_1\, l_{(a}m_{b)} \pm l_a l_b + \rho_3\, x_a x_b + \rho_4\, y_a y_b + \rho_5\, z_a z_b,$	(2.5)
[311]	$R_{ab} = 2\rho_1\, l_{(a}m_{b)} + 2 l_{(a}x_{b)} + \rho_1\, x_a x_b + \rho_4\, y_a y_b + \rho_5\, z_a z_b,$	(2.6)
[$z\bar{z}$111]	$R_{ab} = 2\rho_1\, l_{(a}m_{b)} + \rho_2\, (l_a l_b - m_a m_b) + \rho_3\, x_a x_b + \rho_4\, y_a y_b + \rho_5\, z_a z_b,$	(2.7)

and the twenty-two degeneracies thereof. Here $\rho_1, \cdots, \rho_5 \in \mathbb{R}$ and $\rho_2 \neq 0$ in (2.7).

References

[1] G. S. Hall, *Diff. Geom.* 12, 53 (1984). This reference contains an extensive bibliography on the classification of the Ricci tensor on 4-dimensional Lorentzian space-times manifolds.

[2] R. V. Churchill, *Trans. Amer. Math. Soc.* 34, 784 (1932).

[3] J. Plebański, *Acta Phys. Pol.* 20, 963 (1964).

[4] W. J. Cormack and G. S. Hall, *J. Phys.* A 12, 55 (1979).

[5] G. S. Hall and D. A. Negm, *Int. J. Theor. Phys.* 25, 405 (1986).

[6] G. S. Hall, *Arab. J. Sci. Eng.* 9, 87 (1984).

[7] J. J. Ferrando, J.A. Morales and M. Portilla, *Gen. Rel. Grav.* 22, 1021 (1990).

[8] M. J. Rebouças and A. F. F. Teixeira, *J. Math. Phys.* 32, 1861 (1991).

[9] M. J. Rebouças and A. F. F. Teixeira, *J. Math. Phys.* 33, 2855 (1992).

[10] J. Santos, M. J. Rebouças and A. F. F. Teixeira, *J. Math. Phys.* 34, 186 (1993).

[11] G. S. Hall, M. A. H. MacCallum, F. M. Paiva and M. J. Rebouças, "Limits in the Segre Classification of the Energy-momentum Tensor in General Relativity," in preparation (1995).

[12] For a fairly extensive bibliography on this subject see, for example. M. A. H. MacCallum and J. E. F. Skea, "SHEEP: A Computer Algebra System for General Relativity", in *Algebraic Computing in General Relativity, Lecture Notes from the First Brazilian School on Computer Algebra.* Vol. II, edited by M. J. Rebouças and W. L. Roque. Oxford U. P., Oxford (1994).

[13] See, for example, R. J. Gleiser and M. C. Diaz, *Phys. Rev.* D 37, 3761 (1988) and references therein quoted on this subject.

[14] G. S. Hall, *J. Phys.* A 9, 541 (1976).

[15] G. S. Hall, T. Morgan and Z. Perjés, *Gen. Rel. Grav.* 19, 1137 (1987).

[16] J. Santos, M. J. Rebouças and A. F. F. Teixeira, "Classification of Second Order Symmetric Tensors in 5-Dimensional Kaluz-Klein-Type Theories," to appear in *J. Math. Phys.* (1995).

On perturbation theory for the cosmological standard model

Mario Novello, Renato Klippert Barcellos

Centro Brasileiro de Pesquisas Físicas - Laboratório de Cosmologia e
Física Experimental de Altas Energias - Brasil

The field equations of Einstein are nonlinear, and so there is no known method to obtain solutions for them. Hence the theory of perturbations is a powerful tool in gravitational and cosmological research. However, there are some difficulties known as "gauge problems": there is no unique way to map the background solution onto the perturbed one. We have used the Hawking's point of view to describe the perturbations only in terms of objects that vanish in the background, to get solutions for the vectorial and tensorial components of the perturbations of the Universe of Friedman-Robertson -Walker, the "Standard Model" of cosmology today. The formalism so obtained is translated to Hamiltonian language, making possible the quantization of the perturbations of a classical cosmological solution. Some remarks are made on the stability of the model being considered.

Estudo qualitativo de teorias
do tipo Kaluza-Klein

Antonio B. Batista, Júlio C. Fabris e Eduardo V. Tonini

Departamento de Física - Centro de Ciências Exatas
Universidade Federal do Espírito Santo, Vitória

1. Introdução

Em teorias do tipo Kaluza-Klein, formuladas em $(n = 4 + D)$ dimensões, as dimensões extras sofrem uma compactificação, isto é, suas escalas características são da ordem do comprimento de Planck [1]. Estudamos as possíveis soluções cosmológicas da teoria de Kaluza-Klein para um modelo sem matéria, mas com dimensão arbitrária. Com a adoção da métrica espacialmente plana de Robertson-Walker reduzimos as equações diferenciais a um sistema planar e autônomo cujas soluções são analisadas utilizando a teoria dos sistemas dinâmicos [2].

2. Equações de Campo

A densidade lagrangeana e a métrica adotada são

$$\ell = \sqrt{g}R \tag{1}$$

$$ds^2 = g_{\mu\nu}dx^\mu dx^\nu - \phi^2 \gamma_{ij}dx^i dx^j . \tag{2}$$

onde $\mu, \nu = 0, 1, 2, 3$ e $i, j = 1, 2, ..., D$.

Considerando $g_{\mu\nu}$ como a métrica espacialmente plana de Robertson-Walker, definindo $U = \phi^D$, substituindo $x = \frac{\dot{a}}{a}$, onde a é o fator de escala para o espaço físico, e $y = \frac{\dot{U}}{U} = D\frac{\dot{\phi}}{\phi} = -\frac{\dot{G}}{G}$ [3], onde G é o acoplamento gravitacional, as equações de campo tomam a forma de um sistema planar e autônomo

$$3x^2 + \frac{(D-1)}{2D}y^2 + 3xy = -k\frac{D(D-1)}{2}U^{-\frac{2}{D}} . \tag{3}$$

$$\dot{x} + \frac{3}{2}x^2 + \frac{(D+1)}{4D}y^2 + xy + \frac{1}{2}\dot{y} = -k\frac{D(D-1)}{4}U^{-\frac{2}{D}} . \tag{4}$$

$$\dot{y} + y^2 + 3xy = -kD(D-1)U^{-\frac{2}{D}} . \tag{5}$$

3. Caso $FRW(K = 0)$ x $T^D(\bar{K} = 0)$

Considerando a curvatura do espaço interno nula encontramos apenas duas soluções, sob a forma de lei de potência, compatíveis com as equações de campo. Estas soluções são representadas no diagrama de fase por retas passando pela origem do plano (raios invariantes). Para $D = 1$, temos o primeiro raio invariante descrevendo um universo onde o espaço-tempo é Minkowskiano, mas com acoplamento gravitacional variando. No segundo raio invariante temos um segmento que representa um modelo Big-Bang evoluindo para o espaço-tempo de Minkowski

com acoplamento gravitacional crescente e contração das dimensões internas. O outro segmento representa um Big-Crunch com acoplamento gravitacional decrescente. Para $D \geq 2$, a solução fisicamente aceitável é semelhante à descrita pelo segundo raio invariante para $D = 1$.

4. Caso $FRW(K = 0) \times S^D(\bar{k} \neq 0)$

Para $\bar{k} = 1$ e $D = 1$ temos as mesmas soluções que o caso $\bar{k} = 0$ e $D = 1$. Para $\bar{k} = 1$ e $D \geq 2$ não há soluções fisicamente aceitáveis.

Para $\bar{k} = -1$ e $D = 1$ temos novamente as mesmas soluções encontradas no caso $\bar{k} = 0$ e $D = 1$. Para $D \geq 2$, a região física do espaço de fase apresenta soluções que representam um universo partindo de uma singularidade do tipo Big-Bang com contração, no início, do espaço interno mas com o espaço físico expandindo para Minkowski.

5. Modelo Derivado da Supergravidade à onze dimensões

Finalmente consideramos uma densidade lagrangeana derivada da supergravidade a 11−dimensões [4]

$$\mathcal{L} = \sqrt{g}(R + \frac{1}{12}F_{ABCD}F^{ABCD})$$ (6)

onde $F_{\mu\nu\lambda\gamma} = f(t)\epsilon_{\mu\nu\lambda\gamma}(\mu,\nu,\lambda,\gamma = 0,1,2,3)$ [5].Com a mesma escolha da métrica e das definições de x e y nós obtemos o sistema planar

$$3x^2 + 21xy + 21y^2 = 4\pi G f^2 .$$ (7)

$$\dot{x} + 2x^2 + 6xy + 2\dot{y} + 7y^2 = -\frac{4}{3}\pi G f^2 .$$ (8)

$$2\dot{x} + 3x^2 + 14xy + 7\dot{y} + 28y^2 = 4\pi G f^2 .$$ (9)

As soluções do tipo lei de potência só são compatíveis com as equações de campo para f imaginário ou nulo. As soluções físicas representam modelos partindo de uma singularidade e evoluindo para o espaço-tempo de Minkowski com contração do espaço interno no início da evolução.

6. Conclusão

Em geral as soluções encontradas indicam que deve ocorrer uma singularidade ou no passado ou no futuro. A presença dessa singularidade é inevitável neste caso. Encontramos também que nas soluções físicas o universo começa sua evolução com o espaço interno contraindo-se.

Bibliografia

(1) A. Chodos e S. Detweiler, *Where's Gonne the Fifth Dimension*, Phys. Rev. D21, 2167(1980);

(2) G. Sansone e R. Conti,*Non-Linear Differential Equations*, Pergamon Press, Oxford(1964);

(3) J.C. Fabris, *A Cosmological Solution from the Generalized Marwell-Einstein Theory*, Phys. Lett. B267, 30(1991);

(4) E. Cremmer, B. Julia e J. Scherk, *Eleven Dimensional Supergravity*, Phys. Lett. 76B, 409(1979);

(5) P.G.O. Freund,*On Kaluza-Klein Cosmology*,Nuclear Physics B209, 146(1982).

Perturbações de Densidade com Pressões Negativas

Júlio César Fabris*e Jérôme Martin†

9 de Janeiro de 1995

1. Introdução

O problema da formação das estruturas em larga escalas observadas no Universo, é um dos mais relevantes atualmente em Cosmologia. O tratamento clássico para este problema foi inicialmente feito por Lifschitz e Khalatnikov (E.M. Lifschitz, JETP 16. 587(1946); E.M. Lifschitz and I. Khalatnikov, Adv. Phys. 12, 185(1963)). através do estudo da evolução de pequenas perturbações na densidade em um Universo homogeneo e isótropo em expansão. A conclusão a que foram levados é a de que o crescimento de tais perturbações é insuficiente para explicar a existência das aglomerações de matéria em galáxias e aglomerados de galáxias. De qualquer forma, aqueles autores estabeleceram um método padrão para o estudo deste tipo de problema. Apesar de críticas posteriores que foram feitas ao método empregado, devido à não-invariância das quantidades físicas em relação à escolha do sistema de coordenadas, o método de Lifschitz-Khalatnikov, utilizando o calibre sincrônico, forneceu todas as informações físicas básicas existentes sobre este problema.

Nós nos propomos a utilizar o método de Lifschitz-Khalatnikov no estudo de perturbações de densidade com pressões negativas. O interesse de tal estudo reside no fato que, durante a fase inflacionária, quando $p = -\rho$, as perturbações de densdidade são estritamente nulas; para se obter inhomogeneidades na distribuição de matéria, é preciso se afastar da condição de inflação. Logo, a questão da existencia de pressões negativas outras que a de inflação adquire sua relevancia. Nós mostraremos que, as perturbações de densidade se dividem em tres tipos, segundo o valor da equação de estado, que nós assumiremos como do tipo barotrópica ($p = \alpha\rho$): Para $1 \geq \alpha > -\frac{1}{3}$, existe um modo crescente e um decrescente; para $-\frac{1}{3} > \alpha > -1$, existem apenas modos descrecentes; para $-1 > \alpha$ existem modos que crescem a uma taxa do tipo exponencial. Existem dois valores críticos ($\alpha = -\frac{1}{3}, -1$). que serão discutidos mais abaixo.

2. As Equações Perturbadas e suas Soluções

Nós consideramos as equações de Einstein, às quais impomos uma métrica espacialmente plana e um conteúdo material dado por um fluido perfeito com uma equação de estado barotrópica. Obtemos então as seguintes equações diferenciais conectando $a(t)$ (fator de escala) e $\rho(t)$ (densidade):

$$3(\frac{\dot{a}}{a})^2 = 8\pi G\rho \quad . \tag{1}$$

$$\dot{\rho} + 3\frac{\dot{a}}{a}(1+\alpha)\rho = 0 \quad . \tag{2}$$

onde α é uma constante que define a equação de estado ($p = \alpha\rho$). A solução geral para $a(t)$ é:

$$a(t) = a_0 t^{\frac{2}{3(1+\alpha)}} \quad . \tag{3}$$

*Departamento de Física, Universidade Federal do Espírito Santo, Goiabeiras, Vitória - CEP29060-900 - Espírito Santo - Brasil.
†Laboratoire de Gravitation et Cosmologie Relativistes, Université Pierre et Marie Curie - CNRS/URA 769, 4, Place Jussieu - Tour 22/12 - 4ème Étage - Boîte Courrier 142, 75252 Paris Cedex 05 - França.

Observamos que para $\alpha > -\frac{1}{3}$ o fator de escala cresce mais lentamente que o horizonte: para $\alpha < -\frac{1}{3}$ o fator de escala cresce mais rapidamente que o horizonte. Quando $\alpha = -\frac{1}{3}$ o fator de escala cresce à mesma taxa que o horizonte.

Para estudar a evolução das perturbações de densidade, nós introduzimos as quantidades

$$\tilde{g}_{\mu\nu} = \overset{o}{g}_{\mu\nu} + h_{\mu\nu} \quad , \tilde{\rho} = \overset{o}{\rho} + \delta\rho \quad , \tilde{p} = \overset{o}{p} + \delta p \quad , \tag{4}$$

onde $\overset{o}{g}_{\mu\nu}$, $\overset{o}{\rho}$ e $\overset{o}{p}$ são as soluções de base descritas acima e $h_{\mu\nu}$. $\delta\rho$ e δp são pequenas perturbações em torno delas. Nós impomos o calibre sincrônico $h_{\mu 0} = 0$. Visto que estamos interessados em perturbações de densidade. nós podemos manipular as equações perturbadas, desacoplando os modos escalares e exprimindo-as em termo das quantidades $h = \frac{h_{kk}}{a^2}$, $\Delta = \frac{\delta\rho}{\rho}$ e $\Theta = \delta u^i_{,i}$. Uma combinação das equações resultantes permite determinar uma única equação para Δ:

$$\dddot{\Delta} + \frac{11 - 3\alpha}{3(1+\alpha)} \frac{\ddot{\Delta}}{t} + \left(\alpha(\frac{q}{a})^2 - \frac{2}{9} \frac{(9\alpha^2 + 24\alpha - 5)}{(1+\alpha)^2} \frac{1}{t^2} \right)\dot{\Delta} +$$
$$\left(\alpha(\frac{q}{a})^2 \frac{1}{t} - \frac{2}{9} \frac{(1+3\alpha)(1-9\alpha)}{(1+\alpha))^2} \frac{1}{t^3} \right)\Delta = 0 \quad . \tag{5}$$

Essa equação admite uma solução geral, quando α é positivo, sob a forma.

$$\Delta = \frac{1}{x^{\frac{1}{p}}} \int x^{\frac{4}{3}} \left(c_1 J_\nu(\sqrt{q}\frac{q}{p}x) + c_2 N_\nu(\sqrt{\alpha}\frac{q}{p}x) \right) dx \quad . \tag{6}$$

Em (6). os J_ν são funções de Bessel de ordem ν. Por outro lado. se α é negativo. nós encontramos.   !

$$\Delta = \frac{1}{x^{\frac{1}{p}}} \int x^{\frac{4}{3}} \left(c_1 K_\nu(\sqrt{q}\frac{q}{p}x) + c_2 I_\nu(\sqrt{\alpha}\frac{q}{p}x) \right) dx \quad . \tag{7}$$

Em (7), $K_\nu(x)$ e $I_\nu(x)$ são funções de Bessel modificadas.

3. Análise dos Resultados

O estudo assintótico das soluções permite compreender de forma mais simples o comportamento das perturbações de densidade segundo o valor de α. Nós nos limitaremos aqui a resumir os resultados. Fazendo $t \to 0$, observamos que para $\alpha > -\frac{1}{3}$, existem um modo crescente e outro decrescente; mas. se $-\frac{1}{3} > \alpha > -1$, existem apenas modos decrescentes; por outro lado, para $\alpha < -1$, existem modos que crescem fortemente. No caso em que $\alpha = -1$, as perturbações de densidade são nulas; por outro lado. quando $\alpha = -\frac{1}{3}$. obtemos $\Delta_\pm = t^{-1\pm\sqrt{1+q}}$, onde q é o número de onda da perturbação. Observamos, finalmente, que as perturbações de densidade oscilam. com modo crescente ou decrescente, quando entram dentro do horizonte, apenas quando a pressão é positiva: quando a pressão é negativa. tais oscilações não ocorrem.

Perturbações Cosmológicas na Teoria de Brans-Dicke

J. Plínio Baptista, Júlio C. Fabris, Sergio V. B. Gonçalves*

Departamento de Física, Universidade Federal do Espírito Santo, Goiabeiras

Vitória, Espírito Santo, Brasil

9 de Janeiro de 1995

É analisado o desenvolvimento de perturbações escalares na Teoria de Brans-Dicke(TBD). Assumindo a equação barotrópica $p = \alpha\rho$, estudamos os seguintes casos: vácuo($p = 0$), inflação ($\alpha = -1$), radiação ($\alpha = \frac{1}{3}$), matéria incoerente ($\alpha = 0$).

1. Descrição do Modelo

O ponto de partida da TBD é de se considerar G dependente do tempo através da introdução de um campo escalar ϕ.

A ação na TBD é dada por:

$$A = \int d^4x \sqrt{g}[-\phi R + w(\frac{\phi_{,\mu}\phi^{,\mu}}{\phi}) + 16\pi L_{mat}] \tag{1}$$

Através do Princípio Variacional, impondo a métrica de Robertson-Walker e exprimindo a matéria em termos de um fluido perfeito, obtemos as equações de movimento:

$$\frac{\ddot{R}}{R} + 2\frac{\dot{R}^2}{R^2} + 2\frac{k}{R^2} = \frac{8\pi}{\phi}[\frac{\rho + w(\rho - p)}{3 + 2w}] - \frac{\dot{\phi}}{\phi}\frac{\dot{R}}{R} \tag{2}$$

$$\frac{-3\ddot{R}}{R} = \frac{8\pi}{\phi}[\rho - \frac{(1+w)}{(3+2w)}(\rho - 3p)] + \frac{w}{\phi^2}\dot{\phi}^2 + \frac{1}{\phi}\ddot{\phi} \tag{3}$$

$$\ddot{\phi} + \frac{3\dot{R}}{R}\dot{\phi} = \frac{8\pi}{3+2w}(\rho - 3p) \tag{4}$$

$$\dot{\rho} = -3\frac{\dot{R}}{R}(\rho + p) \tag{5}$$

Perturbando as equações de base, considerando $k = 0$, $p = \alpha\rho$ e o calibre síncrono, temos as três equações para as componentes da perturbação na métrica, h_{ij}, h_{it}, h_{tt}, além das equações perturbadas para o campo ϕ e da conservação da energia:

$$\frac{1}{2R^2}[\nabla^2 h_{ij} - h_{jk,i,k} - h_{ik,j,k} - h_{kk,i,j}] - \frac{1}{2}\ddot{h}_{ij} - \frac{\dot{R}}{2R}[\delta_{ij}\dot{h}_{kk} - \dot{h}_{ij}] -$$

$$-\frac{\dot{R}^2}{R^2}[2h_{ij} - \delta_{ij}h_{kk}] = -\frac{8\pi}{\phi^2}\rho R^2 \delta_{ij}\delta\phi\frac{(w - w\alpha + 1)}{(3+2w)} + \frac{8\pi}{\phi}\{\rho h_{ij}[-\alpha - \frac{(1+w)}{(3+2w)}(1 - 3\alpha)] +$$

$$+R^2\delta_{ij}\delta\rho[\alpha + \frac{(1+w)}{(3+2w)}(1 - 3\alpha)]\} + \frac{1}{\phi}\delta\phi_{,i,j} \tag{6}$$

*E-mail: SERVITO@NPD2.UFES.BR

$$-\frac{1}{2}\{\frac{1}{R^2}(-h_{kk,i}+h_{ik,k})\}_{,t} = \frac{8\pi}{\phi}\rho\delta U^i(1+\alpha) + \frac{w}{\phi^2}\delta\phi_{,i}\dot{\phi}_{,t} + \frac{1}{\phi}\delta\phi_{,i}\,;_t \tag{7}$$

$$\frac{1}{2R^2}[\ddot{h}_{kk} - 2\frac{\dot{R}}{R}\dot{h}_{kk} + 2\frac{(\dot{R}^2 - R\ddot{R})}{R^2}h_{kk}] = -\frac{8\pi}{\phi^2}\rho\delta\phi[\frac{(3w\alpha + w + 2 + 3\alpha)}{(3+2w)}]+$$

$$+\frac{8\pi}{\phi}[\delta\rho\frac{(3w\alpha + w + 2 + 3\alpha)}{(3+2w)}] - \frac{2w}{\phi^3}\delta\phi\dot{\phi}^2 + \frac{2w}{\phi^2}\delta\phi\dot{\phi} - \frac{1}{\phi^2}\delta\phi\ddot{\phi} + \frac{1}{\phi}\delta\ddot{\phi} \tag{8}$$

$$\delta\ddot{\phi} + \frac{\dot{R}}{R^3}h_{kk}\dot{\phi} - \frac{1}{R^2}\nabla^2\delta\phi - \frac{1}{2R^2}\dot{h}_{kk}\dot{\phi} + 3\frac{\dot{R}}{R}\delta\dot{\phi} = \frac{8\pi}{3+2w}\delta\rho(1-3\alpha) \tag{9}$$

$$\delta\dot{\rho} + 3\delta\rho(1+\alpha)\frac{\dot{R}}{R} - \rho(1+\alpha)[\frac{1}{2R^2}\dot{h}_{kk} - \frac{\dot{R}}{R^3}h_{kk} - \delta U^i_{,i}] = 0 \tag{10}$$

Descrevemos agora as soluções para o modo escalar.

- Universo sem matéria($\rho = 0$):

$$\lambda = \frac{1}{t}\{\int[C_1 t^{1-r}J_1(\frac{t^{1-r}q}{1-r}) + C_2 t^{1-r}N_1(\frac{t^{1-r}q}{1-r}]dt + C_3\} \tag{11}$$

onde $\lambda = \frac{\delta\phi}{\phi}$.

- Universo com matéria ($\rho \neq 0$)

•• Inflação ($\alpha = -1$):

$$\lambda = \frac{1}{t}\{\int[C_1 t^{\frac{r-3r^2}{2}}J_k(\frac{t^{1-r}q}{1-r}) + C_2 t^{\frac{r-3r^2}{2}}N_k(\frac{t^{1-r}q}{1-r})]dt + C_3\} \tag{12}$$

$$\Delta = 0 \tag{13}$$

onde $\Delta = \frac{\delta\rho}{\rho}$.

•• Radiação ($\alpha = \frac{1}{3}$):

$$\Delta(t) = \frac{6r^2 - 13r + 6}{qt^{\frac{1}{2}}}\{J_\nu(\xi)\int\frac{1}{t^{2-3r}}[\frac{N_\nu(\xi)}{N_\nu(\xi)J'_\nu(\xi) - N'_\nu(\xi)J_\nu(\xi)}]dt+$$

$$+N_\nu(\xi)\int\frac{1}{t^{2-3r}}[\frac{J_\nu(\xi)}{J_\nu(\xi)N'_\nu(\xi) - J'_\nu(\xi)N_\nu(\xi)}]dt\} + C_1 J_\nu(\xi)+$$

$$+C_2 N_\nu(\xi) + t^{2-2r} \tag{14}$$

onde $\xi = \frac{qt^{1-r}}{1-r}$.

•• Matéria Incoerente ($\alpha = 0$):

$$\Delta(t) = \frac{1}{t}\{\int t^{\frac{3}{2}}[\frac{q}{\sqrt{3}}J_\nu(\xi)\int F(\lambda)\frac{t^{-\frac{1}{2}}N_\nu(\xi)}{N_\nu(\xi)J'_\nu(\xi) - N'_\nu(\xi)J_\nu(\xi)}dt + C_1 J_\nu(\xi)+$$

$$+\frac{q}{\sqrt{3}}N_\nu(\xi)\int F(\lambda)\frac{t^{-\frac{1}{2}}J_\nu(\xi)}{J_\nu(\xi)N'_\nu(\xi) - J'_\nu(\xi)N_\nu(\xi)}dt + C_2 N_\nu(\xi)]dt\}+$$

$$+\frac{1}{t}C_3 \tag{15}$$

onde $\xi = \frac{2qt^{\frac{1}{2}}}{\sqrt{3}}$, $\qquad F(\lambda) = \frac{1}{3t}\dot{f}(\lambda) + \frac{1}{6t^2}f(\lambda)$, e $f(\lambda) = 4t\ddot{\lambda} - \frac{3}{t}\lambda$.

Em relação aos resultados correspondentes da Relatividade Geral, observamos a existência de oscilações para o caso $p = 0$. Entretanto, para os outros casos as características gerais são as mesmas. Em particular, as perturbações de densidade são nulas para o caso de inflação.

Um Cenário Cosmológico Anti-Big Bang

Flávio Gimenes Alvarenga e Júlio César Fabris

Departamento de Física, Universidade Federal do Espírito Santo - UFES

Av. Fernando Ferrari s/n , CEP 29060-900 Vitória - ES, Brasil

Introdução

Uma generalização do campo de maxwell escrito sob uma 3-forma, que preserva sua invariância conforme à seis dimensões, pode ser acoplada à gravitação nesta dimensão. A redução dimensional ao espaço físico revela um cen ário cosmológico com gravitação ordinária e dois campos escalares: um campo é originado da métrica relativa ao espaço-interno e o outro deriva do campo conforme.

As soluções cosmológicas, classificadas em função da natureza da matéria acoplada, descrevem um Universo Primordial infinito em sua origem e caracterizado por uma fase inicial de contração. Tal comportamento define uma Cosmologia Anti-Big Bang.

Analisa-se no âmbito deste modelo a produção de entropia no Universo físico.

O Modelo

As equações de Einstein em presença de um campo conforme (3-forma $F_{A_1 A_2 A_3}$) podem ser escritas à seis dimensões como:

$$R_{MN} - \frac{1}{2}g_{MN}R = 8\pi G T_{MN} + F_{M A_1 A_2}F_N{}^{A_1 A_2} - \frac{1}{6}g_{MN}F_{A_1 A_2 A_3}F^{A_1 A_2 A_3} \tag{1}$$

A métrica hexadimensional descrevendo um Universo físico homogêneo e isotrópico assume a forma

$$ds^2 = g_{MN}dx^M dx^N \qquad , \qquad M,N = 0,1,....5. \tag{2}$$

$$g_{MN} = \begin{cases} g_{00} = +1 \\ g_{ij} = -a(t)^2(1 + kr^2)^{-1}\delta_{ij} & (i,j = 1,2,3) \\ g_{ab} = -u(t)\delta_{ab} & (a,b = 4,5) \end{cases}$$

Esta métrica nos permite definir a geometria do espaço-tempo em termos de g_{ab} e $u = \phi^2$, o campo de gravitação e o campo escalar associado às dimensões internas, respectivamente.

O tensor momento-energia T_{MN} deverá conter as pressões p e p' relativas aos espaços físico e interno:

$$T_{MN} = \begin{cases} T_{00} = \epsilon(t) \\ T_{ij} = -p(t)g_{ij} & (i,j = 1,2,3) \\ T_{ab} = -p'(t)g_{ab} & (a,b = 4,5) \end{cases} \tag{3}$$

A definição de $F_{oab} = \Psi_{;a}$ como a única componente não-nula do campo de maxwell generalizado determina um sistema de equações acopladas para a, u e Ψ:

$$3\frac{a''}{a} - 9\frac{a'^2}{a^2} = -2\pi G(3\epsilon + 3p + 2p')a^6 - \frac{u''}{u} + 3\frac{a'}{a}\frac{u'}{u} + \frac{1}{2}\frac{u'^2}{u^2} - \frac{1}{2}A^2 \tag{4}$$

$$\frac{a''}{a} - \frac{a'^2}{a^2} = 2\pi G(\epsilon + p - 2p')a^6 - \frac{a'}{a}\frac{u'}{u} + \frac{1}{2}A^2 \qquad (5)$$

$$u'' + A^2 u = 4\pi G(\epsilon - 3p + 2p')a^6 u \qquad (6)$$

$$\Psi' = \frac{A}{\sqrt{2}}u \qquad (7)$$

As linhas indicam as derivadas em relação à coordenada reparametrizada θ ($dt = a^3 d\theta$).

Soluções Cosmológicas

As equações de movimento podem ser agora resolvidas de acordo com a forma da matéria acoplada, através de equações de estado barotrópicas $p = \alpha\epsilon$ e $p' = \alpha'\epsilon$. Uma classe de soluções analíticas pode ser obtida para os casos $\alpha = \alpha' = 0$; $\alpha = 1$, $\alpha' = 0$; $\alpha = \frac{1}{3}$, $\alpha' = 0$ e $\alpha = \alpha' = 1$. Neste paper analisaremos os dois últimos casos:

a) **Fluido de Radiação** $(p = \frac{\epsilon}{3}$, $p' = 0)$

$$a(\theta) = \frac{a_0}{\sqrt{sen\theta}} \frac{tan^{1/\sqrt{6}}\frac{\theta}{2}}{1 - tan^{2/\sqrt{6}}\frac{\theta}{2}} \qquad (8)$$

$$u(\theta) = u_0 sen\theta \qquad (9)$$

O estudo assintótico da solução (8) exibe mais claramente o comportamento do fator de escala relativo ao espaço-físico. O fator de escala a evolui inicialmente segundo

$$a \propto t^{-0.12} \qquad , \qquad t \to 0 (\theta \to 0)$$

revelando um Universo que começa infinito, mas com uma rápida fase inicial de contração. Para tempos maiores a evolução do Universo modifica-se para

$$a \propto t^{+0.52} \qquad , \qquad t \to \infty (\theta \to \pi)$$

de modo tal que o Universo passa a expandir-se à uma taxa próxima a descrita pelo Modelo Padrão. Portanto, o Universo possui distância própria inicial infinita entre quaiquer pontos do espaço-tempo, contraindo-se rapidamente até que seu fator de escala atinja um valor mínimo diferente de zero, a partir do qual o Universo evolui em expansão. Essa forma de evolução cosmológica determina um cenário Anti-Big Bang.

O campo escalar u associado ao espaço-interno evolui de modo a compactificar as dimensões internas.

b) **Matéria Rígida** $(p = \epsilon$, $p' = \epsilon)$

$$\epsilon a^6 u^2 = M = cte.$$

$$a(\theta) = \frac{a_0}{\sqrt{senA\theta}} tan^s \frac{A\theta}{2} \qquad (10)$$

$$u(\theta) = u_0 senA\theta \qquad (11)$$

$$s = \frac{1}{\sqrt{3}A}(\frac{16\pi M + A^2 u_0^2}{2u_0^2})^{1/2}.$$

Uma análise da solução para o raio do Universo (10) revela uma forte dependência do parâmetro de massa M. Esse parâmetro constante está associado ao produto da massa total do Universo pelo volume espacial.

Para estudar tal dependência é conveniente adotar os valores $A = 1$ e $u_0 = 1$ para as constantes de integração. Como a massa é sempre positiva, pode-se estimar que todas as soluções fisicamemte aceitáveis correspondem a $s \geq \frac{1}{\sqrt{6}}$.

A evolução assintótica da solução (10) é descrita por

$$a \propto t^{\frac{(s-1/2)}{(3s-1/2)}} \qquad (t \to 0)$$

$$a \propto t^{\frac{(s+1/2)}{(3s+1/2)}} \qquad (t \to \infty)$$

Observa-se um Universo com fase inicial de contração apenas para $s < \frac{1}{2}$. Para $s = \frac{1}{2}$ o fator de escala $a(t)$ é inicialmente constante. Para $s > \frac{1}{2}$ o Universo expande continuamente desde a sua origem.

Visto que o parâmetro M está diretamente relacionado ao valor de s, a quantidade de matéria é responsável por notáveis modificações na natureza das soluções cosmológicas. Para valores de M não suficientemente grandes. o c enário Anti-Big Bang é preservado, entretanto, quando seu valor é suficiente para quebrar o acoplamento gravitação+campo conforme, o cenário Big Bang prevalece.

Problema da Entropia

Estima-se a produção de entropia no Universo segundo este modelo, considerando a entropia total do espaço-tempo hexadimensional constante. A entropia do espaço-externo tridimensional pode ser escrita como

$$dS_3 = -\frac{(\bar{\epsilon} + p') V_3}{T} \frac{V_3}{V_2} dV_2 \qquad (12)$$

onde $\bar{\epsilon} = \frac{\epsilon}{u}$ é a densidade de matéria à seis dimensões, enquanto $V_3 = a^3$ e $V_2 = \phi^2 = u$ são respectivamente os volumes dos espaços físico e interno. Ao considerarmos o Universo dominado pela radiação poderemos estabelecer as relações de conservação $\epsilon a^4 = cte$ e $aT = cte$. Esta última define para o Universo uma origem fria (o Universo é infinito em $t = 0$) e uma temperatura máxima (associada ao momento em que o fator de escala a atinge seu valor mínimo). Sob estas considerações a entropia total à três dimensões não é constante. mas sim determinada por

$$S_3 \propto \frac{1}{u} \qquad (13)$$

Como u é zero no origem do Universo ($\theta = 0$) e é praticamente zero hoje ($\theta - \pi$), a entropia produzida no Universo físico é extremamente grande para pequena dimensão interna observada hoje.

Cosmic spinning string and causal protecting capsules

Mario Novello, Martha Christina Motta da Silva

Centro Brasileiro de Pesquisas Físicas, Rio de Janeiro, RJ, Brasil

O problema da causalidade (do qual a geometria de Gödel [1] é o paradigma) tem sido tratado, na literatura científica, à luz de duas atitudes:

1. Geometrias apresentando curvas tipo tempo fechadas (CTC's) são fisicamente inadequadas — CTC's estariam relacionadas a violações da condição fraca de energia [2]

2. Geometrias com CTC's mantidas em uma forma que preserve o máximo da Física tradicional, conforme trabalhos de Gibbons e Russell [3], Novikov [4], Morris, Thorne e Yurtsever [5].

A posição (1) foi criticada por Jensen e Soleng [6], que apresentaram uma solução na qual a existência ou não de CTC's *não* está relacionada às condições de energia. Baseados nisso, apresentamos um modelo teórico, independente, das condições de energia, que pode apresentar CTC's ou não. Introduzimos, nesse ponto, o conceito de *Cápsulas de Proteção Causal* [7]. Procuramos, portanto, obter soluções das equações de Einstein com constante cosmológica que sejam extensões analíticas (mediante o emprego das condições de Darmois-Lichnerowicz de junção de métricas [8]) de uma geometria com CTC's (Gödel nesse caso), de modo a eliminar a sua ocorrência. Ambos os modelos obtidos têm simetria cilíndrica.

O primeiro modelo obtido tem a solução de Gödel unida analiticamente a uma geometria exterior denominada "Gödel-generalizada, já que recai em Gödel para um caso especial. Esta solução externa tem fluxo de calor nulo e o modelo possui vorticidade constante. A existência ou não de CTC's depende da escolha do raio de junção e dos valores da pressão anisotrópica e da constante cosmológica.

O segundo modelo tem três regiões: Gödel (com vorticidade constante), solução de "string" girante generalizada (com fluxo de calor não nulo e vorticidade variando com a coordenada radial entre os valores de Gödel e zero) e Minkowski com defeito topológico (apresentando um "deficit" angular e vorticidade nula). A existência ou não de CTC's no modelo depende da novamente da escolha dos dois raios de junção e do tipo de matéria existente na região intermediária.

Ambas as soluções acima são independentes das condições de energia no sentido em que soluções com CTC's não implicam em violação destas condições. Temos, portanto, que soluções apresentando CTC's não precisam ser necessariamente descartadas de modelos fisicamente razoáveis, desde que elas estejam "encapsuladas" (logo inacessíveis) dentro de outras soluções sem problemas de causalidade. Este conceito de *cápsulas de proteção causal* seria então uma alternativa às duas visões mencionadas anteriormente em relação à questão da causalidade.

References

[1] K.Gödel. Rev.Mod.Phys. **21**, 3 (1949).

[2] S.W.Hawking. Phys.Rev.D **40**, 603 (1992).

[3] G.W.Gibbons, A.Russell. Phys.Rev.Lett. **30**, 398 (1973).

[4] I.D.Novikov. Zh.Eksp.Teor.Phys. **95**, 769 (1989) [Sov.Phys.JETP **68**, 439 (1989)].

[5] M.S.Morris, K.S.Thorne, U.Yurtsever. Phys.Rev.Lett. **61**, 13 (1988).

[6] B.Jensen, H.H.Soleng. Phys.Rev.D **45**, 3528 (1992).

[7] M.Novello, M.C.Motta da Silva. Phys.Rev.D **49**, 2 (1994).

[8] K.Lake, in *Cosmology and Gravitation*, Proceedings of the Vth Brazilian School of Cosmology and Gravitation, Rio de Janeiro, Brasil, 1987. Ed. M.Novello. World Scientific, singapore, 1988.

Non linear non local theory of gravity

M. Novello and V. A. De Lorenci

LAFEX/Centro Brasileiro de Pesquisas Fisicas —Rio de Janeiro

Deser and Laurent (1968) explored an alternative linear theory for spin-two field using a nonlocal divergence-free projection operator on the matter energy-momentum tensor. Here, we extend this theory by including non-linearity of the gravitational field. We show that such extended model is indistinguishable from General Relativity, as far as the four standard tests of gravity are concerned.

Any theory that aims to be competitive as a possible description of gravitational interaction should provide an explanation at least as good as General Relativity (GR) does for the so-called four traditional tests.

We have presented a non-local theory[1] of gravity which was based on an ancient idea of Deser and Laurent (DL)[2].

The main appeal of DL model was related to the possibility of dealing with a consistent closed field theory without recurrence into the traditional geometrical scheme, which deals with the summation of an infinite series as it has been shown by many authors (see, for instance, Feynmann [3]).

Although DL model has been successful to describe some properties of the motion of a material particle in a gravitational field it contains a fatal drawback that appears when gravitational waves are present. The reason for this is precisely related to the linearity of DL model, that treats gravity as transparent to gravitons. So, in order to solve such difficulty and in the same vein to keep its good properties it seems that a very natural way should be the construction of a theory that incorporates both features:

- non locality;

- non linearity.

Following the procedure outlined in DL paper we take as the true equations of motion for the gravitational field the non-local for:

$$G_L^{\mu\nu} = -k(\hat{T}^{\mu\nu} + n\,\hat{t}^{\mu\nu}).\tag{1}$$

Deser-Laurent model corresponds to the case in which the adimensional constant n takes the value zero. Here we will set $n = 1$. $G_L^{\mu\nu}$ is the linear Fierz-Pauli expression for the spin-two field and $t^{\mu\nu}$ represents the corresponding Gupta [4] energy-momentum tensor, which is quadratic in the gravitational variable $\phi_{\mu\nu}$. A hat above a tensor, as it appears in the above equation, represents the result of the application of the operator $P_{\mu\nu}$ that projects any tensor on the divergenceless space.

This is worth considering that our model is compatible with observations, as far as the four standard tests of gravitational processes are concerned.

References

[1] M. Novello e V. A. De Lorenci, *Non Linear Non Local Theory of Gravitation.* Notas de Física, CBPF-NF-070/94, Dez/94.{Submitted to publication.}

[2] S. Deser and B. E. Laurent, *Gravitation Without Self-Interaction.* Ann. Phys., 50, 76 (1968).

[3] R. P. Feynman, *Lectures on Gravitation.* California Inst. Techonology. (1962-3).

[4] S. N. Gupta, *Quantization of Einstein's Gravitational Field: Linear Approximation.* Proc. Phys. Soc., A 65, 162 (1952).

Relatividade Geral e Implementação Geométrica Local da Causalidade

Manoelito Martins de Souza e Robson Nascimento Silveira

Departamento de Física, Universidade Federal do Espírito Santo

A Teoria da Relatividade Geral de Einstein pressupõe uma estrutura de espaço tempo descrita por uma variedade semi-riemannian quadridimensional. Assim a interação gravitacional, segundo Einstein, é descrita por um tensor simétrico de segunda ordem clássico, o tensor métrico. Isto a torna fundamentalmente distinta das outras 3 interações elementares observadas na natureza. A interação forte, a fraca e a eletromagnética são , todas, teorias locais de calibre, quânticas, descritas por campos vetoriais.

A despeito de seu grande sucesso experimental e teórico, a Relatividade Geral é uma teoria clássica, e como tal, acredita-se, trata-se apenas de uma forma limite e aproximada de uma descrição mais fundamental, quântica. Mas não existe uma teoria quântica para a gravitação.

Por outro lado, a Relatividade Geral é uma teoria com implementação global de causalidade, configurada na adoção de uma variedade semiriemanniana, que corresponde a uma geometria de espaçotempo estruturada sobre superfícies características. A adoção de estruturas geométricas de espaçotempo mais fundamentais, definidas sobre congruências de curvas bicaracteriísticas e que correspondem a uma implementação local (ponto a ponto) da causalidade, pode gerar um formalismo onde o campo gravitacional é expresso em termos de um campo vetorial, como nas demais interações elementares. O carater tensorial da gravitação adviria da estrutura da métrica, definida por um produto tensorial deste campo vetorial. Mas nestas teorias não existe singularidade. A Relatividade Geral é reobtida como uma teoria efetiva de valores médios definidos sobre superfícies características.

Busca-se, neste trabalho, re-escrever as equações de Einstein no contexto destas novas estruturas de espaçotempo, encontrar suas soluções com simetria esférica, mostrar que elas não têm singularidades, e obter, então, a solução de Schwarzschild como uma média definida sobre as superfícies características.

O que se pretende, em síntese, é extender para a gravitação o que se fez para as equações de Maxwell. Neste caso, o grupo de simetria é o grupo de Poincarè e a variedade é o espaçotempo de Minkowski, que corresponde a uma impl ementação global da causalidade através de sua estrutura de cones de luz. Trata-se de uma implementação global porque se exige apenas que os objetos físicos permaneçam em seus respectivos cones de luz; o espaçotempo acessiv el a um objeto físico é formado por uma foliação desses cones de luz. Mostra-se que uma implementação local da causalidade requer uma estrutura de espaçotempo mais complexa, definida em termos de congruências das geratrizes dos co nes de luz. As equações de Maxwell neste contexto têm funções de Green que:

1. são lineais (definidas ao longo de uma linha)

2. são conformemente invariantes

3. não têm singularidades

4. reproduzem as soluções usuais, com suas singularidades, como soluções efetivas.

Classical Equivalence of $\lambda R \phi^2$ Theories and Bekenstein's Theorems

U. F. Wichoski[*]

Depto. de Física Matemática, Instituto de Física

Universidade de São Paulo, Caixa Postal 20516 - CEP 01452-900 São Paulo, SP - Brazil

and

A. J. Accioly

Instituto de Física Teórica, Universidade Estadual Paulista

Rua Pamplona, 145 - CEP 01405-000, São Paulo SP. Brazil

(October 1994)

We discuss, in the context of theories involving a massless scalar field non-minimally coupled to Einstein gravity, the classical equivalence of $\lambda R \phi^2$ theories and Bekenstein's theorems.

1. Introduction

In the early seventies, Bekenstein [1] demonstrated two theorems which embody a technique of generating exact solutions of Einstein's equations; using conformal transformations, he showed that one can generate solutions for a conformally coupled scalar field case from a minimally coupled one.

On the other hand, a scalar nonminimal coupled theory can be represented by a minimal coupled one in the so called Einstein frame [2, 3]. As in the case of the solution generating technique above, conformal transformations play a crucial role in the method of finding the equivalent minimally coupled theory from the nonminimally coupled one. This second technique is particularly useful in the context of the cosmological inflationary models where we can analyze the dynamical behavior of the scalar field from the potential term without the inconvenient presence of the extra curvature terms [4, 5].

Our aim here is to point out that despite some authors [6] combine these two techniques to extend Bekenstein's results. based on the fact that they both use the same conformal transformation and apparently lead to the same results. the classical equivalence emerges only in the context of the represetation technique.

2. Bekenstein's Theorems

Originally in his theorems, Bekenstein has taken into account scalar field as well as electromagnetic fields. However. we are only interested in the scalar field case. so that the theorems are enunciated as follows

Theorem 1. If $\tilde{g}_{\mu\nu}$ and ϕ form a solution of Einstein's equations for a spacetime containing an ordinary scalar field ϕ. then $g_{\mu\nu} = \Omega^{-2}\tilde{g}_{\mu\nu}$ and $\psi = \lambda^{-1}\tanh\lambda\phi$, is the corresponding solution for a conformal scalar field ψ, where $\Omega^{-1} = \cosh\lambda\phi$.

Theorem 2. If $g_{\mu\nu}$ and ψ form an Einstein-conformal solution then $\tilde{g}_{\mu\nu} = \lambda^2\psi^2 g_{\mu\nu}$ and $\tilde{\psi} = \lambda^{-2}\psi^{-1}$ form a second solution.

Clearly the conditions imposed by the second theorem imply that $\Omega^{-2} = -(\sinh\lambda\phi)^2$. So. we can not consider $g_{\mu\nu} = \Omega^{-2}\tilde{g}_{\mu\nu}$ as conformal transformations anymore.

3. Minimally Coupled Representation

Let us consider nonminimal interaction of a scalar field ϕ with gravity given by the action

$$\tilde{S}[\tilde{g}_{\alpha\beta}, \phi] = \int d^4x \sqrt{-\tilde{g}} \left[\frac{\tilde{R}}{k} + \tilde{g}^{\mu\nu}\phi_\mu\phi_\nu + \lambda\tilde{R}\phi^2 - \tilde{V}(\phi) \right]. \tag{1}$$

where $k = 8\pi G$ in natural units and λ is a dimensionless coupling constant [7].
We now perform the following conformal transformation in the action (1)

$$\tilde{g}_{\mu\nu} = (1 + k\lambda\phi^2)g_{\mu\nu} ,$$ (2)

with the condition

$$(1 + k\lambda\phi^2) > 0 .$$ (3)

After some algebraic manipulations we obtain

$$S[g_{\alpha\beta}, \phi] = \int d^4x \sqrt{-g} \left[\frac{R}{k} + T^2(\phi)g^{\mu\nu}\phi_\mu\phi_\nu - V(\phi)\right] .$$ (4)

where R is the curvature scalar with respect to $g^{\mu\nu}$,

$$T^2(\phi) = \frac{1 + \lambda(1 + 6\lambda)k\phi^2}{(1 + \lambda k\phi^2)^2}$$ (5)

and

$$V(\phi) = \frac{\tilde{V}(\phi)}{(1 + \lambda k\phi^2)^2} .$$ (6)

By a redefinition of the scalar field as

$$\Phi = \int d\phi\, T(\phi) .$$ (7)

we find the desired minimally coupled action in the Einstein frame

$$S[g_{\alpha\beta}, \Phi] = \int d^4x \sqrt{-g} \left[\frac{R}{k} + g^{\mu\nu}\Phi_\mu\Phi_\nu - V(\Phi)\right] .$$ (8)

It is important to notice that theories with different coupling constants λ will generate different theories in the Einstein frame, so that the dynamical behavior of the theory will depend on λ even in the Einstein frame.

The advantage of this process resides in the fact that instead of dealing with a nonminimally coupled theory, where direct coupling of the scalar field with background curvature does not allow us from making simple arguments using the potential, we can study a minimal coupled theory and analyze its dynamical behavior from the potential. However, the dynamical dependence on the coupling constant remains in the Einstein frame.

4. The Classical Equivalence

Let us take into account action (1) and suppose that: i-) ϕ is massless and ii-) there is no potential term $(V(\phi) = 0)$.

Again, we perform the transformation (2) along with the field redefinition (7), but now considering them as a change of variables. We also suppose that the condition (3) holds.

We point out that the boundary conditions on the new field Φ are determined from those on the old one ϕ. Hence, we arrive to the following action in the Einstein frame

$$S[g_{\alpha\beta}, \Phi] = \int d^4x \sqrt{-g} \left[\frac{R}{k} + g^{\mu\nu}\Phi_\mu\Phi_\nu\right] .$$ (9)

The new feature is that, independently of the coupling constant λ, all actions are equivalent to the same action in the Einstein frame. In other words, whatever the value of the coupling constant λ we have, the same classical theory will be described [8].

5. Conclusion

In the case of the solution generating technique, considering theorem 1, we can map solutions from the minimally coupled case into solutions of the nonminimally coupled case or, correspondingly from the representation technique point of view, we can map solutions of the theory in the Einstein frame into solutions of the equivalent theory in the physical frame. Hence, if the object of interest is to find new solutions of Einstein's equations, the two techniques, in principle, lead to the same results.

But, if we take into account theorem 2, there is no such correspondence. i.e., there is no equivalent minimally coupled theory in the Einstein frame because the transformation performed is not a conformal one.

So, in addition to the fact that the solution generating technique deals with solutions and the representation technique deals with the theory itself, the former do not necessarily obeys the important condition (3) (cf. theorem 2) which is fundamental to the classical equivalence.

From what we have seen, the conclusion is that the classical equivalence appears only in the context of the representation technique and it means more than a mapping between conformally related solutions.

References

[1] J.D. Bekenstein. Ann. Phys. **82**, 535 (1974).

[2] H.-J. Schmidt. Phys. Lett. **B 214**, 519 (1988).

[3] K. Maeda, Phys. Rev. **D 39**, 399 (1989).

[4] T. Futamase and K. Maeda, Phys. Rev. **D 39**, 399 (1989).

[5] K. Maeda, J.A. Stein-Schabes and T. Futamase. Phys. Rev. **D 39**, 2848 (1989).

[6] J.P. Abreu, P. Crawford and J.P. Mimoso, Class. Quantum Grav. **11**. 1919 (1994).

[7] M.S. Madsen. Class. Quantum Grav. **5**, 627 (1988).

[8] A.J. Accioly, U.F. Wichoski, S.F. Kwok and N.L.P. Pereira da Silva. Class. Quantum Grav. **10**. L215 (1993).

Simetria e Gravidade em Espaços de Finsler

Solange F. Rutz

Laboratório Nacional de Computação Científica, LNCC - CNPq

Rua Lauro Müller 455, CEP: 22290, Rio de Janeiro, RJ - e-mail: rutz@lncc.br

Espaços de Finsler são variedades onde define-se como métrica

$$ds = F(x^i, dx^i), \tag{1}$$

onde F é positiva, homogênea de grau um em dx^i e convexa em dx^i. Espaços Riemannianos são casos particulares onde $F = \sqrt{g_{ij}(x^k)\, dx^i dx^j}$. Define-se como tensor métrico

$$g_{ij}(x^k, \dot{x}^k) = \frac{1}{2}\frac{\partial^2 F^2(x^k, \dot{x}^k)}{\partial \dot{x}^i \partial \dot{x}^j} \implies ds^2 = g_{ij}(x^k, dx^k)dx^i dx^j, \tag{2}$$

onde $\dot{x}^i = dx^i/dt$ e a implicação segue-se da homogeneidade de F. As equações das geodésicas podem ser dadas de forma similar ao caso Riemanniano:

$$\frac{d^2 x^i}{ds^2} + \gamma^i_{jk}\frac{dx^j}{ds}\frac{dx^k}{ds} = 0; \quad \gamma^i_{jk} = \frac{1}{2}g^{ih}\left(\frac{\partial g_{hj}}{\partial x^k} + \frac{\partial g_{hk}}{\partial x^j} - \frac{\partial g_{jk}}{\partial x^h}\right). \tag{3}$$

Dentre os processos de derivação covariante possíveis, temos a *derivada gamma*:

$$\frac{\delta X^i}{\delta t} = \frac{dX^i}{dt} + \Gamma^i_{jk}\dot{x}^j X^k, \quad \Gamma^i_{jk} = \gamma^i_{jk} - \frac{1}{2}g^{ih}\frac{\partial g_{jl}}{\partial \dot{x}^h}\gamma^l_{pk}\dot{x}^p; \tag{4}$$

$$X^i_{;j} = \frac{\partial X^i}{\partial x^j} + \Gamma^i_{hj}X^h, \quad \Gamma^i_{hj} = g^{ik}\left[\gamma_{hkj} - \frac{1}{2}\left(\frac{\partial g_{jk}}{\dot{x}^i}\Gamma^i_{hl} + \frac{\partial g_{kh}}{\partial \dot{x}^i}\Gamma^i_{jl} - \frac{\partial g_{hj}}{\partial \dot{x}^i}\Gamma^i_{kl}\right)\dot{x}^l\right]. \tag{5}$$

A relação entre os processos (4) e (5) é dada naturalmente por $\delta X^i/\delta t = X^i_{;j}\, dx^j/dt$. A equação do desvio geodésico é dada então por:

$$\frac{\delta^2 \xi^i}{\delta s^2} + K^i_{jhk}\dot{x}^j \dot{x}^h \xi^k = 0, \quad K^i_{jhk} = \left(\frac{\partial \Gamma^{\cdot i}_{jh}}{\partial x^k} - \frac{\partial \Gamma^{\cdot i}_{jh}}{\partial \dot{x}^l}\frac{\partial G^l}{\partial \dot{x}^k}\right) - \left(\frac{\partial \Gamma^{\cdot i}_{jk}}{\partial x^h} - \frac{\partial \Gamma^{\cdot i}_{jk}}{\partial \dot{x}^l}\frac{\partial G^l}{\partial \dot{x}^h}\right) + \Gamma^{\cdot i}_{mk}\Gamma^{\cdot m}_{jh} - \Gamma^{\cdot i}_{mh}\Gamma^{\cdot m}_{jk}, \tag{6}$$

onde $G^l = 1/2\,(\gamma^l_{jk}\,\dot{x}^j \dot{x}^k)$.

Sob uma transformação de ponto infinitesimal ($d\tau = $ const.)

$$\tilde{x}^i = x^i + v^i(x^r)d\tau; \quad \dot{\tilde{x}}^i = \dot{x}^i + \left(\frac{\partial v^i}{\partial x^h}\dot{x}^h\right)d\tau \tag{7}$$

um campo escalar $S(x^i, \dot{x}^i)$ se transforma como $\tilde{S}(\tilde{x}^i, \dot{\tilde{x}}^i) = S(x^i, \dot{x}^i)$, ou

$$S(x^i, \dot{x}^i) = \hat{S}(x^i, \dot{x}^i) + \frac{\partial S}{\partial x^i}v^i d\tau + \frac{\partial S}{\partial \dot{x}^i}\frac{\partial v^i}{\partial x^j}\dot{x}^j d\tau + O(d\tau)^2. \tag{8}$$

Logo. a função métrica F será invariante sob a transformação se

$$\pounds_v F = \lim_{d\tau \to 0}\left[\frac{F(x^i, \dot{x}^i) - F(x^i, \dot{x}^i)}{d\tau}\right] = \frac{\partial F}{\partial x^i}v^i + \frac{\partial F}{\partial \dot{x}^i}\frac{\partial v^i}{\partial x^j}\dot{x}^j = 0. \tag{9}$$

A equação acima é equivalente às equações de Killing $\pounds_v g_{ij}(x^k, \dot{x}^k) = 0$. Definindo-se simetria esférica como invariancia sob $SO(3)$, temos que a função métrica $F^2(x^i, \dot{x}^i) = G(r, \theta, \varphi, t, R, \alpha, \beta, \gamma)$, onde

$$\begin{cases} r = \sqrt{x^2 + y^2 + z^2} \\ \tan\theta = \sqrt{x^2 + y^2}/z \\ \tan\varphi = y/x \\ t = t \end{cases} ; \begin{cases} R = \sqrt{\dot{r}^2 + r^2\left(\dot{\theta}^2 + \sin\theta\dot{\varphi}^2\right)\dot{t}^2} \\ \tan\alpha = \sqrt{\dot{r}^2 + r^2(\dot{\theta}^2 + \sin\theta\dot{\varphi}^2 t)}/\dot{t} \\ \tan\beta = r\sqrt{\dot{\theta}^2 + \sin\theta\dot{\varphi}^2}/\dot{r} \\ \tan\gamma = r\dot{\theta}/r\sin\theta\dot{\varphi} \end{cases} \tag{10}$$

invariante sob o grupo será dada por $F^2(x^i, \dot{x}^i) = G(r, t, R, \alpha, \beta)$. Impondo ainda o requerimento de homogeneidade sobre F. temos que a forma geral da métrica Finsleriana quadri-dimensional esfericamente simétrica é dada por

$$F^2(x^i, \dot{x}^i) = R^2Q(r, t, \alpha, \beta) \tag{11}$$

ou, alternativamente,

$$ds^2 = g_{11}dr^2 + g_{22}r^2(d\theta^2 + \sin^2\theta d\varphi^2) + g_{44}dt^2 +$$
$$+ 2\left[g_{12}r\sqrt{d\theta^2 + \sin^2\theta d\varphi^2}dr + g_{24}r\sqrt{d\theta^2 + \sin^2\theta d\varphi^2}dt + g_{14}drdt\right] \tag{12}$$

onde $g_{ij} = g_{ij}(r, t, \alpha, \beta)$. Note que só é possível fazer $g_{22} \equiv 0$. $g_{14} \equiv 0$ para valores fixos de α e β.

Afim de propor equações de campo em espaços de Finsler. extendemos uma analogia entre as teorias gravitacionais de Newton e Einstein, conforme apontada por Pirani. Na primeira teoria, se subtrairmos as equações de movimento de duas partículas infinitesimalmente próximas, submetidas a um campo gravitacional dado por um potencial ϕ.

$$\frac{d^2x^i}{dt^2} = -\eta^{ij}\frac{\partial\phi}{\partial x^j}. \quad \frac{d^2x^i}{dt^2} + \frac{d^2\xi^i}{dt^2} = -\eta^{ij}\frac{\partial\phi}{\partial x^i} - \xi^k\eta^{ij}\frac{\partial^2\phi}{\partial x^j\partial x^k},$$

obtemos que o vetor separação deve obedecer a equação diferencial

$$\frac{d^2\xi^i}{dt^2} + H^i_k\xi^k = 0, \quad H^i_k = \eta^{ij}\frac{\partial^2\phi}{\partial x^j\partial x^k} \tag{13}$$

e que a equação de Laplace. $\nabla^2\phi = \eta^{ij}\partial^2\phi/\partial x^i\partial x^j = 0$. válida no vácuo. implica que $H^i_i = 0$. Na teoria de Einstein. a mesma situação é representada pela equação do desvio geodésico, e o tensor de desvio. pelas equações de Einstein para o vácuo. também deve ser sem traço

$$\frac{D^2\xi^i}{DS^2} + H^i_k\xi^k = 0. \quad H^i_k = R^i_{jlk}\dot{x}^j\dot{x}^l; \quad R_{jl} = R^i_{jli} = 0 \quad \Rightarrow \quad H^i_i = 0. \tag{14}$$

Em espaços de Finsler, propomos como equação de campo para o vácuo que o tensor de desvio seja também sem traço:

$$\frac{\delta\xi^i}{\delta S^2} + H^i_k\xi^k = 0, \quad H^i_k = K^i_{jlk}\dot{x}^j\dot{x}^l. \quad H = 0. \tag{15}$$

Se definirmos um tensor tipo-Ricci. $K_{jl} = K^i_{jli}$. podemos escrever $H = K_{jl}\dot{x}^j\dot{x}^l$ e logo obter $H = 0 \Rightarrow K_{jl} = R_{jl} = 0$ se a métrica for Riemanniana. mas tal implicação não é verdadeira no caso geral Finsleriano.

Afim de obter-se uma solução não-Riemanniana, perturbaremos em primeira ordem a solução de Schwarzschild

$$ds^2 = gdr^2 + r^2d\Omega^2 - hdt^2; \quad d\Omega = \sqrt{d\theta^2 + \sin^2\theta d\varphi^2}. \tag{16}$$

onde $g(r,t,\alpha,\beta) = g_0(r,t) + \varepsilon[g_1(r,t)\alpha + g_2(r,t)\beta]$, $h(r,t,\alpha,\beta) = h_0(r,t) + \varepsilon[h_1(r,t)\alpha + h_2(r,t)\beta]$, $g_0 = 1/h_0$, $h_0 = 1 - 2m/r$ e tomaremos $\alpha = rd\Omega/dt$, $\beta = dr/dt$. Obtemos então (via computação algébrica) uma equação diferencial linear de segunda ordem de 636 termos que conseguimos dividir num sistema de equações uma vez que as funções g_i e h_i independem de dx^j. Esse sistema tem como *solução geral* $g_1 = g_2 = 0$, $h_1 = (2m - r)/r^2$, $h_2 = h_2(r)$, sendo que podemos ainda escolher r, t tal que $h_2(r) \equiv 0$. Logo nosso exemplo de solução não-Riemanniana é dado por

$$ds^2 = \frac{dr^2}{(1 - 2m/r)} + r^2 d\Omega^2 - \left(1 - \frac{2m}{r}\right)\left(1 + \varepsilon\frac{d\Omega}{dt}\right) dt^2. \tag{17}$$

As conseqüências físicas trazidas por esta métrica, conforme descritas pelos Testes Clássicos da Relatividade geral, são tais que o avanço do periélio de Mercúrio e o raio médio de sua órbita sofrem uma correção de $(1 + \varepsilon B/A)$, onde B e A são constantes do movimento, correspondentes à energia e momento angular do sistema (para Mercúrio, $B = 1$, $A = 9 \times 10^3$Km, em unidades geométricas).

$$\Delta\varphi_P = \frac{6\pi m^2}{A^2}\left(1 - \varepsilon\frac{B}{A}\right), \quad <r> = \frac{1}{<u>} = \frac{A^2}{m}\left(1 - \varepsilon\frac{B}{A}\right). \tag{18}$$

Podemos utilizar o erro observacional para limitar o valor da correção Finsleriana em $|\varepsilon| = |c\varepsilon| < 94.5$ Km ou $|\varepsilon| < 3.15 \times 10^{-4}$s. A solução não-Riemanniana acima não apresenta correções adicionais ao comportamento da luz, conforme descrito nos Testes Clássicos.

Bibliografia

McCarthy, P. J. & Rutz, S. F. 1993, Gen. Rel. Grav., **25**, 589

Rutz, S. F. 1993, Gen. Rel. Grav., **25**, 1139

Rund, H. 1959, *The Differential Geometry of Finsler Spaces*, Springer-Berlin

Conjunto Mínimo Fechado de Observáveis na Teoria de Perturbações Cosmológicas

M. Novello, J.M. Salim, M.C. Motta da Silva, S.E. Jorás. R. Klippert

Centro Brasileiro de Pesquisas Físicas — Rio de Janeiro

Tem sido uma prática comum (desde o trabalho original de Lifshitz em 1963) iniciar o estudo de perturbações na teoria da Relatividade Geral de Einstein considerando variações de quantidades não-observáveis. como $\delta g_{\mu\nu}$. A principal desvantagem deste método é a mistura de verdadeiras perturbações com transformações arbitrárias infinitesimais de coordenadas. Este é o chamado problema de *gauge* da teoria de perturbação. Uma solução para esta dificulade foi encontrada por vários autores (J.Bardeen. 1980: B.J.T.Jones. 1976: S.W.Hawking. 1966. D.W. Olson. 1976. J.C.Hwang e E.T.Vishiniac. 1976: R.Khan e W.H.Press. 1983: R.Brandenberger. Mukhanov e Feldman. 1992) procurando por combinações independentes de *gauge* que poderiam ser escritas em termos do tensor métrico e suas derivadas. O próximo passo seria então fornecer a dinamica destes objetos através das equações de Einstein. que seriam então utilizadas para descrever quantidades fisicamente interessantes.

Aqui seguiremos o caminho inverso. mais simples e direto. Isto é, escolheremos desde o inicio como base da nossa análise um certo conjunto de objetos independentes de *gauge* fisicamente observáveis. A dinamica destes objetos será fornecida pelas equações Quasi-Maxwellianas da gravitação. Além disto, qualquer quantidade dependente de *gauge* com a qual usualmente lidamos — por exemplo, as perturbações na expansão θ ou na densidade de energia ρ — podem ser obtidas a partir deste conjunto. através da equação de conservação de energia e da equação de Raychaudhuri.

A métrica de fundo é Friedman-Robertson-Walker escrita em coordenadas gaussianas: $ds^2 = dt^2 + g_{ij} dx^i dx^j$. $g_{ij} = -A(t)^2 \gamma_{ij}(x^k)$. Nesta métrica, o tensor de Weyl $W_{\alpha\beta\mu\nu}$ e suas partes elétrica $E_{\mu\nu}$ e magnética $H_{\mu\nu}$ são nulas: são, portanto, objetos independentes de *gauge* (vide Stewart. 1974).

Seguindo Lifshitz. expandiremos todas as quantidades perturbadas na base de harmônicos. Nos restringiremos ao caso de harmonicos escalares $Q(x^k)$, $\dot{Q} = 0$. isto é, não consideraremos as contribuições rotacionais nem de ondas gravitacionais às perturbações[1]. Desta forma, qualquer objeto poderá ser escrito como

$$F(x^\mu) = \sum_m \mathcal{F}^{(m)}(t) Q^{(m)}(x^i) \ .$$

Para não sobrecarregar a notação, daqui por diante omitiremos o somatório e o índice (m). Usaremos as seguintes definições: $Q_i := Q_{,i}$ e $Q_{ij} := Q_{,ij}$, onde o escalar Q obedece à equação $\nabla^2 Q = mQ$, com símbolo ∇^2 denotando o Laplaciano tridimensional. O operador sem traço Q_{ij} é definido como $Q_{ij} := \frac{1}{m}Q_{ij} - \frac{1}{3}Q\gamma_{ij}$.

Desta forma. expandimos as perturbações na parte elétrica do tensor de Weyl, na 4-aceleração, no *shear* e na expansão:

$$\delta E_{ij} \equiv E(t)\dot{Q}_{ij}(x^k), \quad \delta a_i \equiv \Psi(t)Q_i(x^k), \quad \delta\sigma_{ij} \equiv \Sigma(t)\dot{Q}_{ij}(x^k), \quad \delta\theta \equiv H(t)Q(x^k).$$

Consideraremos que o fluido perturbado obedece à mesma equação de estado antes e depois da perturbação: $p = \lambda\rho$; basta então escrevermos a perturbação na densidade de energia na base de harmônicos: $\delta\rho \equiv \mathcal{N}(t)Q(x^k)$. Admitindo um fluido onde a pressão anisotrópica Π_{ij} seja proporcional ao *shear* σ_{ij}. escrevemos $\delta\Pi_{ij} \equiv \xi \Sigma(t)Q_{ij}(x^k)$. Admitiremos ainda que a perturbação não provoca fluxo de energia.

---

[1] Note que isto implica a inexistência de perturbações na parte magnética do tensor de Weyl.

Agora, podemos perturbar as equações Quasi-Maxwellianas e substituir as expansões na base dos harmônicos. Admitindo que $(1 + \lambda) \neq 0$, obtemos um sistema dinâmico fechado para as variáveis E e Σ:

$$\dot\Sigma = -E - \frac{1}{2}\xi\Sigma + m\Psi .$$

$$\dot E = -\left(\frac{1}{3}\Theta + \frac{1}{2}\xi\right) E - \left(\frac{1}{4}\xi^2 + \frac{(1+\lambda)}{2}\rho + \frac{1}{6}\xi\Theta\right)\Sigma + \frac{m}{2}\xi\Psi$$

onde

$$\Psi = \frac{2}{\rho(1+\lambda)}\left(1 - \frac{3K}{m}\right) A^{-2}(-\lambda E + \frac{1}{2}\lambda\xi\Sigma + \frac{1}{3}\xi\Sigma).$$

onde K é a 3-curvatura do espaço-tempo de fundo. Se $(1 + \lambda) = 0$, torna-se necessária a existência de um fluxo de energia $q_i \equiv q(t)Q_i(x^k)$. As equações Quasi-Maxwellianas fornecem, então:

$$\dot N = \frac{m}{A^2}q . \qquad \dot q + \theta q + N = \frac{2\xi}{3A^2}\left(1 - \frac{3K}{m}\right)\Sigma .$$

$$(E - \frac{\xi}{2}\Sigma)\dot{} + \frac{\theta}{3}(E - \frac{\xi}{2}\Sigma) = -\frac{m}{2}q . \qquad \frac{2}{A^2}\left(1 - \frac{3K}{m}\right)(E - \frac{\xi}{2}\Sigma) = -\dot N - \theta q .$$

que também formam um sistema dinâmico fechado, mas para as variáveis N, q, E e Σ.

Esta abordagem permite uma formulação hamiltoniana das perturbações. Apesar de E e Σ não serem variáveis canonicamente conjugadas, as novas variáveis[2] $P := A(t)E$ e $Q := \Sigma$ o são, e obedecem à dinâmica fornecida pela Hamiltoniana abaixo no caso $\xi = 0$:

$$\mathcal{H} = -\frac{1}{2A}\left(1 + \frac{2m\lambda}{(1+\lambda)\rho A^2}\left(1 - \frac{3K}{m}\right)\right) P^2 + \left(\frac{1+\lambda}{4}\right)\rho A Q^2 .$$

Esta Hamiltoniana é do tipo $\mathcal{H} = -\frac{1}{2\mu^2}P^2 + \frac{1}{2}\omega^2 Q^2$ — um oscilador invertido — se, para $\lambda < -1$ ou $\lambda > 0$ tivermos

$$1 - \frac{3K}{m} > -\frac{1+\lambda}{\lambda}\frac{\rho A^2}{2m} .$$

ou, para $-1 < \lambda < 0$, tivermos

$$1 - \frac{3K}{m} < -\frac{1+\lambda}{\lambda}\frac{\rho A^2}{2m} .$$

Isto indica a instabilidade do universo de Friedman-Robertson-Walker sob perturbações de um fluido sem pressão anisotrópica ($\xi = 0$) e sem fluxo de energia.

---

[2] Note que a variável Q apresentada a seguir não tem relação alguma como harmônico $Q(x^k)$.

Classification of Second Order Symmetric Tensors in Kaluza-Klein-Type Theories

J. Santos, M.J. Rebouças, and A.F.F. Teixeira [‡]

* *Universidade Federal do Rio G. do Norte. Departamento de Física.*
Caixa Postal 1641, 59072-970 Natal - RN. Brazil

† ‡ *Centro Brasileiro de Pesquisas Físicas, Departamento de Relatividade e Partículas*
Rua Dr. Xavier Sigaud 150. 22290-180 Rio de Janeiro - RJ, Brazil

Using the theory of Jordan matrices we discuss the algebraic classification of second order symmetric tensors (Ricci tensor) on five-dimensional (5-D) Lorentzian manifolds M, extending previous results on this issue. We show that a symmetric two-tensor R can be classified in four Segre types and their twenty-two degeneracies. Using real half-null pentad bases for the tangent space $T_p(M)$ to M at p we derive a set of canonical forms for R_{ab}, generalizing the canonical forms for a symmetric two-tensor on 3-D and 4-D space-times manifolds.

Introduction

The algebraic classification of the Ricci part S_{ab} of the Riemman tensor in 4-D space-times (Segre classification) has been discussed by several authors [1] and is of interest in understanding some purely geometrical features of space-times [2] – [4], in classifying and interpreting matter field distributions [5] – [10], in determining limits of non-vacuum space-times [11], and as part of the procedure for checking the local equivalence of space-times [12].

Kaluza-Klein-type theories in five and more dimensions is of interest in at least two contexts. In gauge theories they have been used as a way to unify the fundamental interactions in physics. From a technical viewpoint, on the other hand, they have been employed as a tool for obtaining exact solutions in four dimensions [13].

In this work we briefly discuss the algebraic classification of second order symmetric tensors defined on 5-D Lorentzian manifolds M, extending previous results on this subject [14, 15]. For a detailed account of our results see ref. [16].

Classification and Canonical Forms

In this work M is a real 5-D manifold endowed with a Lorentzian metric g of signature $(- + + + +)$. $T_p(M)$ denotes the tangent vector space to M at a point $p \in M$, and any tensorial lower case latin indices range from 0 to 4.

Let R_{ab} be the covariant components of a second order symmetric tensor R at $p \in M$. Given R_{ab} we may use the metric tensor to have the mixed form $R^a{}_b$ of R at $T_p(M)$. In this form the symmetric two-tensor R may be looked upon as a real linear operator $R : T_p(M) \longrightarrow T_p(M)$. If one thinks of R as a matrix $R^a{}_b$, one can formulate

the eigenvalue problem

$$R^a{}_b V^b = \lambda \delta^a{}_b V^b.\tag{0.1}$$

where λ is scalar and V^b are the components of a generic eigenvector $\mathbf{V} \in T_p(M)$. The fact that we have $\delta^a{}_b$ rather than g_{ab} on the right hand side of equation (0.1) makes apparent that we have cast the non-standard eigenvalue problem involving the hyperbolic (real) metric $R_{ab} V^b = \lambda g_{ab} V^b$ into the standard form (0.1) well known in linear algebra textbooks. However, $R^a{}_b$ is no longer symmetric in general and the eigenvalue problem (0.1) gives rise to the Jordan block diagonal matrices.

When all eigenvalues of R are real similarity transformations exist under which $R^a{}_b$ takes at p either one of the following Jordan canonical forms [16]:

$$\begin{pmatrix} \lambda_1 & 1 & 0 & 0 & 0 \\ 0 & \lambda_1 & 1 & 0 & 0 \\ 0 & 0 & \lambda_1 & 0 & 0 \\ 0 & 0 & 0 & \lambda_2 & 0 \\ 0 & 0 & 0 & 0 & \lambda_3 \end{pmatrix}, \quad \begin{pmatrix} \lambda_1 & 1 & 0 & 0 & 0 \\ 0 & \lambda_1 & 0 & 0 & 0 \\ 0 & 0 & \lambda_2 & 0 & 0 \\ 0 & 0 & 0 & \lambda_3 & 0 \\ 0 & 0 & 0 & 0 & \lambda_4 \end{pmatrix}, \quad \begin{pmatrix} \lambda_1 & 0 & 0 & 0 & 0 \\ 0 & \lambda_2 & 0 & 0 & 0 \\ 0 & 0 & \lambda_3 & 0 & 0 \\ 0 & 0 & 0 & \lambda_4 & 0 \\ 0 & 0 & 0 & 0 & \lambda_5 \end{pmatrix}.$$

(a) Segre type [311]   (b) Segre type [2111]   (c) Segre type [1,1111]

or one of the possible block-degenerated Jordan matrices. Here $\lambda_1, \cdots, \lambda_5 \in \mathbb{R}$. The Segre type is a list of digits inside square brackets, where each digit refers to the multiplicity of the corresponding eigenvalue, which clearly is equal to the dimension of the corresponding Jordan block. The comma in type [1,1111] is used to separate eigenvalues associated to timelike and spacelike eigenvectors. We remark that the Lorentzian character of the metric g on M, together with the symmetry of R_{ab}, rule out the Segre types [5], [41], [32] and [221] and degeneracy thereof (see ref. [16] for details).

When $R^a{}_b$ complex eigenvalues one can show [16] that it is necessarily diagonalizable over the complex field and possesses three real eigenvalues, i.e., only the Segre type $[z \bar z 111]$ and its specializations are permitted.

As far as the canonical forms are concerned, although the most general decomposition for the Ricci tensor in 5-D is given by

$$\begin{aligned}
R_{ab} = {} & 2\rho_1 l_{(a}m_{b)} + \rho_2 l_a l_b + \rho_3 x_a x_b + \rho_4 y_a y_b + \rho_5 z_a z_b + \rho_6 m_a m_b \\
& + 2\rho_7 l_{(a}x_{b)} + 2\rho_8 l_{(a}y_{b)} + 2\rho_9 l_{(a}z_{b)} + 2\rho_{10} m_{(a}x_{b)} + 2\rho_{11} m_{(a}y_{b)} \\
& + 2\rho_{12} m_{(a}z_{b)} + 2\rho_{13} x_{(a}y_{b)} + 2\rho_{14} x_{(a}z_{b)} + 2\rho_{15} y_{(a}z_{b)}.
\end{aligned}\tag{0.2}$$

with $\rho_1, \ldots, \rho_{15} \in \mathbb{R}$, it is possible to show [16] that semi-null pentad bases with non-zero inner product

$$l^a m_a = x^a x_a = y^a y_a = z^a z_a = 1\tag{0.3}$$

can be introduced at a point $p \in M$, such that the possible Segre types and the corresponding canonical forms for a second order symmetric tensor R at $p \in M$ are given by

Segre type	Canonical form	
[1,1111]	$R_{ab} = 2\rho_1 l_{(a}m_{b)} + \rho_2 (l_a l_b + m_a m_b) + \rho_3 x_a x_b + \rho_4 y_a y_b + \rho_5 z_a z_b.$	(0.4)
[2111]	$R_{ab} = 2\rho_1 l_{(a}m_{b)} \pm l_a l_b + \rho_3 x_a x_b + \rho_4 y_a y_b + \rho_5 z_a z_b.$	(0.5)
[311]	$R_{ab} = 2\rho_1 l_{(a}m_{b)} + 2l_{(a}x_{b)} + \rho_1 x_a x_b + \rho_4 y_a y_b + \rho_5 z_a z_b.$	(0.6)
[z z̄ 111]	$R_{ab} = 2\rho_1 l_{(a}m_{b)} + \rho_2 (l_a l_b - m_a m_b) + \rho_3 x_a x_b + \rho_4 y_a y_b + \rho_5 z_a z_b,$	(0.7)

and the twenty-two degeneracies thereof. Here $\rho_1, \cdots, \rho_5 \in \mathbb{R}$ and $\rho_2 \neq 0$ in (0.7).

References

[1] G. S. Hall, *Diff. Geom.* 12, 53 (1984). This reference contains an extensive bibliography on the classification of the Ricci tensor on 4-dimensional Lorentzian space-times manifolds.

[2] R. V. Churchill, *Trans. Amer. Math. Soc.* 34, 784 (1932).

[3] J. Plebański. *Acta Phys. Pol.* **26**, 963 (1964).

[4] W. J. Cormack and G. S. Hall. *J. Phys. A* **12**, 55 (1979).

[5] G. S. Hall and D. A. Negm, *Int. J. Theor. Phys.* **25**, 405 (1986).

[6] G. S. Hall. *Arab. J. Sci. Eng.* **9**, 87 (1984).

[7] J. J. Ferrando, J.A. Morales and M. Portilla, *Gen. Rel. Grav.* **22**, 1021 (1990).

[8] M. J. Rebouças and A. F. F. Teixeira. *J. Math. Phys.* **32**, 1861 (1991).

[9] M. J. Rebouças and A. F. F. Teixeira. *J. Math. Phys.* **33**, 2855 (1992).

[10] J. Santos, M. J. Rebouças and A. F. F. Teixeira. *J. Math. Phys.* **34**, 186 (1993).

[11] G. S. Hall. M. A. H. MacCallum, F. M. Paiva and M. J. Rebouças, "Limits in the Segre Classification of the Energy-momentum Tensor in General Relativity," in preparation (1995).

[12] For a fairly extensive bibliography on this subject see, for example, M. A. H. MacCallum and J. E. F. Skea. "SHEEP: A Computer Algebra System for General Relativity", in *Algebraic Computing in General Relativity. Lecture Notes from the First Brazilian School on Computer Algebra*, Vol. II, edited by M. J. Rebouças and W. L. Roque. Oxford U. P., Oxford (1994).

[13] See, for example, R. J. Gleiser and M. C. Diaz. *Phys. Rev. D* **37**, 3761 (1988) and references therein quoted on this subject.

[14] G. S. Hall. *J. Phys. A* **9**, 541 (1976).

[15] G. S. Hall. T. Morgan and Z. Perjés. *Gen. Rel. Grav.* **19**, 1137 (1987).

[16] J. Santos, M. J. Rebouças and A. F. F. Teixeira. "Classification of Second Order Symmetric Tensors in 5-Dimensional Kaluz-Klein-Type Theories," to appear in *J. Math. Phys.* (1995).

Distribuição Angular de Múons
Próximo ao Nível do Mar

E.G.S. Luna, A.C. Fauth, H. Nogima

Instituto de Física 'Gleb Wataghin' Universidade Estadual de Campinas. Unicamp
13083-970, Campinas, São Paulo, Brasil

May 30, 1995

Utilizando um aparato experimental composto de detectores tipo "streamer", obtemos o fluxo diferencial de múons próximo ao nível do mar entre os ângulos zenitais $0°$ - $30°$

I. Introdução

Múons da radiação cósmica produzidos na atmosfera terrestre são facilmente detectáveis e podem ser usados como uma fonte de informação a respeito da direção de chegada e composição dos raios cósmicos primários. Utilizando um módulo de trajetografia composto de detectores tipo "streamer"[1], determinamos a distribuição angular de múons próximo ao nível do mar (937 g/cm^2). Para tais medidas torna-se importante um sistema experimental que possua como uma de suas principais características a possibilidade de observação visual de trajetórias de partículas. O registro da trajetória possibilita de uma forma direta a determinação da distribuição angular de raios cósmicos, sendo esta informação necessária na transformação de taxas de contagem em intensidades e na identificação de eventos de múons individuais, eventos de chuveiros atmosféricos densos, elétrons altamente energéticos, etc. Os detectores tipo "streamer", operando em regime saturado com auto-apagamento [2], fornecem uma ótima medida de densidade de partículas, além de uma excelente resolução angular.

2. Aparato Experimental e Medidas

O aparato experimental consiste de 5 planos horizontais de área $\approx$ 1m^2 cada, sobrepostos a uma distancia de 50cm um do outro. Cada plano contém 96 tubos "streamer" de secção transversal 1x1cm^2, cuja tensão de trabalho é 4590V. O detector utiliza uma mistura ternária de gases consistindo de Ar/iC$_4$H$_{10}$CO$_2$ na proporção 2.5/9.5/88, respectivamente. A informação necessária para obtenção das coordenadas (x,y) de cada plano onde há a passagem de partícula através do detector, indispensável para a reconstrução das trajetórias, é obtida através da leitura digital de sinais induzidos em fitas metálicas colocadas externamente e ortogonalmente sobre cada plano. A discriminação dos sinais é feita por cartões de leitura LeCroy 4200, onde o limiar de discriminação do sinal do fio anodo é 20mV/50 Ω e limiar de formatação 400ns. Os dados dos eventos registrados pelo aparato são decodificados e interpretados para a reconstrução das trajetórias das partículas. Tais dados são obtidos originalmente através das coordenadas x e y, sendo por este motivo que os traços são reconstruídos em dois planos independentes, ZX e ZY, sendo Z a coordenada vertical do telescópio (fig.1). A reconstrução dos eventos é feita por um programa de computador desenvolvido pelo nosso grupo [3], cujo algoritmo verifica o paralelismo de todas as retas entre quaisquer dois pontos em planos diferentes.

O fluxo estimado de partículas ao nível do mar é da ordem de 500/m^{2}s. Isto representa uma alta taxa de eventos a serem detectados e a inviabilidade (devido a enorme capacidade de armazenamento requerida) de operação do telescópio por um tempo prolongado, necessário na observação de anisotropias [4]. Entretanto, o alto fluxo de partículas permite a verificação da distribuição angular em poucos dias, além de fornecer dados suficientes para a

DATA:25-03-94 HORA 09:34:38:4900
PLANO 2Y   PLANO 2X   Evento= 11
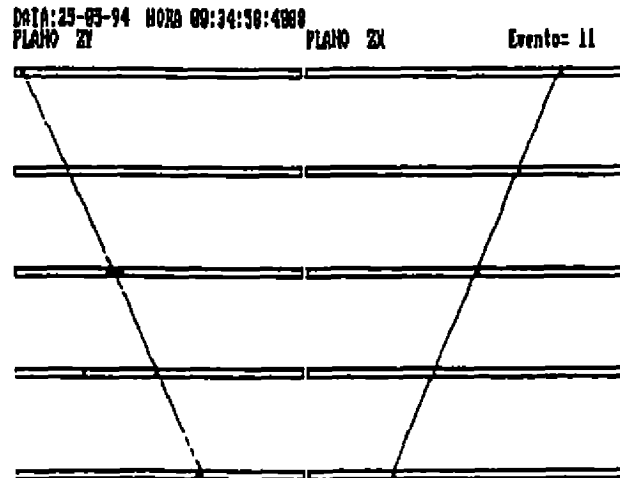
Figura 1: Cópia da tela gráfica gerada pelo programa de reconstrução de trajetórias.

Ângulo Zenital, Θ (graus)
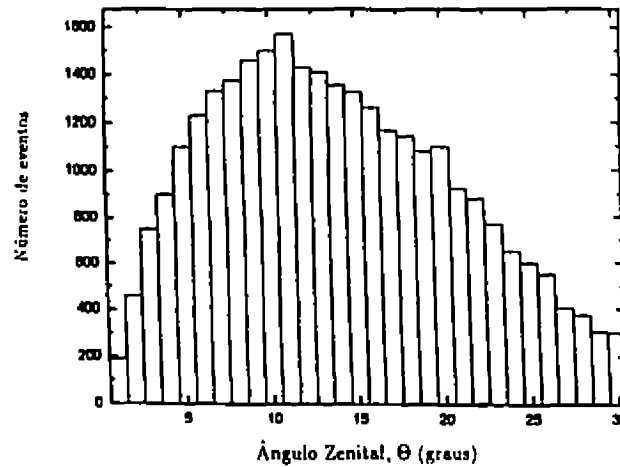
Figura 2: Histograma dos ângulos zenitais de múons a 937 g/cm^2.

estatística de desempenho do detector. Para limitar o fluxo de eventos no telescópio, introduzimos um tempo morto que representa o dobro do tempo em que o experimento fica em aquisição. Os dados foram colhidos durante 20 dias ininterruptos. Neste período selecionamos e reconstruimos $\approx$ 31000 eventos de múons individuais, equivalendo a uma taxa de eventos de 65/h, permitindo obter a distribuição diferencial de múons (fig.2).

3. Conclusão

Montamos e calibramos um telescópio de múons composto de detectores tipo "streamer" de secção transversal 1x1cm^2. Testamos e monitoramos seus 800 canais digitais de cartões de leitura, onde verificamos a melhor relação entre a largura dos clusters e eficiência de detecção. Colocamos o telescópio em funcionamento por 20 dias ininterruptos e selecionamos cerca de 31000 eventos de múons que satisfizeram as condicoes de "trigger".

A distribuição experimental angular diferencial de múons é influenciada fortemente pela geometria do telescópio. Atualmente estamos estudando tal efeito através do desenvolvimento de expressões analíticas para a abertura de telescópios retangulares, o que nos permitirá obter a distribuição angular integral e o valor do expoente n na expressão $I(\Theta) = I()) \cos^n \theta$ [5], usualmente utilizada em distribuições deste tipo.

Agradecimentos

References

[1] E. Iarocci, Nucl. Inst. and Meth., **217**(1983)30.

[2] E.G.S. Luna, A.C. Fauth, *XIV Brazilian National Meeting on Particles and Fields*, Caxambu (1993)284.

[3] Grupo de Léptons, DRCC-UNICAMP.

[4] G. Bressi, et al, Europhys. Lett., **11**(1990)287.

[5] J.N. Crookes e B.C. Rastin, Nucl. Phys. **B39**(1972)493.

Medida da dependência temporal
a oscilação $b_D^0 - \bar{b}_D^0$

Denison Souza-Santos, Ronald Cintra Shellard

Depto de Física - PUC-Rio

Miriam Mendes Gandelman, Luiz Martins Mundim

LAFEX - CBPF

A oscilação entre os mésons $B_d^0 - \bar{B}_d^0$ é um dos dois exemplos de oscilação partícula-antipartícula, um fenômeno quântico, com consequências macroscópicas, o outro sendo a oscilação $K^0 - \bar{K}^0$. Este fenômeno foi observado pela primeira vez no sistema B em 1987, pelos experimentos ARGUS, no DESY e UA1 no CERN.

A origem de tal fenômeno pode ser traçada ao carácter quântico dos estados físicos associados aos B^0s. Os estados mensuráveis, com massa bem definida, são autoestados do operador CP, enquanto que os estados B^0, com sabores de quarks bem definidos, existem como superposição quântica,

$$B^0 = \frac{B_1 + B_2}{\sqrt{2}} \qquad \bar{B}^0 = \frac{B_1 - B_2}{\sqrt{2}},$$

onde B_1 e B_2 são os autoestados físicos. Ao serem formados, por exemplo, na aniquilação e^+e^-, os mésons B tem um sabor bem definido, ou B^0 ou $\bar{B}^0$, uma mistura de B_1 e B_2. No entanto, se B_1 e B_2 tiverem massas diferentes irão decair com vidas médias diferentes, portanto a composição de um estado (não físico) B^0 irá modificar-se ao longo do tempo. Quando o méson decair, o fará com sabor bem definido. A probabilidade de um méson B decair com seu sabor original e tendo oscilado para o anti-sabor é dada pelas expressões

$$\mathcal{P}_{B \to B}(t) = \frac{1}{2} \exp^{-\frac{\Gamma t}{\hbar}} \left(1 + \cos(\frac{\Delta m\, t}{\hbar}) \right)$$
$$= \exp{-\frac{t}{\tau}} \cos^2 \left(\frac{xt}{2\tau} \right)$$

e

$$\mathcal{P}_{B \to \bar{B}}(t) = \frac{1}{2} \exp^{-\frac{\Gamma t}{\hbar}} \left(1 - \cos(\frac{\Delta m\, t}{\hbar}) \right)$$
$$= \exp{-\frac{t}{\tau}} \sin^2 \left(\frac{xt}{2\tau} \right)$$

onde δm é a diferença de massa $m_{b_1} - m_{B_2}$, $x = \frac{\Delta m}{\Gamma}$ e $\tau = \frac{\hbar}{\Gamma}$.

A probabilidade integrada total do méson B^0 decair como $\bar{B}^0$ é então

$$x = \frac{1}{2} \frac{(\frac{\Delta m}{\Gamma})^2}{1 + (\frac{\Delta m}{\Gamma})^2}.$$

Há dois tipos de mésons B neutros, dependendo do sabor do quark que acompanha o b, $B_d^0(d\bar{b})$ e o $B_s^0(s\bar{b})$. A diferença de massa entre os estados físicos podem ser calculadas teoricamente, a partir dos diagramas de transição $(q\,\bar{b}) - (\bar{q}\,b)$ e tem a forma, em primeira aproximação,

$$\Delta m_q = \frac{G_F^2}{6\pi^2}\, m_B m_t^2\, F\left(\frac{m_t^2}{m_W^2}\right)\, \eta_{QCD}\, Bf_B^2\, |V_{tb}^* V_{tq}|^2 .$$

onde $q = d, s$.

$$F(x) = \frac{1}{4} + \frac{9}{4(1-x)} - \frac{3}{2}\frac{1}{(1-x)^2} - \frac{3}{2}\frac{x^2\ln x}{(1-x)}.$$

η_{QCD} é um fator de correção devido à QCD, tendo valor $\eta_{QCD} \simeq 0.55$ na aproximação do próximo termo logaritmicamente dominante. B é um parâmetro associado ao modelo de sacolas (com valor $B = 1.0 \pm 0.2$ em simulações na rede). $f_{B_d} \simeq 180 \pm 50$ MeV e V_{tb} e V_{tq} são os parâmetros de Kobayashi-Maskawa. A medida de Δm permite acesso aos parâmetros de Kobayashi-Maskawa associados ao quark top.

Os experimentos com a colisão e^+e^- a baixas energias (ARGUS e CLEO), produzem apenas B_d^0, pelo decaimento do estado Υ''', em contraste com o LEP onde no decaimento do Z^0 são produzidos ambos sabores dos B^0. O valor experimental medido para a diferença de massa para o B_d, pelo experimento CLEO, $x_d = 0.69 \pm 0.10$ é compatível com o valor medido por DELPHI, $x_d = 0.77 \pm 0.18(estat) \pm 0.09(sist)$ ou

$$\Delta m_d = [3.29 \pm 0.79 \pm 0.39]\; 10^{-4}\; eV/c^2 .$$

O valor de x_s é muito maior do que x_d portanto o período de oscilação dos B_s é menor do que para B_d e mais difícil de ser observado. O intervalo de valores para x_s compatíveis com o modelo padrão é $5 < x_s < (\sim 100)$.

Na medida do valor de δm_b mencionada acima, DELPHI usou a estratégia de identificar o sabor do méson B^0 em cada hemisfério e medir a distância do decaimento ao vértice principal. Neste trabalho estamos usando uma estratégia diferente, medindo a dependência dos sabores decaindo, como função da distância entre os vértices de decaimento, ajustando os dados à convolução das probabilidades de decaimento com e sem oscilação.

$$\mathcal{P}_{OSC}(d) = \int_0^\infty dl\,dl'\,\delta(l+l'-d)\;[\mathcal{P}_{B-B}(l)\,\mathcal{P}_{\bar{B}-B}(l') + \mathcal{P}_{B-B}(l)\,\mathcal{P}_{\bar{B}-B}(l')] .$$

Este método reduz o erro sistemático quando comparado com o método convencional e as distâncias a serem medidas tem um fator duas vezes maior. Este método é dependente da precisão na medida dos parâmetros de impacto das trajetórias carregadas e torna-se particularmente útil com o novo detetor de microvértices de DELPHI, que mede todas as coordenadas dos parâmetros de impacto, quando aplicado à medida de x_s. Os resultados preliminares obtidos até agora são bastante encorajadores.

Identificação de partículas pela medida da perda de energia em detetores de silício

Denison Souza-Santos, Ronald Cintra Shellard

Depto de Física - PUC-Rio

A perda de energia de uma partícula carregada, por ionização, ao atravessar a matéria, é fortemente dependente da sua velocidade. Se a velocidade da partícula for muito maior do que a velocidade orbital dos elétrons no material atravessado, a perda média de energia por ionização é dada pela equação de Bethe-Bloch,

$$-\frac{dE}{dx} = 4\pi N_A r_e^2 m_e c^2 z^2 \frac{Z}{A} \frac{1}{\beta^2} \left[\ln \left(\frac{2m_e c^2 \gamma^2 \beta^2}{I} \right) - \beta^2 - \frac{\delta}{2} \right].$$

sendo os termos relevantes desta fórmula, a dependência em β e γ.

Esta dependência na velocidade da perda de energia por ionização tem sido usada para identificar partículas com massas diferentes, nas regiões de momento entre algumas centenas de MeV/c^2 até cerca de 2 GeV/c^2, em detetores destinados a medir a trajetória de partículas. Tipicamente tem sido usadas para este fim câmaras do tipo TPC *(Time Projection Chambers)* ou câmaras de jatos, onde os sensores da ionização apanham um sinal proporcional à quantidade de elétrons ionizados, consequentemente um sinal proporcional à perda de energia da partícula.

O experimento DELPHI, tomando dados no anel de colisões LEP, no CERN, tem na sua parte central um detetor de alta resolução, para medir a passagem de partículas carregadas. A principal função deste detetor é a de discriminar os vértices primário e secundários, formados na reação, na região de central de colisão, permitindo a resolução entre vértices separados por dezenas de microns. Este detetor é formado por três camadas concêntricas de detetores de microfitas de silício. Cada detetor de silício tem a espessura de cerca de 300 microns, atravessadas pelas partículas carregadas. O sinal colhido pelas fitas é proporcional à quantidade de elétrons liberados na ionização dos átomos de silício. Normalmente, no uso deste detetor, a altura dos pulsos é usada apenas para calcular a posição relativa da trajetória, em relação a duas fitas contíguas.

Neste trabalho demonstramos que este detetor pode ser usado também no modo de identificação, pela discriminação de píons, kaons e prótons, na região de momento abaixo de 1 GeV/c^2. A motivação para este trabalho vem do seu aspecto complementar à identificação das partículas pela perda de energia na TPC de DELPHI. Por outro lado, no novo detetor planejado para a região frontal do experimento, composto apenas por detetores de silício, este modo oferece a oportunidade única de identificação de partículas. A perda de energia por ionização tem um comportamento estatístico, tendo caracteristicamente uma distribuição de Landau em torno da perda média, descrita pela equação de Bethe-Bloch. Quando da leitura da perda de energia na TPC de DELPHI, são tomadas 196 amostragens da quantidade de elétrons ionizados, permitindo então a reconstrução da perda média, ajustando-se uma gaussiana à região de perda de energia mais provável. Em contraste, no detetor de microvértice são tomadas apenas três amostragens da perda de energia, exigindo um tratamento mais criterioso dos dados.

Para corrigir os dados e calibrá-los são necessários vários passos:

1. Definimos o pulso associado a uma trajetória tomando o valor do pulso na fita com maior razão sinal/ruído somado aos pulsos nas duas fitas adjacentes.

2. As trajetórias são normalizadas para aquelas atravessando a placa normalmente à superfície, multiplicando-se o pulso por um fator $1/\cos(\theta)$, onde θ é o ângulo formado pela trajetória com a normal ao plano da placa de silício.

3. Para calibrar os ganhos da eletronica de cada amplificador, o detetor é subdividido nos módulos de cada placa amplificadora. O detetor de microvértices está dividido em 24 módulos em cada uma das 3 camadas, cada módulo em 4 placas de silício independentes e cada 128 fitas é lida por um amplificador, num total de 5 por placa. Para cada uma destas 1440 unidades fazemos um levantamento do espectro de Landau dos pulsos. Cada pulso físico é então renormalizado para uma curva de Landau padrão.

4. Para encontrar a perda de energia média associada a uma determinada trajetória, coletamos os tres pulsos renormalizados e aplicamos um algoritmo que ajusta uma distribuição de Landau mais provável à série, extraindo, então, o valor médio da perda de energia.

Neste algoritmo construimos a probabilidade:

$$\mathcal{P}(X) = \prod_{i=1}^{3} f_L(B_0 * (X_i - X) - b_0).$$

onde B_0 e b_0 são parâmetros que caracterizam a distribuição de Landau de referencia. f_L é a distribuição de Landau. X_i são os valores dos pulsos coletados e X é a variável em relação à qual $\mathcal{P}$ é maximizada. O valor máximo de $\mathcal{P}$ é dado pela solução da equação:

$$\sum_{i=1}^{3} \frac{f_L'(B_0 * (X_i - X) - b_0)}{f_L(B_0 * (X_i - X) - b_0)} = 0$$

onde $f_L' = \frac{df_L}{dx}$.

MICROSUL: A Cosmic Ray Muon Monitor
Um Monitor de Raios Cósmicos

Equipe Microsul: Eduardo J. Pacheco (IAGUSP). Elly Silva(CBPF) Ernst W. Hamburger (IFUSP)
Hélio M. Portela(IFUFF), José A. F. Pacheco (IAGUSP). Jorge Horvath (IAGUSP). Luis
Galhardo (IAGUSP), Manoel T. F. da Cruz (IFUSP), Margaret. O. Silva (CBPF). Nilton
A. Alves (CBPF). Olácio Dietzsch (IFUSP), Regina H. C. Maldonado(IFUFF).
Walter Velloso (IAGUSP). A. F. Assis (CBPF), C. A. M. Mesquita (CBPF).
E. M. Kubo (IFUSP), F. Salemme (IFUSP). Laura M. R. Falco (IFUSP).
M. A. R. Guimarães (CBPF). Marco A. Schmidt (IFUSP).
Marcos Mansueto (IFUSP), S. A. Pereira (IFUSP)

1.Experimento Microsul é um telescópio eletrônico de muons de alta energia

Muons produzidos por Raios Cósmicos primários na alta atmosfera.

Mede distribuição angular dos muons cósmicos ao nível do solo. Ficará ligado permanentemente.

Experimento inspirado em MICRO de Frascati, Italia, 1987. (G.Battistoni et al. Nuovo Cimento 11C (1988) 175)

Em altas energias: direção do muon = direção do R.C.

Precisão na determinação da direção $\sim 1°$

2.Monitor do fluxo de muons de alta energia em função da direção e do tempo

Os Raios Cósmicos Primários são $\sim$ isotrópicos

Anisotropias estreitas (= fontes discretas) foram relatadas por vários grupos nos anos 80, mas não foram confirmadas em experimentos posteriores; somente uma, localizada na nebulosa do Caranguejo, foi encontrada em 1992, mas com pouca intensidade, muito menor que relatada anteriormente [v. revisão de T.C. Weekes . Space Sci. Rev. 59 (1992) 315].

MICRO (Frascati) procurou fontes discretas, mas não encontrou; estabeleceu limite superior $\sim 10^{-5} cm^{-2} s^{-1}$.

Se houver anisotropia estreita intensa no hemisfério Sul. Microsul deve identificá-la. Além disso, vai medir a distribuição angular. o espectro de energia e a variação com o tempo dos muons de $E > 10$ GeV.

3. Aparelho

Seis planos paralelos cada um de 1m x 1m

Dispostos em faces opostas de um cubo $1m^3$

Cada plano contém 96 tubos de 1cm x 1cm x 100cm

Tres planos em cada face do cubo (Ver fig.1).

Partícula que atravessa os planos produz ionização

Permite determinar coordenadas x_i , y_i das interseções

Seis pontos, um em cada plano, determinam trajetória (Se não estiverem em linha reta, evento é rejeitado).
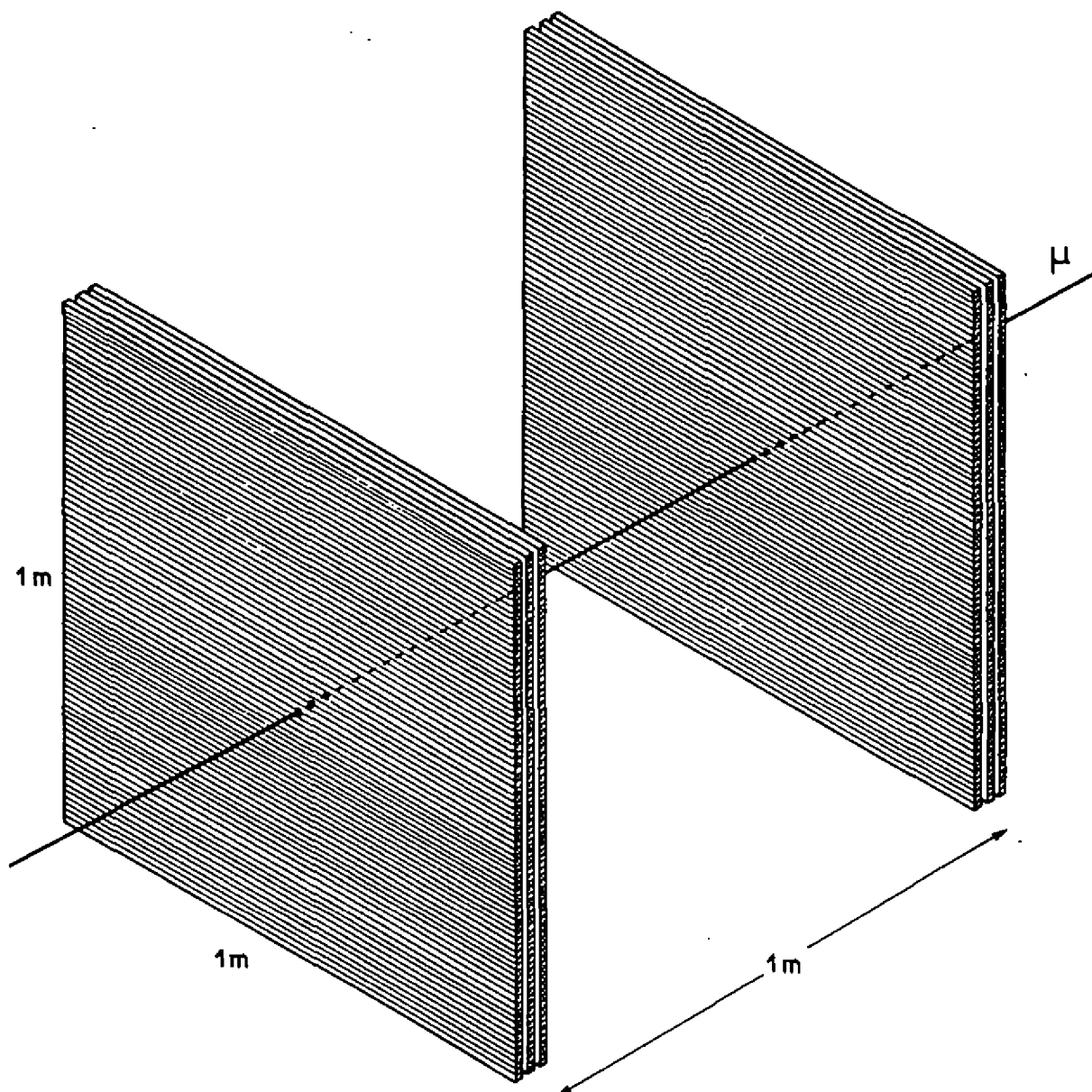
96 tubos de 1 x 1 x 100 cm³
em cada plano

esc. 1: 100

Fig.1.

4. Muons Horizontais

Absorção Atmosférica elimina elétrons e outras partículas. só muons acima de ~ 10 GeV podem penetrar até o contador (Ver fig.2).
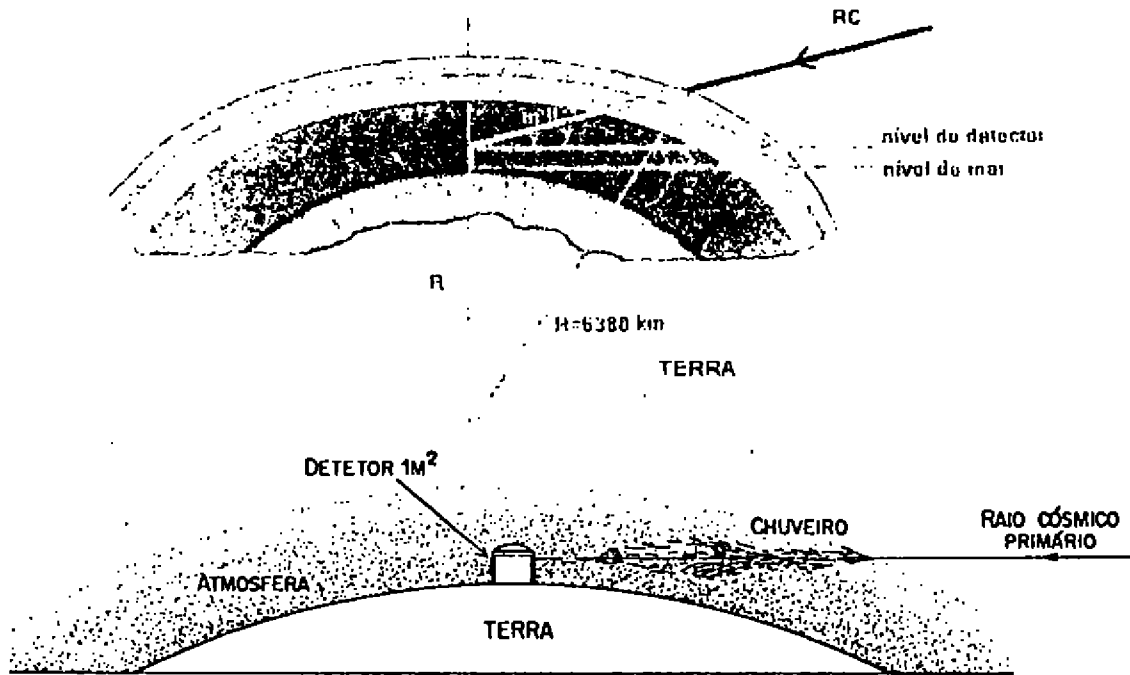
Fig.2.

A espessura da atmosfera verticalmente é ~ 1 kg/cm^2, que absorve muons abaixo de ~ 2 GeV.

Horizontalmente a espessura é 36 kg/cm^2 , E >75 GeV

O fluxo de muons horizontais é >> verticais para $E > 1$TeV (v.p.ex. P. Lipari, Astrop.Phys. **1** (1993)195). (Ver fig.3).
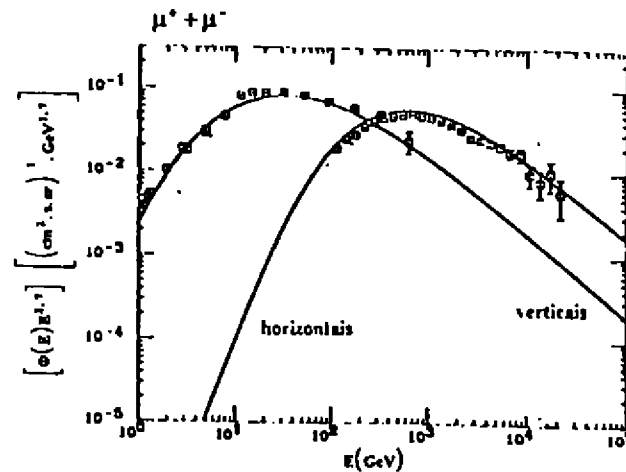
Fig. 3.

5. Local

Cúpula de telescópio ótico desativado no IAGUSP

Horizonte livre em 360°. Altitude 780m.

Infraestrutura instalada: ar condicionado, eletricidade, para raios, sistema de gases, etc. (Ver fig.4).

Fig. 4.

6. Contadores doados por INFN-Padova

Peças fabricadas por Pol.Hi.Tech., Italia

Contadores a gás, tipo 'streamer' limitado (tubo Iarocci)

Estrutura de plástico isolante (PVC.Noril)

Mistura 88% gás carbonico, 4% Argonio, 8% Isobutano

Pressão atmosférica, fluxo continuo 1vol/48h ~ 1.5 l/h

Anodo fio central 100 micra, tensão continua 5000V.

Catodo resistivo de carbono depositado sobre o plástico. Sendo resistivo, permite passagem de sinal por indução ("pickup") do interior para eletrodo externo (faixa ou banda metálica colada sobre plástico do contador).

Ionização provoca multiplicação ('streamers')localizada

Carga local no tubo induz cargas em bandas externas 96 bandas x , acima , e 96 bandas y abaixo de cada plano. Bandas metálicas isoladas, ~ 1cm x 1m cada.

Sinais das bandas ~ 5 mV, duração ~ 60 ns (v.M.Tecchio, Tese de Laurea, Padova, 1989; E.Iarocci, Nucl. Inst. Met. **217** (1983) 30; A.C.Fauth et al. Rev.Fis. Apl.Instr. 7 (1992)31) (Ver figs. 5 e 6).
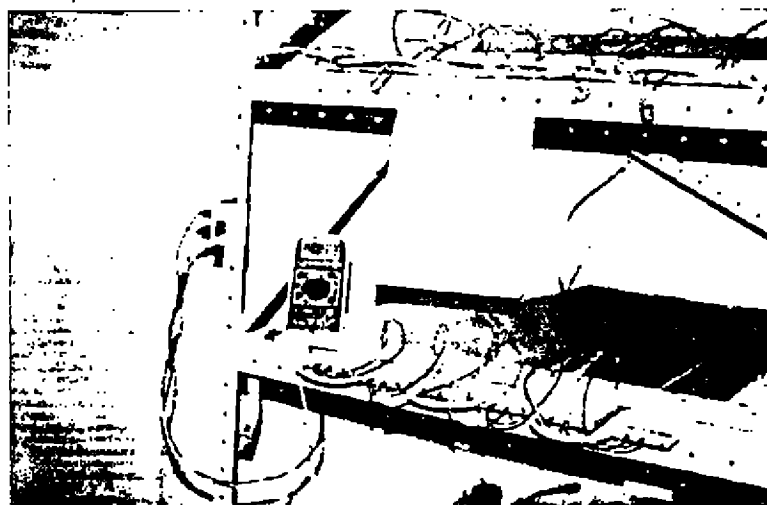
Fig. 5.
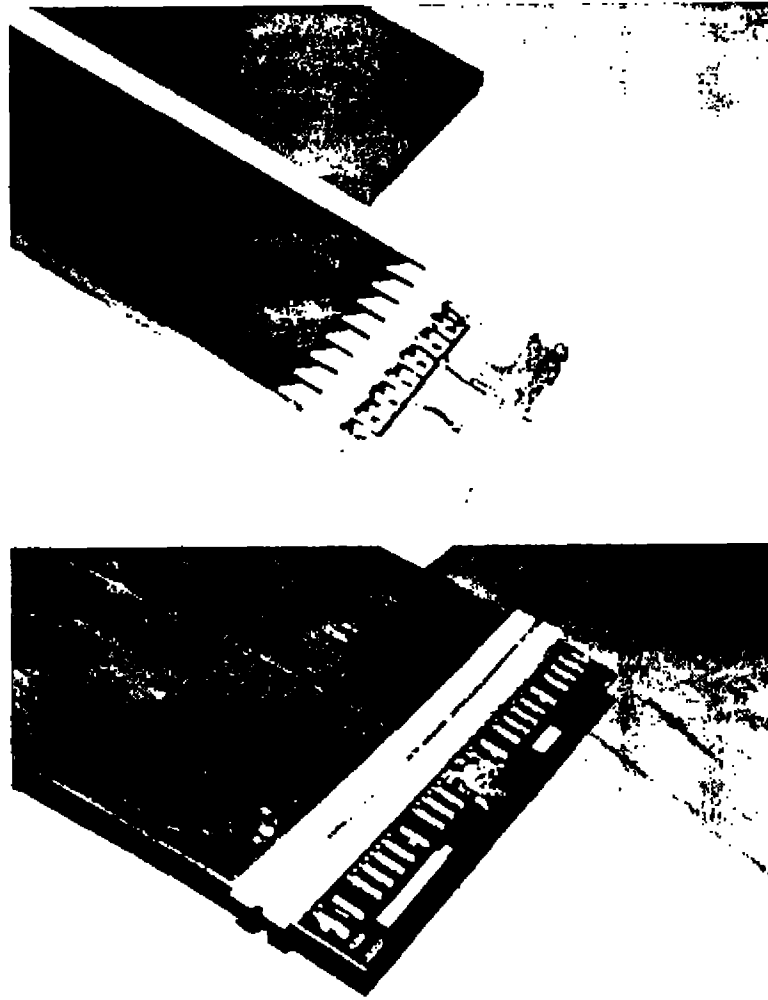
Fig. 6.

7.Montagem dos contadores:

Oito tubos em cada peça

Verificação da resistividade do catodo

Montagem das basetas e dos anodos

Colagem e teste de vazamento

(Foi produzido um vídeo de 11 minutos de duração em que se mostra, em detalhe, a montagem dos contadores: o vídeo foi pensado para instrução de montadores de tubos no futuro).

8. Condicionamento de Alta Tensão

Fluxo de gás para eliminar oxigênio

Mistura CO_2, Ar (e isobutano)

Eleva gradualmente A.T. até 4800 Volts

Em cada tensão, aguarda corrente diminuir

Valor ideal abaixo de 120 nA/m ou 1mA/octotubo

Aceitável até 3mA/octotubo.

Efeito do isobutano sobre corrente média: diminue de 0% a 20%, depois quase constante. (Ver fig.7).

9. Misturador de Gases

Pulmão misturador com palha de aço inox. Fluxômetro de massa com controle automático. (Ver figs 8 e 9).

No CBPF, rotametros calibrados

10. Efeito do isobutano no gás do contador

Nove octotubos, já condicionados em Alta Tensão durante vários dias, tiveram a proporção de isobutano variada de 0 a 59% várias vezes durante algumas semanas. A tensão foi fixada em 4800V, e a figura mostra a corrente, em função do fluxo de isobutano e da data. A corrente é baixa, de nanoampères, e flutua muito a cada instante - até um fator dois. Os valores mostrados são médios. Para cada valor do fluxo de isobutano, observa-se uma redução da corrente ao longo do mês. Além disso, há uma nítida diminuição da corrente quando o isobutano aumenta, de ~ 18nA a 0% até ~ 5nA a 59%, como se espera para um gás apagador ("quenching") (Ver fig. 7).

A densidade da atmosfera ρ em função da altitude z acima do nível do mar pode ser bem aproximada pela exponencial (T.K.Gaisser, Cosmic Rays and Particle Physics. Cambridge Univ.Press. 1990; P. Lipari, loc.cit..1993): $\rho(z) = \rho_0 e^{-z/A}$ onde $\rho_0 = 1030g/cm^2$, $A = 7300m$

À altitude do detetor no IAG/USP $z_0 = 780m$, $\rho(z_0) = 0.904\rho_0 = 931g/cm^2$

A espessura de ar atravessada pelo muon que incide em angulo γ com a horizontal, em g/cm^2, é dada por

$$D(\gamma) = \rho_0 A \sqrt{\frac{\pi R}{2A}} e^{-z_0/A} F(\gamma)$$

onde $R = 6380km$ é o raio da Terra e $F(\gamma)$ dá a variação angular:

$$F(\gamma) = e^{\Gamma^2}\left[1 - \frac{2}{\sqrt{\pi}}\int_0^\Gamma e^{-t^2}dt\right]$$

onde

$$\Gamma = \frac{sen\gamma}{\sqrt{\frac{2A}{R}}}$$

A variação angular de $F(\gamma)$ é muito acentuada, de modo que a espessura de atmosfera atravessada pelo muon é função crítica de γ, como mostra a tabela abaixo e o gráfico

Plan1 Gráfico 9
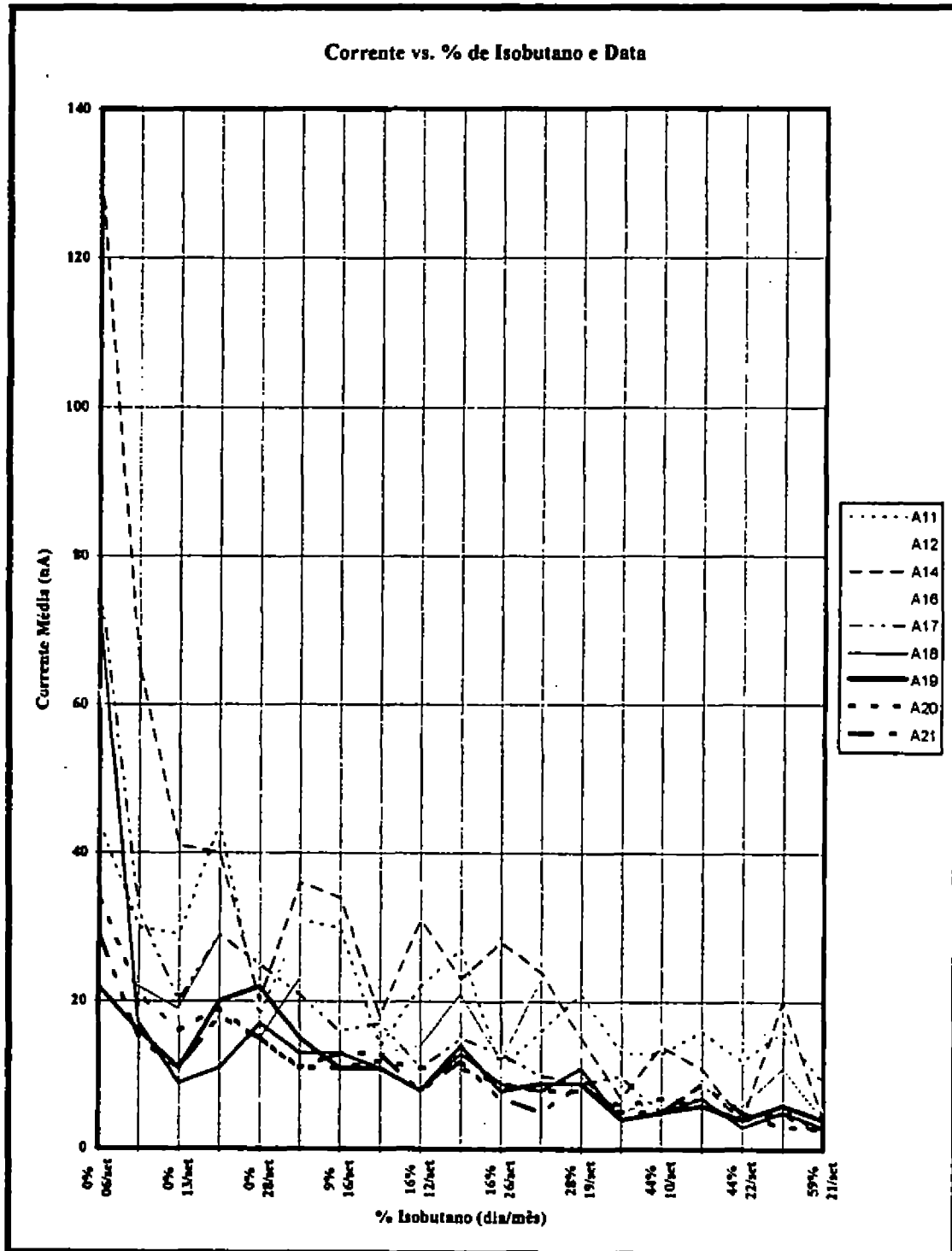
Fig. 7.
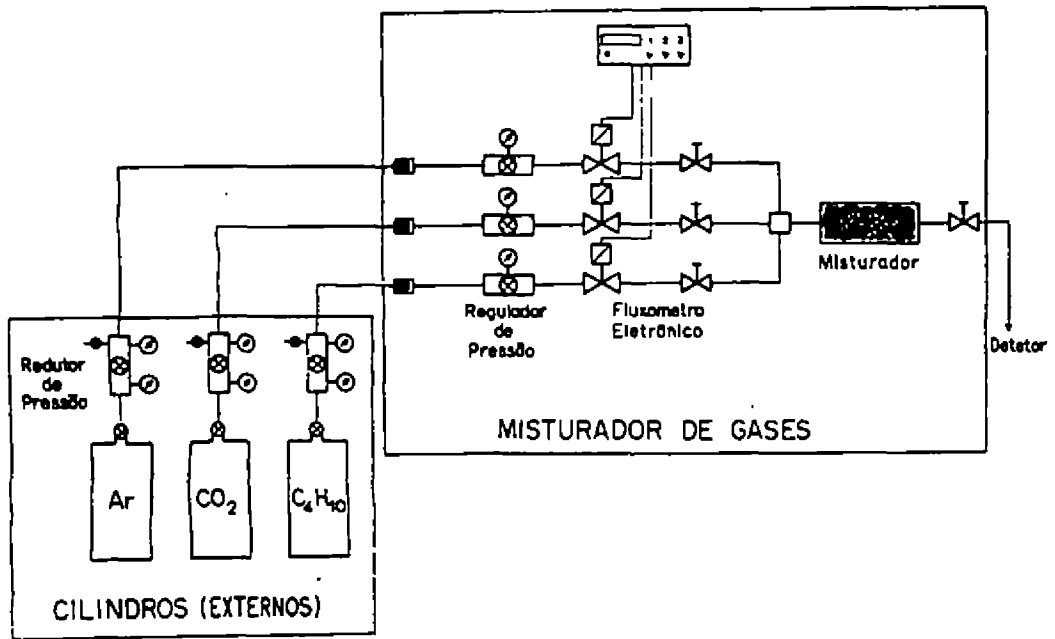
Fig. 8.
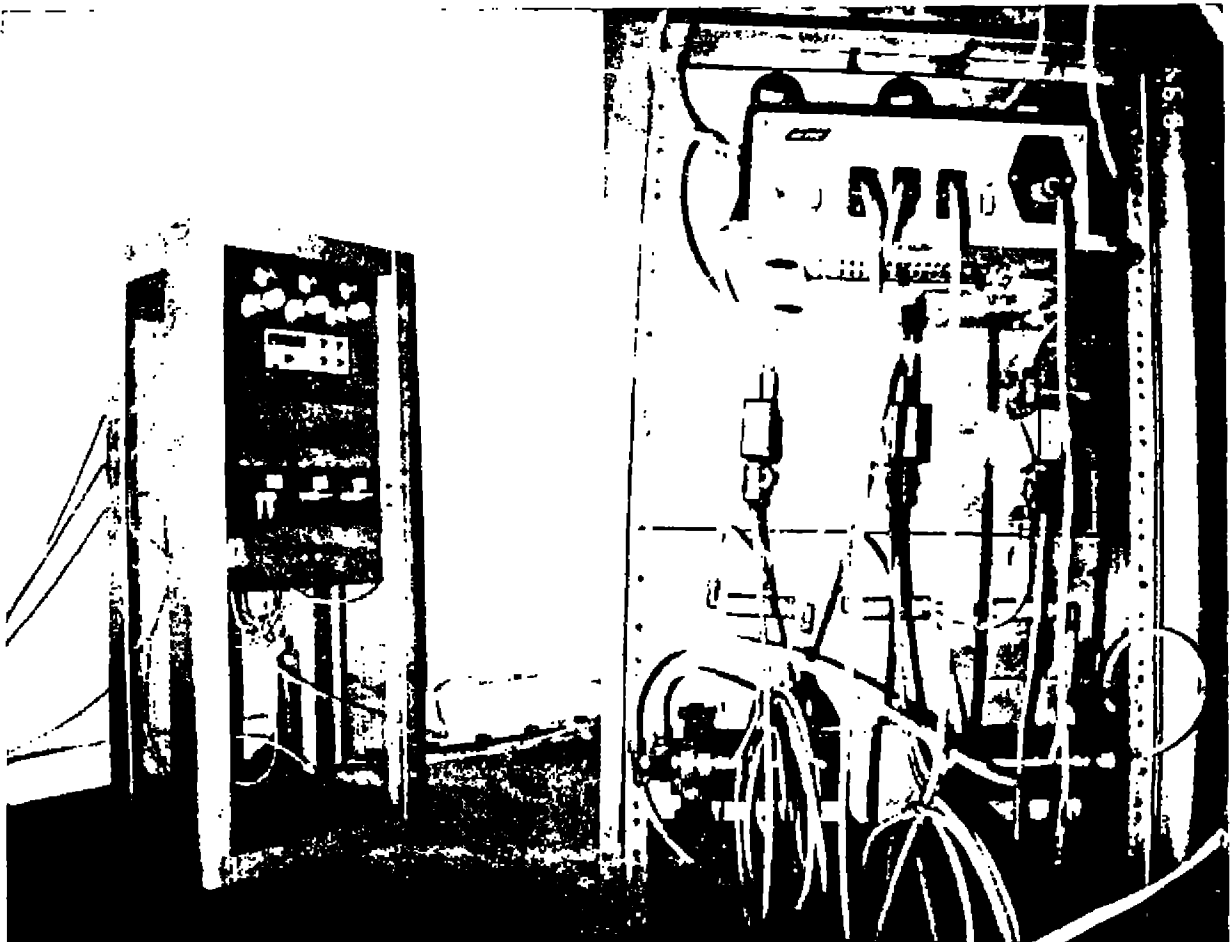
Fig. 9.

11. Espessura da atmosfera em função do ângulo de incidência dos muons

γ	$0°$	$2°$	$4°$	$6°$	$8°$	
$F(\gamma)$	270	139	88	65	53	
$D(\gamma)$	35	18	11	8.4	6.9	kg/cm^2
$E_{min}(\gamma)$	87	43	26	19	16	GeV
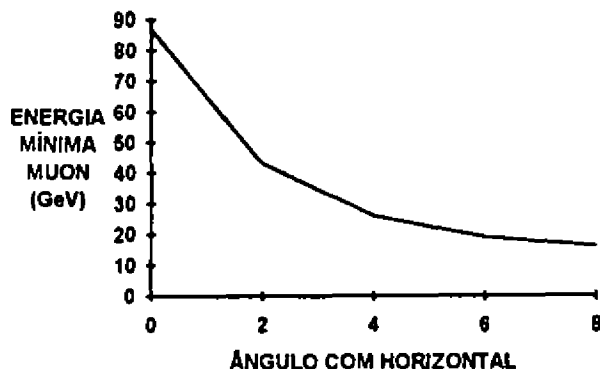
onde a última linha dá a energia mínima de muons que atravessam a espessura D, calculada a partir da perda de energia de muons relativísticos em Nitrogenio líquido (W.Lohmann et al. CERN 85-03 Report,1985).

A $0°$ só podem chegar ao detetor muons que na alta atmosfera tinham mais do que 87 GeV. A $2°$ o valor mínimo é 43 GeV, e assim por diante.

A medida da distribuição angular dos muons é portanto equivalente a uma medição do espectro integral de energia no intervalo de 10 a 87 GeV.

Estamos admitindo que os muons produzidos na alta atmosfera são isotrópicos, assim como os raios cósmicos que os produzem. Anisotropias, se existirem, são pequenas.

12. Estrutura Mecânica

Fase de Projeto

13. Eletrônica

Cartões "front end" LeCroy 4200 testados

Sistema de Aquisição de Dados em fase de projeto

Eletronica CAMAC, computador PC386 Descrição detalhada no trabalho que acompanha este: "Sistema automatizado para teste,calibração e aquisição de dados para eletronica "FRONT-END"em tubos de Iarocci". Equipe MICROSUL: E. W. Hamburger, E. Silva , et.al.

14. Cálculos espalhamento múltiplo, Monte Carlo

Efeito do Campo Magnético da Terra:

Em andamento.

Teste de resolução angular: sombras do Sol e da Lua.

15. Nova doação do INFN/Padova

Estamos recebendo ~ 10 000 tubos de 1cm x1cm x 5m

Eletronica (cartões) associada e suporte mecanico.

Provenientes de experimento $N\bar{N}$

É possível construir telescópio de volume ~80 vezes maior ou quatro telescópios vinte vezes maiores.

16. Agradecimentos

Busca de Mésons η

S. L. C. Barroso, P. C. Beggio, A. O. de Carvalho, M. D. D. Marques.
R. de Oliveira, F. R. A. Revollo, E. H. Shibuya

Instituto de Física Gleb Wataghin. Universidade Estadual de Campinas. Campinas. SP

C. R. A Augusto, C. E. Navia, F. A. Pinto

Instituto de Física, Universidade Federal Fluminense. Niterói. RJ

Os dados experimentais da colaboração Brasil - Japão de Raios Cósmicos (CBJ) mostram a ocorrencia da produção múltipla de mésons π em interações hadrônicas (IH). Entretanto. como estes mésons são detectados através de seu decaimento em γ's. é possível que outros mésons que não o π possam ser identificados. Este trabalho descreve os esforços feitos no sentido de identificar a produção de mésons η em IH usando os dados da CBJ.

A CBJ utiliza como detectores pilhas de materiais fotosensíveis (filmes de Raios-X e placas de emulsão nuclear) intercaladas com placas de chumbo. As IH podem ocorrer na atmosfera (A-Jatos) ou em alvo localizado (C-Jatos). Os A-Jatos são normalmente identificados no conjunto de detectores chamados de câmara superior, e os C-Jatos na camara inferior (o alvo localizado. uma placa de material rico em carbono, se localiza entre a camara inferior e a superior). Os detectores estão arranjados de tal forma a permitir a identificação do vértice da IH e a energia dos γ's resultantes desta interação. Conhecendo a energia dos γ's e altura da IH (posição do vértice) é possível, através da cinemática do decaimento $\pi^0 \to \gamma + \gamma$. identificar estatisticamente os pares de γ's provenientes de um méson π^0. O acoplamento estatístico consiste das seguintes etapas. Primeiro. usando a relação:

$$H_I = \frac{\sqrt{E_1 E_2}\, R_{12}}{M_{méson}}$$

(que relaciona a altura da interação H_I com a energia dos γ's E_1 e E_2 produzidos, a distância R_{12} entre os γ's e a massa de repouso do méson $M_{méson}$ que decaiu nestes dois γ's). determina-se o valor de H_I para todas as combinações binárias dos γ's, supondo que todos foram produzidos por π^0's. Como a altura da interação H é conhecida[1]. seleciona-se os pares de γ's que apresentam valores de H_I compatíveis com H . Em seguida o valor médio dos H_I selecionados é calculado e o valor obtido é usado na expressão acima para se obter o valor de M_η para todas as combinações binárias dos γ's não utilizados para a determinação da altura. Com isso obtém-se a distribuição de M_η. Os histogramas seguintes mostram as distribuições assim obtidas usando-se os dados experimentais de A-Jatos e C-Jatos. Nota-se que nas IH do tipo Mirim não aparece sinal dos η's. enquanto que nas do tipo Açú surge um sinal. A CBJ. através de estudos da distribuição angular. momento transversal. massa invariante. etc. dos dados experimentais. verificou que as IH podem ser classificadas em tres tipos. Mirim. Açú e Guaçú.

---

[1] Nos C-Jatos H é conhecida com boa precisão. visto que o alvo é localizado.

Sistema automatizado para teste, calibração e aquisição de dados para eletrônica "front-end" em tubos de Iarocci

M. P. Albuquerque. N. Alves. G. Cernicchiaro. M. Q. N S. Silva. E. Silva
Centro Brasileiro de Pesquisas Físicas

O. Dietzsch. E. W Hamburger
Instituto de Física da Universidade de São Paulo

L. Galhardo. J. Horvalho. E. J. Pacheco. J. A. F. Pacheco. W Velloso
Instituto Astronômico e Geofísico - USP

R. Maldonado. H. Portella
Universidade Federal Fluminense

Dois tipos de cartões foram estudados: LeCroy e SGS-SLD. Apresentamos as características desses cartões e do funcionamento conjugado com os controladores STOS e STAS em barramento CAMAC. controlados por um microcomputador através de interface GPIB. Para o gerenciamento dos sistemas foram desenvolvidos softwares em linguagem C. Para cada tipo de cartão (LeCroy e SGS-SLD Caen) desenvolvemos sistemas especiais que exercem as seguintes funções: a)teste de funcionamento de cartões: b)calibração do limiar de corte: c)obtenção de curvas, para cada cartão, da eficiência em função de threshold e curvas de tensão de entrada em função de tensão de limiar para eficiência máxima. Para este fim utilizamos geradores de pulso e voltímetros programáveis por GPIB. desenvolvemos interfaces DAC e ADC e o software de controle e teste da simulação. Foram criados métodos de controle de aquisição e desenvolvimento de bibliotecas de funções de programação para futuros trabalhos no experimento.

Análise do Evento do Tipo Centauro

S.L.C. Barroso, P.C. Beggio, A.O. de Carvalho, M.D.O Marques
R. de Oliveira, F.R.A. Revollo, E.H. Shibuya
Instituto de Física 'Gleb Wataghin'
Universidade Estadual de Campinas, Unicamp, Campinas - SP

and

C.R.A. Augusto, C.E. Navia, F.A. Pinto
Instituto de Física, Universidade Federal Fluminense, Niterói-RJ

Apresentamos alguns resultados de análise preliminar efetuada em evento com características diferentes dos eventos de Produção Múltipla de Mésons.

Durante a exposição da câmara de Emulsões 16 (CE-16), pela Colaboração Brasil-Japão de Raios Cósmicos, foi detectado um particular tipo de Interação Nuclear que, após várias remedições e análises constatou-se características diferentes de outras interações normalmente detectadas.

A câmara de emulsões em questão ficou exposta à Radiação Cósmica durante 370 dias e continha 7,8 cm de placas de chumbo. alternadas com filmes de R-X tipos N e 100 cm sua estrutura superior (câmara superior), enquanto que na parte inferior (câmara inferior) foram utilizados 15,0 cm de chumbo alternados com 15 filmes de R-X tipo N e 100.

Algumas características que diferem essa interação nuclear (denominada Centauro V) das interações normais (resultado da Produão Múltipla de Mésons) são a seguir apresentadas:

a) Presença de grande número de chuveiros eletromagnéticos (63%) originados por hádrons (diferentes de π^o). Os critérios utilizados para identificar chuveiros eletromagnéticos originados por hádrons foram:

a.1 - chuveiros detectados só na câmara inferior;

a.2 - chuveiros com curvas de transição com 2 máximos;

a.3 - chuveiros iniciados após 4 cm de chumbo na câmara superior e

a.4 - chuveiros detectados na câmara superior e que continuam na câmara inferior.

Nas interações normais o número de chuveiros originados por hádrons é menor do que 30%

b) Distribuição de energia fracional, que corresponde ao parâmetro x de Feymman, concentrada numa numa região diferente das interações normais, [1].

c) Expoente do espectro de energia fracionária integral (de chuveiros originados por gamas e hádrons juntos) diferente das interações normais. Os valores encontrados foram:

$$\beta_{Centauro\,V} = 1.33 \pm 0.17$$

$$\beta_{Int.\,Normais} = 1.06 \pm 0.09$$

calculados pelo método de máxima verosimilhança.

d) Alto valor de momento linear transversal dos hádrons ($p_t^{(\gamma)}$) indicando possível mecanismo de Produção Múltipla de Partículas diferentes de Mésons, que são as partículas predominantemente produzidas nas interações normais. O valor determinado, por máxima verosimilhança, foi:

$$p_t^{(\gamma)} = 267 \pm 43 \frac{MeV}{c}$$

Conclusão

O evento classificado como do tipo Centauro apresentou várias características que o excluem da categoria de eventos de Produção Múltipla de Mésons (eventos normais). A análise indicou também que esse evento é compatível com a formação e decaimento isotrópico de estado intermediário.

Referência

[1] - Re-analysis of Exotic event - S.L.C. Barroso et al . VIII Int. Symposium on Very High Energy Cosmic-Ray Interactions - Julho/1994 - Tóquio-Japão.

Detector for Measurements of Cosmic Ray Tev Electrons Based on their Synchrotron Radiation in Geomagnetic Field

A.A.Gusev, I.M.Martin, G.I.Pugacheva, A. Turtelli Jr.

Unicamp, IFGW, Campinas, SP, Brazil

1.Introduction

The primary cosmic electrons appear to be small part of the total cosmic ray flux, ~ 1%. But its spectrum reflects important astrophysical processes in the sources of particles, their lifetime, properties of the interstellar media where electrons propagate on the way to the Earth. During the lifetime the electrons fill in the storage region. The interstellar media of the region contains magnetic fields, interstellar matter of a small density and radiation fields of star light and blackbody photons. Passing this space electrons loss the energy by ionization, reverse Compton scattering on star light and blackbody photons and emitting of synchrotron radiation photons in magnetic fields. The scale of the electron energy losses in the Galactic Disk is shown in Fig.1.
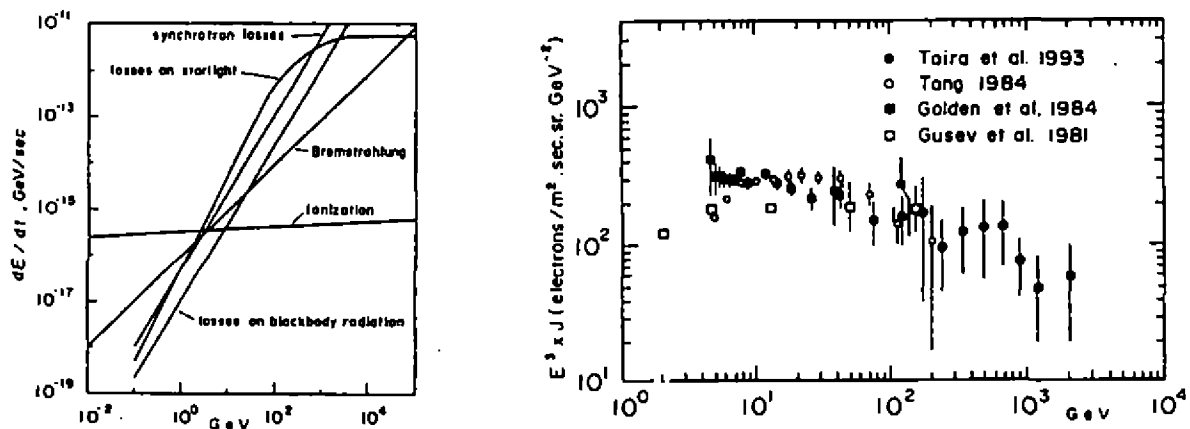
Fig.1. The electron energy losses in the Galactic Disk. Fig.2. The high energy side of primary electron spectrum.

The electron spectral shape is changed by propagation that described by two models: Leaky Box and Diffusion Models. The Leaky Box model suggests the regions of origin and storage of electrons are the same: the electrons are moving in the space freely, without diffusion, only interacting with the media and leaking out from the storage region. The equation for Leaky Box model is

$$d(N(E) \cdot dE/dt)/dE + N(E)/T_L = K E^{-\gamma} \qquad (1)$$

dE/dt, T_L, $KE^{-\gamma}$-energy losses, leakage lifetime and a production spectrum. The solution of equation for high energy electrons:

$$N(E)dE = K E^{-\gamma-1}/b(-\gamma + 1)dE \qquad (2)$$

A Leaky Box model is criticized because it suggests homogenic space distribution of electrons at a storage region, just as for all galaxies, seen by observers on the edges, have the intensity of radio emission (generated by synchrotron radiation of relativistic electrons) decreasing with the distance from the galaxy plane.

Ginzburg et al.(1990) work out the Diffusion Model with a stationary diffusion equation:

$$d(N(E) \cdot dE/dt)/dE + Div(D \cdot grad(N(E))) + N(E)/T_L = K E^{-\gamma} \qquad (3)$$

Here $D = D_o E^\mu z^\delta$ - a diffusion coefficient depending on an electron energy E and on a distance of galactic plane z. The modern values of μ=0.4 - 0.6, δ = 0.3, γ = 2.2 ± 0.2. The solution of the equation is:

$$N(E) \sim E^{-(\gamma+\mu/2+0.5)}, \quad E < 10TeV \quad N(E) \sim E^{-(\gamma+1)}, \quad E > 10TeV \quad (4)$$

Thus, the exponent of electron spectrum near the Earth is Γ = 3.0 ± 0.2, Γ = 3.2 ± 0.2 for Diffusion and Leaky-Box Models. The primary electron spectrum is measured with a good statistic accuracy in the range of 30 - hundreds GeV (Taira et. al. 1993; Gusev A.A. et al, 1981; Golden et al. 1984; Tang. 1984, Fig.2) but it is not enough to distinguish between two Models.

Diffusing, the particles go the distance of $\lambda = \int D(E)dE/bE^2$. With $D_o \sim 10^{29}$. cm^2/sec electrons at 1 TeV have $\lambda \sim 450$ pc. and could not arrive to the Earth from other galaxies or Metagalaxy, they are born in our Galaxy. The lifetime of electrons due to the energy losses is $\tau = 1/bE$. here E in GeV, thus at E=1 TeV $\tau = 3 \cdot 10^5$ years. During this time near the Earth's vicinity at a distances less than 450 pc 5-15 Supernova (SN) flashed up (Nishimura et al, 1980) that could be the sources of the particles. When the range of electrons has the same scale as a distance from the source, peculiarities of the spectrum connected with the particular sources could appear. Thus, measurements of the electron spectrum at several TeV promise an excellent astrophysical information.

At several TeV energy range an exposure factor of $3 \cdot 10^8 m^2 sr \cdot sec$ is needed to get 100 electron events at more 2-3 TeV (see Fig.2). Thus we must measure one year with an instrument of 100 $m^2 sr$. Traditional spectrometers with the lead-scintillator shower calorimeter (see Fig.3) of such enormous geometrical factor are too heavy, about 30 ton, to be launched with a balloon or satellite. Taira et. al. (1993) use the emulsion camera with a geometry factor $\sim 0.1 m^2 sr$ and during 11 flights from 1968 up to now (25 years!) have only an exposure factor 588848 $m^2 sr \cdot sec$.
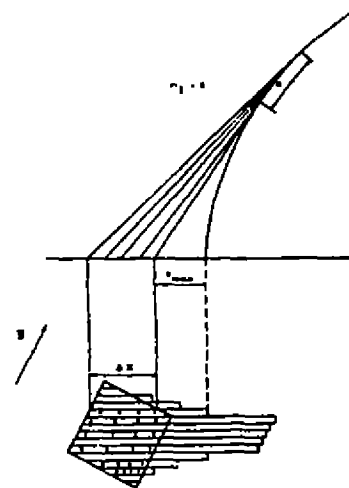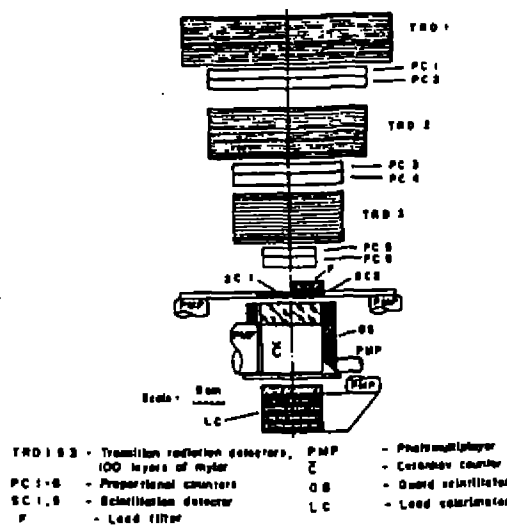
Fig.3 The electron spectrometer used on "INTERCOSMOS-17" satellite.   Fig.4 The illustration of the method.

2.The detection of synchrotron radiation photons emitted by electron in geomagnetic field

Below we discuss characteristics of a device based on a detection of synchrotron radiation of an electron, moving in geomagnetic field (Prilutsky, 1972). The proposed detector is of 2x2 square meters size and consists of 400 CsI crystals of 10x10x15 cm^3. The set of crystals is shielded by an anticoincidence plastic scintillator to reject charged particles. The weight of detector is 3 tons and planned to be installed on board russian heavy satellite "ENERGIA", providing exposure time of several years. The main feature of this method is a sharp increase of sensitive area of detector with an increase of particle energy in comparison with the propriate area of detector. Spectrum of synchrotron photons is described by:

$$dN/dE = 3.56 \cdot 10^4 B_\perp \cdot \chi \int_\chi^\infty K_{5/3}(\eta)d\eta \quad (5)$$

here $\chi = E_\gamma/E_{crit}$, $E_{crit} = 6.67 \cdot 10^{-2}B_\perp E^2$ (E_γ, E_{crit} - MeV, E - electron energy in TeV), $B_\perp$- projection of geomagnetic induction vector on a vector of electron velocity. The mean energy of synchrotron photons depends on E and $B_\perp$: $E_\gamma = 0.019B_\perp E^2$.MeV. the electron energy in TeV. For B=0.3-0.5 Gauss. typical value of magnetic

field for altitudes 100 - 1000 km, and E more than several TeV, photons have energy from hundreds of keV to several MeV. The photons are emitted in an extremely narrow cone around electron velocity direction. Mean length between photon emission points on the electron trajectory is $l = 1.5 \cdot 10^3 B$, m. The registration of 3, 4, 5 or more photons (each one registered by separate CsI crystal) simultaneously in points, belonging to a strait line permits to attribute this special picture to a high energy electron, coming near (or cross) the detector. Fig.4 illustrates calculation procedure of detector sensitive area. Vector B belongs to the detector plane. Effective (sensitive) detector area is defined by the most remote crossing point of detector plane by electron (x_{max}). from which n_γ photons can still be placed in the propriate area of detector ($2 \cdot 2$ m^2); $n_\gamma = 3$, 4, 5 or more, depending on selection criterion. The distance from such a crossing point to the detector, x_{max}, depends on the trajectory of electrons. The effective geometrical factor $\Omega(E)$ is calculated by numerically integration of x_{max} along the line been in detector plane and perpendicular to the line that is created by registered photons. Also an integration along solid angle is made. For $E \sim 1$ TeV and $n_\gamma > 3$ effective geometrical factor is equal the physical geometry factor with solid angle 1 steradian. At $E \sim 5$ and 20 TeV Ω sharply increases 10 and 50 times physical geometry factor.

The estimation of the electron flux of discrete sources at 5-25 TeV using the solution of diffusion equation (Berezinsky et al. 1990) was made.

$$dN/dt - d(N(E) \cdot dE/dt)/dE + Div(D \cdot grad(N(E))) = \delta(t - to)\delta(r - ro)\delta(z - zo)A_0E^{-\gamma_0} \qquad (6)$$

$$N(r, t, E) = AE^{-\gamma} \cdot [1 - Et]^{\gamma-2} \cdot exp(-\lambda \cdot k^2 - r^2/4\lambda)/4\pi \cdot \lambda \cdot h \qquad (7)$$

here to, ro, zo, γ_0, Ao - moment of SN burst, distance SN from Solar System and Galactic plane, exponent and intensity of electron spectrum from given SN; h=1kpc - Galo size, k = r/2h. The electron count rate of the device from 11 SN recently burst in the Solar vicinity with main contribution from Vela permits to feel the boundary of electron spectra at E=20-25 TeV.

E. TeV	6	7	10	15	20	25
N. 1/year	1030	760	325	110	35	5

References

Berezinsky V.S., et al. Astrophysics of Cosmic Rays, Moscow, Nauka, 524pp, 1990.

Nishimura J., Fujii M. and Taira T. Electron Spectrum at the High Energy Side, 16 Int.Cosm.Ray Conf.,V.1, 488, 1979.

Taira T., et al, Energy Spectrum and Confinement time of Cosmic Ray Electrons, 23 Int.Cosm. Ray Conf., V.2, 128, 1993.

Prilutsky O.F., Pisma v JETP, V.16, 452, 1972.

Gusev A.A., et al, Study of High-Energy Electrons Onboard "Intercosmos-17", 17-th Int.Cosm.Ray Conf.,V.1, 89, 1981.

Tang K.-K., The Energy Spectrum of Electrons and Cosmic Ray Confinement, Astroph.J., V.278, 881.1984.

Golden R.L., et al, A Measurement of Absolute Flux of Cosmic Ray Electrons, Astrop.J., V.287, 622, 1984.

Performance de Detectores "Streamer" em Medidas de EAS

A.R.P.Biral, J.A.Chinellato, A.C.Fauth, E.Kemp, M.A.Leigui de Oliveira,
H.Nogima, R.C.Rigitano, L.G. dos Santos, E.L.F.Silva. N.Mengoti Silva.
M.C.Souza Jr., A.Turtelli Jr.

Instituto de Física 'Gleb Wataghin' Universidade Estadual de Campinas (Unicamp)

1. Introdução

Os grandes experimentos de raios cósmicos são comumente compostos por várias estações detectoras à base de cintiladores plásticos para a detecção de chuveiros atmosféricos extensos (ou EAS, extensive air shower). Mais recentemente, eles estao sendo também integrados por detectores de "tracking", por meio dos quais é possível um maior refinamento pela análise de traços de múons constituintes dos chuveiros. Os múons possuem a interessante característica de preservarem a direção da partícula primária, e a sua identificação é feita através da implementação de camadas absorvedoras de elétrons e pósitrons.

A correlação de traços de elétrons de alta energia com a direção do chuveiro é também bastante estreita (cerca de 100 mrad). Isto possibilita a comparação das direções obtidas do tempo de voo da frente de partículas de chuveiros com as dos traços de tais elétrons. No presente trabalho apresentamos resultados preliminares desta comparação. realizadas no ambito do experimento EASCAMP [1].

2. O Sistema de Aquisição

Foram usados para este trabalho quatro detectores tipo piramide contendo cada uma material cintilador plástico NE102 e fotomultiplicadoras Philips XP2040. Este conjunto serviu para a determinação da direção de chegada da frente do chuveiro através do método do tempo de vôo. A parte de "tracking" foi realizada por um módulo de cinco planos de tubos "streamers" de célula 1x1 cm² (Figura 1). Cada plano possui uma área sensível de 96x77 cm² e são distribuídos esquidistantemente na altura total de dois metros. Sobre a parte superior do módulo foi colocada uma piramide idêntica às outras com o propósito de obter uma curva de calibração do número de partículas (registradas no módulo) em função dos canais de ADC [2]. Propositalmente não foi colocado material absorvedor sobre os detectores para não materializar fótons do chuveiro e detectar os elétrons mais energéticos [3]. O "trigger" para a aquisição de dados do módulo "streamer" (Figura 2) permite tanto o registro de eventos de múons isolados [4]. dado pela coincidência de tres planos. como os de EAS, que é dado pela coincidencia das quatro piramides. A leitura de carga da piramide sobre o módulo está submetida a este mesmo "trigger".

3. Análise dos Resultados

- Na análise dos dados devemos destacar um aspecto fundamental: quanto mais energético o chuveiro e quanto mais próximo do seu centro, maior é a densidade de partículas. Neste caso a resposta da direção pelo método de tempo de voo produz o seu melhor desempenho. uma vez que fica menos susceptível às flutuações do número de partículas na frente do chuveiro. Mas, em contrapartida compromete a reconstrução de eventos por "tracking" com uma enorme quantidade de pontos, o que possibilita um número muito grande de traços falsos. por vezes saturando completamente o detector.

À medida que se reduz a densidade de partículas as flutuações da frente do chuveiro produzem maior efeito na resposta do tempo de vôo. e o sistema de "tracking" por sua vez obtém melhores resultados.

Analisamos 25963 eventos adquiridos entre 01/06/94 a 25/07/94. Na Figura 3 e 4 temos os gráficos da diferença do ângulo zenital e azimutal respectivamente. Embora a correlação seja notada pelos picos próximos de zero, nao foi ainda possível determinar onde ela é melhor ou pior.

4. Conclusão

É possível a correlação de dados entre o sistema de "tracking" e o método de tempo de vôo como observamos nos picos das distribuições dos ângulos zenitais e azimutais. Na sequência deste trabalho procurar-se-á definir uma região comum (em número de partículas) onde os dois métodos funcionem em conjunto. Haverá também outras duas regiões: uma superior à região comum, onde a reconstrução por tempo de vôo seja mais confiável que a de "tracking": e outra inferior, onde o "tracking" forneça resultados com qualidade melhor que o de tempo de vôo. Assim teremos os dois métodos funcionando de forma complementar e uma melhor determinação da direção de chegada para o experimento.

References

[1] A. Turtelli Jr et al. Proc. of 21st Int. Cosmic Ray Conf., Adelaide - Austrália. Vol 3. 184 (1990).

[2] A.R.P. Biral et al. Proc. XIV Encontro Nacional de Física de Partículas e Campos. Caxambú - MG. 247 (1993).

[3] A.R.P. Biral et al. Proc. XIV Encontro Nacional de Física de Partículas e Campos. Caxambú - MG. 243 (1993).

[4] E.G.S. Luna et al. Proc. XV Encontro Nacional de Física de Partículas e Campos. Angra dos Reis - RJ (1994).
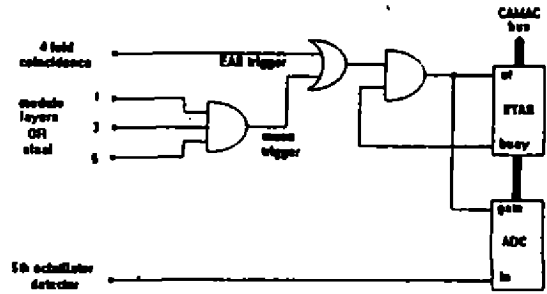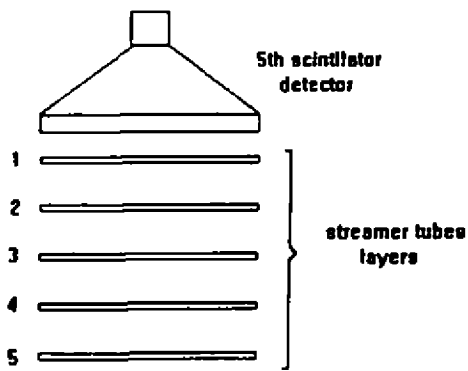
Figura 1: Perfil do módulo de trajeto-
grafia com o detector "pirâmide" na
parte superior.

Figura 2: Diagrama básico do trigger
utilizado.
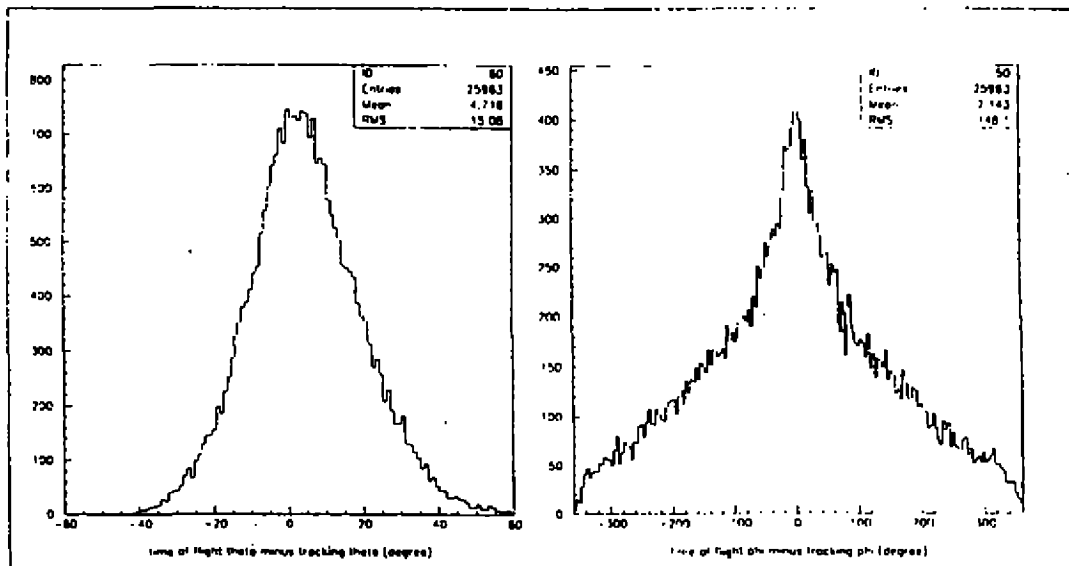
Figura 3: Histograma da diferença
entre os ângulos zenitais obtidos pe-
los métodos de tempo de vôo e "trac-
king".

Figura 4: Histograma da diferença
entre os ângulos azimutais obtidos pe-
los métodos de tempo de vôo e "trac-
king".

Análise de um Evento Multi-Halo

N. Amato

Centro Brasileiro de Pesquisas Físicas

R. H. C. Maldonado, H. M. Portella

Universidade Federal Fluminense, UFF

1. Introdução

Uma característica interessante observada nas experiências que utilizam câmaras de emulsão nuclear e chumbo expostas em altitudes de montanha é a existência de eventos com "halo" na região de energia > 1000 TeV. A Colaboração Brasil-Japão de Raios Cósmicos, CBJ, já publicou resultados de seis eventos com "halo" (1.2). A colaboração Pamir observou vários eventos com "halo" e vários "multi-halo" que apresentam grande alinhamento entre seus constituintes (3).

No CBPF foi feita uma análise sistemática de 50 blocos da câmara número 24 da CBJ, observando-se um evento com características de "multi-halo". O evento é constituído de dois "halos" na região central (500 e 501) e vários chuveiros que se espalham numa área de 11 cm × 18 cm. Os resultados preliminares desta análise são apresentados neste trabalho.

2. Medida do raio dos halos

Nos filmes de raios X tipo N foram feitas medidas da opacidade $D(r,t)$ para várias distâncias laterais r e nas várias profundidades t da câmara. Para isso usou-se o fotomicrodensitómetro com fenda 200 μm × 200 μm. A partir daí, obteve-se a densidade de elétrons $p(r,t)$ usando-se as curvas características dos filmes de raios X. As curvas da densidade ρ (elétrons/cm^2) para várias distâncias r do centro do halo nas diferentes profundidades t, foram construídas separadamente e os resultados são apresentados nas figuras A e B.
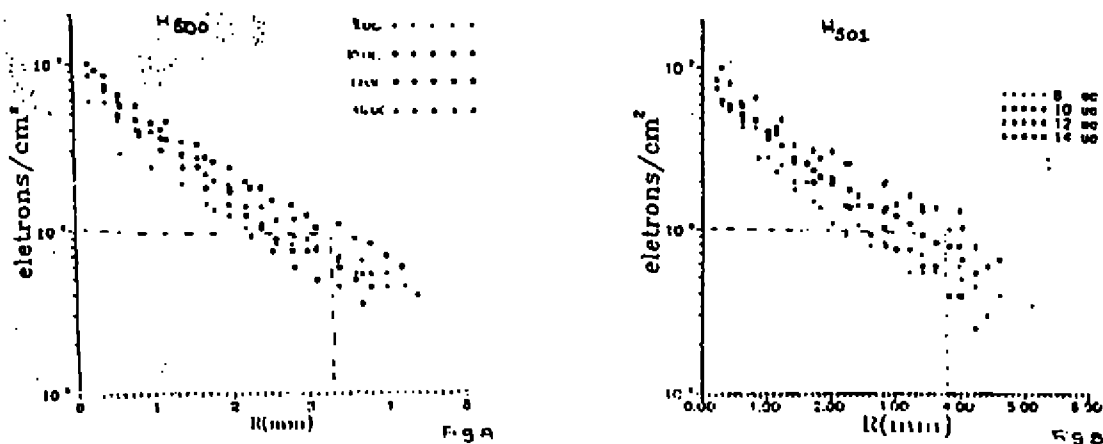
Define-se o raio do halo como a distância lateral (na profundidade onde o chuveiro atinge o máximo) onde a densidade de elétrons atinge o valor de 10^6 elétrons/cm^2. Os resultados obtidos para este evento foram: $R_{500} = 3.3$mm; $R_{501} = 3.8$mm.

3. Medida da Energia

3.1 Energia do Halo

O número de elétrons na profundidade t, $N_e(t)$, foi obtido integrando-se a densidade de elétrons, $\rho(r,t)$, em relação a r. Construiu-se a curva de transição do número de elétrons, $N_e(t)$, em diferentes profundidades t, para a parte dos "halos" 500 e 501. Integrou-se o número de elétrons em relação a t, e obteve-se o comprimento total do traço, $\sum Z_{500} = 3.15 \times 10^7$ e $Z_{501} = 1.79 \times 10^7$

A energia contida no halo, E, foi obtida através da relação $E_{halo} = \epsilon Z$, onde $\epsilon = 7.4$MeV. Os resultados calculados para cada halo são $E_{500} = 233.3$TeV e $E_{501} = 132.5$TeV.

3.2 Energia dos Chuveiros Individuais

A busca dos chuveiros está sendo feita nos filmes de raios X tipo N, tanto na parte dos "halos", usando o microscópio, quanto na parte externa aos mesmos. O método rotineiro de medida de energia está sendo aplicado usando-se um fotômetro simples adaptado num microscópio triocular, com fenda de 230 μm. A curva de transição $D \times t$ é construída e a partir da opacidade máxima determina-se a energia através da curva de calibração. Em alguns chuveiros, devido ao seu tamanho, utilizou-se a abertura da fenda de 475 μm e 935 μm.

Neste evento foram identificados 157 chuveiros, dos quais 29 estão situados na região do "halo" 500, 21 na região do "halo" 501 e 107 na parte externa aos "halos". Dessas medidas preliminares estima-se que a energia dos chuveiros individuais seja da ordem de 1000 TeV.

4. Conclusão

Através do estudo de famílias de alta energia como a deste evento detetados em câmara de emulsão, pode-se obter informações sobre fenômenos de raios cósmicos em região fora do domínio alcançado pelos presentes aceleradores e que tem sido estudado somente através de experiências de chuveiros atmosféricos extensos, EAS. A análise deste evento "multi-halo" permitirá obter informações para a interpretação de fenomenos que ocorrem nesta faixa de energia.

Referência

[1] - S.Yamashita, J. Phys. Soc. Japan, 54 (1985) 529.

[2] - N.Amato, N.Arata e R.H.C.Maldonado, Il Nuovo Cimento 10C (1987) 559.

[3] - Pamir Collaboration - Proc. 5th I.S.V.H.E.C.R.I.- Lodz(1988)9

Estudo e Avaliação do Desempenho do Experimento CLUE, Usando Simulações da Geometria do Detector e Respostas da Fotocâmara TMAE

B. Bartoli (INFN-Nápolis, Itália), D. Alexandreas, D. Bastieri, G. Busetto, S. Centro,
M. Cresti, M. Mariotti, M. Nicoletto, L. Peruzzo, A. Pesci, R. Pugno,
A. Saggion, G. Sartori (INFN-Pádua, Itália), F. Bedeschi, E. Bertolucci, C. Bigongiari,
G. Chiarelli, E. Cocca, G. Marsella, A. Menzione, C. Sbarra, D.A. Smith,
F. Zetti (INFN-Pisa, Itália), F. Liello (INFN- Trieste, Itália), D.J. O'Connor,
R. Paoletti, A. Scribano (Università di Siena, Itália), A.R.P. Biral,
J.A. Chinellato, E. Tamura, A.Turtelli Jr (Universidade Estadual de Campinas, Brasil)

1. Introdução

A colaboração CLUE (Cerenkov Light Ultraviolet Experience) propõe-se a estudar chuveiros extensos através da detecção da luz Cerenkov produzida durante o desenvolvimento desses chuveiros. O detector do CLUE[1] consiste em câmaras MWPC contendo gás TMAE, sensíveis à região espectral do ultravioleta médio (1900 - 2400 Å). Sendo desse modo insensível à radiação de fundo do céu noturno e com um limiar de energia próximo ao de detectores Cerenkov convencionais, se espera que o CLUE (atualmente com dois módulos instalados na ilha de La Palma, no arquipélago das ilhas Canárias) tenha um ciclo de operação e um taxa de dados maior.

Devido à características intrínsicas da luz Cerenkov emitida por chuveiros atmosféricos (como seu carácter altamente direcional) temos o CLUE como um experimento adequado a procura de fontes, como por exemplo através de técnicas de *on/off*. Esse trabalho tem como objetivo uma discussão, através de simulações de imagens na fotocâmara do CLUE produzidas por cascatas eletromagnéticas, das capacidades e das características particulares do experimento em questão.

2. Estudo da imagem obtida em uma fotocamara de experimentos Cerenkov

Através da técnica de detecção de chuveiros por sua luz Cerenkov, os fótons Cerenkov incidentes sobre um espelho sao refletidos em direção a um detector colocado no seu foco. Porém, independente do ponto onde o fóton atinja o espelho, esse fóton será refletido a um determinado ponto do detector de modo que a posição deste ponto seja função da *direção* (ângulos zenital e azimutal) que esse fóton faz com o eixo do espelho (fig 1).

Mesmo porém considerando o caso de espelhos esféricos, como é o caso do CLUE, pode-se afirmar que, para fótons com pequenos ângulos zenitais de incidência, a distância entre o ponto onde o fóton atinge a fotocâmara e o centro da mesma é linearmente proporcional ao ângulo zenital de incidência (fig 2).

Isso nos leva a uma característica comum a todos os experimentos Cerenkov: em experimentos Cerenkov, a extensão do detector fotosensível determina um ângulo zenital máximo (ângulo com o eixo ótico do espelho) que o fóton pode ter para ser observado.

---

[1] A. Menzione et all. Nucl. Instrum. Methods Phys. Res. A263, 255 (1988)

Figura 1:

r ∝ θ_
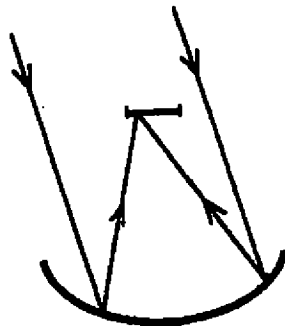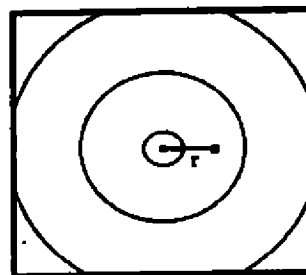
Figura 2:

3. Avaliação da imagem obtida pela fotocâmara

Esse ângulo zenital máximo, no caso do CLUE (raio do espelho = distância focal = 90 cm; comprimento da fotocâmara = 22 cm) tem um valor de $\theta_{max} \approx 4$ graus. Esse fato acaba por não apenas excluir uma certa porcentagem dos fótons Cerenkov incidentes de serem detectados, mas também inviabilizar uma estimativa da distância entre o centro do chuveiro e o espelho através de uma única imagem de fotocâmara (fig 3).
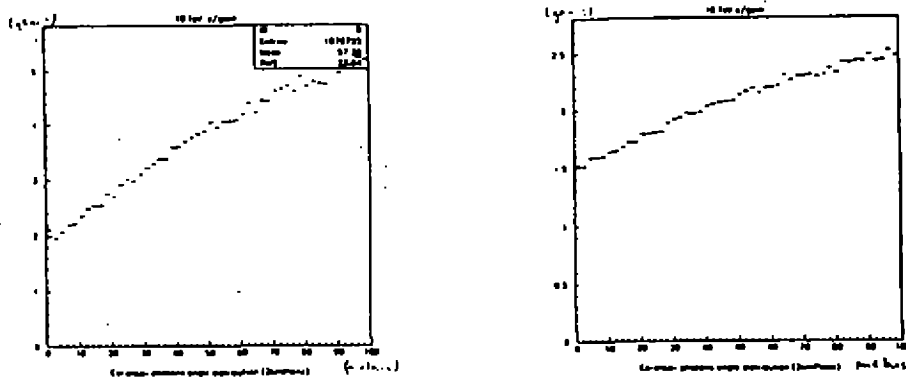
Figura 3: Distr. angular *versus* distância radial: a) sem restrições: b) onde $\theta < \theta_{max}$.

Com relação a análise de algumas características individuais do chuveiro incidente através da imagem na fotocâmara, vemos que no tocante ao CLUE, dificilmente poderemos dispor de características semelhantes ao *azwidth*, concebido pelo grupo de Whipple em imagens obtidas usando fótons Cerenkov no visível?

No caso de Cerenkov no visível, os fótons que atingem a fotocâmara são produzidos nas vizinhanças do máximo do chuveiro na atmosfera (cerca de 8 km de altura). Desse modo, apenas fótons que obedecerem a um estreito critério de ângulos azimutais com relação ao eixo do espelho conseguirão ser refletidos e atingir a fotocâmara (proporcionando a tradicional "elipse" observada).

Com relação ao CLUE porém, devido à atenuação constante dos fótons Cerenkov ultravioleta na atmosfera (onde o oxigênio é o principal absorvedor)[3], serão registrados na fotocâmara principalmente fótons produzidos nas vizinhanças do espelho (nos últimos 500 metros). Desse modo, poderão ser registrados pela fotocâmara fótons com distribuição azimutal muito mais larga, resultando assim em uma imagem na fotocâmara menos definida (fig 4).

[2]T.C. Weeks et all, The Astrophysical Journal 342, 379 (1989)

[3]A.R.P. Biral, J.A. Chinellato, A. Turtelli Jr.,*Atas do XI Encontro Nacional de Partículas e Campos*, 207 (1990)
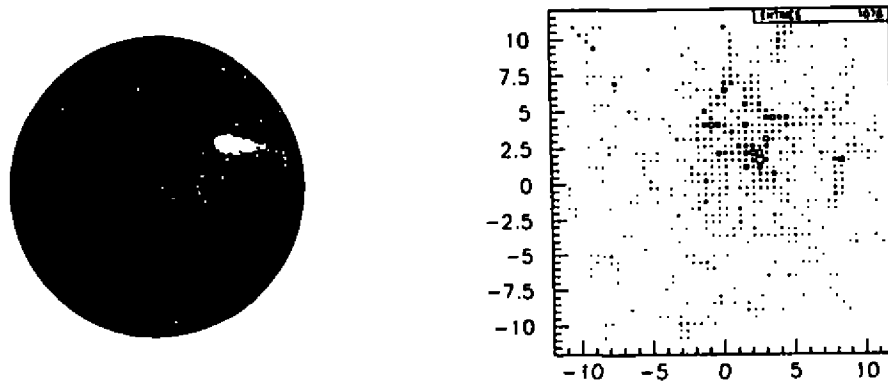
Figura 4: a) imagem Cerenkov no visível; b) para o CLUE (simulação).

4. Conclusões

Esse estudo mostra que somente pelo cruzamento de diversas imagens produzidas em um *array* de espelhos será possível a estimativa das características de um chuveiro tais como a energia e a posição de seu centro. Somente depois se poderá pensar em um maneira de conseguir um tão desejado critério de separação entre chuveiros eletromagnéticos e chuveiros hadrônicos.

Foi verificado também que, através de simulações de chuveiros eletromagnéticos verticais, em uma configuração de array onde a distância entre os diversos módulos fosse da ordem de 20 metros, o CLUE se mostraria sensível a primários com energia entre 5 e 10 TeV. De qualquer forma, estudos *on/off* de fontes γ poderiam ser levados a cabo com apenas um módulo. O limiar de detecção, nesse caso, cairia para próximo de 1 TeV.

Phenomenological 2D-χ^2 Analysis of AGS Pion Interferometry Data

Sandra S. Padula*

Instituto de Física Teórica/UNESP

Rua Pamplona 145, 01405-900, São Paulo, SP, Brasil

We here investigate the resolving power of multi-dimensional interferometry by considering two dynamical scenarios that predict similar correlation functions, even though the underlying decoupling geometries differ considerably. Preliminary E802 $\pi^-\pi^-$ correlation data[1]-[3] on central $Si + Au$ reactions at 14.6 AGeV/c are considered for illustrating the method. We use the non-ideal inside-outside cascade model of Refs. [4, 5]. In one scenario long lived resonances are neglected while in the other the resonance fractions as taken from the Lund model[6]. At the AGS energy range there is only some fragmentary data[7] indicating that resonance production could be suppressed, whereas the Lund model predicts similar resonance yields as at higher SPS energies (i.e., $f(\pi^-/\omega) = 0.16$, $f(\pi^-/K^*) = f(\pi^-/(\eta + \eta')) = 0.09$, where $f(\pi^-/r)$ is the fraction of the observed π^-'s arising from the decay of a resonance of type r).

Under idealized conditions the correlation function, $C_2(k_1, k_2)$, of two identical pions probes the decoupling or freeze-out space-time distribution of pions, $\rho(x)$, through $C_2(k_1, k_2) = 1 + \lambda|\rho(k_1 - k_2)|^2$, where λ is the so-called *chaoticity parameter*. In the analysis discussed here we assume implicitly that $\lambda = 1$ because, as we have extensively emphasized in [4, 5], fits to data treating λ as a free parameter distort the geometrical scales in a further uncontrolled way.

In actual high energy reactions, however, final state interactions, correlations between coordinate and momentum variables and resonance production may distort this ideal Bose-Einstein interference pattern (see e.g. [4, 5]). The correlation function in this more general case can be expressed as[4]

$$C(k_1, k_2) = \Upsilon(q)\left(1 + \frac{|G(k_1, k_2)|^2}{G(k_1, k_1)G(k_2, k_2)}\right) . \tag{1}$$

where $\Upsilon(q) = (q_c/q)/(e^{q_c/q} - 1)$ is the Gamow factor that distorts the pattern due to Coulomb effects, with $q_c = 2\pi\alpha m$ and $q = (-(k_1 - k_2)^2)^{1/2}$. The complex amplitude, $G(k_1, k_2)$, the single-particle probability $P_1(k) \propto G(k, k)$, the parameterizations and kinematical cuts adopted when fitting to the correlation data are discussed in detail elsewhere[4, 5, 8, 11].

To assess the statistical significance of the differences between the fits obtained assuming resonance and non-resonance dynamics, we compute the χ^2 goodness of fit on a two-dimensional grid in the (q_T, q_L) plane, binned with $\delta q_T = \delta q_L = 0.01$ GeV/c. In our preliminary analysis reported in Ref.[8], we compared the square of the difference between the theoretical and experimental correlation functions and found an unexpected ridge of high variance along the $q_T = q_L$ diagonal. However, Zajc[9] pointed out that this feature could have been an artifact of statistical fluctuations in ratios of random variables, and suggested that the following χ^2 variable

$$\chi^2(i, j) = \frac{[A(i, j) - \mathcal{N}_\chi^{-1}C_{th}(i, j)B(i, j)]^2}{\{[\Delta A(i, j)]^2 + [\mathcal{N}_\chi^{-1}C_{th}(i, j)\Delta B(i, j)]^2\}} . \tag{2}$$

should be used instead. In eq. (2), $\mathcal{N}_\chi$ is a normalization factor which is chosen to minimize the average χ^2 and depends on the range in the q_T, q_L plane under analysis. The indices i, j refer to the the corresponding q_T, q_L bins. in each of which the experimental correlation function is given by $C_{exp}(i,j) = \mathcal{N}_\chi \times \frac{A(i,j)}{B(i,j)}$: $\Delta C_{exp}(i,j) =$ $C_{exp}(i,j)\sqrt{\left(\frac{\Delta A(i,j)}{A(i,j)}\right)^2 + \left(\frac{\Delta B(i,j)}{B(i,j)}\right)^2}$ The data for the numerator $A(i,j)\pm\Delta A(i,j)$ and denominator $B(i,j)\pm\Delta B(i,j)$ were obtained from R. Morse[3] with an understanding that the data in this form are preliminary and subject to further final analysis.

The goal of the present interferometry analysis is to extract the rms transverse radius, R_T. at decoupling and the rms decoupling proper time interval, $\Delta\tau$. Minimization of the average χ^2 is performed by exploring the parameter space of R_T and $\Delta\tau$ and computing the $\langle\chi^2\rangle$. averaging over a 30x30 grid in the relative momentum region $q_T, q_L < 0.3$ GeV/c. In the vicinity of the minimum, $R_{T_0}, \Delta\tau_0$. we determine the parameters of the quadratic surface

$$\langle\chi^2(R_T, \Delta\tau)\rangle = \chi^2_{min} + \alpha(R_T - R_{T_0})^2 + \beta(\Delta\tau - \Delta\tau_0)^2 .$$ (3)

Recall that the average χ^2 over N bins is a random variable with unit mean and rms width $\sigma = \sqrt{2/N}$ if the $\chi(i,j)$ are normal random variables with zero mean and unit rms width. For large N, the distribution of the mean χ^2 per bin is $P(\chi^2) \propto \exp[-(\chi^2 - 1)^2/2\sigma^2]$. For the $N = 900$ grid under consideration, $\sigma \approx 0.047$.

The most direct measure of the goodness of the fit in this case is $n_\sigma = |(\chi^2_{min}) - 1|/\sigma$, the number of standard deviations from unity of the average χ^2 per degree of freedom. For a detailed discussion see Ref.[11] The results of this statistical analysis are as follows: for the non-resonance case. with Gamow correctd E802 data. we found that $R_{T_0} = (4.6\pm 0.9)$ fm. $\Delta\tau_0 = (3.4 \pm 0.7)$ fm/c, corresponding to $\langle\chi^2_{min}\rangle = 1.098$ and $n_\sigma = 2.1$. For the full Lund resonance fraction, however. $R_{T_0} = (3.1\pm 1.3)$ fm, $\Delta\tau_0 = (1.6\pm 1.0)$ fm/c. with $\langle\chi^2_{min}\rangle = 1.104$ and $n_\sigma = 2.2$.

The lego plots of the Gamow corrected data and the theoretical correlation functions with and without resonances, corresponding to the optimized geometrical parameters, are shown in Figure 1 for the restricted range $0.005 < q_T, q_L < 0.125$ GeV/c. Part a) shows the 2-D data in the above range. Part (d) shows the corresponding experimental errors. In part (b) the best fit (with $R_T = 4.6$ fm and $\Delta\tau = 3.4$ fm/c over the wider domain $q_T, q_L < 0.3$ GeV/c) assuming no resonance production is shown. In part (c) the best fit with Lund resonance fractions ($R_T = 3.1$ fm and $\Delta\tau = 1.6$ fm/c again over the wider range) is shown. Finally the $\chi^2(i,j)$ for the non-resonance scenario is shown in (e), whereas that corresponding to the full resonance fit is shown in part (f). Similar large fluctuations close to the edge of small q_T and large q_L is seen in both cases. However, the overall trend suggests that the no resonance fit is closer to the data in the region of small q even though the global χ^2 is about the same for both fits.

The average χ^2 per degree of freedom, or equivalently the number of its standard deviations from unity, depends on the range of q under analysis. We have tested this by varying the range of the analysis to restricted q_T, q_L domains, ranging from a 1 × 1 grid corresponding to $0.005 < q_T, q_L < 0.015$ GeV/c, to 2 × 2, etc. For each $n \times n$ grid, $N = n^2$ is the number of degrees of freedom and the standard deviation is expected to be $\sigma = \sqrt{2}/n$. We observed[11] a strong dependence of the number of standard deviations from unity as a function of the range of the analysis. We find that the optimal fit including Lund resonances is much worse than the fit without long lived resonance distortions when the analysis is restricted to the domain $q_L, q_T \leq Q_{max} \approx 100$ MeV/c. where the correlation function deviates significantly from unity.

We conclude that. multi-dimensional analysis has high resolving power in the domain of physical interest. and if these data are confirmed, the present analysis would rule out long lived resonance production models in this energy range. However, we note that recent preliminary analysis in ref. [10] seems to give systematically lower correlation function values in the small q_T, q_L domain, in which case the resonance or an alternate long lived source geometry would be needed. In any case, the results show that 2-D χ^2 analysis can be used to improve considerably the resolving power of interferometry by amplifying in a quantitative way the differences between the data and calculations. In general, the analysis could be sharpened considerably by independent measurements of long lived

resonance abundances to reduce that source of interferometric distortions.

This work was developed in collaboration with Miklos Gyulassy, Columbia University, N.Y., U.S.A.

References

[1] T. Abbott, et al (E802 Collab.), Phys. Rev. Lett. 69 (1992) 1030.

[2] T. Abbott et al (E802 collab) Phys. Rev. Lett., 64 (1990) 847; Phys. Rev. Lett. 66 (1991) 1567.

[3] R.J. Morse, MIT thesis 1990, Nucl.Phys. A525 (1991) 531c : W. Zajc, Proc. QM91.

[4] M. Gyulassy, S. S. Padula, Phys. Lett. 217B (1989) 181; S.S. Padula, M. Gyulassy, S. Gavin, Nucl. Phys. B329 (1990) 357.

[5] S. S. Padula and M. Gyulassy, Nucl. Phys. B339 (1990) 378.

[6] B. Andersson, et al., Nucl. Phys. B281 (1987) 289;
M. Gyulassy, CERN-TH.4794 (1987), published in Proc. Eight Balaton Conf. on Nucl. Phys. (ed. Z. Fodor, KFKI, Budapest 1987).

[7] V. Blobel, et al.Phys. Lett. 48B (1974) 73.

[8] M. Gyulassy and S. S. Padula, CU-TH-593 (93), Proc. of the HIPAGS '93 Workshop. MIT, Jan 13-15, 1993.

[9] W. Zajc. Proc. of CAMP (LESIP IV), p. 439, ed. by M. Plümer, S. Raha and R. M. Weiner, World Scientific (1991).

[10] R.A.Soltz, MIT thesis (1994) unpublished.

[11] M. Gyulassy and S. S. Padula, IFT-P.036/94 - CU-TP-670 preprint, to appear in Phys. Lett. B.
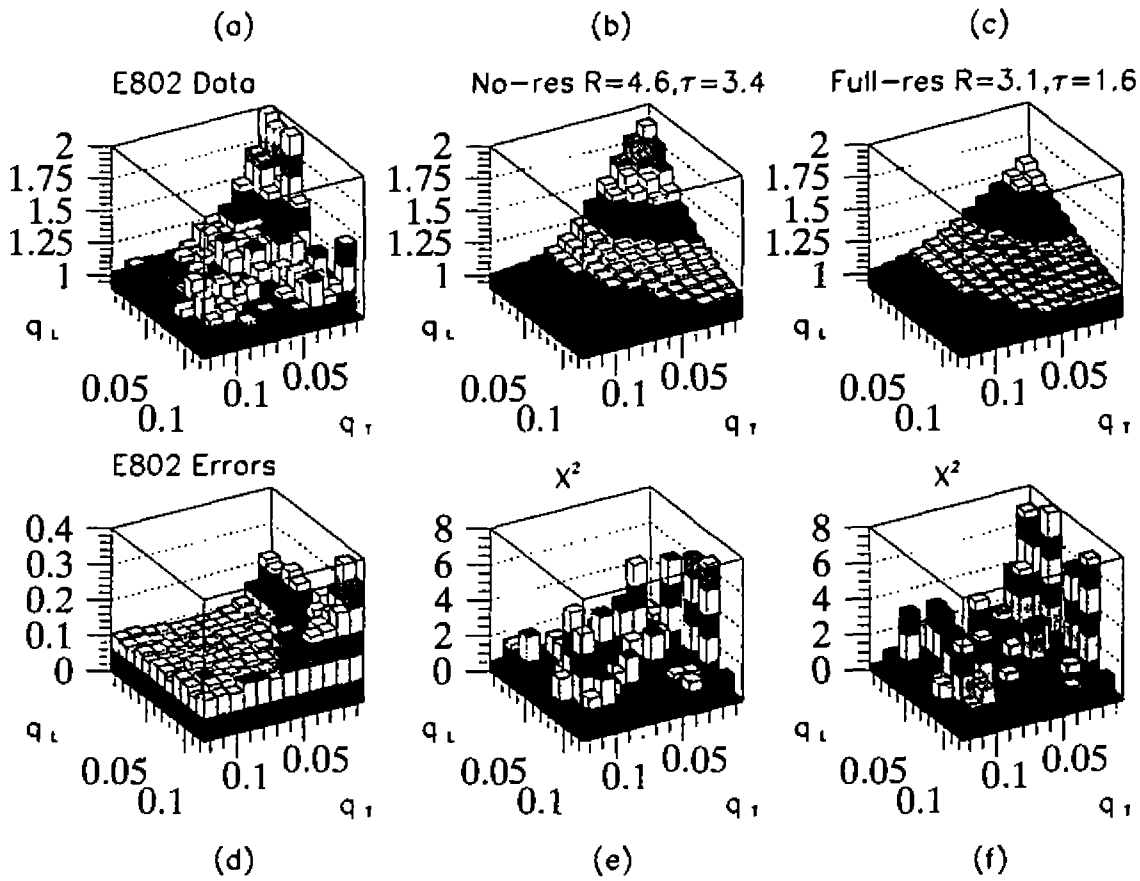
Figure 1. $C(q_T, q_L)$ is shown as a function q_T, q_L for negative pions produced in central Si+Au reactions[1]. The preliminary E802 data corrected for acceptance and Coulomb effects are shown in part (a), with corresponding errors in (d). Parts (b) and (c) show theoretical correlation functions filtered with the E802 acceptance for cases without and with resonance production, respectively. The corresponding distribution of $\chi^2(q_T, q_L)$ are respectively shown in parts (e) and (f).

The reason behind the Gell-Mann-Okubo mass formula

Mário Everaldo de Souza

Departamento de Física, Universidade Federal de Sergipe

Campus Universitário, 49000 Aracaju, SE

The Gell-Mann-Okubo mass formula has been widely used as a phenomenological tool in particle physics but the underlying basis for it has not been known. This paper reveals its basis and generalizes the formula to $SU(n)(n = 3, 4, 5, 6)$.

The Gell-Mann-Okubo mass formula

$$M = M_0 + M_1 Y + M_2 \left(I(I+1) - \frac{Y^2}{4} \right) \qquad (1)$$

where M_0, M_1 and M_2 are suitable constants, I is the isospin, and Y is the hypercharge, has been widely used as a relation among the masses of baryon states belonging either to an octet or to a decuplet. This is a phenomenological formula "with no clear physical reasons for the assumptions on which it is based"[1]. As we will show shortly the reason behind the above mass formula is the general formula for the mass of a baryon

$$E_{n,m,k} = h\nu_1(n+1) + h\nu_2(m+1) + h\nu_3(k+1). \qquad (2)$$

found by De Souza, M.E.[2,3,4]. In the above formula n, m and k are the integers 0,1,2,3,4,etc., and $h\nu_i$ are the quark masses taken as $m_u = m_d = 0.31 \text{Gev}$, $m_s = 0.5 \text{Gev}$, $m_c = 1.7 \text{Gev}$, $m_b = 5 \text{Gev}$ and $m_t = 174 \pm 17 \text{Gev}$.

For the decuplet of SU_3(u,d,s) Eq. (1) becomes

$$M = M_0 + M_1 Y \qquad (3)$$

where Y is the hypercharge. The relation among the masses of baryons of the decuplet of SU_3(u,d,s) is given by

$$M_\Sigma - M_\Delta = M_\Xi - M_\Sigma = M_{\Omega^-} - M_\Xi. \qquad (4)$$

According to Eq. (2) and to the considerations given by references 2, 3 and 4, M_Σ, M_Δ, M_Ξ and M_{Ω^-} are given by

$$M_\Sigma = M_\Delta = 0.31(n+m+2) + 0.5(k+1) \qquad (5)$$

$$M_\Delta = M_N = 0.31(n+m+k+3) + m_\pi I \qquad (6)$$

$$M_\Xi = 0.31(n+1) + 0.5(m+k+2) \qquad (7)$$

$$M_\Omega = 0.5(n+m+k+3) + m_\pi I \qquad (8)$$

where $I = 0, 1$ and m_π is the pion mass. It represents an intrinsic pion oscillation in the effective potential formed from the strong and superstrong interactions. The equality of the first two terms of Eq. (4) is given by

$$0.31(n+1) + 0.5(m+k+2) + 0.31(n+m+k+3) =$$
$$2(0.31(n+m+2) + 0.5(k+1)) \qquad (9)$$

which is satisfied for any n, and $m = k$. Actually, instead of Δ we may have either Δ or N. For example,

- $n = 0, k = m = 0, 1.12 - 0.93 = 1.31 - 1.12 = 0.19$;

- $n = 0, k = m = 1, 1.93 - 1.55 = 2.31 - 1.93 = 0.38$;

- $n = 1, k = m = 0, 1.43 - 1.24 = 1.62 - 1.43 = 0.19$;

- $n = 1, k = m = 1, 2.24 - 1.86 = 2.62 - 2.24 = 0.38$;

- $n = 2, k = m = 0, 1.74 - 1.55 = 1.93 - 1.74 = 0.19$;

- $n = 3, k = m = 0, 2.05 - 1.86 = 2.24 - 2.05 = 0.19$;

- ... ad infinitum

The equality of the first term with the third term of Eq. (4) yields

$$0.31(n + m + 2) \quad + \quad 0.5(k + 1) - 0.31(n + m + k + 3) =$$
$$0.5(n + m + k + 3) \quad - \quad 0.31(n + 1) - 0.5(m + k + 2) \tag{10}$$

which is satisfied for any n, m, k. Again, instead of Δ we may have N. For example,

- $n = m = k = 0, 1.12 - 0.93 = 1.5 - 1.31 = 0.19$;

- $n = 0, m + k = 1, 1.43 - 1.24 = 2.0 - 1.81 = 0.19$;

- $n = k = 0, m = 2, 1.74 - 1.55 = 2.5 - 2.31 = 0.19$;

- ... ad infinitum

Finally, equaling the second and third terms of Eq. (4) one obtains

$$0.5(n + m + k + 3) \quad + \quad 0.31(n + m + 2) + 0.5(k + 1) =$$
$$2(0.31(n + 1) + 0.5(m + k + 2)) \tag{11}$$

which is satisfied if $n = m$ for any value of k. As examples one finds

- $n = m = k = 0, 1.31 - 1.12 = 1.5 - 1.31 = 0.19$;

- $n = m = 0, k = 1, 1.81 - 1.62 = 2 - 1.81 = 0.19$;

- $n = m = 1, k = 0, 2.12 - 1.74 = 2.5 - 2.12 = 0.38$;

- ... ad infinitum

For an octet of $SU_3(u,d,s)$ one obtains

$$3M_\Lambda + M_\Sigma = 2M_N - M_\Xi \tag{12}$$

which in terms of Eq. (2) becomes

$$2(0.31(n + m + 2) \quad + \quad 0.5(k + 1)) =$$
$$0.31(n + m + k + 3) \quad - \quad 0.31(n + 1) - 0.5(m + k + 2). \tag{13}$$

This equation is satisfied if $k = m$ for any n. For example, one has

- $n = m = k = 0$, $2 \times 1.12 = 0.93 + 1.31$;

- $n = 1$, $m = k = 0$, $2 \times 1.43 = 1.24 + 1.62$;

- $n = 2$, $m = k = 0$, $2 \times 1.74 = 1.55 + 1.93$;

- $n = 3$, $m = k = 0$, $2 \times 2.05 = 1.86 + 2.24$;

- $n = 0$, $m = k = 1$, $2 \times 1.93 = 1.55 + 2.31$;

- $n = k = m = 1$, $2 \times 2.24 = 1.86 + 2.62$:

- ... ad infinitum.

Let us now try to relate the constants M_0 and M_1 to the quark masses. Let us consider, for example, the decuplet of $SU_3(u,d,s)$. In terms of the hypercharge the masses of the particles are described by

$$M_{\Omega^-} = M_0 - 2M_1; \tag{14}$$

$$M_{\Xi} = M_0 - M_1; \tag{15}$$

$$M_{\Sigma} = M_0; \tag{16}$$

$$M_{\Delta} = M_0 + M_1. \tag{17}$$

As we calculated above from the masses of Ξ, Σ and Δ one finds that $m = k$(any n) and from the masses of Ω^-, Ξ and Σ one has $n = m$(any k). Therefore, in terms of Y the masses of Ξ, Σ and Δ are given by

$$M_{n,m}(Y) = 0.31(n + m + 2) + 0.5(m + 1) - 0.19(m + 1)Y \tag{18}$$

and the mass of Ω^- is the above formula with $n = m$, that is,

$$M_{\Omega^-}(Y) = (1.12 - 0.19Y)(n + 1). \tag{19}$$

It is easy to observe that the composite baryons which contain pion oscillations and whose energies are given by $E = E_{n,m,k} + \pi$ do not obey the Gell-Mann-Okubo mass formula.

From the $SU(4)$ multiplets of baryons made of u, d, s, and c quarks and considering Eq. (2) one obtains, for example.

$$M_{\Omega_{ccc}} - M_{\Xi_{cc}} = M_{\Xi_{cc}} - M_{\Sigma_c} = M_{\Sigma_c} - M_{\Delta}; \tag{20}$$

$$M_{\Omega_{cco}} - M_{\Omega_{cc}} = M_{\Omega_{cc}} - M_{\Omega_c} = M_{\Omega_c} - M_{\Omega} \tag{21}$$

and

$$2M_{\Xi_{cc}} = M_{\Omega_{ccc}} + M_{\Sigma_c} \tag{22}$$

or more generally, one obtains

$$M_{q_1 q_1 q_1} - M_{q_2 q_1 q_1} = M_{q_2 q_1 q_1} - M_{q_2 q_2 q_1} = M_{q_3 q_2 q_1} - M_{q_2 q_2 q_2} \tag{23}$$

and

$$2M_{q_1 q_1 q_2} = M_{q_1 q_1 q_1} + M_{q_1 q_2 q_2} \tag{24}$$

in which we can consider $SU(6)$. that is, q_i may be u. d. c. s b, and t. In the case of considering u and d. we may have the combinations ud, uu, and dd for $q_i q_j$. We also may have

$$M_{q_1 q_2 q_3} - M_{q_4 q_2 q_3} = M_{q_1 q_i q_j} - M_{q_4 q_i q_j}.$$ (25)

One comes right off to the conclusion that the above formulas look like chemical reactions, such as, for example, the reaction

$$2NaOH = Na_2O + H_2O.$$ (26)

Concluding on realizes that the Gell-Mann-Okubo mass formula is a natural consequence of the pairwise interacting harmonic potential among quarks, which has its origin in the strong and superstrong interactions.

References

1. D. II. Perkins, *Introduction to High Energy Physics*(Addison-Wesley Publishing Company, Inc., Menlo Park, California), 1987.

2. M. E. de Souza, *The Energies of Baryons.* XIV Encontro Nacional de Física de Particulas e Campos. Caxambu. MG, Brazil. September, 1993.

3. M. E. de Souza. *The Energies of Hadrons.* International Symposium Physics Doesn't Stop: Recent Developments in Phenomenology. Madison, Wisconsin, USA. April. 1994.

4. M. E. de Souza. *The Six Fundamental Forces of Nature.* Report no. 02.1994.MES, July, 1994.

Modeling Higher Twist Contributions to Deep Inelastic Scattering with Diquarks

M.Anselmino[1], F.Caruso[2,3], J.R.T. de Mello Neto[3], A. Penna Firme[2], J. Soares[2,3]

[1] Dipartimento di Fisica Teorica dell' Università di Torino and INFN/Sezione Torino

[2] Centro Brasileiro de Pesquisas Físicas

[3] Instituto de Física. Universidade do Estado do Rio de Janeiro

The most recent detailed data on the unpolarized nucleon structure functions allow a precise determination of higher twist contributions. Quark-quark correlations induced by colour forces are expected to be a natural explanation for such effects; indeed, a quark-diquark picture of the nucleon, previously introduced in the description of several exclusive processes at intermediate Q^2 values, is found to model the proton higher twist data with great accuracy. The resulting parameters are consistent with the diquark properties suggested by other experimental and theoretical analyses.

Recent data from Deep Inelastic Scattering (DIS) experiments at CERN and SLAC have provided precise information on the unpolarized proton structure function $F_2(x,Q^2)$ and have allowed a quantitative estimate of higher twist terms [1].

Higher twist contributions to DIS are expected to originate from quark and gluon correlations; we model them here with a quark-diquark picture of the nucleon which effectively takes into account quark-quark correlations. This model has been previously introduced and succesfully applied to many physical processes [2], mainly at moderate Q^2 values, precisely the region where the higher twist effects have been observed (Q^2 up to $\simeq 10 \div 20$ GeV^2).

The diquark contributions to DIS have been studied in several papers, mainly taking into account only scalar diquarks. A most general analysis of spin 0 and spin 1 diquark contributions to DIS has been performed in [3], allowing for a vector diquark anomalous magnetic moment and for scalar-vector and vector-scalar diquark transitions.

Let us assume the nucleon to be a quark-diquark state. When probing the nucleon with the virtual photon in DIS we have then three kinds of contributions: the scattering off the single quark, the elastic scattering off the diquark, and the inelastic diquark contribution.

The expression of the structure functions F, in the quark-diquark parton model, is then given in general by:

$$F(\quad x \quad,Q^2) = \sum_q F^{(q)} + \sum_S F^{(S)} + \sum_V F^{(V)} + \sum_{q_s} F^{(q_s)}$$
$$+ \sum_{q_v} F^{(q_v)} + \sum_{S,V} F^{(S-V)} + \sum_{S,V} F^{(V-S)} \qquad (1)$$

where (q) denotes the single quark contribution, (S) and (V) the scalar and vector diquark, and (q_s) $((q_v))$ the contribution of the quark inside the scalar (vector) diquark. We have also allowed for elastic diquark contributions with a scalar-vector $(S - V)$ or vector- scalar $(V - S)$ transition.

Considering only the unpolarized structure function $F_2(x, Q^2)$, the single quark contributions is the usual one,

$$F_2^{(q)}(x, Q^2) = e_q^2 x q(x, Q^2) \tag{2}$$

where the quark density number $q(x, Q^2)$ evolves according to perturbative QCD. The elastic diquark contributions have been computed in [3] and for F_2 they read:

$$
\begin{aligned}
F_2^{(S)}(\quad x \quad, Q^2) &= e_S^2 S(x) x D_S^2 \\
F_2^{(V)}(\quad x \quad, Q^2) &= \frac{1}{3} e_V^2 V(x) x \left\{ \left[\left(1 + \frac{\nu}{m_N x} \right) D_1 \right. \right. \\
&\quad - \frac{\nu}{m_N x} D_2 + 2 m_N \nu x \left(1 + \frac{\nu}{2 m_N x} \right) D_3 \right]^2 \\
&\quad \left. + 2 \left[D_1^2 + \frac{\nu}{2 m_N x} D_2^2 \right] \right\} \\
F_2^{(S-V)}(\quad x \quad, Q^2) &= \frac{1}{2} e_S^2 S(x) x^2 m_N \nu D_T^2 \\
F_2^{(V-S)}(\quad x \quad, Q^2) &= \frac{1}{6} e_S^2 V(x) x^2 m_N \nu D_T^2
\end{aligned}
\tag{3}
$$

where D_S is the scalar diquark form factor, $D_{1,2,3}$ are vector form factors, and D_T is the transition form factor [3]. $S(x)$ and $V(x)$ are, the scalar and vector diquark density numbers.

The inelastic diquark contributions are given by:

$$F_2^{(qs,v)} = e_{qs,v}^2 x q_{S,V}(x, Q^2) \left(1 - D_{S,V}^2 \right) \tag{4}$$

for scalar and vector diquark respectively.

From Eqs.(2)-(4) one can obtain the full contribution of the quark-diquark nucleon model to F_2. The terms proportional to diquark form factors model higher twists in DIS. Explicitely they are given by:

$$
\begin{aligned}
F_2^{HT} &= \sum_S e_S^2 S(x) x D_S^2 + \sum_V \frac{1}{3} e_V^2 V(x) x \left\{ \left[\left(1 + \frac{\nu}{m_N x} \right) \right. \right. \\
&\times \quad D_1 - \frac{\nu}{m_N x} D_2 + 2 m_N \nu x \left(1 + \frac{\nu}{2 m_N x} \right) D_3 \right]^2 \\
&+ \quad 2 \left[D_1^2 + \frac{\nu}{2 m_N x} D_2^2 \right] \right\} + \frac{1}{2} \sum_S e_S^2 S(x) x^2 m_N \nu D_T^2 \\
&+ \quad \frac{1}{6} \sum_V e_S^2 V(x) x^2 m_N \nu D_T^2 - \sum_{q_s} e_{q_s}^2 x q_s(x, Q^2) D_S^2 \\
&- \quad \sum_{q_v} e_{q_v}^2 x q_v(x, Q^2) D_V^2
\end{aligned}
\tag{5}
$$

Depending on the form factors, one may obtain contributions decreasing like $1/Q^2$ or higher powers, which might be important in the lowest Q^2 range of data. The proton's flavour and spin wave function in the quark-diquark model is:

$$
\begin{aligned}
|p, S_z &= \pm 1/2 > = \pm \frac{1}{3} \left\{ \sin \Omega \left[\sqrt{2} V_{(ud)}^{\pm 1} u^{\mp} - 2 V_{(uu)}^{\pm 1} d^{\mp} \right. \right. \\
&+ \quad \sqrt{2} V_{(uu)}^0 d^{\pm} - V_{(ud)}^0 u^{\pm} \right] \mp 3 \cos \Omega \, S_{(ud)} u^{\pm} \right\}.
\end{aligned}
\tag{6}
$$

where $V_{(ud)}^{\pm 1}$ stays for a (ud) vector diquark with $S_z = \pm 1$, $u^{\mp}$ is a u quark with $S_z = \mp 1/2$ and so on. The probabilities of finding a vector or scalar diquark in the proton are $\sin^2 \Omega$ and $\cos^2 \Omega$ respectively. Eq.(7) fixes the normalization of the distribution functions:

$$S(x) = \cos^2 \Omega f_S(x)$$

$$V_{(ud)}(x) = \frac{1}{3} \sin^2 \Omega f_{V_{(ud)}}(x)$$

$$V_{(uu)}(x) = \frac{2}{3} \sin^2 \Omega f_{V_{(uu)}}(x)$$

$$u_s(x) = \cos^2 \Omega f_{u_s}(x)$$

$$d_s(x) = \cos^2 \Omega f_{d_s}(x)$$

$$u_{V_{(uu)}}(x) = \frac{4}{3} \sin^2 \Omega f_{u_{V_{(uu)}}}(x)$$

$$u_{V_{(ud)}}(x) = d_{V_{(ud)}}(x) = \frac{1}{3} \sin^2 \Omega f_{u_{V_{(ud)}}}(x)$$

(7)

where all f's are normalized as $\int_0^1 f dx = 1$.

Eqs. (5)-(7) then give, for a proton.

$$
\begin{aligned}
(F\ _2^{HT})_p = & \frac{1}{9} \cos^2 \Omega \left[f_S(x) - [4 f_{u_s}(x, Q^2) \right. \\
& \left. + f_{d_s}(x, Q^2)] \right] x D_S^2 + \frac{1}{81} \sin^2 \Omega [f_{V_{(ud)}}(x) \\
& + 32 f_{V_{(uu)}}(x)] x \left\{ \left[\left(1 + \frac{\nu}{m_N x} \right) D_1 - \frac{\nu}{m_N x} D_2 \right. \right. \\
& \left. + 2 m_N \nu x \left(1 + \frac{\nu}{2 m_N x} \right) D_3 \right]^2 + 2 \left[D_1^2 + \frac{\nu}{2 m_N x} D_2^2 \right] \right\} \\
& - \frac{1}{27} \sin^2 \Omega [16 f_{u_{V_{(uu)}}}(x, Q^2) + 5 f_{u_{V_{(ud)}}}(x, Q^2)] x D_V^2 \\
& + \frac{1}{18} \left[\cos^2 \Omega f_S(x) + \frac{1}{9} \sin^2 \Omega f_{V_{(ud)}}(x) \right] x^2 m_N \nu D_T^2.
\end{aligned}
$$

(8)

The distribution functions are parametrized as:

$$f_S(x) = N_S x^{\alpha_S} (1 - x)^{\beta_S}$$

$$f_{V_{(u;d,u)}}(x) = N_{V_{(u;d,u)}} x^{\alpha_{V_{(u;d,u)}}} (1 - x)^{\beta_{V_{(u;d,u)}}}$$

$$f_{(u;d)_s}(x) = N_{(u,d)_s} x^{\alpha_{(u,d)_s}} (1 - x)^{\beta_{(u,d)_s}}$$

$$f_{u_{V_{(u;d,u)}}}(x) = N_{u_{V_{(u;d,u)}}} x^{\alpha_{V_{(u;d,u)}}} (1 - x)^{\beta_{V_{(u;d,u)}}}$$

(9)

The form factors are the most simple in agreement with the asymptotic conditions:

$$D_S = \frac{Q_S^2}{Q_S^2 + Q^2}, \quad D_1 = \left(\frac{Q_V^2}{Q_V^2 + Q^2} \right)^2, \quad D_2 = (1 + \kappa) D_1$$

$$D_3 = \frac{Q^2}{m_N^4} D_1^2, \quad D_V = D_1, \quad D_T = \frac{\sqrt{Q^2}}{m_N} D_1$$

(10)

where κ is the vector diquark anomalous magnetic moment.

Using the MINUIT program we could fit the higher twist contributions, with great accuracy. The parameters are consistent with other applications of the diquark model. The scalar diquarks are more abundant and point like

than vector ones. Also the average x carried by diquarks is smaller for scalar than for vector. The momentum fraction of diquarks is about 0.24 [4].

References

1. M. Virchaux and A. Milsztajn, *Phys. Lett* **B274** (1992) 221.

2. For a Review on Diquarks see, *e.g.*, M. Anselmino, S. Ekelin, S. Fredriksson, D.B. Lichtenberg and E. Predazzi, *Rev. Mod. Phys.* **65** (1993) 1199.

3. M. Anselmino, F. Caruso, E. Leader and J. Soares, *Z. Phys.* **C48** (1990) 689.

4. For further details see M. Anselmino, F. Caruso, J.R.T. de Mello Neto, A. Penna Firme and J. Soares *preprint* CBPF-NF-024-94 and A. Penna Firme, *Da contribuição dos diquarks à descrição de efeitos de "higher twist" observados no espalhamento profundamente inelástico*, Thesis, CBPF (1994), and all the references within.

A Contribuição dos Diquarks ao Espalhamento Profundamente Inelástico $\nu p \to \nu X$

M.Anselmino[1], E.Barone[2], F.Caruso[3,4], E.Cheb-Terrab[4]
P.C.R.Quintairos[3]

[1]*Departamento de Física Teórica, Universidade de Torino e Instituto Nacional de Física Nuclear*

[2]*Universidade de Alessandria e Instituto Nacional de Física Nuclear*

[3]*Centro Brasileiro de Pesquisas Físicas*

[4]*Instituto de Física, Universidade do Estado do Rio de Janeiro*

Neste trabalho apresentam-se os resultados do cálculo da contribuição dos diquarks às funções de estrutura do próton no espalhamento profundamente inelástico neutrino-próton ($\nu p - \nu X$), com troca de corrente neutra, no caso em que o feixe e o alvo não são polarizados.

A partir dos vértices mais gerais possíveis para o acoplamento Z^0-diquark calculam-se as contribuições dos diquarks escalares, vetoriais e das transições entre diquarks (processos do tipo escalar ↔ vetor) às funções de estrutura do próton.

A seção de choque do processo $\nu p - \nu X$, em primeira ordem das amplitudes de espalhamento, é dada por [4]:

$$\frac{d^2\sigma_{CN}}{d\Omega dE'} = \frac{1}{2m_p}\left(\frac{G_F}{2\pi}\right)^2\left(\frac{M_Z^2}{Q^2+M_Z^2}\right)^2\frac{E'}{E}L_{\alpha\beta}(\nu)W^{\alpha\beta} \tag{1}$$

Onde m_p, G_F, M_Z, $L_{\alpha\beta}$ e $W^{\alpha\beta}$ são, respectivamente, a massa do próton. a constante de Fermi. a massa do Z^0, o tensor leptônico e o tensor hadrônico. Estes tensores são definidos por [4]:

$$L_{\alpha\beta}(\nu) = k_\alpha k_\beta' + k_\alpha' k_\beta - g_{\alpha\beta}k.k' + i\epsilon_{\alpha\beta\gamma\delta}k^\gamma k^{\delta'} \tag{2}$$

$$\frac{1}{2m_p}W_{\alpha\beta} = -g_{\alpha\beta}W_1 + \frac{p_\alpha p_\beta}{m_p^2}W_2 - \frac{i\epsilon_{\alpha\beta\gamma\delta}p^\gamma q^\delta}{2m_p^2}W_3 + \frac{q_\alpha q_\beta}{m_p^2}W_4 + \frac{p_\alpha q_\beta + p_\beta q_\alpha}{2m_p^2}W_5 + i\frac{p_\alpha q_\beta - p_\beta q_\alpha}{2m_p^2}W_6 \tag{3}$$

k. k'. p e q são. respectivamente, os quadri-momenta inicial e final do neutrino, o momentum do próton e o momentum transferido. Apenas os termos propocionais à W_1, W_2 e W_3 contribuem à eq.(1) [7,4]. A expressão da seção de choque fica [4].

$$\frac{d^2\sigma_{CN}}{d\Omega dE'} = \frac{G_F^2}{2\pi^2}\left(\frac{M_Z^2}{M_Z^2 + Q^2}\right)^2 E'^2\left[2W_1 sen^2(\theta/2) + W_2 cos^2(\theta/2) - W_3\frac{E + E'}{m_p}sen^2(\theta/2)\right]. \tag{4}$$

No modelo a *partons*, desprezando-se o momentum de Fermi dos constituintes. o tensor hadrônico é dado por [1]:

$$W^{\alpha\beta}(N) = \frac{1}{2}\frac{1}{2m_p\nu x}\sum_{j,s;S} n_j(x,S;s)W_{\alpha\beta}(j,j';s). \tag{5}$$

onde $n_j(x,S;s)$ é a densidade de *partons* do tipo j, com spin s e quadri-momentum $k = xp$, no interior do nucleon de momentum p e spin S. $W_{\alpha\beta}(j,j';s)$ é o tensor que descreve a interação entre o Z^0 e o diquark.

A seguir vamos apresentar os resultados obtidos para $W_{\alpha\beta}(j,j')$ no caso dos diquarks escalares, vetoriais e das transições .

A contribuição do diquark escalar é do mesmo tipo da encontrada no espalhamento $ep - eX$ [1]. ou seja:

$$W_1^{(S)} = 0 \tag{6}$$

$$W_2^{(S)} = \frac{e_D^2}{\nu} S(x) x D_S^2 \tag{7}$$

onde $S(x)$ é a densidade de diquarks escalares com momentum $k = xP$. $D_S(Q^2)$ é o fator de forma do diquark, o qual descreve sua estrutura interna e e_D sua carga elétrica (em unidades da carga do próton).

No caso dos diquarks vetoriais a corrente $V - A$ é dada por [2]:

$$V^\mu = i e_D \left[V^{\eta\mu\rho} + A^{\eta\mu\rho} \right] \epsilon_{2\rho}^*(\lambda_1) \epsilon_{1\eta}(\lambda_2) \tag{8}$$

onde.

$$V^{\eta\mu\rho} :\equiv b_1(2k+q)^\mu g^{\rho\eta} - b_2(k+q)^\eta g^{\rho\mu} - b_3 k^\rho g^{\eta\mu} + b_4(2k+q)^\mu (k+q)^\eta k^\rho \tag{9}$$

$$A^{\eta\mu\rho} :\equiv [a_1(2k+q)_\sigma - a_2 q_\sigma]\epsilon^{\sigma\eta\mu\rho} - a_3 q_\sigma(2k+q)_\delta \epsilon^{\eta\rho\sigma\delta}(2k+q)^\mu \tag{10}$$

k é o momentum do diquark, q o momentum transferido e os ϵ's são os vetores de polarização dos diquarks vetoriais, e os λ's suas helicidades. Os fatores de forma a_i e b_i, $i = 0, 1, 2, 3$ são constantes reais para não violar a simetria CPT [2]. Como vamos tratar do caso não polarizado, temos que o tensor partônico será dado por:

$$\sum_{\lambda_1} W^{\mu\nu}(V,V) = \sum_{\lambda_1,\lambda_2} V^{\mu*} V^\nu \tag{11}$$

Logo:

$$\sum_{\lambda_1} W^{\mu\nu}(V,V) = e_v^2 [V^{\eta\mu\rho} + A^{\eta\mu\rho}][V^{\alpha\nu\beta} + A^{\alpha\nu\beta}] \times \left[\sum_{\lambda_2} \epsilon_{1\eta}^*(\lambda_2)\epsilon_{1\alpha}(\lambda_2) \right] \left[\sum_{\lambda_1} \epsilon_{2\beta}^*(\lambda_1)\epsilon_{2\rho}(\lambda_1) \right] \tag{12}$$

Sabemos ainda que [2]:

$$\sum_\lambda \epsilon_\mu^*(k,\lambda)\epsilon_\nu(k,\lambda) \longrightarrow -g_{\mu\nu} + \frac{1}{m^2}k_\mu k_\nu \tag{13}$$

Substituindo (12) em (11) e efetuando a contração dos tensores obtemos o tensor hadrônico em termos das funções de estrutura, as quais são:

$$W_1^{(V)} = e_D^2 V(x) \left[\frac{1}{4m_p^2} \left[\frac{b_2^2}{2} + \frac{b_3^2}{2} + a_1^2 + a_2^2 \right] \frac{Q^4}{x^2 m_p} + \left[4a_1^2 + b_2^2 + b_3^2 \right] \frac{Q^2}{2m_p} + 4x^2 m_p a_1^2 \right] \tag{14}$$

$$
\begin{aligned}
W_2^{(V)} = \; & e_D^2 V(x) \left[\frac{b_4^2 Q^8}{8m_p^3 x^2} + \left[\left[-\frac{b_4 b_3}{4m_p^3} + \left(-\frac{b_2}{4m_p^3} \right. \right. \right. \right. \\
& + \left. \frac{b_1}{2m_p^3} \right) b_4 \right] + \frac{b_4^2 x^2}{m_p} \left. \right] \frac{Q^6}{x^2} + \left[\left[\frac{b_3^2}{2m_p^3} + \left(-\frac{b_1}{2m_p^3} \right. \right. \right. \\
& + \left. \frac{b_2}{8m_p^3} \right) b_3 + \left(\frac{b_2}{4m_p^3} - \frac{b_1}{2m_p^3} + \frac{b_3}{8m_p^3} \right) b_3 \right] \\
& + \left[\frac{1}{m_p} \left((-b_2 + 3b_1)b_4 - b_3 b_4 \right) + (2b_4^2 \right. \\
& + \left. 4a_3^2)x^2 \right] m_p x^2 \right] Q^4 x^2 + \frac{1}{m_p} \left[\left(2b_4^2 + a_2^2 + a_1^2 \right. \right. \\
& + \left. \left(-b_1 + \frac{b_2}{2} \right) b_2 + \left(-b_1 + \frac{b_3}{2} \right) b_3 \right)
\end{aligned}
$$

$$+ \quad 4(-2m_p a_2 a_3 + m_p b_1 b_4 + 4m_p^3 a_3^2 x^2)x^2 \Big] Q^2$$

$$+ \quad 2m_p(2a_1^2 + 3b_1^2)x^2 \Big] \tag{15}$$

$$W_3^{(V)} = 0 \tag{16}$$

onde $V(x)$ é a densidade de diquarks vetoriais com momentum $k = xp$ e $Q^2 = -q^2$, onde q é o quadri-momentum transferido. Estes resultados foram obtidos com o auxílio do *Maple* (versão V.2).

Os diquarks não contribuem à W_3 porque ao efetuarmos a soma sobre todos os estados de polarização as contribuições antissimétricas se anulam, e esta função contém somente termos deste tipo.

Por último, apresentamos a contribuição dos processos onde ocorrem transições dos diquarks, às funções de estrutura do próton. A corrente para esta interação é dada por [2]:

$$T_\nu^{(S-V)} = -e_D \Big[g_1 g_{\gamma\nu} + g_2 k_\gamma k_\nu + g_3 \epsilon_{\alpha\beta\gamma\nu} q^\alpha k^\beta \Big] \epsilon^\gamma \tag{17}$$

$$T_\nu^{(V-S)} = -e_D \Big[g_1 g_{\gamma\nu} + g_2 (k+q)_\gamma (k+q)_\nu - g_3 \epsilon_{\alpha\beta\gamma\nu} q^\alpha k^\beta \Big] \epsilon^\gamma \tag{18}$$

Os g's são reais pelo mesmo argumento que os a's e os b's o são. Obtemos para as funções de estrutura.

$$W_1^{(T)} = D_T(x) \frac{e_D^2}{2m_p} \Big[g_1^2 + g_3^2 Q^2 \Big(m_p^2 x^2 + \frac{Q^2}{4} \Big) \Big] \tag{19}$$

$$W_2^{(T)} = D_T(x) \frac{e_D^2 x^2}{2m_p} \Big[\frac{1}{x^2} \Big[g_1 + g_2 \Big(m_p^2 x^2 + \frac{Q^2}{2} \Big) \Big]^2 - g_2^2 m_p^4 x^2 + g_3^2 m_p^2 Q^2 - 2 g_1 g_2 m_p^2 \Big] \tag{20}$$

$$W_3^{(T)} = 0. \tag{21}$$

onde para $T = S - V$, $D_T = S(x)$ e para $T = V - S$, $D_T = V(x)$. As funções $W_3^{(S-V)}$ e $W_3^{(V-S)}$ são nulas pelo mesmo motivo que $W_3^{(V)}$.

References

1. M. Anselmino. F. Caruso. E. Leader. J. Soares; *Z. Phys.* **48**, 689 (1990).
2. M. D. Scadron: *Physical Review* **165** (5). 1640 (1967)
3. M. Anselmino, E. Predazzi. S. Ekelin. S. Fredriksson. D.B. Lichtenberg: *Reviews of Modern Physics* **65** (4). (1993).
4. E. Leader & E. Predazzi, *Gauge Theories and The New Physics*, Cambridge University Press, Cambridge, 1982.
5. F. Halzen and A. D. Martin. *Quarks & Leptons: An Introductory Course in Modern Particle Physics*: John Willey & Sons, Singapore. 1984.
6. Bjorken and Drell. *Relativistic Quantum Mechanics*; McGraw-Hill, New York. 1964.
7. F. E. Close. *An Introduction to Quarks and Partons*: Academic Press. 1979.

Could we understand the $^1D_2 \to p\bar{p}$ charmonium decay?

M. Anselmino[1], F. Caruso[2,3], F. Murgia[4] and
M. R. Negrão[2]

[1]*Dipartimento di Fisica Teorica, Università di Torino*
and Istituto Nazionale di Fisica Nucleare. Sezione di Torino
Via Pietro Giuria 1. I-10125 Torino, Italy

[2]*Centro Brasileiro de Pesquisas Físicas/CNPq*
Rua Dr. Xavier Sigaud 150, 22290-180, Rio de Janeiro, RJ, Brazi

[3]*Instituto de Física, Universidade do Estado do Rio de Janeiro, Brazil*
Rua São Francisco Xavier 524, 20550-011, Rio de Janeiro, RJ, Brazil

[4]*Istituto Nazionale di Fisica Nucleare. Sezione di Cagliari*
Via A. Negri 18, I-09127 Cagliari, Italy

Massless perturbative QCD forbids, at leading order, the exclusive annihilation of proton-antiproton into some charmonium states, which, however, have been observed in the $p\bar{p}$ channel, indicating the significance of higher order and non perturbative effects in the few GeV energy region. The most well known cases are those of the $^1S_0$ (η_c) and the $^1P_1$. We consider here the $^1D_2$ state, whose coupling to $p\bar{p}$ in equally forbidden in pQCD, and study several possible non perturbative contributions. It turns out that the observation of the $p\bar{p} \to {}^1D_2$ process would be very intriguing indeed.

Let us consider the $^1D_2$ state created in $p\bar{p}$ annihilations, choosing the z-axis as the proton direction in the $p\bar{p}$ centre of mass frame. Quantum numbers only allow the $^1D_2$ state to be created with the spin third component $J_z = 0$ [1]; such charmonium state is then purely polarized and its spin density matrix has only one non zero component.

$$\rho_{00}(^1D_2) = 1 . \tag{1}$$

This peculiar property reflects into the decay angular distributions of the $^1D_2$. One radiative decay which is expected to be observed with a large branching ratio is

$$^1D_2 \to {}^1P_1\gamma \tag{2}$$

which is dominated by an electric dipole transition. The angular distribution of the photon, as it emerges in the rest frame of the $^1D_2$, is then simply given by [2]

$$W_\gamma(\theta) = \frac{1}{8}(5 - 3\cos^2\theta) \tag{3}$$

where θ is the photon polar angle and an integration has been performed over the azimuthal angle.

The observation of such an angular distribution in $p\bar{p}$ exclusive annihilations should then be a clear signal of the formation and decay of the $^1D_2$ state. The expected mass of the $^1D_2$ state is $M_D = (3788 \pm 7)$ MeV [3].

As charmonium states with $J_z = 0$ cannot decay into $p\bar{p}$ according to massless pQCD, we examine several possible non perturbative contributions. Mass corrections to 'forbidden' charmonium decays have been considered in Ref. [4] for η_c, $\chi_{c0} \to p\bar{p}$. Following the same procedure and notations as in Ref. [4] we have computed the helicity amplitudes for the decay $^1D_2 \to p\bar{p}$.

From the knowledge of the decay helicity amplitudes one obtains the decay rate.

One can get an estimate of the branching ratio $BR(^1D_2 \to p\bar{p})$ by taking the ratio of $\Gamma(^1D_2 \to p\bar{p})$ and $\Gamma(^1D_2 \to gg)$. According to the different choices adopted in Ref. [4] one obtains

$$BR(^1D_2 \to p\bar{p}) \sim 10^{-8} \div 10^{-12}. \tag{4}$$

Eq. (4) clearly shows how mass corrections could not account for the eventual observation of the $^1D_2 \to p\bar{p}$ decay with a branching ratio similar to that measured for other charmonium decays into $p\bar{p}$ ($\sim 10^{-4}$).

One can similarly show that also two quark correlations could not explain a branching ratio for the $^1D_2 \to p\bar{p}$ decay of the order of 10^{-4}; a vector diquark component of the proton allows the decay, by allowing helicity flips at the gluon-vector diquark coupling [5], but, once more, the numerical values turn out to be too small. One finds, with little dependence on the choice of the distribution amplitudes,

$$BR(^1D_2 \to p\bar{p}) \sim 10^{-6}. \tag{5}$$

As a further possible explanation [6,7], the presence of a 2^{-+} glueball with a mass close to 3.8 GeV, does not look much natural and realistic.

Let us consider finally the instanton induced mechanism proposed in Ref. [8] for the $\eta_c \to p\bar{p}$ decay: we know that its contribution decreases very rapidly with increasing Q^2 and, indeed, already for the decay of η_c', with a mass $\simeq 3.6$ GeV, is much smaller than for the η_c [8]. Considering the still higher mass of the $^1D_2$, $M_D \simeq 3.8$ GeV, we cannot expect this non perturbative contribution to be large enough to produce a branching ratio for the process $^1D_2 \to p\bar{p}$ similar to those observed for the other charmonium states.

We have thus seen how several possible non perturbative effects cannot contribute significantly to the $^1D_2$ coupling to $p\bar{p}$; on the other hand we know that leading order pQCD predicts no coupling at all, whereas higher order corrections are difficult to evaluate and have never been computed. A similar situation occurs with the η_c, with the difference that for such particle one might expect a significant gluonic contribution [6,7]. Therefore, the eventual observation of a $BR(^1D_2 \to p\bar{p}) \sim 10^{-4}$, analogous to the values observed for all other charmonium states which can couple to $p\bar{p}$, would pose an intriguing challenge to the theory.

The $^1D_2$ state could be looked for in the mass region $M_D \simeq 3788$ MeV [3]. In fact the $^1D_2$ created in $p\bar{p}$ annihilation is in a pure spin state with $J_z = 0$ and its decay into $^1P_1\gamma$, dominated by an $E1$ transition, has the simple angular distribution given in Eq. (3). Actually, even if other multipole amplitudes contribute to this decay, their relative weights can be evaluated by looking at the angular distribution of the subsequent decay of the $^1P_1$ [9].

An interested reader can find more information in Ref. [1] or contact "guiduska@lafex.cbpf.br".

References

1. M. Anselmino, F. Caruso, F. Murgia and M.R. Negrão, *preprint* CBPF-NF-014-94.
2. See, *e. g.*, T.A. Armstrong *et al.*, *Phys. Rev.* **D48** (1993) 3037; M. Anselmino, F. Caruso and R. Mussa, *Phys. Rev.* **D45** (1992) 4340.
3. D.B. Lichtenberg, R. Roncaglia, J.G. Wills, E. Predazzi and M. Rosso, *Z. Phys.* **C46** (1990) 75.
4. M. Anselmino, R. Cancelliere and F. Murgia. *Phys. Rev.* **D46** (1992) 5049.
5. M. Anselmino, F. Caruso and S. Forte, *Phys. Rev.* **D44** (1991) 1438.
6. M. Anselmino, M. Genovese and E. Predazzi, *Phys. Rev.* **D44** (1991) 1597.
7. M. Anselmino, M. Genovese and D.E. Kharzeev, *Phys. Rev.* **D50** (1994) 595.
8. M. Anselmino and S. Forte, *Phys. Lett.* **B323** (1994) 71.
9. F.L. Ridener and K.J. Sebastian, *Phys. Rev.* **D49** (1994) 4617.

Férmions Excitados em Colisões
eγ Polarizados

O. J. P. Éboli

Instituto de Física - USP

and

E.M. Gregores, J.C. Montero, S.F. Novaes e D. Spehler

Instituto de Física Teórica - UNESP

Investigamos algumas consequências da existência de léptons excitados de spin $\frac{1}{2}$ e $\frac{3}{2}$ preditos por modelos compostos em colisões $e\gamma$. Examinamos a potencialidade da próxima geração de aceleradores lineares com feixes polarizados de fornecer informações sobre o spin e acoplamento destas partículas.

Neste trabalho, procuramos possíveis desvios do Modelo Padrão nas reações $e\gamma \to e\gamma$ quando um férmion excitado de spin $\frac{1}{2}$ ou $\frac{3}{2}$ é trocado como uma contribuição adicional à QED. Em particular, concentramos nossa atenção na possibilidade de distinguir o spin de tais estados e a natureza quiral de seu acoplamento através do uso de feixes polarizados.

A dinâmica a nível preônico não é especificada pelos modelos que prevêm a existência de tais ressonâncias [1] e portanto, nos ativemos a Lagrangianas efetivas para descrever o acoplamento dos estados excitados aos férmions usuais e bósons vetoriais. Consideramos um acoplamento tipo momento magnético entre o férmion excitado de spin $\frac{1}{2}$ ($\Psi^*_{1/2}$), o férmion no estado fundamental (ψ) e o fóton, descrito pela Lagrangiana efetiva

$$\mathcal{L}^{1/2}_{\text{eff}} = \frac{e}{2\Lambda} \bar\Psi^*_{1/2} \sigma^{\mu\nu}(A + B\gamma_5)\psi \, F_{\mu\nu} + \text{h.c.} \tag{1}$$

Para o acoplamento do férmion excitado de spin $\frac{3}{2}$ ($\Psi^{*\mu}_{3/2}$), adotamos a Lagrangiana efetiva de mais baixa ordem invariante de gauge que descreve seu acoplamento com os férmions usuais e o fóton [2]

$$\mathcal{L}^{3/2}_{\text{eff}} = \frac{e}{\Lambda} \bar\Psi^{*\mu}_{3/2} \gamma^\nu(C + D\gamma_5)\psi \, F_{\mu\nu} + \text{h.c.}, \tag{2}$$

onde $F_{\mu\nu}$ é o tensor do campo eletromagnético, $\sigma^{\mu\nu} = \frac{1}{2}[\gamma_\mu, \gamma_\nu]$, e Λ é a escala de composição.

Os limites experimentais mais restritivos para a existência destes férmions provêm das medidas de $(g-2)$, momento magnético anômalo dos elétrons e múons [3,4]. Estes limites podem no entanto ser evitados se considerarmos apenas acoplamentos quirais. Nestes casos, as contribuições dos estados excitados de spin $\frac{1}{2}$ e spin $\frac{3}{2}$ para o momento magnético anômalo serão proporcionais a $\alpha/\pi(m_l/M_{1/2(3/2)})^2$, onde $M_{1/2(3/2)}$ é a massa dos estados excitados e $l = e, \mu$. Para preservar a invariância de CP, as constantes $A, \ldots, D$ são consideradas reais. Os acoplamentos que nós consideramos aqui são uma generalização de outros geralmente usados em trabalhos correlatos [5].

A existência de férmions excitados com massa abaixo do limite cinemático *i.e.* $M_{1/2(3/2)} < \sqrt{s_{max}}$, pode ser facilmente estabelecida através do pico de Breit-Wigner que aparece na distribuição da massa invariante do par elétron-fóton mesmo para casos não polarizados conforme apresentado na Fig. 1.
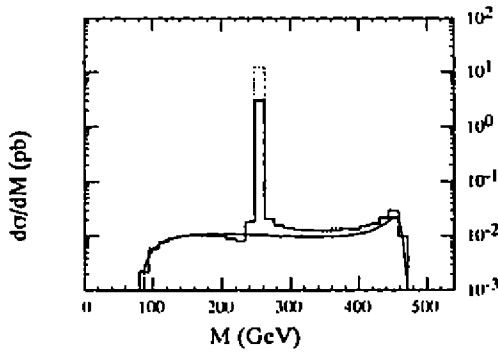
Figura 1: *Distribuição da massa invariante do par elétron-fóton para* $\sqrt{s}$ = 500 GeV. *Estados excitados de spin$\frac{1}{2}$ são indicados pelo histograma cheio, os de spin$\frac{3}{2}$ pelo pontilhado e o* background *(*Λ = ∞*) é indicado pela linha contínua.*

A natureza quiral do acoplamento (LH ou RH) pode ser identificada polarizando-se apenas o feixe de elétrons, mantendo-se o laser e o feixe de pósitrons, sobre o qual o laser incide, sem polarização. Nestas condições, o feixe de fótons se manterá não polarizado e a seção de choque assume a forma

$$d\sigma_{P,0} = d\sigma_{00}(1 + P_e A_{P,0}) \ . \tag{3}$$

onde $d\sigma_{P,0}$ é a seção de choque para elétrons iniciais com polarização longitudinal P_e e fótons não polarizados. $d\sigma_{00}$ é a seção de choque não polarizada e $A_{P,0}$ o fator de assimetria dado por

$$A_{P,0} = \frac{d\sigma_{+0} - d\sigma_{-0}}{d\sigma_{+0} + d\sigma_{-0}} \ . \tag{4}$$
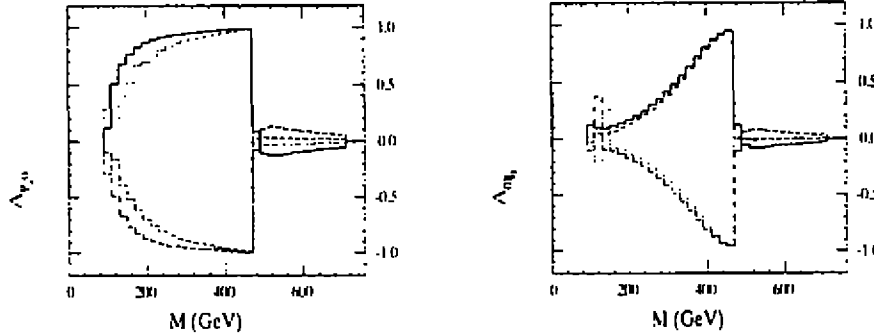
Figura 2: *Gráfico de* $A_{P,0}$ *e* $A_{0\xi_2}$ *em função da massa do estado excitado, assumindo um grau de polarização de 90% e* Λ = 1 TeV *para LH-spin$\frac{1}{2}$ (cheio), RH-spin$\frac{1}{2}$ (traços), LH-spin$\frac{3}{2}$ (pontos), RH-spin$\frac{3}{2}$ (traços-pontos). Note-se o abrupto corte que ocorre ao se atingir o limite cinemático imposto pela distribuição de energia do laser-backscattering, para* $\sqrt{s}$ = 500 GeV.

Como se pode ver na Fig. 2, a medida de $A_{P,0}$ distingue claramente o acoplamento de mão esquerda (LH) do de mão direita (RH). Esta medida de assimetria, no entanto, não é capaz de distinguir o spin da ressonancia.

O spin do estado excitado pode ser determinado polarizando-se apenas o feixe de pósitrons sobre o qual incide o laser não polarizado. Nesta situação, obtem-se um feixe de fótons com polarização circular ξ_2 e a seção de choque se torna

$$d\sigma_{0\xi_2} = d\sigma_{00}(1 + \xi_2 A_{0\xi_2}) \ . \tag{5}$$

onde $A_{0\xi_2}$ é o fator de assimetria dado por

$$A_{0\xi_2} = \frac{d\sigma_{0+} - d\sigma_{0-}}{d\sigma_{0+} + d\sigma_{0-}} \ . \tag{6}$$

A medida desta assimetria, conforme pode ser visto na Fig. 2 distingue os estados LH-spin$\frac{1}{2}$ e RH-spin$\frac{3}{2}$ dos estados RH-spin$\frac{1}{2}$ e LH-spin$\frac{3}{2}$. Como a quiralidade da partícula terá sido, a esta altura, determinado pela medida de $A_{P,0}$, obtem-se deste modo a determinação de seu spin.

Além da determinação do *spin* e *quiralidade* do estado excitado, a polarização dos feixes iniciais também pode proporcionar um aumento considerável na seção de choque para um dado *spin* e acoplamento. Este aumento na seção de choque se torna importante ao se desejar ajustar os parâmetros do acelerador para uma produção abundante de tais estados, uma vez que ele tenha sido descoberto e sua massa, *spin* e acoplamento determinado. Outra razão para se desejar tal aumento na seção de choque para um particular *spin* e acoplamento é a de aumentar a região de descoberta no plano $A \times M$ se nenhuma ressonância for encontrada com os feixes não polarizados.

References

1. M. Suzuki, "Survey of Composite Particle Models of Electroweak Interaction", Proceedings International Symposium on Bound Systems and Extended Objects, Karuizawa, Japan, March, 1992 (preprint UCB-PTH-92-17, May 1992)

   R. D. Peccei, "The Mass Problem and the Issue of Compositeness", Lectures given at Lake Louise Winter Institute: Selected Topics in Electroweak Interactions, Lake Louise, Canada, Feb 15-21, 1987 (preprint DESY 87-050, May 1987)

2. J. Kühn and P. Zerwas, Phys. Lett. **B147**, 189 (1984).

3. F. M. Renard, Phys. Lett. **B116**, 264 (1982).

4. M. Suzuki, Phys. Lett. **B143**, 237 (1984); F. M. Renard, Phys. Lett. **B139**, 449 (1984).

5. A. Feldmaier, H. Salecker and F. C. Simm, Phys. Lett. **B223**, 234 (1989).

Coulomb interference and bending slope
in hadron-hadron scattering

Flávio I. Pereira

Observatório Nacional . CNPq, Rio de Janeiro. Brazil

and

Erasmo Ferreira

Universidade Federal do Rio de Janeiro. 21945-970 RJ. Brazil

With the purpose of testing the results of QCD calculations on the structure of the forward elastic scatering cross-section, we analyse the coulombic-nuclear interference ocurring at small values of the momentum transfer. We enphasize the influence of the hadronic structures on the determination of the Coulomb phase and consequently on the t-dependence of the strong interaction slope parameter.

Soft hadron-hadron scattering at high energies presents features which are the same for every pair of interacting hadrons : a forward peak in the differential elastic cross-section, and a total cross-section which rises slowly with the energy. This universal behaviour says that the underlying dynamics determining the elastic amplitude rests on fundamental properties of the strong interaction; actually it is due to the peculiar structure of the physical vacuum of QCD. The differential elastic cross-section can be parametrized in the form [1]

$$\frac{d\sigma}{dt} = \frac{d\sigma}{dt}\bigg|_{t=0} e^{[B(0)+ct+dt^2]t} .$$ (1)

At very small values of the momentum transfer t (notice that the physical values of t are negative) the first term in the exponent dominates. and the shape of the differential cross-section looks as almost linear in a log scale. With the definition of the logarithmic slope at any t

$$B(t) = \frac{d}{dt}\left(\ln \frac{d\sigma^{el}}{dt}\right) .$$ (2)

we have as a parametrization for $B(t)$

$$B(t) = B(0) - 2c|t| + 3d|t|^2 .$$ (3)

In the experimental observations of elastic scattering, the slope $B(0)$ has been measured in several instances. The coefficient c, which tells how the slope bends, has not been often measured. and the reliability of the determinations is not always satisfactory. The measurements are difficult. as they require good accuracy at very small angles, and a very good extraction of the effects of the interference between the strong and the Coulomb interactions.

The Model of the Stochastic Vacuum applied to high-energy scattering [2] describes the values of the total cross-section $\sigma^T(s)$ and of the slope parameter of the elastic differential cross-section. which are the basic characteristic quantities of hadronic elastic processes at very low momentum transfers, in terms of non-perturbative properties of the QCD vacuum . The ingredients are the value of the gluon condensate $(0|g^2 FF|0)$ and the characteristic correlation length a. According to this model. experimental determination of parameters in elastic and total cross-setions at high energies provide essential information on these fundamental QCD properties. The model predicts

correctly the observed relation between $\sigma^T(s)$ and $B(0)$ at all energies. For the parameter c of the bending slope the model predicts values of about

$$c \approx B(0) \ 0.5 \ a^2 t^2 \ . \tag{4}$$

Thus the determination of shape of the forward peak gives direct information on the correlation length a. The experimental information obtained at ISR energies [1] are in agreement with eq (4). However, in the more recent CERN experiments at $\sqrt{s} = 541$ GeV at very low t ($|t| = 0.00075 - 0.12$ GeV^2) the reported value for the parameter c is compatible with zero. We wish to call attention for a difficulty in the analysis of the data, due to the interpretation of the Coulomb-strong interference at such low t values.

The strong amplitude leading to the parametrization in eq (1) is of the form

$$f_S(t) = \frac{\sigma_{tot}}{4\sqrt{\pi}} \ (i + \rho) \ G_p^2(t) \ e^{\frac{1}{2}[B(0)+ct+dt^2]t} \ . \tag{5}$$

where

$$\rho = \frac{Re \ f_S(0)}{Im \ f_S(0)} \ .$$

and $G_p(t)$ is the proton form factor

$$G_p(q^2) = \left(\frac{\Lambda^2}{q^2 + \Lambda^2}\right)^2 \ . \qquad \Lambda^2 = 0.71 \ \text{GeV}^2 \ . \tag{6}$$

The total (strong plus coulombic) differential elastic cross-section for $\bar{p}p$ scattering is written

$$\frac{d\sigma}{dt} = |f_S + e^{i\alpha\phi}f_C|^2 \ . \tag{7}$$

where the Coulomb amplitude is

$$f_C = 2\alpha\sqrt{\pi} \ \frac{G_p^2(t)}{|t|} \tag{8}$$

and ϕ is the Coulomb phase. In general, ϕ is considered as numerically small. However, taking into account the proton form factor, the expression for ϕ is written [3]

$$\phi(q^2) = -\int_0^\infty dq'^2 \ \ln\frac{q'^2}{q^2} \ \frac{d}{dq'^2}[G_p^2(q'^2)\frac{f_S(q'^2)}{f_S(0)}] \ + \ \nu(q^2) \ . \tag{9}$$

where

$$\nu(q^2) = \frac{2q^2}{\Lambda^2}[2 \ \ln\frac{\Lambda^2}{4q^2} \ - \ 1] \ . \tag{10}$$

If we now consider the form of the amplitude (5) with a positive value of c , we see that the integral in the expression for the phase ϕ diverges. In these circumstances, the parametrization of the amplitude with a power series in t in the exponent becomes unacceptable. The determination of the value for the parameter c using data at very low values of t, where the Coulomb interaction is important, becomes meaningless as soon as c takes positive values. Thus to evaluate anything beyond the first term $B(0)$ we need an explicit form for the t-dependence of the amplitude, generated through some model, and this form must be such that the integration in eq (9) be defined. In the fittings of experimental data made at ISR energies ($\sqrt{s} \approx 20$ GeV), the Coulomb interference region was not really important in the analysis, but this is not the case with the new $\sqrt{s} = 541$ GeV data.

References

1. J.B.Burq et al, *Nucl. Phys.* **B217** (1983) 285.

2. H.G.Dosch, E.Ferreira and A.Krämer, *Phys. Rev.* **D50** (1994) 1992.

3. G.B.West and D.R.Yennie, *Phys. Rev.* **172** (1968) 1413; R. Cahn, *Z. Phys.* **C15** (1982) 253.

Estudos de Simulação para
Produção de Bárions Charmosos

Fernanda Gallinucci Garcia, Carlos O. Escobar

Instituto de Física - Universidade de São Paulo

A produção soft de multipartículas é uma característica dominante na maioria dos eventos em colisões hadrônicas a altas energia. Processos com muitas partículas no estado final são intrinsicamente complicados, desde que muitas variáveis são envolvidas. Mesmo assim, seria possível utilizar a Lagrangiana da QCD para estudar estes processos soft. Entretanto, uma característica destes processos é que não envolve grandes momentos transferidos e sendo assim, a constante de acoplamento forte α_s é muito grande para que a teoria de perturbação possa ser usada. Consequentemente, procedimentos não perturbativos devem ser adotados. Então, atualmente, a melhor coisa a se fazer em descrever a física hadrônica soft é construir modelos que incorporam todas as idéias teóricas acessíveis, motivadas tanto pelos estudos não-perturbativos da QCD quanto pelas propriedades gerais da matriz-S (dualidade e unitariedade).

Uma abordagem não perturbativa altamente estudada consiste em expansões em N^{-1}, onde N pode ser tanto o número de cor N_c ou o número de sabores N_f. Este tipo de expansão fornece uma classificação topológica de diagramas.

Um modelo que tem obtido grande sucesso na produção de partículas leves é o Quark Gluon String Model (QGSM). Este modelo usa a idéia de *strings* de Pomeron *quark*-glúon para descrever a produção múltipla de hádrons com baixo p_t a altas energias. O que se pretende com este modelo é poder descrever o espectro das partículas, isto é, obter a secção de choque inclusiva dos hádrons (σ^{in}) em termos das funções de estrutura e funções de fragmentação dos *quarks* *vestidos*; distribuições de multiplicidade e rapidez; explicar o crescimento observado experimentalmente na região central do espectro, com o aumento da energia.

Na abordagem baseada na expansão $1/N_f$, o polo de Pomeranchuk é descrito por gráficos do tipo cilíndrico e os Reggeons secundários por gráficos planares.

(a) **Gráficos planares:** o processo de interação envolve a aniquilação dos *quarks* de valência dos hádrons que colidem e uma configuração do tipo tubo de cor (um *string* $q\bar{q}$) aparece. A quebra deste *string* leva a criação dos hádrons brancos.

(b) **Gráficos cilíndricos:** os hádrons iniciais trocam vários glúons, em um estado singleto de cor e os *quarks* de valência dos hádrons, que estão num estado branco, são ligados a *string* *quark*-glúon. Quando *quarks* são emitidos, estes *strings* são quebrados e resultam em chuveiros de hádrons.

Os parâmetros da trajetória do Pomeron, $\alpha_P(0)$ e $\alpha'_P(0)$ são determinados pela dinâmica do glúon e interações entre os *quarks*, ou seja, pela contribuição de todos os diagramas. Como a soma de todos estes gráficos não pode ser resolvida teoricamente, então escolhemos os parâmetros com base na análise dos dados experimentais.

A contribuição mais simples e dominante para amplitude de espalhamento elástico que não desaparece em energias assintóticas é de um único Pomeron, que tem a topologia de um cilindro. Figura 1.

Um corte através de um Pomeron resulta em dois canais de hádrons, correspondentes as duas intersecções através da superfície do cilindro. Estes canais são esticados entre q_v dos hádrons iniciais para formarem singletos de cor.
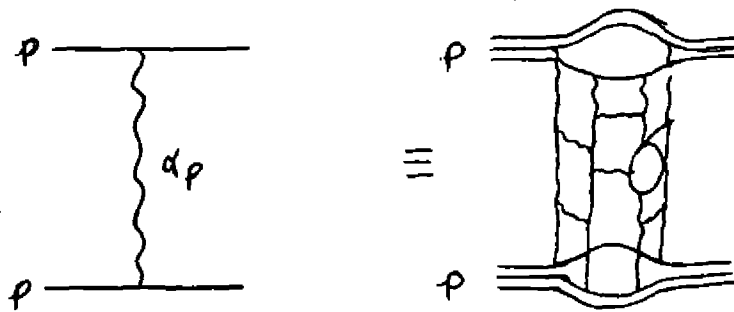
Figura 1. Uma única troca de Pomeron e sua topologia cilíndrica.

Dentro de cada diagrama, as frações do momento levados pelos constituintes nas extremidades de um canal são determinadas pelas funções de distribuições e a produção de partículas num dado canal é dada pelas funções de fragmentação. Em essência, fazemos uso da estrutura partônica dos hádrons e tratamos cada diagrama como um processo de dois passos:

1. Separação de cor na colisão;

2. Fragmentação de objetos coloridos que resulta na produção de canais hadrónicos.

Basicamente, o modelo necessita apenas de dois ingrediente:

1. Funções de distribuição de momento;

2. Funções de fragmentação.

O espectro inclusivo de partículas secundárias é determinado pela convolução da distribuição de momento de diquarks, *quarks* de valência e *quarks* do mar nas partículas incidentes e as funções para fragmentação destes diquarks e *quarks* em hádrons secundários. As distribuições de momento dos diquarks e *quarks* dependem do número n de Pomerons cortados no diagrama em questão. No caso de um alvo de nucleon, o espectro inclusivo de hádron secundário h tem a forma:

$$\frac{x}{\sigma^{inel}}\frac{d\sigma}{dx} = \sum_{n=1}^{\infty} w_n \varphi_n^h(x) + V_D^{(1)}\varphi_D^{(1)}(x) + V_D^{(2)}\varphi_D^{(2)}(x).$$ (1)

onde as funções $\varphi_n^h(x)$ determinam as contribuições dos diagramas com n Pomerons cortados e $w_n = \sigma_n / \sum_{n=1}^{\infty}\sigma_n$ é a probabilidade de cortar precisamente n Pomerons. Os últimos dois termos levam em conta as contribuições dos processos de dissociação difrativa. No caso de produção de hádrons contendo *quarks* u e b, estas contribuições são desprezíveis.

No caso de interações $\pi^+ p$ temos então a expressão

$$\varphi_n^h(x) = f_{\bar{q}}^h(x_+, n)f_q^h(x_-, n) + f_q^h(x_+, n)f_{qq}^h(x_-, n) + 2(n-1)f_s^h(x_+, n)f_s^h(x_-, n)$$ (2)

$$x_\pm = \frac{1}{2}(\sqrt{[\frac{4m_\perp^2}{s} + x^2]} \pm x).$$ (3)

As quantidades $f_{qq}, f_q, f_{\bar{q}}$ e f_s correspondem as contribuições dos diquarks, *quarks* e antiquarks de valência e *quarks* do mar, enquanto que as contribuições da partícula incidente e do alvo dependem das variáveis x_+ e x_- respectivamente.

Assim sendo, as seções de choque para produção de n chuveiros de Pomeron, σ_n, são determinadas de acordo com as regras de Abramovskii-Gribov-Kancheli pelas contribuições da parte imaginária da amplitude de espalhamento elástico proveniente de gráficos contendo k Pomerons. Então, na aproximação quasi-eikonal, a seção de choque σ_n e a probabilidade de processos com n Pomerons cortados tem a forma

$$w_n = \sigma_n / \sum_{n=1}^{\infty} \sigma_n \tag{4}$$

$$\sigma_n = \frac{\sigma_P}{nz}(1 - e^{-z})\sum_{k=0}^{n-1} \frac{z^k}{k!}. \tag{5}$$

onde

$$\sigma_P = 8\pi\gamma e^{\zeta\Delta}. \tag{6}$$

$$\zeta = ln(s/1GeV^2). \tag{7}$$

$$z = \frac{2C\gamma}{R^2 + \alpha'_P\zeta}e^{\zeta\Delta}. \tag{8}$$

Os valores dos parâmetros apresentados para descrever a totalidade dos dados são:

$$\Delta = 0.139, \quad \alpha'_P = 0.21 GeV^{-2}. \tag{9}$$

$$\gamma_{\pi p} = 1.07 GeV^{-2}, \quad R^2_{\pi p} = 2.48 GeV^{-2}, \quad C_{\pi p} = 1.65 \tag{10}$$

Finalmente, as funções f que aparecem na descrição da expressão da seção de choque têm a forma, no caso do espectro em colisões $\pi^+ p$,

$$f_q^h(x_+, n) = \int_{x_+}^1 u_d(x_1, n)G_d^h(x_+/x_1)dx_1. \tag{11}$$

$$f_{\bar{q}}^h(x_+, n) = \int_{x_+}^1 u_{\bar{u}}(x_1, n)G_{\bar{u}}^h(x_+/x_1)dx_1. \tag{12}$$

A forma das funções $u(x, n)$ é determinada no modelo de *quark – gluonstrings* pelo comportamento assintótico de Regge na região $x \to 0$ e $x \to 1$ e para valores intermediários de x por meio de uma simples interpolação.

Uma motivação para este tipo de estudo e a incapacidade da QCD em descrever estes processos encontra-se na nítida discrepância que há nos dados experimentais a respeito do *leading particle effect*. Para pequeno $x?F$ há uma certa concordância com a teoria e os dados experimentais, mas para grande $x?F$, a discordância é brutal. É claro que para processos, onde os hádrons incidentes contêm os sabores de quarks iguais aos da partícula formadas, a seção de choque tem um comportamento mais suave na queda, comparado a processos onde os hádrons incidentes não possuem quarks semelhantes. A figura que demonstra este efeito esta mostrada abaixo.

Sendo assim, mostraremos os resultados apresentados em Angra para mésons D^+, utilizando o Quark Gluon String Model para achar as seções de choque desejadas.

□ E769
△ WA82
● combined data
·- QCD
·-- PYTHIA

Asymmetry

0   0.5   1

0   0.2   0.4   0.6   0.8

Feynmon−x
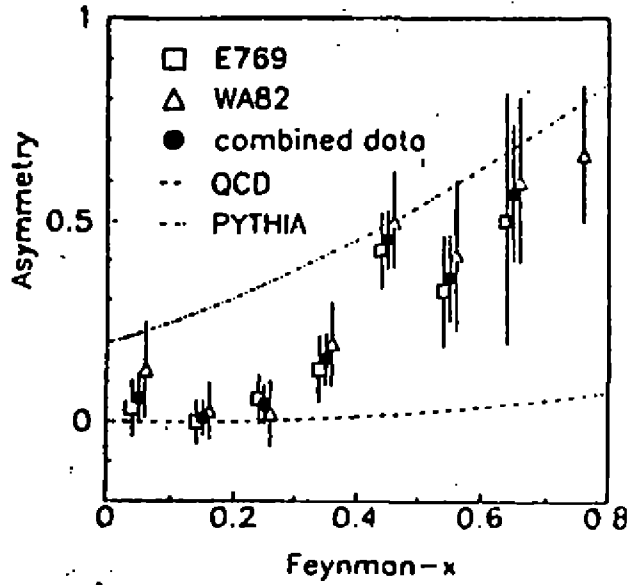
$A \equiv \dfrac{\sigma(leading) - \sigma(noleading)}{\sigma(leading) + \sigma(noleading)}$

Phys. Rev. Letters 72 (1994) 812 - 815

(a)

dN/dx (arbitrary units)

○ WA82 D°
● PYTHIA D°
△ NTLO c

(b)

dN/dx (arbitrary units)

○ WA82 D⁻
● PYTHIA D⁻
△ NTLO c̄
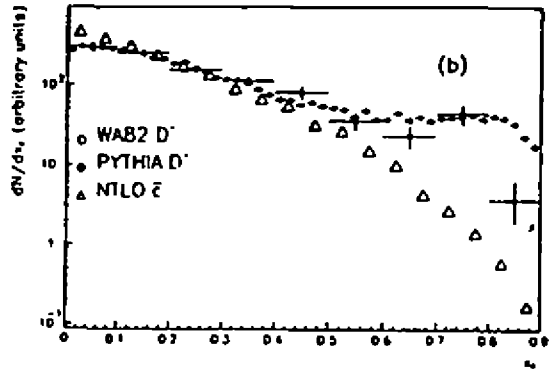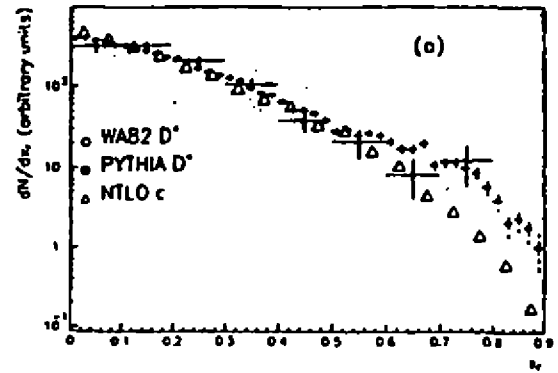
Fig 3. x distributions from π⁻ interactions. (a) D⁺, (b) D⁻.

$D^+ (c\bar{d})$

$D^- (\bar{c} d)$

Phy. Letters B 305 (1993) 402-406

SECAO DE CHOQUE INCLUSIVA 29/09/94 17.14

dσ/dx

n = 1
αₓ(0) = 0

0.1 0.2 0.3 0.4 0.5 0.6 0.7

SECAO DE CHOQUE INCLUSIVA 29/09/94 16.35

dσ/dx

n = 2
αₓ(0) = 0

0.1 0.2 0.3 0.4 0.5 0.6 0.7
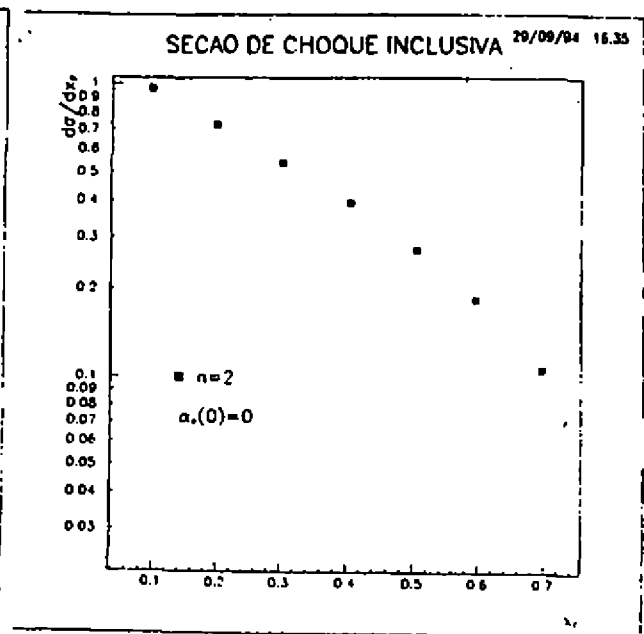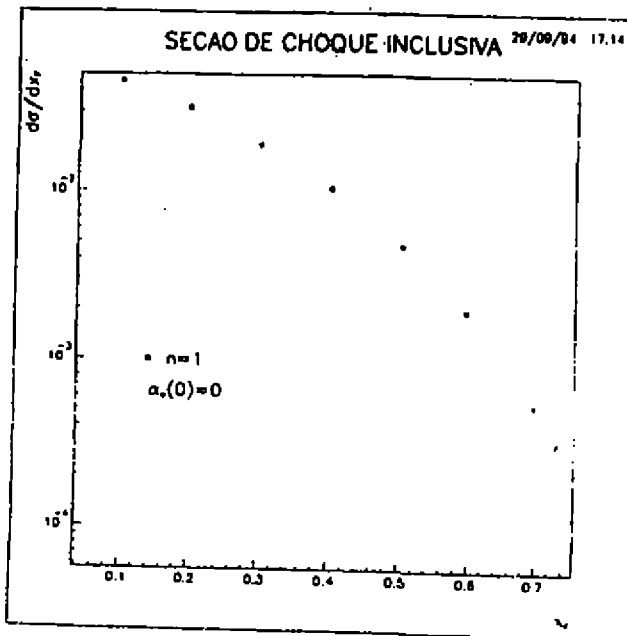
Resonance Production in Peripheral Heavy Ion Collisions

A. A. Natale

Instituto de Física Teórica, Universidade Estadual Paulista

Rua Pamplona, 145, 01405, São Paulo, SP, Brazil

We compute the rates for pseudoscalar meson production through two-photon and two-pomeron scattering, at energies that will be available at RHIC and LHC. Light mesons will mostly be produced by pomeron fusion at large rates, the two processes are comparable for charmed mesons, while electromagnetic production will be dominant for bottom mesons. We discuss the possibility of observing the reaction $PP \to \sigma \to \gamma\gamma$.

Relativistic heavy-ion colliders are planned and considered in Brookhaven (RHIC) and at CERN (LHC), with the main interest in the search of a quark-gluon plasma in central nuclear reactions. In addition to this important feature of heavy-ion colliders, peripheral collisions may be extremely useful to study hadronic resonances with $J^{PC} = 0^{-+}, 0^{++}, 2^{-+}, 2^{++} ....$, and here we will compute resonance production through $\gamma\gamma$ fusion, and double-pomeron exchange. Although pomeron-pomeron scattering is not important for heavy final states, we shall see that it is dominant for light resonances, and will produce such amount of mesons that will allow the study of decays with very small branching ratios.

The rate of ressonance production through photon fusion in heavy-ion collisions is determined through the equivalent photon or Weizsäcker-Williams approximation, and the total cross section $ZZ \to ZZ\gamma\gamma \to ZZR$ can be written as

$$\sigma(s) = \int d\tau \frac{dL}{d\tau} \hat\sigma(\hat s). \tag{1}$$

where $dL/d\tau$ is the photon luminosity and $\hat\sigma(\hat s)$ is the cross section of the subprocess $\gamma\gamma \to R$. The differential luminosity can be obtained through standard methods, and was determined according to a conservative prescription discussed by Cahn and Jackson [1]. The resulting cross sections for a series of resonances are shown in the following table [2]. In this table the columns with the cross sections for photon and pomeron scattering at RHIC and LHC

Meson	$RHIC_{\gamma\gamma}$	$RHIC_{PP}$	$LHC_{\gamma\gamma}$	LHC_{PP}
π^0	7.1	124	40	386
η	1.5	92	17	351
η'	1.1	99	22	125
η_c	0.32×10^{-2}	0.11	0.5	0.8
η_c'	0.36×10^{-3}	0.83×10^{-2}	0.1	0.06
η_b	0.13×10^{-7}	0.41×10^{-6}	0.37×10^{-3}	0.8×10^{-6}

are identified by the indices $\gamma\gamma$ and PP respectively, and the values are in mb. We assumed collisions of ^{238}U at RHIC ($\sqrt{s} = 0.2TeV/nucleon$), and ^{206}Pb at LHC ($\sqrt{s} = 6.3TeV/nucleon$). These machines will operate with luminosities $\mathcal{L}_{RHIC} \simeq 10^{27} cm^{-2}s^{-1}$ and $\mathcal{L}_{LHC} \simeq 10^{26} cm^{-2}s^{-1}$.

The pomeron distribution in a nucleus can be obtained folding the pomeron distribution function in a nucleon with the elastic nuclear form factor [3], and is given by

$$F_P(x) = \left(\frac{3A\beta_0 Q_0^2}{2\pi}\right)^2 \frac{1}{x} \left(\frac{s'}{m^2}\right)^{2\epsilon} e^{-(\frac{xM}{Q_0})^2}. \tag{2}$$

where A is the atomic mass, β_0 is the quark-pomeron coupling, $\beta_0^2 = 3.93 GeV^{-2}$. The factor $s'^{2\epsilon}$ in Eq.(2), where s' denotes the invariant mass of the subprocess with which the pomeron participates, comes from the Regge behavior of the pomeron, whose trajectory is given by $\alpha_P(t) = 1 + \epsilon + \alpha'_P t$, with $\epsilon = 0.085$. In Eq.(2) $Q_0 \approx 60$ MeV determines the width of the nuclear gaussian form factor used to obtain the Pomeron distribution.

To compute the subprocess cross section in the case of double-pomeron scattering, we use the phenomenological fact that the pomeron couples to quarks like a isoscalar photon [4], and treat the pomeron-quark coupling according to a prescription of Donnachie and Landshoff [5]. Our results for the double diffractive resonance production are displayed in the table shown previously [2]. We verify that light resonances in peripheral heavy ion collisions will be basically produced by double-pomeron scattering. The rate of meson production decrease with the increase of the meson mass, with the pomeron and photon initiated processes becoming of the same magnitude for charmed mesons. The main reason for this behavior lies in the fast decrease of the pomeron-quark coupling for "off-shell" quarks.

To show how large is the meson production in these peripheral reactions we will discuss about the observation of the elusive σ meson. Although several experiments claim about the presence of a resonance (σ) in the region of 600 – 700 MeV [6], the existence of such a meson is quite controversial. The σ partial widths into electroweak interacting particles are very small when compared with the hadronic one, and the hope to discover this particle may be connected with the possibility of observing the resonance in these other channels. The cross section for photon-photon production of σ mesons at RHIC(LHC) is equal to 0.39(5.3) mb, while the double pomeron rate for σ production at RHIC(LHC) is 28(110) mb. These values correspond to 8.7×10^5 and 3.4×10^{10} events/year at RHIC and LHC respectively, assuming 100% efficiency. The number of σ mesons decaying into two photons will be a very small fraction of all the mesons produced. For a $q\bar{q}$ σ-meson with 650 MeV, the linear σ-model predicts a hadronic width as large as its mass, $\Gamma_\sigma \sim m_\sigma$. Therefore, most of the σ's will decay into two pions, only 340 and 1.3×10^4 mesons (respectively at RHIC and LHC) will decay into two photons, and these values assume one year of operation with full efficiency for detecting the photons, and tagging the intact ions in the peripheral collision. The chances are clearly better for LHC. Therefore, the σ meson can be produced in the reaction $PP \to \sigma \to \gamma\gamma$, and we verified that the background does not spoil this signal [2].

In conclusion, we computed the rates for light resonance production in relativistic peripheral heavy ion collisions. The processes considered were double photon or double pomeron fusion. The pomeron-pomeron scattering, in the case of light resonances, give cross sections at least one order of magnitude larger than the electromagnetic one. These rates are of the same order for charmed mesons, and the photon-photon production dominates for bottom mesons. In particular, these machines operating in the heavy ion mode, will be able to shed light on the existence of a σ meson with a mass near 650 MeV, observing it in the reaction $PP \to \sigma \to \gamma\gamma$, as long as the efficiency for separating the peripheral collision is not too low.

References

[1] R. N. Cahn and J. D. Jackson, Phys. Rev. D42, 3690 (1990).

[2] A. A. Natale, Mod. Phys. Lett. A9, 2075 (1994).

[3] B. Muller and A. J. Schramm, Nucl. Phys. A523, 677 (1991).

[4] A. Donnachie and P. V. Landshoff, Nucl. Phys. B244, 322 (1984); B267, 690 (1985).

[5] A. Donnachie and P. V. Landshoff, Phys. Lett. B185, 403 (1987); 207, 319 (1988); Nucl. Phys. B311, 509 (1988/89).

[6] P. Estabrooks et al., Phys. Rev. D19, 2678 (1979); N. Biswas et al., Phys. Rev. Lett. 47, 1378 (1981); T. Akesson et al., Phys. Lett. B133, 241 (1983); N. Cason et al., Phys. Rev. D28, 1586 (1983); A. Courau et al., Nucl. Phys. B271, 1 (1986); M. Svec et al., Phys. Rev. D45, 55 (1992).

Oscilações de neutrinos na matéria
no contexto de três famílias

J. Bellandi (a), M.M.Guzzo (a) e V.M.Aquino (a,b)

(a) Instituto de Física Gleb Wataghin - Unicamp, 13083-970 Campinas - SP - Brasil

(b) Universidade Estadual de Londrina, 86051-970, Londrina, Pr, Brasil

Partindo da equação de evolução temporal de um sistema de três famílias de neutrinos na presença da matéria, derivamos uma solução analítica para as amplitudes de probabilidade de transição entre sabores. Casos particulares da solução, mixing entre duas famílias a densidade de matéria constante e oscilações entre três famílias no vácuo, são obtidos a partir da solução geral.

1. Introdução

O efeito da matéria na propagação de neutrinos tem sido estudado como proposta de solução ao problema do neutrino solar. Em regime não adiabático, na maioria dos trabalhos, a probabilidade de transição é calculada utilizando-se a fórmula de Landau-Zener [1]. Uma interessante análise no contexto de duas famílias é apresentada por Palash B. Pal [22]. Em trabalho recente [3] apresentamos uma proposta alternativa para o cálculo das transições em regime não adiabático por utilização do método dos operadores exponenciais ordenados de Feynman e do método da fase estacionária. A extensão para o caso de três famílias é analisada nas referências [4] e [5]. Neste trabalho abordamos o caso da evolução do sistema a densidade de matéria constante. O caso do vácuo e o conhecido caso de mixing entre duas famílias sendo obtidos a partir da solução geral.

2. Oscilações no contexto de três famílias

Partindo da equação de evolução temporal para um sistema de três neutrinos conforme referência [5],

$$i\frac{d}{dt}\nu_f(t) = (UM^2U^{-1} + A)\nu_f(t)$$

onde:

$$\nu_f = U_{fi}\nu_i; f = e,\mu,\tau; i = 1,2,3; U = exp[i2\psi T_7]exp[i2\phi T_5]exp[i2\omega T_2]$$

ϕ, ω e ψ sendo os ângulos de mixing, A sendo a matriz de interação com a matéria, e as matrizes T_i sendo definidas a partir das matrizes de Gell-Mann λ_i por $\lambda_i = 2T_i$, definindo um novo espinor $\Psi(t)$ dado por:

$$\nu_f(t) = exp[i2\psi T_7]exp[i2\phi T_5]exp[-i\int(A3T_3 + A8T_8)d\lambda]\Psi(t)$$

sendo A3 e A8 os coeficientes da expansão da hamiltoniana do sistema em matrizes T_i, a equação de evolução em função das componentes de Ψ para um neutrino criado como eletrônico em $t_0 = 0$ pode ser resolvida efetuando-se transformações de Laplace sobre as mesmas, resolvendo para $\Psi_i(p)$ e efetuando-se as antitransformações. A solução para $\Psi(t)$ é obtida em função das raízes λ_1 λ_2 e λ_3 do polinômio característico do sistema Q(p). Apresentamos a seguir o resultado obtido para a componente eletrônica

$$\nu_e(t) = exp\left[-i\left(A0 + \frac{A3}{2} + \frac{A8}{2\sqrt{3}}\right)t\right](\cos^2\phi D11 + \cos\phi\sin\phi D13)$$
$$+ exp\left[i\left(\frac{A8}{\sqrt{3}} - A0\right)t\right](\cos\phi\sin\phi D31 + D33\sin^2\phi)$$

onde, definindo $\xi_4 = -i\frac{A4}{2}$; $B = \frac{A3}{2} + \frac{A5\sqrt{3}}{2}$ e $F(t)$:

$$F(t) = \exp\left[\frac{\lambda_1 t}{(\lambda_1 - \lambda_2)(\lambda_1 - \lambda_3)}\right] + \exp\left[\frac{\lambda_2 t}{(\lambda_2 - \lambda_1)(\lambda_2 - \lambda_3)}\right] + \exp\left[\frac{\lambda_3 t}{(\lambda_1 - \lambda_3)(\lambda_2 - \lambda_3)}\right]$$

os coeficientes Dij serão

$$D11 = F''(t) - i(A3 + B)F'(t) - A3BF(t); D13 = \xi_4(F'(t) - iA3F(t))$$

$$D31 = \xi_4 \int \exp[-1B\lambda]D11(\lambda)d\lambda; D33 = 1 + \xi_4 \int \exp[-1B\lambda]D13(\lambda)d\lambda$$

3. Análise dos resultados

A partir da solução obtida e da forma explícita das raízes do polinômio $Q(p)$ uma análise numérica desta solução pode ser efetuada. A obtenção de quantidades como angulos de mixing na matéria $\dot{o}$, $\dot{\omega}$ e as corretas condições de ressonância não podendo no entanto ser efetuadas diretamente. Em algumas situações particulares no entanto. (onde o polinômio $Q(p)$ pode ser fatorado), tal análise pode ser efetuada algebricamente. Assim ocorre no caso do vácuo e no caso em que $\psi = \dot{o} = 0$ onde os conhecidos resultados de mixing entre duas famílias $(\nu_e.\nu_\mu)$ são recuperados.

Referências

1. C.Zener, Proc. R. Soc. London A137, 696 (1932); L. Landau. Phys. Z. Sow. 2, 46 (1932).
2. Palash B. Pal, International Journal of Modern Physiscs A. Vol 7, N 22 (1992).
3. M. M. Guzzo, J. Bellandi e V. M. Aquino, Phys. Rev. D, 49. 1404 (1994).
4. V. Barger and K. Whisnant, Physical Rev. D. Vol 22, N 11 (1980).
5. T.K.Kuo and James Pantaleone. Physical Review D. Vol 35, N 11 (1987).

Vínculos aos Leptoquarks Escalares a partir dos Dados do LEP

O. J. P. Éboli, J. K. Mizukoshi

Instituto de Física, Universidade de São Paulo
Caixa Postal 20516, 01452-990 São Paulo, Brazil

M. C. Gonzales-Garcia

Theory Division, CERN, CH-1211 Geneva 23, Switzerland

Embora o Modelo Padrão (MP) das interações eletrofracas descreva com grande sucesso os fenômenos de origem eletrofraca, ele não explica algumas questões, tais como o número de gerações fermionicas, bem como o mecanismo para a geração de massa aos férmions e bósons de gauge. Além disso, o MP não apresenta uma estrutura muito elegante para descrever a fenomenologia, pois contém muitos parametros livres. Com isto, foram propostos extensões a este modelo, como a teoria grande unificada (GUT), o $SU(4)$ e os modelos compostos. Nestes modelos, existem campos bosônicos que mediam as transições entre léptons e quarks, os chamados leptoquarks.

As procuras diretas dos sinais dos leptoquarks escalares em aceleradores estabeleceram limites inferiores para as suas massas. Nas experiências realizadas no Large Electron-Positron (LEP) do CERN, o limite é de $M_{LQ} \geq$ 45 - 73 GeV, dependendo do tipo de leptoquark. Neste artigo vamos estudar os vínculos vindos das contribuições das correções radiativas da física do Z ao leptoquark escalar singleto, com acoplamento "right". Calculamos os parâmetros S, T e U e as correções radiativas em um loop para o vértice $Z \to e\bar{e}$.

A lagrangiana mais geral que exibe a simetria $SU(3)_C \otimes SU(2)_L \otimes U(1)_Y$, com as conservações dos números bariônico (B) e leptônico (L), da carga e cor, é dada por

$$\mathcal{L} = g_{1R}\bar{u}^c_R e_R S_1 + (D^\mu S_1)^\dagger D_\mu S_1 - M_{LQ}^2 S_1{}^\dagger S_1 \tag{1}$$

com

$$D_\mu S_1 = (\partial_\mu + ie\frac{s_W}{c_W}Q^\gamma Z_\mu + ieQ^\gamma A_\mu)S_1 \tag{2}$$

onde u_R e e_R denotam os campos singletos do quark e do lépton, respectivamente , $f^c = Cf^T$ denota o campo conjugado de carga e Q^γ é a unidade de carga elétrica. Por simplicidade, os índices de cor e família foram suprimidos.

A parte que contribui para as correções oblíquas é originada exclusivamente do segundo termo em (1). Fazendo os cálculos, obtemos $S = T = U = 0$. Como o resultado obtido está dentro dos limites experimentais permitidos para o MP, nós não conseguimos impor vínculos restritivos para a massa do leptoquark através das correções oblíquas.

O próximo passo consiste em calcular as correções de vértice para o processo $Z \to e\bar{e}$. O leptoquark dá origem às contribuições não universais para ρ_f e κ_f, parametrizados por

$$\Delta\rho_{non}^{LQ} = -\frac{\Gamma_{LQ}(M_Z^2)}{a_f} . \tag{3}$$

$$\Delta\kappa_{non}^{LQ} = -\frac{1}{2s_W^2 Q^J}(1 + \frac{v_J}{a_J})F_{LQ}(M_Z^2) .$$ (4)

com

$$
\begin{aligned}
F_{LQ}^Z(M_Z^2) =\ & \frac{g_{1R}^2}{16\pi^2}N_C\Big\{ m_u^2 g_R^2 C_0(0, M_Z^2, 0, M_{LQ}^2, m_u^2, m_u^2)\\
& +g_L^u\Big[(2-D)C_{00}(0, M_Z^2, 0, M_{LQ}^2, m_u^2, m_u^2)\\
& +M_Z^2 C_{12}(0, M_Z^2, 0, M_{LQ}^2, m_u^2, m_u^2)\Big]\\
& +2\frac{s_W}{c_W}Q^\gamma C_{00}(0, M_Z^2, 0, m_u^2, M_{LQ}^2, M_{LQ}^2) + g_L^e B_1(0, m_u^2, M_{LQ}^2)\Big\} .
\end{aligned}
$$

onde nós usamos a regularização dimensional ($D = 4 - \epsilon$) para calcularmos as integrais dos loops. B_1, C_0, C_{00} e C_{12} são os coeficientes de Passarino-Veltman e $g_{L/R}^f = v^f \mp a^f$, onde os acoplamentos axial e vetorial de corrente neutra são dados por $a^f = I_3^f$ e $v^f = I_3^f - 2Q^\gamma s_W^2$. Antes de prosseguirmos com o fitting dos dados do LEP, temos que calcular as correções para o vértice eletromagnético, com o intuito de verificar se o leptoquark modifica a carga elétrica no acoplamento.

Para calcular o vértice $\gamma - e\bar{e}$, basta fazermos $M_Z^2 - q^2$, $g_L = g_R - -Q^\gamma$ e $\frac{s_W}{c_W}Q^\gamma - Q^\gamma$. Nós obtemos que no limite $q^2 - 0$, a contribuição do leptoquark para este vértice é nula, o que significa que a carga elétrica não é alterada com a inclusão do leptoquark na teoria.

Tendo em vista que a contribuição do vértice $\gamma - e\bar{e}$ é nula, podemos nos concentrar nas expressões (3) e (4), que podem dar vínculos para a constante de acoplamento g_{1R} e a massa do leptoquark, já que tanto $\Delta\rho_{non}$ como $\Delta\kappa_{non}$ estão relacionados com as assimetrias no pico do Z.

Nós analisamos o caso em que o leptoquark se acopla com a terceira geração de férmions, portanto com a contribuição do quark top nos loops. Impondo que o acoplamento férmion-leptoquark seja do tipo eletromagnético ($g_{1R} = \frac{e}{s_W}$), nós obtemos o limite inferior $M_{LQ} \geq 350$ GeV, com 90 % C.L. para o top com a massa $m_t = 174$ GeV e o Higgs com $M_H = 250$ GeV. Verifica-se portanto que as correções radiativas deram vínculos mais restritivos do que a procura direta dos leptoquarks nos aceleradores.

REFERÊNCIA

O. J. P. Éboli, M. C. Gonzalez-Garcia e J. K. Mizukoshi, preprint CERN-TH.7508/94, IFUSP-P 1129.

Vínculos de Lagrangianas Efetivas
à Partir de Correções Oblíquas

A. Brunstein, M. B. Magro, P. G. Mercadante

Instituto de Física, Universidade de São Paulo

Caixa Postal 20516, 01452-990 São Paulo, Brazil

Denominamos correções oblíquas as correções de auto-energia dos propagadores dos bósons de gauge. Essas correções podem fornecer-nos vínculos para novos acoplamentos que eventualmente caracterizem uma Nova Física além do Modelo Padrão. Uma maneira de parametrizar os possíveis desvios em relação ao Modelo Padrão é através dos parâmetros S,T e U [1], que podem ser associados com os observáveis físicos Δr, $\Delta \rho$, Δk e Δn. Assim, comparando os dados experimentais com as predições do Modelo Padrão, podemos impor vínculos para a contribuição da Nova Física.

Um modo de estudarmos os efeitos de novos acoplamentos além do Modelo Padrão é a utilização de teorias efetivas, onde construímos operadores de dimensão 4 invariantes por $SU(2)_L \odot U(1)_Y$ e por CP. Essas teorias podem ser realizadas de forma linear ou não-linear no que diz respeito às transformações dos campos considerados. Nesse trabalho utilizamos o formalismo de realizações não-lineares e nos restringimos ao setor bosonico da teoria eletrofraca. Denominamos as lagrangianas construídas dessa forma de lagrangianas quirais.

Calculamos S, T e U para os operadores efetivos descritos em [2] e detalharemos o cálculo para o caso de $\mathcal{L}_6$

$$\mathcal{L}_6 = \alpha_6 Tr(V_\mu V_\mu) Tr(T V^\mu) Tr(T V^\nu) \ .$$

onde

$$T = U\tau_3 U^\dagger \ ;$$
$$V_\mu = (D_\mu U)U^\dagger \ ;$$
$$D_\mu U = \partial_\mu U - g W_\mu U + g' U B_\mu \ .$$

com as definições

$$\hat{W}_\mu = \frac{1}{2i}\vec{W}_\mu \vec{\tau} \ ;$$
$$\hat{B}_\mu = \frac{1}{2i}B_\mu \tau^3 \ .$$

que produz os vértices W^+W^-ZZ e $ZZZZ$ com as respectivas regras de Feynman

$$\frac{ig^4}{128c_w^2}2(g^{\alpha\mu}g^{\beta\nu} + g^{\alpha\nu}g^{\beta\nu}) \ ;$$

$$\frac{ig'^4}{128s_w^4}8(g^{\mu\nu}g^{\alpha\beta} + g^{\mu\alpha}g^{\nu\beta} + g^{\mu\beta}g^{\alpha\nu}) \ .$$

Estamos interessados na obtenção de vínculos para estes novos acoplamentos. Como estes são acoplamentos quárticos, ainda não é possível testá-los diretamente a nível de árvore. Temos então que olhar para uma ordem acima a fim de podermos calcular os efeitos destes novos acoplamentos no Modelo Padrão. Olhamos então para as correções radiativas dos propagadores do W e do Z, que a priori geram os vínculos pretendidos.

Assim, escrevemos explicitamente a contribuição de cada loop

$$-i\Sigma_{ZZ}^{(Z)} = \frac{-ig^4 4M_Z^2}{128c_w^4(4\pi)^2}\left(-\frac{9}{2}\ln\frac{\Lambda^2}{M_Z^2} + 2\frac{\Lambda^2}{M_Z^2} + \frac{\Lambda^4}{M_Z^4} + \frac{9}{4}\right) ;$$

$$-i\Sigma_{ZZ}^{(W)} = \frac{-ig^4}{128c_w^4(4\pi)^2}\left(-3\ln\frac{\Lambda^2}{M_W^2} + 2\frac{\Lambda^2}{M_W^2} + 2\frac{\Lambda^4}{M_W^4} + \frac{1}{4}\right) ;$$

$$-i\Sigma_{WW}^{(Z)} = \frac{-ig^4}{128c_w^4 2(4\pi)^2}\left(-3\ln\frac{\Lambda^2}{M_Z^2} + 2\frac{\Lambda^2}{M_Z^2} + 2\frac{\Lambda^4}{M_Z^4} + \frac{1}{4}\right) ,$$

onde Λ é a escala da nova física.

No entanto, quando calculamos as funções renormalizadas [1], não obtivemos o cancelamento das divergências quadráticas e quárticas, conforme esperávamos. Essas divergências também aparecerão no cálculo dos observáveis físicos, e não soubemos ainda interpretar esse resultado coerentemente. Alguns autores [3] afirmam que as divergências quadráticas remanescentes são absorvidas na renormalização do acoplamento do W, ou, equivalentemente, na renormalização da constante de Fermi, G_F.

References

[1] B. A. Kniehl e H. G. Kohrs, Phys. Rev. D48 (1993) 225.

[2] T. Appelquist e G. Wu, Phys. Rev. D48 (1993) 3235.

[3] K. Hagiwara, S. Ishihara, R. Szalapski e D. Zeppenfeld, Phys. Lett. B283 (1992) 353, Phys. Rev. D48 (1993) 2182.

Color transparency and nuclear sahdowing

A. G. Grunfeld

Departamento de Física, Fac. de Cs. Ex.. Universidad
Nacional de La Plata. La Plata. Argentina

In a recent work (D.Kharzeev and H.Satz, Phys. Lett. B 327. 361 (1994)) it has been shown that shadowing effects observed in hadron and photon interactions with nuclei are due to quantum-mechanical coherence and interference. For $q\bar{q}$ production on nuclear targets, this model allows to estimate nuclear cross-sections in a direct way.

In the present work this procedure has been used in order to compute cross-sections corresponding to $c\bar{c}$-nucleon interactions for a range of photon energies and nuclear targets.

The model describes the relation between

$$\sigma(\gamma A \longrightarrow q\bar{q})$$

and

$$A\sigma(\gamma N \longrightarrow q\bar{q})$$

in terms of the size of coherence Z_c relative to nuclear parameters as the mean free path λ of the $q\bar{q}$ fluctuation. the average internucleonic distance d and the uniform-equivalent volume nucleus radious R, for the regimes of shadowing, antishadowing, incoherence and vector meson dominance.

The basic quantity to study is the transparency ratio

$$T_n(X_t) = \frac{\sigma(\gamma A \longrightarrow q\bar{q})}{A\sigma(\gamma p \longrightarrow q\bar{q})}$$

in the regimes mentioned above.

In the VMD. shadowing and antishadowing regions T_n is expressed in terms of x_t, m_p (proton mass) and λ. To estimate the value of λ

$$\lambda = \frac{d^3}{\sigma}$$

it is necessary to calculate the cross-section for the interaction of the virtual system on nucleons.

σ was computed taking into acount the behaviour

$$\sigma(\rho) \approx C\rho^2$$

$$C = \frac{\sigma(J/\Psi N)}{<\rho^2>_{J/\Psi}}$$

($\rho =$ transverse separation of $c\bar{c}$)

In the case of VMD, the transparency rate was calculated for nuclear targets of Be. Fe and Pb and the results are:

$$Be \quad T_n = 40$$
$$Fe \quad T_n = 9.6$$
$$Pb \quad T_n = 4.26$$

These results are in contradiction with the model, because in this regime T_n must be a constant less than one. If this condition is imposed by hand, the value obtained for σ does not obey the quadratic behaviour shown above, which is a fundamental property of Color Transparency.

In conclusion, the present results seems to indicate that there exists an internal inconsistency in the starting model. The origin of this contradiction is not clear yet. We are currently working on this subject.

ϵ_b Constraints on Self–Couplings of Vector Bosons

O. J. P. Éboli, S. M. Lietti

Instituto de Física, Universidade de São Paulo,

C.P. 20516, 01452-990 São Paulo, Brazil

M. C. Gonzalez-Garcia

Physics Department, University of Wisconsin.

Madison, Wisconsin 53706, USA

S. F. Novaes

Instituto de Física Teórica, Universidade Estadual Paulista,

Rua Pamplona 145, 01405-900 São Paulo, Brazil.

We analyze the constraints on possible anomalous contributions to the W^+W^-Z vertex coming from non-universal radiative corrections to the $Z - b\bar{b}$ width. We parametrize these corrections in terms of ϵ_b and use the LEP data to establish the allowed values for the anomalous triple couplings.

The Standard Model (SM) of electroweak interactions has so far explained extremely well all the available experimental measurements. However, some elements of the SM, such as the symmetry breaking mechanism and the interaction among the gauge-bosons, have not been object of direct experimental observation yet.

One of the main goals of LEP II at CERN will be the investigation of the reaction $e^+e^- \to W^+W^-$, which can furnish direct bounds on anomalous $W^+W^-\gamma$ and W^+W^-Z interactions.

Other valuable indirect sources of information on anomalous interactions are the low energy data and the results of LEP, which can also constrain substantially the possible deviations of the gauge boson self-interactions from the SM predictions through their contribution to the electroweak radiative corrections.

In this work we concentrate on non–universal effects due to the non-vanishing masses of the virtual particles running in the loop corrections to vertices. These non–universal contributions to the $Zb\bar{b}$ couplings have been parametrized in a model independent way in terms of the parameter ϵ_b, which is defined as

$$\epsilon_b = \frac{g_A^b}{g_A^\ell} - 1 \, ,$$

where g_A^b (g_A^ℓ) is the axial coupling of the Z to the pair $b\bar{b}$ ($\ell\bar{\ell}$).

The most general polynomial CP conserving and Lorentz invariant structure of the W^+W^-Z vertex is associated to the effective Lagrangian,

$$\mathcal{L}_{eff}^{WWZ} = -ie\frac{c_W}{s_W}\left[g_1^Z(W_{\mu\nu}^+W^{-\mu} - W_{\mu\nu}^-W^{+\mu})Z^\nu + \kappa_Z W_\mu^+ W_\nu^- Z^{\mu\nu} + \frac{\lambda_Z}{m_W^2}W_\mu^{+\nu}W_\nu^{-\rho}Z_\rho^\mu \right] \tag{1}$$

with $s_W(c_W) = \sin(\cos)\theta_W$ and $g = e/s_W$. The terms in Eq. (1) are C and P invariant.

We will concentrate on terms that conserve CP since the contribution of CP violating interactions to the decay width $Z - b\bar{b}$ is suppressed by powers of m_b^2/M_W^2.

The effects of the anomalous couplings are related to the quantities Δg_1^Z, $\Delta\kappa_Z$ and λ_Z, and their respective standard model values are

$$\begin{aligned}
\Delta g_1^Z &= g_1^Z - 1 = 0 \, , \\
\Delta\kappa_Z &= \kappa_Z - 1 = 0 \, , \\
\lambda_Z &= 0 \, .
\end{aligned} \tag{2}$$

We are now in position to evaluate the non-universal contributions to the decay width $Z \to f_i \bar{f}_i$ associated to the anomalous interactions described above. As a consequence of the V-A structure of the W coupling to fermions, this anomalous amplitude also presents this structure. Neglecting the external fermion masses, can be written as

$$\Gamma^\mu_{ANO}(Zf\bar{f}) = i\frac{e}{4 s_W c_W} \sum_i V_{ij} V^\dagger_{ij} F(m_j)\gamma^\mu(1 - \gamma^5) ,$$ (3)

where $V_{ij} = \delta_{ij}$ for leptons and it is the Cabibbo-Kobayashi-Maskawa mixing matrix for quarks. Neglecting the mixings V_{tj} ($j = 1, 2$) and all the internal fermions masses but m_{top}, it is clear that this amplitude will be equal for all final fermions except for the b-quark. The universal part, $F(0)$, affects the values of $\Delta\rho$ and $\sin\bar\theta_W$. Non-universal effects appear in the $Z \to b\bar{b}$ width and they can be parametrized by the parameter ϵ_b which takes the form

$$\epsilon_b = \Delta F \equiv [F(m_{top}) - F(0)] .$$

The anomalous interactions give rise to new contributions to ϵ_b, in addition to the SM ones (ϵ_b^{SM}), that are given, in terms of the anomalous couplings (2) by

$$\epsilon_b - \epsilon_b^{SM} = \Delta\kappa_Z \Delta F_{\kappa_Z} + \Delta g_1^Z \Delta F_{g_1^Z} + \lambda_Z \Delta F_{\lambda_Z}$$ (4)

where the form factors are given by

$$\Delta F_{\kappa_z} = -\frac{g^2 c_W^2}{16\pi^2} \left\{ \frac{zt}{4w^2}[1 + B_0(z, w, w)] + 2[B_0(0, 0, w) - B_0(0, t, w)] \right.$$

$$+ \frac{t(t - w)}{2w^2}[B_0(z, w, w) - B_0(0, t, w)] - 2w[C_0(0, z, 0, t, w, w) - C_0(0, z, 0, 0, w, w)]$$

$$\left. + t\left[\frac{(t - w)^2 + tz - 2zw + 4w^2}{2w^2}\right] C_0(0, z, 0, t, w, w) \right\} ,$$ (5)

$$\Delta F_{g_1^Z} = -\frac{g^2 c_W^2}{16\pi^2} \left\{ -\frac{t}{2w} + \frac{3t}{2w} B_0(z, w, w) + 2\left(1 + \frac{w}{z}\right)[B_0(0, 0, w) - B_0(0, t, w)] \right.$$

$$+ 2\frac{t}{w}\left(1 \div \frac{t + w}{2z}\right)[B_0(0, t, w) - B_0(z, w, w)] + 2w\left(1 + \frac{w}{z}\right) C_0(0, z, 0, 0, w, w)$$ (6)

$$\left. - \left[2\frac{(t - w)^2 + tz + wz}{z} + \frac{t}{w}\frac{(t - w)^2 + tz - 2wz + z^2}{z}\right] C_0(0, z, 0, t, w, w) \right\} ,$$

$$\Delta F_{\lambda_z} = -\frac{g^2 c_W^2}{16\pi^2 w}\{2w[B_0(0, 0, w) - B_0(0, t, w)] + (2w - z)t\, C_0(0, z, 0, t, w, w)$$

$$- 2w^2[C_0(0, z, 0, t, w, w) - C_0(0, z, 0, 0, w, w)]\} .$$ (7)

B_0 and C_0 are the Passarino-Veltman two and three-point functions respectively. We used the short hand notation $z = m_Z^2$, $w = m_W^2$, and $t = m_{top}^2$. The Passarino-Veltman two-point functions are divergent and were evaluated using dimensional regularization that is a gauge-invariant regularization scheme. The above expressions have poles only in $d = 4$ dimensions that are identified with the logarithmic dependence on the cutoff, i.e.,

$$\frac{2}{4 - d} - \gamma_E + \ln(4\pi) + 1 = \ln\frac{\Lambda^2}{\mu^2} .$$ (8)

The form factor ΔF_{λ_z} is independent of the cutoff while the others have a logarithmic dependence of the form

$$\Delta F_{\kappa_z} = -\frac{g^2 c_W^2}{64\pi^2}\frac{zt}{w^2}\ln\frac{\Lambda^2}{w} ,$$

$$\Delta F_{g_1^Z} = -\frac{3g^2 c_W^2}{32\pi^2}\frac{t}{w}\ln\frac{\Lambda^2}{w} .$$

In order to obtain the bounds on the anomalous triple gauge-boson vertices, we evaluated these form factors as a function of m_{top}, neglecting all other fermion masses. Our results are shown in Table 1 which also contains the SM prediction for ϵ_b.

m_{top}	$c_b^{SM} \times 10^3$	$\Delta F_{\kappa_z} \times 10^3$	$\Delta F_{g_1^z} \times 10^3$	$\Delta F_{\lambda_z} \times 10^3$
125	−2.82	−7.43	−27.98	−1.68
150	−4.88	−9.94	−36.93	−2.10
175	−7.13	−12.62	−46.26	−2.51
200	−9.79	−15.41	−55.77	−2.90
225	−12.80	−18.29	−65.33	−3.26

Table 1: SM model predictions for c_b and anomalous form factors as a function of m_{top}, assuming $\Lambda = 1$ TeV.

m_{top}	$\Delta\kappa_z$	Δg_1^z	λ_z
125	(−1.4, 0.43)	(−0.38, 0.11)	(−6.3, 1.9)
150	(−1.3, 0.11)	(−0.34, 0.030)	(−6.0, 0.53)
175	(−1.2, −0.091)	(−0.32, −0.025)	(−6.0, −0.46)
200	(−1.1, −0.25)	(−0.32, −0.068)	(−6.1, −1.3)
225	(−1.1, −0.37)	(−0.32, −0.10)	(−6.3, −2.1)

Table 2: 90 % CL limits on the anomalous couplings, assuming $\Lambda = 1$ TeV.

An analysis of the available LEP and SLC data in terms of the oblique parameters ϵ_i ($i = 1, 2, 3$) and c_b has been performed in the literature, which led to

$$c_b = (0.9 \pm 4.2) \times 10^{-3} .\tag{9}$$

This experimental result together with Eq. (4) and Table 1 can be used to constrain the "blind" directions of the low-energy effective Lagrangian. We list in Table 2 the bounds at 90% CL obtained for the parameters g_1^z, κ_z, λ_z.

At this point it is worth comparing our results with the bounds obtained from the universal radiative corrections, which can be found in the literature. A crude comparison shows that our constraints are comparable to the universal bounds for g_1^z and κ_z. Moreover, our results for λ_z, are of the same order for a heavy top after considering the strong correlation existing in the universal constraints.

For more details and references see:

O. J. P. Éboli, S. M. Lietti, M. C. Gonzalez-Garcia and S. F. Novaes. Phys. Lett. **B339** (1994) 119-126.

Elastic proton-proton scattering
and complex parton-parton amplitude

A.F. Martini and M.J. Menon

Instituto de Física 'Gleb Wataghin'. Unicamp

13083-970 Campinas. São Paulo. Brasil

Starting from a simple phenomenological relation between real and imaginary parts of the elementary (parton-parton) amplitude, improvements in an eikonal approach to elastic hadron scattering is presented. It is shown that the model reproduces the pp differential cross section data at ISR energies.

In the Glauber's Multiple Diffraction Theory the scattering amplitude between two hadrons. F_{AB}. is connected with the form factors, G_A and G_B and the elementary parton-parton amplitude, f, through the well known formulas [1]

$$F_{AB} = i \int b \, db \, J_0(qb)[1 - e^{-\Omega(b,s)}] \equiv i < 1 - e^{-\Omega(b,s)} > . \qquad \Omega(b,s) = C < G_A G_B f > . \qquad (1)$$

where C is transferred momentum independent. In a diffractive model to elastic hadron scattering the following choices have been used [2]:

$$G_j = [(1 + q^2/\alpha_j^2)(1 + q^2/\beta_j^2)]^{-1}. \quad j = A. B. \quad f = [1 - q^2/a^2]/[1 + q^4/a^4]. \qquad (2)$$

In this model the eikonal is purelly imaginary, $\chi = i\Omega$, so that the amplitude F_{AB} is purelly imaginary too. In the original formulation the real part of F_{AB} is estimated through the Martin's prescription.

$$\frac{d\sigma}{dt} = \{\phi^2(q,s) + \rho^2(s)[\frac{d}{dt}[t\phi(q,s)]]^2\}.$$

with $\phi(q,s) = F_{AB}(q,s)/F_{AB}(0,s)$ and where ρ is the ratio of the real to the imaginary part of the forward elastic scattering amplitude. With the experimental ρ-value at each energy as input. elastic pp scattering may be well described at ISR energies with the following values and dependences for the free parameters [3]:

$$\alpha^2 = 0.42 \; GeV^2. \qquad a^2 = 0.483 + 0.124[lns]^2 \; (GeV^2),$$

$$\beta^2 = 1.80 \; GeV^2, \qquad C(s) = 7.814 + 0.0518[lns]^2 \; (GeV^{-2}). \qquad (3)$$

However Martin's formula has limited validity [4] and also the ρ-parameter can not be predicted since it is an input variable at each energy. In order to avoid the use of this prescription we introduced a complex elementary amplitude through a very simple anzats:

$$\frac{1 - q^2/a^2}{1 + q^4/a^4} \equiv Im\{f(q,s)\}, \qquad Re\{f(q,s)\} \equiv \lambda(s)Im\{f(q,s)\}, \tag{4}$$

where $\lambda(s)$ is a free parameter to be determined at each energy. With (1) to (4) the differential cross section may be calculated by $d\sigma/dq^2 = \pi|F_{AB}(q,s)|^2$. Fitting to pp at $\sqrt{s} = 53$ GeV reproduces the same result as that obtained with the Martin's prescription for $\lambda = 0.055$, as can be seen in Figures 1 and 2. Attempts to reproduce the results with the Martin's prescription in the ISR energies have lead to the following preliminary parametrization:

$$\lambda(s) = -0.04829 + 0.01262[lns]. \tag{5}$$

With this we have a complet predictive formalism. Figure 3 shows the comparison of the predictions through (1) to (5) and experimental data at all ISR energies.
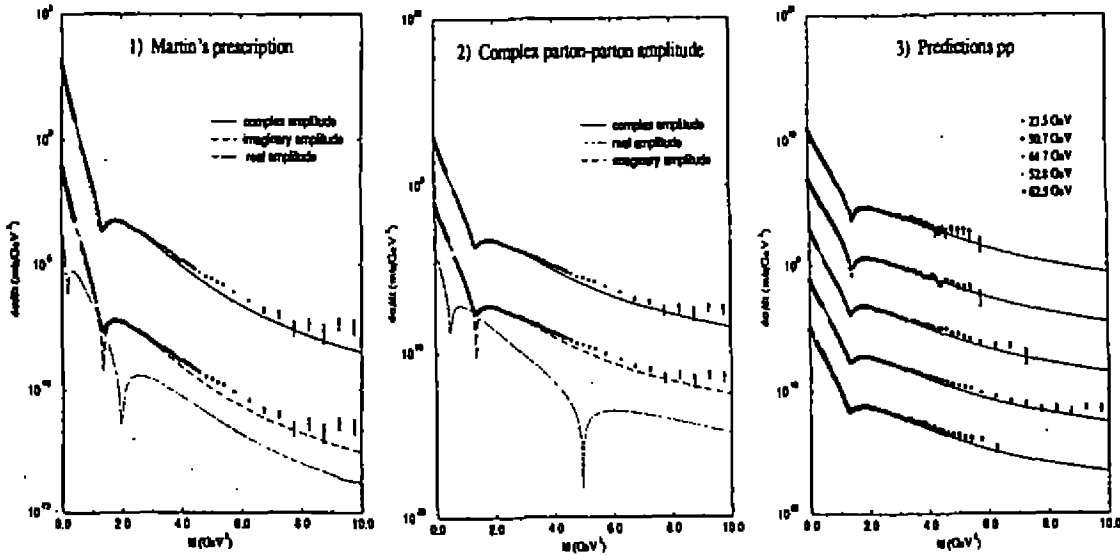
References

1. M.J. Menon, Phys. Rev. D48 (1993) 2007.

2. M.J. Menon and B.M. Pimentel,Hadronic J. 16 (1993) 137; M.J. Menon, Nucl. Phys. B (Prooc. Supp.)B25 (1992) 94.

3. M.J. Menon, Proc. Vth Int. Conf. on Elastic and Diffractive Scattering (World Scientific, Singapore, 1994) 188.

4. R. Henzi and P. Valin, Phys. Lett. B149 (1984) 239.

A Single Quark Effective Potential Model

B. E. J. Bodmann*, M. Dillig**, C. A. Z. Vasconcellos*

*Instituto de Física, UFRGS, Porto Alegre, Brazil

**Institut für Theoretische Physik III, FAU, Erlangen, Germany

In the present work we construct a radial spherical symmetric single quark potential model for the nucleon, consistent with asymptotic freedom and confinement. The quark mass enters as a potential parameter and that way induces indirectly an isospin dependence in the interaction. As a consequence, a contribution to the negative charge square radius of the neutron arises as an effect of the quark core, which simulates an isospin symmetry breaking effect in the nucleon due to strong interaction.

Our Lagrangian is represented by a massless fermion field (the quark field), which has to be extended by a vector potential, according to local $U(1)$-invariance. The massless Lagrangian however is symmetric under chiral transformation, which is known to be an approximate symmetry in spite of the u and d mass difference being small on the typical strong interaction scale. Various models of the nucleon based on chiral symmetry violation on the quark level (c.f. [1] and refs. therein), result in quantitative agreement with experimental results, such as electromagnetic form factors, for instance. Thus we take chiral symmetry and its violation on the quark level as a guiding principle to construct the "complete" model-Lagrangian.

We choose the chiral group in its simplest form, i.e. isospin representation. The generators can be associated with isospin raising, isospin lowering and the third component of the isospin axial vector current, respectively. In our case, we regard isospin symmetry as an approximate one only, with symmetry breaking due to the possible mass difference $m_u - m_d \neq 0$. In order to violate chiral symmetry explicitly, we introduce a scalar term into our Lagrangian, which contains Lorentz scalar and vector potentials. The scalar potential is of the same order in magnitude as the vector potential, to combine the success of nonrelativistic quark models with a relativistic one. To be more specific, we use the approximation $\gamma^\mu V_\mu \to \gamma^\mu \delta^0_\mu V_0$, with $V_0 = U$, with U a Lorentz scalar, such that we gain an equally mixed scalar vector potential $\gamma^\mu V_\mu + U \to (1 + \gamma^0) V$. Further we introduce a mass term, which shifts the mixture between the scalar and vector potential contribution and leads to a different "overall effect" in the upper and lower component. The mass thus appears as a potential parameter. In this way the effective potential acts dominantly on the upper component of the spinor, and this way reduces in the nonrelativistic limit and for $m_q \to M_q \approx \frac{M_N}{3}$, to a nonrelativistic description. In the present work we do not discuss the Lagrangian in its complete (i.e. approximate chiral symmetric) beauty, but restrict our present discussion to the possible role of the quark mass as a potential parameter in a relativistic model.

To get a convenient potential, we use the relation between a modulation function and a potential as shown in ref. [1]. The spinor wavefunction in the Dirac equation is taken to be a product of the free quark spinor q and a modulation amplitude $\sqrt{F}$, which modulates the quark wavefunction and is determined by physical boundary conditions. F in general exhibits a space-time dependence. The relation between the modulation function F and the potential V in our spherical symmetric and static approximation is taken to be $V = -\frac{1}{2} \frac{d}{dr} \ln F$ (c.f. refs. [1], [2]). In order to define the potential we use the phenomenological behavior of asymptotic freedom $F \to 1$ as $r \to 0$ and introduce confinement tentatively via $F^{(n)} \to 0$ as $r \to \infty$. For convenience we take the simplest solution, which seems to be appropriate for our purpose, that is a solution to the above cited relation including the boundary

conditions yielding: $V = G(r)r^2$ with $V = 2\hbar c \frac{r^3}{r^4-R_q^4}$, where G represents a variable coupling constant of the harmonic oscillator potential. The variable R_q represents an expansion parameter, which depends on the energy eigenvalue and the quark mass.

The Dirac equation for the upper and lower components ϕ and χ then reads

$$(\underline{\sigma} \cdot \underline{p})\chi + (m_q + 2V)\phi = E_q\phi, \qquad (\underline{\sigma} \cdot \underline{p})\phi - m_q\chi = E_q\chi.$$

After separation of the angular part of the Dirac equation, there remain the differential equations for the upper and lower radial components g_κ and f_κ,

$$f_\kappa = \frac{\hbar c}{E_q + m_q c^2}\left[\frac{dg_\kappa}{dr} + \frac{\kappa+1}{r}g_\kappa\right], \qquad 0 = \left(\frac{d^2}{dr^2} - \frac{\epsilon_K}{r^2} - \frac{\epsilon_V r^{2n-1}}{r^{2n}-R_q^{2n}} + \epsilon_E\right)(rg_\kappa(r)) \qquad (1)$$

with κ being the eigenvalues of the invariant quantity $K = \gamma_0(\underline{\Sigma}\cdot\underline{l}+1)$ and the abbreviations $\epsilon_V = \frac{2n(E_q+m_qc^2)}{\hbar c}$, $\epsilon_E = \frac{E_q^2-(m_qc^2)^2}{\hbar^2c^2}$, $\epsilon_K = \kappa(\kappa+1)$. In order to fix the expansion parameter R_q, we set the second derivative of the wave function to a minimum in analogy to the phenomenology of potential scattering and obtain:

$$R_q = 3\frac{\hbar c}{E_q - 3m_qc^2}\left[-1 + \sqrt{1 + \frac{2}{9}(\epsilon_\kappa + 6)\frac{E_q - 3m_qc^2}{E_q + m_qc^2}}\right]. \qquad (2)$$

This formula has physical solutions for $E_q > 3m_qc^2$ only. A simultaneous solution of equation (1) and (2) yields the values for $R_q \approx 1fm$ (R_q seems to be constant even for $|\kappa| > 1$) and the energy eigenvalues for $\kappa = -1$: $E_{-1}^u \approx 300MeV$ and $E_{-1}^d \approx 310MeV$ with $\Delta m = 3MeV$ (c.f. ref. [2]). It should be mentioned, that equation (1), with the simplest form of a potential leads to normalization problems, which is clearly a consequence of the static approximation with expansion at $r = R_q$. However if time dependence is taken into account, it can be shown that R_q is related to a "natural cutoff" (a future paper, in preparation). To demonstrate the effect of the quark mass dependence, we calculate the charge square radius for the proton and neutron, taking into account the quark core only (i.e. $0 \leq r < R_q$).

$$\langle r^2\rangle_p = 0.53fm^2 < 0.74fm^2 \ (exp.) \qquad \langle r^2\rangle_n = -0.04fm^2 > -0.12fm^2 \ (exp.)$$

For exact isospin symmetry the expression $\langle r^2\rangle_n$ is zero as expected, or in turn the negative sign appears as a consequence of isospin symmetry breaking (compare ref. [3]).

We demonstrated, that with a potential model of the kind proposed, even a small isospin symmetry breaking, in our case we used $\frac{2\Delta m}{m_u+m_d} \approx 0.05$, can lead to a negative sign of the charge square radius for the neutron. This property is a consequence of the quark mass, which enters as a parameter into the potential and thus induces indirectly a small isospin symmetry breaking. Finally the question arises: Can the experimental fact of the negative charge square radius of the neutron be understood in terms of "proper" isospin breaking?

References

1. H.T. Coelho et al. *Current Topics in Nuclear Physics and Quantum Field Theory* ed. D. Dillenburg et al., Editora da Universidade UFRGS, Porto Alegre, Brasil (1994) 241

2. B.E.J. Bodmann, C.A.Z. Vasconcellos, M. Dillig *in Proceedings of the* HADRON 94 *Conference*, ed. C.A.Z. Vasconcellos et al., World Scientific (1994)

3. S. Théberge et al. *Can. J. Phys.* 60 (1982) 59.

Oblique corrections in a model with neutrino masses and strong CP resolution

A. A. Natale and P. S. Rodrigues da Silva

Instituto de Física Teórica, Universidade Estadual Paulista
Rua Pamplona, 145, 01405, São Paulo, SP. Brazil

There has been recently some interest on the implications of one loop corrections due to majorana particles on the electroweak measurements [1, 2, 3]. Most of this interest was focused on the consequences of the Hill and Paschos model [4], where it is introduced a fourth generation of leptons, which accomodates a heavy neutral member with a majorana mass of $O(G_\mu^{-1/2})$, and where the light neutrinos obtain small masses through the see-saw mechanism. Computing the oblique corrections for such a model, it was verified that a heavy majorana neutrino in the third generation decouples from electroweak physics and cannot be excluded experimentally [3].

The one-loop corrections in these type of models have been parametrized in terms of the heavy (or fourth generation) charged lepton mass, and of the light and heavy neutrino mass eigenstates (see, for instance, Refs. [2, 3]), and they show some intricate behavior as these masses are variated [2]. Although the introduction of a new generation is phenomenologically attractive [5], there is a much wider class of models, where we have majorana neutrinos without the company of the fourth generation charged lepton, and where we expect that the contribution of the new physics to the oblique parameters S, T and U [6], will be described only in terms of the light and heavy neutrino mass eigenstates. Therefore, we expect to constrain directly the neutrino masses, when we compute and compare their contribution to the radiative corrections with the experimental data.

Our intention in this work is to verify what is the order of the limits we obtain on the light neutrino masses, through the calculation and comparison of the oblique corrections with the experimental data. The calculation will be performed for a specific model, although we expect it to be sufficiently general to give one idea of the limits that can be obtained on neutrino masses in this class of models.

The model we will consider has been proposed by Shin [7], and besides the standard generations of quarks and leptons, it contains three generations of right-handed neutrinos (N_{0R}), one superheavy quark, and one $SU(3)_c \otimes SU(2)_L \otimes U(1)_Y$ singlet complex scalar σ. One of the interesting points of the model is that the σ boson carry nonzero Peccei-Quinn charge [8], i.e. the σ boson will acquire a large vacuum expectation value (vev), which will be identified with the scale of Peccei-Quinn symmetry breaking, which resolve the strong CP problem. At the same time the σ will give large majorana masses to the right-handed neutrinos (N_{0R}), therefore, as it carries lepton-number and PQ charge, the Goldstone boson associated with this symmetry breaking was called "majoraxion". As occurs with the ordinary axion, the vev of this scalar boson (V_{PQ}) will be limited to $10^{10} - 10^{12}$ GeV [9]. Further details about the model can be found in Ref. [7], and here we will restrict ourselves only to what is necessary to

compute the oblique corrections in this model.

In a general way, we can write the neutrinos mass matrix as follows,

$$
\left(\bar{\nu}_{0L} \ \ \bar{N}_{0L}^{c}\right)
\begin{bmatrix} 0 & m_D \\ m_D^T & M_N \end{bmatrix}
\left(\begin{array}{c} \nu_{0R}^{c} \\ N_{0R} \end{array}\right) + H.c.
\tag{1}
$$

This procedure allows us to consider an arbitrary number of lepton families, i.e., for n families the mass matrix elements, m_D and M_N, are indeed $n \times n$ matrices, with

$$
(m_D)_{ij} \equiv (\frac{v}{\sqrt{2}})y_{ij}^{(\nu)} \quad \text{e} \quad (M_N)_{ij} \equiv (\frac{V_{PQ}}{\sqrt{2}}) \times \exp(i\theta_0)y_{ij}^{(N)}.
\tag{2}
$$

where θ_0 is the vev phase of σ, which must be fixed according to the strong CP problem.

In the case we want to deal only with the three Standard Model generations, the matrices m_D and M_N will assume a 3×3 form. To obtain the neutrinos mass eigenstates, we have to diagonalize the mass matrix in Eq.(1). This was done introducing a 6×6 matrix, V. In order to make the computation of the diagonalization matrix feasible, we need to introduce some assumptions on the model proposed by Shin [7], which are summarized in the following. Only the tau neutrino (ν_τ) will acquire mass via the seesaw mecanism. The heavy neutrinos (N_1, N_2, N_3) are expected to have masses of the same order of V_{PQ} (the Peccei-Quinn symmetry scale). We will assume mixing just between ν_τ and N_3, and the mass matrix of charged leptons is assumed to be diagonal. These assumptions retain most of the physics of the problem, and at the same time greatly simplify the calculation, because we get rid of a complicated mixing matrix, which, if we do have a mass hierarchy in the Dirac neutrino sector, will not modify significantly our results. This yelds the mixing angle as a function of the ν_τ mass (m_1) and N_3 mass (m_2),

$$
s_\theta^2 = \frac{m_1}{m_1 + m_2} \quad \text{and} \quad c_\theta^2 = \frac{m_2}{m_1 + m_2}
\tag{3}
$$

which are related to Dirac and Majorana masses by

$$
m_D = \sqrt{m_1 m_2} \quad \text{and} \quad M_N = m_2 - m_1.
\tag{4}
$$

With these results we can write the interaction Lagrangian in terms of these mixing angles, recalling some properties of majorana particles, which lead us to

$$
\mathcal{L}_{Z\nu_\tau N} = -\frac{g_2}{4c} Z_\mu \left\{ -c_\theta^2 \bar{\nu}_\tau \gamma^\mu \gamma_5 \nu_\tau - s_\theta^2 \bar{N}_3 \gamma^\mu \gamma_5 N_3 + 2is_\theta c_\theta \bar{N}_3 \gamma^\mu \nu_\tau \right\}
\tag{5}
$$

and,

$$
\mathcal{L}_{W^\pm \nu N} = -\frac{g_2}{\sqrt{2}} W_\mu^- \left\{ -ic_\theta \bar{\tau}^- \gamma^\mu (1 - \gamma_5)\nu_\tau + s_\theta \bar{\tau}^- \gamma^\mu (1 - \gamma_5)N_3 \right\} + H.c.
\tag{6}
$$

where we are abreviating the notation for the weak mixing angle, $c = \cos\theta_w$ and $s = \sin\theta_w$.

Now we are able to compute the oblique radiative corrections to this model. We have adopted the parametrization given by Kniehl e Kohrs [3]. We computed the oblique parameters, and after some algebra we obtained the analytic form of S, T and U [10], which allows us to plot the oblique parameters in terms of neutrino masses (the figures are available via mail: FEDEL@uspif.if.usp.br). Using a very recent fit of the oblique parameters for the experimental data [11], we have got some constraints on the light neutrino mass, assuming a Top quark of mass $m_t = 175$ GeV.

In the model we are discussing the heavy Majorana mass is related to V_{PQ}, and we have naturally that $m_2 \approx M_N = O(V_{PQ})$, therefore, when we computed numerically the values of S, T and U, we assumed m_2 to be in the

interval $10^{10} - 10^{12}$ GeV. The parameter S gives the most stringent limit on the mass m_1, and our results are as follows: for $m_2 = 10^{10}$ GeV we obtain that $m_1 \leq 3.2$ KeV, whereas for $m_2 = 10^{12}$ GeV we obtain $m_1 \leq 32$ eV, which is a limit smaller than the experimental value of the ν_τ mass. This limit is a direct consequence of the fact that the experimental data still allow for a heavy Dirac neutrino with $m_D \leq 178$ GeV. With the U parameter we obtain a limit that is at least one order of magnitude worse, whereas the T calculation does not give any meaningful result.

As the Majorona mass is of the order of the Peccei-Quinn scale we obtain an extremely small mixing angle between the neutrino eigenstates, therefore our limits can be easily related to a limit on the Dirac neutrino mass. If we had a much lighter Majorana mass we would have the same constraint on the Dirac one, however, no limit would be obtained for the ν_τ, i.e. better than the present experimental limit on m_{ν_τ}. Notice that even if we had not simplified the mixing matrix we would obtain a similar result, as long as there is a mass hierarchy for the Dirac neutrino masses.

References

[1] S. Bertolini and A. Sirlin, Phys. Lett. B257, 179 (1991).

[2] E. Gates and J. Terning, Phys. Rev. Lett. 67, 1840 (1991).

[3] B. A. Kniehl and H. -G. Kohrs, Phys. Rev. D48, 225 (1993).

[4] C. T. Hill and E. A. Paschos, Phys. Lett. B241, 96 (1990).

[5] W. Buchmuller, C. Greub, and H. -C. Kohrs, Nucl. Phys. B370, 3 (1992).

[6] M. E. Peskin and T. Takeuchi, Phys. Rev. Lett. 65, 964 (1990); Phys. Rev. D46, 381 (1992); D. C. Kennedy and B. W. Lynn, Nucl. Phys. B322, 1 (1989).

[7] Michael Shin, Phys. Rev. Let. 59, 2515 (1987).

[8] R. Peccei and H. Quinn, Phys. Rev. Lett. 38, 1440 (1977); Phys. Rev. D16, 1791 (1977).

[9] M. S. Turner, Phys. Rep. 197, 67 (1990).

[10] P. S. R. Silva, Dissertação de Mestrado pela Universidade de São Paulo (1994).

[11] R. Barbieri, Talk given at the Rencontres de la Valles d'Aoste, La Thuile, Italy, March 1994, Preprint IFUP-TH 28/94.

Neutrinos Atmosféricos e a Razão ν_e/ν_μ

H. M. Portella, R. H. C. Maldonado, A. Gomes

Instituto de Física, Universidade Federal Fluminense

N. Amato, C. E. C. Lima

Centro Brasileiro de Pesquisas Físicas

1. Introdução

Os neutrinos atmosféricos são produzidos nos chuveiros hadrônicos induzidos pelos raios cósmicos primários e são observados em detetores subterrâneos de grande massa de água (Cerenkov), através de suas interações no interior destes detetores. Da medida dos elétrons e dos muons contidos nestes detetores estima-se para a razão $(\nu_e + \bar{\nu}_e)/(\nu_\mu + \bar{\nu}_\mu)$ um valor acima de 1, o que está em total desacordo com estimativas teóricas que sugerem um valor de aproximadamente 1/2.

Neste trabalho calculamos analiticamente o fluxo de neutrinos atmosféricos resolvendo as equações unidimensionais que descrevem a difusão dos hadrons e leptons na atmosfera e comparamos nossos resultados com os obtidos através de cálculos de simulação por Gaisser e colaboradores e obtidos analiticamente por Bugaev e Naumov.

2. Fluxo de neutrinos

O "Rate" de um detetor de Cerenkov é função do fluxo dos neutrinos atmosféricos que entram no detetor, da massa de água, da seção de choque dos diferentes tipos de neutrinos que interagem dentro do detetor e também da eficiência do Cerenkov em identificar um evento do tipo eletrônico ou muônico cujo o vértice da interação está contido no detetor.

Neste trabalho nós nos limitamos a calcular o fluxo de neutrinos atmosféricos na região de energia, 500 MeV $\leq E_\nu \leq 2$ GeV.

Na primeira parte do trabalho obtivemos o fluxo de mesons ($\pi^\pm$, $K^\pm$, K_0^L) levando-se em conta a distribuição zenital e os efeitos geomagnéticos sobre os raios cósmicos primários. Usamos em nossos cálculos uma atmosfera isotérmica e para grandes ângulos zenitais ($\theta > 70°$) se fez a correção no fluxo de muons do efeito da curvatura da Terra.

Tendo-se obtido os fluxos mesônicos, calculamos o fluxo integral de muons levando-se em conta os efeitos do decaimento dos muons em elétrons e da perda de energia por ionização dos muons na atmosfera. Para esse efeito usamos a seguinte expressão $-dE/dx = a + bE$. a e b constantes. Essa perda de energia foi considerada contínua.

Para a região de energia considerada os neutrinos são originados em sua maioria dos decaimentos dos pions, kaons e muons.

3 Resultados e Conclusões

As razões entre os neutrinos e antineutrinos muônicos foi estimada em 1.15 e entre os neutrinos e antineutrinos eletrônicos em 2.1. Para a direção vertical e para a energia dos neutrinos menor que 2 GeV, os fluxos de neutrinos e antineutrinos muônicos vindos dos decaimentos dos pions e kaons, tem a mesma ordem de grandeza. Para a

direcção horizontal e para energias menores que 10 GeV o decaimento dos muons em elétrons é bastante importante, tornando-se dominante na produção dos antineutrinos muônicos.

O fluxo de neutrinos por nós calculados é comparado com o obtido por Gaisser para as coordenadas geomagnéticas de Kamiokande. Da figura vemos que o fluxo dos neutrinos e antineutrinos eletrónicos coincidem com os obtidos por Gaisser, enquanto que para os neutrinos e antineutrinos muônicos há uma direrença de cêrca de 8% (nossos cálculos fornecem um fluxo menor).

Fizemos uma estimativa do "Rate" do detetor de Kamiokande e o resultado é apresentado na tabela abaixo.

tipo do evento	dados experimentais	Gaisser et al.	Portella et al.
e-like	122	127	125
μ-like	103	175	143

Fluxo de Neutrinos
(Kamiokande)
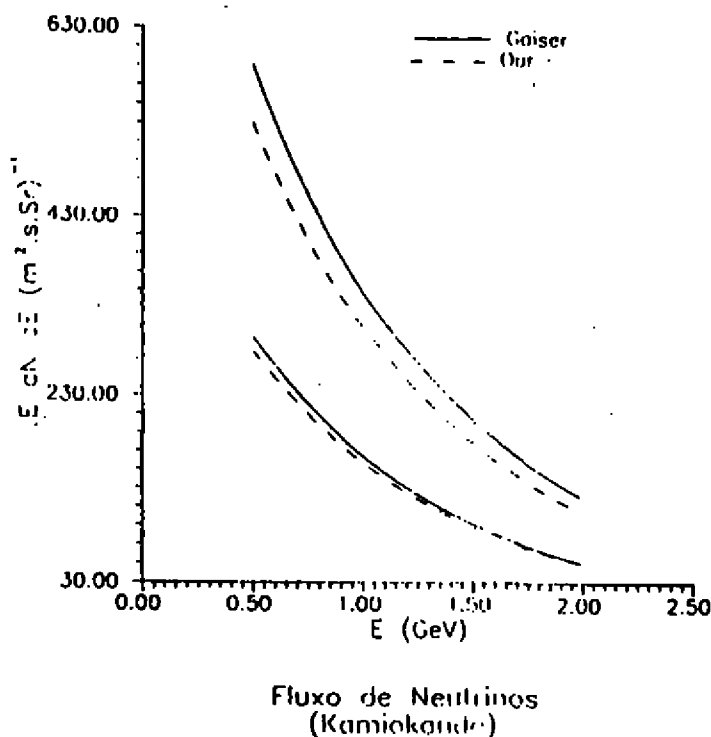
Referência

T.K. Gaisser - Cosmic Ray and Particle Physics - Cambridge University Press (1992).

Numerical analysis of the elastic parton-parton profiles in eikonal models

M. J. Menon and D. S. Thober

Instituto de Física 'Gleb Wataghin' Universidade Estadual de Campinas (Unicamp)

We present a numerical analysis of the two-dimensional Fourier transform connecting parton-parton profile functions and scattering amplitudes from five pure geometrical (eikonal) models. Making use of three numerical programs we show the cases in which the transform may be computed.

Elementary (parton-parton) amplitudes in pure geometrical models has recently been discussed in reference [1]. We shall assume the knowledge of this analysis and recall that a necessary condition for a consistent use of the Glauber's multiple diffraction theory is the existence of a well defined Fourier transform for the elementary amplitude. Current models make use of the following choices for this amplitude [1]:

- Chou and Yang: $f_{CY} = 1$.
- Glauber and Velasco: $f_{GV} = e^{i(b_1 q^2 + b_2 q^4)}/(1 + (q/a)^2)^{\frac{1}{2}}$.
- Saleem, Aleem and Alzhar: $f_{SAA} = 1 - (q/a)^2/(1 + (q/a)^2)^{\frac{1}{2}}$.
- Bourrely, Soffer and Wu: $f_{BSW} = 1 - (q/a)^2/(1 + (q/a)^2)$.
- Menon and Pimentel: $f_{mBSW} = 1 - (q/a)^2/(1 + (q/a)^4)$.

where q^2 is the transferred momentum and a^2 a free parameter in each model. We recall also that f_{BSW} corresponds to an interpretation made by some authors and that the subscript in f_{mBSW} means *modified* - BSW [1].

Our aim is to investigate the integral

$$D(b) = \int_0^\infty q dq J_0(qb) f(q) \equiv < f(q) >. \tag{1}$$

where b is the impact parameter. Ordinary two-dimensional Fourier transform may be found in two cases,

$$D_{GV} = < |f_{GV}| > = a e^{-ab}/b, \tag{2}$$

$$D_{mBSW} = < f_{mBSW} > = -a^2 [Kei(ab) + Ker(ab)] \tag{3}$$

and generalized Fourier transform in the case of the Chou and Yang model, $D_{CY} = < f_{CY} > = \delta(b)$.

Integration of equation (1) was tested by means of fast Fourier transform in XVGR, and Mathematica programs, [2, 3, 4], as well as through the NAG library for direct numerical integration. Due to slow convergence all cases presented fast oscilations. The same happens if a cut-off in the integral limit is introduced.

In order to obtain a fast convergence we carried out an integration by parts,

$$D(b) = \frac{q J_1(qb) f(q)}{b} \Big|_0^\infty - \frac{1}{b} \int_0^\infty dq q J_1(qb) f'(q). \tag{4}$$

The first term vanishes in the case of $|f_{GV}|$ and f_{mBSW} and with a cut-off above 30 GeV^2 the second term reproduces the analytical results (equations (2) and (3)), as can be seen in Figure 1.a. In the case of f_{BSW} the first term diverges at infinity and the second one can be calculated, as shown in Fig. 1.b. A cut-off above 30 GeV^2 does not change the numerical results up to four digits. The analysis was made with a cut-off at 100 GeV^2. In the case of f_{SAA} the first term diverges and the second one presents fast oscilations and so could not be calculated. The novel results we arrived was: (a) a separation of the finite and divergent parts in the case of f_{BSW}: (b) numerical integration throught the programs referred is not possible in the case of f_{SAA}.

Acknowledgments

References

1. M. J. Menon, Physical Review D **48**, 2007 (1993).

2. W. II. Press, B. P. Flannery, S. A. Teukolsky. e W. T. Vetterling. *Numerical Recipies in C*. (Cambridge University Press, Cambridge, England, 1988).

3. S. Wolfram, *Mathematica*, (Addison - Wesley Publishing Company, 1991).

4. S. M. Rossi. *PC-Laser: Um software para simulação de lasers semicondutores*. Master Thesis FEE-Unicamp (1993).
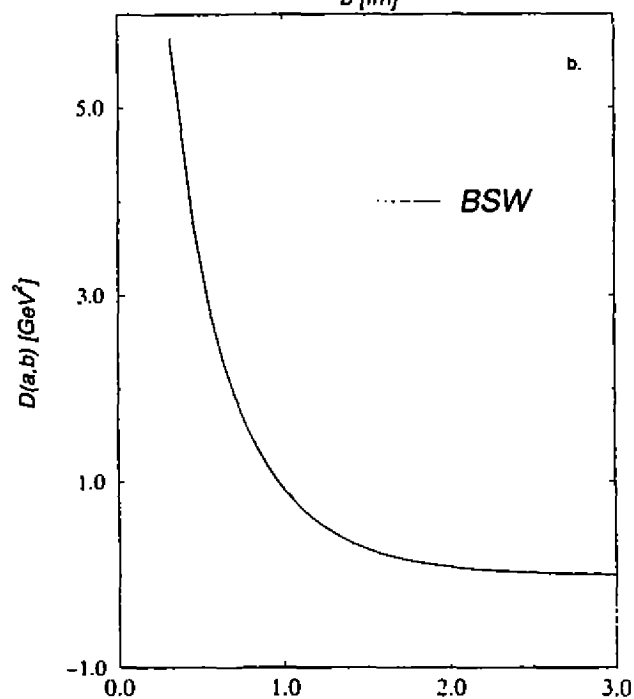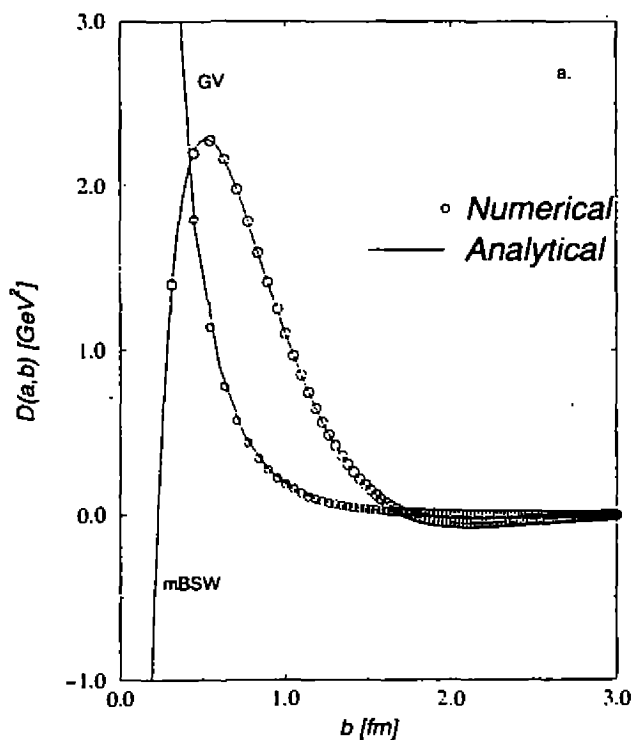
(a) Numerical integration of (4) and analytical results (2) $b[fm]$ (b) Numerical integration of the second term of (4).

Nucleon Mass Splitting in Thermo Field Dynamics

H. R. Christiansen*

Departamento de Física, Universidad Nacional de La Plata

C.C. 67. (1900) La Plata, Argentina

The finite temperature and finite density dependence of the neutron-proton mass difference is analyzed in a purely hadronic framework where the $\rho - \omega$ mixing is crucial for this isospin symmetry breakdown. The problem is handled within Thermo Field Dynamics. The present results, consistent with partial chiral and charge symmetry restoration, improve the experimental data fit for the energy difference between mirror nuclei.

In recent years. the possibility of producing quark-gluon plasma by means of very energetic nucleus-nucleus collisions [1] opened a rather important program of investigation of matter under extreme conditions that could shed light on various fundamental problems of field theory and nuclear physics.

In the present work we analyze the behavior of the neutron-proton mass difference with temperature and density within meson theory. Our results are consistent with both partial chiral and charge symmetry restoration with increasing temperature and density. In particular, the density effects are in order to exhibit the expected tendency to clear away the Nolen-Schiffer Anomaly (NSA).

Although a full description of the neutron-proton mass difference calls for essentially non perturbative techniques. one may gain qualitative understanding of the problem. relying on the perturbative methods used in many body nuclear physics. There, relativistic perturbation theory (RPT) is mainly used for the analysis of hadron interactions [2]. In Ref. [3] we have obtained a good result for the n-p mass splitting using RPT at the hadronic level. In that work we have shown that the role of the $\rho - \omega$ mixing interaction is crucial in the understanding of the n-p mass difference, in a hadronic context. We have concluded that the mixing of the vector mesons is the main non-electromagnetic charge symmetry breaking (CSB) contribution to be considered. We recall that $\Delta M_{n-p}^{exp} = 1.29$ MeV while $\Delta M_{n-p}^{em} = -0.66$ to -0.76 MeV [4]. implying a 2 MeV strong contribution.

Here we obtain the finite temperature and density (FTD) dependence of the nucleon mass splitting using the same framework as in Ref. [3] where we have considered nucleons and mesons as the fundamental dynamical degrees of freedom.

A natural framework for the study of matter under FTD conditions is the so-called Thermo Field Dynamics (TFD) [5]. TFD is a real time formalism of the statistical field theory. very powerful for describing non-isolated many body systems. It is a canonical field theory formulation in which the Hilbert space is doubled and each field operator has two independent components belonging to the thermal doublet. Correspondingly, the Green's functions. self-energies etc., are expressed by the thermal matrices. Moreover, the usual perturbation theory at zero temperature and density can be easily extended to FTD. This formalism is also particularly useful to perform both high and low temperature expansions, a feature much less accesible in the imaginary time formalism. Consequently, perturbation theory is at hand using the Feynman diagrams technique proper of RPT. Moreover, the TFD free propagators can be explicitly separated into two parts: one term being the usual one and the other part. depending on temperature and density. TFD establishes that inner vertices of a diagram can be of either type, physical or ghost while the external ones ought to be physical. In view of this, and up to second order perturbation. only the mixing vertex involve both kind of terms. However, for the ghost type, the product of meson propagators

will produce a vanishing contribution to the loop. The contribution coming from antiparticles can be omitted for temperatures β^{-1} below pair production. Furthermore, as the presence of real mesons calls for extreme conditions, its effect shall be neglected.

We perform a low temperature expansion of the remaining self energy expression with a relativistic chemical potential depending on both temperature and density. The corresponding equations are adequate for astrophysical temperatures (a couple of MeV's) and baryon densities in the range of the nuclear matter density $\delta_0 = 0.1934 fm^{-3}$. Under these conditions, the T^2-dependent term of the corrected self energy is negligible. Hence the main contribution comes from the term which only depends on δ. In connection with this result let us finally comment on the NSA. The anomaly is the failure of theory to explain the mass differences between mirror nuclei, a gap amounting to a few hundred keV. The mass difference of mirror nuclei can be written as $M_{Z>} - M_{Z<} = \Delta E_{em} - (M_n - M_p)^\delta$ where $M_{Z>}$ is the mass of the nucleus with the larger charge, ΔE_{em} is the e-m self energy difference between the nuclei and $(M_n - M_p)^\delta$ is the nucleon mass difference inside the nucleus. Since ΔE_{em} has been exhaustively analyzed [6], in recent years particular attention has been paid to the second term. Our numerical results of $(M_n - M_p)^\delta - (M_n - M_p)^0$ for $T = 0$ and baryon densities ranging from $\delta_0/2$ to $1.5\delta_0$, go from -100 to -250 keV with a set of coupling constants chosen in order to saturate the 2 MeV hadron contribution to the vacuum nucleon mass difference within the model [7] (This election is well inside the accepted range of variation of these parameters [8]). The final result is in the right direction to remove the anomaly.

In conclusion, we have shown that the extension of canonical Quantum Field Theory in vacuum to FTD media, provides sensible results for the nucleon mass splitting under extreme conditions. For standard astrophysical temperatures we find a negligible temperature contribution to the nucleon self masses. On the other hand, within the present framework, the hadronic model predicts the hoped trends to remove the NSA. Our numerical results for the nucleon mass splitting in dense media, suggest that one should include (besides $\rho - \omega$ mixing) some other contribution being of minor importance to the n-p mass difference in vacuum but relevant inside nuclei.

Acknowledgments

References

[1] Proceedings of Quark Matter '90, Nucl. Phys. **A525** (1991).

[2] R. Machleidt, K. Holinde and Ch. Elster, Phys. Rep. **149**, 1 (1987).

[3] H. R. Christiansen, L. N. Epele, H. Fanchiotti and C. A. Garcia Canal, Phys. Lett. **B267** (1991), 164.

[4] M. Cini, E. Ferrari and R. Gatto, Phys. Rev. 2 (1959), 7; J. Gasser and H. Leutwyler. Phys. Rep. **87** (1982), 77.

[5] Y. Takahashi, H. Umezawa, Collect. Phen. 2, (1975), 55; H. Matsumoto, Fortschr. Phys. **25** (1977), 1.-N. P. Landsman and Ch. G. van Weert, Phys. Rep. **145** (1987), 141.

[6] S. Shlomo, Rep. Progr. Phys. **41**, (1978), 957.

[7] We have used the vacuum values for masses and couplings. The deviation from these numbers, a higher order correction, is negligible at low temperatures and densities. See e.g. C. Adami and G. E. Brown, Phys. Rep. **234** (1993), 1; S. Gao, R-K. Su and P. K. N. Yu, Phys. Rev. **C49** (1994), 40, and references therein.

[8] M. Beyer and A. G. Williams, Phys. Rev. **C38**, 779 (1988); P. C. Mc Namee, M. D. Scadron and S. A. Coon, Nucl. Phys. **A249** 483 (1975); **A287** 381 (1977); S. Coon and R. Barret, Phys. Rev. **C36** 2189 (1987).

Phenomenology of the Spontaneous CP Violation in $SU(3)_L \otimes U(1)_Y$ Electroweak Models

Luis N. Epele and Daniel A. Gómez Dumm*

Departamento de Física, Universidad Nacional de La Plata

C.C. 67, (1900) La Plata, Argentina

We study the phenomenological consequences of the spontaneous CP violation in an $SU(3)_L \otimes U(1)_Y$ model with three Higgs triplets and one sextuplet, which has been recently proposed by Pisano and Pleitez [1] and Frampton [2]. Since this CP-violating effects are due to the presence of complex vacuum expectation values in the Higgs sector, our analysis requires a detailed study of the enlarged scalar potential.

As we have previously shown [3], this potential yields a spontaneous CP-breakdown mechanism for a certain region in the space of parameters. The question now is, whether the model can reproduce the observed CP violation phenomenology or not. To find the answer, we firstly identify the scalar mass eigenstates, and then calculate the main contributions to the mass difference $m_{K_L} - m_{K_S}$ and the CP-violation parameters ε and ε' related to the Kaon decays.

The diagonalization of the neutral and charged scalar mass matrices does not represent a trivial task, in view of the many terms entering the Higgs potential. In our work, we proceed first by identifying the scalar mass eigenstates when CP is conserved, and then we approximately find the physical scalars when CP is spontaneously broken. In order to deal with the large number of unknown parameters, we take as an assumption that the only scales introduced by the potential are those given by the vacuum expectation values of the neutral higgs (say, v_χ and v_η), and a global coupling constant scale λ. After considering the spontaneous breakdown of the gauge symmetry $SU(3)_L \otimes U(1)_Y$ to $U(1)_{em}$, we find that the mass eigenstates interact with the fermions through CP-violating Yukawa couplings.

The most important contributions of the new physical scalars to Δm_K, ε and ε' are given by tree-level diagrams, together with the well-known "box" and "penguin"-like graphs, involving in this case neutral and charged scalar mediators. In the corresponding calculations, once again we have to deal with many unknown parameters. However, their order of magnitude can be computed. Thus, if there are no cancellation and enhancement effects, it is possible to obtain meaningful numerical estimations.

The main contribution to Δm_K is found to be proportional to the product $(V_L^d)_{11}(V_L^d)_{12}$, where V_L^d is the mixing matrix for the down-like quarks, d, s and b[1]. Assuming that the masses of the light scalars are not greater than 150 GeV, our result is that the condition

$$(V_L^d)_{11}(V_L^d)_{12} \leq 0.01$$

has to be satisfied if we require the $SU(3)_L \otimes U(1)_Y$ contribution to be lower than the standard prediction by at least one order of magnitude.

---

*e-mail: dumm@venus.fisica.unlp.edu.ar

[1] As usual, it is satisfied the relation $V_L^{u\dagger} V_L^d = V_{CKM}$. However, in this model both V_L^d and V_L^u also appear in a separate way in the Lagrangian.

The value of ε receives contributions from both tree-level and box diagrams. Here, in order to get the experimental value $|\varepsilon| \simeq 2.26 \times 10^{-3}$, the angles in V_L^d must obbey the stronger constraint

$$(V_L^d)_{11}(V_L^d)_{12} \leq 4 \times 10^{-3}$$

Moreover, we find that other contributions are negligible when compared with this one. In this way, the d-quark mixing angles should reach the upper limit in the above equation if the phases coming from the scalar potential are responsible for the observed CP violation.

Finally, for the calculation of the ε' parameter it is necessary to consider both tree-level and penguin diagrams. Here even the experimental data are not conclusive: they just agree with the upper bound $|\varepsilon'/\varepsilon| \leq 5 \times 10^{-3}$. The evaluation of the diagrams gives in this case the approximate result $|\varepsilon'/\varepsilon|_{SU(3)} \sim \mathcal{O}(10^{-4})$. Therefore, once we have fixed the value of ε, both Δm_K and $|\varepsilon'|$ fall very well within the experimental bounds.

It is interesting to remark that similar calculations have been performed for a two-Higgs-doublet model [4]. However, in that case, the introduction of arbitrary small parameters in the Lagrangian has been necessary in order to reproduce the observed CP violation and flavor-changing phenomenological effects. In the $SU(3)_L \otimes U(1)_Y$ model, as stated above, the corresponding "small" parameter appears naturally as a mixing angle in V_L^d, and could be explained in terms of the hierarchical structure of the quark-mixing matrices.

References

[1] F. Pisano y V. Pleitez. *Phys. Rev.* **D46** (1992) 410.

[2] P. H. Frampton. *Phys. Rev. Lett.* **69** (1992) 2889.

[3] L. Epele, H. Fanchiotti. C. García Canal and D. Gómez Dumm. *Phys. Lett.* **343B** (1995) 291.

[4] J. Liu and L. Wolfenstein. *Nucl. Phys.* **B280** (1987) 1.

Fluctuation and Dissipation in Nonequilibrium Quantum Field Theory

Rudnei O. Ramos*

Instituto de Física, Universidade de São Paulo
C.P. 20516. 01452-990 São Paulo, SP. Brazil

The nonequilibrium dynamics of a scalar field is studied using perturbation theory and a real time finite temperature formulation. The evolution equation for the scalar field is explicitly obtained and terms responsible for noise (fluctuations) and dissipation are identified and studied in the high temperature limit.

I. Introduction

The understanding of a very large amount of physical phenomena depends on the understanding of the dynamics associated to them. In the early Universe. for example. it is fundamental the study of the dynamics associated to the cosmological phase transitions, that possible happened at early times. which could lead to answers to most of the current questions in cosmology, like the origin of the large-scale structure of the Universe to the excess of baryonic matter [1]. In inflationary models the dynamics of some quantum field driven inflation (the inflaton) it is also fundamental. More at laboratory scales, we can also probe nontrivial dynamical effects through experiments of heavy ions collisions. The study of all these cases involve the understanding of nonequilibrium aspects of phase transitions in quantum field theory.

In the study of any nonequilibrium system is important to identify what we call by "system" and to what this system is coupled to, usually called the "thermal bath". which drives the system into equilibrium [3]. For a scalar quantum field, we can identify its short wavelength modes as a thermal bath driving the longer wavelength modes, which have slower dynamics, into equilibrium. We can also identify other fields coupled to the background scalar field as being part of the bath.

The separation between "system" and "bath" is implemented here by perturbation theory, where the effective action is obtained by integrating over small fluctuations about the field configuration we are interested in. From the effective action we derive the effective equation of motion which we will show here up to two-loops. The Schwinger's closed time path scheme [2] at finite temperature is used as an appropriate formalism to study nonequilibrium field theory. In this formalism the time path goes from $t = -\infty$ to $t = \infty$ and then it turns back to $t = -\infty$. As a result of this choice of time path we have a doupling of field variables: we identify the fields in one time path branch as φ_+, for $t \in [-\infty, +\infty]$, and φ_-, for $t \in [+\infty, -\infty]$. The real-time propagators on the contour are therefore given in terms of a 2×2 matrix. $[G(x, x')]_{m,n}$, where $m, n = +, -$. The physical (casual) propagator is $G^{+,+}$. The momentum space Fourier transform of $[G(x, x')]_{m,n}$ is given by [2]

$$G^{++}(\vec{k}, t - t') = G^{>}(\vec{k}, t - t')\theta(t - t') + G^{<}(\vec{k}, t - t')\theta(t' - t)$$

$$G^{--}(\vec{k}, t - t') = G^{>}(\vec{k}, t - t')\theta(t' - t) + G^{<}(\vec{k}, t - t')\theta(t - t')$$

$$G^{+-}(\vec{k}, t - t') = G^{>}(\vec{k}, t - t')$$

$$G^{-+}(\vec{k}, t - t') = G^{<}(\vec{k}, t - t') \tag{1}$$

where, for free propagators at finite temperature,

$$G^{>}(\vec{k}, t - t') = \frac{1}{2\omega(\vec{k})}\left[(1 + 2n(\omega))\cos[\omega(t - t')] - i\sin[\omega(t - t')]\right]$$

$$G^{<}(\vec{k}, t - t') = G^{>}(\vec{k}, t' - t), \tag{2}$$

where $n(\omega) = \left(e^{\beta\omega} - 1\right)^{-1}$ is the Bose distribution and $\omega \equiv \omega(\vec{k})$ is the free particle energy.

Let us now consider a self-interacting $\lambda\phi^4$ model with classical action $S[\phi]$. The effective action $\Gamma[\phi]$ up to two-loops and order λ^2, can be represented graphically as

$$\Gamma[\varphi_+, \varphi_-] = S[\varphi] + \quad \bigcirc\!\!\!\!\!< \quad + \quad \times\!\!\!\!\!< \quad + \quad \bigcirc\!\!\!\!\!\bigcirc\!\!\!< \quad + \quad -\bigcirc\!\!- \quad + \mathcal{O}(\lambda^3), \tag{3}$$

where, in the graphic representation, all the possible combinations of $\varphi_{+,-}$ are in the external legs and the internal propagators are given by $G^{m,n}$ ($m, n = +, -$). $S[\varphi]$ is given by $S[\varphi] = S[\varphi_+] + S[\varphi_-]$. The identification of fluctuations and dissipations in the equation of motion for a field configuration φ, derived in terms of the effective action, it is usually easier when expressing $\Gamma[\varphi_+, \varphi_-]$ in terms of new field variables denoted by φ_c and φ_Δ (known as center of mass coordinate, or system field, and the relative coordinate, or the response field, respectively) expressed in terms of the old variables as $\varphi_c = \frac{1}{2}(\varphi_+ + \varphi_-)$; and $\varphi_\Delta = \varphi_+ - \varphi_-$. In terms of φ_c, φ_Δ and expressing the propagators in (3) in terms of the casual propagator G^{++}, we get the following expression for the effective action (3) (for details see [6])

$$\begin{aligned}
\Gamma[\varphi_\Delta, \varphi_c] &= \int d^4x \left\{ \varphi_\Delta(x)\left[-\Box - m^2 - \frac{\lambda}{2}\int\frac{d^3k}{(2\pi)^3}\frac{(1 + 2n(\omega))}{2\omega(\vec{k})} - \right.\right. \\
&\quad - \left. \frac{\lambda^2}{2}\int dt'\int\frac{d^3q}{(2\pi)^3}\mathrm{Im}\left\{G_\phi^{++}(\vec{q}, t - t')\right\}^2 \theta(t - t')\int\frac{d^3k}{(2\pi)^3}\frac{(1 + 2n(\omega))}{2\omega(\vec{k})}\right] \varphi_c(x) - \\
&\quad - \left. \frac{\lambda}{4!}\left(4\varphi_\Delta(x)\varphi_c^3(x) + \varphi_\Delta^3(x)\varphi_c(x)\right)\right\} + \\
&\quad + \int d^4x d^4x' \int\frac{d^3k}{(2\pi)^3}e^{i\vec{k}\cdot(\vec{x} - \vec{x}')}\left\{-\frac{\lambda^2}{8}\left[\varphi_\Delta(x)\varphi_c(x)\varphi_\Delta^2(x') + \right.\right. \\
&\quad + \left. 4\varphi_\Delta(x)\varphi_c(x)\varphi_c^2(x')\right]\int\frac{d^3q}{(2\pi)^3}\mathrm{Im}\left[G_\phi^{++}(\vec{q}, t - t')G_\phi^{++}(\vec{q} - \vec{k}, t - t')\right]\theta(t - t') - \\
&\quad - \frac{\lambda^2}{3}\varphi_\Delta(x)\varphi_c(x')\mathrm{Im}\left[\prod_{j=1}^3\int\frac{d^3q_j}{(2\pi)^3}G_\phi^{++}(\vec{q}_j, t - t')\right]\theta(t - t')\delta(\vec{k} - \vec{q}_1 - \vec{q}_2 - \vec{q}_3) + \\
&\quad + i\frac{\lambda^2}{4}\varphi_\Delta(x)\varphi_c(x)\varphi_\Delta(x')\varphi_c(x')\mathrm{Re}\int\frac{d^3q}{(2\pi)^3}\left[G_\phi^{++}(\vec{q}, t - t')G_\phi^{++}(\vec{q} - \vec{k}, t - t')\right] + \\
&\quad + i\frac{\lambda^2}{12}\varphi_\Delta(x)\varphi_\Delta(x')\mathrm{Re}\left[\prod_{j=1}^3\int\frac{d^3q_j}{(2\pi)^3}G_\phi^{++}(\vec{q}_j, t - t')\right]\delta(\vec{k} - \vec{q}_1 - \vec{q}_2 - \vec{q}_3)\right\}. \tag{4}
\end{aligned}$$

The last two terms in $\Gamma[\varphi_\Delta \varphi_c]$, Eq. (4), give the imaginary contributions to the effective action at the order of perturbation theory considered. It is straightforward to associate the imaginary terms in (4) as coming from functional integrations over Gaussian fluctuation fields ξ_1 and ξ_2 [4,5,6]

$$\Gamma[\varphi_\Delta, \varphi_c] = \frac{1}{i} \ln \int D\xi_1 \, P[\xi_1] \int D\xi_2 \, P[\xi_2] \exp\{iS_{\text{eff}}[\varphi_\Delta, \varphi_c, \xi_1, \xi_2]\} \, , \tag{5}$$

where

$$S_{\text{eff}}[\varphi_\Delta, \varphi_c, \xi_1, \xi_2] = \text{Re}\Gamma[\varphi_\Delta, \varphi_c] + \int d^4x \left[\varphi_\Delta(x)\varphi_c(x)\xi_1(x) + \varphi_\Delta(x)\xi_2(x)\right] \, . \tag{6}$$

and $\text{Re}\Gamma[\varphi_\Delta, \varphi_c]$ is the real part of Eq. (4). In (6), ξ_1 and ξ_2, are fields with probability distributions given by

$$P[\xi_1] = N_1^{-1} \exp\left\{ -\frac{1}{2} \int d^4x \, d^4x' \xi_1(x) \left(\frac{\lambda^2}{2} \text{Re} \left[G_\phi^{++}\right]_{x,x'}^2\right)^{-1} \xi_1(x') \right\} \, . \tag{7}$$

$$P[\xi_2] = N_2^{-1} \exp\left\{ -\frac{1}{2} \int d^4x \, d^4x' \xi_2(x) \left(\frac{\lambda^2}{6} \text{Re} \left[G_\phi^{++}\right]_{x,x'}^3\right)^{-1} \xi_2(x') \right\} \, . \tag{8}$$

where N_1^{-1} and N_2^{-1} are normalization factors, and in (7-8) we introduced the compact notation,

$$\left[G_\phi^{++}\right]_{x,x'}^2 = \int \frac{d^3k}{(2\pi)^3} \exp\left[i\vec{k}.(\vec{x} - \vec{x}')\right] \int \frac{d^3q}{(2\pi)^3} G_\phi^{++}(\vec{q}, t - t') G_\phi^{++}(\vec{q} - \vec{k}, t - t') \tag{9}$$

and

$$\left[G_\phi^{++}\right]_{x,x'}^3 = \int \frac{d^3k}{(2\pi)^3} \exp\left[i\vec{k}.(\vec{x} - \vec{x}')\right] \left[\prod_{j=1}^{3} \int \frac{d^3q_j}{(2\pi)^3} G_\phi^{++}(\vec{q}_j, t - t')\right] \delta(\vec{k} - \vec{q}_1 - \vec{q}_2 - \vec{q}_3) \, . \tag{10}$$

ξ_1 and ξ_2 act as fluctuation sources for the scalar field configuration φ. ξ_1 couples with both the response field φ_Δ and with the physical field φ_c, leading to a coupled (multiplicative) noise term $(\varphi_c\xi_1)$ in the equation of motion for φ_c, while ξ_2 gives origin to an additive noise term.

The equation of motion for φ_c (the physical field) is defined by

$$\frac{\delta S_{\text{eff}}[\varphi_\Delta, \varphi_c, \xi_1, \xi_2]}{\delta \varphi_\Delta}\Big|_{\varphi_\Delta=0} = 0 \, . \tag{11}$$

Restricting to situations near equilibrium and for nearly homogeneous fields, and using a Dyson equation for the propagators (or equivalently, by the use of full propagators), it was shown in [6] that the effective equation of motion for φ_c would be given consistently up to order λ^2 by the following equation

$$[\Box + m_T^2]\varphi_c(\vec{x}, t) + \frac{\lambda_T}{3!}\varphi_c^3(\vec{x}, t) + \eta_1\varphi_c^2\dot{\varphi}_c(\vec{x}, t) = \varphi_c(\vec{x}, t)\xi_1(\vec{x}, t) \, . \tag{12}$$

where m_T and λ_T are the finite temperature effective mass and coupling constant, respectively, η_1 is a dissipation coeficient given in the high T limit by

$$\eta_1 \stackrel{T \gg m_T}{\simeq} \frac{96}{\pi T} \ln\left(\frac{T}{m_T}\right) \, . \tag{13}$$

In (12) we have dropped the aditive fluctuation field ξ_2 and the associated dissipation term due to the fact that they can only be consistently defined at order $\mathcal{O}(\lambda^4)$ since it associated dissipation term is effectively of order λ^4 and therefore they are subdominant in the effective equation of motion for weak couplings.

From (7) we get that

$$\langle\xi_1(x)\xi_1(x')\rangle = \frac{\lambda^2}{2}\text{Re}\left[G^{++}\right]_{x,x'}^2 \, , \tag{14}$$

meaning that the fluctuation field ξ_1 is non-Markovian (it is not delta correlated) although it is Gaussian distributed. In [6] it was shown that a Markovian limit exists for (14) at very high temperatures ($T \to \infty$):

$$\langle \xi_1(x)\xi_1(x')\rangle \overset{T\to\infty}{=} 2T\eta_1\delta(x - x') \, . \tag{15}$$

From (12) we can see that in nonlinear quantum field theories, the equation of motion describing the approach to equilibrium of field configurations, do not usually assume a simple form as given by the standart Langevin equation, with dissipation term given by $\Gamma\dot\varphi$ and additive stochastic noise term. Instead, the dissipation kernels depend on the amplitude of the field configuration under study and fluctuations are of multiplicative nature. Also, usually we are only able to get a Markovian limit for the fluctuation correlation function at some nontrivial limit, as a very high temperature limit as shown for the case above. These differences in relation to the standart Langevin equation can lead to many new phenomena, when studing the nonequilibrium dynamics in physical systems. For example, multiplicative noises, as opposite to additive noises, are able to change the minima of the field potential of the configuration under study and preliminary results in the subject have shown nontrivial effects [7]. Dissipative kernels dependent on the amplitude of the field can also be very important in the study of inflation, being able may be, to lessen the constraints on the shape of the inflaton potential and leading to an improved study of particle production at reheating [8].

As a final comment, we must say that although we have used a perturbative study for dissipation and fluctuation, these are intrinsicaly nonperturbative effects. It is not discarded the fact that higher order loop corrections could give same order corrections as the one leading to (13). In fact, in ref. [9] it was shown that there are an infinity series of diagrams contributing at the same order to transpot coefficients (e.g., the dissipation coeficient). These however can be evaluated by a resumation approach, leading to an effective vertex computed at two-loop order and the full contribution to the transport coefficients evaluated. Work in order to study corrections to the equation of motion (12) and the study of the effects of the coupling of others fields are under progress [10].

References

1. E. W. Kolb and M. S. Turner, *The Early Universe*, Addison-Wesley 1990.

2. J. Schwinger, *Jour. Math. Phys.* 2, 407 (1961). See also: K. Chou, Z. Su, B. Hao and L. Yu, *Phys. Rep.* 118, 1 (1985); N. P. Landsman and Ch. G. van Weert, *Phys. Rep.* 145, 141 (1987).

3. A. O. Caldeira and A. J. Leggett, *Physica* 121A, 587 (1983).

4. M. Morikawa, *Phys. Rev.* D29, 2228 (1984).

5. D. Lee and D. Boyanovsky, *Nucl. Phys.* B406, 631 (1993).

6. M. Gleiser and R. O. Ramos, *Phys. Rev.* D50, 2441 (1994).

7. S. Habib, in *Stochastic Processes in Astrophysics*, Proc. Eighth Annual Workshop in Nonlinear Astronomy (1993), Los Alamos Report No. LA-UR-93-2105.

8. D. Boyanovsky, H. J. de Vega, R. Holman, D. S. Lee and A. Singh, Univ. Pittsburgh, Report no. PITT-94-07.

9. S. Jeon, *Phys. Rev.* D47, 4586 (1993); University of Washington report no. UW/PT 94-09.

10. R. O. Ramos, work in progress.

Interações Não Lineares entre Campos Eletromagnéticos em Altas Temperaturas

F. T. Brandt e J. Frenkel

Instituto de Física, Universidade de São Paulo

São Paulo. 01498 SP. Brasil

Investigamos o comportamento das interações não lineares entre campos eletromagnéticos no limite de altas temperaturas. Mostramos que, em geral, não há contribuições proporcionais à T^2. e que a dependência em $\log(T)$ se relaciona de maneira simples com o comportamento ultravioleta em temperatura zero. Apresentamos argumentos indicando que a ação térmica tende para o valor negativo da ação, em temperatura zero. quando $T \to \infty$.

1. Introdução

Campos eletromagnéticos exibem um comportamento *não-linear* (auto interagente) quando *efeitos quânticos* são levados em conta. As contribuições dominantes para este efeito podem ser calculadas utilizando-se o formalismo da *eletrodinâmica quântica*, e são descritas pelos diagramas mostrados na figura abaixo.
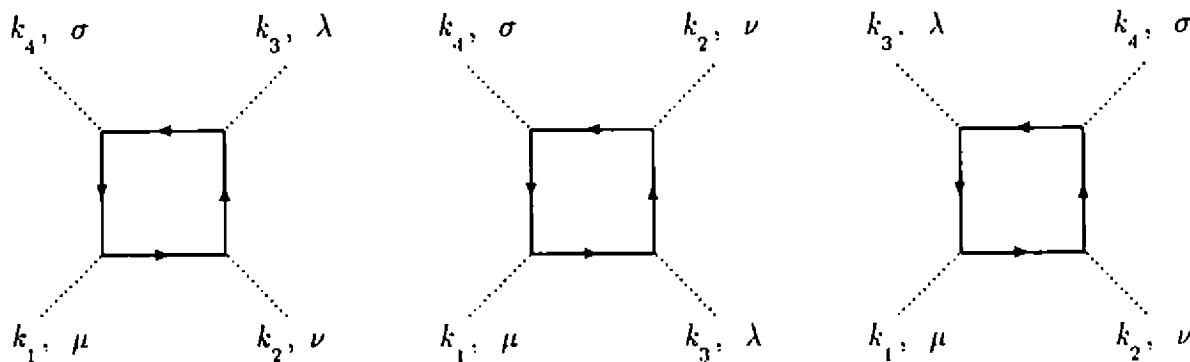
Diagramas descrevendo as interações não lineares entre campos eletromagnéticos. Linhas pontilhadas representam fótons e linhas cheias representam eletrons ou pósitrons

O trabalho mais conhecido, onde este efeito foi calculado usando a eletrodinâmica quântica, foi publicado em 1950 por Karplus e Neuman [1]. Anos antes. este efeito já havia sido calculado no limite não relativístico por H. Euler e B. Kockel em 1935 [2].

Em trabalhos recentes [3] (veja também [4]), estudamos as interações fóton-fóton. levando em conta os efeitos térmicos. Ou seja, os fótons interagem com os elétrons do vácuo e com *elétrons térmicos*. Nossa motivação foi entender o comportamento da interação fóton-fóton em função da temperatura.

Este tipo de estudo requer um formalismo onde sejam levados em conta efeitos quânticos e *efeitos térmicos*. Por isso, faremos a seguir um brevíssimo resumo do formalismo da *teoria de campos a temperatura finita*. Ao mesmo tempo, apresentaremos uma técnica de cálculo de funções de Green térmicas que simplifica muito os cáculos envolvidos.

$$k_2, \mu_2 \qquad\qquad k_3, \mu_3$$

$$\vdots \quad = \pm \frac{1}{(2\pi)^3} \int \frac{d^3\vec{q}}{2\sqrt{\vec{q}^2 + m^2}} N_{F,B}\left(\sqrt{\vec{q}^2 + m^2}\right) A_{\mu_1\mu_2\cdots\mu_N}(k_1, k_2, \cdots, k_N)_{q^2=m^2}$$

$$q \qquad\qquad + (\text{Funcao de } N \text{ Pontos em } T = 0)$$

$$k_1, \mu_1 \qquad\qquad k_N, \mu_N$$

2. Campos a Temperatura Finita - Formalismo do tempo imaginário

No *formalismo do tempo imaginário*, as funções de Green térmicas são calculadas *perturbativamente* de maneira muito semelhante ao que é feito em cálculos a temperatura zero. *mas*, com uma "pequena" (mas não trivial) modificação:

$$\int \frac{d^4 q}{(2\pi)^4} \mathcal{D}_0(q_0, \vec{q}) \to T \sum_n \int \frac{d^3\vec{q}}{(2\pi)^3} \mathcal{D}_0(\omega_n, \vec{q}), \tag{1}$$

onde T é a temperatura e $\omega_n = \pi T(2n+1)$ para férmions ou $\omega_n = 2\pi T n$ para bosons: $\mathcal{D}_0$ é o propagador associado à partícula do "loop".

Cálculos de funções de Green térmicas, em geral, envolvem complicações técnicas que tendem a obscurecer a interpretação física. Em trabalhos recentes, temos utilizados uma técnica que, além de simplificar em muito os cálculos, fornece uma interpretação física bastante clara. Além disto, esta técnica permite que a ação efetiva da teoria seja construida de maneira sistematica.

Cosidere uma função de Green térmica com n partículas externas. Utilizando as regras de Feynman a temperatura finita $T \neq 0$, (com a modificação descrita acima), é possível mostrar que

onde $A_{\mu_1\mu_2\cdots\mu_N}(k_1, k_2, \cdots, k_N)$ é a amplitude *em ordem de árvore* dada por

$$A_{\mu_1\mu_2\cdots\mu_N}(k_1, k_2, \cdots, k_N) \equiv$$

$$k_1, \mu_1 \qquad k_2, \mu_2 \qquad k_3, \mu_3 \qquad k_N, \mu_N$$

$$\cdots$$

$$q$$

$$+ \quad (\text{permut. ciclic.}) + (q \to -q),$$

e

$$N_{F,B}(q_0) = \frac{1}{\exp(q_0/T) \pm 1}$$

é a distribuição de Fermi/Bose.

Portanto, a interpretação física é bastante clara:

"Uma função de Green térmica, com N partículas externas, e um "loop" interno fermiônico (bosônico), é obtida subtraindo-se (somando-se) à função de Green do vácuo ($T = 0$) a amplitude de espalhamento, para frente, de um

férmion (bóson) térmico, na camada de massa, multiplicada pela distribuição de Fermi-Dirac (Bose-Einstein), e integrada sobre o 3-momentum do férmion (bóson)" [5].

A amplitude de espalhamento $\mathcal{A}$ goza de todas as propriedades de invariância da teoria dos campos envolvidos (invariância de gauge abeliana ou não abeliana, transformação geral de coordenadas, transformações de Weyl, etc). Em particular, $\mathcal{A}$ é invariante por transformações de Lorentz.

Temos portanto um cenário onde um sistema de partículas térmicas (plasma) interage com campos externos, mas não exsite interação *entre* as partículas térmicas.

A interação das partículas térmicas com os campos externos é descrita pela teoria *quântica* dos campos envolvidos. Conhecendo-se estas interações (regras de Feynman, e.g. QED) podemos calcular $\mathcal{A}$ e obter a interação não linear entre os campos externos, devida às interações com o plasma. A parte quântica deste efeito "termo-quantico" esta contida em $\mathcal{A}$ e na estatística das partículas térmicas.

3. Altas temperaturas

Usando as regras de Feynman da QED, a parte térmica da interação não linear é dada por

$$\frac{e^4}{(2\pi)^3} \int_0^\infty \frac{q^2}{2Q^0} dq N(Q^0) \int d\Omega \sum_{ijkl} \left(B^{\mu\nu\lambda\sigma}_{(ijkl)}(k_1, k_2, k_3; Q) + B^{\mu\nu\lambda\sigma}_{(ijkl)}(k_1, k_2, k_3; -Q) \right). \tag{2}$$

onde $q = |Q|$, $Q^0 = (q^2 + m^2)^{1/2}$, $N(Q^0) = (1 + e^{Q^0/T})^{-1}$. $\int d\Omega$ é a integral sobre as direções de Q, e a soma é sobre as permutações cíclicas $(ijkl)$ de (1234). Cada B tem um numerador que é um traço de Dirac. Por exemplo

$$B^{\mu\nu\lambda\sigma}_{(1234)} = \frac{\text{tr}\left[(\mathcal{Q} + m)\gamma^\mu(\mathcal{Q} + \not{k}_1 + m)\gamma^\nu(\mathcal{Q} + \not{k}_{12} + m)\gamma^\lambda(\mathcal{Q} + \not{k}_{123} + m)\gamma^\lambda(\mathcal{Q} + \not{k}_{123} + m)\gamma^\sigma\right]}{(2Q.k_1 + k_1^2)(2Q.k_{12} + k_{12}^2)(2Q.k_{123} + k_{123}^2)}, \tag{3}$$

onde $k_{12} = k_1 + k_2$, etc.

A série em potências da temperatura é obtida expandindo-se os denominadores,

$$(2Q.k + k^2)^{-1} = (2Q.k)^{-1} - k^2(2Q.k)^{-2} + k^4(2Q.k)^{-3} + \cdots, \tag{4}$$

e os numeradores de B. Obtemos assim termos que são funções homogêneas em Q de grau 1, 0, -1, -2, $\cdots$.

Termos de grau $n = 1, 0, -1$ produzem as potências T^3, T^2 e T, de acordo com a equação

$$\int_0^\infty \frac{q^{n+2} dq}{q_0 (\exp(q_0/T) + 1)} = (1 - 2^{-n-1})\Gamma(n + 2)\zeta(n + 2)T^{n+2} + \mathcal{O}(m). \tag{5}$$

Termos de grau -2 porduzem uma contribuição $\log(T)$, mais termos indepentes de T; potências ímpares cancelam-se na soma $\left(B^{\mu\nu\lambda\sigma}_{(ijkl)}(k_1, k_2, k_3; Q) + B^{\mu\nu\lambda\sigma}_{(ijkl)}(k_1, k_2, k_3; -Q) \right)$.

Contribuições $\mathcal{O}(T^2)$ *também se calcelam*. Este cancelamento é uma pouco mais sutil, envolvendo identidades tais como

$$\frac{k_1^2}{K_1^2}\left[\frac{1}{K_{23}}\left(\frac{1}{K_2} + \frac{1}{K_3}\right) + \frac{1}{K_{34}}\left(\frac{1}{K_3} + \frac{1}{K_4}\right) + \frac{1}{K_{42}}\left(\frac{1}{K_4} + \frac{1}{K_2}\right)\right] + (3 \text{ permut. ciclic.})$$

$$-\frac{k_{12}^2}{K_{12}^2}\left(\frac{1}{K_3} + \frac{1}{K_4}\right)\left(\frac{1}{K_1} + \frac{1}{K_2}\right) + (2 \text{ cyclic perms. of } 2,3,4) \tag{6}$$

$$= \frac{1}{K_1 K_2 K_3 K_4}(k_1^2 + k_2^2 + k_3^2 + k_4^2 - k_{12}^2 - k_{13}^2 - k_{14}^2) = 0,$$

onde $K_i \equiv k_i \cdot Q$. Neste exemplo, consideramos somente os termos proporcionais a $Q^\mu Q^\nu Q^\lambda Q^\sigma$. Um cálculo explícito mostrou que todas as contribuições proporcionais a T^2 se anulam. Note que este tipo de cancelamento ocorre ao nível do integrando em $d\Omega$.

O cancelamento da $\mathcal{O}(T^2)$ é por si só intrigante, pois mostra que não existe uma contribuição dominante para a não linearidade. Isto contratsta com o comportamento da parte quadrática da ação efetiva, que é proporcional à T^2. De fato, o comportamento dominante da função de 2 pontos é de $\mathcal{O}(T^2)$.

Este resultado nos leva a suspeitar que, talvez, não exista nem mesmo uma contribuição proporcional ao $\log(T)$. O cálculo explícito mostrou que os termos em $\log(T)$ não se anulam ao nível do integrando em $d\Omega$. A fim de obter um resultado conclusivo, teríamos que calcular estas integrais angulares explicitamente. Este cálculo se mostrou impraticável, mesmo utilizando-se os recursos de *computação algébrica* (Mathematica, Maple, Reduce, Form).

No limite de *grandes comprimentos de onda* ($\vec{k} \to 0$) e no limite *estático* ($k_0 \to 0$), foi possível verificar o cancelamento dos termos em $\log(T)$. Isto aumentou ainda mais a suspeita de que a não-linearidade possa ter um limite finito quando $T \to \infty$.

Esta suspeita é reforçada quando analisamos o comportamento das funções de $n > 2$ pontos, na QED em $T = 0$. Sabemos que a *invariância de gauge* elimina as divergências ultravioletas, exceto no caso da auto-energia do fóton ($n = 2$). Lembrando que $A_{\mu_1 \cdots \mu_n}(k_1 \cdots k_n)$ é invariante de gauge, poderíamos esperar que todas as funções com $n > 2$ pontos fossem finitas.

4. Teoria clássica de transporte

Usando a teoria clássica de trasnporte, mostraremos que existe uma razão física muito clara para a inexistência da não linearidade no limite $T \to \infty$. Veremos que, as funções de Green térmicas com um número $n > 2$, par (n impar é trivial, pelo teorema de Furry), de fótons externos, não podem se comportar como T^2. Nosso ponto de partida é semelhante ao utilizado na referência [6].

No limite clássico, um sistema de partículas térmicas é descrito pela densidade de probabilidade no espaço de fase $f(x,p)$. No caso em que as partículas *não colidem*, f obedece a equação de Boltzmann

$$\frac{df}{d\tau} = C[f] = 0, \tag{7}$$

onde $C[f]$ é a integral de colisão.

Usando as equações de movimento *clássicas* para um elétron de massa m

$$m\frac{dx^\mu}{d\tau} = p^\mu$$

$$m\frac{dp^\mu}{d\tau} = eF^{\mu\nu}p_\nu, \tag{8}$$

a equação de transporte pode ser escrita como

$$p^\mu \left[\frac{\partial}{\partial x^\mu} - eF_{\mu\nu}\frac{\partial}{\partial p_\nu} \right] f(x,p) = 0 \tag{9}$$

Neste ponto, é possível fazer a conexão com a teoria de campos a temperatura finita. Vimos que a expansão em potências da temperatura é tambem uma série em potências dos momenta externos. Portanto, pelas relações de Einstein-de Broglie, temos uma expansão em potencias de $\hbar$. *A contribuição dominante corresponde ao limite clássico*. A aproximação de um "loop" coresponde à ausência de colisões na equação de Boltzmann.

Sendo Γ o funcional gerador das funções de Green térmicas no limite de altas temperaturas (portanto clássico), teremos

$$\frac{\delta\Gamma}{\delta A_\mu} = J^\mu = e \int \frac{d^4p}{(2\pi)^3} 2\theta(p_0)\delta(p^2 - m^2)p^\mu f(x,p). \tag{10}$$

Deste modo, é possível obter as funções de n pontos usando derivação funcional da equação acima. Isto pode ser feito de maneira sistemática expandindo perturbativamente a função de distribuição, de modo que

$$p_\mu f^{(0)} = N(p_0) P_\mu, \tag{11}$$

$$\vdots$$

$$p_{\mu_n} f^{(n-1)} = f^{(0)} C_{\mu_1 \cdots \mu_n} A^{\mu_1} \cdots A^{\mu_{(n-1)}}, \tag{12}$$

onde as funções $C_{\mu_1 \cdots \mu_n}$ são obtidas resolvendo-se a equação de transporte perturbativamente

$$p_{\mu_n} f^{(n-1)} = p_{\mu_n} \left(\frac{1}{p \cdot \partial} p^\mu (\partial_\mu A_\nu - \partial_\nu A_\mu) \frac{\partial}{\partial p_\nu} \right)^{(n-1)} f^{(0)} \tag{13}$$

Portanto, podemos escrever

$$\Pi_{\mu_1 \cdots \mu_n} \equiv \frac{\delta^n \Gamma}{\delta A^{\mu_1} \cdots \delta A^{\mu_n}} = \int \frac{d^4 p}{(2\pi)^3} 2\theta(p_0) \delta(p^2 - m^2) f^{(0)} (n-1)! C_{\mu_1 \cdots \mu_n} \tag{14}$$

A dimensão das funções $C_{\mu_1 \cdots \mu_n}$ é $p^{(2-n)}$. Portanto, o integrando das funções de n-pontos tem dimensão $p^{(4-n)}$. Isto mostra que a função de 2 pontos é proporcional à T^2, e a função de 4 pontos *pode* crescer no máximo logaritimicamente para $T \to \infty$.

Os coeficientes $C_{\mu_1 \cdots \mu_n}$ são sistematicamente obtidos, usando integração por partes em $d^4 p$. Por exemplo, para $n = 2$ obtemos a auto-energia do fóton

$$\Pi_{\mu\nu}(k) = \frac{T^2}{24} \int \frac{d\Omega}{4\pi} \left[\frac{k_\nu Q_\mu}{k \cdot Q} + \frac{k_\mu Q_\nu}{k \cdot Q} - \frac{k^2 Q_\mu Q_\nu}{k \cdot Q^2} - \eta_{\mu\nu} \right]. \tag{15}$$

onde a integral é sobre as direções de $\vec{p}/|\vec{p}|$ e $Q \equiv p/|\vec{p}|$. Este resultado concorda com o cálculo (muito mais complicado) utilizando teoria quântica de campos a temperatura finita no limite $T \to \infty$.

Portanto, a ação efetiva da QED a temperatura finita é dominada pela contribuição quadrática nos campos, sendo proporcional à T^2. Os termos não-lineares são subdominantes em T. Isto concorda com o argumento intuitivo, segundo o qual a não-linearidade é produzida por um efeito puramente quântico. Deste modo, como no limite $T \to \infty$ as interações do plasma com o campo externo são descritas classicamente, seria de se esperar que a não-linearidade desaparecesse.

Embora a teoria clássica de transporte explique a supressão da não-linearidade, de maneira direta, ela não nos fornece uma resposta sobre a existência ou não dos termos logaritimicos para funções de Green de $n > 2$ pontos.

5. Comportamento das funções de $n > 2$ pontos no limite $T \to \infty$

Usando regularização dimensional, a função de n fótons, *total* (térmica + $T = 0$), é dada por [3]

$$A^{\mu_1 \mu_2 \cdots \mu_N}(k_i, k_i^0, T) = M^\epsilon T \sum_{Q_0 = \pi i T(2n+1)} \int d^{3-\epsilon} Q F^{\mu_1 \mu_2 \cdots \mu_N}(Q^0, Q, k_i, k_i^0). \tag{16}$$

É possível mostrar que o termo proporcional à $1/\epsilon$ pode ser escrito como

$$A_\epsilon^{\mu_1 \mu_2 \cdots \mu_N}(k_i, T) = f^{\mu_1 \mu_2 \cdots \mu_N}(k_i) \left[\frac{1}{\epsilon} + \log\left(\frac{M}{T} \right) \right]. \tag{17}$$

Ou seja, o $\log(T)$ sempre aparece combinado com $1/\epsilon$.

Como as funções de $n > 2$ fótons são todas finitas no ultravioleta, as funções $f^{\mu_1 \mu_2 \cdots \mu_{N>2}}(k_i)$ devem se anular. Consequentemente, os termos $\log(T)$ também desaparecem. Este resultado foi explicitamente verificado, no limite de grandes comprimentos de onda, para a função de 6 pontos. Mesmo neste caso relativamente simples, um único diagrama de 6 fótons possui 975 termos. Depois de somar as 6! permutações, obtivemos zero.

Finalmente, resta saber qual é o valor, independente de T, que a função de n fótons assume no limite $T \to \infty$ No limite de grandes comprimentos de onda, foi possível mostrar que a ação térmica não linear tende para o valor negativo da ação térmica em $T = 0$

Referências

1. R. Karplus e M. Neuman, Phys Rev. 80, 380 (1950); 83, 776 (1951).

2. H. Euler e B. Kockel, *Naturwiss.* 23. 246 (1935).

3. F. T. Brandt, J. Frenkel e J. C. Taylor. Phys. Rev. D 50, 4110 (1994).

   F. T. Brandt e J. Frenkel, preprint IFUSP/p-1118, a ser publicado no Phys. Rev. Lett..

4. P. Elmfors, D. Persson e B.-S. Skagerstam, Phys. Rev. Lett. 71, 480 (1993); P. Elmfors, D. Persson e B.-S. Skagerstam, Institut Report 93-11, Götenborg e NORDITA -93/78 P; P. Elmfors, P. Liljenberg, D. Persson e B.-S. Skagerstam, Institut Report 94-13, Götenborg 1994; P. Elmfors e B.-S. Skagerstam, NORDITA - 94/18 P; W. Dittrich, Phys. Rev. D 19, 2385 (1979); M. Loewe e J. C. Rojas, Phys. Rev. D 46. 2689 (1992); R. Tarrach, Phys Lett. 133B, 259 (1983).

5. G. Barton, Ann. Phys. 200, 271 (1990).

6. P.F. Kelly, Q. Liu, C. Lucchesi e C. Manuel, Phys. Rev. Lett. 72, 3461, (1994).

Nonrelativistic Quantum Particle in a Curved Space as a Constrained System

A. Foerster, H. O. Girotti and P. S. Kuhn

Instituto de Física da UFRGS, Porto Alegre, Brasil

The canonical quantization of a nonrelativistic particle moving in a curved space is a long standing problem. Indeed, for such a system the classical-quantum correspondence does not define a unique Hamiltonian operator. The free massive particle already serves to illustrate this point; the corresponding classical Hamiltonian is $h = \frac{1}{2M} p_i g^{ij} p_j$, implying that the classical-quantum transition $h \to H$ is afflicted by ordering ambiguities. Moreover, not all quantum mechanical counterparts of h possess a coordinate representation behaving as scalar under generalized coordinate transformations. The canonical quantization procedure is, then, plagued with ambiguities which are not harmless, since they affect the energy spectrum of the physical system.

The outcomes from the path-integral approach can be summarized as follows

$$< q \mid H \mid \phi > = - \frac{\hbar^2}{2M\sqrt{g}} \partial_i \left[\sqrt{g} g^{ij} \partial_j \phi(q) \right] + \frac{\kappa \hbar^2}{M} R \phi(q) . \tag{1}$$

where $g = \det g_{ij}$ and $\partial_i \equiv \partial/\partial q^i$. As can be seen, besides the Laplace-Beltrami operator, a term proportional to the scalar curvature R arises in the structure of H. For the dimensionless constant κ several different values can be found in the literature.

Therefore, an unambiguous determination of the Hamiltonian operator describing the quantum dynamics of a free particle moving in a curved space is still lacking. Here we make a proposal pointing towards such determination. First we work out the problem within the operator approach and then separetely, within the functional approach.

Our main idea consists in treating the curved manifold as a hypersurface (U_{N-1}) embedded in an Euclidean space. To secure that the motion takes place on U_{N-1} we let the Cartesian equation of the hypersurface act as a constraint. The whole problem of formulating the quantum dynamics of a free particle in a curved space reduces then, essentially, to solve for the motion of a constrained quantum system in an Euclidean space. Afterwards, we undo the embedding in order to recover the original problem (for more details, see Ref.[1]).

Within the canonical approach we obtain

$$H_E = \frac{1}{2M} g^{-\frac{1}{4}} \Pi_i g^{\frac{1}{2}} g^{ij} \Pi_j g^{-\frac{1}{4}} + V_Q , \tag{2}$$

where the Π' are momenta operators,

$$V_Q = \frac{\hbar^2}{8M} \frac{(\partial_n f)(\partial^n f)}{M} \bar{\Gamma}^i_{0i} \bar{\Gamma}^j_{0j} , \tag{3}$$

and $\hat{\Gamma}^{\mu}_{\nu\rho}$ is the Christoffel symbol associated with the metric $\bar{g}_{\mu\nu}$, and g designates the *reduced* determinant $g \equiv \det g_{ij}$.

The first term in Eq.(2) is the standard Laplace-Beltrami operator. It only contains quantities intrinsic to the surface. On the other hand, V_Q represents the contribution to the Hamiltonian arising from the quantum fluctuations of the normal vector. It is easy to see that V_Q behaves as scalar under *reduced* coordinate transformations.

This result can not be considered as final since, for recovering the original system, one must first remove the spurious degree of freedom. We start by recalling that the intrinsic geometry of a surface is based on the inner product as applied only to its tangent vectors, which belong to the calculus of the surface itself. This is not the case with normal vectors, which enter in the structure of V_Q as $(\partial_a f)(\partial^a f)$.

Hence, by isolating from H_E the piece intrinsic to the surface one arrives to

$$H = \frac{1}{2M} g^{-\frac{1}{4}} \Pi_i g^{\frac{1}{4}} g^{ij} \Pi_j g^{-\frac{1}{4}}. \tag{4}$$

Thus we have $\kappa = 0$ for H, determining the Hamiltonian operator of a free particle in a curved space without ambiguities.

In the functional formalism we have

$$H'_E = H + V'_Q, \tag{5}$$

where

$$V'_Q = \frac{\hbar^2}{8M} \left\{ R + \frac{(\partial_a f)(\partial^a f)}{4M} \left[3 g^{ij}_{,0} g_{ij,0} - (g^{ij} g_{ij,0})^2 \right] \right\}. \tag{6}$$

Again,we undo the embedding by removing from H'_E all the terms which are not intrinsic to the surface. In this way we obtain

$$H' = H + \frac{\hbar^2}{8M} R, \tag{7}$$

as the Hamiltonian operator of a free particle in a curved space. This result arised unambiguously within the functional approach and is seen not to coincide with that obtained in the operatorial scheme (see Eq.(4), the difference being the term proportional to the scalar curvature.

To summarize. we have shown how the operator and functional formulations of the dynamics of constrained systems can be used for obtaining the quantum Hamiltonian of an unconstrained nonrelativistic particle in a curved space.

[1] A. Foerster, H. O. Girotti and P. S. Kuhn, to appear in Phys. Lett.A

A Questão do Ordenamento na Quantização dos Skyrmions

Jorge Ananias Neto

Centro Brasileiro de Pesquisas Físicas, D.C.P.

R. Dr. Xavier Sigaud 150 22290-180 Rio de Janeiro, Brasil

Quantizando através das coordenadas coletivas, mostramos que existe um problema de orde-
namento na definição do operador momento. Então, sugerimos uma nova definição para este
operador que pode resolver o problema de infravermelho que se apresenta quando tentamos
minimizar todo o Hamiltoniano Quântico.

I. Introdução

O modelo de Skyrme é uma teoria de campos não linear que apresenta soluções clássicas tipo sóliton. O seu sucesso consiste na possibilidade de ser uma teoria alternativa à QCD no limite de baixas energias, ou seja, no limite não perturbativo. Inicialmente, a Lagrangiana estática é escrita como

$$L = \frac{F_x}{e} \int d^3x \left[-\frac{1}{16} Tr \left(\partial_i U \partial_i U^+ \right) + \frac{1}{32} Tr \left[U^+ \partial_i U, U^+ \partial_j U \right]^2 \right] , \tag{1}$$

onde F_x é a constante de decaimento dos pions, e é um parâmetro adimensional e U é um campo pertencente a SU(2), ou seja, $UU^+ = 1$. Introduzindo as coordenadas rotacionais coletivas através da substituição $U(x)$ por $U(x,t) = A(t)U(x)A^+(t)$ onde A é uma matriz SU(2) escrita como $A = a_0 + ia.\tau$, podemos escrever o Hamiltoniano através da relação $H = \pi\dot{a} - L$, como

$$H = M + \frac{1}{8\lambda} \sum_i \pi_i^2$$

$$= M + \frac{1}{8\lambda} \sum_{i=0}^{3} \left(-\frac{\partial}{\partial a_i^2} \right) , \tag{2}$$

onde M é a massa do sóliton e λ é o momento de inércia. A quantização canônica é feita substituindo π_i por $-i\partial/\partial a_i$, com o vínculo $\sum_{i=0}^{i=3} a_i^2 = 1$. O operador $\sum_{i=0}^{3} \left(-\frac{\partial}{\partial a_i^2} \right)$ é conhecido como laplaciano na triesfera, com autovalores $l(l+2)$ $l = 1, 2 \dots$ e autovetores polinômios em a_i. Se o nosso propósito é trabalhar com as coordenadas a_i, a expressão para o operador momento conjugado a a_i devido ao vínculo é

$$\pi_j = \frac{1}{i} \left[\delta_{i,j} - a_j a_i \right] \partial_i . \tag{3}$$

Consequentemente $\pi_j \pi_j$ pode ser escrito como

$$\pi_j \pi_j = -\partial_j \partial_j + 3 a_j \partial_j + a_i a_j \partial_i \partial_j . \tag{4}$$

Cabe agora mencionar o problema de ordenamento que aparece na definição (3). Tentando contornar esta questão e o problema de infravermelho que surge quando tentamos minimizar todo o Hamiltoniano Quântico sugerimos uma nova definição para o operador momento dada por

$$\pi_j = \frac{1}{(1+\alpha)i}\left[(\delta_{i,j} - a_j a_i)\partial_i + \alpha\,\partial_i(\delta_{i,j} - a_i a_j)\right] \, , \tag{5}$$

onde α é um parâmetro real livre. Consequentemente $\pi_j \pi_j = -\partial_j \partial_j + 3a_j \partial_j + a_j a_i \partial_j \partial_i - \frac{5\alpha(2\alpha-3)}{(1+\alpha)^2}$, e os autovalores do Hamiltoniano Quântico extendido são dados por

$$E = M + \frac{1}{8\lambda}\left[l(l+2) - \frac{5\alpha(2\alpha-3)}{(1+\alpha)^2}\right] \, . \tag{6}$$

Na equação acima quando l=1 nós verificamos que para $\alpha > \frac{21+5\sqrt{21}}{14}$ ou $\alpha < \frac{21-5\sqrt{21}}{14}$ desaparece o problema infravermelho. Assim, é possível procurar configurações de campo que minimizem todo o Hamiltoniano Quântico. Com estas novas soluções esperamos obter consideráveis melhoras no espectro físico do modelo de Skyrme. Mais referências podem ser encontradas em Remarks on the Collective Coordinates Quantization of the SU(2) Skyrme Model, preprint CBPF(1994), a ser publicado no Journal of Physics G.

Integrais Múltiplas de Grassmann e a Expansão em β do modelo de Hubbard em d=2(1+1).

I.C.Charret e M.T.Thomaz,

Instituto de Física - Universidade Federal Fluminense

Av. Litorânea s/nº, Campus da Praia Vermelha

Niterói, R.J., 24310-340

E.V.Corrêa Silva e S.M. de Souza

Instituto de Física - Universidade Federal do Rio de Janeiro

Caixa Postal: 68528, Rio de Janeiro, R.J., 21945-970

Calculamos em ordem β a função de partição grã-canônica do modelo de Hubbard em $d = 2(1 + 1)$ usando integrais múltiplas de Grassmann.

É usual no cálculo de integrais funcionais de sistemas fermiônicos a utilização de formas bosonizadas. Neste trabalho utiliza-se a Álgebra de Grassmann para calcular de forma não-perturbativa as integrais funcionais fermiônicas via integrais múltiplas de Grassmann. Mostramos anteriormente [1] que integrais múltiplas de Grassmann da forma:

$$I_l = \int \prod_{i=1}^{N} d\bar{\eta}_i d\eta_i exp\{-[\eta A\bar{\eta} + (\eta B\bar{\eta})^l]\}, \quad l \leq N, \tag{1}$$

possuem expressões exatas.

As integrais funcionais de modelos fermiônicos interagentes escritas sobre uma rede pode m ser colocadas numa forma similar a I_l.

Para um sistema em equilíbrio termodinâmico com um reservatório a temperatura T podendo trocar partículas com esse reservatório, toda informação está contida na função de partição grã-canônica, $Z = Tr[exp(-\beta K)]$, onde $\beta = 1/kT$ e $K = H - \mu N$.

Para sistemas fermiônicos interagentes a função de partição grã-canônica é dada por [2]:

$$Z(\beta,\mu) = \int \mathcal{D}\psi(\vec{x},\tau)\mathcal{D}\bar{\psi}(\vec{x},\tau)e^{-\int d\vec{x}\int_0^\beta d\tau\bar{\psi}(\vec{x},\tau)\theta_\tau\psi(\vec{x},\tau)}e^{-\int_0^\beta d\tau K}, \tag{2}$$

onde $\psi(\vec{x},\tau)$ e $\bar{\psi}(\vec{x},\tau)$ são funções anticomutantes, $\vec{x}$ e τ são parâmetros contínuos. Por outro lado podemos pensar em um sistema fermiônico descrito por parâmetros discretos. No caso de uma rede unidimensional, a cadeia contém N sítios espaciais. O intervalo de temperatura pode ser particionado em M subintervalos de módulo ε, onde $M\varepsilon = \beta$. A versão discreta da eq.2 corresponde a $\vec{x}$ e τ assumirem valores discretos sobre uma hiper-rede. A forma discreta de $Z(\beta,\mu)$ é similar as integrais I_l.

Para qualquer valor de ε finito tal que $M\varepsilon = \beta$ é verdadeira a igualdade: $Z = Tr[e^{-M\varepsilon K}] = Tr[(e^{-\varepsilon K})^M]$. A expansão no parâmetro ε em alta temperatura até primeira ordem fica:

$$Z = Tr[(1 - \varepsilon K)^M + O(\varepsilon^2)] = Tr[1 - M\varepsilon K + O(\varepsilon^2)] = Tr[1 - \beta K + O(\varepsilon^2)] \tag{3}$$

A equivalência das duas expansões é verdadeira em todas as ordens de ε.

Aplicamos esse método para obter a função de partição grã-canônica do modelo de Hubbard [3] de dimensão $d = 2(1 + 1)$. Consideramos o modelo com interação entre primeiros vizinhos na presença de um campo magnético externo.

Trabalhando com uma rede espacial unidimensional sujeita a condições de contorno espaciais periódicas e com um intervalo de temperatura particionado em M subintervalos de módulo ε sujeito a condições de contorno antiperiódicas, podemos escrever os geradores da álgebra em função da posição no sítio x_i e do intervalo de temperatura τ_j: $\eta(x_i, \tau_j)$.

A função de partição grã-canônica discretizada possui uma forma esquemática dada por:

$$Z = \int d\eta d\bar{\eta} e^{-\eta \mathbf{A}\bar{\eta}} e^{-(U\eta_1 \bar{\eta}_1 \eta_1 \bar{\eta}_1)} \tag{4}$$

Na eq. (4) a matriz $\mathbf{A}$ contém as informações sobre as interações quadráticas incluindo as condições de contorno antiperiódicas na temperatura. A expressão dá o resultado exato da função de partição grã-canônica até ordem β.

Com o auxílio de computação algébrica (MAPLE) encontramos uma expressão geral para a função de partição para sistemas fermiônicos a altas temperaturas:

$$Z = 2^{2N} \{ 1 + N\beta(\mu - E_0 - U/4) \} \tag{5}$$

No limite de altas temperaturas $(T \to \infty)$ encontramos que a energia média por sítio é $(E_0 + U/4)$, o número médio de partículas com spin σ é $1/2$ e a magnetização média é zero.

Em resumo, temos que esse método nos fornece a função de partição grã-canônica para altas temperaturas de sistemas fermiônicos interagentes de modo não-perturbativo. O método se aplica a qualquer sistema de férmions interagentes.

References

1. S.M. de Souza e M.T. Thomaz, J. Math. Phys. **31** (1990) 6.

2. U.Wolf, Nucl. Phys. **225** (1983) 391.

3. J.Hubbard, Proc. Roy. Soc. **A277** (1963) 237; **A281** (1964) 401.

A superspace formulation of the BV action

Nelson R. F. Braga and Ashok Das[*]

Instituto de Física, Universidade Federal do Rio de Janeiro

Rio de Janeiro 21945 Caixa Postal 68.528. Brasil

We show that for a general gauge fixing Lagrangian, the BV action can be written in a manifestly generalized BRST invariant manner in a superspace with one Grassmann coordinate.

Generalized BRST Invariant Superspace Formulation

Let us consider the theory defined by

$$\tilde{\mathcal{L}} = \mathcal{L}(\phi_\mu - \dot{\phi}_\mu , \eta - \tilde{\eta} , \overline{\eta} - \dot{\overline{\eta}}) \tag{4.6}$$

and note that when the tilde superfields vanish, this Lagrangian reduces to our original theory. In this case, we can define

$$\Phi_\mu(x,\theta) = \phi_\mu(x,\theta) - \dot{\phi}_\mu(x,\theta) \tag{1}$$

$$\Lambda(x,\theta) = \eta(x,\theta) - 4\tilde{\eta}(x,\theta) \tag{2}$$

and note that if the field strength associated with the 1-form $\Omega = \Phi_\mu dx^\mu + \Lambda d\theta$ vanishes along the θ direction, then we can determine

$$\Phi_\mu(x,\theta) = (A_\mu - \tilde{A}_\mu) + \theta D_\mu^{(A - \tilde{A})}(c - \tilde{c})$$

$$\Lambda(x,\theta) = (c - \tilde{c}) - \frac{1}{2}\theta[c - \tilde{c}, c - \tilde{c}]_+$$

This, however, does not determine the individual superfields ϕ_μ, $\dot{\phi}_\mu$, η and $\tilde{\eta}$ uniquely and this is the arbitrariness in the generalized BRST transformations that we discussed earlier.

In addition, let us introduce the superfields

$$\begin{aligned}
\dot{\phi}_\mu^*(x,\theta) &= A_\mu^* - \theta B_\mu \\
\tilde{\eta}^*(x,\theta) &= c^* - \theta B \\
\tilde{\overline{\eta}}^*(x,\theta) &= \overline{c}^* - \theta \overline{B} \\
\dot{f}(x,\theta) &= \tilde{F} + \theta c_F \\
\dot{f}^*(x,\theta) &= F^* - \theta B_F
\end{aligned} \tag{3}$$

It is clear now that with these choices of the superfields, the generalized BRST transformations of Eq. (2.11) arise as translations of the θ coordinate. Thus, we see that the gauge fixing Lagrangian of Eq. (2.12) for the shift symmetry can be written in this superspace as

[*]Permanent address: Department of Physics and Astronomy, University of Rochester, Rochester, NY 14627, USA.

$$\bar{\mathcal{L}}_{gf} = \frac{\partial}{\partial\theta} \, \mathrm{Tr} \left(\dot{\phi}^*_\mu \dot{\phi}^\mu + \bar{\eta}^* \dot{\eta} - \dot{\bar{\eta}}\eta^* - \dot{f}^* f \right)$$

Being the θ component of a superfield, this is manifestly invariant under the generalized BRST transformations.

The gauge fixing Lagrangian for the original symmetry can also be written in this space in a straight forward manner. Let $\psi = \psi(A_\mu, c, \bar{c}, F)$ denote an arbitrary gauge fixing fermion. We assume this to depend only on the original fields. Then, we can define a fermionic superfield as

$$\Psi = \psi + \theta\delta\psi = \psi + \theta\left(-\frac{\delta\psi}{\delta A_\mu} \psi_\mu + \frac{\delta\psi}{\delta c} c + \frac{\delta\psi}{\delta\bar{c}} \bar{c} - \frac{\delta\psi}{\delta F} c_F \right)$$

For the gauge choice presented before this superfield will be of the form

$$\Psi = -\mathrm{Tr} \, \partial_\mu \bar{c} A^\mu + \theta \, \mathrm{Tr} \left(\partial_\mu \bar{c} \psi^\mu + \partial_\mu A^\mu \bar{c} \right)$$

We see that the gauge fixing Lagrangian for the original symmetry can be written as

$$\mathcal{L}_{gf} = \frac{\partial\Psi}{\partial\theta}$$

for any arbitrary fermionic gauge fixing term. Once again, being the θ component of a superfield, this is manifestly invariant under the generalized BRST transformations.

The complete Lagrangian can now be written as

$$
\begin{aligned}
\mathcal{L} &= \mathcal{L}_o(\phi_\mu - \dot{\phi}_\mu) + \bar{\mathcal{L}}_{gf} + \mathcal{L}_{gf} \\
&= \mathcal{L}_o(A_\mu - \dot{A}_\mu) + \frac{\partial}{\partial\theta} \, \mathrm{Tr} \left(\dot{\phi}^*_\mu \dot{\phi}^\mu + \bar{\eta}^* \dot{\eta} - + \dot{\bar{\eta}}\eta^* - \dot{f}^* f \right) + \frac{\partial\Psi}{\partial\theta}
\end{aligned}
\tag{4}
$$

which is manifestly invariant under the generalized BRST symmetry and upon elimination of the auxiliary fields and ghosts associated with the shift symmetry, leads to the BV action.

Bibliography

1. I. A. Batalin and G. A. Vilkovisky, Phys. Lett. **B102** (1981) 27; Phys. Rev. **D28** (1983) 2567.

2. J. Alfaro and P. H. Damgaard, Phys. Lett. **B222** (1989) 425; J. Alfaro, P. H. Damgaard, J. I. Latorre and D. Montano, Phys. Lett. **B233** (1989) 153; J. Alfaro and P. H. Damgaard, Nucl. Phys. **B404** (1993) 751.

Macroscopic manifestations of nondistributive structures, the wave function of macroscopic quantum automata

Andrey A. Grib[*]

Departamento de Matemática Aplicada - IMECC
Universidade Estadual de Campinas - UNICAMP
CP. 6065: 13.081-970. Campinas. SP. Brasil

Examples of macroscopic structures "macroscopic quantum computers", described by wave functions due to nondistributive logics of work of these computers are discussed. It is shown for the lattice of topologies for 3 points that due to its nondistributivity and nonmodularity it can't be described either by Kolmogorovian probability or by the wave function.

As it is well known usual Kolmogorovian probability measure doesn't work for quantum systems. Instead one must use "probability amplitude" – the wave function, being vector in some Hilbert space. So in physics we have – "classical macroscopic systems", when one has the usual probability measure defined on the phase space and "quantum microscopic" systems described by wave functions.

It was in the paper of Birkgoff and von Neumann [1] that the reason of use of the "probability amplitude" in microphysics was understood. This reason is nondistributivity of the lattice of properties ("yes-no" questions) of the micro-systems ("quantum logic"). Nondistributivity means that if a, b, c are some properties and we define "disjunction" $\vee$ corresponding to such property. $d = a \vee b$ that if a-"true" then d "true", if b"true" then d"true", and conjunction $\wedge$ as $\ell = a \wedge b$ so that ℓ-"true" leads to a "true", ℓ-"true" leads to b-"true", then in general $a \wedge (b \vee C) \neq (a \wedge b) \vee (a \wedge C)$.

Birkgoff, von Neumann, K. Piron and others then proved that nondistributivity of abstract lattices of properties leads to noncommuting operators in Hilbert space.

One can ask, are there other systems (macroscopical ones) described by probability amplitude ?.

As it was shown in our papers [2, 3] the answer is "yes". The example of such a system is "macro-scopical quantum computer", the system, "hardware" of which is described by classical physics, but "sofware" due to "quantum logic" used for attributing symbols to states of "hardware" is described by the wave function. To construct such automata one must look for graphs of these automata and to use the rule: the state of the system is identified if there is negative answer on the question about some complementary state: "a" is not "not a". Rules for constructing Hasse diagram for such automata were given in [2, 3] and it was shown that one comes to the usual Hilbert space formulation for their work, to Heisenberg uncertainty relation, without Planck's constant and to Schrödinger equation for the evolution of state. Bell's inequalities can be broken for such automata but surely without any reference to relativity theory. So besides superconductivity and superfluidity one can have other examples of systems described by wave functions. There is the possibility of interactions of microscopical quantum systems with such automata due to usual rules of quantum physics. The intriguing possibility to look for such systems in nature is the work of human brain ("quantum brain"). Other question is: are there stochastic systems which can't be described either by probability measure or by the probability amplitude ?. The answer is "yes": such system is the lattice of topologies

[*]On leave from A.A. Friedmann Laboratory for Theoretical Physics. 191023 St. - Petersburg. Griboyedov can. 30/32. Russia

for 3 points [4], due to its nondistributivity if topology is random one can't have usual probability measure, and due to nonmodularity there is no wave function. One can find some realization of this lattice in terms of idempotent operators as some 6 × 6 noncommunting matrices and two "bra" and "ket" Hilbert spaces. This realization shows as some resemblance (noncommutativity) to quantum systems as some difference (two Hilbert spaces instead of one) of the lattice of topologies from other known stochastic systems, all this shows that "quantum topology" must be founded on some other grounds than usual quantum theory.

Literature

1. Birkgoff E., von Neumann J., Ann. of Math. **37**, 823 (1936).

2. Grib A.A., Zapatrin R.R., Intern. Journal of Theor. Phys. **29**, 113 (1990).

3. Grib A.A.. Zapatrin R.R. Intern. Journal of Theor. Phys. **30**, 949 (1991).

4. Grib A.A., Zapatrin R.R. Intern. Journal of Theor. Phys. **31**, 1093 (1992).

Physical interpretation of Schwinger's formula for effective actions

L. C. de Albuquerque,[*] C. Farina,[†] Silvio J. Rabello[‡]
and
Arvind N. Vaidya[§]

Instituto de Física, Universidade Federal do Rio de Janeiro

Caixa Postal 68.528-CEP 21945-970, Rio de Janeiro, RJ. Brasil

We show explicitly that Schwinger's formula for one-loop effective actions corresponds to the summation of energies associated with the zero-point oscilations of the fields. We begin with a formal proof, and after that we confirm it using a regularization prescription.

Although the result we shall prove is quite general, we shall choose, for simplicity, a definite problem in order to emphasize the basic points of our demonstration without getting involved with mathematical details.

Considerer then a massive scalar field in a $(3 + 1)$-dimensional space-time (the extension to $d + 1$ dimensions is trivial) and suppose we are interested in computing the Casimir energy $\varepsilon[1]$, where the boundary conditions are chosen to be of Dirichlet type in only one of the axis, say, the OX_3 axis. So, the fields must vanish at $z = 0$ and $z = a$, where two plates of area $A >> a$ paralell to each other are placed.

In a recent paper, J. Schwinger[2] showed, for the massless case, how this calculation could be done through the formula (which we will call Schwinger's formula for now on)

$$\omega^{(1)} = -\frac{i}{2} \int_{s_0}^{\infty} \frac{ds}{s} Tr e^{-is(\mathcal{H} - i\varepsilon)}, \tag{1}$$

where $\omega^{(1)}$ is the one-loop effective action and $\mathcal{H}$ is the proper-time Hamiltonian for the system at hand. Then, the casimir energy is simply given by $\varepsilon = -\frac{\omega^{(1)}}{T}$, where T can be viewed as the time interval. In equation (1). the regularising cut-off s_0 must be put to zero only after a suitable subtraction of non-physical terms is madeAn application of this formula for the same problem but with a different regularization prescription can be found in [3]. See also [4] for the massive case...

Since Schwinger's formula had also been aplied with sucess for the cases of effective actions for QED in the old fifties [5], we thought it would be interesting to give a physical interpretation of it through a connection with the more intuitive picture of the mode summation approach.

We shall firstly establish a formal connection and after that, we shall confirm our result in a more rigorous way, using a regularization procedure.

Let us start with the formal expression

$$\omega^{(1)} = -\frac{i}{2} \int_{0}^{\infty} \frac{ds}{s} Tr e^{-is(\mathcal{H} - i\varepsilon)}, \tag{2}$$

[*] e-mail:ift10030@ufrj.bitnet
[†] e-mail:farina@vms1.nce.ufrj.br
[‡] e-mail:goldegol@vms1.nce.ufrj.br
[§] e-mail:ift10034@ufrj.bitnet

where $\mathcal{H} = \vec{p}^2 - \omega^2 + m^2$, with $\vec{p} = -i\vec{\nabla}$, $\omega = i\partial_t$. Taking a derivative with respect to m^2 on both sides of (2), we get

$$\frac{\partial \omega^{(1)}}{\partial m^2} = -\frac{1}{2} \int_0^\infty ds Tr e^{-is(\mathcal{H}-i\epsilon)}. \tag{3}$$

Computing the trace, and making the identification $\epsilon = -\omega^{(1)}/T$, we have

$$\frac{1}{A}\frac{\partial \epsilon}{\partial m^2} = \frac{1}{2}\sum_{n=1}^\infty \int \frac{dk_1 dk_2 dk_0}{(2\pi)^3} \int_0^\infty ds e^{-is(-k_0^2+k_1^2+k_2^2+\frac{n^2\pi^2}{a^2}-i\epsilon+m^2)}. \tag{4}$$

Integration over s imediatly leads to

$$\frac{1}{A}\frac{\partial \epsilon}{\partial m^2} = \frac{i}{2}\sum_{n=1}^\infty \int\int \frac{dk_1 dk_2}{(2\pi)^2} \int \frac{dk_0}{2\pi} \frac{1}{k_0^2 - [k_1^2 + k_2^2 + \frac{n^2\pi^2}{a^2} - i\epsilon + m^2]}. \tag{5}$$

Now, with the aid of residua theorem, we can integrate over k_0 to get

$$\frac{1}{A}\frac{\partial \epsilon}{\partial m^2} = \frac{1}{2}\sum_{n=1}^\infty \int\int \frac{dk_1 dk_2}{(2\pi)^2} \frac{1}{\sqrt{k_1^2 + k_2^2 + \frac{n^2\pi^2}{a^2} + m^2}}. \tag{6}$$

Then, making the integration over m^2 we obtain,

$$\frac{\epsilon}{A} = \sum_{n=1}^\infty \int\int \frac{dk_1 dk_2}{(2\pi)^2} \frac{1}{2}\omega(k_1, k_2, n), \tag{7}$$

apart from an additive irrelevant constant, and where we defined the eigenfrequencies (zero-point energies of the field) $\omega(k_1, k_2, n) = \sqrt{k_1^2 + k_2^2 + \frac{n\pi^2}{a} + m^2}$. Expression (7) is precisely the usual (unregularized) mode summation expression for the Casimir energy of a massive scalar field between two paralell plates distant apart a distance a [6].

Since in our previous deduction manipulations with divergent terms were made, let us now reobtain the same result, but this time in a more rigorous way. What we mean is that we shall establish a connection between two regularized expressions, Schwinger's one and a (regularized) mode summation expression, with some kind of regularization prescription adopted.

However, instead of starting with the regularized expression (1) (with the cut-off s_0), we shall adopt the following regularization prescription

$$\omega^{(1)} = -\frac{i}{2}\int_0^\infty ds s^{\nu-1}Tr e^{-is(\mathcal{H})}, \tag{8}$$

where ν is large enough to make the integral well defined. In this approach, after the integral is computed an analytical continuation to the whole complex plane of ν must be done and then the limit $\nu \to 0$ must be carefully taken (sometimes appropriate subtractions have shall to be made, see [3, 4] for more details of this approach)

As before we start taking the derivative of (8) with respect to m^2. After evaluating the trace, we get

$$\frac{\partial \omega^{(1)}}{\partial m^2} = -\frac{AT}{2}\sum_{n=1}^\infty \int \frac{dk_1 dk_2 dk_0}{(2\pi)^3} \int_0^\infty ds s^\nu e^{-is(-k_0^2+k_1^2+k_2^2+\frac{n^2\pi^2}{a^2}+m^2)}. \tag{9}$$

Using the definition of the Euler Gamma function, the integration over s readily yields

$$\frac{\partial \omega^{(1)}}{\partial m^2} = (i)^{\nu+1}\frac{-1}{2}AT\Gamma(\nu+1)\sum_{n=1}^\infty \int\int \frac{dk_1 dk_2}{(2\pi)^2} \int \frac{dk_0}{2\pi}[k_0^2 + (i)^2(k_1^2 + k_2^2 + \frac{n^2\pi^2}{a^2} + m^2)]^{-(\nu+1)}. \tag{10}$$

Using   now   that $\int_{\infty}^{\infty} dx(x^2 + a^2)^{-\sigma} = (a^2)^{\frac{1}{2}-\sigma} B(\frac{1}{2}, \sigma - \frac{1}{2})$,   where $B(p,q) = \frac{\Gamma(p)\Gamma(q)}{\Gamma(p+q)}$, we get

$$\frac{\partial \omega^{(1)}}{\partial m^2} = \frac{-1}{2} i^{-\nu} A T \Gamma(\frac{1}{2}) \Gamma(\nu + \frac{1}{2}) \sum_{n=1}^{\infty} \int \int \frac{dk_1 dk_2}{(2\pi)^2} \frac{1}{2\pi} [k_1^2 + k_2^2 + \frac{n^2\pi^2}{a^2} + m^2]^{-(\nu+\frac{1}{2})}. \tag{11}$$

Integrating on m^2 and identifying $\varepsilon = -\frac{\omega^{(1)}}{T}$, we finaly obtain apart from an irrelevant additive constant

$$\frac{\varepsilon}{A} = \sum_{n=1}^{\infty} \int \int \frac{dk_1 dk_2}{(2\pi)^2} \frac{1}{2} \omega(k_1, k_2, n) F(\nu), \tag{12}$$

where we defined

$$F(\nu) = \frac{i^{-\nu}}{1-2\nu} \frac{\Gamma(\nu + \frac{1}{2})}{\sqrt{\pi}} \omega^{-2\nu}(k_1, k_2, n). \tag{13}$$

Some comments are in order here. Expression (12) is nothing but the usual mode summation with the presence of the regulator function $F(\nu)$, once $F(\nu)$ contains the negative power $\omega^{-2\nu}$. So, for ν large enough expression (12) is well defined and after an analytical continuation to the whole complex ν plane is made the limit $\nu \to 0$ can be (carefully) taken to yield the physical Casimir energy per unit area. One could object by saying that, besides $\omega^{-2\nu}$, the regulator $F(\nu)$ contains the other factors $\frac{i^{-\nu}}{1-2\nu} \frac{\Gamma(\nu+\frac{1}{2})}{\sqrt{\pi}}$. However, this causes no problem at all, since for $\nu \to 0$ this factor turns to be 1. Hence, we have established the equivalence between the modified Schwinger's formula (8) and the (regularized) mode summation aproach. Although we have choosen a definite problem, eg. the Casimir energy for a massive scalar field with Dirichlet boundary condition in one direction, our deduction is general, and therefore the Schwinger's formula for (one-loop) effective action could be physically interpreted as the summation of zero-point energies of the field.

References

[1] H. G. B. Casimir, *Proc. K. Ned. Akad. Wet* 51, (1948) 793.

[2] J. Schwinger, *Lett. Math. Phys.* 24 (1992) 59.

[3] M. V. Cougo-Pinto, C. Farina and A. J. Segui-Santonja. *Lett. Math. Phys.* (1994), in press.

[4] M. V. Cougo-Pinto, C. Farina and A. J. Segui-Santonja, to appear in *Lett. Math. Phys.* (1994).

[5] J. Schwinger, *Phys. Rev.* 82 (1951) 664.

[6] Plunien, G., Muller, B. and Greiner, W., *Phys. Rep.* 134 (1986) 87.

BRST quantization of anomalous gauge theories

Nelson R. F. Braga[*]

Instituto de Física, Universidade Federal do Rio de Janeiro
Caixa Postal 68528- 21945 Rio de Janeiro-Brasil

It is shown how the BRST quantization can be applied to a gauge invariant sector of theories with anomalously broken symmetries. This result is used to shown that shifting the anomalies to a classically trivial sector of fields (Wess Zumino mechanism) makes it possible to quantize the physical sector in a standard BRST way as for a non anomalous theory. The trivial sector plays the role of a topological sector if the system is quantized without shifting the anomalies.

1. Introdução

Let us assume that we have a theory described by:

$$S = S_{Phys.}(\Phi^a, \Phi^{*a}) + S_T(\vartheta^b, \vartheta^{*b}, c^\alpha) \qquad (1)$$

Subject to the boundary conditions $S_{Phys.}(\Phi^a, \Phi^{*a} = 0) = S(\phi^i)$ and $S_T(\vartheta^b, \vartheta^{*b} = 0, c^\alpha) = 0$ The set ϑ^b includes at least the fields θ^j and the ghosts d^β. Assuming that the new fields in S_T have an invariant path integral measure. we get: $\Delta S = \Delta S_{Phys.} = c^\gamma A_\gamma$

Wess-Zumino mechanism: $\frac{1}{2}(W, W) - i\hbar \Delta W = d^\gamma \overline{A}_\gamma$

The anomalies have not been canceled. They have just been shifted to the symmetries associated to the trivial sector.

Example

$$S_{Phys.} = \int d^2x\{S_0 + i\psi^*\psi c - i\overline{\psi}\,\overline{\psi}^*c\} \qquad (2)$$

$$S_T = \int d^2x\{\theta^*c + \theta^*d + \overline{c}^*\pi + \overline{d}^*\lambda\} \qquad (3)$$

The action $S_{Phys.}$ corresponds to the gauge fixed BV action for the chiral Schwinger model. whose classical action is S_0. S_T corresponds to the gauge fixed action for a theory of a scalar field that transforms with the gauge group of the Schwinger model

We can write S_T as a BRST variation, showing explicitly it's topological character:$S_T = \delta\Omega$ with

$$\Omega = -\theta^*\theta + \overline{c}^*\overline{c} + \overline{d}^*\overline{d} \qquad (4)$$

Two different approaches are possible then. First approach:

$$\overline{S}_T(\phi^a, \phi^{*a}) = \int d^2x\{\theta^*d + \overline{d}^*\lambda + d^*\eta\} \qquad (5)$$

With $\Psi = \overline{d}(\theta - \theta_o)$ that leads to the action

[*]braga@vms1.nce.ufrj.br

$$\overline{S}_T(\phi^a, \phi^{*a} = \frac{\partial \Psi}{\partial \phi^a}) = \int d^2x \{\overline{d}d + \lambda(\theta - \theta_o)\} \tag{6}$$

Second approach: (Wess Zumino mechanism)

$$M_1 = -\frac{1}{4\pi} \int d^2x \left\{ \frac{(a-1)}{2} \partial_\mu \theta \, \partial^\mu \theta + \theta \left[(a-1)\partial_\mu A^\mu + \epsilon^{\mu\nu}\partial_\mu A_\nu\right] \right\} \tag{7}$$

That satisfies $(M_1, S) = i\Delta S_{Phys.} + \int d^2x \overline{A}(\theta, A_\mu)d$ Now the quantum action $W = S_{Phys.} + S_T + hM_1$ gets

$$\overline{W} = S_{Phys.} + \int d^2x \{\theta^* c + \overline{c}^* \pi\} + M_1(A_\mu, \theta) \tag{8}$$

that corresponds to the Schwinger model with it's standard Wess Zumino term.

Conclusion

It is interesting now to make a parallel with the original discussion of Faddeev and Shatashvili. There, the anomalies are interpreted as not breaking the gauge symmetry but just inducing a different representation for the group, in which the WZ fields are also present. We can say that in order to build up this representation for the gauge group we are borrowing some fields from a sector that behaves as a topological theory if the WZ mechanism is not implemented.

Bibliography:

"BRST quantization of anomalous gauge theories" N.R.F.Braga - HEP-TH 9405088.

Equivalence of Classical Spins and Hartree-Fock-Bogoliubov Approximation of the Fermionic Anharmonic Oscillator

M. T. Thomaz

Instituto de Física, Universidade Federal Fluminense, Av. Litorânea s/nº.
Campus da Praia Vermelha Niterói, R.J., 24310-340   Brazil

A. F. R. de Toledo Piza

Instituto de Física, Universidade de São Paulo
São Paulo, S.P., 01452-990   Brazil

We show that the Hartree-Fock-Bogoliubov (alias Gaussian) approximation of the initial condition problem of the Fermionic Anharmonic Oscillator is equivalent to a bosonic hamiltonian system of two classical spin.

It has been shown that the Hartree-Fock approximation of fermionic many-body system can be mapped into an equivalent hamiltonian classical system[1]. This equivalence allows to derive physical properties of fermionic quantum systems by studying the classical equation of the equivalent system. It is not an obvious statement that all fermionic quantum system can be mapped onto a classical model.

The Fermionic Anharmonic Oscillator (FAO) is the zero spatial realization of the Hubbard model[2] describing the itinerant magnetism. Even though this model is exactly soluble[3] its approximate treatment allows one to associate to it a classical dynamic system. In the general initial condition problem we study the dynamical evolution under the FAO dynamics of a given initial condition. Restricting ourselves to the extended mean field approximation we have to consider the pairing correlation effect and the Bogoliubov transformation is used to diagonalize the generalized matrix operator.

All the one-particle information is contained in the one-particle density matrix and in the pairing tensor. $\mathcal{F}(t)$ is the full density matrix of the system of identical fermionic particles.

A generalized density matrix can be defined[4] and it is diagonalized by a similarity transformation $W^t \mathcal{R} W = N$. The matrices W and N are of the form

$$W = \begin{pmatrix} \Omega & Z^* \\ Z^* & \Omega \end{pmatrix}, \text{ and, } N = \begin{pmatrix} p & 0 \\ 0 & \mathbb{1} - p \end{pmatrix}, \tag{1}$$

p being a diagonal matrix.

We use the projector operator method[5] to get an approximation to $\mathcal{F}(t)$: $\mathcal{F}(t) = \mathcal{F}_0(t) + \mathcal{F}'(t)$, where $\mathcal{F}_0(t)$ should contain the complete information of one-quasi-particle operators, the two-quasi-particle density is approximated by the product of one-particle functions and finally we impose that $Tr(\mathcal{F}(t)) = Tr(\mathcal{F}_0(t)) = 1$. $\mathcal{F}_0$ gives the Hartree-Fock-Bogoliubov approximation. The expression of $\mathcal{F}_0(t)$ for a system of identical fermions is known[6].

The most general initial state vector for the FAO is,

$$| \Psi \rangle = \frac{1}{\sqrt{N}} (\rho \mathbb{I} + \beta a_1^\dagger + \alpha a_1^\dagger + \tau a_1^\dagger a_1^\dagger) | 0 \rangle, \tag{2}$$

where the coefficients ρ, β, α and τ are complex numbers and the normalization constant N is: $N = |\rho|^2 + |\beta|^2 + |\alpha|^2 + |\tau|^2$.

The matrices Ω and Z can be written as

$$\Omega(t) = \begin{pmatrix} \cos\gamma(t)\cos\xi(t) & e^{-i\varphi(t)}\sin\gamma(t)\cos\xi(t) \\ e^{i\varphi(t)}\sin\gamma(t)\cos\xi(t) & \cos\gamma(t)\cos\xi(t) \end{pmatrix}, \tag{3}$$

and

$$Z(t) = \begin{pmatrix} e^{i\theta(t)}\sin\gamma(t)\sin\xi(t) & e^{i(\theta(t)-\varphi(t))}\cos\gamma(t)\sin\xi(t) \\ -e^{i(\theta(t)-\varphi(t))}\cos\gamma(t)\sin\xi(t) & e^{i(\theta(t)-2\varphi(t))}\sin\gamma(t)\sin\beta(t) \end{pmatrix}. \tag{4}$$

The dynamical evolution of the parameters $\gamma(t), \xi(t), \theta(t)$ and $\varphi(t)$ gives

$$\dot{\gamma}(t) = 0, \quad \dot{\xi}(t) = 0, \quad \dot{\theta}(t) = 2\lambda_B B + 2\hbar\omega + \quad \dot{\varphi}(t) = 2\lambda_B B. \tag{5}$$

The above equations of motion are equivalent to the classical system of two spins. To see this we define conjugate momenta of variables $\theta(t)$ and $\varphi(t)$,

$$j_\theta(t) = \cos\gamma(t) \qquad \text{and} \qquad j_\varphi(t) = \cos\xi(t). \tag{6}$$

The hamiltonian

$$H = 2\lambda_B B(j_\varphi + j_\theta) + (2\hbar\omega + U)j_\theta \tag{7}$$

gives the same equation of motion as (5). The hamiltonian (7) describes the paired mean-field dynamics of the FAO. It has the form of the action-angle classical hamiltonian for two precessing angular momenta of magnitude one.

References

[1] A.K. Kerman and S.E. Koonin, Ann. of Phys. 100 (1976) 332 .

[2] J. Hubbard, Proc. Roy. Soc. A277 (1963) 237 ; A281 (1964) 401.

[3] S.M. de Souza, S. Moss de Oliveira and M.T. Thomaz, Am. J. Phys. 60 (1992) 1122;
M.C.D. Barrozo, M.T. Thomaz and A.F.R. de Toledo Piza, *Dynamical Evolution of a Fermionic Anharmonic Oscillator*, Am. J. of Phys.(to be published).

[4] P. Ring and P. Schuck, *The Nuclear Many-Body Problem*, (Springer-Verlag, New York, 1980), pp. 245-248 and 251-252.

[5] C.R. Willis and R.H. Picard, Phys. Rev. A9(1974) 1343 ; A16 (1977) 1625 .
M.C. Nemes and A.F.R. de Toledo Piza, Phys. Rev. C27 (1983) 862; Physica 137A (1986) 367.

[6] J. Des Cloiseaux, *Many-Body Physics*, C. de Witt and R. Balian (eds.), Gordon and Breach (1968), pp.5.

Schwinger's formula and the partition function for the bosonic and fermionic harmonic oscillator

L. C. Albuquerque. C. Farina·and S. J. Rabello

Instituto de Física, Universidade Federal do Rio de Janeiro

Rio de Janeiro, R.J. CEP - 21.945-970 - Brazil

We use Schwinger's formula. introduced by himself in the early fifties to compute effective actions for QED, and recently applied to the Casimir effect, to obtain the partition functions for both the bosonic and fermionic harmonic oscillator.

The computation of the partition function of the usual harmonic oscillator is probably one of the most elementary exercises in a Statistical Mechanics course. There are many ways of making this calculation. and undoubtedly the easiest is the direct one, that is,

$$
\begin{aligned}
Z(\beta) &:= Tr\, e^{-\beta H} \\
&= \sum_{n=0}^{\infty} e^{-\beta(n+\frac{1}{2})\omega} \\
&= \frac{e^{-\frac{\beta\omega}{2}}}{1 - e^{-\beta\omega}} \\
&= \frac{1}{2\sinh(\frac{\beta\omega}{2})}.
\end{aligned}
\tag{1}
$$

where we simply used that the eigenvalues of the Hamiltonian operator for the harmonic oscillator are given by $(n + \frac{1}{2})\omega$. with $n = 0, 1, 2, ...$ (we are using $h = 1$) and summed the infinite terms of a geometric series.

However, it is exactly the simplicity of handling with this example that makes it a perfect "laboratory" to test or develop other methods of computation. as for instance, the path integral method[1]. the Green function method[2]. etc..

Our purpose in this letter is to apply a formula invented by Schwinger in 1951[3] to compute effective actions for QED, and recently applied with success in the computation of the Casimir energy for both the massless and massive scalar field[4-6]. to obtain not only the result of equation (1), but also the partition function for a fermionic harmonic oscillator. Curious as it may seem, this approach has never appeared in the literature.

Let us start with the bosonic case. It is well known that the corresponding partition function can be written as[7]

$$
Z(\beta) = \det{}^{-\frac{1}{2}} (\omega^2 - \partial_\tau^2)|_{\mathcal{F}_p},
\tag{2}
$$

where the subscript $\mathcal{F}_p$ means that the operator $\omega^2 - \partial_\tau^2$ acts only on a set of functions which are periodic, with period β. In ref. [7], Gibbons used the generalized ζ-function method to compute such a determinant. Here, we shall use Schwinger's formula (deduced in the Appendix A):

$$
\ln Z(\beta) = \frac{1}{2}Tr \int_0^\infty ds\, s^{\nu-1}\, e^{-i s L}.
\tag{3}
$$

·e-mail: farina@vms1.nce.ufrj.br

where $\hat{L}_\omega := \omega^2 - \partial_\tau^2$ and we chose the regularization based on the analytical continuation, instead of Schwinger's one.

For periodic boundary conditions we have

$$Tr\, e^{-is\hat{L}_\omega} = \sum_{n=-\infty}^{\infty} e^{-is[\omega^2 + n^2(\frac{2\pi}{\beta})^2]}.$$ (4)

so that

$$
\begin{aligned}
\ln Z(\beta) &= \frac{1}{2} \sum_{n=-\infty}^{\infty} \int_0^\infty ds\, s^{\nu-1} e^{-is[\omega^2 + (n\frac{2\pi}{\beta})^2]} \\
&= \frac{1}{2}\Gamma(\nu) \sum_{n=-\infty}^{\infty} \left[\omega^2 + \left(n\frac{2\pi}{\beta}\right)^2\right]^{-\nu} \\
&= \frac{1}{2}\omega^{-2\nu}\Gamma(\nu) + \left(\frac{\beta}{2\pi}\right)^{2\nu} \Gamma(\nu) E_1^{\mu^2}(\nu,1).
\end{aligned}
$$ (5)

where we introduced the one-dimensional inhomogeneous Epstein function

$$E_1^{\mu^2}(\nu,1) := \sum_{n=1}^{\infty} \left(n^2 + \mu^2\right)^{-\nu} \quad ; \quad Re\,\nu > \frac{1}{2},$$ (6)

defined $\mu = \frac{\beta\omega}{2\pi}$ and used the well known integral representation of the Euler Gamma function $\int_0^\infty dt\, t^{\nu-1} e^{-\alpha t} = \alpha^{-\nu}\Gamma(\nu)$.

Although the above series converges only for $Re\,\nu > \frac{1}{2}$, it can be analytically continued to a meromorphic function in the whole complex plane given by[8]

$$
\begin{aligned}
E_1^{\mu^2}(\nu,1) &= -\frac{1}{2\mu^{2\nu}} + \frac{\sqrt{\pi}\Gamma(\nu-\frac{1}{2})}{2\Gamma(\nu)\mu^{2\nu-1}} \\
&\quad + \frac{2\sqrt{\pi}}{\Gamma(\nu)} \sum_{n=1}^{\infty} \left(\frac{n\pi}{\mu}\right)^{\nu-\frac{1}{2}} K_{\nu-\frac{1}{2}}(2\pi n\mu).
\end{aligned}
$$ (7)

It is worth noting that the structure of poles of $E_1^{\mu^2}(\nu,1)$ is governed by the poles of $\Gamma(\nu - \frac{1}{2})$. Hence, they are located at $\nu = \frac{1}{2}, -\frac{1}{2}, -\frac{3}{2}, \dots$, and so on. As we see, $E_1^{\mu^2}(\nu,1)$ is analytic at the origin.

Substituting (7) into (5), taking the limit $\nu \to 0$ and observing that the divergent terms cancel without any further subtraction, we get

$$\ln Z(\beta) = -\frac{\omega\beta}{2} + 2\sqrt{\frac{\omega\beta}{2\pi}} \sum_{n=1}^{\infty} \sqrt{\frac{1}{n}} K_{-\frac{1}{2}}(n\omega\beta).$$ (8)

In order to compute the summation on the r.h.s. of (8), we appeal to the formula[9]

$$K_{-\frac{1}{2}}(n\omega\beta) = \sqrt{\frac{\pi}{2n\omega\beta}} e^{-n\omega\beta}.$$ (9)

Inserting (9) into (8), and using equation (B.1) (see **Appendix B**), we obtain the final result

$$\ln Z(\beta) = -\ln\left[2\sinh\left(\frac{\omega\beta}{2}\right)\right] \quad \Rightarrow \quad Z(\beta) = \frac{1}{2\sinh\left(\frac{\omega\beta}{2}\right)}.$$ (10)

in perfect agreement with (1).

For the fermionic case, it can be shown that

$$Z^f(\beta) = \det{}^{+1}(\omega^2 - \partial_\tau^2)|_{\mathcal{F}_a}.$$ (11)

where the subscript $\mathcal{F}_a$ now means that the operator L_ω acts only on a set of antiperiodic functions. As a consequence, the eigenvalues turn to be $\lambda_n = \omega^2 + \left(p\frac{\pi}{\beta}\right)^2$, with p an odd integer. Then, using these eigenvalues in the analogue of equation (3), but remembering that for the fermionic case, instead of the factor $\frac{1}{2}$ we must write (-1), we get

$$\ln Z^J(\beta) = -\Gamma(\nu) \sum_{p=odd} \left[\omega^2 + \left(p\frac{\pi}{\beta}\right)^2\right]^{-\nu}. \tag{12}$$

Adding and subtracting $\Gamma(\nu) \sum_{p=even} \left[\omega^2 + \left(p\frac{2\pi}{\beta}\right)^2\right]^{-\nu}$ to the r.h.s. of last equation, we may write

$$\ln Z^J(\beta) = 2\Gamma(\nu) \left[\left(\frac{\beta}{2\pi}\right)^{2\nu} E_1^{\mu^2}(\nu, 1) - \left(\frac{\beta}{\pi}\right)^{2\nu} E_1^{\mu^2}(\nu, 1)\right], \tag{13}$$

where now $\mu = \frac{\beta\omega}{\pi}$. Following exactly the same steps as before, that is, using the analytical continuation of the one-dimensional inhomogeneous Epstein function given by (7) and taking the limit $\nu \to 0$, we get

$$\ln Z^J(\beta) = \beta\omega + 4\sqrt{\frac{\omega\beta}{2\pi}} \sum_{n=1}^{\infty} \sqrt{\frac{1}{n}} K_{-\frac{1}{2}}(n\omega\beta) - 4\sqrt{\frac{\omega\beta}{\pi}} \sum_{n=1}^{\infty} \sqrt{\frac{1}{n}} K_{-\frac{1}{2}}(2n\omega\beta). \tag{14}$$

Using equations (9) and (B.1) we finally obtain.

$$\ln Z^J(\beta) = \ln \left[\frac{\sinh(\omega\beta)}{\sinh\left(\frac{\omega\beta}{2}\right)}\right]^2 \implies Z^J(\beta) = 4\cosh^2\left(\frac{\omega\beta}{2}\right). \tag{15}$$

This result can be checked easily in the following way: the fermionic oscillator that is being considered here is the second order Grassmann oscillator studied by Finkestein and Villasante[10] (in fact, we are dealing here with the particular case of $N = 2$ of their work). In this case, it can be shown that there are only three energies: 0 (double degenerated),

$+\beta\omega$, $-\beta\omega$, so that, if we use directly the definition for $Z^J(\beta)$, we will obtain

$$\begin{aligned}
Z^J(\beta) &= Tr\, e^{-\beta H^J} \\
&= 2 + e^{\beta\omega} + e^{-\beta\omega} \\
&= 4\cosh^2\left(\frac{\beta\omega}{2}\right).
\end{aligned} \tag{16}$$

In this paper we applied the Schwinger's formula for the one-loop effective action to the computation of the partition function for both the bosonic and Grassmann harmonic oscillator. Regularization by analytical continuation was adopted. We note that depending on the boundary condition choice (eg. Dirichlet condition), new subtractions (renormalizations) can be needed. But this is easily done remembering that the Schwinger's formula contains an integration constant, which can be used to subtract these divergent terms.

Appendix A

Let

$$e^{\Gamma(\omega)} = \det L_\omega|_{\mathcal{F}} = \exp Tr \ln L_\omega|_{\mathcal{F}}. \tag{A.1}$$

where $\dot{L}_\omega = \omega^2 - \partial_r^2$, and the subscript $\mathcal{F}$ means that some boundary condition is assumed. Hence

$$\Gamma(\omega) = Tr \ln(\omega^2 - \partial_r^2)|_{\mathcal{F}} \qquad (A.2)$$

Taking the variation with respect to ω^2 (the subscript $\mathcal{F}$ will be omitted but the boundary condition is understood). we obtain

$$
\begin{aligned}
\delta_{\omega^2}\Gamma(\omega) &= Tr \dot{L}_\omega^{-1} \delta \dot{L}_\omega \\
&= iTr \int_0^\infty ds\, e^{-is(\dot{L}_\omega - i\epsilon)} \delta \dot{L}_\omega \\
&= \delta \left[-Tr \int_0^\infty \frac{ds}{s} e^{-i(\dot{L}_\omega - i\epsilon)} \right]
\end{aligned}
\qquad (A.3)
$$

Apart from an additive constant to be fixed by normalization, integration leads to

$$\Gamma(\omega) = -Tr \int_0^\infty \frac{ds}{s} e^{-is\dot{L}_\omega}. \qquad (A.4)$$

where the $i\epsilon$ factor of convergence is tacitly assumed. Last equation is clearly ill-defined. One way to circumvent this problem was pointed out by Schwinger: one introduces a cut-off s_0, so that the integral can be performed. Then, subtracting the divergent terms for $s_0 = 0$, the remaining integral is finite. However, there is another possible choice[5], which consists in replacing expression (A.4) by

$$\Gamma(\omega) = -Tr \int_0^\infty ds\, s^{\nu-1} e^{-is\dot{L}_\omega}. \qquad (A.5)$$

with ν big enough, such that integral (A.5) is well defined. Then, after the integral is made, we perform an analytical continuation to the whole complex plane. After subtracting the poles at $\nu = 0$ (when they exist), we take the limit $\nu \to 0$, and this way we get a finite prescription for the integral (A.4). In the main text we adopt this approach instead Schwinger's one.

Appendix B

In this Appendix we shall prove that

$$\sum_{n=1}^\infty \frac{1}{n} e^{-n\alpha} = \frac{\alpha}{2} - \ln \left[2\sinh\left(\frac{\alpha}{2}\right) \right] \quad : \quad \alpha > 0. \qquad (B.1)$$

With this purpose, we will define $S(\alpha)$ such that

$$S(\alpha) := \sum_{n=1}^\infty \frac{1}{n} e^{-n\alpha}. \qquad (B.2)$$

Diferentiating both sides of (B.2) with respect to α and using the well known result of the sum of the infinite terms of a geometrical series, we get

$$-\frac{dS(\alpha)}{d\alpha} = \frac{e^{-\frac{\alpha}{2}}}{2\sinh\left(\frac{\alpha}{2}\right)}. \qquad (B.3)$$

Now, integrating in α we readly get

$$S(\alpha) = \frac{\alpha}{2} - \ln\left[2\sinh\left(\frac{\alpha}{2}\right)\right]. \qquad (B.4)$$

where we used that $S(\infty) = 0$. This completes the desired proof.

References

1. R.P. Feynman and A.R. Hibbs, **Quantum Mechanics and Path Integrals**, Mc. Graw Hill, Inc., New York, 1965.

2. For the problem at hand, this method can be found in the following reference: H. Boschi, C. Farina and A. de Souza Dutra; submitted for publication

3. J. Schwinger, Phys. Rev. **82** (1951) 664.

4. J. Schwinger, Lett. Math. Phys. **24** (1992) 59.

5. M. V. Cougo-Pinto, C. Farina and A. J. Segui-Santonja, to appear in the Lett. Math. Phys..

6. M. V. Cougo-Pinto, C. Farina and A. J. Segui-Santonja, to appear in Lett. Math. Phys..

7. G.W. Gibbons, Phys. Lett. **A60** (1977) 385.

8. J. Ambjorn and S. Wolfran, Ann. Phys. **147** (1983) 1; Elizalde and Romeo, J. Math. Phys. **30** (1989) 1133.

9. I.S. Gradstheyn and I.M. Ryzhik **Table of Integrals, Series and Products**, Academic Press, Inc. (NY). 1980, formula 8.469.3.

0. R. Finkelstein and M. Villasante, Phys. Rev. **D33** (1986) 1666.

Statistical interpretation of the heat kernel regularization

Henrique Boschi-Filho[*]

Instituto de Física - Universidade Federal do Rio de Janeiro

In this communication we are going to show that the heat kernel regularization has a clear and beautiful statistical meaning. This will be shown explicitly for the chiral anomaly for general Yang-Mills fileds with Fujikawa's approach [1]. Let us start remembering that the chiral anomaly appears non-perturbatively in the path integral framework as the Jacobian of the fermionic measure which is noninvariant under infinitesimal chiral rotations. This Jacobian results in an additional term for the Lagrangian and can be written, in $D = 2m$ dimensions, as

$$\mathcal{A}(x) = \sum_n \phi_n{}^\dagger(x)\gamma_D^5 \phi_n(x) \tag{1}$$

where $\gamma_D^5 = i\gamma_0\gamma_1\gamma_2 \cdots \gamma_{D-1}$; γ_μ are the usual Dirac matrices in D dimensions and ϕ_n are the eigenstates of the Dirac operator $\not{p}$, such that $\not{p}\phi_n = \lambda_n\phi_n$.

The expression (1) for the anomaly is not well defined since the trace of γ_D^5 is zero but the product of fields in the same space-time point diverges. Thus, a regularization is needed in order to calculate it. Here, we will proceed with the heat kernel method introducing a damping factor and defining the regularized anomaly as

$$
\begin{aligned}
\mathcal{A}^R(x) &= \lim_{\epsilon \to 0} \sum_n \phi_n{}^\dagger(x)\gamma_D^5 \exp\{-\epsilon\lambda_n^2\}\phi_n(x) \\
&= \lim_{\epsilon \to 0} \sum_n \phi_n{}^\dagger(x)\gamma_D^5 \exp\{-\epsilon \not{p}^2\}\phi_n(x) \\
&= \lim_{\epsilon \to 0} \lim_{x' \to x} tr[\gamma_D^5 H(x, x'; \epsilon \not{p}^2)]
\end{aligned}
\tag{2}
$$

where $H(x, x'; \epsilon \not{p}^2) = \langle x| \exp\{-\epsilon \not{p}^2\}|x'\rangle = \exp\{-\epsilon \not{p}^2\}\delta^{(D)}(x - x')$ is the heat kernel.

Let us now reobtain the above results in the light of a statistical mechanics approach. To see how one can get it, let us discuss a theory at finite temperature in D dimensional space-time, using the Euclidean time approach. This is done simply by restriting the time integration in the action to the finite interval $(0, \beta]$, where β is the inverse temperature. In this picture, the thermal expectation value of an operator $\mathcal{O}$, assuming thermal equilibrium, is

$$< \mathcal{O} >_\beta = Z(\beta)^{-1} \sum_n < n| \exp\{-\beta H\}\mathcal{O}|n >. \tag{3}$$

where $Z(\beta) = \sum_n < n| \exp\{-\beta H\}|n >$ is the usual partition function, which normalizes the expectation value $< \mathcal{O} >_\beta$. H is the Hamiltonian and $|n>$ are its eigenstates, such that $H|n> = E_n|n>$. Note also that

$$\sum_n < n| \exp\{-\beta H\}\mathcal{O}|n > = tr < n'| \exp\{-\beta H\}\mathcal{O}|n > = Tr\left(\exp\{-\beta H\}\mathcal{O}\right). \tag{4}$$

[*]e-mail: boschi@ufrj.bitnet   boschi@vms1.ncc.ufrj.br

where tr means trace over matrix elements and Tr over both matrices and states. For simplicity, we described discrete basis $|n>$, but in general, these can be continous as $|x>$ and the trace Tr would imply an integration over x. In order to connect the thermal expectation value and the anomaly, we choose the Hamiltionian $H \equiv \not{D}^2$ so that the eigenstates $|n>$ are identified with the ones given in the Fujikawa's analysis, $\phi_n(x)$. The thermal expectation value becomes

$$< \mathcal{O} >_\beta = Z(\beta)^{-1} \sum_n \phi_n(x)^\dagger \exp\{-\beta\not{D}^2\}\mathcal{O}\phi_n(x) \tag{5}$$

and the partition function is $Z(\beta) = \sum_n \phi_n(x)^\dagger \exp\{-\beta\not{D}^2\}\phi_n(x)$. Now, identifying the operator $\mathcal{O}$ with γ_D^5 we have that the anomaly is just the unrenormalized thermal expectation value when the temperature approaches infinity $(\beta \to 0)$

$$A(x)|_{reg} = \lim_{\beta\to 0} Z(\beta) < \gamma_D^5 >_\beta . \tag{6}$$

Here, the inverse temperature β plays the role of the heat kernel cutoff. Note that we have obatined explicitly through this picture that the naive form of the anomaly is $0 \times \infty$, since in th limit $\beta \to 0$, $Z(\beta) \to \infty$ and $< \gamma_D^5 >_\beta \to 0$ and the product of these, which is just eq. (6), is finite. The analysis presented above can also be extended to anomalous models.

As the heat kernel method is related to the zeta function and stochastic quantization these later methods could also, in principle, have a statistical interpretation in the above sense.

References

[1] K. Fujikawa, Phys. Rev. Lett. **42** (1979) 1195; Phys. Rev. D **21** (1980) 2848.

[2] L. Alvarez-Gaumé and E. Witten, Nucl. Phys. B **234** (1983) 269.

[3] G. Münster and M. Reuter. Phys. Lett. B **198** (1987) 73.

Chiral Schwinger model with a Podolsky
term at finite temperature

C.P. Natividade*, A. de Souza Dutra* and H. Boschi-Filho†

*Universidade Estadual Paulista - Campus de Guaratingueld
†Instituto de Física, Universidade Federal do Rio de Janeiro

In this communication we will use the path integral formalism to discuss the chiral Schwinger model (CSM) [1] plus the Podolsky term and its anomalous chiral fermionic Jacobian in a finite temperature approach [2] [3]. As in the usual CSM, the fermionic measure is noninvariant under chiral rotations, so that we expect that this Jacobian will give rise to dynamically generated masses for the gauge field. Let us start, writing the Lagrangian density for CSM with the Podolsky term

$$\mathcal{L} = -\frac{1}{4} F_{\mu\nu} F_{\mu\nu} - b^2 \partial_\nu F_{\mu\nu} \partial_\sigma F_{\mu\sigma} + i\bar{\psi}\not{D}\psi , \qquad (1)$$

where $b > 0$ is the Podolsky coupling constant. As we are going to discuss the finite temperature theory corresponding to the above Lagrangian we demand that the bosonic and fermionic fields obey the usual periodic and antiperiodic conditions in the imaginary time formalism. Implementing infinitesimal chiral transformations in the fermion fields this lead to a change in fermionic measure of the partition function $D\bar{\psi}D\psi = D\bar{\psi}'D\psi' J_\beta(\varepsilon(x))$, where $J_\beta(\varepsilon(x))$ is a non-trivial Jacobian. In order to discuss the dynamical mass generation through obtaining this Jacobian at finite temperature we use the Fujikawa procedure with the operator $\not{D} = \gamma_\mu(\partial_\mu - ie\xi A_\mu + ie\eta\gamma_5 A_\mu)$, being η and ξ real parameters. Now, following Ref. [4] we find that the anomalous Jacobian is given by

$$J_\beta(\varepsilon(x)) = \exp\left\{-\frac{ie^2}{\pi} \int_\beta d^2x \varepsilon(x) \, (\eta g_{\mu\nu} + \xi\epsilon_{\mu\nu})\partial_\mu A_\nu\right\} \qquad (2)$$

which implies an anomalous divergence for the axial-vector current $\partial_\mu[\bar{\psi}\gamma_\mu(1-\gamma_5)\psi] = (e/\pi)(\eta g_{\mu\nu} + \xi\epsilon_{\mu\nu})\partial_\mu A_\nu$, which is explicit β-independent. To find the dynamically generated mass for CSM with the Podolsky term we decompose the vector field as usual and iterate the infinitesimal Jacobian to find

$$J_\beta(x) = \exp\left\{-\frac{i}{2\pi} \int_\beta d^2x [\eta\sigma \,\Box\, \sigma - \xi\rho \,\Box\, \rho - (\eta - \xi)\sigma \,\Box\, \rho]\right\} . \qquad (3)$$

such that, the effective Lagrangian is given by

$$\mathcal{L}_{eff} = \frac{1}{2\,e^2}\rho \,\Box\, \Box\, \rho + \frac{b^2}{e^2}(\Box\, \partial_\mu\rho)^2 + i\bar{\psi}'\gamma_\mu\partial_\mu\psi' - \frac{1}{4\pi}[\eta \,\sigma \,\Box\, \sigma - \xi\rho \,\Box\, \rho - (\eta - \xi)\sigma \,\Box\, \rho] . \qquad (4)$$

Now, using the Euler-Lagrange equations for higher-order derivative systems [5] we get the equation of motion for the $\rho(x)$ field

$$\left(\Box - 2b^2 \Box\, \Box + \frac{e^2}{4\pi}\frac{(\eta + \xi)^2}{\eta}\right)\Box\, \rho = 0 . \qquad (5)$$

This equation can be rewritten as $\Box(\Box + \mu^2)(\Box - M_t^2)\rho(x) = 0$ and the field $\rho(x)$ can be expressed as a linear combination of three other fields: a massless free excitation, a pseudo-scalar field with mass μ and a tachyonic mode

with mass M_t

$$\mu^2 = \frac{1}{4b^2}\left[(1+8b^2\mu_0^2)^{1/2}-1\right] \; ; \qquad M_t^2 = \frac{1}{4b^2}\left[(1+8b^2\mu_0^2)^{1/2}+1\right] \tag{6}$$

where $\mu_0{}^2 = e^2(\eta+\xi)^2/4\pi\eta$. These masses are β-independent. Taking $b - 0$ we find that μ^2 coincides with zero temperature result of Jackiw and Rajaraman [1] (identifying $2a^2/(a-1) = (\eta+\xi)^2/\eta$) and the Podolsky tachyon M_t^2 vanishes in this limit. As we can see, the higher order derivative term is not sufficient to restore the symmetry which was destroyed at quantum level. So, the basic properties of the usual CSM persist despite the additive Podolsky term. In fact, its usual mass was redefined by the Podolsky coupling b and we get also a tachyonic mode M_t^2.

In a more complete version of this work, following ref. [6], we have also calculated the zero temperature propagators of the model, i. e., the gauge field propagator in the nonsingular $(a > 1)$ and singular $(a = 1)$ cases and the relevant fermionic propagator. We also extended these calculations to the finite temperature case in two frameworks: imaginary time and thermofield dynamics. The analysis of the propagators lead to the same conclusions as presented above. This work was partially supported by CNPq - Brazilian agency.

References

[1] R. Jackiw and R. Rajaraman, Phys. Rev. Lett. 54 (1985) 1219; 54 (1985) 2060 (E).

[2] K. Fujikawa, Phys. Rev. Lett. 42 (1979) 1195; Phys. Rev. D21 (1980) 2848.

[3] H. Boschi-Filho, C.P. Natividade and C. Farina. Phys. Rev. D45 (1992) 586.

[4] H. Boschi-Filho and C.P. Natividade, Mod. Phys. Lett. A 7 (1992) 3303

[5] J. Barcelos-Neto and N.R.F. Braga, Phys. Rev. D 39 (1989) 494.

[6] A. de Souza Dutra, Int. J. Mod. Phys. A 9 (1994) 2229.

Teoria de Maxwell-Podolsky com termo
de Chern-Simons de ordem superior:
um modelo sem táquions?

A. de Souza Dutra e C. P. Natividade

Depto. de Física e Química: UNESP - Campus de Guaratinguetá

DUTRA@GRT000.UESP.ANSP.BR

Vamos considerar inicialmente o caso de um modelo cuja densidade de lagrangiana é dada por:

$$\mathcal{L} = -\frac{a\,F_{\mu\nu}^2}{4} + b\,\partial_\mu F^{\mu\lambda}\partial^\nu F_{\nu\lambda} + \theta_1\,\epsilon^{\mu\nu\rho}A_\mu\partial_\nu A_\rho + \theta_2\,g^{\sigma\delta}\epsilon^{\mu\nu\rho}\partial_\sigma A_\mu\partial_\nu\partial_\delta A_\rho. \tag{1}$$

sendo a, b, θ_1 e θ_2 os parâmetros arbitrários que nos permitem tomar os vários limites da teoria.

O propagador no gauge de Lorentz, e na representação de momentum, é dado por:

$$D_{\mu\nu} = \frac{1}{(\theta_2 k^2 + 2\theta_1)^2 - (a - 2bk^2)^2 k^2}\Bigg\{ (a - 2bk^2)g_{\mu\nu} +$$

$$+ \frac{a}{k^4}\left[(a - 2bk^2)\left(\left(a - \frac{1}{\alpha}\right)k^2 - 2bk^4\right) - (\theta_2 k^2 + 2\theta_1)^2\right]$$

$$- i(\theta_2 k^2 + 2\theta_1)\frac{\epsilon_{\mu\nu\theta}k^\theta}{k^2}\Bigg\}. \tag{2}$$

onde α é o parâmetro de gauge.

O propagador acima tem seus polos definidos através da equação de terceiro grau: $x^3 + a_1 x^2 + a_2 x + a_3 = 0$. ($x \equiv k^2$), onde $a_1 \equiv -\frac{(\theta_2^2 + 4ab)}{4b^2}$ $a_2 \equiv \frac{(a^2 - 4\theta_1\theta_2)}{4b^2}$ e $a_3 \equiv -\frac{\theta_1^2}{4b^2}$.

A equação do terceiro grau acima tem um discriminante D tal que, se $D \geq 0$, nos levam a situações não físicas. A única possibilidade seria aquela em que $D < 0$, onde definimos: $D \equiv Q^3 + R^2$, onde $Q \equiv \frac{(3a_2 - a_1^2)}{9}$ e $R \equiv \frac{(9a_1 a_2 - 27a_3 - 2a_1^3)}{54}$.

Temos a solução da equação polinomial acima dada por ($D < 0$):

$$x_0 = m_0^2 = 2\rho^{1/3}\cos(\frac{\alpha}{3}) - \frac{a_1}{3}.$$

$$x_\pm = m_\pm^2 = -\rho^{1/3}\{\cos(\frac{\alpha}{3}) \pm \sqrt{3}sen(\frac{\alpha}{3})\} - \frac{a_1}{3}. \tag{3}$$

onde $\rho = \sqrt{R^2 + L^2}$, com $L \equiv \sqrt{|D|}$ e $\alpha = arctan(L/R)$. Para eliminar-se a possibilidade da existência de táquions ou ghosts, impomos que as três massas ao quadrado acima sejam reais, positivas e diferentes entre si.

Um caso particular interessante é aquele em que não existe o termo de Chern-Simons usual ($\theta_1 = 0$). Neste caso a equação (3) fica sendo: $x(x^2 + a_1 x + a_2) = 0$, logo os polos estarão dados por: $m_0 = 0$, $m_\pm = \frac{1}{2}\left[-a_1 \pm \sqrt{a_1^2 - 4a_2}\right]$.

A imposição que as massas ao quadrado sejam positivas, nos leva à restrição sobra a região de validade do parâmetro θ_2: $\theta_2^2 > -8ab$,

como usualmente toma-se $a = 1$ e $b = -c^2$, teremos: $\theta_2^2 > -\frac{8}{c^2}$.

Podemos agora passar a fazer a quantização canônica da teoria acima descrita com $a = 1$, $b = -c^2$ e θ_2 obedecendo à desigualdade (8).

Inicialmente fazemos a variação funcional da densidade de lagrangiana (1) [1]. de onde obtemos a equação de movimento, $(1 - 2c^2\square)\partial_\mu F^{\mu\nu} + \theta_1 \epsilon^{\mu\nu\alpha}\partial_\mu A_\alpha - 2\theta_2\epsilon^{\mu\nu\beta}\partial_\mu\square A_\beta = 0$. além dos momenta:

$$\pi^\nu = -F^{0\nu} - 2c^2\left(\partial^k\partial^\lambda F_{0\lambda}\delta_k^\nu - \partial^0\partial^\lambda F_\lambda^\nu\right) + \theta_1\epsilon^{\beta\nu}A_\beta + 2\theta_2\epsilon^{\beta\mu\nu}\partial_\mu\partial^0 A_\beta.$$

$$s^\nu = 2c^2\left(\partial_\mu F^{\mu\nu} - \delta_0^\nu\partial_\rho F^{0\rho}\right) + \theta_2\epsilon^{\beta\nu}\partial_0 A\beta. \tag{4}$$

como $\epsilon^{\beta\nu} \equiv \epsilon^{0\beta\nu}$, é fácil concluir que temos a densidade Hamiltoniana canônica $\mathcal{H}_c = \pi_\mu\dot{A}^\mu + s_\mu\dot{A}^\mu - \mathcal{L}$ (com $\dot{A} \equiv \ddot{A}$), tal que:

$$\mathcal{H}_c = \pi_i\dot{A}^i - \frac{1}{4c^2}s_is^i + s_i\partial_k F^{ik} - \dot{A}_0\partial_k s^k 0 + \frac{1}{2}\left(\dot{A}_i - \partial_i A_0\right)^2 +$$

$$-c^2\left(\partial_i\dot{A}^i - \nabla^2 A_0\right)^2 + \frac{1}{4}F^{ij}F_{ij} - 2\theta_1\epsilon_{ki}A^i\dot{A}^k - 2\theta_1\epsilon_{ij}A_0\partial^i A^j +$$

$$-\theta_2\epsilon_{ij}\dot{A}^j\left(\frac{1}{(2c^2)}s^i + \partial_k F^{ik} + \partial^i\dot{A}_0 + \theta_2\epsilon_{ik}\dot{A}^k\right) +$$

$$-2\theta_2\left(\epsilon_{sl}\partial^k A^s\partial_k\dot{A}^l + \epsilon_{ki}\dot{A}_0\partial^k A^i + \epsilon_{ij}\partial_k A_0\partial^k\partial^l A^j\right). \tag{5}$$

Impondo a consistência temporal dos vínculos. obtém-se o seguinte vínculo secundário:

$$\Omega_2 = \partial_i s^i - \pi^0 - \theta_2\epsilon_{ij}\partial^i\left(A^j + 2\dot{A}^j\right) \approx 0 .$$

$$\Omega_3 = \partial_k\pi^k + 2\theta_1\epsilon_{ij}\partial^j A^i \approx 0. \tag{6}$$

Pode-se verificar os limites de modo a se convencer que os vínculos acima são os corretos. É fácil ver que temos uma teoria com vínculos de primeira classe. Dessa forma devemos buscar uma fixação de calibre conveniente. Como é típico de modelos com derivadas de ordem superior. vamos escolher um vínculo fixador de calibre de ordem superior:

$$\Upsilon_1 = \left(1 - 2c^2\square\right)\partial_k A^k \approx 0, \tag{7}$$

de cuja consistência são gerados os seguintes vínculos:

$$\Upsilon_2 = A^0 + \mathcal{P}\epsilon_{ij}\partial^i A^j \approx 0 \tag{8}$$

$$\Upsilon_3 = \dot{A}^0 + \mathcal{P}\epsilon_{ij}\partial^i\dot{A}^j \approx 0. \tag{9}$$

onde $\mathcal{P} \equiv 2(\theta_1 - \theta_2\square)(1 - 2c^2\square)^{-1}\nabla^{-2}$. Os parênteses de Poisson não - nulos são :

$$\{\Omega_1(\vec{x}), \Upsilon_3(\vec{y})\} = -\delta^2(\vec{x} - \vec{y}).$$

$$\{\Omega_2(\vec{x}), \Upsilon_2(\vec{y})\} = \delta^2(\vec{x} - \vec{y})$$

$$\{\Omega_3(\vec{x}), \Upsilon_1(\vec{y})\} = (1 - 2c^2\nabla^2)\nabla^2\delta^2(\vec{x} - \vec{y}). \tag{10}$$

Podemos então construir a matriz de Dirac e, após inverte-la, obtemos os seguintes parênteses de Dirac não -nulos:

$$\{A_i(\vec{x}), \pi_j(\vec{y})\}^* = \delta_{ij}\delta^2(\vec{x} - \vec{y}) - (1 - 2c^2\nabla^2)\partial_i\partial_j G(\vec{x} - \vec{y}).$$

$$\{\dot{A}_i(\vec{x}), s_j(\vec{y})\}^* = \delta_{ij}\delta^2(\vec{x} - \vec{y}),$$

$$\{\pi_i(\vec{x}), \pi_j(\vec{y})\}^* = (1 - 2c^2\nabla^2)(2\theta_1\epsilon_{ki}\partial_j - \theta_2\epsilon_{kj}\partial_i)\partial^k\delta^2(\vec{x} - \vec{y}). \tag{11}$$

onde $G(\vec{x} - \vec{y})$ satisfaz à equação : $(1 - 2c^2\nabla^2)\nabla^2 G(\vec{x} - \vec{y}) = \delta^2(\vec{x} - \vec{y})$. Novamente quando se tomam os limites apropriados, podemos verificar os nossos resultados comparando-os com aqueles presentes na literatura.

Na seqüência, devemos verificar se os polos encontrados são dinâmicos. Em seguida deveremos construir modelos com interação da teoria aqui desenvolvida com a matéria. verificando se as correções radiativas não reintroduzem os táquions ou os fantasmas. Além de procurar por estados ligados que possam ser responsáveis por fenômenos como a supercondutividade.

References

[1] J. Barcelos-Neto e C. P. Natividade. Z. Phys. C 51 (1991) 313.

Some Remarks on the Algebra of Supercharges in D=(1+2)

L. P. Colatto*

DCP, Centro Brasileiro de Pesquisas Físicas
CEP 22290-180 Rio de Janeiro, RJ, Brazil

One shows that 3-dimensional $N=1$-supersymmetric models with non-trivial topological field configurations develop a central charge in the supersymmetry algebra. This result is also discussed in the presence of a Chern-Simons term, keeping supersymmetry non-extended.

Ordinary and supersymmetric Abelian gauge models in 3D space-times have been fairly-well investigated over the past years [1]. Besides their relevance in connection with the possibility of getting non-perturbative results more easily, the ultraviolet finiteness of Chern-Simons (including the case of gravity) theories is a remarkable feature of field theories defined in $D=(1+2)$ [2]. Also, Abelian Chern-Simons models with matter couplings seem to be the right way to tackle exciting topics in Condensed Matter Physics, such as high-T_c superconductivity and Fractional Quantum Hall Effect [3]. Our purpose in this note is to assess a typical three-dimensional gauge model with $N=1$-supersymmetry from the point-of-view of the algebra of the supersymmetry generators. We actually wish to present here a few remarks on the connection between topologically non-trivial solutions, the Chern-Simons term, and the presence of a central charge operator in the algebra of *simple* supersymmetry.

The ($N=1$)-super-Poincaré algebra in $(1+2)$ dimensions is generated by a real two-component spinorial charge, Q_a, whose the operatorial relations are given by $\{Q_a, Q_b\} = 2 i P_{ab}$ and $[Q_a, P_{ab}] = 0$, P_{ab} being the translation generator [4]. This super-Poincaré algebra has been generalized in [5] for extended supersymmetries. But, in fact, to recognize if a quantum field theory is consistent with supersymmetry, we need to obtain the Noether's (super)charges for the specific model, and the local features of a system are presented by the current algebra, that depends, as we will see, on the details of the model [6]. It is worthwhile to mention that this is one way to detect the symmetry at the quantum level; another approach would be through the analysis of the Ward identities for the symmetry under consideration. With this point-of-view, we shall analyse how the various terms (consistent with the symmetries of the (1+2)-dimensional supersymmetric model) contribute to the equal-time commutators. The motivation to use the canonical formulation in our analysis is that we actually wish to identify a central charge in the algebra and, in case it appears, it can be read off from the RHS of the anticommutators between the supersymmetry charges.

The models we shall contemplate here include an $N=1$-supersymmetric self-interacting matter model, its coupling to gauge fields and an $N=1$-supersymmetric Abelian Chern-Simons model. The main result we find is that a central charge appears, even if the supersymmetry is simple, provided that topologically non-trivial solutions are present in the model.

The explicit representation we adopt for the symmetric $\tilde{\gamma}$-matrices ($\tilde{\gamma} \equiv C\gamma$) reads:

$$(\tilde{\gamma}^0)_{ab} = \begin{pmatrix} 1 & 0 \\ 0 & 1 \end{pmatrix} , \quad (\tilde{\gamma}^1)_{ab} = \begin{pmatrix} 1 & 0 \\ 0 & -1 \end{pmatrix} , \quad (\tilde{\gamma}^2)_{ab} = \begin{pmatrix} 0 & -1 \\ -1 & 0 \end{pmatrix} ,$$

*e-mail: colatto@cbpfsu1.cat.cbpf.br

where C is the charge conjugation:

$$C = \begin{pmatrix} 0 & -i \\ i & 0 \end{pmatrix} .$$

(1)

As a notational convention, we shall denote spinor indices by early latin characters (a,b,...).

1. The Self-Interacting Matter Model

Matter fields are assembled in scalar superfields, whose representation in terms of a θ-expansion (θ is a two-component Grassmann-valued Majorana spinor) is given by $\Phi(x,\theta) = \phi(x) + \theta^a \psi_a(x) - \theta^2 F(x)$, where $\phi(x)$ is a physical scalar, $\psi_a(x)$ is a physical fermion and $F(x)$ is an auxiliary field. Now, it is possible to write an action that is invariant with respect to the symmetries (supersymmetry, Lorentz) and that is power-counting renormalizable:

$$S_{matter} = \int d^3x\, d^2\theta \left\{ -\frac{1}{2}(D_a \Phi)^2 + \frac{1}{2} m\Phi^2 + \frac{\lambda}{8}\Phi^4 \right\} ,$$

$$D_a \equiv \left(\frac{\partial}{\partial\theta^a} - i\theta^b \frac{\partial}{\partial x^{ab}} \right) \Phi \equiv (\partial_a - i\theta^b \partial_{ab})\Phi .$$

(2)

The supercharge is obtained via Noether theorem and reads as below:

$$Q_c = \int d^2\vec{x}\, J^0{}_c$$

$$= \int d^2\vec{x} \left\{ -i\psi^a (\bar\gamma^0)_{ac} \left(m\dot\phi + \frac{\lambda}{2}\phi^3 \right) + \frac{1}{2}\psi_c \partial^0 \phi + \frac{1}{2}\phi\partial^0 \psi_c + \right.$$

$$\left. -\frac{i}{2}\epsilon^{0\nu\rho}\psi^a (\bar\gamma_\rho)_{ac}\partial_\nu \phi + \frac{i}{2}\epsilon^{0\nu\rho}\phi\partial_\nu \psi^a (\bar\gamma_\rho)_{ac} \right\} .$$

(3)

By using the graded canonical commutation relations for ϕ and ψ_a, the anticommutator defining the super-Poincaré algebra turns out to be:

$$\{Q_a, Q_b\} = -2i P^\mu (\bar\gamma_\mu)_{ab} + i\epsilon^{ij} \int d^2\vec{x}\, \partial_i \left[(\bar\gamma_j)_{ab} \left(m\phi^2 + \frac{\lambda}{2}\phi^4 \right) \right] ,$$

(4)

where P^μ is obtained as the 0μ component of the "improved" energy-momentum tensor. Observe that the mass and self-interaction terms both contribute to a central charge in the supercharge algebra. The case we study here is just the 3-dimensional counterpart of the model considered by Olive and Witten in the paper of ref. [7], where the topological origin for the central charge is first pointed out. In our case, proceeding along the same lines as done in ref. [7], it is shown that the second term in the RHS of eq. (4) is non-trivial by virtue of the contributions coming from soliton-like configurations associated to the ϕ-field. However, it should be stressed that these static configurations are not the straightforward generalization of the kinks to two space dimensions, for they have an energy that is divergent. They simply signal the presence of field configurations with non-trivial topology and only upon the introduction of gauge fields, as we shall proceed to in the next section, they will lead to static configurations of *finite energy*; they are the so-called solitons with a magnetic flux, or vortices [8].

2. Matter–Gauge Background Coupling

The next step of our discussion consists in complexifying the matter model of the previous section and then performing the gauging of the $U(1)$-symmetry it possesses [4]. The degrees of freedom in the gauge sector are accommodated in a Majorana spinor superfield, $\Gamma_a(x;\theta)$, whose θ-expansion reads [4]:

$$\Gamma_a = \chi_a + \theta^b(C_{ab}B + iV_{ab}) + \theta^2(2\lambda_a - i\partial_a{}^b\chi_b) ,$$

(5)

where V_{ab} is the usual $U(1)$-gauge field, λ_a is its physical supersymmetric partner (the photino), whereas χ_a and B are non-physical components; C_{ab} denotes the elements of the charge conjugation matrix. The action that accomplishes the minimal coupling between the matter and gauge sectors is given by [4]

$$S_{matter-gauge} = \int d^3x\, d^2\theta \left\{ -\frac{1}{2}(\nabla^a \bar{\Phi})(\nabla_a \Phi) \right\} , \qquad (6)$$

whith $\nabla_a \Phi \equiv (D_a - i\Gamma_a)\Phi = (\partial_a - i\theta^b \partial_{ba} - i\Gamma_a)\Phi$. The Noether supersymmetry charge turns out to be

$$
\begin{aligned}
Q_c &= \int d^2\vec{x}\, J^0{}_c = \\
&= \frac{1}{4} \int d^2\vec{x} \left\{ i\,\epsilon^{0ij} [\bar\psi^a\,(\tilde\gamma_j)_{ac}\,\nabla_i\,\phi + \psi^a\,(\tilde\gamma_j)_{ac}\,\nabla_i\,\bar\psi] - (\psi_c\,\nabla^0\,\bar\psi + \bar\psi_c\,\nabla^0\,\phi) + \right. \\
&\quad \left. - (\bar\phi\,\nabla^0\,\psi_c + \phi\,\nabla^0\,\bar\psi_c) + i\,\epsilon^{0ij}\,(\bar\phi\,\nabla_i\,\psi^a + \phi\,\nabla_i\,\bar\psi^a)(\tilde\gamma_j)_{ac} \right\} :
\end{aligned}
\qquad (7)
$$

∇^0 and ∇^i stand for the gauge-covariant derivatives with space-time indices. Also, we should mention that our component fields are defined through the action of the (spinorial) gauge-covariant derivatives on the superfield Φ, according to:

$$
\begin{aligned}
\Phi|_{\theta=0} &= \phi . \\
\nabla_a \Phi|_{\theta=0} &= \psi_a , \\
\nabla^2 \Phi|_{\theta=0} &= F .
\end{aligned}
\qquad (8)
$$

After a lengthy computation and the use of well-known algebraic relations among the $\tilde\gamma$-matrices, we obtain that

$$\{Q_a\,,\,Q_b\} = -2\,i\,P^\mu(\tilde\gamma_\mu)_{ab} . \qquad (9)$$

where te momentum operator P^μ appearing in the RHS includes now contributions from the gauge field minimally coupled to matter through (6). Nevertheless, no term in the form of a central charge arises from the action (6); this means taht the central charge operator of eq. (4) is not modified by the introduction of the $U(1)$ gauge superfield. The role of the latter is to stabilize the topological configurations associated to the action (2) in the form of vortex-like solitons, as already known from the works quoted in ref. [8].

3. The N=1 Abelian Chern-Simons Term

The gauge sector discussed in the previous section was treated as a background; since no Maxwell-like dynamical term was added to the action (6) that gives propagation to the physical fields V_{ab} and λ_a. We have now in mind to introduce a Chern-Simons (CS) term for the latter and we shall compute how it contributes to the algebra of eq. (9). We begin with the gauge-invariant CS term written up in superspace [4]:

$$S_{CS} = \frac{M}{g^2} \int d^3x\, d^2\theta\; \Gamma^a W_a , \qquad (10)$$

where M is a mass parameter, g is the gauge coupling constant and the field-strength superfield W_a is defined as $W_a = \frac{1}{2}D^b D_a \Gamma_b$ [4]. The CS term above contributes the piece

$$(Q_{CS})_c = \int d^2\vec{x}\,(J_{CS})^0_c = \int d^2\vec{x} \left\{ \frac{i}{2}V^0\,(\psi_c\bar\phi - \bar\psi_c\phi) \right\} , \qquad (11)$$

to be added to the RHS of the supersymmetry charge of eq. (7). The reader should be warned for the fact that the contribution given in eq. (11) is true once one has chosen to work in the Wess-Zumino gauge. Moreover, also

restricting the supercharge of eq. (7) to the Wess-Zumino gauge, one computes the anticommutator (9) with the CS piece and verifies that <u>no</u> new contribution appears that modifies the central charge.

4. Conclusions

The work of Haag, Lopusanski and Sohnius [5] yields a theorem stating that a central charge in a supersymmetric model in four dimensions can only appear whenever supersymmetry is extended. In two dimensions, Olive and Witten [7] showed how configurations with non-trivial topology (namely, kinks) could be the source for a central charge operator in the framework of a simple supersymmetry. In this letter, we presented some results on the algebra of supercharges for a self-interacting matter model and an Abelian gauge theory in $D=(1+2)$. Our results indicate that the conclusion drawn from the two-dimensional case persists in three dimensions, i. e., 3-dimensional models with topologically non-trivial field configurations develop a central charge in the algebra of *simple supersymmetry*. The central charge appears indeed as a space integral that probes the behaviour of the fields at infinity.

This result differs from the one presented in the paper of ref. [9], where the authors consider an Abelian ($N=2$)-supersymmetric model with a ϕ^6-potential and a Chern-Simons term for the gauge potential. They conclude that the non-trivial topological contribution to the central charge is nothing but the magnetic flux associated to the gauge field.

References

[1] A. Linde, *Rep. Progr. Phys.* **42** (1979) 389;
    S. Deser, R. Jackiw and S. Templeton, *Phys. Rev. Lett.* **48** (1982) 975;
    S. Deser, *Three Topics in Three Dimensions*. in the proceedings of the Trieste Conference on Supermmenbranes and Physics in 2+1 Dimensions, eds. M.J. Duff *et al.*, World Scientific (Singapore, July 1989);

[2] F. Delduc, C. Lucchesi, O. Piguet and S.P. Sorella, *Nucl.Phys.* **B346** (1990) 313;
    A. Blasi, O. Piguet and S.P. Sorella, *Nucl.Phys.* **B356** (1991) 154;
    C. Lucchesi and O. Piguet, *Nucl.Phys.* **B381** (1992) 281;

[3] J. Schonfeld, *Nucl. Phys.* **B185** *(1981) 157*;
    Fractional Statistics and Anyon Superconductivity, ed. by Franck Wilczek, World Scientific (Singapore), 1990;

[4] S. J. Gates, M. T. Grisaru. M. Roček and W. Siegel, *Superspace*,
    Benjamin/Cummings Publishing Company (1983);

[5] S. Coleman and J. Mandula, *Phys. Rev.* **159** (1967) 1251;
    R. Haag. J. T. Lopuszanski and M. Sohnius, *Nuc. Phys.* **B88** (1975) 257;

[6] R. Jackiw, *Field Theoretic Investigation in Current Algebra, Current Algebra and Anomalies*. S. B. Treiman. R. Jackiw. B Zumino and E. Witten (eds.), World Scientific Publishing Co. (1985);

[7] E. Witten and D. Olive, *Phys. Lett.* **B78** (1978) 97;
    P. Di Vecchia and S. Ferrara, *Nuc. Phys.* **B130** (1977) 93;
    A. D'Adda and P. Di Vecchia, *Phys. Lett.* **B73** (1978) 162;

[8] H. B. Nielsen and P. Olesen, *Nucl. Phys.* **B61** (1973) 45;
    see also L. H. Ryder, *Quantum Field Theory* - Chapter 9, Cambridge University Press, 1985;

[9] C. Lee, K. Lee and E. Weinberg. *Phys. Lett.* **B243** (1990) 105.

The partition function for an anyon-like oscillator

H. Boschi-Filho*, C. Farina* and A. de Souza Dutra†

*Instituto de Física - Universidade Federal do Rio de Janeiro

†Universidade Estadual Paulista - Campus de Guaratinguetá

We want to compute the following determinant

$$\exp[\Gamma_s^\theta(\omega)] = \det{}^s \left(\omega^2 + \partial_t^2\right)_\theta \equiv \det{}^s (L)_\theta . \tag{1}$$

where L acts on functions that satisfy some given boundary condition specified by the label θ. The power of the determinant given by the parameter s is left completely arbitrary to take into account the cases that interpolate between the fermionic and the bosonic oscillators. Hence, playing with the boundary condition and the parameter s we can pass continuously from the bosonic to the fermionic oscillator. That is why we refer to this determinant as the partition function of an "anyon-like" oscillator.

Suggested by the Green function method usually employed in quantum field theory, we write

$$\frac{\partial}{\partial\omega}\Gamma_s^\theta(\omega) = 2s\omega Tr\left(L^{-1}\right)_\theta = 2s\omega \int_0^\tau G_\omega^\theta(t,t)dt , \tag{2}$$

where the Green function $G_\omega^\theta(t,t')$ satisfies $\left(\omega^2 + \partial_t^2\right)G_\omega^\theta(t,t') = \delta(t-t')$, as well as some boundary condition (to be given in a moment). Integrating this equation we obtain

$$\Gamma_s^\theta(\omega) - \Gamma_s^\theta(0) = 2s \int_0^\omega d\omega'\omega' \int_0^\tau dt G_{\omega'}^\theta(t,t) . \tag{3}$$

Since our purpose here is to use a generalized boundary condition in the sense that the periodic and antiperiodic cases will appear as particular cases, and in order to make connection with the behavior of correlation functions of anyon-like systems, it is natural to impose the following θ-dependent condition

$$G_\omega^\theta(t + \tau, t') = e^{-i\theta}G_\omega^\theta(t,t'). \tag{4}$$

It is clear that this boundary condition becomes periodic for $\theta = 0$ and antiperiodic for $\theta = \pi$. Depending on these conditions and the value of the parameter s, which can be thought as a "statistical" parameter, this determinant will be mapped into different partition functions. As these particular cases are related to bosonic and fermionic systems, this condition of general periodicity could, in principle, be related to particles whose statistics interpolates bosons and fermions, i. e., anyons [2].

It is straightforward to construct the Green function $G_\omega^\theta(t - t')$. Using basically the same technique that Kleinert [3] employed for the simpler cases of periodic and antiperiodic boundary conditions, it can be shown that

$$G_\omega^\theta(t - t') = \frac{e^{-i\theta/2}}{4\omega}\left[\frac{e^{i\omega(t-t'-\tau/2)}}{\sin(\frac{\omega\tau+\theta}{2})} + \frac{e^{-i\omega(t-t'-\tau/2)}}{\sin(\frac{\omega\tau-\theta}{2})}\right] ; \quad t - t' \in [0,\tau) \tag{5}$$

Substituting this Green function in Eq. (3), for the interval $[0, \tau)$ and with $t = t'$, we have

$$\Gamma_s^\theta(\omega) - \Gamma_s^\theta(0) = 2s \int_0^\tau dt \int_0^\omega d\omega' \omega' \left\{ \frac{e^{-i\theta/2}}{4\omega'} \left[\frac{e^{-i\omega'\tau/2}}{\sin(\frac{\omega'\tau+\theta}{2})} + \frac{e^{i\omega'\tau/2}}{\sin(\frac{\omega'\tau-\theta}{2})} \right] \right\}$$

$$= \ln \left\{ e^{i\theta} \left[-1 + e^{-i(\theta+\omega\tau)} \right] \left[1 - e^{-i(\theta-\omega\tau)} \right] \right\}^s . \tag{6}$$

Recalling Eq.(1) we see that the exponential of $\Gamma_s^\theta(\omega)$ is the desired determinant. Identifying $\tau = -i\beta$ ($\hbar = 1$), taking $\theta = 0$ (periodic boundary condition) and $s = -1/2$, this determinant reduces to the partition function for a bosonic oscillator [1], [3]. Analogously, for a fermionic oscillator, we just make $\theta = \pi$ (antiperiodic boundary condition) and $s = +1$, so that the above determiant reduces to the partition function of a fermionic oscillator.

For the general case, the partition function reads

$$Z_s^\theta(\beta) \equiv \exp \left[\Gamma_s^\theta(\omega) \right] = 4^s \left[\cosh^2 \frac{\omega\beta}{2} - \cos^2 \frac{\theta}{2} \right]^s . \tag{7}$$

Note that, in Eq. (7), we left the statistics parameter s free. In fact, it may be a function of the periodicity parameter θ, interpolating between $s(\theta = 0) = -1/2$ (bosonic case) and $s(\theta = \pi) = +1$ (fermionic case), as for example $s(\theta) = -1/2 + 3/2f(\theta)$, where $f(\theta)$ may be a function which satisfies $f(0) = 0$ and $f(\pi) = +1$. We wonder if this factor can be obtained from the functional integration of a generalized variable, with arbitrary commutation relation, interpolating the cases of bosonic (c-number) and Grassmannian variables, as a kind of a q-deformed calculation [4],[5].

This work was partially supported by Conselho Nacional de Desenvolvimento Científico e Tecnológico (CNPq).

References

[1] G.W.Gibbons, Phys. Lett. **A60**, 385 (1977).

[2] F. Wilczek, *Fractional statistics and anyon superconductivity*, (ed.) World Scientific, Singapore, 1990.

[3] H. Kleinert, *Path Integrals in Quantum Mechanics, Statistics, and Polymer Physics*, World Scientific Publishing, Singapore (1990).

[4] A. Lerda and S. Sciuto, Nucl. Phys. B **401** (1993) 613.

[5] J.L. Matheus-Valle and M.A.R. Monteiro, Mod. Phys. Lett. A **9** (1994) 945.

Estados Ligados na Eletrodinâmica Quântica Massiva Bi-Dimensional (QED_2)*

V. S. Alves[‡], M. Gomes[†]

[‡]Universidade de São Paulo. Departamento de Física-Matemática. Instituto de Física
Caixa Postal 20516 - CEP 01452-900 São Paulo-SP. Brasil
on leave of absence from Universidade Federal do Pará.
e-mail:vansergio@uspif.if.br.

it [†]Universidade de São Paulo. Departamento de Física-Matemática, Instituto de Física
Caixa Postal 20516 - CEP 01452-900 São Paulo-SP. Brasil

O trabalho consiste no estudo de estados ligados férmion-anti-férmios na eletrodinâmica quântica massiva bi-dimensional em $(1 + 1)D$ na expansão $1/N$ [1]. Foram calculadas via TQC as matrizes de espalhamento na aproximação não relativística, e comparada com a secão de choque na aproximação de Born, e obtemos desta forma, o potencial responsável pela interação nos processos de espalhamento. Via equação de Schrödinger foram investigadas a existência de possíveis estados ligados.

Introdução

A importância do estudo de modelos Bi-dimensional com N campos fermiônicos, reside no fato que em baixas dimensões algumas teorias (o caso da QED_2) são mais facilmente investigada, sendo portanto um bom laboratório para o estudo de propriedades gerais e também para a descoberta de novos aspectos possivelmente relevantes em dimensões superiores. O aspecto não relativístico desta teoria será analisada na ordem mais baixa, $O(\frac{1}{M})$.

Estados Ligados na QED_2 Massiva

A QED_2 com N campos fermiônicos é descrita pela seguinte densidade de Lagrangiana:

$$\mathcal{L} = -\frac{1}{4}F_{\mu\nu}F^{\mu\nu} + \bar{\psi}(i\partial_\mu\gamma^\mu - M)\psi - \frac{\lambda}{2}(\partial_\mu A^\mu)^2 + eA_\mu\bar{\psi}\gamma^\mu\psi , \tag{1}$$

onde $\underline{\lambda}$ é o parâmetro de fixação de gauge, M a massa do férmion e $\underline{e}$ é a constante de acoplamento (que neste caso possui dimensão de massa[1]). e existe uma soma implícita nos índices de simetria interna dos campos fermiônicos. i.e, ψ_a ($a = 1,...,N$). que neste espaço-tempo, possuem duas componentes. O tensor $F_{\mu\nu}$ é o usual. ou seja, $F_{\mu\nu} = \partial_\mu A_\nu - \partial_\nu A_\mu$, com $\mu,\nu = 0,1$. O campo A_μ é um campo de gauge. e as matrizes de Dirac são matrizes 2x2. Para a massa do férmion diferente de zero a teoria não possui uma solução exata[2]: apesar de ser super-renormalizável na constante de acoplamento. No entanto, na teoria de perturbação ordinária existem uma série infinita de diagramas de Feynman que contribuem para um dado processo de espalhamento. Dentre esse conjunto infinito de diagramas

---

[1]Lembre-se que no sistema de unidades naturais. $c = \hbar = 1$. $[\mathcal{L}] = M^D$. onde D é a dimensão do espaço-tempo. Como a dimensão canônica do campo de Dirac é $[\psi] = [\bar{\psi}] = M^{\frac{D-1}{2}}$ e a do campo bosônico $[A_\mu] = M^{\frac{D-2}{2}}$. implica que para $D = 2$. $[e] = M$.

[2]Para $M = 0$ e $N = 1$. temos o chamado "modelo de Schwinger" [2,3] . que é exatamente solúvel. i.e, as suas funções de Green podem ser calculadas de forma fechada[4].

podemos escolher aqueles que possuem uma mesma ordem em N. Pode-se fazer isto introduzindo uma nova constante de acoplamento

$$a = e\sqrt{N} , \qquad (2)$$

onde a é mantida fixa para N grande. Com esta mudança a Lagrangiana de interação em (1) fica: $\mathcal{L}_{int} = \frac{a}{\sqrt{N}}A_\mu\bar\psi\gamma^\mu\psi$. Incorporando o efeito de polarização do vácuo ao propagador do campo de gauge A_μ na expansão $1/N$, que na teoria livre é dado por[3] $\Delta_{\mu\nu F}(k) = -i[\frac{g_{\mu\nu}-\frac{k_\mu k_\nu}{\lambda^2}}{k^2-m^2+i\epsilon}]$ (no gauge de Landau $\lambda \to \infty$), encontra-se a seguinte expressão:

$$\Delta'_{\mu\nu F}(k) = -i(g_{\mu\nu} - \frac{k_\mu k_\nu}{k^2})\frac{1}{k^2 - m^2 + \frac{a^2}{\pi}(-1 + f(k^2))} . \qquad (3)$$

com

$$f(k^2) = \frac{4M^2}{\sqrt{4M^2k^2 - k^4}} arctg(\frac{k^2}{\sqrt{4M^2k^2 - k^4}}) , \quad 0 < k^2 < 4M^2 \qquad (4)$$

e

$$f(k^2) \simeq \frac{2M^2}{k^2\sqrt{1-\frac{4M^2}{k^2}}}ln(\frac{1-\sqrt{1-\frac{4M^2}{k^2}}}{1+\sqrt{1-\frac{4M^2}{k^2}}}) + \frac{2i\pi M^2}{k^2\sqrt{1-\frac{4M^2}{k^2}}} . \quad k^2 > 4M^2 \qquad (5)$$

Utilizando o formalismo de redução [5,6] encontra-se a seguinte amplitude de espalhamento férmion-anti-férmion:

$$\mathcal{M}_{fi} = (2\pi)^2\delta(p'_1 - p'_2 - p_1 + p_2) \left[\mathcal{M}_{fi}^{direto} - \mathcal{M}_{fi}^{aniq.}\right] , \qquad (6)$$

onde

$$\mathcal{M}_{fi}^{direto} = \frac{a^2}{N}\bar u(\vec p_1\,')\gamma^\mu u(\vec p_1)\Delta'_{\mu\nu F}(k)\bar v(\vec p_2\,')\gamma^\nu v(\vec p_2), \qquad (7)$$

e

$$\mathcal{M}_{fi}^{aniq.} = \frac{a^2}{N}\bar u(\vec p_1\,')\gamma^\mu v(\vec p_2\,')\Delta'_{\mu\nu F}(k)\bar v(\vec p_2)\gamma^\nu u(\vec p_1). \qquad (8)$$

Com ajuda das soluções da equação de Dirac em $(1 + 1)D$ [1]. e fazendo uma aproximação não relativística até $\mathcal{O}(p/M)$ na expressão (3) e nas correntes espinoriais em (7). a amplitude de espalhamento do termo direto fica:

$$\mathcal{M}_{fi}^{direto} = i\frac{a^2}{N}\frac{1}{(1 + \frac{a^2}{6\pi M^2})\vec k^2 + m^2} \qquad (9)$$

onde foi levado em consideração que o quadrado do bi-momento transferido $k^2 = k_0^2 - |\vec k|^2 \simeq -|\vec k|^2$ até $\mathcal{O}(p/M)$ [1]. Observe que o termo constante $\frac{a^2}{M^2}$ no denominador de (9) pode ou não ser desprezado. No que segue, vamos considerar $\frac{a^2}{M^2} \geq 1$ de tal forma que a contribuição advinda da polarização do vácuo é relevante [4]. Por outro lado, para o termo de aniquilação $k^2 \simeq 4M^2$. e a função $f(k^2)$ dada por (5) diverge para $k^2 = 4M^2$. Isto implica que $\Delta'_{F\mu\nu}(k) \to 0$, e consequentemente $\mathcal{M}_{fi}^{aniq.}$ se anula para este valor do momento. Vemos assim que não há contribuição para o potencial proveniente do termo de aniquilação. Deste modo. encontra-se a seguinte expressão para o potencial efetivo, no limite para $m \to 0$.

---

[3] O termo de massa $\underline{m}$ foi introduzido a fim de evitar possíveis divergências infra-vermelhas nos cálculos intermediários.

[4] Na situação oposta. i.e, para $\frac{a^2}{M^2} \ll 1$, o cálculo reproduz, no limite $m \to 0$, somente o potencial coulombiano clássico.

$$V_{eff}(x) = \frac{\alpha^2}{2N\left(1 + \frac{\alpha^2}{6\pi M^2}\right)}|x|,$$ (10)

que representa o potencial coulombiano em 2D, atrativo, responsável pela interação entre o par férmion–anti-férmion.

Resolvendo-se a equação de Schrödinger para o problema de dois corpos de massa reduzida $\mu = m_1 m_2/(m_1 + m_2) = \frac{M}{2}$, submetidos ao potencial (10), obtém-se as seguintes funções de onda:

$$\Psi = \begin{cases} a_1 A_i\left[\left(x - \frac{E}{\rho}\right)(M\rho)^{1/3}\right] = \Psi_+, & x > 0 \\ a_2 A_i\left[\left(-x - \frac{E}{\rho}\right)(M\rho)^{1/3}\right] = \Psi_-, & x < 0 \end{cases}$$ (11)

com $\rho = \frac{\alpha^2}{2N\left(1 + \frac{\alpha^2}{6\pi M^2}\right)}$, e também a equação que determina os auto-valores da energia E,

$$A_i'\left(-\frac{E}{\rho}(M\rho)^{1/3}\right) = 0$$ (12)

onde A_i é a função de Airy.

Conclusão

Na QED_2 massiva estudamos a existência de estados ligados entre férmion–anti-férmion. É possível obter estados ligados variando a constante de acoplamento, ou a massa do férmion, para um determinado valo de N (a princípio grande). Esses resultados foram obtidos na região de acoplamento forte ($\frac{\alpha^2}{M^2} \geq 1$), onde o efeito de polarização do vácuo não pode ser desprezado. Esse modelo exibe características semelhantes à QCD, como o confinamento do par férmion–anti-férmion. Observa-se também, através da expressão do potencial efetivo (equação (10)), que o confinamento só ocorre se os férmions são massivos. Caso contrário, se $M \rightarrow 0$, não existem estados ligados. Devemos enfatizar que o limite quando $M \rightarrow 0$ aqui considerado não corresponde ao modelo de Schwinger, pois o limite não relativístico que temos pressupõe que M^2 é grande. O modelo de Schwinger é obtido se tomarmos $M = 0$ de início na teoria de campos, i.e, fazendo este limite no propagador do campo A_μ, dado por (3). Podemos analisar os resultados dessas duas teorias rapidamente. Pela expressão (3) verifica-se imediatamente que o fóton adquire uma massa $\frac{e}{\sqrt{\pi}}$ quando fazemos $M \rightarrow 0$ [5]. Dessa forma, a energia do estado ligado que se formaria teria exatamente o valor $\frac{e}{\sqrt{\pi}}$. No nosso caso, isto não acontece, mais precisamente esta energia é nula. O motivo dessa diferença de resultados está no fato de que o limite não relativístico do modelo de Schwinger perde o seu significado (este limite corresponderia ao caso $\alpha^2 >> k^2$, pois α^2 é o único parâmetro de massa desta teoria). É oportuno ressaltar que os estados ligados obtidos nesse modelo tiveram como contribuição apenas o termo direto do espalhamento, visto que os gráficos de aniquilação não contribuem.

References

[1] V. S. Alves. *Estados Ligados em Modelos Bi-Dimensionais: o caso da QED₂ e de um Modelo com Interações Fermiônicas*, Dissetação de Mestrado, IFUSP, (1993);

[2] J. Schwinger, Phys. Rev. 128, 2425, (1962);

[3] S. Coleman, Ann. Phys. 101, 239, (1976);

[4] J. H. Lowenstein and J. A. Swieca, Ann. Phys. 68, 172, (1970);

[5] Lehman, Symanzik and Zimmermann, Nuov. Cimen. I. 205, (1955);

[6] M.Gomes, *Apostila do Curso de Introdução à Teoria Quântica de Campos I e II*, IFUSP. (1993);

---

⁵Historicamente quem obteve primeiramente esse resultado foi Schwinger[2], e ilustra o fenômeno de Higgs, ou seja, a quebra espontânea de simetria de gauge local sem o surgimento de um bóson de Goldstone.

Aproximação 1/n no modelo Nambu-Jona-Lasinio (NJL) $SU(3)$ generalizado*

F. A. Peña[†], M. C. Nemes[‡]

[†]Universidade de São Paulo, Departamento de Física–Matemática, Instituto de Física
Caixa Posta 20516 - CEP 01452-990, São Paulo-SP, Brasil,
on leave of absence from Universidad de La Frontera, Temuco. Chile.
[‡]Universidade Federal de Minas Gerais, Departamento de Física, Instituto de Ciências Exatas.
C.P. 702. 31270 Belo Horizonte-MG, Brasil.

Introdução

No presente trabalho, considera-se a expansão $1/N$ do modelo Nambu-Jona-Lasinio (NJL) $SU(3)$ sabor generalizado das interações quárticas fermiônicas em 4D no formalismo da integral funcional, sendo N o parâmetro livre que representa o número de cores. O modelo apresenta as propriedades básicas de simetrias da QCD. é não-renormalizável e contém o termo sugerido por t'Hooft que quebra a simetria axial $U_A(1)$.

O trabalho consiste em obter o espectro de massas dos hádrons mais leves como pólos do inverso da matriz função vértice e as constantes de acoplamento méson-quark-antiquark na aproximação árvore da matriz de espalhamento T.

O Modelo e a Expansão $1/N$

O modelo NJL para estudar as propriedades dos mésons mais leves na escala hadrônica compatível com as simetrias da QCD e incorporando o termo de quebra da simetria axial $U_A(1)$ é dado pela seguinte densidade de Lagrangiana generalizada,

$$\mathcal{L}_{NJL} = \overline{\psi}\,[i\partial\!\!\!/ \ - m_0]\,\psi + \mathcal{L}_{4f} + \mathcal{L}_{t'Hooft} \tag{1}$$

onde

$$\mathcal{L}_{4f} = \frac{1}{2}G_1\left[(\overline{\psi}\lambda_a\psi)^2 + (\overline{\psi}\lambda_a i\gamma_5\psi)^2\right] - \frac{1}{2}G_2\left[(\overline{\psi}\lambda_a\gamma^\mu\psi)^2 + (\overline{\psi}\lambda_a\gamma^\mu\gamma_5\psi)^2\right] \tag{2}$$

e

$$\mathcal{L}_{t'Hooft} = K\left[det\frac{1}{2}\left[\overline{\psi}(1+\gamma_5)\psi\right] + det\frac{1}{2}\left[\overline{\psi}(1-\gamma_5)\psi\right]\right]. \tag{3}$$

As matrizes λ_a são os geradores do grupo $SU(3)$ sabor, $a = 0,1,2,....8$ e m_o é a matriz diagonal cujos elementos correspondem as massas correntes de quarks. A dimensão das duas constantes de acoplamento G_i é $[L]^2$ e da constante K é $[L]^5$.

A interação de seis campos, $\mathcal{L}_{t'Hooft}$ precisa ser reduzida a uma interação quártica fechando num "loop de férmions", formando assim, um condensado de quarks $\langle\overline{\psi}_i\psi_i\rangle$. Usa-se um "cutoff" euclidiano covariante, Λ, que define o esquema de regularização .

Assim, a densidade de Lagrangiana efetiva quártica vem dada por

$$\mathcal{L} = \overline{\psi}\,[i\partial\!\!\!/ \ - m_0]\,\psi + \frac{1}{2}K_a^{(-)}(\overline{\psi}\lambda_a\psi)^2 + \frac{1}{2}K_a^{(+)}(\overline{\psi}\lambda_a i\gamma^5\psi)^2$$

$$+ \frac{1}{2}K_{08}^{(-)}\left[(\overline{\psi}\lambda_0\psi)(\overline{\psi}\lambda_8\psi) + (\overline{\psi}\lambda_8\psi)(\overline{\psi}\lambda_0\psi)\right]$$

$$+ \frac{1}{2} K_{08}^{(+)} \left[(\overline{\psi}\lambda_0 i\gamma^5 \psi)(\overline{\psi}\lambda_8 i\gamma^5 \psi) + (\overline{\psi}\lambda_8 i\gamma^5 \psi)(\overline{\psi}\lambda_0 i\gamma^5 \psi) \right]$$

$$- \frac{1}{2} G_2 \left[(\overline{\psi}\lambda_a \gamma^\mu \psi)^2 + (\overline{\psi}\lambda_a \gamma^\mu \gamma^5 \psi)^2 \right] \tag{4}$$

onde

$$K_0^{(\mp)} = G_1 \pm \frac{1}{4} K [2\langle \overline{u}u \rangle + \langle \overline{s}s \rangle]; \qquad K_1^{(\mp)} = K_2^{(\mp)} = K_3^{(\mp)} = G_1 \mp \frac{3}{8} K \langle \overline{s}s \rangle;$$

$$K_4^{(\mp)} = K_5^{(\mp)} = K_6^{(\mp)} = K_7^{(\mp)} = G_1 \mp \frac{3}{8} K \langle \overline{u}u \rangle; \qquad K_8^{(\mp)} = G_1 \mp \frac{1}{8} K [4\langle \overline{u}u \rangle - \langle \overline{s}s \rangle]:$$

$$K_{08}^{(\mp)} = \mp \frac{\sqrt{2}}{8} K [\langle \overline{u}u \rangle - \langle \overline{s}s \rangle]$$

Na expansão $1/N$ escrevemos (4) como,

$$\mathcal{L} = \left[-\frac{1}{2\overline{k}_a^{(-)}}\sigma_a^2 - \frac{1}{2\overline{k}_a^{(+)}}\pi_a^2 - \frac{1}{4g_2}tr V^2 - \frac{1}{4g_2}tr A_5^2 + C_1\sigma_0\sigma_8 + C_2\pi_0\pi_8 \right] +$$

$$\sqrt{N}\left[C_3\sigma_0 + C_4\sigma_8 \right] + \overline{\psi}K\psi + cte \tag{5}$$

onde C_1, C_2, C_3 e C_4 dependem das constantes de acoplamento e

$$\overline{k}_0^{(\mp)} = k_0^{(\mp)} - \frac{k_{08}^{(\mp)2}}{k_8^{(\mp)}}$$

$$\overline{k}_8^{(\mp)} = k_8^{(\mp)} - \frac{k_{08}^{(\mp)2}}{k_0^{(\mp)}}$$

$$\overline{k}_j = k_j$$

com $j = 1, \ldots, 7$ e

$$K = [i\partial\!\!\!/ - m]\left[1 + \frac{1}{\sqrt{N}}(i\partial\!\!\!/ - m)^{-1}(\sigma + \pi i\gamma^5 + iV_\mu\gamma^\mu + iA_{\mu5}\gamma^\mu\gamma^5)\right]$$

com $\sigma = \sigma_a\lambda^a$, $\pi = \pi_a\lambda^a$, $V_\mu = -iV_{\mu a}\lambda^a$, $A_{\mu5} = -iA_{\mu5a}\lambda^a$.

Utilizando o formalismo da integral funcional obtem-se as equações de "gap" ("tad-pole").

$$m_u = m_d = m_u^0 - 2\langle \overline{u}u \rangle \left(g_1 + \frac{3}{4}k\langle \overline{s}s \rangle \right)$$

$$m_s = m_s^0 - 2g_1\langle \overline{s}s \rangle - \frac{3}{2}k\langle \overline{u}u \rangle^2 \tag{6}$$

e a função vértice

$$\Gamma = \begin{pmatrix} \Gamma_{\sigma\sigma} & \Gamma_{\sigma V}^\nu & 0 & 0 \\ \Gamma_{V\sigma}^\mu & \Gamma_{VV}^{\mu\nu} & 0 & 0 \\ 0 & 0 & \Gamma_{\pi\pi}^5 & \Gamma_{\pi A}^{\nu5} \\ 0 & 0 & \Gamma_{A\pi}^{\mu5} & \Gamma_{AA}^{\mu\nu5} \end{pmatrix} \tag{7}$$

que é uma matriz em blocos diagonais. Cada bloco vem ser tratado independente e os elementos tem a estrutura

$$\Gamma_j = (1 - J\Omega)\Omega^{-1} \tag{8}$$

o simbolo J refere-se às integrais fermiônicas em "um-loop" do tipo

$$J_{ab}(\Xi, \Xi') = 2iTr \int^{\Lambda} \frac{d^4p}{(2\pi)^4} \left[\Xi \lambda_a S_F \left(p + \frac{q}{2} \right) \bigotimes \Xi' \lambda_b S_F \left(p - \frac{q}{2} \right) \right] . \tag{9}$$

Ω é uma matriz na qual contém as constantes de acoplamento e Ξ é uma matriz de Dirac.

Os propagadores mesônicos estão dados pelo inverso da função vértice e as massas dos campos auxiliares são determinadas pelo conjunto de condições

$$\mathcal{D}(q^2) = det(I - J\Omega) = 0 \tag{10}$$

para $q^2 = m_h^2$, onde cada canal é determinado pela forma específica de J e Ω compatível com os números quânticos da partícula.

Para obter a matriz de espalhamento, usaremos a fórmula de redução com a densidade de Lagrangiana de interação dada por

$$\mathcal{L}_{int} = \frac{1}{\sqrt{N}} \bar{\psi} \mathcal{K} \psi. \tag{11}$$

Na ordem N. podemos escrever a matriz de espalhamento na forma

$$T = M_{ij}(\Xi, \Xi') \cdot \left(\Xi \lambda_i \bigotimes \Xi' \lambda_j \right) \tag{12}$$

com as matrizes M dadas por

$$M = (1 - \Omega J)^{-1} \Omega . \tag{13}$$

Expandindo o denominador da matriz M em torno do pólo $q^2 = m_h^2$ para um canal hadronico. a matriz T corresponde ao termo de Born representado na forma

$$\langle \bar{b}d \, | T | \, \bar{c}a \rangle \cong J_{db}(-q) \frac{1}{q^2 - m_h^2 + i\epsilon} J_{ca}(q) . \tag{14}$$

onde

$$J_i(q) = g(q^2) \, \Xi \, \lambda_i \tag{15}$$

e $g(q^2)$ o fator de forma quark-antiquark-méson.

As constantes de acoplamento quark-antiquark-méson são definidas para os pólos mesônicos $g = g(m_h^2)$.

Resultados Numéricos

As constantes de acoplamento do modelo são obtidas como na referência (12) : g_1 é essencialmente fixada pelas equações de "gap" as quais geram as massas dos quarks constituintes m_i. O parametro g_2 vem ser obtido através da massa do méson ρ. A constante k é determinada do levantamento $\eta\eta'$. O "cutoff" covariante é $\Lambda = 1\,GeV$. Os valores das constantes são : $g_1 \Lambda^2 = 7.858$, $g_2 \Lambda^2 = 10.998$, $k \Lambda^2 = 336$. As massas dos quarks constituintes são $m_u = m_d = 385.9\,GeV$ e $m_s = 529.0\,GeV$.

O espectro de massas pseudoescalares associado a este conjunto de parâmetros são

$$m_{\pi^0} = m_{\pi^+} = m_{\pi^-} = 139.5\,MeV \; (exp.\ 139.56\,MeV)$$

$$m_{\kappa^+} = m_{\kappa^-} = 491.5\,MeV \; (exp.\ 497.67\,MeV)$$

$$m_{\pi_0} = 545\,MeV \; (exp.\ 548.8\,MeV)$$

$$m_{\pi_h} = 928\,MeV \; (exp.\ 957.5\,MeV) .$$

Conclusões

A implementação formal da expansão $1/N$ com a introdução dos campos auxiliares bosónicos usados para a derivação de uma densidade de Lagrangiana efetiva com interações mesónicas, têm como teoria "macroscópica" fundamental o modelo NJL $S\dot{U}(3)$ e portanto as apropriadas simetrias da QCD. Esta implementação permite obter uma densidade de Lagrangiana que preserva a dinâmica original do modelo.

Têm-se demonstrado. que na ordem dominante da expansão $1/N$. exibe a geração dinâmica de massa dos campos fermiônicos. As equações de "gap" que achamos são precisamente as obtidas no formalismo Bethe-Salpeter. Os campos bosónicos auxiliares pseudoescalares mostram ser bem representados por estados ligados $q - \bar{q}$. As massas são obtidas como pólos da inversa da matriz função vértice. Estes resultados são muito bons com os dados experimentais.

A discusão anterior é básicamente dedicada à derivação da densidade de Lagrangiana mesónica. Isto representa um primeiro paso em obter as correções na aproximação de "um-loop" como um caminho sistemático e consistente. Por exemplo, para os efeitos de ordem mais altas, temos diagramas "triângulo" relativo aos processos de decaimento e "quadrados" relativo a espalhamento.

Outra contribuição importante da presente densidade de Lagrangiana é relativo a $q^2=0$ na expansão local dos campos auxiliares. Neste caso, obtevesse uma interação local efetiva dos campos mesonicos incorporando termos cinéticos destes campos. Temos a confiança que as aproximações "$K - \bar{K}$ molecules" e outros sistemas compostos. sejam bem descritos. Estas investigações estão em desenvolvimento.

Agradecimentos : agradecemos a B. Hiller e A. H. Blin. da Universidade de Coimbra. Portugal e M. O. Gomes. R. Mendes. V. S.Alves. S. V. L. Pinheiros. L. C. Malacarne. da Universidade de São Paulo. Brasil. pelas sempre boas discusões.

References

[1] Y. Nambu and G. Jona-Lasinio. Phys.Rev.122 (1961) 345; 124 (1961) 246

[2] G. t'Hooft. Phys.Rev.Lett.37. (1976) 8 ;Phys.Rev.D14 (1976) 3432

[3] S. P. Klevansky. Rev.of Mod.Phys.. 64 3 (1992) 649

[4] V. Bernard. R. L. Jaffe and U.-G. Meißner. Nucl.Phys.B308 (1988) 753;
    V. Bernard and U.-G. Meißner,Phys. Lett. B223 (1989) 439

[5] V. Bernard, U.-G. Meißner and I. Zahed. Phys. Lett.59 (1987) 966;
    V. Bernard and U.-G. Meißner. Nucl.Phys. A489 (1988) 647

[6] J. da Providencia, M. C. Ruivo and C. A. de Sousa. Phys. Rev. D36 (1987] 1882

[7] S. Klimt. M. Lutz. U. Vogl and W.Weise. Nucl.Phys. A516 (1990) 429;
    U. Vogl. M. Lutz. S. Klimt and W. Weise. Nucl.Phys. A516 (1990) 469

[8] M. Takizawa. K. Tsushina. Y. Kohyama and K. Kubodera. Nucl.Phys. A507 (1990) 611

[9] H. Hatsuda and K. Kunhiro. Prog.Theor. Phys. 91 (1987) 284

[10] V. Bernard. A. H. Blin. B. Hiller. U.-G. Meißner and M.C. Ruivo. Phys. Lett. B305 (1993) 163

[11] J. Weinstein, N. Isgur. Phys.Rev. D12 (1975) 3770; Phys.Rev. D41 (1990) 2236

[12] D. Lhose. J. W. Durso. K. Holinde. J. Speth. Nucl.Phys. A516 (1990) 513

[13] F. Cannata. J. P. Dedonder and L. Lesniak. Z.Phys. A343 (1992) 451

[14] R. L. Jaffe. Phys.Rev. D15 (1977) 267

[15] E. van Beveren. G. Rupp, T. A. Rijken and C. Dullemond. Phys.Rev. D27 (1983) 1527; E. van Beveren. Nucl.Phys. B21(proc.Suppl.) (1991) 43

[16] H. Reinhardt and R. Alkofer, Phys.Lett.B (207).4 (1988)

[17] Van Sérgio Alves. Estados Ligados em Modelos Bi-Dimensionais : O caso da QED_2 e de um Modelo com Interações Quárticas Fermiônicas. Dissertação de Mestrado. Instituto de Física da USP.1993.

[18] G. t'Hooft. Nucl.Phys. B72 (1974) 461; B75 (1974) 461

[19] M. K. Volkov. Ann.Phys.(N.Y) (1984) 157

Uma prova original para os teoremas
de Vandermonde e Saalschutz

R. M. Ricotta* e A. T. Suzuki**

* Faculdade de Tecnologia de São Paulo. CEETPS-UNESP
** Instituto de Física Teórica-UNESP

O Método de Integração a Dimensão Negativa (NDIM). [1], foi originalmente concebido através da seguinte integral:

$$\int d^d k (k^2)^n = (-\pi)^{d/2} n! \delta_{n+d/2,0} \quad n \in Z \tag{1}$$

O ponto fundamental aqui é que agora valores negativos da dimensão d são admitidos, o que torna a integral acima não trivial, com d/2 inteiro. Este resultado é compatível com o limite da integral (d > 0):

$$\int d^d k (k^2)^n = \lim_{m \to 0} \int d^d k \frac{(k^2)^n}{(k^2 + M^2)^m} = \lim_{m \to 0} \left(\pi^{d/2} (M^2)^{n+d/2-m} \frac{\Gamma(n + d/2)\Gamma(m - n - d/2)}{\Gamma(d/2)\Gamma(m)} \right) \tag{2}$$

o que significa que, se n > 0 necessariamente d < 0.

Uma outra maneira possível de se obter este resultado é através de projeção de potências da integral Gaussiana em d dimensões, [2]:

$$\int d^d k e^{-\lambda k^2} = \left(\frac{\pi}{\lambda} \right)^{d/2}. \tag{3}$$

Considerando-se uma continuação analítica para d < 0, podemos expandir o lado esquerdo da equação (3).

$$\sum_{n=0}^{\infty} \frac{(-\lambda)^n}{n!} \int d^d k (k^2)^n = \left(\frac{\pi}{\lambda} \right)^{d/2} \tag{4}$$

e concluir que a igualdade só se dá se a integral em (4) tomar o valor de (1). Em outras palavras. só um termo da série contribui para o resultado conhecido, dando à integral Gaussiana um caráter fermiônico, característico do método.

A integral (1) define portanto o método, permitindo o cálculo de integrais d-dimensionais, comumente utilizadas para resolver integrais de Feynman dimensionalmente regularizadas. . Os cálculos envolvidos baseiam-se fundamentalmente na expansão binomial em série de potências e as manipulações são puramente algébricas: frequentemente temos que fazer somas de funções hipergeométricas generalizadas. É neste ponto que aplicamos a integral definidora (1) para demonstrar, de forma original, teoremas bastante conhecidos. Apresentamos aqui os nossos resultados.

Considere a série hipergeométrica truncada, cuja soma é dada pelo Teorema de Vandermonde (1770). (caso particular da Soma de Gauss, [3]) :

$$_2F_1(a,b;c;1) = \sum_{n=0}^{\infty} \frac{(a)_n (b)_n}{(c)_n n!} = \frac{(c-a)_{-b}}{(c)_{-b}}, \tag{5}$$

onde $c - a - b > 0$, $c > 0$, $b < 0$ e $(b)_n = (-1)^n/((1 - b)_{-n}$ é uma propriedade do símbolo Pochhammer.

Introduzimos uma variável vinculada: $k = -b - n$ de forma que

$$\sum_n \rightarrow \sum_{n,k} \delta_{k+n+b,0} \tag{6}$$

Usamos então o parâmetro negativo b como a dimensão negativa da integral definidora do método, (1)

$$\delta_{n+k+b,0} = \frac{1}{(-\pi)^b(n+k)!} \int d^{2b}k(k^2)^{n+k}. \tag{7}$$

A partir dai usamos somente as séries binomiais,

$$(1 - q^2)^{-a} = \sum_n \frac{(a)_n}{n!}(q^2)^n = \sum_n \frac{\Gamma(a+n)}{\Gamma(a)n!}(q^2)^n \tag{8}$$

$$(1 - q^2)^\alpha = \sum_n \frac{\Gamma(\alpha+1)}{\Gamma(\alpha+1-n)n!}(q^2)^n \tag{9}$$

obtendo finalmente o resultado acima.

O Teorema de Saalschutz refere-se à soma da função hipergeométrica $_3F_2(a,b,c;d,e;1)$, quando vale a relação : $a + b + c + 1 = d + e$ entre os seus coeficientes e um dos parâmetros do numerador é inteiro negativo. [4]

$$_3F_2(a,b,c;d,e;1) = \sum_{n=0}^{\infty} \frac{(a)_n(b)_n(c)_n}{(d)_n(e)_n n!} = \frac{\Gamma(d)\Gamma(1+a-e)\Gamma(1+b-e)\Gamma(1+c-e)}{\Gamma(1-e)\Gamma(d-a)\Gamma(d-b)\Gamma(d-c)} \tag{10}$$

No nosso caso, consideramos os parâmetros b, c e e negativos, de forma que introduzimos duas variáveis vinculadas, $-c - n = l$ e $-b - n = k$,

$$\sum_n \rightarrow \sum_{n,l,k} \delta_{l+n+c,0} \, \delta_{k+n+c,0} \tag{11}$$

Usamos a integral definidora do método (1) duas vezes, onde $(-b)$ e $(-c)$ fazem o papel da dimensão negativa. Através das séries binomiais obtemos o resultado desejado, (10).

References

[1] I. G. Halliday and R. M. Ricotta, Phys. Lett. B193 (1987) 241

[2] R. M. Ricotta, J. J. Giambiagi Festschrift, ed. por H. Falomir et al, World Scientific, Singapura, 1990

[3] C. F. Gauss, Ges. Werke, 3 (1866), 123 e 207

[4] L. Saalschutz, Zeitschrift fur Math. u. Phys., 35 (1890), 186

$N = 1$ Super-τ_3QED from Atiyah-Ward Space-Time *

M. A. De Andrade and O. M. Del Cima

Centro Brasileiro de Pesquisas Físicas (CBPF)

Departamento de Teoria de Campos e Partículas (DCP)

Rua Dr. Xavier Sigaud, 150 - Urca

22290-180 - Rio de Janeiro - RJ - Brasil

In this letter, we present the action for the massive super-QED$_{2+2}$. A pair of chiral and a pair of anti-chiral superfields with opposite $U(1)$-charges are required. We also carry out a dimensional reduction à la Scherk from (2+2) to (1+2) dimensions, and we show that, after suitable truncations are performed, the supersymmetric extension of the τ_3QED$_{1+2}$ naturally comes out.

The idea of considering space-times with several time directions and indefinite signature has deserved a great deal of attention since a self-dual Yang-Mills theory in (2+2) dimensions [1] has been related to the Atiyah-Ward conjecture [2]: this theory might be the source for various integrable models in lower dimensions, after appropriate dimensional reductions are carried out.

More recently, Gates, Ketov and Nishino [3] have pointed out the existence of Majorana-Weyl spinors in the Atiyah-Ward space-time, and $N=1$ self-dual supersymmetric Yang-Mills theories and self-dual supergravity models have been formulated for the first time in this particular space [4].

Since over the past years 3-dimensional field theories [5] have been shown to play a central rôle in connection with the behaviour of 4-dimensional theories at finite temperature [6], as well as in the description of a number of problems in Condensed Matter Physics [7, 8, 9], it seems reasonable to concentrate efforts in trying to understand some peculiar features of gauge-field dynamics in 3 dimensions. Also, the recent result on the Landau gauge finiteness of Chern-Simons theories is a remarkable property that makes 3-dimensional gauge theories so attractive [10]. Very recently, this line of investigation has been well-motivated in view of the possibilities of providing a gauge-theoretical foundation for the description of Condensed Matter phenomena, such as high-T_c superconductivity [8], where the QED$_3$ and τ_3QED$_3$ [8, 9] are some of the theoretical approaches that been forwarded as an attempt to understand more deeply about high-T_c materials.

Our purpose in the present letter is to show the relationship between massive Abelian $N=1$ super-QED$_{2+2}$ [11] and $N=1$ super-τ_3QED, after a dimensional reduction à la Scherk is carried out and suitable supersymmetry-preserving truncations are made in order to suppress non-physical propagating modes in three dimensions.

The supersymmetric extension of the massive QED in $D=1+3$ requires two chiral superfields carrying opposite $U(1)$-charges [12]. On the other hand, to introduce mass in the matter sector in $D=2+2$, without breaking gauge-symmetry, we have to introduce four scalar superfields: a pair of chiral and a pair of anti-chiral superfields; the supermultiplets of each pair exhibit opposite $U(1)$-charges.

The massive Abelian $N=1$ super-QED$_{2+2}$ is described by the action : [1]

$$S_{inv}^{AW} = -\frac{1}{8}\left(\int ds\, W^c W + \int d\tilde{s}\, \widetilde{W}^c\widetilde{W}\right) + \int dv\,\left(\Psi_+^\dagger e^{4qV}\tilde{X}_+ + \Psi_-^\dagger e^{-4qV}\tilde{X}_-\right) +$$

$$+ im\left(\int ds\,\Psi_+\Psi_- - \int d\tilde{s}\,\tilde{X}_+\tilde{X}_-\right) + \text{h.c.} \quad , \tag{1}$$

where q is a dimensionless coupling constant and m is a parameter with dimension of mass. The $+$ and $-$ subscripts in the matter superfields refer to their respective $U(1)$-charges. To build up the interaction terms, we have used a mixing between the chiral and anti-chiral superfields (in order to justify such a procedure, we refer to the works of Gates, Ketov and Nishino [4]). This mixed interaction term establishes that the vector superfield be *complex*.

In the action (1), the chiral ($\Psi_\pm$) and the anti-chiral ($\tilde{X}_\pm$) superfields are defined as follows:

$$\Psi_\pm(x,\theta,\tilde{\theta}) = e^{i\theta\tilde{\partial}\theta}\left[A_\pm(x) + i\theta\psi_\pm(x) + i\theta^2 F_\pm(x)\right] \quad , \quad \tilde{D}_{\dot\alpha}\Psi_\pm = 0 \quad , \tag{2}$$

$$\tilde{X}_\pm(x,\theta,\tilde{\theta}) = e^{i\theta\partial\tilde{\theta}}\left[B_\pm(x) + i\tilde{\theta}\tilde{\chi}_\pm(x) + i\tilde{\theta}^2 G_\pm(x)\right] \quad , \quad D_\alpha\tilde{X}_\pm = 0 \quad ; \tag{3}$$

where

$$\tilde{\partial}_{\dot\alpha\alpha} \equiv \tilde{c}_{\dot\alpha\dot\beta}\tilde{\sigma}^{\mu\,\dot\beta}{}_\alpha\partial_\mu \quad \text{and} \quad \tilde{\sigma}^{\mu\,\dot\beta}{}_\alpha = (i\sigma_x, -\sigma_y, \sigma_z, 1_2)^{\dot\beta}{}_\alpha \quad ; \tag{4}$$

$$\partial_{\alpha\dot\alpha} \equiv c_{\alpha\beta}\sigma^{\mu\,\beta}{}_{\dot\alpha}\partial_\mu \quad \text{and} \quad \sigma^{\mu\,\beta}{}_{\dot\alpha} = (-i\sigma_x, \sigma_y, -\sigma_z, 1_2)^\beta{}_{\dot\alpha} \quad . \tag{5}$$

$A_\pm$ and $B_\pm$ are complex scalars, $\psi_\pm$ and $\tilde{\chi}_\pm$ are Weyl spinors. and $F_\pm$ and $G_\pm$ are complex auxiliary scalars.

In the Wess-Zumino gauge [12], a complex *vector* superfield, V, is written as

$$V(x,\theta,\tilde{\theta}) = \frac{1}{2}i\theta\sigma^\mu\tilde{\theta}B_\mu(x) - \frac{1}{2}\tilde{\theta}^2\theta\lambda(x) - \frac{1}{2}\theta^2\tilde{\theta}\tilde{\rho}(x) - \frac{1}{4}\theta^2\tilde{\theta}^2 D(x) \quad , \tag{6}$$

where D is a complex auxiliary scalar, λ and $\tilde{\rho}$ are Weyl spinors and B_μ is a *complex* vector field.

The field-strength superfields, W_α and $\widetilde{W}_{\dot\alpha}$, defined by

$$W_\alpha = \frac{1}{2}\tilde{D}^2 D_\alpha V \quad \text{and} \quad \widetilde{W}_{\dot\alpha} = \frac{1}{2}D^2\tilde{D}_{\dot\alpha}V \quad , \tag{7}$$

respectively, satisfy the chiral and anti-chiral conditions, $\tilde{D}_{\dot\beta}W_\alpha=0$ and $D_\beta\widetilde{W}_{\dot\alpha}=0$.

. By considering the superfields defined above, the following component-field action stems from the superspace action of eq.(1) :

$$S_{inv}^{AW} = \int d^4x\left\{-\frac{1}{4}i\left(\lambda^c\partial\tilde{\rho} + \tilde{\rho}^c\tilde{\partial}\lambda\right) - \frac{1}{8}G^*_{\mu\nu}G^{\mu\nu} - \frac{1}{4}D^*D +\right.$$

$$- F_+^*G_+ - A_+^*\Box B_+ - \frac{1}{2}i\psi_+^c\partial\tilde{\chi}_+ - qB_\mu\left(\frac{1}{2}i\psi_+^c\sigma^\mu\tilde{\chi}_+ + A_+^*\partial^\mu B_+ - B_+\partial^\mu A_+^*\right) +$$

$$+ iq\left(A_+^*\tilde{\chi}_+\tilde{\rho} + B_+\psi_+^c\lambda\right) - (qD + q^2B_\mu B^\mu)A_+^*B_+ +$$

$$- F_-^*G_- - A_-^*\Box B_- - \frac{1}{2}i\psi_-^c\partial\tilde{\chi}_- + qB_\mu\left(\frac{1}{2}i\psi_-^c\sigma^\mu\tilde{\chi}_- + A_-^*\partial^\mu B_- - B_-\partial^\mu A_-^*\right) +$$

$$- iq\left(A_-^*\tilde{\chi}_-\tilde{\rho} + B_-\psi_-^c\lambda\right) + (qD - q^2B_\mu B^\mu)A_-^*B_- +$$

$$\left.+ m\left(\frac{1}{2}i\psi_+\psi_- - \frac{1}{2}i\tilde{\chi}_+\tilde{\chi}_- - A_+F_- - A_-F_+ + B_+G_- + B_-G_+\right)\right\} + \text{h.c.} \quad , \tag{8}$$

---

[1] In this letter, we are adopting $\eta_{\mu\nu}=(+,-,-,+)$ for the A-W space-time metric, $ds\equiv d^4x\,d^2\theta$, $d\tilde{s}\equiv d^4x\,d^2\tilde{\theta}$ and $dv\equiv d^4x\,d^2\theta d^2\tilde{\theta}$, where θ and $\tilde{\theta}$ are Majorana-Weyl spinors. Notice that we are using the following convention for charge conjugation of all Weyl spinors: $\psi^c\equiv i\sigma_z\psi^*$ and $\tilde{\chi}^c\equiv i\sigma_z\tilde{\chi}^*$. Our conventions for the supersymmetry covariant derivatives are: $D_\alpha=\partial_\alpha-i\partial_{\alpha\dot\alpha}\tilde{\theta}^{\dot\alpha}$ and $\tilde{D}_{\dot\alpha}=\tilde{\partial}_{\dot\alpha}-i\tilde{\partial}_{\dot\alpha\alpha}\theta^\alpha$. The spinor indices are raised and lowered with the help of the following antisymmetric tensors: $c_{\alpha\beta}=-c^{\alpha\beta}=i\sigma_y$ and $\tilde{c}_{\dot\alpha\dot\beta}=-\tilde{c}^{\dot\alpha\dot\beta}=-i\sigma_y$. We use the abbreviations $\theta\sigma^\mu\tilde{\theta}\equiv\theta^\alpha\sigma^\mu_{\alpha\dot\alpha}\tilde{\theta}^{\dot\alpha}$, $\theta\psi\equiv\theta^\alpha\psi_\alpha$ and $\tilde{\theta}\tilde{\chi}\equiv\tilde{\theta}^{\dot\alpha}\tilde{\chi}_{\dot\alpha}$. For more details about notation and conventions in $D=2+2$, see ref.[11].

where $G_{\mu\nu}$ is the usual field-strength associated to B_μ.

Due to the fact that in massive super-QED$_{2+2}$ one must have two opposite $U(1)$-charges to introduce mass at tree-level, and a complex vector superfield in order to build up the gauge invariant interactions, we can read directly from the action (1), the following set of local $U(1)_\alpha \times U(1)_\gamma$ trasformations :

$$\delta_g A^*_\pm = \pm iq\beta(x)A^*_\pm \quad , \quad \delta_g \psi^c_\pm = \pm iq\beta(x)\psi^c_\pm \quad \text{and} \quad \delta_g F^*_\pm = \pm iq\beta(x)F^*_\pm \quad ; \tag{9}$$

$$\delta_g B_\pm = \mp iq\beta(x)B_\pm \quad , \quad \delta_g \bar\chi_\pm = \mp iq\beta(x)\bar\chi_\pm \quad \text{and} \quad \delta_g G_\pm = \mp iq\beta(x)G_\pm \quad , \tag{10}$$

where $\beta \equiv \alpha - i\gamma$ is an arbitrary infinitesimal complex function. Notice that the complexified gauge transformations (10) read as above because one has previously fixed to work in the Wess-Zumino gauge. As for the gauge superfield components surviving the Wess-Zumino gauge, we have :

$$\delta_g \lambda = \delta_g \bar\rho = 0 \quad , \quad \delta_g D = 0 \quad \text{and} \quad \delta_g B_\mu = i\,\partial_\mu\beta \quad . \tag{11}$$

Therefore, in the Wess-Zumino gauge, the real part of B_μ gauges the $U(1)_\gamma$-symmetry with real gauge function γ, whereas its imaginary part gauges the $U(1)_\alpha$-symmetry with real gauge function α. The latter is an ordinary phase symmetry, and we associate it with the electric charge. Indeed, as we will see later on, the imaginary component of B_μ will be taken as the photon field. The parameter γ generates a local Weyl-like invariance [13]. However, the vector field that gauges such a symmetry, namely the real part of B_μ, will be suppressed in the process of dimensional reduction, so that such an invariance will not leave track in $D=1+2$. It should be emphasized that the mass bilinears in the action given by eq.(8) preserve the local $U(1)_\alpha \times U(1)_\gamma$-symmetry, since their component matter fields (fermion and scalar) carry opposite charges.

It is well-known that outstanding supersymmetric models with extended supersymmetry are closely related to simple supersymmetries in higher dimensions [14, 15]. As we are interested in simple supersymmetric models in $D=1+2$, since those should be more relevant for applications in Condensed Matter Physics [7, 8, 9], we concentrate our efforts to investigate which sort of model comes out after a suitable compactification from Atiyah-Ward space-time to 3-space-time dimensions is accomplished. Therefore, it will be interesting to carry out a dimensional reduction (à la Scherk [14]) of the massive $N=1$ super-QED$_{2+2}$. Bearing in mind that this procedure should extend the supersymmetry [14, 15] to $N>1$, truncations will be needed in order to remain with a simple supersymmetry and to suppress unphysical modes, i.e. spurious degrees of freedom coming from $D=2+2$ dimensions.

Performing the dimensional reduction[2] of the action (8) to $D=1+2$ [11], the following result comes out :

$$
\begin{aligned}
S^{D=3}_{\text{inv}} &= \int d^3x \left\{ -\frac{1}{4}i\left(\bar\lambda\gamma^m\partial_m\rho + \bar\rho\gamma^m\partial_m\lambda \right) - \frac{1}{8}\left(G^*_{mn}G^{mn} + 2\partial_m\phi^*\partial^m\phi \right) - \frac{1}{4}D^*D + \right. \\
&\quad - F^*_+ G_+ - A^*_+ \Box B_+ - \frac{1}{2}i\bar\psi_+\gamma^m\partial_m\chi_+ - qB_m\left(\frac{1}{2}i\bar\psi_+\gamma^m\chi_+ + A^*_+\partial^m B_+ - B_+\partial^m A^*_+ \right) + \\
&\quad + \frac{1}{2}q\phi\bar\psi_+\chi_+ + q\left(A^*_+\bar\chi_+\rho - B_+\bar\psi_+\lambda \right) - \left(qD + q^2 B_m B^m + q^2\phi^2 \right)A^*_+ B_+ + \\
&\quad - F^*_- G_- - A^*_-\Box B_- - \frac{1}{2}i\bar\psi_-\gamma^m\partial_m\chi_- + qB_m\left(\frac{1}{2}i\bar\psi_-\gamma^m\chi_- + A^*_-\partial^m B_- - B_-\partial^m A^*_- \right) + \\
&\quad - \frac{1}{2}q\phi\bar\psi_-\chi_- - q\left(A^*_-\bar\chi_-\rho - B_-\bar\psi_-\lambda \right) + \left(qD - q^2 B_m B^m - q^2\phi^2 \right)A^*_- B_- + \\
&\quad \left. - m\left(\frac{1}{2}\bar\psi^c_+\psi_- + \frac{1}{2}\bar\chi^c_+\chi_- + A_+F_- + A_-F_+ - B_+G_- - B_-G_+ \right) \right\} + \text{h.c.} \quad ,
\end{aligned}
\tag{12}
$$

---

[2]One uses the trivial dimensional reduction where the time-derivative, ∂_3, of all component fields vanishes, $\partial_3\mathcal{F}=0$. Also, it was assumed that B_μ is reduced in the following manner: $B^\mu = (B^m, \phi)$, where ϕ is a complex scalar field and the 3-dimensional metric becomes $\eta_{mn} = (+,-,-)$. Note that, λ, ρ, ψ and χ are now Dirac spinors in $D=1+2$.

where, after dimensional reduction, the coupling constant q acquires dimension of $(\text{mass})^{\frac{1}{2}}$.

Analysing the 3-dimensional action given by eq.(12), it can be easily shown that the spectrum will unavoidably be spoiled by the presence of ghost fields, since the free sector of the action is totally off-diagonal. Therefore, truncations are needed in order to remove the spurious degrees of freedom, as well as to give rise to a simple supersymmetric action in $D=1+2$. First of all, to make the truncations possible, we need to diagonalize the whole free sector, in order that the ghost fields be identified.

The diagonalization is achieved by looking for suitable linear combinations of the fields which yield a diagonal form for the free action (12). After extremely tedious algebraic manipulations, we find the following transformations which diagonalize the action $S_{\text{inv}}^{D=3}$:

1. gauge sector :

$$\lambda = \frac{1}{\sqrt{2}}\left(\widehat{\rho}+\widehat{\lambda}\right) \quad \text{and} \quad \rho = \frac{1}{\sqrt{2}}\left(\widehat{\rho}-\widehat{\lambda}\right) \ ; \tag{13}$$

2. fermionic and bosonic matter sector :

$$\psi_\pm = \frac{1}{\sqrt{2}}\left(\widehat{\psi}_\pm \mp \widehat{\psi}_\mp^c + \widehat{\chi}_\pm \pm \widehat{\chi}_\mp^c\right) \quad \text{and} \quad \chi_\pm = \frac{1}{\sqrt{2}}\left(\widehat{\chi}_\pm \pm \widehat{\chi}_\mp^c - \widehat{\psi}_\pm \pm \widehat{\psi}_\mp^c\right) \ ; \tag{14}$$

$$A_\pm = \frac{1}{\sqrt{2}}\left(\widehat{A}_\pm - \widehat{B}_\pm\right) \quad \text{and} \quad B_\pm = \frac{1}{\sqrt{2}}\left(\widehat{A}_\pm + \widehat{B}_\pm\right) \ ; \tag{15}$$

$$F_\pm = \frac{1}{\sqrt{2}}\left(\widehat{F}_\pm + \widehat{G}_\pm\right) \quad \text{and} \quad G_\pm = \frac{1}{\sqrt{2}}\left(\widehat{G}_\pm - \widehat{F}_\pm\right) \ . \tag{16}$$

On the other hand, to simplify the Yukawa-interaction terms (gaugino-matter couplings), we find that the following field redefinitions for the bosonic matter sector are convenient :

$$\widehat{A}_\pm = \frac{1}{\sqrt{2}}\left(\breve{A}_\pm \mp \breve{A}_\mp^*\right) \quad \text{and} \quad \widehat{F}_\pm = \frac{1}{\sqrt{2}}\left(\breve{F}_\pm \mp \breve{F}_\mp^*\right) \ . \tag{17}$$

By replacing these field redefinitions into the action (12), one ends up with a diagonalized action, where the fields, ϕ, $\widehat{\rho}$, $\widehat{\chi}_+$, $\widehat{\chi}_-$, $\widehat{B}_+$ and $\widehat{B}_-$ appear like ghosts in the framework of an $N=2$-supersymmetric model. Therefore, in order to suppress these unphysical modes, truncations must be performed. Bearing in mind that we are looking for an $N=1$ supersymmetric 3-dimensional model (in the Wess-Zumino gauge), truncations have to be imposed on the ghost fields, ϕ, $\widehat{\rho}$, $\widehat{\chi}_+$, $\widehat{\chi}_-$, $\widehat{B}_+$ and $\widehat{B}_-$. To keep $N=1$ supersymmetry in the Wess-Zumino gauge, we must simultaneously truncate the component fields, $\widehat{G}_+$, $\widehat{G}_-$, D, a_m and τ [3] . The truncation of τ is dictated by the suppression of a_m. Now, the choice of truncating a_m, instead of A_m, is based on the analysis of the couplings to the matter sector: A_m couples to both scalar and fermionic matter and we interpret it as the photon field in 3 dimensions.

After performing these truncations, and omitting the ($\widehat{}$) and ($\breve{}$) symbols, we find the following action in $D=1+2$:

$$S_{N=1}^{\tau_3\text{QED}} = \int d^3\widehat{x}\left\{\frac{1}{2}i\overline{\lambda}\gamma^m\partial_m\lambda - \frac{1}{4}F_{mn}F^{mn} + \right.$$
$$- A_+^*\Box A_+ - A_-^*\Box A_- + i\overline{\psi}_+\gamma^m\partial_m\psi_+ + i\overline{\psi}_-\gamma^m\partial_m\psi_- + F_+^*F_+ + F_-^*F_- +$$
$$- qA_m\left(\overline{\psi}_+\gamma^m\psi_+ - \overline{\psi}_-\gamma^m\psi_- + iA_+^*\partial^m A_+ - iA_-^*\partial^m A_- - iA_+\partial^m A_+^* + iA_-\partial^m A_-^*\right) +$$

---

[3] The a_m field is the real part of B_m, since we are assuming $B_m = a_m + iA_m$. Also, as $\widehat{\lambda}$ is a Dirac spinor, it can be written in terms of two Majorana spinors in the following manner: $\widehat{\lambda} = \tau + i\lambda$.

$$- iq\left(A_+\overline{\psi}_+\lambda - A_-\overline{\psi}_-\lambda - A_+^*\overline{\lambda}\psi_+ + A_-^*\overline{\lambda}\psi_-\right) + q^2 A_m A^m \left(A_+^* A_+ + A_-^* A_-\right) +$$

$$- m\left(\overline{\psi}_+\psi_+ - \overline{\psi}_-\psi_- + A_+^* F_+ - A_-^* F_- + A_+ F_+^* - A_- F_-^*\right)\Big\}\quad , \tag{18}$$

where it can be easily concluded that this is a supersymmetric extension of a parity-preserving action, namely, τ_3QED [9]. However, to render our claim more explicit, we are going next to rewrite (18) in terms of the superfields of $N=1$ supersymmetry in 3 dimensions.

In order to formulate the $N=1$ super-τ_3QED action (18) in terms of superfields, we refer to the work by Salam and Strathdee [16], where the superspace and superfields in $D=1+3$ were formulated for the first time. Extending their ideas to our case in $D=1+2$, the elements of superspace are labeled by (x^m, θ), where x^m are the space-time coordinates and the fermionic coordinates, θ, are Majorana spinors, $\theta^c=\theta$. [4]

Now, we are ready to introduce the formulation of $N=1$ super-τ_3QED in terms of superfields. We define the complex scalar superfields with opposite $U(1)$-charges, $\Phi_\pm$, as

$$\Phi_\pm = A_\pm + \overline{\theta}\psi_\pm - \frac{1}{2}\overline{\theta}\theta F_\pm \quad \text{and} \quad \Phi_\pm^\dagger = A_\pm^* + \overline{\psi}_\pm\theta - \frac{1}{2}\overline{\theta}\theta F_\pm^* \quad , \tag{19}$$

where A_+ and A_- are complex scalars, ψ_+ and ψ_- are Dirac spinors and F_+ and F_- are complex auxiliary scalars. Their gauge-covariant derivatives read :

$$\nabla_a \Phi_\pm = (D_a \mp iq\Gamma_a)\Phi_\pm \quad \text{and} \quad \overline{\nabla}_a \Phi_\pm^\dagger = (\overline{D}_a \pm iq\overline{\Gamma}_a)\Phi_\pm^\dagger \quad , \tag{20}$$

where $D_a \equiv \overline{\partial}_a - i(\gamma^m\theta)_a\partial_m$ and $\overline{D}_a \equiv \partial_a - i(\overline{\theta}\gamma^m)_a\partial_m$. The gauge superconnection, Γ_a, is written in the Wess-Zumino gauge as

$$\Gamma_a = i(\gamma^m\theta)_a A_m + \overline{\theta}\theta\lambda_a \quad \text{and} \quad \overline{\Gamma}_a = -i(\overline{\theta}\gamma^m)_a A_m + \overline{\theta}\theta\overline{\lambda}_a \quad , \tag{21}$$

with field-strength superfield, W_a, given by

$$W_a = \frac{1}{2}\overline{D}_b D_a \Gamma_b \quad . \tag{22}$$

By using the previous definitions of the superfields, (19), (21) and (22), and the gauge-covariant derivatives, (20), we found how to build up the $N=1$ super-τ_3QED action, given by eq.(18), in superspace; it reads :

$$S_{N=1}^{\tau_3\text{QED}} = -\int d\hat{v}\left\{\frac{1}{2}\overline{W}W + (\overline{\nabla}\Phi_+^\dagger)(\nabla\Phi_+) + (\overline{\nabla}\Phi_-^\dagger)(\nabla\Phi_-) - m(\Phi_+^\dagger\Phi_+ - \Phi_-^\dagger\Phi_-)\right\} . \tag{23}$$

where the superspace measure we are adopted is $d\hat{v}\equiv d^3\hat{x}d^2\theta$ and the Berezin integral is taken as $\int d^2\theta = -\frac{1}{4}\overline{\partial}\partial$.

Our final conclusion is that the massive Abelian $N=1$ super-QED$_{2+2}$ proposed in ref.[11] shows interesting features when an appropriate dimensional reduction is performed. The dimensional reduction à la Scherk we have applied to our problem becomes very attractive, since, after doing some truncations to avoid non-physical modes, the $N=1$ super-τ_3QED is obtained as a final result. In fact, the Atiyah-Ward space-time shows to be very fascinating as a starting point to formulate models to be studied in lower dimensions.

Acknowledgements

---

[4] The adjoint and charge-conjugated spinors are defined by $\overline{\psi}=\psi^\dagger\gamma^0$ and $\psi^c=-C\overline{\psi}^T$, repectively, where $C=\sigma_y$. The γ-matrices we are using arised from the dimensional reduction to $D=1+2$ are: $\gamma^m=(\sigma_x, i\sigma_y, -i\sigma_z)$. Note that for any spinorial objects, ψ and χ, the product $\overline{\psi}\chi$ denotes $\overline{\psi}_a\chi_a$.

References

[1] A. A. Belavin, A. M. Polyakov, A. S. Schwartz and Y. S. Tyupkin, *Phys. Lett.* B59 (1975) 85 ; R. S. Ward, *Phys. Lett.* B61 (1977) 81 ; M. F. Atiyah and R. S. Ward. *Comm. Math. Phys.* 55 (1977) 117 ; E. F. Corrigan, D. B. Fairlie, R. C. Yates and P. Goddard, *Comm. Math. Phys.* 58 (1978) 223 ; E. Witten, *Phys. Rev. Lett.* 38 (1977) 121.

[2] M. F. Atiyah, *unpublished*; R. S. Ward, *Phil. Trans. R. London* A315 (1985) 451 ; N. J. Hitchin, *Proc. London Math. Soc.* 55 (1987) 59.

[3] S. J. Gates Jr., S. V. Ketov and H. Nishino, *Phys. Lett.* B307 (1993) 323.

[4] S. J. Gates Jr., S. V. Ketov and H. Nishino, *Phys. Lett.* B297 (1992) 99 and *Nucl. Phys.* B393 (1993) 149.

[5] W. Siegel, *Nucl. Phys.* B156 (1979) 135 ; J. Schonfeld, *Nucl. Phys.* B185 (1981) 157 ; R. Jackiw and S. Templeton, *Phys. Rev.* D23 (1981) 2291 ; S. Deser and R. Jackiw, *Phys. Lett.* B139 (1984) 371 ; S. Deser. R. Jackiw and S. Templeton, *Phys. Rev. Lett.* 48 (1982) 975 and *Ann. Phys. (N.Y.)* 140 (1982) 372.

[6] S. Weinberg, *Understanding the Fundamental Constituents of Matter*, ed. A. Zichichi, Plenum Press (New York, 1978) ; A. Linde, *Rep. Progr. Phys.* 42 (1979) 389 ; D. Gross, R.D. Pisarski and L. Yaffe *Rev. Mod. Phys.* 53 (1981) 43.

[7] O. Foda, *Nucl. Phys.* B300 (1988) 611 ; Y.H. Chen, F. Wilczek, E. Witten and B.I. Halperin, *Int. J. Mod. Phys.* B3 (1989) 1001 ; J.D. Lykken, *Chern-Simons and Anyonic Superconductivity*, talk given at the fourth annual Superstring Workshop, "Strings 90", Texas A & M University (Texas, March 1990).

[8] N. Dorey and N. E. Mavromatos. *Phys. Lett.* B226 (1991) 163 and *Nucl. Phys.* B386 (1992) 614.

[9] R.D. Pisarski, *Phys. Rev.* D29 (1984) 2423 ; T.W. Appelquist, M. Bowick, D. Karabali and L.C.R. Wijewardhana. *Phys. Rev.* D33 (1986) 3704 ; R. Mackenzie and F. Wilczek, *Int. J. Mod. Phys.* A3 (1988) 2827 ; G.W. Semenoff and P. Sodano, *Nucl. Phys.* B328 (1989) 753 ; G.W. Semenoff and L.C.R. Wijewardhana, *Phys. Rev. Lett.* 63 (1989) 2633 ; A. Kovner and B. Rosenstein, *Mod. Phys. Lett.* A5 (1990) 2661.

[10] F. Delduc, C. Lucchesi, O. Piguet and S.P. Sorella, *Nucl. Phys.* B346 (1990) 313 ; A. Blasi, O. Piguet and S.P. Sorella, *Nucl. Phys.* B356 (1991) 154 ; C. Lucchesi and O. Piguet, *Nucl. Phys.* B381 (1992) 281.

[11] M.A. De Andrade, O.M. Del Cima and M.N.P. Magalhães, $N=1$ *Supersymmetry and Super-QED in Atiyah-Ward Space-Time*, CBPF preprint, CBPF-NF-065/94 (1994).

[12] J. Wess and B. Zumino, *Nucl. Phys.* B70 (1974) 39 ; *Phys. Lett.* B49 (1974) 52 and *Nucl. Phys.* B78 (1974) 1 ; S. Ferrara and B. Zumino, *Nucl. Phys.* B79 (1974) 413.

[13] O. Piguet, J.A. Helayël-Neto and S.P. Sorella, *private communications*.

[14] J. Scherk, *Extended Supersymmetry and Extended Supergravity Theories*, Recent Developments in Gravitation. Cargèse 1978, Ed. M. Lévy and S. Deser, Plenum Press ; L. Brink, J.H. Schwarz and J. Scherk, *Nucl. Phys.* B121 (1977) 77 ; F. Gliozzi, J. Scherk and D. Olive, *Nucl. Phys.* B122 (1977) 253 ; J. Scherk and J.H. Schwarz, *Nucl. Phys.* B153 (1979) 61.

[15] M.F. Sohnius, *Phys. Rep.* 128 (1985) 39 ; P. van Nieuwenhuizen, *An Introduction to Simple Supergravity and the Kaluza-Klein Program*, Relativity, Groups and Topology II, Les Houches 1984, Ed. B.S. de Witt and R. Stora, North-Holland.

[16] A. Salam and J. S. Strathdee, *Phys. Rev.* D11 (1975) 1521.

Anomalies in chiral $\mathcal{W}$—gravity

Marcelo Carvalho, Luiz Claudio Queiroz Vilar and S.P. Sorella

CBPF - Centro Brasileiro de Pesquisas Físicas,

Rua Xavier Sigaud 150, 22290-180 Urca, Rio de Janeiro, Brazil

$\mathcal{W}$—algebras [1] are an extension of the Virasoro algebra. They describe the commutation relations between the components of the stress-energy tensor (T_{++}, T_{--}) and currents $(W_{++++\ldots}, W_{-----\ldots})$ of higher spin (see ref. [2] for a general introduction).

Among the various $\mathcal{W}$—algebras considered in the recent literature, the so called $\mathcal{W}_3$—algebra plays a rather special role, due to the fact that it has a simple field theory realization. The corresponding field model, known as $\mathcal{W}_3$—gravity, yields a generalization of the usual bosonic string action. In its chiral version, the starting field content of the model is given by a set of free scalar fields $\phi^i (i = 1, ..., D)$ which are used to study the current algebra of the spin-two and spin-three operators T_{++} and W_{+++}

$$T_{++} = \frac{1}{2}\partial_+\phi^i\partial_+\phi^i . \qquad W_{+++} = \frac{1}{3}d_{ijk}\partial_+\phi^i\partial_+\phi^j\partial_+\phi^k . \qquad (1)$$

The operators in (1) can be included in the initial free scalar action by coupling them to external fields h_{--}, B_{---}. It is a remarkable fact then that the resulting action exhibits a set of local invariances which can be gauge fixed using the Batalin-Vilkovisky procedure. The gauged fixed action with the external fields (Y^i, τ_+, ρ_{++}) coupled to the nonlinear BRS transformations of the fields $(\phi^i, c_-, \gamma_{--})$ then reads

$$\Sigma = \int d^2x \left(\frac{1}{2}\partial_+\phi^i\partial_+\phi^i - h_{--}T_{++} - B_{---}W_{+++} \right)$$
$$+ \int d^2x \, s\,(b_{++}h_{--} + \beta_{+++}B_{---}) + \int d^2x \, (Y^i s\phi^i + \tau_+ sc_- + \rho_{++}s\gamma_{--}) , \qquad (2)$$

where (c_-, γ_{--}) and (b_{++}, β_{+++}) are respectively a pair of ghost and antighost fields and s denotes the BRS operator (see [7] for the details).

The model is thus constrained by the Slavnov-Taylor identity $S(\Sigma) = 0$, with

$$S(\Sigma) = \int d^2x \left(\frac{\delta\Sigma}{\delta Y^i}\frac{\delta\Sigma}{\delta\phi^i} + \frac{\delta\Sigma}{\delta\tau_+}\frac{\delta\Sigma}{\delta c_-} + \frac{\delta\Sigma}{\delta\rho_{++}}\frac{\delta\Sigma}{\delta\gamma_{--}} - \frac{\delta\Sigma}{\delta b_{++}}\frac{\delta\Sigma}{\delta h_{--}} - \frac{\delta\Sigma}{\delta\beta_{+++}}\frac{\delta\Sigma}{\delta B_{---}} \right) . \qquad (3)$$

This identity is the starting point for studying the properties of the Green's functions of the model with insertion of the composite operators (T_{++}, W_{+++}), i.e. it yields an algebraic characterization of the $(T-W)$-current algebra. As it is well known, the existence of anomalies in the quantum extension of the Slavnov-Taylor identity turns out to be related to the presence of central charges in the corresponding current algebra.

At the quantum level the classical action (2) gives rise to an effective action $\Gamma = \Sigma + O(\hbar)$, which obeys the broken Slavnov-Taylor identity

$$S(\Gamma) = \hbar \mathcal{A} \cdot \Gamma , \qquad (4)$$

where the insertion $\mathcal{A} \cdot \Gamma$ represents by the radiative corrections. According to the Quantum Action Principle the lowest order nonvanishing contribution to the breaking $\mathcal{A} \cdot \Gamma = \mathcal{A} + O(\hbar\mathcal{A})$, is an integrated local functional of the fields and their derivatives with dimension three and ghost number one which obeys the consistency condition

$$\mathcal{B}_\Sigma\mathcal{A} = 0 , \qquad (5)$$

where $\mathcal{B}_\Sigma$ is the nilpotent linearized Slavnov-Taylor operator.

Setting $\mathcal{A} = \int A_2^1$, condition (5) yields the nonintegrated equation [1],

$$\mathcal{B}_\Sigma A_2^1 + dA_1^2 = 0 ,\tag{6}$$

where d denotes the exterior space-time derivative. A solution A_2^1 of eq. (6) is said nontrivial if

$$A_2^1 \neq \mathcal{B}_\Sigma \hat{A}_2^0 + d\hat{A}_1^1 ,\tag{7}$$

with $\hat{A}_2^0$ and $\hat{A}_1^1$ local functionals of the fields. In this case the integral of A_2^1 on space-time, $\int A_2^1$, identifies a cohomology class of the operator $\mathcal{B}_\Sigma$ in the sector of the integrated local functionals with ghost number one.

Equation (6), due to the anti-commutation property between $\mathcal{B}_\Sigma$ and d, and to the algebraic Poincaré Lemma, generates a tower of descent equations

$$\mathcal{B}_\Sigma A_2^1 + dA_1^2 = 0 ,$$
$$\mathcal{B}_\Sigma A_1^2 + dA_0^3 = 0 ,\tag{8}$$
$$\mathcal{B}_\Sigma A_0^3 = 0 .$$

In order to solve the ladder (8) we follow the algebraic setup proposed by one of the authors [4] and successfully applied to the study of the Yang-Mills [5] and of the gravitational anomalies [6]. The method is based on the introduction of an operator δ which decomposes the extea $\mathcal{B}_\Sigma$ commutator, i.e.

$$d = -[\mathcal{B}_\Sigma, \delta] .\tag{9}$$

Defining the two operators δ_+, δ_- as

$$\delta_+ = \frac{\partial}{\partial c_-} ,\tag{10}$$

$$\delta_- = \sum_{p=0}^{\infty}\sum_{q=0}^{\infty} \left(\partial_-^p \partial_+^q h_{--}\frac{\partial}{\partial\partial_-^p \partial_+^q c_-} + \partial_-^p \partial_+^q B_{---}\frac{\partial}{\partial\partial_-^p \partial_+^q \gamma_{--}} - \partial_-^p \partial_+^q \tau_+ \frac{\partial}{\partial\partial_-^p \partial_+^q b_{++}} \right.$$
$$\left. -\partial_-^p \partial_+^q \rho_{++}\frac{\partial}{\partial\partial_-^p \partial_+^q \beta_{+++}} - \partial_-^p \partial_+^q Y^i \frac{\partial}{\partial\partial_-^p \partial_+^{q+1}\phi^i} \right) ,\tag{11}$$

we see that the operator $\delta = dx^+\delta_+ + dx^-\delta_-$ obeys thus (9) and $[\delta, d] = 0$.

Suppose now that the solution A_0^3 of the last equation of the tower (8) has been found, it is apparent then to check that the higher cocycles A_2^1, A_1^2 can be identified with the δ-transform of A_0^3 [4]:

$$A_1^2 = \delta A_0^3 = dx^+\delta_+ A_0^3 + dx^-\delta_- A_0^3 ,\tag{12}$$

$$A_2^1 = \frac{1}{2}\delta^2 A_0^3 = -dx^+dx^-\delta_+\delta_- A_0^3 .\tag{13}$$

Let us emphasize that solving the last equation of (8) is a problem of local cohomology instead of a modulo d one. One sees thus that, due to the operator δ, the characterization of the cohomology of $\mathcal{B}_\Sigma$ modulo d is essentially reduced to a problem of local cohomology. It is also worth to recall that the latter can be systematically studied by using several methods as, for instance, the spectral sequenctechnique.

Following [7], the final result for the cohomology of $\mathcal{B}_\Sigma$ modulo-d is given by two anomaly cocycles:

$$\mathcal{A}_u = \int u_2^1$$
$$= \int d^2x \left(2c_-\partial_+^3 h_{--} - 4\partial_+^3 h_{--}\gamma_{--}\partial_+\gamma_{--}b_{++} + 4\partial_+^3 c_- B_{---}\partial_+\gamma_{--}b_{++} \right.$$
$$\left. - 4\partial_+^3 c_-\gamma_{--}\partial_+ B_{---}b_{++} - 4\partial_+^3 c_-\gamma_{--}\partial_+\gamma_{--}\tau_+ \right) .\tag{14}$$

---

[1] We adopt here the usual convention of denoting with A_q^p a q-form with ghost number p.

$$\mathcal{A}_T = \int T_2^1$$

$$= \int d^2x \left(2\left(B_{---}\partial_+\gamma_{--} - \partial_+ B_{---}\gamma_{--} \right) \partial_+^3 \phi^i \partial_+ \phi^i \right.$$

$$+ \frac{3}{2}\left(\partial_+^2 B_{---}\partial_+\gamma_{--} - \partial_+ B_{---}\partial_+^2\gamma_{--} \right) T_{++}$$

$$+ \left(\partial_+^3 B_{---}\gamma_{--} - B_{---}\partial_+^3\gamma_{--} \right) T_{++} \tag{15}$$

$$- \gamma_{--}\partial_+\gamma_{--}\partial_+^2 Y^i \partial_+\phi^i - \gamma_{--}\partial_+\gamma_{--} Y^i \partial_+^3 \phi^i$$

$$\left. + 2\gamma_{--}\partial_+\gamma_{--}\partial_+ Y^i \partial_+^2 \phi^i + \frac{1}{2}\partial_+\gamma_{--}\partial_+^2\gamma_{--} Y^i \partial_+\phi^i \right) .$$

Let us remember that, in general [4], eqs. (14), (15) give only a particular solution of the descent equations (8). However, in the present case, they yield the most general solution. This is due to the fact that the cohomology of $\mathcal{B}_\Sigma$ turns out to be vanishing in the sectors of the one forms wtwo forms with ghost number one [7].

Equations (14), (15) give the expressions of the anomalies which arise in chiral W_3—gravity. They agree with the explicit Feynman graphs computation done in ref. [3]. In particular, the term $\mathcal{A}_U$ of (14), also called the universal gravitational anomaly, is easily seen to be a generalization of the usual diffeomorphism anomaly of the bosonic string, while the second term $\mathcal{A}_T$ in eq.(15) is a matter-dependent anomaly whose origin can be traced back to the nonlinearity of the W_3—algebra [3].

As a final observation, we show that the classical action (2) turns out to be cohomologically trivial, i.e. it is a pure $\mathcal{B}_\Sigma$—variation. It is easily checked indeed that

$$\Sigma = \mathcal{B}_\Sigma \int d^2x \left(\frac{1}{2} Y^i \phi^i - \tau_+ c_- - \frac{1}{2}\rho_{++}\gamma_{--} - \frac{1}{2}\beta_{+++} B_{---} \right) . \tag{16}$$

This property allows to interpret in a suggestive way the W_3—gravity as a topological model of the Witten's type.

References

[1] A. B. Zamolodchikov. *Teor. Mat. Fiz* 65 (1985) 205;
    V. A. Fateev and A. B. Zamolodchikov, *Nucl. Phys.* B280 (1987) 644;
    J. Thierry-Mieg, *Phys. Lett.* B197 (1987) 368;
    V. A. Fateev and S. Lykanov, *Int. J. Mod. Phys.* A3 (1988) 507;

[2] C. M. Hull, Classical and Quantum W—gravity. *Summer School in High Energy Physics and Cosmology, Trieste 1992,* I.C.T.P ;

[3] C *Phys. Lett.* 259B (1991) 68; *Nucl. Phys.* 364B (1991) 621;
    Phys. Lett. 269B (1991) 257; *Nucl. Phys.* 367B (1991) 731;
    Comm. Math. Phys. 156 (1993) 245; *Int. J. Mod. Phys.* 8 (1993) 2419;

[4] S. P. Sorella, *Comm. Math. Phys.* 157 (1993) 231;

[5] S. P. Sorella and L. Tataru, *Phys. Lett.* B324 (1994) 351;

[6] M. Werneck de Oliveira and S. P. Sorella, *Int. J. Mod. Phys.* 9 (1994) 2979;
    O. Moritsch, M. Schweda and S. P. Sorella, *Class. Quantum Grav.* 11 (1994) 1225;

[7] M. Carvalho. L. C. Q. Vilar and S. P. Sorella, *preprint* CBPF-NF-042/94.

Particles and Strings
in Degenerate Background Fields

Luís A. Cabral and Victor O. Rivelles

Instituto de Física - Universidade de São Paulo

Caixa Postal 20516, 01498-970 São Paulo - SP

We consider a model that describe a non-relativistic particle immersed in a degenerate gravitational background, where we apply the Hamiltonian for- malism and we obtain the constraints. According to the form of background components, we may have a system with first or second class constraints. We also study string theory in a similar background, where the Hamiltonian analysis is non-trivial because of the new structure of constraints generated in this case.

The formulation of general relativity in terms of tetrads and Lorentz connection. is such that the action and equations of motion remain well defined even when the tetrad (or the metric recovered from that) is degenerate.

An analogous situation occurs when we consider a non-relativistic particle or a bosonic string immersed in a degenerate gravitational background.

For the particle, the action is

$$S = \int \frac{1}{2} m g_{ij} \dot{X}^i \dot{X}^j \, dt \tag{1}$$

where g_{ij} is an spatial metric defined in a D-dimensional space.

Writing $g_{ij} = g_i g_j$, this becomes degenerate. This form of metric was chosen in analogy with the form in the string case, which in this case the background was found in the search for non-perturbative solutions [1].

For the particle we have $D - 1$ constraints:

$$\Phi_\alpha = g_1 P_\alpha - g_\alpha P_1 = 0 \qquad \alpha = 2, ..., D \tag{2}$$

We find that

$$\{\Phi_\alpha, \Phi_\beta\} = P_1(g_\alpha \partial_{[\beta} g_{1]} + g_\beta \partial_{[1} g_{\alpha]} + g_1 \partial_{[\alpha} g_{\beta]}), \tag{3}$$

and,

$$\dot{\Phi}_\alpha = \frac{P_1^2}{m g_1^2} \partial_{[\alpha} g_{1]} + \lambda^\beta \{\Phi_\alpha, \Phi_\beta\} = 0. \tag{4}$$

From this, according to the value of $\partial_{[i} g_{j]}$, we have the following cases.

I) $\partial_{[i} g_{j]} = 0$. In this case $\{\Phi_\alpha, \Phi_\beta\} = 0$ and Φ_α are first class constraints. so that the system has only one degree of freedom.

II) $\partial_{[i} g_{j]} \neq 0$. For odd dimensions $D \geq 3$, we can find λ^α. implying in $(D - 1)$ second class constraints. In this case the theory has $\frac{(D+1)}{2}$ degrees of freedom. For $D = 2$, $\{\Phi_\alpha, \Phi_\beta\} = 0$, implying $P_1 = P_2 = 0$. so the theory doesn't has degrees of freedom. For even dimensions $D \geq 4$, the matrix associated to $\{\Phi_\alpha, \Phi_\beta\}$ cannot be invertible.

so λ^a are not determined completely. In this case there is a linear combination of Φ_α that is a first class constraint. This case deserves additional care since the structure of constraints is non-trivial and will be treated elsewhere.

Let us consider now the action of an string in a gravitational background defined in a D-dimensional space-time, given by

$$S = \frac{-1}{4\pi\alpha'} \int d\sigma d\tau \sqrt{-h} h^{ab} G_{\mu\nu}(X) \partial_a X^\mu \partial_b X^\nu. \tag{5}$$

where h_{ab} is the world-sheet metric. When $G_{\mu\nu}$ is non-degenerate, there are only first class constraints. However, when $G_{\mu\nu}$ is degenerate, we have additional primary constraints and according to the form of the metric components, we will have two class of constraints and their related algebra with a non-trivial structure too. The complete study of that will be presented in the near future in order to study the quantum aspects of the model.

References

[1] O.A.Mattos and V.O.Rivelles, Phys. Rev. Lett. **70** (1993) 1583.

On the Origin of Mass and the Electroweak Mass Spectrum Without Higgs

Manoelito Martins de Souza

Departamento de Física, Universidade Federal do Espírito Santo

In a CAUSALITY PRESERVING MANIFOLD FORMALISM, (CPMF). which is based on a model of spacetime with geometric and strict implementation of causality, masses are consequences of the spacetime symmetries. The mass spectrum of a set of non abelian fields is so lely determined from its Lagrangian kinematics term. in a way independent of any kind of interactions and without any extra field (no Higgs, no Yukawa coupling, etc). The origin and meaning of mass in this formalism is discussed and then illustrated with the vector boson sector of the standard $SU(2) \otimes U(1)$ electroweak theory.

Equações de Maxwell-Dirac Quirais em
(3 + 1)D Exatamente Integráveis

Manoelito Martins de Souza

Departamento de Física, Universidade Federal do Espírito Santo

Estudamos a questão da integrabilidade das equações de Maxwell-Dirac(Weyl) quirais em (3+1) dimensões num formalismo com preservação local de causalidade. Característica destes formalismos é que mesmo em (3+1)D a dinâmica se passa em (1+1)D porque as coordenadas espaciais ortogonais à direção em que se dá a interação (troca de um quantum) não participam. A dinâmica é conformemente invariante e as equações se tornam exatamente integráveis.

Causalidade e Grupos de Isometria em Teoria de Campo

Manoelito Martins de Souza e Gilmar de Souza Dias

Departamento de Física, Universidade Federal do Espírito Santo

O grupo de invariância das teorias físicas (gravitação excluida), das leis da dinâmica das partículas e, também, o grupo de isometrias da estrutura geométrica da variedade espaciotemporal onde estas leis e teorias são definidas, é o grupo de Poincaré. Não é por coincidência que se trata de um mesmo grupo; é uma consequência de relações de causalidade que restringem as regiões acessíveis à evolução e propagação de objetos físicos (campos. partículas, etc) à partir de um ponto da variedade espaciotemporal ao cone de luz deste ponto e ao seu interior. A invariância de Poincaré implica em uma implementação parcial ou global do princípio de causalidade através da estrutura de cones de luz, definida em cada ponto da variedade. Esta implementação parcial da causalidade não é suficiente nem satisfatória, pois pode-se mostrar que ela é fonte de grandes dificuldades no formalismo usual com covariancia de Poincaré. Estas dificuldades podem ser superadas com uma implementação geométrica local da causalidade. Isto corresponde a substituir a descrição do espaçotempo de Minkowski por uma estrutura geométrica definida por congruências de curvas bicaracterísticas, ou seja uma variedade com preservação local de causalidade. Discute-se neste trabalho o grupo máximo de simetrias destas novas estruturas de espaçotempo, sua isometrias, geradores, algebra, bem como suas consequências e interpretações físicas.

Causalidade e Estruturas de Espaço-Tempo
em Eletrodinâmica Clássica

Manoelito Martins de Souza   e   Jair Valadares Costa

Departamento de Física, Universidade Federal do Espírito Santo

A propagação de sinais ou de campos de massa nula em teorias físicas relativísticas é associada às superfícies características de suas respectivas equações de ondas. Estas teorias podem ser re-escritas numa estrutura geométrica de espaço-tempo definida por foliações dessas superfícies e que constituem um implementação geométrica e global da causalidade. Formalismos que adotam a variedade de Minkowski como modelo de estrutura geométrica do espaçotempo são exemplos desta implementação global da causalidade, e são acossados, como se sabe, por vários problemas e patologias, tais como a presença de singularidades e divergências. Mostra-se, por outro lado, que a propagação de campos só se dá ao longo de suas bicaracterísticas, que são as geratrizes de suas superfícies características, são suas curvas elementares constituintes. Isto constitue a base para uma implementação geométrica, local, do princípio da causalidade. A adoção de bicaracterísticas como elementos definidores da estrutura geométrica do espaçotempo leva à construção de formalismos mais fundamentais que os usuais, porque estes podem ser recuperados a partir daqueles como formalismos efetivos definidos sobre valores médios; e mais simples e eficazes, porque não possuem muitos de seus problemas e patologias.

Busca-se, neste trabalho, uma formulação da Eletrodinâmica Clássica no contexto de um modelo de estrutura de espaçotempo com implementação geométrica e local da causalidade. A formulação usual é reobtida com uma integração sobre as bicaracterísticas deste novo formalismo. Discute-se, em particular, o campo, suas simetrias e leis de conservação no ponto limite em que este se confunde com suas fontes; situação em que o suporte experimental da Eletrodinâmica não é tão sólido, e onde grandes problemas ainda persistem.

Boundary Conditions of Bosonic Lagrange Multipliers at Finite Temperature

M. T. Thomaz

Instituto de Física, Universidade Federal Fluminense Av. Litorânea s/nº,
Campus da Praia Vermelha, Niterói, R.J., 24310-340   BRAZIL

and

Y. İpekoğlu

Middle East. Technical University, Ankara, TURKEY

We show that Lagrange multipliers (non-physical bosonic fields) are not constrained to satisfy boundary conditions in the path integral at finite temperature.

It is a common knowledge that to get the partition function of a system at thermal equilibrium we have to integrate over all configurations that are periodic(bosons) or anti-periodic (fermions) in the temperature parameter.

The aim of this communication is to explicitly show a comment made by Toimela[1] that the boundary condition satisfied by a non-physical field is a matter of "gauge" choice.

To exemplify the general result that non-physical field does not have to satisfy any boundary condition in the path integral we consider a quantum mechanical model that is invariant under global translation. The *ansatz* of Bernard[2] and Gross et al.[3] for a physical partition function is used to discuss the boundary conditions of fields associated to Lagrange multipliers which implement the symmetries.

Let us consider a one dimensional quantum model of two particles invariant under global translation[4]:

$$H = \frac{p_1^2}{2m_1} + \frac{p_2^2}{2m_2} + V(q_1 - q_2),\tag{1}$$

where q_i, p_i and m_i are the position operator, momentum operator and mass of particle i, $i = 1, 2$. The potential V depends on the relative position of the two particles.

We denote the position and momentum operators associated with the center of mass (C.M.) of the system by X and P respectively.

In the center of mass frame the total momentum is zero. However this equality can not be imposed to the operator $P = p_1 + p_2$. This requirement can be enforced by demanding that the operator P acting on physical states is zero[4], that is, $P \mid \Psi_{phys}\rangle = 0$.

In the model under consideration, we may construct a "gauge" invariant quantum mechanical model where the "Gauss law" gives the constraint on the total canonical momentum.

The classical analogue of hamiltonian (1) can be obtained from the Lagrangian

$$L = \frac{1}{2}m_1(\dot{q}_1 + eA)^2 + \frac{1}{2}m_2(\dot{q}_2 + eA)^2 - V(q_1 - q_2)\tag{2}$$

that is invariant under the simultaneous transformations $q_i'(t) = q_i(t) - a(t)$ and $A'(t) = A(t) + \frac{1}{e}\dot{a}(t)$, where $a(t)$ is an arbitrary time-dependent function. In particular $a(t)$ can be chosen such that $A'(t) = 0$[1]. Therefore, $A(t)$ is a Lagrange multiplier. The hamiltonian associated with eq. (2) is

$$H = \frac{p_1^2}{2m_1} + \frac{p_2^2}{2m_2} - eA(t)(p_1 + p_2) + V(q_1 - q_2). \tag{3}$$

The equation for the Lagrange multiplier gives a "Gauss law" for $A(t)$: $p_1 + p_2 = 0$.

The *ansatz* of Bernard and Gross et al. for a physical partition function is given by[2, 3]

$$Z = \sum_{|\Psi_{phys}\rangle} \langle \Psi_{phys} | e^{-\beta H} | \Psi_{phys}\rangle = Tr(\wp e^{-\beta H}). \tag{4}$$

where $\beta = \frac{1}{kT}$, k is the Boltzmann constant and T is the absolute temperature. The projecor operator $\wp$ is: $\wp = \int_{-\infty}^{\infty} dw\, e^{iw\mathbf{P}}$.

The calculation of (4) can be simplified if we use the coordinates and momenta operators of the center of mass and the relative motion.

The partition function (4) can be written in terms of the particles positions q_i as

$$Z = \int_{-\infty}^{\infty} dq_1(0)dq_2(0) \int_{\substack{q_1(0)=q_1(\beta)\\q_2(0)=q_2(\beta)}} \mathcal{D}q_1(\tau)\mathcal{D}q_2(\tau) \int_{-\infty}^{\infty} \mathcal{D}A(\tau) e^{\int_0^\infty d\tau L_{eff}(q_1,q_2,A;\tau)}. \tag{5}$$

where, $L_{eff} = -\{\frac{m_1}{2}(\frac{dq_1}{d\tau} - eA(\tau))^2 + \frac{m_2}{2}(\frac{dq_2}{d\tau} - eA(\tau))^2 + V(q_1 - q_2)\}$, and it is the Lagrangian (2) written in the Euclidean space. The "gauge" field $A(\tau)$ does not have to satisfy any boundary condition.

Since L_{eff} is invariant under the simultaneous tranformations $q_i^a(\tau) = q_i(\tau) + a(\tau), i = 1,2$ and $A^a(\tau) = A(\tau) + \frac{1}{e}\dot{a}(\tau)$, we can choose the function $a(\tau)$ such that $A^a(\tau = 0) = A^a(\tau = \beta)$. The function $a(\tau)$ that allows $A^a(\tau)$ to satisfy periodic boundary condition is:

$$a(\tau) = e\left[A(\beta) - A(0)\right]g(\tau), \tag{6}$$

where $g(\tau)$ satisfies the conditions: $g(0) = g(\beta)$ and $\dot{g}(\beta) = -1 + \dot{g}(0)$.

References

[1] T. Toimela, Int. Jor. of Theor. Phys. 24, 901-949 (1985).

[2] C.W. Bernard, Phys.Rev. D9, 3312-3320 (1974).

[3] D.J. Gross, R.D. Pisarski and L.G. Yaffe, Rev. Mod. Phys 53, 43-80 (1981).

[4] R. Jackiw; *Current Algebra and Anomalies*, ed. by S.B. Treiman et al., Princeton University Press (1985), pp. 243-247.

[1]This choice is called the Weyl gauge: A(t)=0

Estados Ligados na Eletrodinâmica Escalar em (2+1)D com Termo de Chern-Simons

M. O. C. Gomes, L. C. Malacarne

Instituto de Física, Universidade de São Paulo

Este Trabalho consiste no estudo da existência de estados ligados para a Eletrodinâmica Escalar. em três dimensões, com o termo de Chern-Simons[1]

O método consiste no cálculo, via teoria quântica de campos, das matrizes de espalhamento $\mathcal{M}_{fi}$ na aproximação não relativística, ou seja, foram calculados os propagadores dos campos responsáveis pela interação nos processos de espalhamento e construídas as matrizes de espalhamento. Uma vez obtida a matriz de espalhamento, comparou-se a secão de choque na teoria quântica de campos com a seção de choque da mecânica quântica na aproximação de Born, obtendo-se assim a forma do potencial responsável pela interação nos processos de espalhamento. Através da equação de Schrödinger analisa-se a possibilidade de estados ligados.

O modelo é descrito pela seguinte densidade de Lagrangeana

$$\mathcal{L}(x) = -\frac{1}{4}aF_{\mu\nu}F^{\mu\nu} + \frac{\theta}{4}\varepsilon^{\mu\nu\lambda}F_{\mu\nu}A_\lambda + (D_\mu\phi)^*(D^\mu\phi) - m^2\phi^*\phi . \tag{1}$$

O propagador para o campo A_μ é

$$D^{\mu\nu}(k) = \frac{-i}{ak^2 - \frac{\theta^2}{a}}\left[P^{\mu\nu} - \frac{i\theta}{a}\varepsilon^{\mu\nu\lambda}\frac{k_\lambda}{k^2}\right] \tag{2}$$

e na ordem mais baixa $[\mathcal{O}(e^2)]$ o potencial obtido é

$$V_T = \frac{e}{2\pi a}K_0(\frac{\theta r}{a}) - \frac{e}{\pi m\theta}\frac{1}{r^2}\left[1 - \frac{\theta r}{a}K_1(\frac{\theta r}{a})\right]\bar{L} \tag{3}$$

que é idêntico (a menos de um termo de interação spin-órbita) ao potencial obtido para a eletrodinâmica fermiônica[2,3].

Em coordenadas polares (r,ϕ) o operador L é representado por $-i\frac{\partial}{\partial\phi}$. Escrevendo $\Psi_{nl}(r\phi) = R_{nl}(r)\Phi_l(\phi)$ com $\Phi_l(\phi) = \frac{1}{\sqrt{2\pi}}e^{il\phi}$ obtemos a correspondente equação radial de Schrödinger

$$\mathcal{H}R_{nl} = -\frac{1}{m}\left(\frac{\partial^2}{\partial r^2} + \frac{1}{r}\frac{\partial}{\partial r}\right)R_{nl} + U_l^{eff}(r)R_{nl} = E_{nl}R_{nl} \tag{4}$$

onde

$$U_l^{eff}(r) = \frac{l^2}{mr^2} + \frac{e^2}{2\pi a}K_0(\frac{\theta r}{a}) - \frac{e^2}{\pi m\theta}\frac{l}{r^2}\left[1 - \frac{\theta r}{a}K_1(\frac{\theta r}{a})\right] . \tag{5}$$

Para o caso que $\theta \longrightarrow 0$, a teoria se reduz a eletrodinâmica escalar pura, e o potencial dado na equação (3). no limite $\theta \longrightarrow 0$, vai para o potencial Coulombiano em três dimensões.

No limite $a \longrightarrow 0$, com $\theta \neq 0$, o termo de Maxwell desaparece da Lagrangiana inicial, e temos uma teoria de Chern-Simons pura. Neste limite o potencial se reduz à

$$V_{CS}(a = 0, \theta, r) = -\frac{e}{\pi\theta m}\frac{l}{r^2} . \tag{6}$$

Quando $l > \frac{e^2}{\pi\theta}$ o potencial U_{CS} é totalmente repulsivo e não possibilita a formação de estados ligados.

Por outro lado se $l < \frac{e^2}{\pi\theta}$, o potencial tem comportamento atrativo com decaimento forte na origem, no entanto as condições de contorno nos leva a uma solução nula para energias negativas não possibilitando a existência de estados ligados.

Para a análise do potencial de Maxwell-Chern-Simons, vamos escrever a equação de Schrödinger em termos das variáveis adimencionais

$$y = \frac{\theta r}{a} \qquad \alpha = \frac{e^2}{\pi\theta} \qquad \beta = \frac{ma}{\theta} \qquad e \qquad \epsilon_{nl} = \frac{ma^2}{\theta^2}E_{nl}$$

obtemos

$$\left(\frac{\partial^2}{\partial y^2} - \frac{1}{y}\frac{\partial}{\partial y}\right) R_{nl}(y) - U'_{eff}R_{nl}(y) + \epsilon_{nl}R_{nl}(y) = 0 \tag{7}$$

onde

$$U'_{eff}(\alpha, \beta, y) = \frac{l^2}{y^2} + \frac{1}{2}\alpha\beta K_o(y) - \frac{\alpha l}{y^2}(1 - yK_1(y)) \tag{8}$$

Pela análise da derivada do potencial U'_{eff} o intervalo onde o potencial apresenta mínimo local (a derivada pode se anular) é dado por $2 < l < \alpha$. Neste intervalo o comportamento de U'_{eff} fornece que, perto da origem, o potencial diverge para $+\infty$, e para grandes valores de y, ele se aproxima de zero por valores negativos. Temos então a possibilidade da existência de estados ligados. Através de análise numérica encontramos valores da energia do estado fundamental para alguns valores dos parâmetros α, β e l.

l	α	β	ϵ_{nl}
6	8	2000	- 0.0221 ± 0.0005
6	12	2000	- 0.1235 ± 0.0005
6	16	2000	- 0.2490 ± 0.0005

l	α	β	ϵ_{nl}
2	8	2000	- 0.0221 ± 0.0005
4	8	2000	- 0.0365 ± 0.0005
6	8	2000	- 0.0221 ± 0.0005

Conclusão

Utilizando a equação de Schrödinger estudamos a possível existência de estados ligados partícula-partícula para o potencial não relativístico obtido. Em primeiro lugar tomando o limite para a teoria de Maxwell pura ($\theta \longrightarrow 0$), obtivemos o potencial Coulombiano em duas dimensões, como era de se esperar. No limite para a teoria de Chern-Simons pura ($\alpha \longrightarrow 0$), obtivemos um potencial atrativo, no entanto fortemente divergente na origem.

Comprovamos assim que é o termo de Chern-Simons que dá o caráter atrativo para o potencial, mas o termo de Maxwell é necessário para eliminar essa divergência. Finalmente, via cálculo numérico do potencial Maxwell-Chern-Simons, confirmamos a existência de estados ligados para vários valores dos parâmetros livres da teoria, com a massa do campo de gauge θ não muito grande.

Certamente o resultado obtido necessita ser complementado, isto é, precisamos comprovar se o caráter atrativo do potencial não é destruido quando incorporamos efeitos de ordem superior em teoria de perturbação (ordem e^4). Também temos que obter uma melhor compreensão da estrutura infravermelha da teoria, o que pode ser feito via análise do tipo Block-Nordsieck.

Bibliografia

1 - L.C. Malacarne, *Estados Ligados na Eletrodinâmica Escalar em* $(2+1)D$ *com Termo de Chern-Simons*. Dissertação de Mestrado, IFUSP. (1994);

2 - H. O. Girotti, M. Gomes and A. J. da Silva, Phys. Lett. B274(1992)357;

3 - H. O. Girotti, M. Gomes, J. L. deLira, R. S. Mendes and J. R. S. Nascimento, Phys. Rev. Lett. 69(1992)2623.

Magnetic Monopoles without Singularity

P.C.R. Cardoso de Mello[1], S. Carneiro[2] and M.C. Nemes[1]

[1]*Departamento de Física - Universidade Federal de Minas Gerais*

[2]*Instituto de Física, Universidade de São Paulo*

In this work, we suggest a lagrangian description for dual electrodynamics, i.e., electrodynamics with electric charges and magnetic monopoles. Calculating the Euler-Lagrange equations, we can obtain the whole set of equations we need, namely the generalized Maxwell and Lorentz equations, without introducing Dirac's string.

The proposed lagrangian density is

$$\mathcal{L} = \mathcal{L}_o - \frac{1}{4}F_{\mu\nu}F^{\mu\nu} - j_\mu A^\mu - g_\mu \tilde{A}^\mu \tag{1}$$

where $\mathcal{L}_o$ is the free lagrangian density for the charge and pole. j^μ and g^μ are, respectively, the electric and magnetic currents, and we define the generalized tensor field

$$F^{\mu\nu} \equiv \partial^\mu A^\nu - \partial^\nu A^\mu - \epsilon^{\mu\nu\alpha\beta}\partial_\alpha \tilde{A}_\beta \tag{2}$$

and the non-local potentials

$$A^\mu \equiv A^\mu + \frac{1}{2}\epsilon^{\mu\gamma\alpha\beta}\int_P^x \partial_\alpha \tilde{A}_\beta \, d\xi_\gamma \tag{3}$$

$$\tilde{A}^\mu \equiv \tilde{A}^\mu - \frac{1}{2}\epsilon^{\mu\gamma\alpha\beta}\int_P^x \partial_\alpha A_\beta \, d\xi_\gamma \tag{4}$$

in terms of the field variables, A^μ and $\tilde{A}^\mu$.

With these definitions, it's ease to check that

$$F^{\mu\nu} = \partial^\mu A^\nu - \partial^\nu A^\mu \tag{5}$$

and that its dual

$$\tilde{F}^{\mu\nu} \equiv \frac{1}{2}\epsilon^{\mu\nu\alpha\beta}F_{\alpha\beta} = \partial^\mu \tilde{A}^\nu - \partial^\nu \tilde{A}^\mu \tag{6}$$

From the density lagrangian (1), using (5), (6) and the identity

$$F^{\mu\nu}F_{\mu\nu} = \tilde{F}^{\mu\nu}\tilde{F}_{\mu\nu} \tag{7}$$

we obtain, for A^μ and $\tilde{A}^\mu$, the Euler-Lagrangian equations

$$\partial^\nu F_{\mu\nu} = j_\mu \tag{8}$$

$$\partial^\nu \tilde{F}_{\mu\nu} = g_\mu \tag{9}$$

That is. precisely the generalized Maxwell equations.

For the charge and pole degrees of freedom. the lagrangian gives the equations

$$m\frac{dU^\alpha}{d\tau} = e(\partial^\alpha A^\beta - \partial^\beta A^\alpha)U_\beta \tag{10}$$

and

$$M\frac{dV^\alpha}{d\tau} = g(\partial^\alpha \tilde{A}^\beta - \partial^\beta \tilde{A}^\alpha)V_\beta \tag{11}$$

Using (5) and (6). we get the wanted generalized Lorentz equations

$$m\frac{dU^\alpha}{d\tau} = eF^{\alpha\beta}U_\beta \tag{12}$$

and

$$M\frac{dV^\alpha}{d\tau} = g\tilde{F}^{\alpha\beta}V_\beta \tag{13}$$

Hierarquia de Schroedinger não Linear Generalizada

H. Aratyn, J.F. Gomes e A.H. Zimerman

Instituto de Física Teórica- UNESP

Rua Pamplona 145, 01405-900, São Paulo. SP

A importância do estudo dos modelos completamente integráveis tem se evidenciado nos ultimos anos principalmente devido ao fato destes apresentarem uma estrutura algébrica extremamente rica fornecendo o cenario natural na descrição de solitons. Estes modelos podem ser descritos através de equações diferenciais não lineares, operadores pseudo diferenciais (formulação de Lax) ou ainda através de uma formulação matricial.

A integrabilidade implica na existência de uma lei de conservação associada a cada grau de liberdade. Cada carga conservada Q_i, por sua vez pode ser associada a uma Hamiltoniana definindo a evolução temporal com respeito a um tempo t_i através da equação de Hamilton.

$$\frac{\partial A}{\partial t_i} = \{A, Q_i\} \tag{1}$$

Em particular, para uma teoria de campos em duas dimensões existem infinitos graus de liberdade e consequentemente infinitas leis de conservação descrevendo a evolução temporal num espaço de infinitos tempos. As equações de evolução (1) definem uma Hierarquia de modelos que apresentam em comum um conjunto infinito de leis de conservação.

Em particular, um modelo integrável de grande interesse devido a suas soluções soliton apresentarem aplicações na construção de laser de solitons utilizado em transmissões telefonicas é o modelo de Schroedinger não linear descrito pelas equações (veja ref. [1])

$$\partial_t q - \partial_x^2 q - 2q(rq) = 0$$
$$\partial_t r + \partial_x^2 r + 2r(rq) = 0 \tag{2}$$

A estrutura algébrica deste sistema é introduzida através da condição de curvatura nula,

$$[\partial_t - B, \partial_x - A] = (q_t - q_{xx} - 2rq^2)E_+ + (r_t + r_{xx} + 2r^2q)E_- = 0 \tag{3}$$

onde os potenciais de gauge são definidos na álgebra $sl(2)$,

$$A = \frac{\lambda}{2}H + qE_+ + rE_- \tag{4}$$

$$B = (\frac{\lambda^2}{2} + qr)H - (\partial_x q - \lambda q)E_+ + (\partial_x r + \lambda r)E_- \tag{5}$$

e os geradores satisfazem $[H, E_\pm] = \pm E_\pm$ e $[E_+, E_-] = H$.

Note que, apesar das equações de movimento independerem do parâmetro espectral λ, este é de crucial importância a nível dos potenciais de gauge como veremos a seguir.

Na realidade, o sistema físico descrito pela eq. (2) é totalmente descrito sómente pelo potencial de gauge A. A outra componente, B, pode ser determinada através da condição de curvatura nula assumindo uma forma polinomial para B em termos do parâmetro espectral λ. Dentro da hierarquia o potencial B contem informação

sobre a evolução temporal com respeito a um determinado tempo. Podemos então descrever toda a hierarquia de Schroedinger através da condição de curvatura nula para um tempo arbitrário t_n.

$$\partial_{t_n} A - \partial_x B_n + [A, B_n] = 0 \tag{6}$$

onde A é dado na eq. (4) e queremos determinar B_n segundo o seguinte ansatz. $B_n = \sum_{i=1}^{n} B_n^i \lambda^i$. A eq. (6) é chamada equação de Zakharov-Shabat cuja solução é conhecida ser da forma $B_n = \lambda B_{n-1} + O(1)$.

A generalização desta estrutura para muitos campos pode ser proposta de várias maneiras utilizando a álgebra de $sl(n+1)$. Entre elas, as de maior interesse físico são

$$A = \sum_{a=1}^{n} q_a E_{\alpha_a + \alpha_{a+1} + \cdots + \alpha_n} + r_a E_{-\alpha_a - \alpha_{a+1} - \cdots - \alpha_n} \tag{7}$$

onde E_α são operadores step de $sl(n+1)$ e o potencial de gauge em (7) define a hierarquia de Schroedinger não linear generalizada, GNLS. Um outro extremo nesta formulação consiste na hierarquia de Toda definida por

$$A = \sum_{a=1}^{n} q_a E_{\alpha_a} + r_a E_{-\alpha_a - \alpha_{a+1} - \cdots - \alpha_n} \tag{8}$$

Uma analise detalhada da solubilidade da equação de Zakharov-Shabat para estes modelos pode ser encontrada na referência [2] onde também exploramos a formulação de Lax, matricial e suas equivalências.

References

[1] A.P. Fordy, "Soliton Theory, a Survey of Results", Manchester University Press, (1990)

[2] II. Aratyn, J.F. Gomes and A.H. Zimerman, "Affine Lie Algebraic Origin of Constrained KP Hierarchies", IFT-P029-94 ou hep-th/9408104

A Study on the Ground State of Heisenberg Antiferromagnetic Chains

J. Rodrigo Parreira* O. Bolina† and J. Fernando Perez‡

Instituto de Física, Universidade de São Paulo
P.O. Box 20516, 01452-990 São Paulo, Brazil

We consider the ground state of one dimensional antiferromagnets with exchange function given by $(-1)^{|x-y|} J |x-y|^{-\alpha}$. We prove Néel order in the ground state for $1 < \alpha < 3$ for a sufficiently large spin and absence of LRO for any spin if $\alpha > 3$.

The model is given by the Hamiltonian:

$$H_\Lambda = \sum_{x \in \Lambda} \left[(-1)^x h S_x + \left(\sum_{n=1}^{L} (-1)^n J n^{-\alpha} S_x . S_{x+n} \right) \right]$$

where $J < 0, \alpha > 0, h \geq 0$ and $\Lambda = \{-\frac{L}{2}, -\frac{L}{2}+1, ..., \frac{L}{2}-1, +\frac{L}{2}\} \subset \frac{1}{2} Z$ (L odd). The S variables are usual spin operators such that $S^2 = s(s+1)$. We define the spontaneous magnetization as:

$$m = \lim_{h \to 0} \sigma(h) = \lim_{h \to 0} \lim_{L \to \infty} \frac{1}{L} \left\langle \sum_{x \in \Lambda} S_x \right\rangle_\Lambda .$$

where $< . > = Tr(.) \exp\{-\beta H\}/Tr \exp\{-\beta H\}$. The first condition to be imposed on the exchange function is due to the thermodynamic stability of the system. We need $\sum_n n^{-\alpha} < \infty \Rightarrow \alpha > 1$.

We introduce the Fourier transform of an arbitrary function f with $k \in \Lambda^*$ (the first Brillouin zone), as

$$\hat{f}(k) = \frac{1}{\sqrt{L}} \sum_{x \in \Lambda} f(x) e^{-ikx} .$$

We also introduce the two-point function $g_k^i = < \hat{S}_k^i \hat{S}_{-k}^i >$.

Theorem 1 *For the model described above, with $h = 0$, for every $1 < \alpha < 3$, there exists $s(\alpha) < \infty$ such that the system will show LRO at zero temperature if $s > s(\alpha)$.*

Proof

We have, as a consequence of the infrared bound [1], [2], the following condition for the existence of Néel order in the ground state:

$$[S(S+1)]^{\frac{1}{2}} > \frac{1}{2\pi} \int_0^{2\pi} dk \left\{ \frac{-6 \sum_n J n^{-\alpha}(-1)^n (1 - \cos kn)}{\sum_n J n^{-\alpha}[1 - (-1)^n \cos kn]} \right\}^{\frac{1}{2}} = I.$$

The numerator is bounded, if $\alpha > 1$ by a positive number, $A(\alpha)$. The term in the denominator, after making can be estimated by a second degree function. At this point we obtain:

$$I \leq \sqrt{\frac{A(\alpha)}{B(\alpha)}} \int_0^\pi dk \frac{1}{(\pi^{3-\alpha} k^{\alpha-1} - k^2)^{1/2}} = \mathcal{I}.$$

where $B(\alpha) = 2 [\pi^2(3-\alpha)]^{-1}$. The integral above is finite if $\frac{\alpha-1}{2} < 1$, implying that the condition for LRO can now be stated as $[s(s+1)]^{\frac{1}{2}} > \mathcal{I}$, which can always be made true if $\alpha < 3$ and s is sufficiently large.

Theorem 2 *If $\alpha > 3$ we have $m = 0$ in the ground state for any value of s.*

Proof

Our proof follows from the following inequality [3]:

$$\langle \{b^*, b\} \rangle \sqrt{[[a^*, H], a](a^*, a)\beta} \geq |\langle [a^*, b] \rangle|^2$$

where a, b are self-adjoint operators, β is the inverse temperature, $\langle . \rangle$ is the usual expected value and $(., .)$ is the Duhamel two-point function [1]. In our case we choose $a^* = \dot{S}^-_{-k}$ and $b = a = \dot{S}^+_k$, where $\dot{S}^\pm_k$ are the Fourier transforms of the operators $S^\pm_x = S^1_x \pm iS^2_x$.

The anticommutator and the double commutator (after an explicit calculation) can be bounded by the norm. The Duhamel two-point function can be estimated by the infrared bound [1].

So we have, when $L \rightarrow \infty$:

$$s(s+1) \geq 4\sigma(h)^2 \int_0^\pi dk \left\{ \frac{2\sum_x [1 - (-1)^x \cos kx] x^{-\alpha}}{4\sum_x [1 - \cos kx] x^{-\alpha} s(s+1) + |h\sigma(h)|} \right\}^{1/2} = 4\sigma(h)^2 I(\alpha, h).$$

We first look at the denominator, where we know that $1 - \cos kx \leq k^2 x^2 / 2$. The numerator can be estimated by a constant, $R(\alpha)$ after throwing away the contribution coming from even values of x. We then have:

$$I(\alpha, h) = \sqrt{R(\alpha)} \int_0^\pi dk \frac{1}{\{4k^2 \sum_x x^{2-\alpha} s(s+1) + |h\sigma(h)|\}^{1/2}}$$

showing a logarythmic divergence when $h \rightarrow 0$ and $\alpha > 3$, which implies $\lim_{h \rightarrow 0} \sigma(h) = 0.$.

References

[1] Dyson. F.: Lieb. E. H.,Simon. B.: *J. Stat. Phys.*, **18**, n. 4, 335 (1978).

[2] Neves, E. J.; Perez, J. F.: *Phys. Lett.*, **114A**, 331 (1988).

[3] Shastry. B. S.: *J. Phys. A*, **25**, L249 (1992).

O Método HMC e Fermions Dinâmicos

Marcia G. do Amaral

Instituto de Física - UFF

Embora o método de Monte Carlo (MC) tenha sido muito usado na simulação de diferentes tipos de teoria, seu sucesso foi estabelecido somente para o estudo de modelos que contenham campos bosonicos. Qualquer simulação que contenha variáveis fermiônicas só pode ser feita, usando-se um MC tradicional, se dispusermos de um tempo infinitamente absurdo de CPU. O aparecimento de máquinas cada vez mais velozes não elimina, sob hipótese nenhuma, a necessidade urgente de se desenvolver algorítmos que sejam mais velozes e eficientes.

Para que possamos entender a natureza dos problemas com os férmions, vamos considerar uma função de partição na qual existam férmions ψ e $\overline{\psi}$ acoplados a um campo bosônico φ, ie:

$$Z = N \int [d\psi d\overline{\psi}][d\varphi] \, \exp\left\{-S_T(\varphi, \psi, \overline{\psi}\,)\right\}.$$

onde

$$S_T = S_0(\varphi) + \overline{\psi} M(\varphi)\psi$$

pode ser escrita como a soma de uma ação puramente bosônica e uma ação fermiônica na qual $M(\varphi)$ contém a ação livre fermiônica e a interação férmion-bóson. Como $\overline{\psi}$ e ψ são variáveis de Grassmann e não sabemos como lidar com um grande número de variáveis anticomutantes, é mais conveniente intrmos os campos fermiônicos diretamente, o que provoca o aparecimento de um termo proporcional a $(\exp\{-S_0(\varphi)\}\, \det\, M(\varphi))$ no integrando. Quando fazemos uma simulação MC precisamos gerar configurações dos campos φ que obedeçam à seguinte distribuição de probabilidade:

$$P_{eq} = \exp\left\{-S_0(\varphi)\right\} \det\, M(\varphi)$$

Em princípio com esta expressão podemos fazer uma simulação MC tradicional, mas o cálculo de $\det M(\varphi)$ é muito lento, exigindo N^3 operações, onde N é o número de sítios da rede. Usando um método de updating Metropolis, teremos de calcular $\det M(\varphi)$ 2 vezes por sítio por passo de MC. A conseqüência disto é que o cálculo do determinante irá exigir um total de N^4 operações para cada passo MC, o que torna impossível em termos práticos usar um MC tradicional.

O método de Monte Carlo Híbrido (HMC) tem a vantagem de combinar todas as boas qualidades de métodos nas quais as equações de movimento são calculadas sem a existência de erros de truncamento com aquelas do MC tradicional. Uma das grandes vantagens do HMC é que os campos são updated de uma maneira paralela sobre todos os sítios e posteriormente a nova configuração será aceita ou rejeitada globalmente. No HMC introduzimos um parâmetro de tempo artificial τ juntamente com uma dinâmica Hamiltoniana especificando a evolução dos campos bosônicos com função de τ. Introduzimos, também, um momento conjugado $\pi(\tau)$ para os campos bosônicos. No caso de férmions usamos a seguinte igualdade,

$$Z = N \int [d\psi d\overline{\psi}\, d\varphi] \, \exp\left\{-S_0(\varphi) - \overline{\psi} M(\varphi)\psi\right\} = N \int [d\varphi] \, \det\, M(\varphi) xp\left\{-S_0(\varphi)\right\}$$

que por sua vez é igual a

$$N \int [d\varphi][d\chi] \, \exp\left\{-S_0(\varphi) - \chi^T \left(M^T(\varphi)M(\varphi)\right)^{-1}\chi\right\}$$

onde introduzimos os campos χ bosônicos - chamados de pseudofermiônicos- e, onde ao invés de usarmos $M(\varphi)$
, usamos $M^T(\varphi)M(\varphi)$ para garantir a convergência das integrais bosônicas. Se $M(\varphi)$ for real (como acontece na
caso do modelo que descreve os polímeros conjugados), os campos χ serão reais e a potência correta do det $M(\varphi)$
é encontrada.

No caso de polímeros, por exemplo, a Hamiltoniana de um problema no qual os férmions são acoplados a um
campo escalar, é dada por.

$$H(\varphi, \pi, \chi) = \frac{1}{2}\pi^2 + S_0(\varphi) + \chi^T \left(M^T(\varphi)M(\varphi)\right)^{-1}\chi$$

O algoritmo de Leap Frog pode ser facilmente adaptado a esta classe de problemas e na evolução de φ e π durante
um intervalo de tempo τ_o, os campos pseudofermiônicos χ são mantidos fixos. Depois de uma evolução de Dinamica
Molecular completa para (π, φ), a nova configuração gerada será aceita ou rejeitada por um Monte Carlo Global.
Durante o processo de evolução, cada vez que os campos φ são updated teremos de modificar $M^T(\varphi)M(\varphi)$ e também
$(M^T(\varphi)M(\varphi))^{-1}\chi$. O updating do primeiro termo é simples já que a matriz $M^T M$ é altamente esparsa, porem a
inversa de uma matriz esparsa não é esparsa. Com isso, temos de definir um campo auxiliar $\Phi = (M^T(\varphi)M(\varphi))^{-1}\chi$
e usamos um resolutor específico (gradiente conjugado) que nos dará o valor correto de Φ para um conjunto de
campos χ e φ.

Causal Theory in (2+1)-dimensional QED

G. Scharf and W. F. Wreszinski*

Institut für Theoretische Physik der Universität Zürich

B. M. Pimentel[†] and J. L. Tomazelli[‡]

Instituto de Física Teórica, Universidade Estadual Paulista
Rua Pamplona 145, 01405-900 - São Paulo, SP - Brazil

The program of constructing the S-matrix by means of causality in quantum field theory goes back to Stueckelberg and Bogoliubov[1]. In the early 70's, Epstein and Glaser[2] proposed an axiomatic construct where ultraviolet divergences do not appear, leading directly to the renormalized perturbation series. They have shown that in the causal theory the UV problem is a consequence of incorrect splitting of distributions.

In the causal theory[3] the S-matrix is viewd as an operator-valued distribution and has the following form

$$S(g) = 1 + \sum_{n=0}^{\infty} \frac{1}{n!} \int d^3 x_1 \dots d^3 x_n \, T_n(x_1 \dots x_n) g(x_1) \dots g(x_n) \, . \tag{1}$$

The n-point operator-valued distributions T_n are the basic objects of the theory. They can be constructed inductively from T_1 through a number of physical requirements, the most essential one being causality. Let the operator-valued distributions $\tilde{T}_n$ be defined by

$$S(g)^{-1} = 1 + \sum_{n=0}^{\infty} \frac{1}{n!} \int d^3 x_1 \dots d^3 x_n \, \tilde{T}_n(x_1 \dots x_n) g(x_1) \dots g(x_n) \, . \tag{2}$$

Then one defines, for arbitrary sets of points X, Y in the (2+1)-dimensional Minkowski space, the following distributions

$$A'_n(x_1 \dots x_n) = \sum_{P_2} \tilde{T}_{n_1}(X) T_{n-n_1}(Y, x_n) \, . \tag{3}$$

$$R'_n(x_1 \dots x_n) = \sum_{P_2} T_{n-n_1}(Y, x_n) \tilde{T}_{n_1}(X) \, . \tag{4}$$

where the sums run over all partitions

$$P_2 : \{x_1, \dots, x_{n-1}\} = X \cup Y \, , \quad X \neq \emptyset$$

into disjoint subsets with $|X| = n_1$, $|Y| \leq n - 2$. We also introduce

$$D_n(x_1 \ldots x_n) = R'_n - A'_n .$$ (5)

If the sums are extended over all partitions P_2^0, including the empty set $X = \emptyset$, we obtain the distributions

$$A_n(x_1 \ldots x_n) = A'_n + T_n(x_1 \ldots x_n) .$$ (6)

$$R_n(x_1 \ldots x_n) = R'_n + T_n(x_1 \ldots x_n)$$ (7)

These distributions are not known by the induction assumption because they contain the unknown T_n. Only the difference

$$D_n = R'_n - A'_n = R_n - A_n$$ (8)

is known. We can determine R_n or A_n separately by investigating the support properties of the various distributions. It turns out that R_n is a retarded and A_n an advanced distribution. Hence by causal distribution splitting of (9) one gets R_n (and A_n), and T_n then folows from (8) (or (7)).

In QED_3, D_n is of the form

$$D_n(x_1 \ldots x_n) = \sum_k : \prod_j \bar{\psi}(x_j) d_n^k(x_1 \ldots x_n) \prod_l \psi(x_l) :: \prod_m A(x_m) : ,$$ (9)

where $\psi(\bar{\psi})$ are *free* fermion field operators and A the *free* radiation field operators. The double dots denote the usual normal ordering. In the above expression, d_n^k are tempered numerical distributions, which have causal support. They must be split as follows:

$$d_n^k = r_n(x) - a_n(x) .$$ (10)

where r_n and a_n have support in the forward and backward light-cone, respectively.

The first order term T_1 of QED_3 is given by

$$T_1(x) = ie : \bar{\psi}(x)\gamma^\mu \psi(x) : A_\mu(x) = -\tilde{T}_1(x)$$ (11)

By using Wick's theorem, the term due to vacuum polarization in (10) is obtained by two fermionic contractions

$$D_2^{vp}(x_1, x_2) = d^{\mu\nu}(x_1, x_2) : A_\mu(x_1) A_\nu(x_2) : ,$$ (12)

In momentum space we find

$$d^{\mu\nu}(k) = d_S^{\mu\nu}(k) + d_A^{\mu\nu}(k) ,$$ (13)

where

$$d_S^{\mu\nu}(k) = (k^\mu k^\nu - k^2 g^{\mu\nu}) B(k^2) .$$ (14)

$$d_A^{\mu\nu}(k) = im\epsilon^{\mu\nu\alpha} k_\alpha \tilde{B}(k^2) .$$ (15)

and

$$r_A^{\mu\nu}(k) = im\epsilon^{\mu\nu\alpha} k_\alpha \Pi^{(2)}(k^2) ,$$ (16)

where

$$\Pi^{(2)}(k^2) = \frac{me^2}{2(2\pi)\sqrt{k^2}} \log \frac{1 - \sqrt{k^2/4m^2}}{1 + \sqrt{k^2/4m^2}} .$$ (17)

The vacuum polarization tensor can be written in the form

$$\Pi_{\mu\nu}(k) = (g_{\mu\nu} - \frac{k_\mu k_\nu}{k^2})\Pi^{(1)}(k^2) + im\epsilon_{\mu\nu\alpha}k^\alpha \Pi^{(2)}(k^2) .$$ (18)

In the limit $k^2 \to 0$ it can be shown that

$$\Pi^{(1)}(0) = 0 ,$$ (19)

and

$$\Pi^{(2)}(0) = \frac{e^2}{4\pi m} .$$ (20)

As a result, the photon propagator modified by proper vacuum polarization insertions have a pole dislocated from the origin, so that the photon acquires a "dinamically generated" mass[4].

References

[1] N. N. Bogoliubov, D. V. Shirkov, Introduction to the Theory of Quantized Fields; New York (1959);

[2] H. Epstein, V. Glaser, Ann. Inst. Poincaré A 19 (1973) 211; .

[3] G. Scharf, Finite Quantum Electrodynamics, Springer Verlag Berlin (1989);

[4] G. Scharf, W. F. Wreszinski, B. M. Pimentel, J. L. Tomazelli, Ann. Phys., vol. 231, 1 (1994) 185,
     B. M. Pimentel, A. T. Suzuki, J. L. Tomazelli, Int. J. Mod. Phys. A7 (1992) 5307.

Path-ordered Phase Factors in Scalar QED

B. M. Pimentel* and J. L. Tomazelli[†]

Instituto de Física Teórica, Universidade Estadual Paulista

Rua Pamplona 145, 01405-900 - São Paulo, SP - Brazil

The main difficulty in dealing with long-range potentials in the relativistic quantum theory is the factorization of infrared divergences out of scattering amplitudes, in order to get finite cross-sections. Who first had a deeper insight to circumvent this problem in spinor QED were Bloch and Nordsieck[1], over fifty years ago. Later, it was shown[2] that if we cast bremsstrahlung contributions in all orders of perturbation theory, we get finite cross-sections. In the same spirit, Kulish and Faddeev[3] and others considered a new space of asymptotic states, containing an infinite number of coherent photons, in order to extract finite elements from the S-matrix. In the early 80's, applying the concept of path-ordered phase factors, usually employed in QCD, Kubo[4] reproduced the Kulish-Faddeev results for spinor QED in the infrared asymptotic region in a simple and straightforward way. We must expect that Kubo's method still applies to scalar QED in order to obtain information about its behavior at the infrared. As we shall see, it is sufficient to write the interaction Hamiltonian of scalar QED in a suitable form.

Keeping this in mind, we will adopt an alternative approach to scalar QED, which is also useful to the investigation of electromagnetic properties of particles of either zero or unity spin. It is specially adequate to the study of the renormalizability of scalar QED as an effective theory[5], equivalent to the original, whose structure is similar to that of spinor QED. For our purposes it is not convenient to start with the usual equations of motion for interacting fields but with the Heisenberg equations

$$[i\beta^\mu(\partial_\mu + ieA_\mu(x)) - m]\psi(x) = 0 , \qquad (1)$$

$$\overline{\psi}(x)[i\beta^\mu(\overleftarrow{\partial}_\mu + ieA_\mu(x)) + m] = 0 , \qquad (2)$$

$$\Box A_\mu(x) = j_\mu(x) . \qquad (3)$$

where β_μ are matrices satisfying the algebra

$$\beta_\mu\beta_\nu\beta_\lambda + \beta_\lambda\beta_\nu\beta_\mu = g_{\mu\nu}\beta_\lambda + g_{\lambda\nu}\beta_\mu . \qquad (4)$$

In the linear equations (1) and (2) the field ψ and its adjoint $\overline{\psi}(x) = \psi^\dagger(x)(2\beta_0{}^2 - I)$ have five components corresponding to the scalar field and its four derivatives with respect to the coordinates and the time, which transform like the components of a vector. They are known as the Duffin-Kemmer equations for scalar fields which interact via the electromagnetic potential $A_\mu(x)$.

In spinor quantum electrodynamics the field operators $\psi(x)$ and $A_\mu(x)$ in the interaction picture have the same form as the operators for the corresponding free fields. The situation is different here, since not all the components of $\psi(x)$ are dynamically independent. As a consequence we can evaluate S-matrix elements from the effective Hamiltonian density

$$\mathcal{H}_{int}^{eff}(x) = -j_\mu^{(0)}(x)A^{\mu(0)}(x) , \tag{5}$$

$$j_\mu^{(0)}(x) = e\overline{\psi}^{(0)}(x)\beta_\mu\psi^{(0)}(x) . \tag{6}$$

In this case the Green's function for the free scalar particle in momentum space is given by

$$S_F(p) = (\not{p} - m)^{-1} = \frac{\not{p}(\not{p} + m) + p^2 - m^2}{m(p^2 - m^2 + i\epsilon)} , \tag{7}$$

with $\not{p} \equiv \beta_\mu p^\mu$.

We now apply Kubo's technique[4] to extract infrared singularities from Green's functions in the effective scalar particle theory described above. So, let us first consider the simplest case of the two-point Green's function $G^c(x-y)$. In the interaction picture, this can be written as

$$G^c(x - y) = \frac{< 0|T\{\psi^{(0)}(x)\overline{\psi}^{(0)}(y)S\}|0 >}{< 0|S|0 >} , \tag{8}$$

with

$$S = T\{\exp[i \int d^4x'\, j_\mu^{(0)}(x')A^{\mu(0)}(x')]\} . \tag{9}$$

As we are mostly interested in the infrared asymptotic behavior of the theory, we replace $j_\mu^{(0)}$ in (9) by

$$j_\mu^{as}(x) = \int d^3\vec{p}\frac{p_\mu}{p_0}\rho(\vec{p})\delta^{(3)}(\vec{x} - \frac{\vec{p}}{p_0}t) , \tag{10}$$

and neglect contributions from vacuum polarization graphs, like in the Bloch-Nordsieck model[1], since there are no antiparticles in the limit of low frequencies. As a result we arrive at

$$G^c(p) =< 0|T\{\exp[ie \int_y^x dx'_\mu\, A^{\mu(0)}(x')]\}|0 > S_F(p) , \tag{11}$$

where $S_F(p)$ is the Feynman propagator for charged mesons, given by (7), and

$$< 0|T\{\exp[ie \int_y^x dx'_\mu\, A^{\mu(0)}(x')]\}|0 >= e^{-f(\frac{r_0-r_0}{p_0})} , \tag{12}$$

where

$$f(\nu) = -\frac{e^2}{8\pi^2}(2p^2 + 1 - a)\{-i\frac{\nu}{\epsilon} + \log[\frac{(i\nu + \epsilon)}{\epsilon}]\} , \tag{13}$$

a standing for the gauge parameter. The last expression also appears in the calculation of the Green's function in the Bloch-Nordsieck model for spinor QED_3[6].

In the same way, we obtain

$$B_\mu(p,p') = \beta_\mu \exp\{ie^2 \int \frac{d^4k}{(2\pi)^4} \frac{p.p'}{(k^2 + i\epsilon)(k.p)(k.p')}\} \tag{14}$$

for the unrenormalized vertex function in the Feynman gauge in the asymptotic limit. This coincides with the infrared singular exponential which factorizes in the vertex function for both spinor and the usual scalar QED. In the former it is obtained via perturbation theory[2], while in the later through an alternative laborious method[7].

.References

[1] F. Bloch and A. Nordsieck. Phys. Rev. 52 (1937) 54;

[2] D. Yennie. S. Frautschi and H. Suura, Ann. Phys. 13 (1961) 379;

[3] P. Kulish and L. Faddeev, Theor. Math. Phys. 4 (1971) 745;

[4] R. Kubo, Prog. Theor. Phys. 66 (1981) 1816;

[5] T. Kinoshita, Prog. Theor. Phys. 5 (1950) 473;

[6] B. M. Pimentel and J. L. Tomazelli. J. Phys. G 20 (1994) 845;

[7] M. C. Bergère and L. Szymanowski, Phys. Rev. D 26 (1982) 3550;

On the Covariantization of the Chiral Constraints

Clovis Wotzasek*

Department of Physics and Astronomy, University of Rochester
Rochester, N.Y. 14627, USA

E.M.C. de Abreu and C.Neves

Instituto de Física, Universidade Federal do Rio de Janeiro ·
21945 Rio de Janeiro, Brasil

We show that a complete covariantization of the chiral constraint in the Floreanini-Jackiw necessitates an infinite number of auxiliary Wess-Zumino fields otherwise the covariantization is only partial and unable to remove the nonlocality in the chiral boson operator. We comment on recent works that claim to obtain covariantization through the use of Batalin-Fradkin-Tyutin method, that uses just one Wess-Zumino field.

The quantization of chiral boson in two-dimensions is a very interesting theoretical problem, which has appeared originaly in the investigation of heterotic string [1], and became quite important in the study of fractional quantum Hall efect [2]. This problem has a simple solution in the Hamiltonian language while it has been beset with enormous difficulties in the Lagrangian side. One of these problems is the covariantization of the second-class chiral constraint. i.e., the transformation from second to first-class, which is the object of investigation in this paper.

In Ref.[3], the FJ chiral boson was iteratively changed to modify the nature of chiral constraint to render it first-class. Following this route the modified Floreanini-Jackiw model with the original chiral field plus the set of Wess-Zumino fields will always have one left over second-class constraint that must as well be converted into first-class if a complete covariantization is desired.

It is our intention in this paper to work out the possibility of stopping the constraint conversion process, mentioned above, at any (finite) stage, say after N iterations, even if a second-class constraint remains, and study its consequences. It is expected that in doing this we would destroy the possibility of obtaining the complete Wess-Zumino Lagrangian, and the theory would only be partially covariantized. We plan to stop the constraint conversion process in two different ways and verify their equivalence. Firstly we will follow a constraint conversion method introduced by one of us some years ago in the context of the chiral Schwinger model [4]. Another way of doing it is by a simple elimination of the left over second-class constraint using Dirac brackets for the variables involved. This can be done after an arbitrary N number of steps. It will then be clear that the results of the first method corresponds to choose to stop at N=1 in the second method.

Let us consider now the case of Floreanini-Jackiw chiral boson. For the case of the (left mover) FJ chiral boson, described by

$$L = \int dx \, (\dot{\phi}\phi' - \phi'^2) \tag{1}$$

the Dirac Hamiltonian reads

$$H = \int dx \, \left[\phi'^2 + \lambda(\pi - \phi') \right]$$

*CLOVIS@URHEP.PAS.ROCHESTER.EDU

$$= \int dx \, \pi \phi' \tag{2}$$

where $\pi = \delta\mathcal{L}/\delta\dot{\phi}$ is the canonical momentum of $\phi(x)$ and $\lambda = \phi'$ has been determined from the consistency condition for the evolution of the chiral constraint $\Omega = \pi - \phi'$. The modified (first-class) constraint is,

$$\Omega \rightarrow \tilde{\Omega} = \pi - \phi' - 2\theta' \tag{3}$$

where θ is the Wess-Zumino field,

$$\{\theta'(x), \theta'(y)\} = \frac{1}{2}\delta'(x-y) \tag{4}$$

which shows that this auxiliary field is itself of chiral nature. The other brackets are canonical

$$
\begin{aligned}
\{\phi(x), \pi(y)\} &= \delta(x-y) \\
\{\phi(x), \theta(y)\} &= 0 \\
\{\pi(x), \theta(y)\} &= 0
\end{aligned}
\tag{5}
$$

To compute $\tilde{H}$ is now a pretty simple algebraic work.

$$\tilde{H} = \int dx \, (\phi'^2 + 2\phi'\theta' + \theta'^2) = \int dx \, (\phi' + \theta')^2 \tag{6}$$

We obtain a first-class algebra for the (modified) chiral constraint

$$\{\tilde{\Omega}(x), \tilde{\Omega}(y)\} = 0 \tag{7}$$

We have thus succeeded in turning into first-class the original second-class constraint of the Floreanini-Jackiw model.

In summary, we have worked the problem of covariantization of the bosonic chiral constraint following the methodology of Ref.[4]. Differently from the approach of [3] where an infinite number of auxiliary fields is necessary, this one only needs one Wess-Zumino field.

References

[1] D.J.Gross, J.A.Harvey, E.Martinec, R.Rhom, Phys.Rev.Lett.54 (1985)502.

[2] See, for instance, "Quantum Hall Effect", M.Stone ed. (World Scientific 1992).

[3] C.Wotzasek, Phys.Rev.Lett.66(1991)129-133.

[4] C.Wotzasek, Intl.J.Mod.PhysA5(1990)1123.

Decaimento por Ativação Térmica em um Sistema Metaestável

E. S. Fraga[†] e C. A. A. de Carvalho[‡]

Instituto de Física, Universidade Federal do Rio de Janeiro

Caixa Postal 68528, CEP 21945-970, Rio de Janeiro, RJ, Brasil

O estudo do decaimento em sistemas metaestáveis vem atraindo um número crescente de pesquisadores devido à sua aplicabilidade nas mais diversas áreas da Física [1, 2, 3, 4]. O método comumente utilizado para tal estudo consiste em forçar uma abordagem de equilíbrio com a intenção de obter um problema estacionário [5,6]. Contudo, começam a surgir na literatura abordagens mais realísticas que se utilizam de métodos de não-equilíbrio resultando, portanto, na obtenção de resultados explicitamente dependentes do tempo [7, 8, 9].

Neste trabalho, estamos interessados em obter a influência da inclusão de férmions, a uma certa temperatura e sujeitos a um dado potencial químico, sobre um sistema metaestável bosônico. Para tal, faremos uso de inúmeros resultados apresentados na referência [7], cuja leitura anterior é fortemente recomendada.

Nosso problema é definido pela Lagrangeana [10, 11] $\mathcal{L} = \frac{1}{2}(\partial_\mu \phi)(\partial^\mu \phi) - [V(\phi) - V(\phi_2)] + \bar{\psi}_a(i\gamma^\mu \partial_\mu - \mu - g\phi)\psi_a + \epsilon_F \bar{\psi}\gamma_0 \psi$, sendo $V(\phi) = \frac{g^2}{2}(\phi - \phi_0)^2 \left(\phi + \phi_0 + \frac{2\mu}{g}\right)^2 + j\phi$, ϕ_2 o mínimo metaestável e ϵ_F o potencial químico. Integrando sobre os férmions no funcional gerador, admitindo a existência de apenas dois estados ligados e adicionando os devidos contra-termos [9, 10, 12], podemos escrever a ação efetiva em termos dos dados de espalhamento [9, 10]. Extremizando a ação efetiva e utilizando a equação do gap, podemos obter a energia das soluções tipo "bolha" [8,9] como função de seu raio, e a taxa de decaimento como função do tempo (vide figs.).

Notamos, então, que no limite de baixa temperatura encontramos tanto estruturas do tipo "sphaleron" [7] quanto estruturas do tipo "bolha" metaestável [8,9]. O limite de alta temperatura forneceria apenas curvas de dissociação. É importante observarmos que o fator determinante no surgimento de "bolhas" metaestáveis é a ocupação relativa dos estados ligados fermiônicos [8,9].

References

[†] e-mail: fraga@if.ufrj.br

[‡] e-mail: aragao@if.ufrj.br

[1] M.E. Shaposhnikov, "Lectures at ICTP Summer School in High Energy Physics and Cosmology", Trieste, 1991. V.V. Khoze, "Proceedings of Yale TEXAS Workshop on Baryon Number Violation", 1992.

[2] D. Boyanovsky, H.J. de Vega and R. Holman, Pittsburgh University preprint PITT-94 01.

[3] A.H. Guth, "The Oskar Klein Memorial Lectures", Vol. 2, Ed. Gösta Ekspong (World Scientific) and references therein.

[4] Yu-Lu, "Solitons and Polarons in Conducting Polymers" (World Scientific), 1988 (and references therein).

[5] J.S. Langer, Ann. Phys. (N.Y.) 41, 108 (1967); 54, 258 (1969).

[6] Sidney Coleman, Phys. Rev. D15, 2929 (1977). Curtis G. Callan, Jr. e Sidney Coleman, Phys. Rev. D16, 1762 (1977).

[7] D. Boyanovsky and C.A.A. de Carvalho, Phys. Rev. D48, 5850 (1993).

[8] D. Boyanovsky, C.A.A. de Carvalho and E.S. Fraga, Phys. Rev. B50, 2889 (1994).

[9] E.S. Fraga and C.A.A. de Carvalho, submitted to Phys. Rev. E.

[10] C.A.A. de Carvalho, Mod. Phys. Lett. B3, 125 (1989); Nucl. Phys. B324, 729 (1989).

[11] C.A.A. de Carvalho, Phys. Rev. D21, 1100 (1980).

[12] R.F. Dashen, B. Hasslacher e A. Neveu, Phys. Rev. D10, 4114 (1974), D10, 4130 (1974), D12, 2443 (1975).
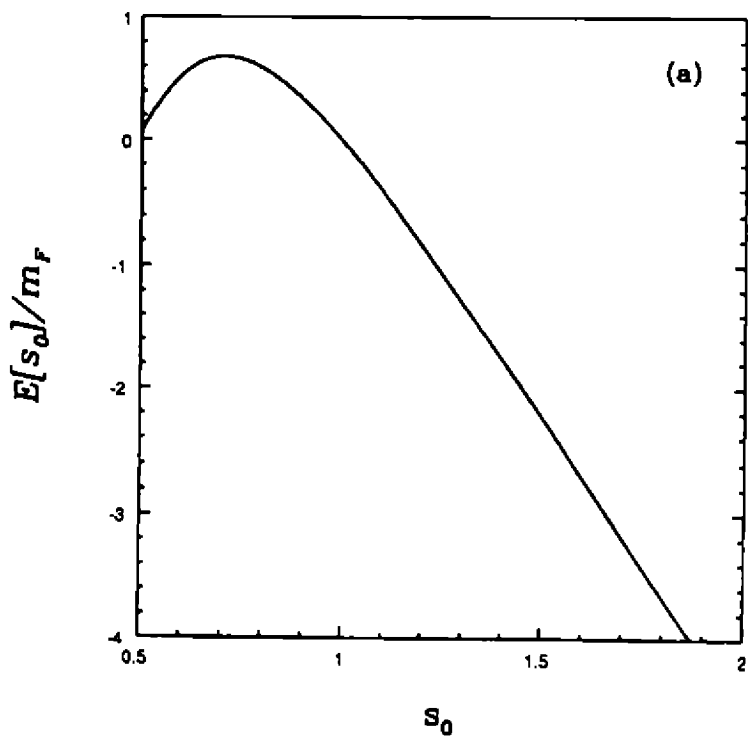
Fig.1a

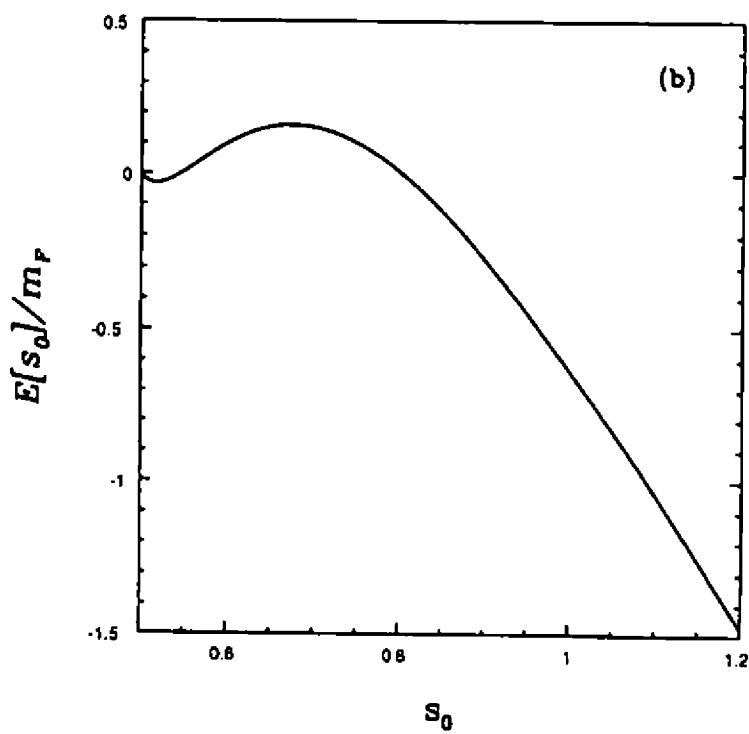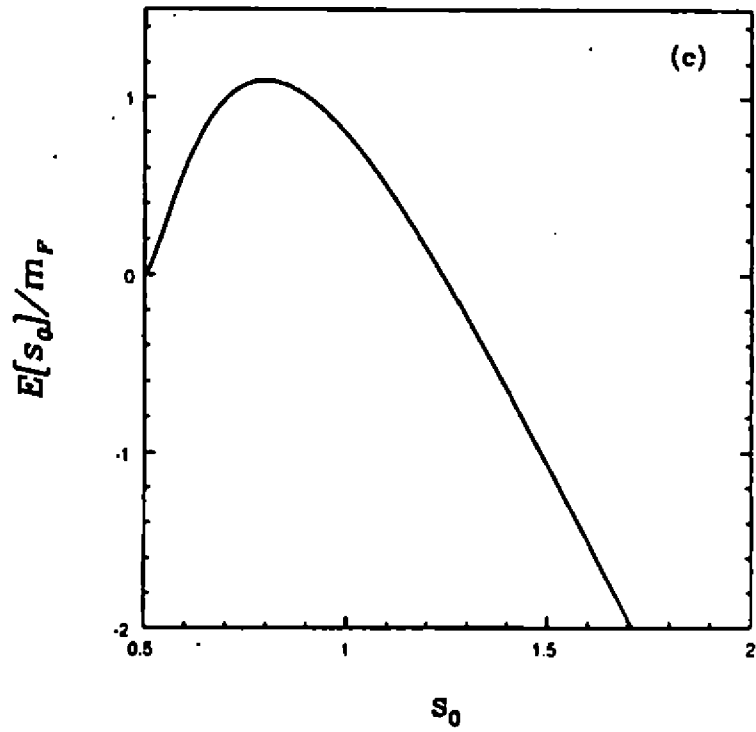
Fig.1b

Figura 1: Energia da "bolha" como função de seu raio no limite de baixa temperatura para (a) $m_F < \epsilon_F < \Omega$. (b) $\omega_0 < \epsilon_F < m_F$. (c) $0 < \epsilon_F < \omega_0$.
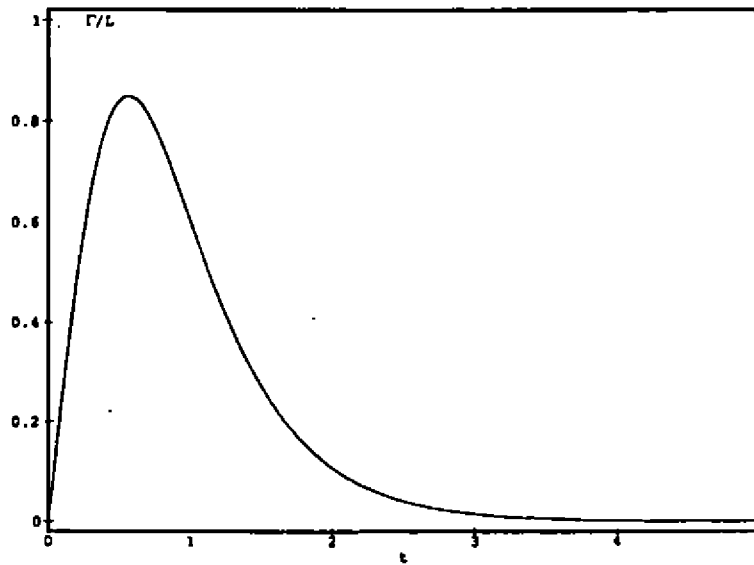

Fig.2. Taxa de decaimento como função do tempo.

Influência das Condições de Contorno sobre o Momento Magnético Anômalo do Elétron

Franz P. A. Farias, A. Matos Neto

Instituto de Física, Universidade Federal da Bahia

Introdução

Nas últimas décadas tem sido publicados diversos trabalhos [1,2] acerca das modificações nas correções radiativas às propriedades do elétron como por exemplo, seu momento magnético e sua massa. Estas modificações tem origem na alteração das condições de contorno impostas sobre o campo de radiação.

O problema de nosso interesse é o do cálculo das correções radiativas às propriedades mencionadas acima quando o elétron se encontra em interação com um campo magnético dado e com o campo de radiação quantizado. Confinamos este campo em uma região delimitada por duas placas paralelas de naturezas distintas, uma sendo perfeitamente condutora e a outra infinitamente permeável.

O cálculo das correções radiativas

O método de abordagem consiste em descrever o elétron como uma excitação elementar do campo elétron-pósitron em interação com o campo de radiação e na presença de um campo externo dado. O elemento básico neste tratamento é a equação de Dirac Generalizada [3]:

$$(i\gamma.\partial - e\gamma.A_e(x))\psi(x) + \int d^4x' M(x,x')\psi(x') = 0. \tag{1}$$

onde, $M(x,x')$ é o operador de massa cuja expressão em ordem mais baixa na constante de acoplamento é:

$$M(x,x') = m_0\delta(x - x') + ie^2\gamma^\mu G(x,x')\gamma_\mu D_0^{(+)}(x - x'), \tag{2}$$

com $G(x,x')$, a função de Green do elétron na presença do campo externo $A_e(x)$ e $D_0^{(+)}(x)$ é a função de Green do fóton livre [4].

Na situação de interesse, ou seja, o confinamento do campo de radiação entre as duas placas, consideramos que a função de Green do elétron não se altera. Por outro lado, a função de Green do fóton se modifica. Esta função Green tem sido obtida através de diversos métodos [5,6].

Temos obtido a função de Green do fóton através de um método que faz uso explícito do fato de que o confinamento estabelece uma mudança de representação dos observáveis quanto-mecânicos [5]. Nestas condições altera-se o espaço de Fock associado ao sistema campo de radiação confinado com relação àquele em que o campo de radiação encontra-se livre. A expressão da função de Green do fóton confinado é:

$$D_d^{(+)}(x) = \sum_{m=-\infty}^{\infty} \exp[im\pi]D_0^{(+)}(x^0, x^1, x^2, x^3 + 2md). \tag{3}$$

Como um primeiro passo na verificação da expressão (3) calculamos a pressão de Casimir entre duas placas de naturezas distintas:

$$P(d) = (7/8)(\pi^2/240d^4), \tag{4}$$

resultado este que concorda com aquele conseguido por Boyer [7] por um outro método.

Com a função de Green (3) conseguimos uma expressão aproximada para o operador de Massa em (2) que, substituida em (1) permite reescrever a equação de Dirac Generalizada com:

$$[\gamma.(-i\partial - eA_e(x)) + m - \mu'(1/2)\sigma F]\psi(x) = 0, \tag{5}$$

sendo m e μ' expressos em função de m_0, μ_0 e das correções radiativas respectivamente. Os resultados dessas expressões integrais serão apresentados posteriormente.

Referências:

1) Bordag, M., Robaschik, D. e Wieczoreck, E. ; Phys. Lett. A, *132* (1988) 145.

2) Bordag, M.; Phys. Lett. B, *171* (1986) 113.

3) Schwinger, J.; Phys. Rev., *82* (1951) 664.

4) Itzykson, C. e Zuber, J.-B.; Quantum Field Theory, (1985).

5) Scharf, G.e Wreszinski, W.; Found. Phys. Lett., *5* (1992) 89.

6) Plunien, G., Müller, B. e Greiner, W.; Phys. Reports, *134* (1986) 89.

7) Boyer, T. H.: Phys. Rev., *A9* (1974) 2078.

Efeito Casimir entre Placas de Materiais Distintos à Temperatura Finita

J.C. da Silva. Hebe Q. Plácido, Ademir E. Santana, A. Matos Neto

Instituto de Física, Universidade Federal da Bahia

I - Introdução

Casimir[1] em 1948, demonstrou que duas placas paralelas. neutras, condutoras atraem-se como resultado da energia (não nula) associada ao estado de vácuo do campo eletromagnético. Desde então o fenômeno tem sido abordado sob uma diversidade de aspectos. Estudos variados sobre o Efeito Casimir em diferentes geometrias, condições de contorno, etc, têm sido realizados[2]. Em particular, efeitos de temperatura foram encorporados adequadamente por Mehra[3].

Estimulado por Casimir, Boyer[4] mostrou que para placas distintas, uma condutora e outra de material permeável a $T = 0K$, a força é repulsiva. Prosseguindo nesta linha de investigação, apresentaremos as correções introduzidas pela temperatura no resultado obtido por Boyer. Este será o objetivo deste trabalho.

II - Correção de Temperatura ao Efeito Casimir

Em analogia com o método utilizado por Plunien et al[2]. consideraremos o campo eletromagnético confinado em caixas de volume $R \times L^2$ constituidas de paredes infinitamente permeáveis. Numa delas inscrimos uma placa condutora a uma distância d e noutra à distância R/η da placa paralela oposta. Esta configuração se encontra imersa num banho térmico, na condição de equilíbrio. Seguindo Mehra[3], devemos obter a diferença entre as energias livres de Helmholtz dos sistemas considerados. Calcularemos, então, para cada cavidade o valor de

$$F = \sum_k \frac{\hbar\omega_k}{2} + \sum_k \beta^{-1} \ln[1 - \exp(-\beta\hbar\omega_k)] = E_0 + F'. \tag{1}$$

com as autofrequências dadas por

$$\omega_k = \pi c \left[\left(\frac{n+1/2}{d}\right)^2 + \left(\frac{n_y}{L}\right)^2 + \left(\frac{n_z}{L}\right)^2 \right]^{1/2}. \tag{2}$$

O primeiro termo da eq.(1), independente da temperatura. foi calculado por Boyer[4]. O segundo termo, F' .representa a correção de temperatura desejada. Após efetuarmos a subtração acima referida, obtemos

$$F'(d,T) = \frac{\pi L^2}{2} \sum_{n=0}^{\infty} \int_0^{\infty} dr \beta^{-1} \ln\left(1 - \exp\left[-\beta\pi hc\left(\left[\frac{n+1/2}{d}\right]^2 + r\right)^{1/2}\right]\right) +$$

$$- \frac{\pi L^2}{2} \int\int_0^{\infty} dx dr \beta^{-1} \ln\left(1 - \exp\left[-\beta\pi hc(x^2+r)^{1/2}\right]\right). \tag{3}$$

Após efetuar as integrações desta eq.(3), a pressão é obtida derivando-se o resultado em relação à separação das placas. Tem-se, então,

$$P = \frac{7}{8}\frac{\pi^2 \hbar c}{240 d^4} - \frac{\pi}{\beta d^3} \sum_{n=0}^{\infty} \left(n + \frac{1}{2}\right)^2 \ln\left[1 - \exp\left(-\frac{\beta\pi\hbar c}{d}\left[n + \frac{1}{2}\right]\right)\right] - \frac{\pi^2}{45\beta^4(\hbar c)^3}. \tag{4}$$

O primeiro termo na eq.(4) corresponde à pressão de radiação em $T = 0K$[4]. O terceiro termo é o usual de Stefan-Boltzmann.

Para uma análise mais detalhada do comportamento da pressão, tomaremos os limites para baixas e altas temperaturas.

a) No limite de baixas temperaturas, uma expansão do logarítmo, na eq.(4), é permitida. obtendo-se para a pressão total entre as placa

$$P_{LT} = \frac{7}{8}\frac{\pi^2\hbar c}{240 d^4} + \frac{\pi}{4\beta d^3}\left[\exp\left(-\frac{\beta\pi\hbar c}{2d}\right) + \frac{1}{2}\exp\left(-\frac{\beta\pi\hbar c}{d}\right) + 9\exp\left(-\frac{3\beta\pi\hbar c}{2d}\right)\right] +$$

$$- \frac{\pi^2}{45\beta^4(\hbar c)^3}. \tag{5}$$

Nesta equação, o segundo termo corresponde à correção devido às condições de contorno utilizadas.

b) Em altas temperaturas, a fórmula da soma de Poisson é utilizada para calcular a soma na eq.(4). Desta Avaliação resulta

$$P_{HT} = \frac{0,9kT}{4\pi d^3} + \frac{kT}{2\pi d^3}\left[1 + \frac{4\pi kTd}{\hbar c} + \frac{1}{2}\left(\frac{4\pi kTd}{\hbar c}\right)^2\right]\exp\left(-\frac{4\pi kTd}{\hbar c}\right). \tag{6}$$

Observa-se que, tanto o termo de Stefan-Boltzmann quanto o de $T = 0K$ são cancelados neste limite. Esta expressão é similar ao caso de placas iguais[3], exceto pelo fator numérico 0,9 e pelo sentido repulsivo da força.

Referências

1. H.B.G. Casimir; Proc. Kon. Nederl. Akad. Wetenschap 51(1948)793.
2. G. Plunien, B. Muller, W. Greiner; Phys. Rep. 134(1984)87.
3. J. Mehra; Physica 37(1967)145.
4. T.H. Boyer; Phys. Rev. A9(1974)2078.

Considerations Related to the
Aharonov-Bohm and Casimir Effects

K. Dechoum, H. M. França

Instituto de Física, Universidade de São Paulo
C.P. 20516, 01498-970. São Paulo, SP. Brasil

A. Maia Jr.

Inst. de Matemática, Estatística e Ciências da
Computação, Univ. Estadual de Campinas. C.P. 6065
13081-970, Campinas. SP, Brasil

We discuss the interaction between a microscopic electric dipole oscillator and a long solenoid which are separated by a small distance. The zeropoint current fluctuations of the solenoid are taken into account. We describe how they affect the ground state and the excited states of the oscillator, thus providing a description of the Casimir interactions of the system. We conclude that the lifetime of the oscillator excited states are modified when the dipole is close enough to the solenoid. We also show that there is an enhancement in the spontaneous emission of the dipole oscillator and also an anysotropy which is related to the dipole orientations [1]. We show that this Casimir interaction always exists, that is, it occurs even when the macroscopic current in the solenoid is zero. The Aharonov-Bohm effect on the oscillator, is interpreted in terms of the solenoid electric field ($c\vec{E}_{sol} \equiv -\partial\vec{A}_{sol}/\partial t$) which acts on the charged oscillating particle. This is possible because, from the microscopic and macroscopic point of view, the fields in the neighbourhood of the solenoid are always time varying due to the discreteness of the electronic charge, the transient behaviour of the macroscopic current and the zeropoint and thermal current fluctuations. We suggest experiments which can exhibit these effects related of the Aharonov-Bohm and Casimir interactions.

[1] H.M. França, T. W. Marshall and E. Santos, "Spontaneous emission in confined space according to stochastic electrodynamics", *Phys. Rev.* **A45**, 6436 (1992).

Lagrangianas Não-Polinomiais
no Modelo de Skyrme

Jorge Ananias Neto

Centro Brasileiro de Pesquisas Físicas, D.C.P.
R. Dr. Xavier Sigaud 150 22290-180 Rio de Janeiro, Brasil

Escolhendo diferentes constantes de acoplamento para termos de derivadas de ordem superior no Modelo de Skyrme, podemos somar a Lagrangiana final numa forma binomial, geométrica e logarítmica que por sua vez apresentam consideráveis melhoras na usual fenomenologia prevista.

O modelo de Skyrme consiste em tratar os Bárions e suas interações através de soluções tipo sóliton num modelo que tem como base o Sigma Não-Linear mais o termo estabilizador de Skyrme. Neste trabalho pretendemos utilizar o quadrado do termo cinético como estabilizador e gerador da forma padrão de termos de derivadas de ordem superior, cuja a expressão final da Lagrangiana contendo todos os termos de derivadas de ordem superior é dada por[1]

$$L = -c_1 \int d^3r \, [2M - I\,Sp] - c_2 \int d^3r \, [2M - I\,Sp]^2$$
$$\ldots - c_n \int d^3r \, [2M - I\,Sp]^n \, , \tag{1}$$

onde $c_1 \equiv F_\pi^2/16$. Escolhemos três diferentes relações, $K_n = \frac{c_n}{c_1}$ que permitem somar a Lagrangiana (1) com termos de derivadas de ordem superior em formas não convencionais, que são:

a) Forma Binomial,

$$K_n \equiv \frac{c_n}{c_1} = \left(\begin{array}{c} s \\ n-1 \end{array} \right) / (2e^2 F_\pi^2)^{n-1}$$

onde s é a potência da forma binomial;

b) Forma Geométrica,

$$K_n \equiv \frac{c_n}{c_1} = \frac{1}{(2e^2 F_\pi^2)^{n-1}} \; ;$$

c) Forma Logarítmica,

$$K_n \equiv \frac{c_n}{c_2} = \frac{(-1)^{n-1}}{(n-2)(2e^2 F_\pi^2)^{n-2}} \quad n = 3, 4, \ldots \; .$$

---

[1] Aqui nós já estamos usando o ansatz hedgehog dado por $U = \exp(i\tau.\hat{r}F(r))$ e expandindo a Lagrangiana através das coordenadas coletivas $U(r,t) = A(t)U(r)A^+(t)$ sendo $A = a_0 + a_i.\tau_i$. M é dado por $M \equiv \frac{2\sin^2 F(r)}{r^2} + F'(r)^2$, I é o momento de inércia $I \equiv \frac{6}{3}\sin^2 F$ e $Sp \equiv Tr \left[\partial_0 A \partial_0 A^{-1} \right]$.

Definindo o Hamiltoniano Qùantico através da relação $H = \pi\dot{a} - L$ e utilizando as massas do Nucleon e da Delta como parámetros de entrada, obtemos os principais resultados físicos, que são mostrados na tabela 1.

TABELA 1- Parámetros Físicos no modelo de Skyrme

	bin.	geo.	log.	Adkins et al	expt.
$F_\pi(Mev)$	143	152	141	129	186
e	21.55	8.48	6.69	5.45	-
$< r^2 >^{\frac{1}{2}}_{l=0}$ (fm)	0.61	0.61	0.60	0.59	0.72
μ_p	1.75	1.75	1.74	1.87	2.79
μ_n	-1.20	-1.21	-1.21	-1.33	-1.91
g_A	0.79	0.84	0.76	0.61	1.23

As três formas da Lagrangiana do modelo de Skyrme aqui apresentadas, binomial, geométrica e logarítmica,representam uma tentativa de se incluir a contribuição de todos os termos de derivadas de ordem superior, numa forma específica, no cálculo de quantidades físicas. Sem dúvida nenhuma, a inclusão destes termos melhoram o espectro físico, cabendo ressaltar que a forma geométrica foi a que mais se aproximou dos resultados experimentais. Mais referencias podem ser encontradas em Jorge Ananias Neto. Non-Polynomial Lagrangians in the Skyrme Model, Preprint CBPF (1994).

Minijets, Inelasticity and Proton-Proton Total Cross Section

A. L. Godoi, J. Bellandi, R. J. M. Covolan and J. Montanha Neto

Instituto de Física 'Gleb Wataghin' Universidade Estadual de Campinas, Unicamp

13083-970, Campinas, São Paulo, Brasil

Inelasticity, the fraction of energy released to the secondary particles produced in a hadronic collision, is an important quantity whose behavior has not been properly established yet. In this paper we show a reanalysis of the Akeno's data [1] on absorption cross section wherein inelasticity is considered to be alternatively an increasing or decreasing function of energy. Our main concern was to extract, from these data, information about the proton-proton total cross section. In our procedure we have used average inelasticities calculated by the Interacting Gluon Model [2], which has been corrected in order to include the air effect [3]. Following results obtained previously [4], we came to an expression that can be solved numerically for the total cross section.

$$(\sigma_{in}^{p-air})^\gamma - \sigma_{abs}^{p-air}(\sigma_{in}^{p-air})^{\gamma-1} - \left\{ \sum_{n=1}^{n_{max}} \left[\int d^2b P_n(b) \right] \right\}^\gamma = 0.$$

In this equation σ_{in}^{p-air} is given by the Glauber formula [5], P_n is the probability of n-fold collisions of the primary nucleon inside the nucleus, n_{max} is the maximum number of collisions. $\gamma = 2.22$ is the slope of the primary flux and σ_{abs}^{p-air} is the absorption cross section given by Akeno's experiment. The results are shown in the figure on the next page.

In this figure, we show data of total cross section from accelerator (squares and circles) [6] and the cosmic-ray points are those obtained in the present analysis by decreasing inelasticity (squares) and increasing inelasticity (circles). The curves, which indicate different rates of increase for σ_{tot}^{pp}, were obtained from a combination of accelerator and cosmic-ray data. Curve A was obtained by fitting all accelerator data up to $\sqrt{s} = 900$ GeV, the CDF point at $\sqrt{s} = 1.8$ TeV and the cosmic-ray data obtained with the $< K >$ which decreases with energy (squares). Curve B, instead, includes the E710 point at $\sqrt{s} = 1.8$ TeV and the cosmic-ray data obtained with the $< K >$, which increases with energy (circles). Thus, we have demonstrated to what extent the change of inelasticity with energy can affect data of σ_{tot}^{pp} extracted from cosmic-ray measurements.

An extended version of this work will appear in ref.[7].

References

1. M. Honda et al., Phys. Rev. Lett. 70 (1993) 525.

2. F. O. Durães et al., Phys. Rev. D 47 (1993) 3049.

3. M. O. Azaryan et al., Sov. J. Nucl. Phys. 20 (1975) 213; S. A. Slavatinskii et al., Sov. Phys. JETP 19 (1964) 1452.

4. J. Bellandi et al., J. Phys. G: Nucl. Part. Phys. 18 (1992) 579; Phys. Lett. B 279 (1992) 149.

5. R. J. Glauber, in *Lectures in Theoretical Physics* ed. W. Britten and L. G. Dunham (Interscience, N. Y., 1959) vol. I, p. 135; R. J. Glauber and G. Matthiae, Nucl. Phys. B 21 (1970) 135.

6. UA4/2 Collab., C. Augier et al., Phys. Lett. B 315 (1993) 503.

7. J. Bellandi et al., Phys. Lett. B (1994), in press.
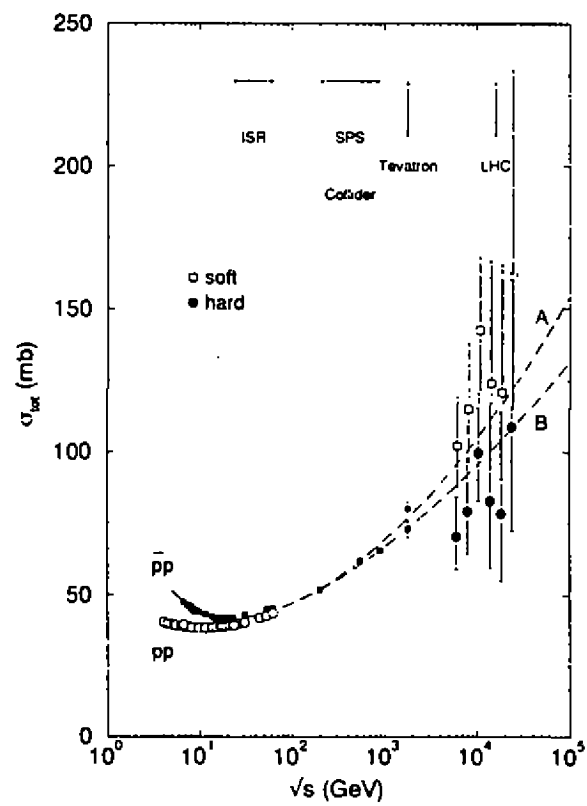
Black Hole Nucleation in 331 Model*

C.B. Peres[†]and F. Pisano

Instituto de Física Teórica - Unesp, S. Paulo, SP

Even though Hawking Radiation may seem a generic feature shared by any theory of gravitation, the consequences that the evaporation of Primordial Black Holes (PBH) can have on our cosmological scenarios differ greatly on the theory assumed to describe the matter fields. Here we investigate some of these consequences on the light of the $SU(3)_C \times SU(3)_L \times U(1)_N$ gauge model for non-gravitational interactions. We reemphasize the peculiarities of this model and make an explicit calculation of the rate at which PBH nucleate in this framework. We contrast our results with the ones coming from the $SU(5)$ GUT, the SUSY-$SU(5)$. the SUSY-Standard Model, and finally from the Standard Model of elementary particles.

Recently there has been a considerable interest in $SU(3)_C \times SU(3)_L \times U(1)_N$ gauge extensions (from now on 331 models) [1]-[4] of the 321 Standard Model (SM) of elementary particles. This kind of models brings to a very interesting new phenomenology and on the theoretical point of view it allows us to give some answers to many fundamental questions which have been left without explanation within the 321 SM, such as the fermion family replication problem [5], the relation between the color degrees of freedom and the flavors, and the possibility of the third family being different [6][7]. Supersymmetric extensions have been also attempted [8].

Here we are concerned with a preliminary attempt of making cosmological applications of a 331 model. In particular, we are interested in calculating the black hole nucleation rate in the very early universe taking into account the fields of the model and then to compare the results with the predictions of the four models: the SM. the SUSY SM, the $SU(5)$ GUT model, and the SUSY GUT $SU(5)$, reported recently in the literature [9].

Let us display the fields of the model in the symmetric phase when the 331 symmetry is preserved. We define the electric charge operator of the theory as

$$\frac{Q}{e} = \frac{1}{2}(\lambda_3 - \sqrt{3}\lambda_8) + N \tag{1}$$

where

$$\frac{\lambda_3}{2} = \frac{1}{2}\,\mathrm{diag}\,(1,-1,0); \quad \frac{\lambda_8}{2} = \frac{1}{2\sqrt{3}}\,\mathrm{diag}\,(1,1,-2) \tag{2}$$

are the diagonal generators of the $SU(3)$ (chiral flavor) group and N denotes $U(1)_N$ charges. We can identify the weak hypercharge of the SM as

$$\frac{Y}{2} = -\frac{\sqrt{3}}{2}\lambda_8 + N; \quad Q = T_3 + \frac{Y}{2}, \tag{3}$$

where T_3 is the diagonal generator of the $SU(2)$ (chiral flavor) group. The gauge symmetry breaking hierarchy is

$$SU(3)_C \times SU(3)_L \times U(1)_N$$
$$|$$
$$SU(3)_C \times SU(2)_L \times U(1)_Y \tag{4}$$
$$|$$
$$SU(3)_C \times U(1)_Q$$

where the first step of the breaking around 3 TeV [10] is due to the VEV of the neutral component of the χ scalar triplet. All masses of the fields in the model are generated with four multiplets of scalar fields with the following transformation properties under the 331 group

$$\eta \sim (1,3,0). \quad \rho \sim (1,3,+1), \quad \chi \sim (1,3,-1)$$
$$S_{ij}^- \sim (1,6_S^*,0) \tag{5}$$

and in the symmetric phase of the theory they are parameterized by 30 real scalar fields.

There are 17 spin-1 gauge fields:

$$
\begin{aligned}
SU(3)_C &: & g_\mu^i &\sim (8,1,0); & i = 1,...,8; \\
SU(3)_L &: & W_\mu^j &\sim (1,8,0); & j = 1,...,8; \\
U(1)_N &: & B_\mu &\sim (1,1,0).
\end{aligned}
\tag{6}
$$

The spin-$\frac{1}{2}$ fermions of the theory consist of three triplets of leptons,

$$
L_l \sim (1,3_L,0), \quad l = e,\mu,\tau
\tag{7}
$$

which contain 9 fields. There are not right-handed leptonic $SU(3)$ flavor singlets. There are also three families of quarks with the transformation properties:

$$
\begin{aligned}
Q_{1L} &\sim (3,3,+2/3), \\
u_R \sim (3,1,+2/3), \quad d_R &\sim (3,1,-1/3), \quad J_{1R} \sim (3,1,+5/3)
\end{aligned}
\tag{8}
$$

for the first family, and

$$
\begin{aligned}
Q_{\alpha L} &\sim (3,3^*,-1/3) \\
J_{\alpha R} \sim (3,1,-4/3), \quad c_{\alpha R} &\sim (3,1,+2/3), \quad s_{\alpha R} \sim (3,1,-1/3),
\end{aligned}
\tag{9}
$$

where $\alpha = 2,3$ labels the second and third families. Taking into account the color degrees of freedom we have an amount of 54 quarks fields. In the model there are not any spin-$\frac{3}{2}$ Rarita-Schwinger fields. Then the total number of massless fields in the 331 model is 110.

The rate of primordial black hole nucleation per unit volume and unit time (with $\hbar = c = k_B = G = 1$) is given by [11][12]

$$
\Gamma(T) = 0.87 \; T \left(\frac{\mu}{T}\right)^\Theta \frac{1}{64\pi^3} \exp\left(-\frac{1}{16\pi T^2}\right)
\tag{10}
$$

where T is the temperature of the thermal bath simulating the very early universe conditions, μ is a mass regulator parameter close to the Planck mass, and Θ is a numerical factor which depends on N_s, the number of spin fields accessible to the system:

$$
\Theta = \frac{1}{45} \left(212 N_{s=2} - \frac{233}{4} N_{s=3/2} - 13 N_{s=1} + \frac{7}{4} N_{s=1/2} + N_{s=0}\right).
\tag{11}
$$

Bellow we list for each theory considered here the number of relatively massless fields (including the graviton) and the associate parameter Θ [9]

Theory	N	Θ
SM	62	3.083
SUSY SM	132	3.656
SUSY $SU(5)$	242	3.000
$SU(5)$	104	0.283
331-Model	111	4.361

Now we will assume that physics holds beyond the Planck scale in order to obtain the behavior of the nucleation rate $\Gamma(T)$ for each of these models under this hypothesis. The results are presented in the graphics where the temperature is given in $\mu = 1$ unities of Planck temperature.
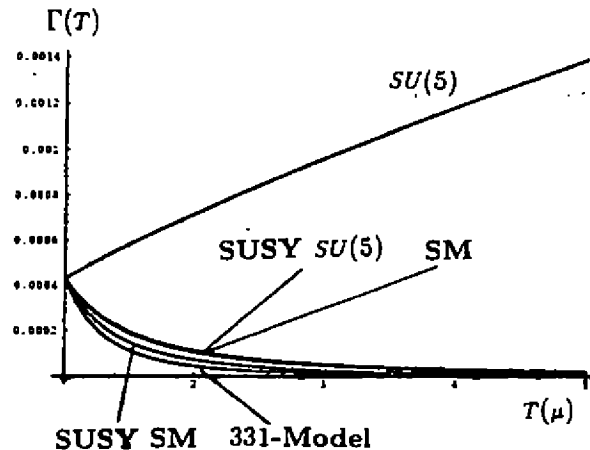
Therefore we summarize the following remarkable results: The nucleation rate for the $SU(5)$ theory increases with the temperature but the rate is essentially the same for both the SM and the SUSY $SU(5)$ model. Finally, in this context the 331 Model provides the smallest nucleation rate.

Acknowledgements

References

1. The original reference is F. Pisano and V. Pleitez, Neutrinoless Double Beta Decay and Doubly Charged Gauge Bosons, IFT-P.017/91 (1991); F. Pisano and V. Pleitez, Phys. Rev. D46 (1992) 410

2. R. Foot, O.F. Hernandez, F. Pisano and V. Pleitez, Phys. Rev. D47 (1993) 4158

3. J.C. Montero, F. Pisano and V. Pleitez, Phys. Rev. D47 (1993) 2918

4. A complete list of references concerning 331 models including the phenomenology can be found in F. Pisano, V. Pleitez and M.D. Tonasse, Chiral Extensions of the Standard Model (Preliminary version), IFT S. Paulo (1994)

5. F. Pisano and Tran A. Tuan, Anomaly Cancellation in a Class of Chiral Flavor Gauge Models, Trieste Report. IC/93/200: Proc. XIV ENFPC. SBF, pp. 322-330 (1993)

6. P.H. Frampton, The Third Family is Different, Univ. of North Carolina Report (1994)

7. D.G. Dumm, F. Pisano and V. Pleitez, Mod. Phys. Lett. A9 (1994) 1609

8. T.V. Duong and E. Ma, Supersymmetric $SU(3) \times U(1)$ Gauge Model: Higgs Structure at the Electroweak Energy Scale, Univ. of California Report, UCRHEP-T111 (1993)

9. G. Hayward and D. Pavon, Phys. Rev. D40 (1989) 1748

10. D. Ng, Phys. Rev. D49 (1994) 4805

11. D. Gross, M.J, Perry and L.G. Yaffe, Phys. Rev. D25 (1982) 330: D36 (1987) 4805

12. J.I. Kapusta, Phys. Rev. D30 (1984) 831

A Radiative Corrections Scheme for Generation of the Lepton Masses*

F. Pisano, V. Pleitez

Instituto de Física Teórica - Unesp, S. Paulo, SP

M. D. Tonasse

Instituto de Física da Universidade de São Paulo, S. Paulo, SP

We consider in the context of 331 model of the electroweak interactions the generation of the lepton masses by introducing a single neutral right-handed singlet in a radiatively corrections scheme. By adding a lepton-barion number violating term in the Higgs potential, we show that one can have the right mass spectrum for the leptons without introducing a sextet of Higgs fields which is present in the original model.

Let us consider the electroweak sector of the model with full gauge symmetry [1]-[2] $G_{331} \equiv SU(3)_C \times SU(3)_L \times U(1)_N$ where the leptons transform under G_{331} as $(1,3,0)$ and the gauge invariant renormalizable Higgs potential is

$$V(\eta, \rho, \chi) = [\lambda'(\eta^\dagger \chi)(\eta^\dagger \rho) + \lambda \epsilon^{ijk} \eta_i \rho_j \chi_k + H.c.]$$
$$+ \text{Hermitian terms} \tag{1}$$

for the Higgs multiplets $\eta \sim (1,3,0)$, $\rho \sim (1,3,1)$, and $\chi \sim (1,3,-1)$. There is the global $\mathcal{F}$-symmetry. $\mathcal{F} = B + L$. which prevent the neutrinos to get a mass. The λ'-term violates the $\mathcal{F}$-symmetry explicitly and contains interactions like $\rho^0 \chi^0 \eta_1^- \eta_2^+$, $\eta^0 \rho^0 \eta_1^- \chi^+$. Now, we introduce a single right-handed neutrino in the same fashion as the Ref.[3]. Two neutrinos and the electron are massless at zeroth order, while the other leptons – two neutrinos. the muon. and the tau – are massive. Fig.1 shows the one-loop contribution to the charged leptons (μ', τ') mass matrix.

$$\begin{pmatrix} m & \xi v_\chi \\ \xi v_\chi & m \end{pmatrix}, \tag{2}$$

with

$$\xi = \lambda^2 \frac{\lambda' f_{\mu\tau}^2}{48\pi^2} \frac{h_\mu h_\tau}{A^2 + m_P'^2} v_\chi^3 v_\rho m_P' \int_0^1 dx \frac{x^3}{[(m_P'^2 - m_\phi^2)x - m_P'^2]^3} \tag{3}$$

where m_ϕ stands for a typical value of the scalar masses, v_ρ and v_χ are the VEV's of the neutral components of the ρ- and χ-triplets, and $A^2 = h_e^2 + h_\mu^2 + h_\tau^2$ (h's have mass dimension). The neutrino mass m_P' follows the see-saw relation $m_F' m_P' = A^2$.

The eigenvalues of the matrix in Eq. (2) are m_μ and m_τ such that $m_\mu + m_\tau = 2m$ and $m_\tau - m_\mu = 2\xi$ being $m = v_\eta f_{\mu\tau}$ ($f_{\mu\tau}$ is an arbitrary dimensionless Yukawa parameter and v_η is the VEV of the neutral η-triplet component). With a reasonable choice of parameters. $v_\eta^2 + v_\rho^2 \approx (246 \text{ GeV})^2$, $v_\eta 10 \text{ GeV}$. that is $f_{\mu\tau} \approx 0.1$: $m_P' \approx 30$ MeV and $v_\chi \approx 1$ TeV. We can also choose the A parameter in such a way that $h_\mu h_\tau/(A^2 + m_P') \leq 0.5$ if $h_\mu \approx h_\tau$ and $\lambda' \approx 0.5$. We assume that $m_\phi \sim 60$ GeV, and evaluating the integral in Eq. (3), from the one-loop diagram in Fig.1 we obtain $m_\mu \approx 105$ MeV and $m_\tau \approx 1777$ MeV [4] when the trilinear mass scale $\lambda \approx 1064$ GeV.

The other two neutrinos get a finite Majorana mass from the diagram of the Fig.2. Finally, the electron get a mass from the diagram of Fig.3.
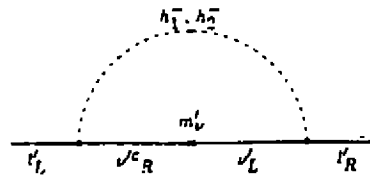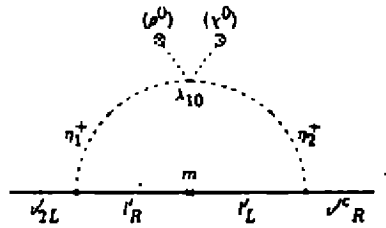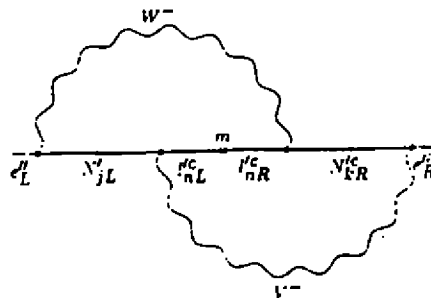
Figure 1

Figure 2

Figure 3

[1] The original reference is F. Pisano and V. Pleitez, Neutrinoless Double Beta Decay and Doubly Charged Gauge Bosons, IFT-P.017/91 (1991); F. Pisano and V. Pleitez, Phys. Rev. D46 (1992) 410

[2] R. Foot, O.F. Hernandez, F. Pisano and V. Pleitez, Phys. Rev. D47 (1993) 4158; J.C. Montero, F. Pisano and V. Pleitez Phys. Rev. D47 (1993) 2918

[3] C. Jarlskog, Nucl. Phys. A518 (1990) 129; Phys. Lett. B241 (1990) 579

[4] Particle Data Group, Review of Particle Properties, Phys. Rev. D50 (1994) 1173

PARTICIPANTES

ADILSON JOSE DA SILVA - IFUSP
ADOLFO MAIA JUNIOR - UNICAMP
ADOLFO PEDRO C. MALBOUISSON - CBPF
ADRIANA BRUNSTEIN - IFUSP
ADRIANA L. GODOI - UNICAMP
ADRIANA PEREIRA DE MEDEIROS - UCP
ADRIANO ANTONIO NATALE - IFT
ADRIANO SANTANA PEDRA - UFES
AGUSTIN R. ZUNIGA GAMARRA - UNICAMP
ALBERTO CORREA DOS REIS - CBPF
ALBERTO FRANCO DE SA SANTORO - CBPF
ALDO SOARES CARDOSO - UFRJ
ALEX ITIRO SHIMABUKURO - UNICAMP
ALEXANDRE GOLDEGOL - UFRJ
ALEXANDRE GOMES MOSCOSO - UCP
ALEXANDRE TORT - UFRJ
ALFREDO TAKASHI SUZUKI - IFT
ALVARO DE SOUZA DUTRA - UNESP-GUAR
ALVARO FAVINHA MARTINI - UNICAMP
ALVARO LEONARDI AYALA FILHO - UFRGS
ANA GABRIELA GRUNFELD - LA PLATA
ANA LUCIA BARBOSA - IFT
ANDERSON CAMPOS FAUTH - UNICAMP
ANDRE BESSADAS PENNA FIRME - CBPF
ANDRE LUIZ C. DE GOUVEA - PUC/RJ
ANDRE LUIZ MOTA - UFMG
ANDRE ZUKOSKI - UCP
ANDREA DE AZEVEDO MOREGULA - UFRJ
ANDREI GRIB - UNICAMP
ANGELA FOERSTER - UFRGS
ANNA MARIA FREIRE ENDLER - CBPF
ANTONIO C. BAPTISTA ANTUNES - UFRJ
ANTONIO EDSON GONCALVES - IFUSP
ANTONIO J. SEGUI-SANTONJA - ZARAGOZA
ANTONIO R.PERISSINOTTO BIRAL - UNICAMP
ANTONIO SOARES DE CASTRO - UNESP-GUAR
ANTONIO TAVARES DA COSTA JR - UFF
ARMANDO TURTELLI JUNIOR - UNICAMP
AZIZ NACIB AB'SABER - SBPC
BARDO ERNST JOSEP BODMANN - UFRGS
BEATRIZ BORGES CASARO - IFUSP
BERNARD MARIE MARECHAL - UFRJ
BRUTO MAX PIMENTEL ESCOBAR - IFT
CARLA VALLE - UCP
CARLOS A.ARAGAO DE CARVALHO FILHO. UFRJ
CARLOS ALBERTO FERREIRA LIMA - CBPF
CARLOS ALBERTO SANTOS E ALMEIDA - UFCE
CARLOS ALBERTO TELLO SAENZ - UNICAMP
CARLOS ENRIQUE NAVIA OJEDA - UFF
CARLOS FARINA DE SOUZA - UFRJ
CARLOS FREDERICO CHARRET BRANDT - UFF
CARLOS M NAON - LA PLATA
CARLOS MERGULHAO JUNIOR - IFUSP
CARLOS OURIVIO ESCOBAR - IFUSP
CAROLA DOBRIGKEIT CHINELLATO - UNICAMP
CESAR AUGUSTO ZEN VASCONCELOS - UFRGS
CESAR P. DA NATIVIDADE - UNESP-GUAR
CEZAR AUGUSTO BONATO - UFPB

CLAUDIO B. S. FURTADO - UFPE
CLAUDIO GONCALVES CARVALHAESUFF
CLIFFORD NEVES PINTO - UFRJ
D. ALTSCHULER - ZURICH
D. NANOPOULOS - TEXAS A&M
DANIEL ALBERTO GOMES DUMM - LAPLATA
DANIEL GUSTAVO BARCI - UFRJ
DARIO SASSI THOBER - UNICAMP
DENIS DALMAZI - UNESP-GUAR
DENISON DE SOUZA SANTOS - PUC/RJ
DING PING LI - CBPF
DMITRI MAKSIMOVITCH GITMAN - IFUSP
EDGAR MARTINEZ MARMOLEJO - UNICAMP
EDMUNDO MARINHO DO MONTE - UNB
EDSON MINORU KUBO - IFUSP
EDUARDO CANTERA MARINO - UFRJ
EDUARDO DE MORAES GREGORES - IFT
EDUARDO SOUZA FRAGA - PUC/RJ
EDUARDO TADEU FERNANDES - IFUSP
EDUARDO VALENTINO TONINI - UFES
EDUARDO VASQUEZ CORREA SILVA - UFRJ
ELLY SILVA - CBPF
EMILIO JORGE LYDIA - UFRJ
ERASMO MADUREIRA FERREIRA - UFRJ
ERNESTO KEMP - UNICAMP
ERNST WOLFGANG HAMBURGER - IFUSP
EUGENE LEVIN - CBPF
EUGENIO RAMOS BEZERRA DE MELLO - UFPB
EVERTON MURILO CARVALHO DE ABREU - UFRJ
F. HALZEN - MADISON
FABIO BOSCO MOURA SALEMME - IFUSP
FELICE PISANO - IFT
FELIX RENE ARIAS REVOLLO - UEL
FERNANDA GALLINUCCI GARCIA - IFUSP
FERNANDO M. LEAO DE ALMEIDA JR - UFRJ
FERNANDO MIGUEL PACHECO CHAVES - IFUSP
FERNANDO PABLO DEVECCHI - UFRGS
FERNANDO RAIMUNDO ARANHA SIMAO - CBPF
FERNANDO TADEU CALDEIRA BRANDT - IFUSP
FLAVIO GIMENEZ ALVARENGA - UFES
FLAVIO IMBERT DOMINGOS - UCP
FRANCISCO ANTONIO PENA CAMPOS - IFUSP
FRANCISCO E. MENDONCA DA SILVEIRA - IFT
FRANCISCUS JOZEF VANHECKE - UFRJ
FRANZ PETER ALVES FARIAS - UFBA
FREDERICO A. JANZON MORENO - IFUSP
GALINA PUGACHEVA - UNICAMP
GALVAO - UNB
GEORGIJ TAKHTAMYSHEV - CBPF
GIL DA COSTA MARQUES - IFUSP
GILMAR DE SOUZA DIAS - UFES
GILVAN AUGUSTO ALVES - CBPF
H. EDWARD SEIDE - LNCSA
HEBE QUEIROZ PLACIDO - UFBA
HELIO MANOEL PORTELLA - UFF
HELIO NOGIMA - UNICAMP
HELIO TEIXEIRA COELHO - UFPE
HENDLY DA SILVA CARVALHO - UFRJ

HENRIQUE BOSCHI FILHO - UFRJ
HERON CARLOS DE GODOY CALDAS - UFMG
HORACIO OSCAR GIROTTI - UFRGS
HUGO ROLANDO CHRISTIANSEN - LA PLATA
HUMBERTO DE MENEZES FRANCA - IFUSP
IGNACIO A.DE BEDIAGA E HICKMAN - CBPF
IRAZIET DA CUNHA CHARRET - UFF
ITZHAK RODITI - CBPF
IVANO DAMIAO SOARES - CBPF
IVONE F. DA MOTA E. ALBUQUERQUE - IFUSP
JAIR VALADARES COSTA - UFES
JANILO SANTOS - UFRN
JEFERSON DE LIMA TOMAZELLI - IFT
JOAO BARCELOS NETO - UFRJ
JOAO CARLOS DOS ANJOS - CBPF
JORGE ABEL ESPICHAN CARRILLO - UNICAMP
JORGE ANANIAS NETO - CBPF
JORGE EDUARDO CIEZA MONTALVO - UERJ
JORGE M. CARVALHO MALBOUISSON - IFUSP
JORGE R. V. DOMINGOS - UCP
JOSE ALEXANDRE NOGUEIRA - UFES
JOSE AUGUSTO CHINELLATO - UNICAMP
JOSE EDUARDO M. HORNOS - IFQSC
JOSE FERNANDO PEREZ - IFUSP
JOSE FRANCISCO GOMES - IFT
JOSE GUILHERME ROCHA DE LIMA - CBPF
JOSE KENICHI MIZUKOSHI - IFUSP
JOSE LEITE LOPES - CBPF
JOSE LUIS VAZQUEZ BELLO - CBPF
JOSE LUIZ MATHEUS VALLE - UFJF
JOSE MONTANHA NETO - UNICAMP
JOSE ROBERTO PINHEIRO MAHON - UERJ
JOSE R. SOARES DO NASCIMENTO - IFUSP
JOSE RODRIGO PARREIRA - IFUSP
JOSE W. F. VALLE - VALENCIA
JUAN ALBERTO MIGNACO - UFRJ
JUAREZ CAETANO DA SILVA - UFBA
JULIO CESAR FABRIS - UFES
JULIO CESAR NEVES PESSANHA - CBPF
KALED DECHOUM - IFUSP
LAURA MARIA RUBI FALCO - IFUSP
LEILA JORGE ANTUNES - IEN
LEONARDO FOGEL - UCP
LIGIA M. COELHO DE SOUZA RODRIGUES - CBPF
LINDOLPHO DE CARVALHO DIAS - CNPQ
LUCIANE RANGEL DE FREITAS - UFRJ
LUCIENE PONTES FREITAS - IFT
LUIS ALBERTO DE OLIVEIRA - CBPF
LUIS ANTONIO CABRAL - IFUSP
LUIS CARLOS MALACARNE - IFUSP
LUIS GALHARDO FILHO - IAG
LUIZ C. MARQUES DE ALBUQUERQUE UFRJ
LUIZ CLAUDIO PEREIRA - UNB
LUIZ CLAUDIO QUEIROZ VILAR - CBPF
LUIZ EDUARDO SILVA SOUZA - UFRJ
LUIZ F.BLOOMFIELD TORRES - UFRJ
LUIZ PAULO COLATTO - CBPF
LUIZ VICTORIO BELVEDERE - UFF
M. ASOREY - ZARAGOZA
MANOELITO MARTINS DE SOUZA - UFES

MAOR URI - CBPF
MARCELLO BARBOSA DA SILVA NETO - CBPF
MARCELO A. LEIGUI DE OLIVEIRA - UNICAMP
MARCELO COSTA DE LIMA - CBPF
MARCELO DE MOURA LEITE - IFUSP
MARCELO DE OLIVEIRA SOUZA - UENF
MARCELO DE SOUZA ALVES - UFRJ
MARCELO EVANGELISTA DE ARAUJO - UNB
MARCELO JOSE REBOUCAS - CBPF
MARCELO OTAVIO CAMINHA GOMES - IFUSP
MARCELO PORTES DE ALBUQUERQUE - CBPF
MARCIA BEGALLI - UERJ
MARCIA GONCALVES DO AMARAL - UFF
MARCIO JOSE MENON - UNICAMP
MARCO ANTONIO DE ANDRADE - CBPF
MARCUS VENICIUS COUGO PINTO - UFRJ
MARGARIDA M. RODRIGUES NEGRAO - CBPF
MARIA ALINE BARROS TRAVESSA - UFRJ
MARIA B. DE LEONE GAY DUCATTI - UFRGS
MARIA C. VON REICHENBACH - LA PLATA
MARIA CRISTINA PEREIRA - G
MARIA ELENA POL - CBPF
MARIA LUIZA BEDRAM - UFRJ
MARIA NATALIA PORTELA MAGALHAES - CBPF
MARIA TERESA C. DOS SANTOS HOMAZ - UFF
MARIO EVERALDO DE SOUZA - UFSE
MARIO NOVELLO - CBPF
MARTA LILIANA TROBO - LA PLATA
MARTHA CHRISTINA MOTTA DA SILVA - CBPF
MARTIN FLECK - UFRGS
MAURICIO BERNARDINO MAGRO - IFUSP
MAURICIO DOS SANTOS BARBI - UFRJ
MAURICIO ORTIZ CALVAO - UFRJ
MAURO DONIZETI TONASSE - IFUSP
MOACYR HENRIQUE GOMES E. SOUZA - CBPF
NAMI FUX SVAITER - CBPF
NATHAN BERKOVITS - IFUSP
NAZIRA ABACHE TOMIMURA - UFF
NELSON RICARDO DE FREITAS BRAGA - UFRJ
NEUSA AMATO - CBPF
O. PIGUET - GENEVE
ORLANDO LUIS GOULART PERES - IFT
OSCAR JOSE PINTO EBOLI - IFUSP
OSWALDO MONTEIRO DEL CIMA - CBPF
P. SODANO - PERUGIA
PATRICIO ALFREDO GAETE DURAN - UFRJ
PAULO CESAR BEGGIO - UNICAMP
PAULO CESAR RIBEIRO QUINTAIROS - CBPF
PAULO ISRAEL TRAJTENBERG - CBPF
PAULO SERGIO KUHN - UFRGS
PAULO SERGIO RODRIGUES DA SILVA - IFT
PEDRO GALLI MERCADANTE - IFUSP
RAFAEL DE LIMA RODRIGUES - UFPB
RAIMUNDO MUNIZ TEIXEIRA FILHO - IFUSP
RAMON MENDEZ GALAIN - URUGUAY
REGINA CELIA ARCURI - UFRJ
REGINA HELENA CEZAR MALDONADO - UFF
REGINA MARIA RICOTTA - FATEC
RENATA DA SILVA ANDRADE - UCP
RENATA ZUKANOVICH FUNCHAL - IFUSP

RENATO KLIPPERT BARCELLOS - CBPF
RENATO MELCHIADES DORIA - UCP
RICARDO R. LANDIM DE CARVALHO - CBPF
ROBERTO JOSE MARIA COVOLAN - UNICAMP
ROBSON NASCIMENTO SILVEIRA - UFES
ROGERIO ROSENFELD - EXTERIOR
ROLAND KOBERLE - IFQSC
RONALD CINTRA SHELLARD - PUC/RJ
RONALDO THIBES - UFRJ
ROSSANA C. FALCAO - CBPF
RUDNEI DE OLIVEIRA RAMOS - IFUSP
SAMUEL ROCHA DE OLIVEIRA - UNB
SANDRA DOS SANTOS PADULA - IFT
SANDRA FILIPPA AMATO - UFRJ
SANDRA SAUTU - CBPF
SANTIAGO PEREZ BERGLIAFFA - LA PLATA
SAULO CARNEIRO DE SOUZA SILVA - IFUSP
SEBASTIAO ALVES DIAS - CBPF
SERGIO ANEFALOS PEREIRA - IFUSP
SERGIO E.DE CARVALHO EYER JORAS - UFRJ
SERGIO FERRAZ NOVAES - IFT
SERGIO LUIZ CARMELO BARROSO - UNICAMP

SERGIO MARTINS DE SOUZA - UFRJ
SERGIO MORAIS LIETTI - IFUSP
SERGIO V. DE BORBA GONCALVES - UFES
SILVESTRE RAGUSA - IFQSC
SILVIO PAOLO SORELLA - CBPF
SOLANGE DA FONSECA RUTZ - LNCC
T. SJOSTRAND - CERN
TANIA GLAUCIA DARGAM - UFRJ
THAIS SCATTOLINI LORENA LUNGOV - IFUSP
UBIRAJARA FERRAIOLO WICHOSKI - IFUSP
VAN SERGIO ALVES - IFUSP
VERISSIMO MANOEL DE AQUINO - UEL
VICTOR DE OLIVEIRA RIVELLES - IFUSP
VITOR EMANUEL RODINO LEMES - CBPF
VITOR OGURI - CBPF
VITORIO ALBERTO DE LORENCI
WALDEMAR MONTEIRO. DA SILVA JR - UFF
WALTER FELIPE WRESZINSKI - IFUSP
WEUBER DA SILVA CARVALHO - UFRJ
Y. NUTKU - MARMARA
YARA DO AMARAL COUTINHO - UFRJ